UNIVERSIDADE FEDERAL DE SÃO CARLOS
CENTRO DE CIÊNCIAS EXATAS E DE TECNOLOGIA
DEPARTAMENTO DE QUÍMICA
PROGRAMA DE PÓS-GRADUAÇÃO EM QUÍMICA

"*Picramnia glazioviana* and *Picramnia bahiensis* as source for new natural products. Insecticidal and fungicidal evaluations and High-Resolution Bioassay/HPLC-HRMS-SPE/NMR studies"

Leila Gimenes*

Thesis presented as part of the requirements to obtain the title of DOCTOR in SCIENCES, concentration area: ORGANIC CHEMISTRY

Supervisor: Prof. Dr. João Batista Fernandes

*** FAPESP sponsorship**

São Carlos - SP
2018

UNIVERSIDADE FEDERAL DE SÃO CARLOS

Centro de Ciências Exatas e de Tecnologia
Programa de Pós-Graduação em Química

Folha de Aprovação

Assinaturas dos membros da comissão examinadora que avaliou e aprovou a Defesa de Tese de Doutorado da candidata Leila Gimenes, realizada em 27/04/2018:

Prof. Dr. João Batista Fernandes
UFSCar

Prof. Dr. João Henrique Ghilardi Lago
UNIFESP

Prof. Dr. Tiago Venâncio
UFSCar

Prof. Dr. Eli Fernando Pimenta
UFSCar

Prof. Dr. Jairo Kenupp Bastos
FCFRP/USP

Aos meus pais Celso e Odila, por estarem sempre presentes em minha vida, por dedicarem tudo de si e me permitirem chegar onde estou. Aos meus irmãos Allyson, Philipi e Leandro, mostrando a verdadeira importância de se ter uma família. Ao meu lindo afilhado Anthony, por ensinar que a vida pode ser leve apenas com um sorriso.

Agradeço ao meu namorado Rodrigo, pelo seu amor, imensa dedicação, companheirismo, apoio e carinho.

“Energy can have two dimensions. One is motivated, going somewhere, a goal somewhere, this moment is only a means and the goal is going to be the dimension of activity, goal oriented--then everything is a means, somehow it has to be done and you have to reach the goal, then you will relax. But for this type of energy the goal never comes, because this type of energy goes on changing every present moment into a means for something else, into the future. The goal always remains on the horizon. You go on running, but the distance remains the same.

No, there is another dimension of energy: that dimension is unmotivated celebration. The goal is here, now; the goal is not somewhere else. In fact, you are the goal. In fact there is no other fulfillment than that of this moment--consider the lilies. When you are the goal and when the goal is not in the future, when there is nothing to be achieved, rather you are just celebrating it, then you have already achieved it, it is there. This is relaxation, unmotivated energy.**”**

“Listen to your being. It is continuously giving you hints; it is a still, small voice. It does not shout at you, that is true. And if you are a little silent you will start feeling your way. Be the person you are. Never try to be another, and you will become mature. Maturity is accepting the responsibility of being oneself, whatsoever the cost. Risking all to be oneself, that's what maturity is all about.**”**

“Sadness gives depth. Happiness gives height. Sadness gives roots. Happiness gives branches. Happiness is like a tree going into the sky, and sadness is like the roots going down into the womb of the earth. Both are needed, and the higher a tree goes, the deeper it goes, simultaneously. The bigger the tree, the bigger will be its roots. In fact, it is always in proportion. That's its balance.**”**

— Osho

"Que os vossos esforços desafiem as impossibilidades, lembrai-vos de que as grandes coisas do homem foram conquistadas do que parecia impossível."
Charles Chaplin

"Conheça todas as teorias, domine todas as técnicas, mas ao tocar uma alma humana, seja apenas outra alma humana"
Carl J. Jung

ACKNOWLEDGMENTS

This work would not have been possible without the financial support from *Fundação de Ámparo à Pesquisa do Estado de São Paulo* – FAPESP (FAPESP Grants: 2013/20458-1 and 2016/18024-1) for the scholarship in Brazil, and abroad. I am also grateful to CNPq (CNPQ Grant: 141754/2013-3) and Capes for the financial support received to the research and instruments.

I would like to thank all those who have helped me in carrying out my research, and those I had the pleasure to meet and work together during this journey. Each of you contributed in some way to my progress, overcoming, motivation, and self-knowledge.

Especially, I am extremely grateful for those that have been close to me, those who gave me kind advices, and cheered for my best and achievements. My sincere thanks to:

Prof. Dr. João Batista Fernandes, who has accepted me in his research group, giving me the generous guidance to the development of this project, and showing how a good scientist (and person) should be. Thank you for the support given, for all opportunities I had to improve myself and my professional life, for all lessons within my research, and during all my academic life. I am also grateful for inspiring me with your serenity, patience, and attentiveness. Thank you for all meetings we had to discuss my work, and for your effort in it. I will bring all the good moments I lived during my PhD to my professional and personal life, along with all the lessons and knowledge I had the pleasure to get from you.

Prof. Dr. Dan Staerk who has accepted me as a visitant student in his research group in Denmark, giving me great suggestions and tips to improve my work. I am also grateful for all opportunities I had during my staying in his group, the courses I took, the study groups and the conferences I joined. I would like to thank for finding time in his busy schedule for the meetings we had. Thank you for trusting me while troubleshooting the NMR. From this internship I could learn not only about the research, but also about life and self-knowledge.

All evaluating members who have accepted my invitation being part of my Thesis Committee, for finding some time to read my Thesis, and give the guidance necessary to improve my work and my scientific research. I am grateful for all suggestions and collaboration.

All Professors of the Natural Products Laboratory for the valuable lessons and extensive knowledge shared, especially to Prof. Dr. Paulo Cezar Vieira, for the discussions about the compounds and for the friendship, and Prof. Dr. Maria Fátima das Graças Fernandes da Silva for the contribution with the biosynthesis of my work.

Prof. Dr. Tiago Venâncio and Prof. Dr. Antônio Gilberto Ferrreira (Giba) for taking care of the NMR instruments, for allowing us to use the space and contributing with tips and knowledge about the technique. Also, for being willing to help, and for the friendship.

Prof. Dr. João Henrique G. Lago for inspiring me to the research of natural products, for teaching me the first steps of my professional life, and to Prof. Dr. Paulete Romoff, for having participated in my academic life and for the lessons as well. I am grateful to you both for the friendship; it is always a pleasure for me to meet you again.

Prof. Dr. Odair Correa Bueno for the insecticide bioassays, together with the students responsible for this work, especially to Marcela Ceccato for all her help.

Technician Ms. Dorai Periotto Zandonai for the fungicide bioassays, for the dedication and commitment. Certainly, an example of kindness and sweetness as a professional. Thanks for your friendship.

Prof. Dr. João Marcos Batista Jr. and Prof. Dr. Fernando Martins dos Santos Jr. for the VCD analysis and DFT calculations.

Technician Arife Onder for the kind help I received during my staying at Copenhagen University, for the friendship and all her effort while taking care of the lab and the

organization of it, allowing everything to be well done. Thanks for your sweetness and patience while helping.

All friends I met during this academic journey, which contributed in a different way of my life and work, and for the good moments and laughs that made my PhD life easier. Especially to my dear friends that helped me a lot during the end of this journey: Alana, Taynara, and Carol. Thank you girls for all good moments we shared together and for the friendship. You are amazing!

All friends I made in KU, especially Hamidreza (Hami) for the antibacterial assay, for the tips about publications and also for being a kind friend, for our conversations, laughs and good moments shared together. I am also grateful to Djóni, Malene and the Chinese team: Tuo Li, Chao, and Yong. Thank you guys for the good moments we shared and for the friendship.

The Brazilian friends I met in Denmark: Thanks my dear friends Fer and Hitty, Fernanda, Sarah, Felipe and Nei, for the moment of relaxing and laughs.

The postgraduate secretaries Cristina, Ariane, and Luciani for taking care of the good work of the postgraduate. I am very grateful to Cristina for all the help with the documentation and attention.

Finally, nobody has been more important to me in the pursuit of this project than the members of my family and my boyfriend:

To my parents, whose love and support are with me wherever I go. Thanks for looking after me, for always giving the best of you, for not giving up on me. For showing me the meaning of love and dedication. Especially to my mom, she has done for me more than I will ever be able to give back. She is my inspiration of strength, caring, and immeasurable love. I love you both!

To my loving and supportive boyfriend Rodrigo, for all his love and dedication, for always worrying about me and my well-being, for giving his best to make me happy. Thank you for being part of my life, for supporting me and understanding the time I

have been abroad. For everything I have learned from you. For always being by my side at all times. For all the good and difficult moments we lived together. I love you!

To God, from whom I got the strength needed to overcome all difficult situations, allowing me to continue moving forward and making progress.

LIST OF MAIN SYMBOLS AND ABBREVIATIONS

δ	Chemical Shift in ppm
ϕ	Diameter
π	Pi bond
μL	Microliter
μm	Micrometer
ºC	Celsius Degree
ACN	Acetonitrile
AcOEt	Ethyl Acetate
atm	Atmosphere
Bis-Tris	bis-(2-hydroxyethyl)-imino-tris-(hydroxymethylmethane)
br s	Broad singlet
C_{18}	Octadecylsilane Phase
CC	Chromatographic Column
$CDCl_3$	Deuterated Chloroform
cm^2	Square Centimeter
COSY	Correlation Spectroscopy
d	Dublet
DAD	Diode Array Detector
DCM	Dichloromethane
dd	Doublet of doublet
ddd	Doublet of doublet of doublet
dt	Doublet of triplet
DEPT	Distortionless Enhancement by Polarization Transfer
DMSO	Dimethyl sulfoxide
dq	Doublet of quartet
DTT	Dithiothreitol
EDTA	N,N,N',N'-ethylenediaminetetraacetate
EI	Eletronic Impact Ionization
ESI	Electrospray Ionization
eV	Eletron Volt
g	Gram

GC/MS	Gas Chromatography/Mass Spectrometry
H	Height
Hex	Hexane
HMBC	Heteronuclear Multiple Bond Correlation
HPLC	High-Performance Liquid Chromatography
HPLC-HRMS-	High-Performance Liquid Chromatography-High-Resolution Mass-
SPE/NMR	Solid-Phase Extraction/Nuclear Magnetic Resonance
HSQC	Heteronuclear Single Quantum Correlation
H2BC	Heteronuclear 2-Bond Correlation
Hz	Hertz
IC_{50}	The Half Maximal Inhibitory Concentration
J	Coupling Constant
m	Multiplet
m/z	Mass-to-charge Ratio
Md	Median Survival of *Atta sexdens rubropilosa*
MeOH	Methanol
MeOD	Deuterated Methanol
mg	Milligram
MHz	Megahertz
mL	Milliliter
mm	Millimeter
MS	Mass Spectrometry
nm	Nanometer
^{13}C NMR	Thirteen Carbon Nuclear Magnetic Resonance
^{1}H NMR	Proton Nuclear Magnetic Resonance
NOESY	Nuclear Overhauser Effect Spectroscopy
pH	Potential of Hydrogen
PNPG	p-nitrophenol α-$_D$-glucopyranoside
PNPP	p-nitrophenyl phosphate
PTFE	Polytetrafluoroethylene
PTP1B	Recombinant Human Protein Tyrosine Phosphatase 1B
PVDF	Polyvinylidene difluoride
ROESY	Rotating-frame Overhauser Spectroscopy
s	Singlet

t	Triplet
td	Triplet of Doublet
THF	Tetrahydrofuran
TIC	Total Ion Current Chromatogram
TLC	Thin Layer Chromatography
Tris	Tris-(hydroxymethyl)-aminomethane
UV	UltraViolet
v/v	Volume/Volume

LIST OF TABLES

LIST OF FIGURES

ABSTRACT

Picramnia glazioviana AND *Picramnia bahiensis* AS SOURCE FOR NEW NATURAL PRODUCTS. INSECTICIDAL AND FUNGICIDAL EVALUATIONS AND HIGH-RESOLUTION BIOASSAYS/HPLC-HRMS-SPE/NMR STUDIES - Leaf-cutting ants of the genus *Atta* and *Acromyrmex* are considered the most important pests in agriculture, pastures, and reforestation programs due to the defoliation caused by the uncontrolled herbivory that the plants undergo, causing damages to the plantations and serious economic losses. In this context, the chemistry of natural products corroborates to minimize this problem with respect to the development of products for the control of leaf-cutting ants with broad spectrum characteristics of biological activities, and low environmental impact. In this work, the insecticide and fungicide profile of the extracts from *P. glazioviana* and *P. bahiensis* were evaluated. *P. glazioviana* showed a promising insecticidal activity to its ethanol extract, and to the dichloromethane (PGD) and ethyl acetate (PGA) phases. *P. bahiensis*, on the other hand, presented excellent activities to its extracts and fractions in both bioassays analyzed. These results encouraged the phytochemical study and isolation of the constituents present in both these species of plants. Thus, the study with *P. bahiensis* yielded the isolation of five known anthraquinones (chrysophanol, aloe-emodin, islandicin, pulmatin and chrysophanein) and two new anthrones C,O-diglycosides. In relation to *P. glazioviana*, from the PGD phase it was isolated twenty two new highly oxygenated nortriterpenes, compounds that present new chemical skeleton, and the biogenesis for the formation of these compounds was proposed. This is the first report of isolation of nortriterpenes in plants of the Picramniaceae family. Once it was discovered a new chemical skeleton of natural products, an achievement that brings huge contribution to the chemosystematics of this plant and to the chemistry of natural products as a whole. The HPLC-HRMS-SPE/NMR technique was also performed to this phase, allowing us to isolate and acquire excellent NMR spectra in few days of experiment, and high degree of purity for each compound. The PGD phase was also analyzed by high-resolution PTP1B, α-glucosidase and antibacterial bioassay. Although the construction of the biochromatogram has not indicated the presence of antidiabetic constituents in this phase, some constituents with antibacterial potential could be pinpointed through the biochromatogram against *Staphylococcus aureus*. This result is very promising

regarding the discovery of new natural products with important biological activities. The high-resolution bioassay was also evaluated to the methanol extract from roots of *P. bahiensis* with the enzymes PTP1B and α-glucosidase, and some constituents could be pinpointed after the construction of the biochromatogram. Thus, this is the first work presenting the evaluation of *Picramnia* species exhibiting an antidiabetic potential.

Keywords: leaf-cutting ants, *Picramnia bahiensis*, *Picramnia glazioviana*, nortriterpenes, anthraquinones, high resolution bioassay, HPLC-HRMS-SPE/NMR

RESUMO

Picramnia glazioviana E *Picramnia bahiensis* COMO FONTE PARA NOVOS PRODUTOS NATURAIS. AVALIAÇÕES INSETICIDA E FUNGICIDA E ESTUDOS DE BIOENSAIOS DE ALTA RESOLUÇÃO/HPLC-HRMS-SPE/NMR – As formigas cortadeiras do gênero *Atta* e *Acromyrmex* são consideradas as principais pragas nos programas de agricultura, pastagens e reflorestamento devido à desfolhação que as plantas sofrem causada pela descontrolada herbivoria, acarretando em danos às plantações e sérias perdas econômicas. Nesse contexto, a química de produtos naturais corrobora para minimizar esse problema no que diz respeito ao desenvolvimento de produtos para o controle de formigas cortadeiras que apresentem características de amplo espectro de atividades biológicas e baixo impacto ambiental. Neste trabalho, o perfil inseticida e fungicida dos extratos de *P. glazioviana* e *P. bahiensis* foram avaliados. *P. glazioviana* apresentou uma atividade inseticida promissora para seu extrato etanólico e para as fases em diclorometano (PGD) e em acetato de etila (PGA). *P. bahiensis*, por outro lado, apresentou excelentes atividades para seus extratos e frações em ambos bioensaios analisados. Estes resultados incentivaram o estudo fitoquímico e isolamento dos constituintes presentes em ambas as espécies de planta. Assim, o estudo com *P. bahiensis* resultou no isolamento de cinco antraquinonas conhecidas (crisofanol, aloe-emodina, islandicina, pulmatina e crisofaneina) e duas novas antronas C,O-diglicosiladas. Em relação à *P. glazioviana*, a partir da fase PGD foram isolados vinte e dois novos nortriterpenos altamente oxigenados, compostos que apresentam um novo esqueleto químico, e a biogênese para formação desses compostos foi proposta. Este é o primeiro relato do isolamente de nortriterpenos em plantas da família Picramniaceae. Uma vez que foi descoberto um novo esqueleto químico de produtos naturais, uma conquista que traz uma enorme contribuição para a quimiosistemática desta planta e para a química de produtos naturais como um todo. A técnica HPLC-HRMS-SPE/NMR foi utilizada com essa fase, permitindo o isolamento e aquisição de excelentes espectros de RMN em poucos dias de experimentos e alto grau de pureza para cada composto. A fase PGD foi também analisada pelo bioensaio de alta resolução com as enzimas PTP1B, α-glucosidase e antibacteriano. Embora a construção do biocromatograma não tenha indicado a presença de constituintes antidiabéticos nesta fase, alguns constituintes com

potencial antibacteriano puderam ser indicados através do biocromatograma contra *Staphylococcus aureus.* Este resultado é bastante promissor no que diz respeito à descoberta de novos produtos naturais com importantes atividades biológicas. O bioensaio de alta resolução também foi avaliado para o extrato metanólico das raízes de *P. bahiensis* frente às enzimas PTP1B e α-glucosidase e alguns constituintes puderam ser indicados após a construção do biocromatograma. Assim, este é o primeiro trabalho apresentando a avaliação de espécies de *Picramnia* exibindo potenticial antidiabético.

Keywords: formigas cortadeiras, *Picramnia bahiensis*, *Picramnia glazioviana*, nortriterpenos, antraquinonas, bioensaio de alta resolução, *HPLC-HRMS-SPE/NMR.*

SUMARY

1 – INTRODUCTION

1.1 – AGRICULTURE AND INSECT PEST

Brazil has a land mass that covers over 8.5 million square kilometers, of which 264 million ha (30%) are classified as agriculture. It is effectively the 5th largest country in the world. The magnitude of Brazilian biodiversity can be perceived in the extraordinary wealth of its ecosystems, with an extremely varied flora and fauna and an incalculable numbers of insects and microbes existing in very different habitats. (NEWMAN, 2017). Due the immense territorial area, Brazil has developed a large-scale commercial agricultural system, recognized worldwide for its role in domestic economic growth and expanding exports (MARTINELLI, 2010). Globally, the country is currently one of the leading manufacturers and exporters of food, fibers, meat and energy, and it is one of the largest producers of coffee, corn, soybeans, sugarcane (sugar and ethanol), oil plants, oranges (fresh fruit and juice), grapes, and bovine, swine, and poultry meat (OLIVEIRA, 2014).

However, the agricultural sector faces systematic annual losses due to pests and diseases. In a general approach, the large supply of food in the agricultural environment favors the emergence of insect pests, leading huge economic losses during the production process of any crop plant species. Losses caused by pests and pathogens in a global agriculture are estimated to account for 37% of production, of which about 13% is due to insects. In Brazil, the results indicate an average annual loss of 7.7% in production, representing approximately 25 million tons of food, fiber, and biofuels and total annual economic losses reaching approximately US$ 17.7 billion (OLIVEIRA, 2014; SILVA-FILHO, 2000; ZARBIN, 2009).

Specie of insect becomes an agricultural pest when its population grows wildly due the absence of the biodiversity found in forests, favoring the disappearance of many insects, also decreasing the population of its natural predators. In this scenario of large food supply, absence of predators, associated with high reproduction rate, polyphagic habit and uncontrolled herbivory, the insect pest is established, whose population growth is almost uncontrollable (ZARBIN, 2009).

In an attempt to eradicate several pests and protecting the crops, the use of pesticides has been the main measure of controlling the population of those at

a non-detrimental level. Currently, the amount of pesticides used varies annually and depends on economic and agronomic factors, and Brazil is one of the largest consumers of pesticides, including insecticides, fungicides, and herbicides. Considering only the insecticides, the country consumed 164 thousand tons in 2011, reaching an annual expenditure of US$ 2.9 billion. Currently, from the 102 active ingredients (insecticides) used in Brazil and 423 commercial products with insecticidal action registered at the Ministry of Agriculture, Livestock and Supply (MAPA), 51.6% of these belong to toxicological class I (extremely toxic) or II (highly toxic, OLIVEIRA, 2014).

However, the continuous and indiscriminate use of synthetic pesticides has intensified, leading to a gradual and almost irreversible contamination of the environment. Negative consequences of the use of these compounds, as persistence in the environment and in the produced food, including contamination of human, reduction of the natural population of predators and the biodiversity and acquisition of resistance of the pest (FORIM, 2010; RIBEIRO, 2008; VIEGAS-JUNIOR, 2003).

By the demand for rational and sustainable solutions for agricultural production, alternatives that reduce the environmental imbalance and potentiate the production become the best strategy with regarding to ecological awareness, leading to improvements in life for both farmers and consumers, besides the environment. Consequently, the use of natural products for agricultural pest control becomes a valuable tool that fits the requirements for efficacy, safety and selectivity. In general, natural insecticides are not persistent, leaving no residues in the foods and environment, and degrade faster than synthetic ones (FORIM, 2010; VIEGAS-JUNIOR, 2003).

This practice has been used since the Middle Age, with more than 2000 species of plants known for their insecticidal properties. As an example, pyrethrin (**1**), a natural compound extracted from the flowers of *Chrysanthemum cinerariaefolium*, used as an insecticide since 1800 in Persia, and it has been commercially produced since 1828 for the control of insects (VIEGAS-JÚNIOR, 2003). Another example of a natural insecticide is the neem, *Azadirachta indica*, a specie belonging to the family Meliaceae and originating from India that has several secondary metabolites, which the main compound with the greatest focus of study is the limonoid azadirachtin (**2**). This compound is active against a large spectrum of insects, non-toxic to natural predators and pollinators; it is rapidly degraded in the environment, being

recommended by several integrated pest management programs around the world. In addition, several other secondary metabolites are reported in the literature for the control of insects, such as alkaloids (nicotine, **3**), rothenoid (rotenone, **4**) and terpenes (2-norbornanol sesquiterpenic derivative, **5**). These and other examples reflect the enormous contribution that nature can provide as an alternative to conventional synthetic products, and highlights the relevance of the research contributing for the development of a sustainable and non-polluting agriculture (BOULOGNE, 2012; FORIM, 2010; VIEGAS-JÚNIOR, 2003; ZARBIN, 2009). FIGURE 1.1 illustrates the examples of natural insecticides cited above.

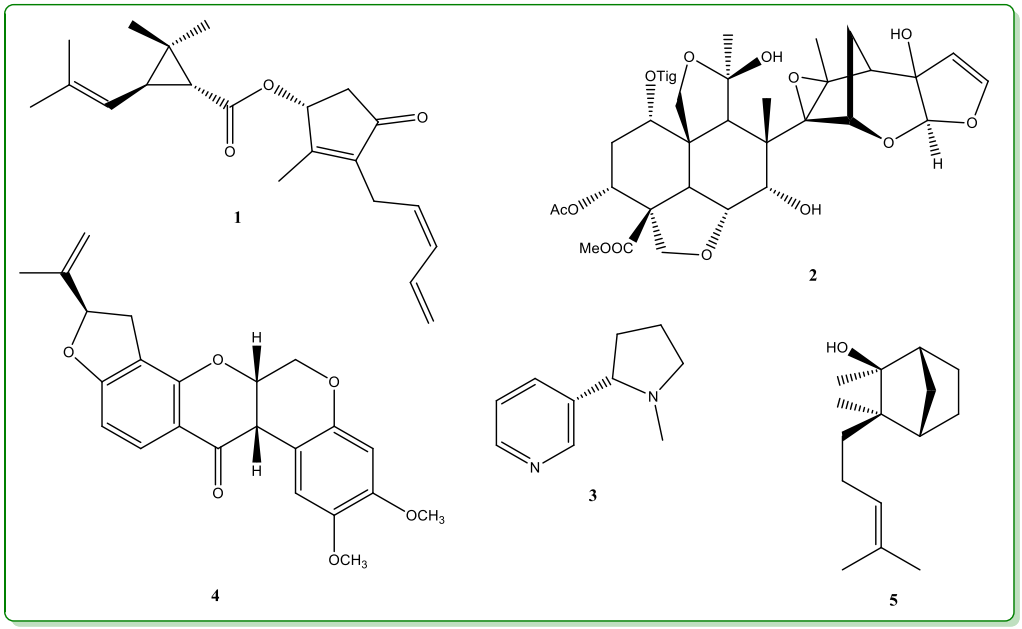

FIGURE 1.1 - Natural Insecticides: Pyrethrin (1), Azadirachtin (2), Nicotine (3), Rotenone (4) e 2-nor-bornanol derivative (5).

1.2 – LEAF-CUTTING ANTS

Ants are one of the most successful and dominant groups of insects, belonging to the class Insecta, order Hymenoptera and family Formicidae (ILHA, 2009; MARINHO, 2006; REIS-FILHO, 2007). The Attini tribe comprises about 13 genera considered leaf cutting-ants, which the genus *Atta*, are popularly known as *saúvas*, and genus *Acromyrmex*, known as *quenquéns*. They have a very wide geographical distribution, occurring throughout the American continent, from the Southern of United States, going through Central America (except for some islands

of the Antilles) and through all countries of South America (except Chile) to the center of Argentina. Brazil is the country with the highest number of *saúvas* in South America, distributed throughout the national territory, with presence of nine species of *Atta* and 21 species of the genus *Acromyrmex* (DE BRITTO, 2016).

The specie *Atta sexdens rubropilosa* lives in a mutualistic symbiosis with the fungus *Leucoagaricus gongylophorus*, which they cultivate as fungal gardens in underground nest chambers. It is a close and fully interdependent relationship. For this association, fresh leaves are brought into the nest, serving as a substrate for maintenance and growth the fungus. The fungus, on the other hand, is the only source of food for larvae and queen, as well as they produce enzymes that degrade foliar polysaccharides into assimilable nutrients for the ants, as glucose for example, serving as food for adult ants workers (FIGURE 1.2; REIS-FILHO, 2007; SCHIOTT, 2010).

(Author's picture) (BOULOGNE, 2012)

FIGURE 1.2 - Leaf-cutting ants and their simbiotic fungus.

Leaf-cutting ants can cut parts of the plants, such as flowers and leaves, corresponding about 29 to 77% of cut plants in natural environments. Chemical and physical features of the plants influence the acceptance by the ants. Generally, the workers select the plants to be cut, choosing those that present the nutritional value required by the symbiotic fungus, and rejecting those that contain toxic substances for themselves and for the fungus (DE BRITTO, 2016; REIS-FILHO, 2007; MARINHO, 2006). However, due their uncontrolled herbivory, serious damage

are caused to agriculture and forest cultivations, such as: loss of productive pasture surface, accidents with animals and farm machinery, weed proliferation, loss of soil fertility and land value, etc. An adult *Atta* nest causes a drop in productivity, for example, of 3.2 t/ha of sugar cane, corresponding of 5.3 of productivity (DE BRITTO, 2016).

Among the biological characteristics that make these insects as pests of difficult control, it can be highlighted: social organization and cooperative care with offspring and nest mates, division of tasks by castes, sterile and reproductive individuals, as well as factors such as the defense ability and chemical communication, olfactory sensitivity, learning ability, selectivity and production of antibiotic substances (which aims to reduce the growth of other fungi and bacteria present in the nest). These characteristics give them advantages over other herbivores, favoring their success, reproduction and survival (MARINHO, 2006).

Thus, the management of leaf-cutting ants is essential for Brazilian agribusiness, once these can bring huge losses to the country. In Brazil, the most used controlling method is the chemical control, highlighting the use of granulated baits containing soybean oil as a carrier, citrus pulp and a toxic active ingredient (usually the most common used are sulfluramid and fipronil, BOARETTO & FORTI, 1997; DE BRITTO, 2016). However, concerns about damage to the environment and to humans made they banned in many countries. From this perspective, an alternative control method would be the use of natural products provided by plants, more specific to leaf-cutting ants, biodegradable and less harmful to humans and the environment.

1.3 – PICRAMNIACEAE FAMILY

Picramniaceae is a family that comprises three genera (*Picramnia*, *Alvaradoa* and *Nothotalisia*) and about 50 known species. They are characterized by trees and shrubs, restricted to the American tropics. In Brazil, the Picramniaceae family represents two genera and 21 species occurring mainly in forests and in all phytogeographical domains, except Pampas. Sixteen species are endemic to the country (PIRANI & DEVECCHI, 2016).

Previously, the genera *Picramnia* and *Alvaradoa* were placed in the Simaroubaceae family due their species present small actinomorphic flower, bitter bark and pinnately compound leaves. However, studies from FERNANDO & QUINN (1995) showed differences in the structure of flowers in Picramniaceae species, leading to removal these genera from the Simaroubaceae family, and establishing a new family, Picramniaceae (LOGACHEVA & SHIPUNOV, 2017; PIRANI & DEVECCHI, 2016). Besides the decisive morphological classification to this establishment, another important aspect contributed to this positioning. Chemically, the Simaroubaceae family is characterized by the production of secondary metabolites as quassinoid, highly oxygenated degraded triterpenes. Although species of both *Picramnia* and *Alvaradoa* are also bitter, further phytochemical investigations of these plant genera reported the absence of quassinoids (JACOBS, 2003). In addition to these information, a third genus, *Nothotalisia* was recently recognized belonging to the family Picramniaceae. In 2011, after a careful examination of the received material previously described as *Talisia peruviana* (Sapindaceae), THOMAS (2011) discovered several features of the flowers and fruits, concluding the recognition of a new genus of Picramniaceae.

1.3.1 – The genus *Picramnia*

Picramnia comprises about 40 species distributed since Florida (USA), Mexico, and West Indies, through Central America to South America (Colombia, Venezuela, Peru, Brazil Paraguay and northern Argentina (FERNANDO & QUINN, 1995; PIRANI & DEVECCHI, 2016). Phytochemical investigations of some species reported the isolation of several metabolites, mainly triterpenes, anthrones, oxanthrones, anthraquinones (besides anthrone, oxanthrones and anthraquinones glycosides), coumarins and flavonoids. Most of these compounds have shown interesting pharmacological activities as fungicide, insecticide and cytotoxic (DIAZ, 2004; KITAMURA, 2013; PHIFER, 2007, ROBLEDO, 2015; RODRIGUEZ-GAMBOA, 1999 and 2000), and it was between the years 1995 to 2001 when the largest sequence of works reporting the isolation of new compounds from *Picramnia* has emerged, mainly associated to the isolation of anthraquinones and anthraquinone derivatives (HERNANDEZ-MEDEL, 1996 and 1998; RODRIGUEZ-GAMBOA, 1999;

2000 and 2001; SOLIS, 1995). Hereby is shown some examples reported in the literature (FIGURES 1.3 and 1.4).

However, although these works have reported the isolation of new compounds, a detailed search in the literature for the scientific papers during the last ten years reveal the small number of studies describing the chemical composition of *Picramnia* species. The most recent work date from 2015, presenting the antileishmanial effect of the flavonoid 5,3'-hydroxy-7,4'-dimethoxyflavanone (ROBLEDO, 2015) while MARTÍNEZ (2013) highlight the antifeedant activity associated to the very known anthraquinones (emodin and chrysophanol). None of these works in the last decade have reported the discovery of new natural products isolated from *Picramnia* species, whereas the last scientific paper published about the isolation of new compounds (new anthrone and oxanthrone C-glycosides from *Picramnia latifolia*) is from the past 14 years (DIAZ, 2004).

Since *Picramnia* species proved to be source of the isolation of new compounds, the continue studies with these species are promising to the discovery of new constituents, besides to contribute to the chemosystematics of the Picramniaceae family.

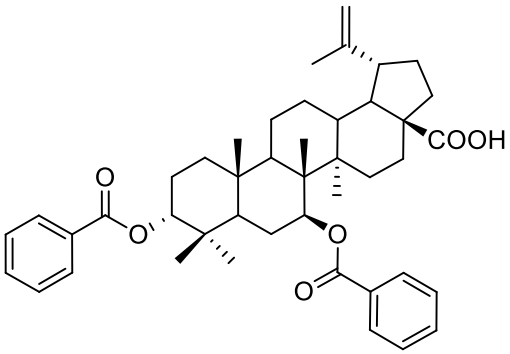

lup-20(29)-en-28-oic acid 3α,7β-dibenzoate

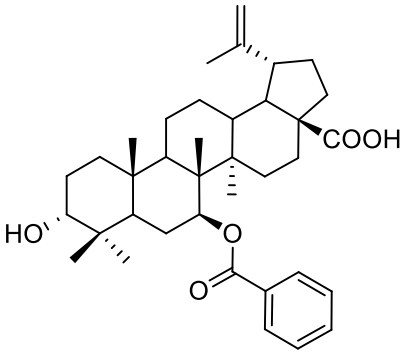

3α–hydroxy-lup-20(29)-en-28-oic acid 7β-benzoate

FIGURE 1.3 - New triterpenes isolated from *Picramnia teapensis* in 2001.

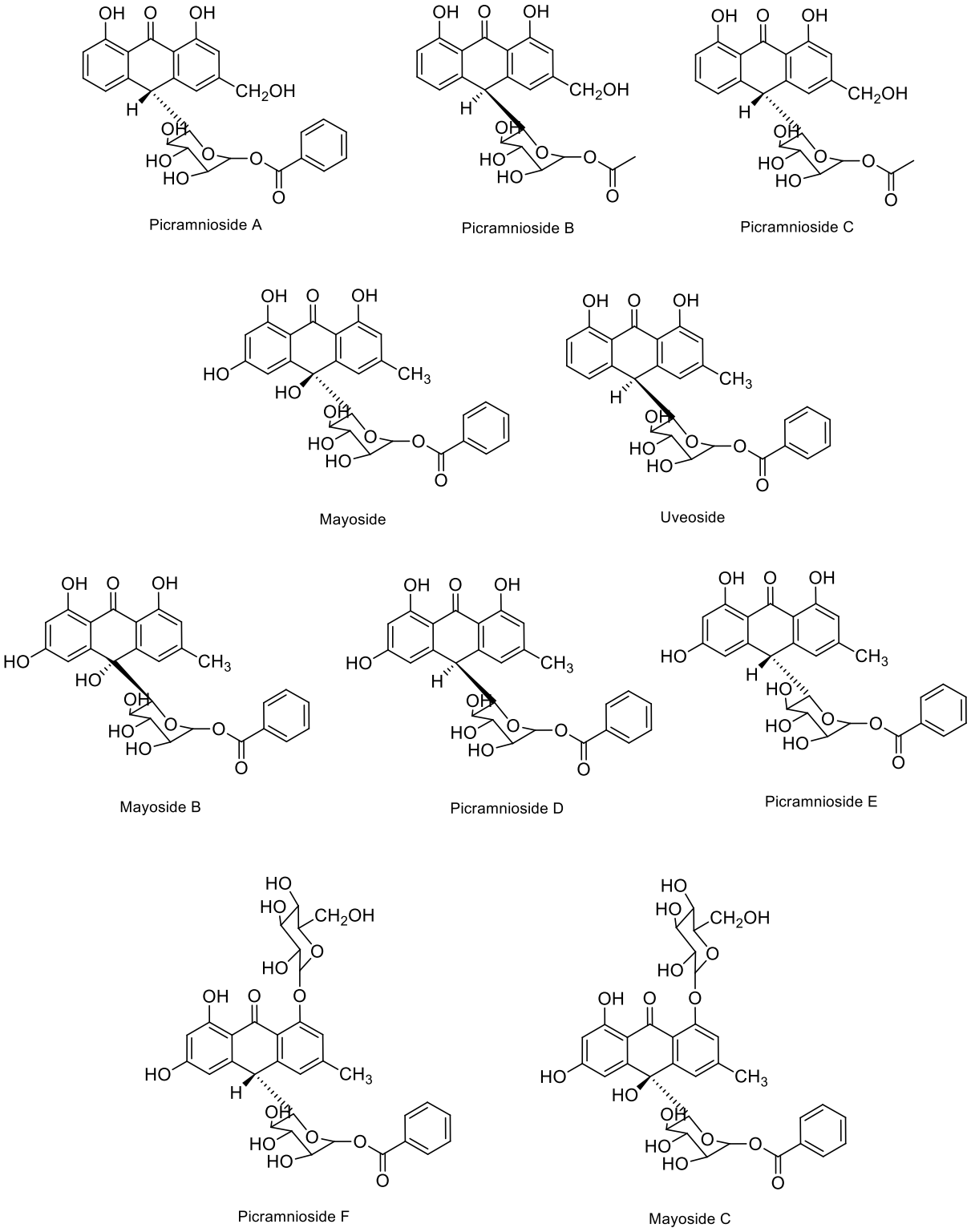

FIGURE 1.4 - New anthraquinones and derivatives isolated from *Picramnia* species between the years 1995 to 2000.

1.4 – HIGH-RESOLUTION BIOASSAYS/HPLC-HRMS-SPE/NMR

Considering the technical barriers and the classical bioassay-guided method used for obtaining pure natural products, new advanced approaches to accelerate the process and to discover a greater number of new chemical entities are urgently needed in natural products research (PAULI, 2012). Two recent technological developments in bioanalytical chemistry have enabled simultaneous chemical and pharmacological profiling of minor and major metabolites direct from crude extracts, without the need of prior isolation and purification of individual compounds. Through high-resolution bioactivity profiling, a biochromatogram of the respective enzyme assaying can be overlaid with the corresponding HPLC chromatogram. For this, the sample is microfractionated by analytical-scale HPLC into microplates followed by enzyme assaying, allowing direct pinpointing of all bioactive constituents. The second important technology is hyphenation of analytical-scale high performance liquid chromatography, high-resolution mass spectrometry, solid-phase extraction, and nuclear magnetic resonance spectroscopy (HPLC–HRMS–SPE/NMR). This technology has proven to be effective for dereplication as well as full structural characterization of individual metabolites in crude plant extracts (LIU, B, 2015; LIU, Y, 2015; TAHTAH, 2016; WUBSHET, 2016). The combination of these two technologies into the high-resolution bioassay/HPLC-HRMS-SPE/NMR bioanalytical platform constitutes a powerful technique for identification and structural characterization of bioactive compounds directly from crude extracts of plants, foods, and microorganisms. One example of the work that has been done with this hyphenated technique and dual high-resolution PTP1B and α-glucosidase enzymes is shown in FIGURE 1.5 (WUBSHET, 2016). For this present work, the bioassays using this technology were performed together with the Department of Drug Design and Pharmacology, Copenhagen University, under supervision of Prof. Dr. Dan Staerk, and are featured below:

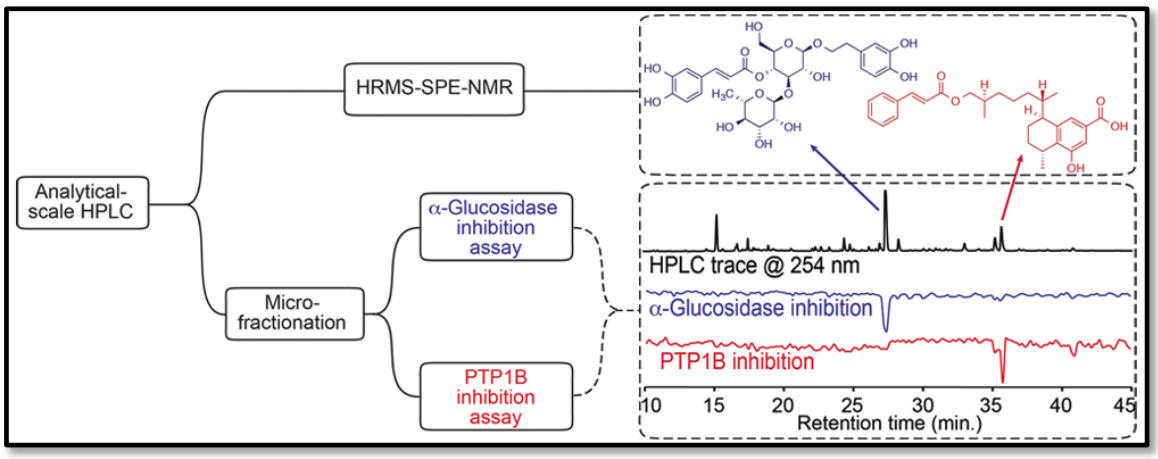

FIGURE 1.5 - Schematic overview of the dual high-resolution PTP1B and α-glucosidase/HPLC-SPE-NMR bioanalytical platform.

1.4.1 α-Glucosidase and PTP1B enzymes

Diabetes is a chronic disease that affected 387 million people worldwide in 2014 and estimations to the next 25 years is to increase to more than 592 million of people (TAHTAH, 2016). In a specific way, all carbohydrate foods are broken down into glucose in the blood. In order the body produces energy, the insulin (a hormone made by the pancreas) lets glucose pass from the blood stream into the cells. When the body present some bad dysfunction of the insulin, the glucose level in the blood is raised (hyperglycemia), being responsible for the two main types of diabetes: Type 1 Diabetes (T1D) and Type 2 Diabetes (T2D, International Diabetes Federation, 2018).

T1D occurs by an auto-immune reaction where the body's defense system attacks the cells that produce insulin, consequently making the pancreas not able to produce insulin, whereas the T2D is characterized by high and/or fluctuating blood glucose due to insulin resistance, when the body cannot make good use of the insulin it produces (International Diabetes Federation, 2018; TRINH, 2016).

Type 2 diabetes is responsible for at least 90% of all cases of diabetes and the diagnosis is often made when a complication appears or when a routine blood or urine glucose test is done. This alarming global health problem emphasizes the need for new and effective therapeutic approaches. In this context, one way of maintaining lower and more stable blood glucose is by inhibiting the α-glucosidase

enzyme in the digestive system. This enzyme is responsible in the carbohydrate hydrolysis, leading to the release of absorbable monosaccharaides to enter the blood stream, thereby elevating the blood glucose level. A second way would be by Protein tyrosine phosphatase-1B (PTP1B), an enzyme responsible for catalyzing the dephosphorylation of the activated insulin receptor, which results in down regulation of the insulin-signaling pathway. Thus, the use of plants as a source for inhibitors of both α-glucosidase and PTP1B enzymes seems as an attractive approach (International Diabetes Federation, 2018; TRINH, 2016; WUBSHET, 2015).

1.4.2 *Staphylococcus aureus*

Staphylococcus aureus is both a commensal bacterium and a human pathogen. Asymptomatic colonization for *S. aureus* in humans is far more common than infection. It is estimated that approximately 30% of the human population is colonized with this bacteria. However, the frequencies of both community-acquired and hospital-acquired staphylococcal infections have increased steadily. Infections are initiated when a breach of skin or mucosal barriers allows staphylococci access to adjoining tissues or the bloodstream. Whether an infection is contained or spreads depends on a complex interplay between *S. aureus* virulence determinants and host defense mechanisms (CHAMBERS, 2001; LOWY, 1998; TONG, 2015).

The majority of these infections occur in persons with multiple risk factors for infection. For example, higher rates than in the general population are observed in injection drug users, person with insulin-dependent diabetes, patients with dermatologic conditions, patients with long-term indwelling intravascular catheters, surgical patients, and patients with the acquired immunodeficiency syndrome. The staphylococcal manifestations can lead a variety of skin and soft tissue infections, until more severe complications as cutaneous abscesses, purulent cellulitis, infective endocarditis (IE), pleuropulmonary and osteoarticular infections. The FIGURE 1.6 presents photos of classical *S. aureus* skin and soft tissue infections (LOWY, 1998; TONG, 2015).

FIGURE 1.6 - *Staphylococcus aureus* skin and soft tissue infections.

Moreover, the abuse and lack of responsibility using antimicrobial agents, in association with the easy adaptability of microbes in all climate and environment on the planet, resulted in the emergence of drug-resistant bacterial infection, an issue that has becoming a life-threatening problem in a public health, with economic, social and medical implications, besides one of the greatest challenges of the modern medicine in the development of antibiotics. Although most antibiotics are still active, the rapid progression of resistance suggests that many of these drugs cannot be effective for so long. Consequently, these negative health trends call for a global initiative for searching of new strategies of prevention and treatment of infectious disease. From this perspective, some naturally occurring chemical compounds serve as model for a large percentage clinically proven drugs. The structural diversity of plant-derived compounds is immense, and many are being assessed as antimicrobial agents (CHAMBERS, 2001; MAHADY, 2008; SPELLBERG, B., 2008). Among the diversity of compounds that can find in the nature, it can be cited flavonoids, terpenes, phenolic acids, anthraquinones and alkaloids as antibacterial agents (GYAWALI, 2014; PACHECO, 2012; WEI, 2015). The FIGURE 1.7 illustrates some triterpenes as examples of natural products with bacterial activity against *S. aureus* (PACHECO, 2012). Thus, the discovery of new antibacterial chemical entities with novel mechanisms of action are urgently needed, and the natural products can play therefore, a significant role such as therapeutic agents.

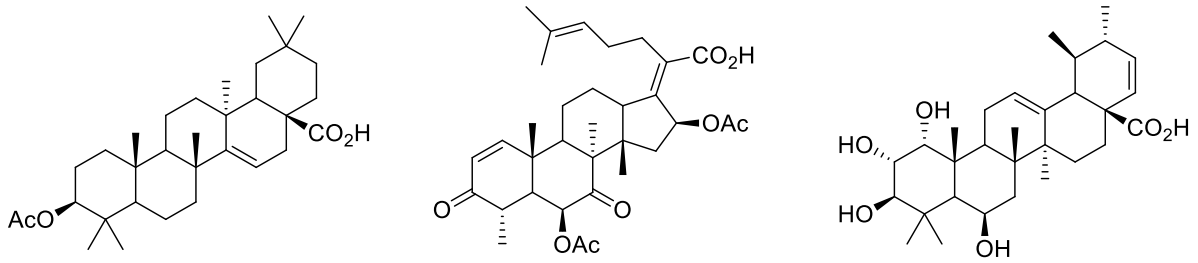

3-Acetyl-Aleuritolic acid | Helvolic acid | Eleganene-A

FIGURE 1.7 - Triterpenes with antibacterial activity against *S. aureus*.

Therefore, the phytochemical study of *Picramnia* species aiming for new natural products, in association with the evaluation of important biological activities, brings the contribution of this genus to the chemistry of natural products.

2 – OBJECTIVES

The present work had the main objective the phytochemical study of two species of *Picramnia*: *P. glazioviana* and *P. bahiensis*; the evaluation of the insecticide and fungicide activities of their extracts and fractions against leaf-cutting ants and the evaluation of their antidiabetic inhibition profiles.

In a specific way, the objectives were:

- The phytochemical study of *P. glazioviana* and *P. bahiensis* - Isolation, purification and structure elucidation of their constituents;
- Evaluation of the inseticide activity against *A. sexdens rubropilosa* and the fungicide activity against *L. gongylophorus* to the extracts and fractions from both plant species;
- Evaluation of the antidiabetic (α-glucosidase and PTP1B enzymes) and antibacterial (*S. aureus*) potential activity of both species of *Picramnia*;
- Performing the high-resolution bioassays and construction of the biochromatograms;
- Evaluation of the dichloromethane partition from *P. glazioviana* by HPLC-HRMS-SPE/NMR

3 – EXPERIMENTAL SECTION

3.1 – MATERIALS

3.1.1 – Chemicals and Reagents

- Water used for HPLC analysis was prepared by a deionization and 0.22 µm membrane filtration system (Milipore, Billerica, MA, USA).
- Analytical grade HPLC solvents (Methanol and Acetonitrile) were obtained from J. T. Baker, Panreac and VWR (Fontenay-sous-Bois, France).
- Formic acid was obtained from Merck (Darmstadt, Germany).
- Analytical grade solvents as hexane, dichloromethane, ethyl acetate, acetone, ethanol and methanol were distilled at Chemistry Department, Federal University of São Carlos.
- Chloroform-d_1 and methanol-d_4 (99.8 atom % D) from Cambridge Isotope Laboratories, Inc. (Andover, MA, USA) and from Sigma-Aldrich (St. Louis, MO, USA).
- Dimethyl sulfoxide, Tris, Bis-Tris, DTT, EDTA, p-nitrophenol α-D-glucopyranoside (PNPG) and α-glucosidase type I (EC 3.2.20, from *Saccharomyces cerevisiae*, lyophilized powder) were purchased from Sigma-Aldrich (St. Louis, MO, USA).
- Recombinant human Protein Tyrosine Phosphatase 1B (PTP1B) (BML-SE332-0050, EC 3.1.3.48) was purchase from Enzo Life Sciences, Inc., (NY, U.S.A.).

3.1.2 – Chromatographic Material

- Aluminum foil coated with sílica gel 60 UV_{254} for Thin Layer Chromatography (TLC) were obtained from Sigma Aldrich and Macherey-Nagel GmbH & Co.

- Silica gel 60 (63 - 230 µm) and silica gel for flash chromatography (40 – 63 µm) used for Column Chromatography (CC) were obtained from Acros Organics. C_{18} reversed phase silica gel (60 A, 40 µm) was obtained from Sorbent Technologies.
- Sephadex® LH-20 was purchased from Amersham Biosciences Inc.

For the HPLC analysis, chromatographic separations were performed using the followed columns:

- Analytical Column Macherey-Nagel GmbH & Co - C_{18} 5 µm (ϕ 4.6 x 150 mm);
- Analytical Column Phenomenex Luna - C_{18} 10 µm (ϕ 4.6 x 250 mm);
- Semi-preparative Phenomenex Luna - C_{18} 10 µm (ϕ 10 x 250 mm);
- Analytical Column Phenomenex Luna - C_{18} (2) 3 µm (ϕ 4.6 x 150 mm) from Copenhagen University.
- Semi-preparative Phenomenex Luna - C_{18} (2) 3 µm (ϕ 10 x 150 mm) from Copenhagen University.

PVDF membrane filters (0.45 µm - ϕ 25 mm) from Agela Technologies and PTFE membrane filters (0.20 µm – ϕ 15 mm) from Macherey-Nagel GmbH & Co, model Chromafil O-20/15 MS were used for filtration of the HPLC samples.

3.2 – INSTRUMENTS

The analysis by GC/MS (Gas Chromatography/ Mass Spectrometry) were acquired with the following instrument:

- Shimadzu MDGC-2010Plus, equipped with a Headspace autoinjector AOC-5000Plus, flame ionization detector FID-2010Plus and Mass Spectrometry TQ8030. The analysis were performed by Eletronic Ionization (EI) at 70 eV, using a Rextek Column Rtx-5MS, 30 m length, 0.25 mm of diameter and

thickness of the 0.25 µm. The software used to analyse the datas was GCMS Postrun Analysis.

NMR spectra were acquired with the following instruments:

- Bruker AvanceTM III NanoBay 9.4 Tesla - 400 MHz equipped with 5 mm BFO (smart probe with ATMA);
- Bruker Avance III Ultrashield Plus 600 MHz equipped with a cryo-probe TCI 5 mm ($^{1}H/^{13}C/^{15}N$) with ATMA (Automatic Tunning Matching);
- Bruker Avance III 600 MHz spectrometer equipped with a Bruker SampleJet sample changer and a cryogenically cooled gradient inverse triple-resonance 1.7 mm TCI probe-head (Bruker Biospin, Rheinstetten, Germany) from Copenhagen University
- Bruker Avance III HD 600 MHz spectrometer equipped with a with a 5 mm cryogenically cooled $^{13}C/^{1}H$ DCH probe head for ^{1}H and ^{13}C NMR spectroscopy and a Bruker SampleCase autosampler with 24 positions from Copenhagen University

The analysis by HPLC were performed using the following instruments:

- Shimadzu LC-10AD system consisting of a LC- 10AD pump (Kyoto, Japan), a SPD 10AD UV-vis detector working with two wavelenghts, SCL 10A VP system controller. This equipment was connected to a CBM – 10A and a Shimadzu Class – VP software was used for data acquisition.
- Agilent 1200 and 1260 series chromatographic HPLC systems consisting of a G1311A quaternary pump with built-in degasser C1322A, a G1367B autosampler, a G1316A thermostatted column compartment, and a G1316A photodiode-array detector (DAD) all controlled by EZI Chrome software.
- Agilent 1200 series chromatographic HPLC system consisting of a G1316A quaternary pump with built-in degasser G1322A, a G1367C high-performance autosampler, a G1316A

thermostatted column compartment, and a G1315C photodiode-array detector (DAD) all controlled by Agilent ChemStation ver. B.03.02 software, from Copenhagen University.

The HPLC-HRMS-SPE/NMR analysis was acquired in Copenhagen University using the hyphenated plattform as described below:

- Agilent 1260 series chromatographic HPLC system consisting of a G1311B quaternary pump with built-in degasser, a G1329B autosampler, a G1316A thermostatted column compartment, and a G1315D photodiode-array detector (DAD), a Bruker micrOTOF-Q II mass spectrometer (Bruker Daltonik GmbH, Bremen, Germany) equipped with an electrospray ionization (ESI) interface (operated via a 1:99 flow splitter), a Knauer Smartline 120 pump for postcolumn flow dilution, a Spark Holland Prospekt 2 SPE unit, a Gilson 215 liquid handler for automated filling of 1.7 mm NMR tubes, and a Bruker Avance III 600 MHz spectrometer.

3.3 – OTHERS APPARATUS

- Rotary evaporator Büchi, models R-200, R-114 and R-205, equipped with Büchi B-490 e B-480 Heating Bath, a Neslab CFT-25 and Neslab Thermo Felx 900 recirculating chillers from Thermo Scientific, kept at 5 °C and coupled to the vacuum pumps from Sibata Scientific Technologies.
- Analytical Balances from Sartorius model BP219S and from A&D Company, model GH-202.
- Laminar flow fume hood Veco, model VLFS-12M;
- Optical rotations were obtained on a polarimeter with sodium light (589nm) by using a Bellingham + Stanley ADP 410 polarimeter – from Copenhagen University.

- Speed Vacuum Savant SPD121P coupled with a RVT400 refrigerated vapor trap and an OFP-400 oil free pump (Hobrook, NY, USA) – from Copenhagen University.
- A Multiskan FC microplate photometer (Thermo Scientific, Waltham, MA, USA) controlled by SkanIt ver. 2.5.1 software was used to read the microplates, from Copenhagen University.

3.4 – METHODOLOGIES

3.4.1 – Insecticidal bioassay against *A. sexdens rubropilosa*

Extracts, partitions and fractions obtained after the chromatographic fractionations were sent for evaluation of the toxicity test (by ingestion), carried out at the Social Insects Study Center, São Paulo State University in Rio Claro (Universidade Estadual Paulista de Rio Claro, UNESP, Rio Claro) under supervision of Prof. Dr. Odair Correa Bueno and his students responsible for the bioassays, coordinated by Marcela Ceccato, according to the established protocol described in BUENO et. al., 1989.

For the assays, *A. sexdens rubropilosa* workers were randomly removed from the laboratory nests. Fifty ants were selected and distributed on 5 Petri dishes (10 cm diameter, ten ants to each dish lined with filter paper) for each treatment. During the experiments, the ants were maintained on an artificial diet established by the group (BUENO, 1997) consisting of glucose 50 g, bacterial peptone 10 g, yeast extract 1 g and agar 15 g/L in distilled water. The diet (0.5 g per dish), which the samples were added, was offered and replaced daily with a new portion. Ants from the control treatment were fed with a diet without any sample (extract, partition and fractions). During the experiments, the material was maintained in an incubator of 24 (±1) °C and relative humidity ranging between 70 and 80%. The experiment was observed during 25 days and the number of dead ants recorded daily. It was estimated the survival curve of leaf-cutting ants for each treatment and

calculated the median longevity. The Log rank-test (α=0.05) was used for statistical analysis of data.

3.4.2 – Fungicidal bioassay against *L. gongylophorus*

The fungicidal bioassay was carried out at Federal University of São Carlos, Natural Products Bioassays Laboratory, under coordination of Ms. Dorai Periotto Zandonai. The fungus was isolated from a nest of *A. sexdens rubropilosa* and maintained in a culture medium consisting of malt extract (20 g/L), peptone (5 g/L) yeast extract (2 g/L) and agar (20 g/L). Samples submitted to the fungal symbiont assay were incorporated into the culture medium and dissolved in distilled water, obtaining a final concentration of 1000 µg/mL for extracts and partitions and 100 µg/mL for pure compounds. Then, in each test tube, 10 mL of the culture medium/extract was added. The test tubes with culture medium/extract and Petri dishes (80 X 15 mm) were autoclaved at 120 °C, 1.0 atm for 20 minutes. After sterilization of the material, the culture media were poured into the Petri dishes using a laminar flow hood, previously sterilized for 30 minutes by ultraviolet light. After solidification of the culture medium, each Petri dish was inoculated at the center position with an 8 mm diameter agar disc previously colonized by the symbiotic fungus *L. gongylophorus*. Each sample was prepared in quintuplicate, with an identical number of replicates for the general control (culture medium and symbiotic fungus). After the 30-day incubation time, at 25 °C (± 2) the final medium diameter measurements were performed and the mycelial growth area of each plate was calculated for each sample. This methodology is an adaptation of MIYASHIRA, (2007). Inhibition percentages were calculated to the mycelial growth area of the symbiont fungus to the controls comparing with the area of the mycelial growth with the plates containing the samples. The control was considered as 0% of the symbiotic fungus inhibition.

3.4.3 – α-Glucosidase and PTP1B Inhibition Assays

The assays for identification of the antidiabetic inhibitors were performed at the Department of Drug Design and Pharmacology, Copenhagen University according with the methodologies described below.

3.4.3.1 – Determination of Inhibitory Concentrations

Dilution series of the crude extract and partitions were dissolved in DMSO and added to 96-well microplates in triplicate. α-glucosidase and PTP1B assay were performed adding the specific reagents in each well following the methodology described below. Dose-response curves and IC_{50} values were obtained using GraphPad prism, version 6.00.283 (GraphPad Software, Inc., La Jolla, CA).

3.4.3.2 – High-Resolution α-Glucosidase and PTP1B biochromatogram

Microfractionation of the dichloromethane partition of *P. glazioviana* (PGD) for the high-resolution α-glucosidase and PTP1B biochromatograms were performed with an Agilent 1200 system (Santa Clara, CA) containing a G1364C fraction collector. Analyses were performed at 40 ºC on a 150 x 4.6 mm i.d. Phenomenex Luna C_{18} (2) reversed-phase column (3 µm particle size) with a flow rate of 0.8 mL/min. The solvents were a binary gradient mixture of water-acetonitrile (95:5 υ/υ) as eluent A and acetonitrile-water (95:5 υ/υ) as eluent B, both with 0.1% formic acid. A single injection of 10 µL of PGD partition was separated using the following gradient elution profile: 0 min, 25% B; 25 min, 30% B; 45 min, 35% B; 53 min, 35% B; 83 min, 40%B; 123 min, 100%B; 132 min, 100% B. The eluent from 10 to 105 min was fractionated into three 96-well microplates (omitting the 8 wells in the last column of each plate for the blank controls), leading to a resolution of 2.78 data

points per min. The content in the microplates were subsequently evaporated to dryness using a SpeedVac concentrator. After evaporation, the α-glucosidase and PTP1B assay were performed on the collected material. The α-glucosidase inhibition assay was performed at 28 °C in 0.1 M phosphate buffer pH 7.5, a final volume of 200 µL, final DMSO = 5%, total enzyme concentration 0.05 U/mL and total substrate concentration (p-NPG) 1.0 mM, according to the previously described procedure (SCHMIDT, 2012). Briefly, the content of each well was dissolved in 100 µL of 0.1 M phosphate buffer containing 10% of DMSO and added 80 µL of the α-glucosidase solution. After incubation at 28 °C for 10 min the reaction was started by addition of 20 µL of p-NPG (10 mM in phosphate buffer). The cleavage product of p-PNPG was monitored at 405 nm every 30 s for 35 min using a Multiskan FC microplate photometer with built-in incubator and the percentage enzyme inhibition was calculated using the equation presented below. Inhibition of α-glucosidase activity was plotted against chromatographic retention time to give α-glucosidase high-resolution biochromatograms. Figure illustrating this procedure is shown below (FIGURE 3.1).

$$\%\text{inhibition} = \left(1 - \frac{\text{SLOPE sample}}{\text{SLOPE blank}}\right) x100$$

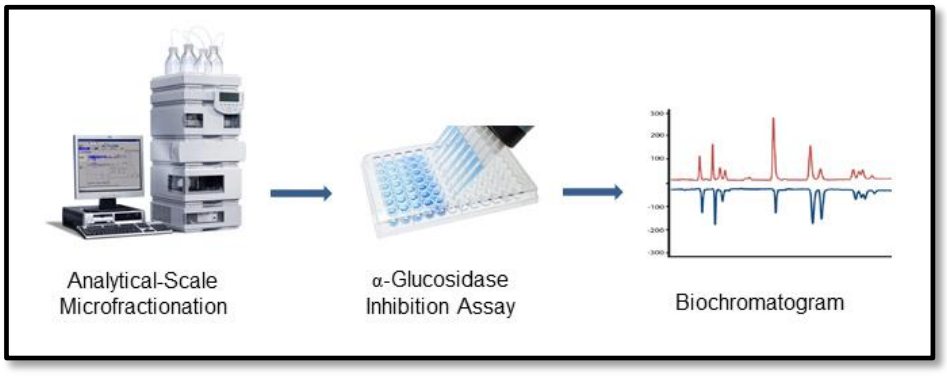

FIGURE 3.1 - Schematic representation of the workflow procedure to perform the α-glucosidase inhibition profile.

The PTP1B inhibition assay was performed at 25 °C using a two component buffer, consisting of 50 mM Tris and 50 mM bis-Tris containing 0.1 M NaCl adjusted to pH 7.0 with acetic acid, using a final reaction volume of 180 µL. The content in each well were dissolved in 18 µL of DMSO followed by the addition of 52 µL of buffer containing 3.46 mM EDTA (final well concentrations 10% DMSO and 1 mM EDTA), and 60 µL of a solution constituted by 1.5 mM pNPP and 6 mM DTT (final well concentrations 0.5 mM pNPP and 2 mM DTT). After preincubation at 25 °C for 10 min, the reaction was started by adding 50 µL of 0.001 µg/µL PTP1B stock solution (final well concentration: 0.05 µg/well). The amount of p-nitrophenol produced was determined by measuring the absorbance at 405 nm every 30 s for 10 min using a Multiscan FC microplate photometer with built-in incubator and the percentage enzyme inhibition was calculated using the same equation presented above. Inhibition of PTP1B activity was plotted against chromatographic retention time to give PTP1B high-resolution biochromatograms (WUBSHET, 2016). The same methodology was used to perform the high-resolution α-glucosidase and PTP1B biochromatograms to the methanol extract from roots of *P. bahiensis* (PBRMe), adjusting the gradient elution profile and the flow rate. The details of each eluent can be found hereafter in the section 3.5.2.6.

3.4.4 –Antibacterial Inhibition Assay

The methodology of the antibacterial bioassay was developed in the Department of Drug Design and Pharmacology at Copenhagen University. Since this methodology is going to be published, the descriptions were not included in this work.

3.5 – PHYTOCHEMICAL STUDIES

3.5.1 – *Picramnia glazioviana*

3.5.1.1 – Plant Material and Extraction

Leaves of *P. glazioviana* were collected in Piuma and Marataizes, Espírito Santo, Brazil and identified by Dr. José Rubens Pirani. A voucher specimen has been deposited at the Botanic Department, São Paulo University, São Paulo, Brazil. The crude extract was prepared at the Laboratory of Natural Products, Chemistry Department, Federal University of São Carlos, São Carlos, SP, Brazil by Ms. Dorai Periotto Zandonai. The leaves of *P. glazioviana* were dried in a circulation oven at 40 °C and subsequently reduced to powder by milling to obtain the dried material (513 g). After milling, the material was subjected to an exhaustive extraction with ethanol and then filtered. The resulting solution was concentrated in a rotary evaporator under reduced pressure obtaining 41.12 g of the crude extract.

The crude ethanol extract was sent to the Social Insects Study Center at São Paulo State University in Rio Claro and to the Natural Products Bioassays Laboratory, Chemistry Department at the Federal University of São Carlos for evaluation of the insecticidal and fungicidal activities against *A. sexdens rubropilosa* and the symbiont fungus *L. gongylophorus*.

3.5.1.2 – Isolation and Purifications Steps

The ethanol crude extract was submitted to a liquid-liquid partition by the preparing of a hydroalcoholic solution of the extract with MeOH:H_2O (1:3) and subsequently extracted with hexane, dichloromethane and ethyl acetate (3 x 400mL, for each solvent) and then, dried under reduced pressure. This procedure resulted in the following phases with their respective mass and codes, as described in TABLE 3.1. All phases were sent to perform the insecticidal and fungicidal bioassays against leaf-cutting ants and the PGD, PGA and PGHi phases had the chromatographic profile analyzed by HPLC.

TABLE 3.1 – Liquid-liquid Partition of the Ethanol Extract from *P. glazioviana* and their respective mass

Phases	Mass (g)	Code
Hexane	2,54	PGHe
Dichloromethane	1,53	PGD
Ethyl Acetate	18,75	PGA
Hydroalcoholic	14,82	PGHi

The results obtained from the bioassays indicated the dichloromethane and ethyl acetate phases as the most promising to the insecticidal activity. Thus, the phytochemical study was initiated with the PGD phase focusing on the isolation the compounds. Consequently, it was developed an isocratic elution methodology for analysis on analytical reversed-phase (RP) HPLC. The best separation condition was carried out using the binary mixture constituted by water-acetonitrile (40:60 υ/υ) on a Phenomenex Luna C_{18} column, (10 µm, 4.6 x 250 mm). Subsequent injections on semipreparative reversed-phase (RP) HPLC using a Phenomenex Luna C_{18} column (10 µm, 10 x 250 mm), concentration of 370 mg/ mL and wavelengths defined to 254 and 220 nm allowed to isolate seven pure compounds. The HPLC chromatogram resulting of this separation is shown in FIGURE 3.2. The letters indicate the isolated compounds and were established provisionally initiating from the right to the left, according the compounds were analyzed. The TABLE 3.2 indicates the compounds isolated with their respective mass.

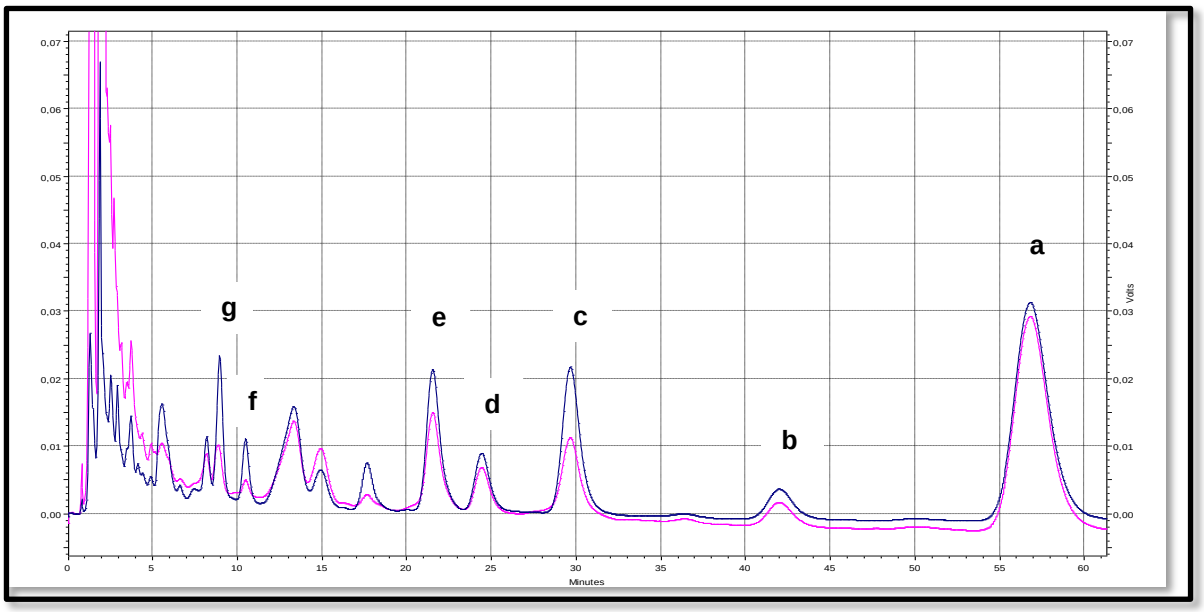

FIGURE 3.2 - HPLC Chromatogram at 254 (blue) and 220nm (pink) using isocratic elution indicating the compounds isolated of PGD partition from *P. glazioviana*.

TABLE 3.2 – Mass of the compounds isolated from the isocratic semi-preparative HPLC purification of the PGD partition

Compounds	a	b	c	d	e	f	g
Mass (mg)	24,4	1,2	8,2	3,6	5,2	1,1	1,4

After isolation the pure compounds, NMR experiments were acquired to the compounds **a**-**e** with a Bruker 400 MHz. The first analysis of the NMR and MS data suggested these compounds as new natural products, and subsequent NMR experiments to compounds **a-g** were acquired with a Bruker 600 MHz. Once it was isolated plenty material of the major compound (**a**), it allowed the acquisition of all 2D NMR experiments, enabling the full structure elucidation to this compound. Furthermore, since the compound **a** is a new natural product presenting a new chemical skeleton, it was proposed a plausible biogenetic pathway to the formation of these structures in the plant. However, the amount isolated for some compounds limited the acquisition of a good quality 2D NMR experiments, as HMBC spectrum for example. Thereafter, further studies with the PGD partition and structure elucidation of these new compounds were proceeded at Copenhagen University, Department of Drug Design and Pharmacology, Copenhagen, Denmark, under the supervision of

Prof. Dr. Dan Staerk. High-resolution α-glucosidade and PTP1B inhibition profile were constructed from this partition, as well the antibacterial inhibition profile. HPLC-HRMS-SPE/NMR was also performed and the procedure from this technique is described hereafter.

3.5.1.3 – HPLC-HRMS-SPE/NMR

The first step before starting the HPLC-HRMS-SPE/NMR analysis was the development of a good chromatographic condition to have the best separation of all constituents present in the sample. For that, a gradient elution with acetonitrile-water exhibited the best choice as eluent, reaching these conditions. Thus, several methodologies were tested using this mobile phase, and after eleven analytical attempts, the best gradient elution was chosen according to the following description: 0 min, 25% B; 25 min, 30% B; 45 min, 35% B; 53 min, 35% B; 83 min, 40% B; 123 min, 100% B; 140 min, 100% B, using acetonitrile-water (5:95) + 0.1% formic acid (eluent A) and acetonitrile-water (95:5) + 0.1% formic acid (eluent B) as a mobile phase. This methodology was the same used to perform the microfractionation for the construction of the biochromatograms, as described in the item 3.3.4.2. Thus, cumulative SPE trappings of the selected peaks on SPE cartridges (Hysphere GP phase, 10 x 2 mm i.d.) were performed for 8 repeated separations using absorption thresholds (254 and 200 nm) and a concentration of the 100 mg/ mL, 20 µL of injection volume and flow rate at 0.8 mL/ min. For all separations, approximately 1 % of the HPLC eluate was directed to a micrOTOF-Q II mass spectrometer. Mass spectra was acquired in positive ion mode, using a drying temperature of 200 °C, capillary voltage of 4100 V, nebulizer pressure of 2.0 bar and a dry gas flow of 7 L/min. The other approximately 99% of the HPLC eluate was directed to the DAD detector and thereafter diluted with Milli-Q water at a flow rate of 1 mL/min, allowing the cumulative SPE trappings of the selected analytes on Hyphere Resin GP cartridges (10 x 2 mm i.d.). Subsequently, each cartridge was dried with pressurized nitrogen gas during 45 min and eluted with 30 µL of $CDCl_3$ into 1.7 mm o.d. NMR tubes (96-positions tube racks). A scheme representing the workflow procedure for HPLC-HRMS-SPE/NMR is shown in FIGURE 3.3.

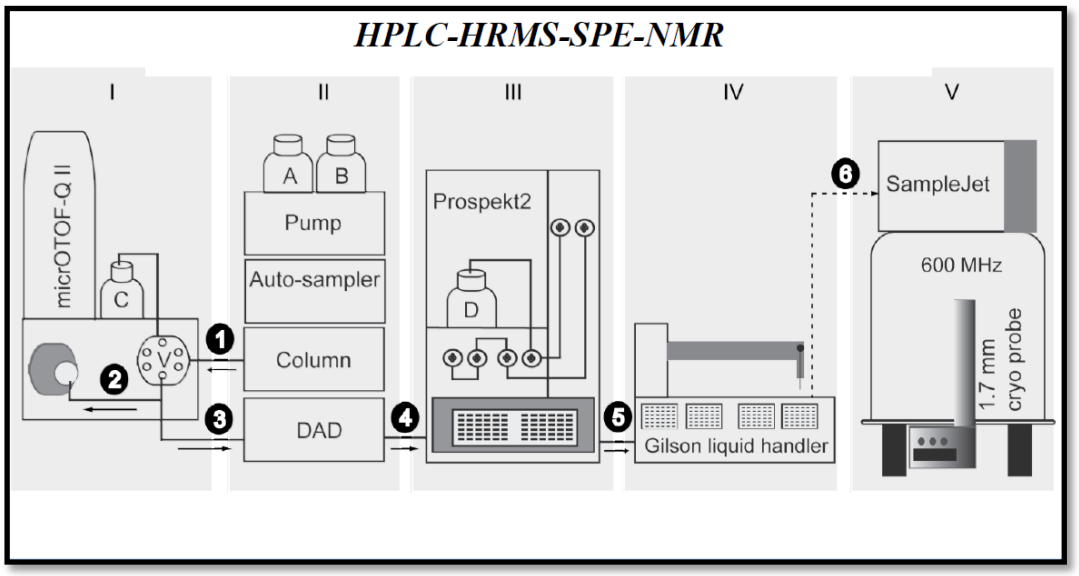

FIGURE 3.3 - Scheme of the hyphenated HPLC-HRMS-SPE/NMR system

The FIGURE 3.4 shows the chromatogram used for trapping the compounds. Thus, the analyses performed from the HPLC-HRMS-SPE/NMR system presented an optimal chromatographic separation and the acquisition of the NMR spectra for some compounds (especially to the major compounds) presented high spectral purity degree and excellent intensity of the signals. However, during the time needed for acquisition of long 2D and ^{13}C NMR experiments, it was noticed an initial decomposition process in some samples solubilized in $CDCl_3$. Moreover, the need of having enough amount of each sample for futures experiments, as optical rotation and circular dichroism (an important experiment for the establishment the absolute stereochemistry of the chiral centers in the structure), a new isolation process was initialized, considering then, a semi-preparative HPLC scale.

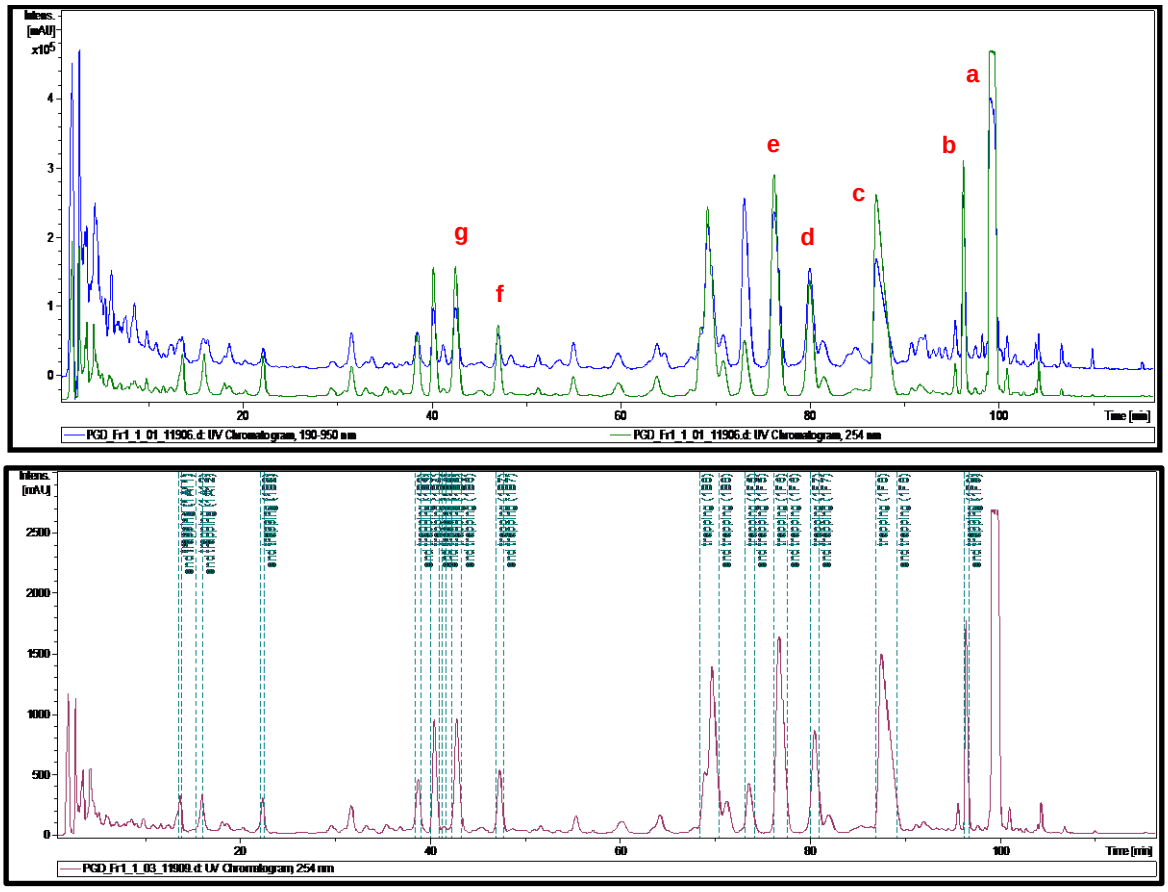

FIGURE 3.4 – HPLC Chromatogram used for trapping the compounds by HPLC-HRMS-SPE/NMR (above) and trapped compounds (green dashed line, below) of PGD partition from *P. glazioviana*. The letters indicate the isolated compounds from the first purification procedures as described in FIGURE 3.2.

3.5.1.4 – Semi-Preparative Scale HPLC fractionation

The separation in semi-preparative scale was performed through a series of repeated injections using the same chromatographic conditions described above, 15 µL of injection volume, concentration of 300 mg/ mL and flow rate at 4.7 mL/ min.

From these procedures, it was possible to separate, isolate and elucidate 22 compounds, including those very minor compounds **7a**, **21** and **24,** according to FIGURE 3.5 (The compounds were numbered as shown in this figure). Besides, the very small volume of injection (15 µL) in a 3 µm HPLC semi-preparative column was efficient to separate the compounds **14**, **15** and **16** that co-eluted during the trapping analyses (See FIGURE 3.4). The TABLE 3.3 indicates the isolated

compounds and their respective mass after 15 injections on semi-preparative column.

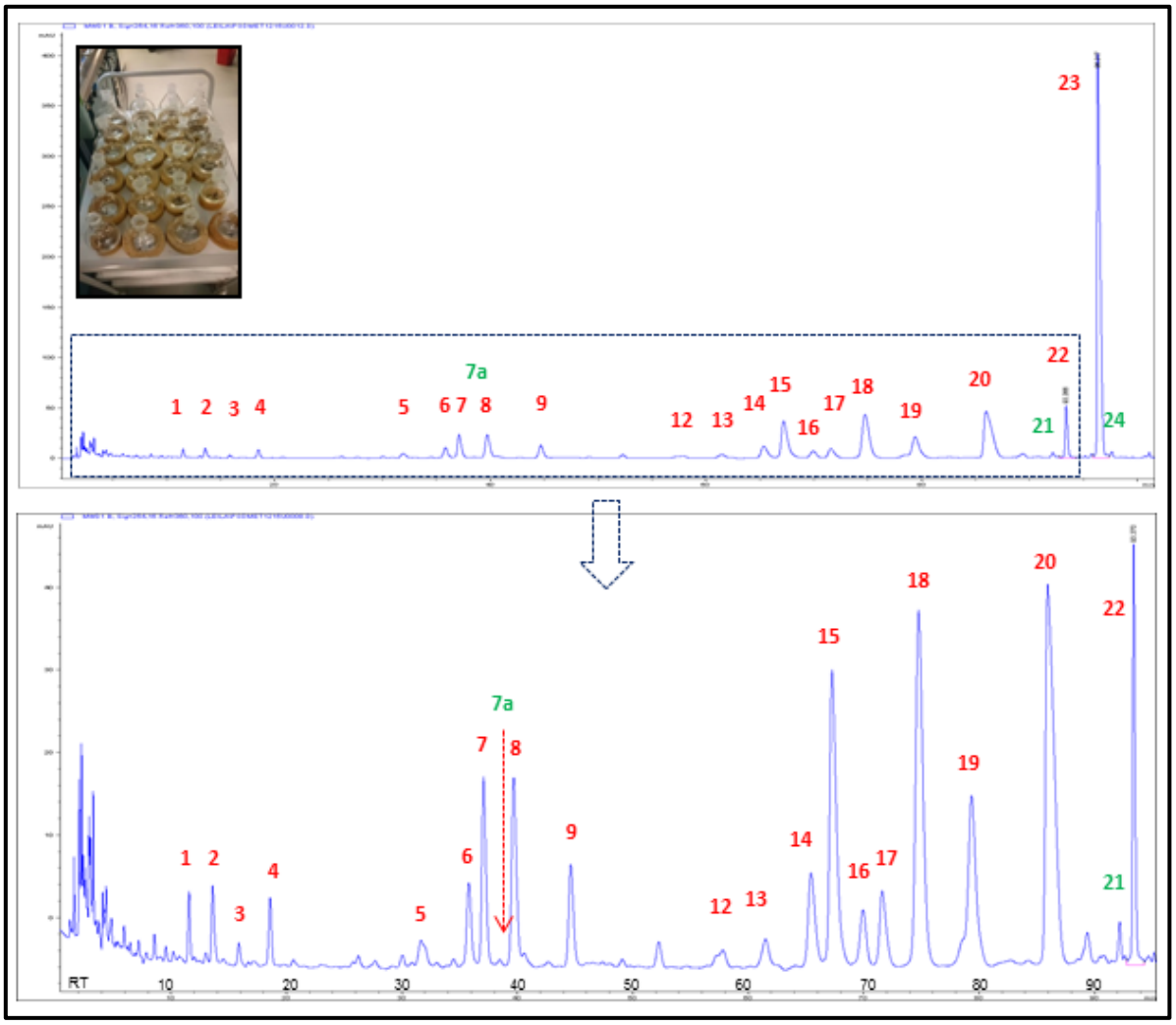

FIGURE 3.5 – Semi-preparative HPLC chromatogram (above) and chromatogram amplification (below) at 254 nm indicating the compounds isolated of PGD phase from *P. glazioviana*.

TABLE 3.3 – Mass of the isolated compounds, as illustrated in Figure 3.5 after 15 injections on semi-preparative HPLC

Compounds*	Mass (mg)
PGD 1	0.48
PGD 2	1.02
PGD 3	0.42
PGD 5	1.14
PGD 6	0.88
PGD 7	0.95
PGD 7a	0.41
PGD 8	0.65
PGD 9	1.47
PGD 12	0.50
PGD 13	0.55
PGD 14	1.16
PGD 15	2.70
PGD 16	0.67
PGD 17	1.75
PGD 18	4.31
PGD 19	2.44
PGD 20	5.49
PGD 21	0.37
PGD 22	2.16
PGD 23	15.17
PGD 24	0.43

* The amount of the compounds after all injections should be confirmed. Compound 4, 10 and 11 were not elucidated.

3.5.1.5 – Purification of the compounds 2 and 5

Compounds **2** and **5** showed some impurities after analyzing the ^{1}H NMR spectrum. Thus, they were consequently submitted to analytical HPLC aiming their purification. For this purpose, the compounds were dried at the bottom of a small insert for HPLC vials and subsequent solubilized with the less volume as

possible of methanol. They were then purified using an isocratic elution of acetonitrile:water (25:75 υ/υ; compound **2**) and (32:68 υ/υ; compound **5**) acidified with 0.1% formic acid. A total of 11 and 9 repeated injections for compound **2** and **5** respectively were performed, using a flow elution rate of 0.6 mg/mL in both analyses. However, some variations in the chromatographic profile were noticed, as a different retention time of the present compounds among the repeated purifications procedures (FIGURES 3.6 and 3.7). The fractions collected from all injections were gathered afterwards, analyzing separately the most intense peak from each chromatogram, and guided by the color of the collected fractions (specifically to purifications of compound **5**). The ^{1}H NMR spectrum for each compound will be acquired in a near future to verify the purity after these procedures. The amount of each compound is represented in TABLE 3.4.

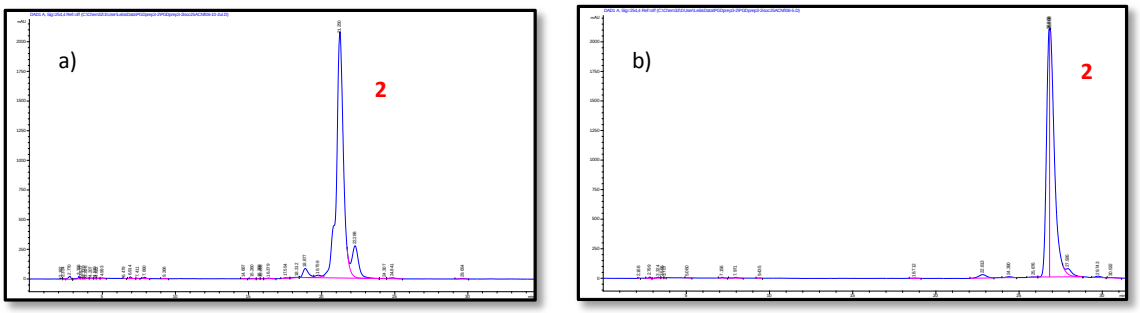

FIGURE 3.6 - Example of different chromatographic profiles obtained with an isocratic elution in the analytical HPLC after repeated injections to purification of compound **2**. a) major compound eluted at 21.2 min b) major compound eluted at 26.9 min.

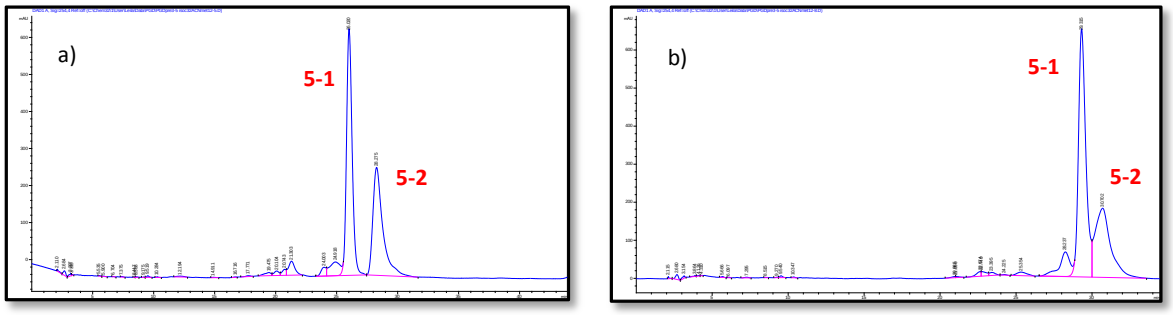

FIGURE 3.7 – Example of different chromatographic profiles obtained with an isocratic elution in the analytical HPLC after repeated injections to purification of compound **5**. a) the first compound eluted at 26.0 min b) the first compound eluted at 29.3 min.

TABLE 3.4– Mass of the compounds 2 and 5 after analytical purifications procedures

Compounds	Mass (mg)
PGD 2	0.76
PGD5-1	0.52
PGD5-2	0.45

3.5.2 – *Picramnia bahiensis*

Leaves, stem and roots of *P. bahiensis* were collected in Piuma and Marataizes, Espírito Santo, Brazil and identified by Dr. José Rubens Pirani. A voucher specimen has been deposited at the Botanic Department, São Paulo University, São Paulo, Brazil. The crude extracts were prepared at the Natural Products Laboratory, Chemistry Department, Federal University of São Carlos, São Carlos, SP, Brazil by Ms. Dorai Periotto Zandonai. The plant materials of *P. bahiensis* were dried in a circulation oven at 40°C and subsequently reduced to powder by milling to obtain the dry materials. After milling, the materials were subjected to exhaustive extraction with solvents of increasing polarity as hexane, dichloromethane and methanol, and then filtered. The resulting solutions were concentrated in a rotary evaporator under reduced pressure obtaining the amount of each respective crude extracts as shown below in TABLE 3.5.

TABLE 3.5 – Prepared extracts from *P. bahiensis*

Vegetal Structures	Dried Material (g)	Hexane Extract (g)	Dichloromethane Extract (g)	Methanol Extract (g)
Leaves	47	1,2504	1,8561	4,3611
Stem	342	0,6931	2,4524	18,9101
Roots	219	0,7475	2,3217	12,5552

All crude extracts were sent to the Social Insects Study Center at São Paulo State University, Rio Claro, SP, Brazil, under responsibility of Dr. Rodrigo O. S. Kitamura for evaluation of the insecticidal activity against leaf-cutting ants, during his PhD study. Once his study was based on the hexane and dichloromethane extracts from roots of *P. bahiensis* and an expressive activity was noticed to all other extracts from this plant, it was chosen to continue the investigation of this plant, focusing firstly on the study of the methanol extract from the stem (PBCMe), since a high amount of the material was available.

Moreover, all extracts were sent to the Natural Products Bioassays Laboratory, Chemistry Department at Federal University of São Carlos for evaluation of the fungicidal activity against the symbiont fungus *L. gongylophorus*, and it was also observed a good percent of inhibition of the selected extract for the initial studies (PBCMe), as well as to the methanol and dichloromethane extracts from leaves.

3.5.2.1 – Methanol Extract from the Stem of *P. bahiensis* (PBCMe)

The methanol extract from the stem of *P. bahiensis* was submitted to fractionation procedures by chromatography column, using Sephadex-LH 20 as stationary phase. A total of 6 consecutives injections of 1.5 g of the extract per column were separated using methanol as mobile phase, resulting in 32 collected fractions (8 fractions per each column, FIGURE 3.8). These fractions were evaluated by analytical TLC but due the high polarity of the fractions, they could not be distinguished to a subsequent combination in groups. The ^{1}H NMR were then acquired for each fraction and afterward they were combined in 5 groups. The groups

01 and 02 were gathered after verifying high similarities in their spectrum. TABLE 3.6 presents the combined groups with their respective mass.

FIGURE 3.8 - Chromatographic separation of the PBCMe extract on Sephadex LH-20.

TABLE 3.6 – Chromatographic separation of the PBCMe extract combined in 05 groups

Groups	Mass (g)
PBCMe 01+02	3.323
PBCMe 03	3.294
PBCMe 04	0,876
PBCMe 05	0,867

The analysis of the group PBCMe 03 by ^{1}H NMR showed signals for aromatic protons besides signals correlated to sugar units. Once several anthraquinone glycosides have been reported in the literature from *Picramnia* species presenting these set of signals, further procedures aiming to purify the constituents from this group were performed, as described below.

3.5.2.2 – PBCMe 03 fractionations

The following fractionation of the group PBCMe 03 was performed using chromatographic column on Sephadex LH-20 as stationary phase. Two injections of 1.5 g of the material was separated using methanol as eluent, resulting in 07 fractions from the first separation, and 9 fractions from the second one. All these fractions were analyzed by TLC and ^{1}H NMR, and combined in 05 groups after the analyses (TABLE 3.7). However, the last fraction collected from the first separation (PBCMe 03/07 col1) was observed as an intense orange color and therefore, it was not combined in groups, being analyzed separately.

TABLE 3.7 - Chromatographic fractionation of the group PBCMe 04/03 combined in 05 groups

Group	Mass (g)
PBCMe 03/01	0,266
PBCMe 03/02	0,412
PBCMe 03/03	0,174
PBCMe 03/04	1,458
PBCMe 03/05	0,686

The ^{1}H NMR spectra for all groups were acquired. The groups PBCMe 03/01 to 03/03 showed plenty signals with the chemical shift at the range of δ_H 4,5 a δ_H 3,0, characteristic of sugars. The analytical chromatographic profiles to the groups PBCMe 03/04 and PBCMe 03/05 were also evaluated by HPLC. PBCMe 03 and all combined groups coming from its fractionation (with exception of the fraction PBCMe 03/07 col1 due its low acquired mass) were sent to the Social Insects Study Center

at São Paulo State University in Rio Claro, and to the Bioassays Laboratory of the Natural Products Group, Chemistry Department at the Federal University of São Carlos for evaluation of their respective insecticidal and fungicidal activities against leaf-cutting ants and the symbiont fungus *L. gongylophorus.* The following purification procedures were performed consequently to the fraction PBCMe 03/07 col1 and to the group PBCMe 03-04 based on the information from the ^{1}H NMR spectrum and also considering the results from the bioassays.

3.5.2.3 – Purification steps of the fration PBCMe 03/07 col1

The fraction PBCMe 03/07 col1 was analyzed by HPLC using reversed-phase column (C_{18}). Two major compounds absorbing at 254 nm were observed besides some minor constituents. The isocratic elution using ACN:H_2O (35:65 v/v), 20 µL volume of injections and flow rate at 1 mL/min presented an excellent separation of the compounds on C_{18}, according to FIGURE 3.9. The initial objective of this procedure was the isolation of the compounds using the HPLC technique, since a better separation and high performance of the chromatographic profile can be reached from this procedure than a simple chromatographic column. However, the low solubility of a more concentrated sample in a polar solvent brought the limitation to this process. Plenty precipitated particles and a non-complete solubility of the sample were observed.

Consequently, the fraction was also evaluated by TLC on silica gel 60, and based on these results, the following purification procedure was performed using a chromatographic column on silica (FIGURE 3.10). A gradient elution was initialized using 100% dichloromethane, gradually increasing the polarity of the solvent to ethyl acetate and then 100% of methanol. A total of 13 fractions were collected, and combined in 08 groups after analysis of their TLC. This procedure allowed the isolation of three known anthraquinones. The TABLE 3.8 indicates the compounds isolated with their respective amounts.

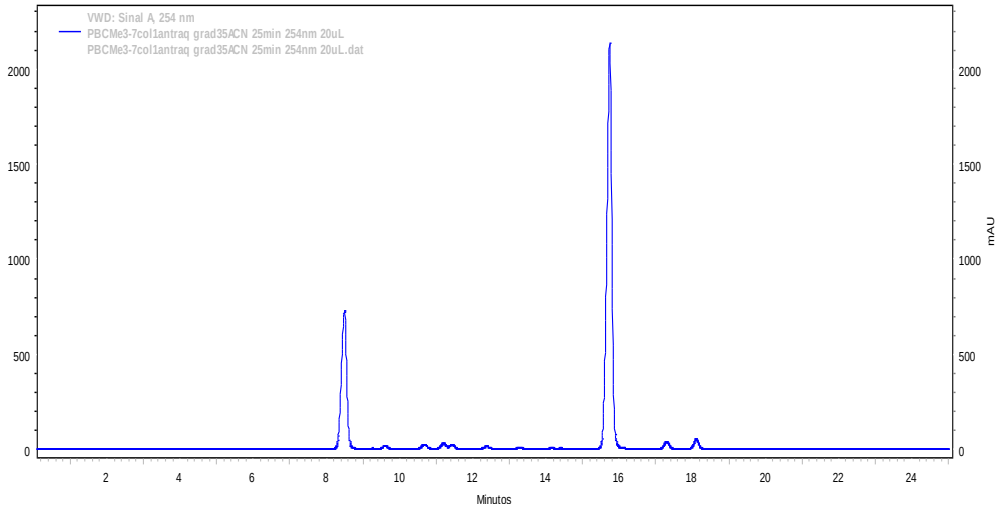

FIGURE 3.9 – Reversed-Phase HPLC Chromatogram at 254 nm using an isocratic elution constituted by ACN:H2O (35:65) of the fraction PBCMe 03/07 col1.

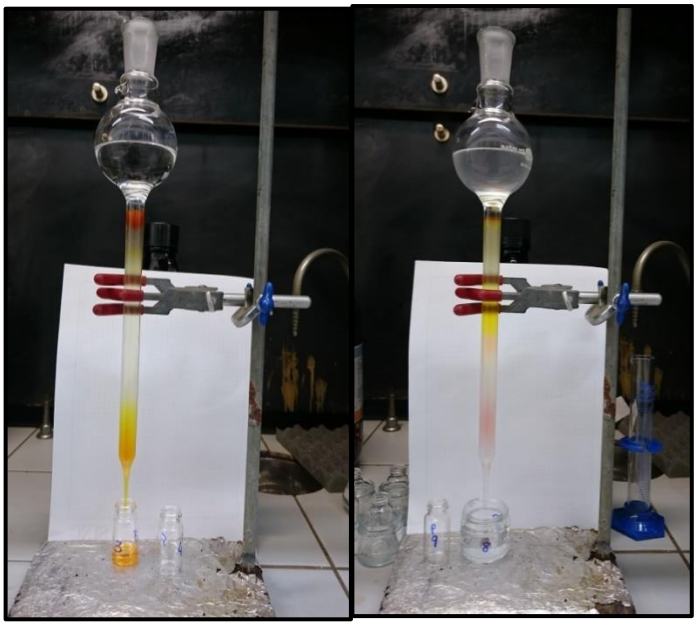

FIGURE 3.10 – Illustration of the chromatographic column performed on silica to the fraction PBCMe 03/07 col1.

TABLE 3.8 – Chromatographic fractionations of PBCMe 03/07col1 combined in 08 groups

Group	Mass (mg)
PBCMe 03/07col1-1 **(compound 25)**	0.5
PBCMe 03/07col1-2+3 **(compound 26)**	3.0
PBCMe 03/07col1-4	0.4
PBCMe 03/07col1-5	0.8
PBCMe 03/07col1-6	0.3
PBCMe 03/07col1-7 **(compound 27)**	1.2
PBCMe 03/07col1-8	1.0

Compounds **25** and **26** were also analyzed by GC-MS. The analyses to the compound **25** were carried out at 80 ºC as initial temperature during 2 minutes, increasing with a rate of 15 ºC/min to the final temperature at 280 ºC, keeping for 8 minutes. The temperature of the injector was 250 °C, the temperature of interface as 280 °C and final flow at 1.2 mL/min in a Split mode. The total time for analysis was 23.33 min. To compound **26**, the analyses were carried out at 80 ºC as initial temperature during 2 minutes, increasing with a rate of 20 ºC/min to 150 ºC, and after increasing 25 ºC/min to the final temperature at 280 ºC, keeping for 8 minutes. The temperature of the injector was 250 °C, the temperature of interface as 280 °C and final flow at 1.0 mL/min in a Split mode. The total time for analysis was 18.70 min.

3.5.2.4 – Analyses of the groups PBCMe 03/04 and PBCMe 03/05

The constituents belonged to the groups PBCMe 03/04 and PBCMe 03/05 were analyzed by HPLC. The presence of two major compounds with the highest absorption at 254 nm wavelength was observed. These compounds presented the same retention time when separated on reversed-phase C_{18} (Macherey-Nagel GmbH & Co column, 5µm, ϕ 4,6 x 150 mm) using a gradient elution constituted by ACN:H_2O (10% to 100% ACN in 50 min) and flow rate at 1 mL/min, which indicated the same major substances were present in each fractions. The group PBCMe 03/05 however, indicated the presence of two further minor

compounds (FIGURE 3.11 and 3.12). The following chromatographic procedures were performed to the group PBCMe 03-04.

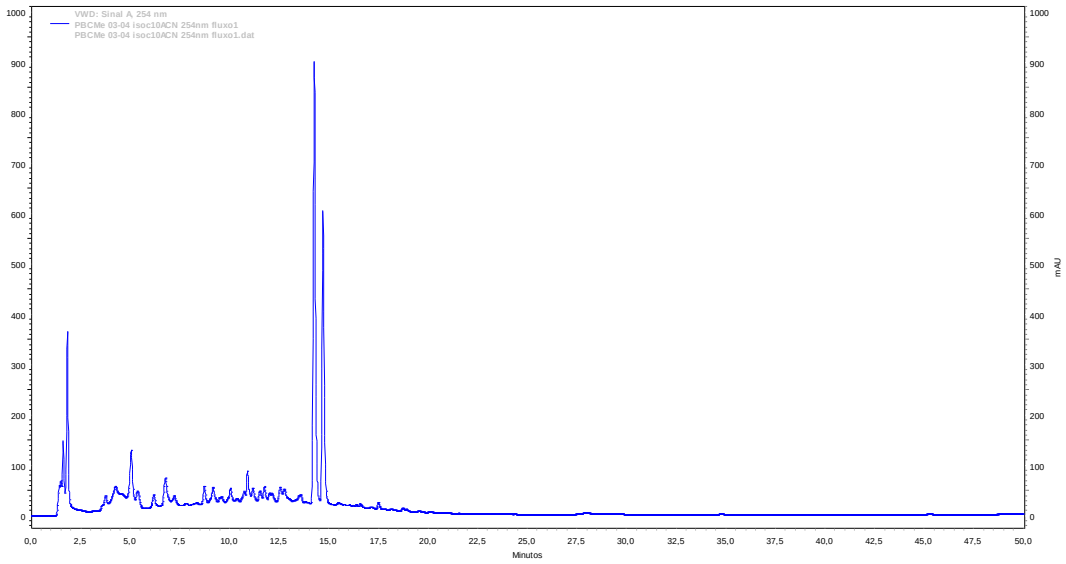

FIGURE 3.11 - Chromatographic profile of the group PBCMe 03/04 on reversed phase C_{18} analytical column.

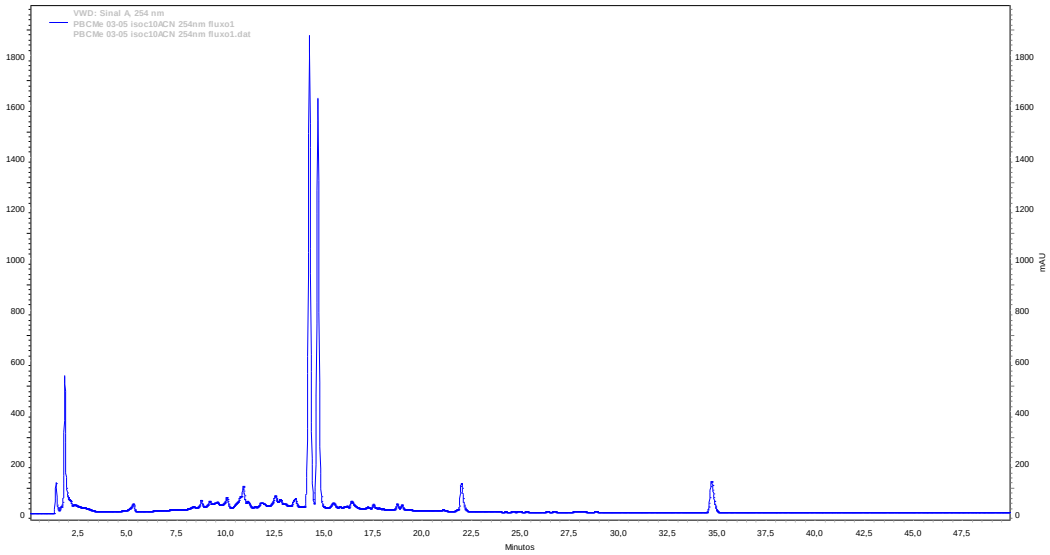

FIGURE 3.12 - Chromatographic profile of the group PBCMe 03/05 on reversed phase C_{18} analytical column.

3.5.2.5 – Purification of the group PBCMe 03/04

Due the high amount of the group PBCMe 03/04, the first purification processes to this sample were performed by chromatographic column on reversed-phase (silica C_{18}) using an isocratic elution constituted by MeOH:H_2O (1:1 v/v) as mobile phase. Nine fractions were collected and combined in 4 groups. However, the two major compounds could not be separated through this fractionation using this elution system.

Thus, it was developed a chromatographic condition on HPLC to a better separation of both compounds, and the best result achieved used an isocratic elution constituted by ACN:H_2O (25:75 v/v) on analytical reversed phase C_{18} at 254 nm and flow rate of 1 mL/min. The compounds were purified afterwards by semi-preparative HPLC using the same conditions described above and a flow rate established to 3 mL/min. These procedures resulted in the isolation of two known anthraquinone glycosides: pulmatin and chysophanein (FIGURE 3.13). The TABLE 3.9 indicates the mass of the isolated compounds.

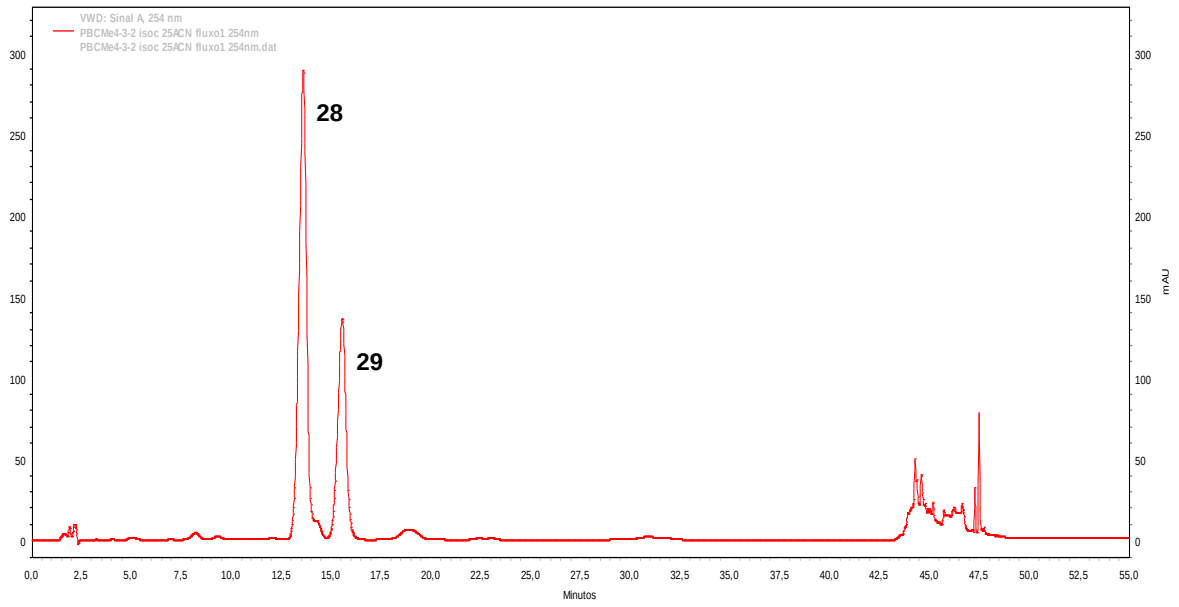

FIGURE 3.13 – Reversed-Phase HPLC Chromatogram at 254 nm using an isocratic elution constituted by ACN:H2O (25:75) for purification of the fraction PBCMe 03/04.

TABLE 3.9 – Isolated compounds from PBCMe 03/04 HPLC purifications

Compounds	Mass (mg)
PBCMe 03/04/01 **(Compound 28 - pulmatin)**	2.5
PBCMe 03/04/02 **(Compound 29 - chrysophanein)**	1.2

3.5.2.6 – Methanol Extract of Roots from *P. bahiensis* (PBRMe)

The study of the methanol extract of roots from *P. bahiensis* (PBRMe) was developed at Copenhagen University, Department of Drug Design and Pharmacology, Copenhagen, Denmark. The extract was evaluated for its antidiabetic potential through the inhibition of the α-glucosidase enzyme, according to the methodology described in item 3.3.4. Although it was verified a medium inhibition value to this extract (IC_{50} = 43.5 µg/mL), as reported by Silva et. al. (2017), an inhibitory concentration value (IC_{50}) of 103.34 µg/mL to *S. americanum* ethyl acetate extract allowed to pinpoint the bioactive compounds through the high-resolution α-glucosidase inhibition profiling after the construction of its biochromatogram, allowing the identification of 4 compounds correlated to this activity. This fact motivated the analysis of the PBRMe chromatographic profile by HPLC aiming a later microfractionation and evaluation of its α-glucosidase inhibition profiling. Thus, a gradient elution constituted by acetonitrile-water (5:95) + 0.1% formic acid (eluent A) and acetonitrile-water (95:5) + 0.1% formic acid (eluent B) as mobile phase exhibited the best separation of the constituents in a reversed-phase C_{18} column (Phenomenex Luna 3 µm), according to the following description: 0 min, 5% B; 15 min, 19% B; 44 min, 40% B; 47 min, 45% B; 52 min, 59% B; 57 min, 59% B; 70 min, 100% B, 80min, 100% B. The column eluent was directed to an automated fraction collector previously established to collect the six well separated major constituents of the chromatogram into a small glass HPLC vials. A concentration of 100 mg/mL, 20 µL volume of injection and an eluent flow rate maintained at 0.6 mL/min, in association with a series of successive injections resulted in the isolation of two new anthrones C,O-diglycosides, PBRMe 02 **(compound 30)** and PBRMe 03 **(compound 31)**. The remaining four major constituents collected from these procedures presented a considerable level of impurities after analyses of the ^{1}H NMR spectrum and consequently the 2D NMR experiments were not acquired to these compounds. The FIGURE 3.14 presents the mass of the isolated compounds.

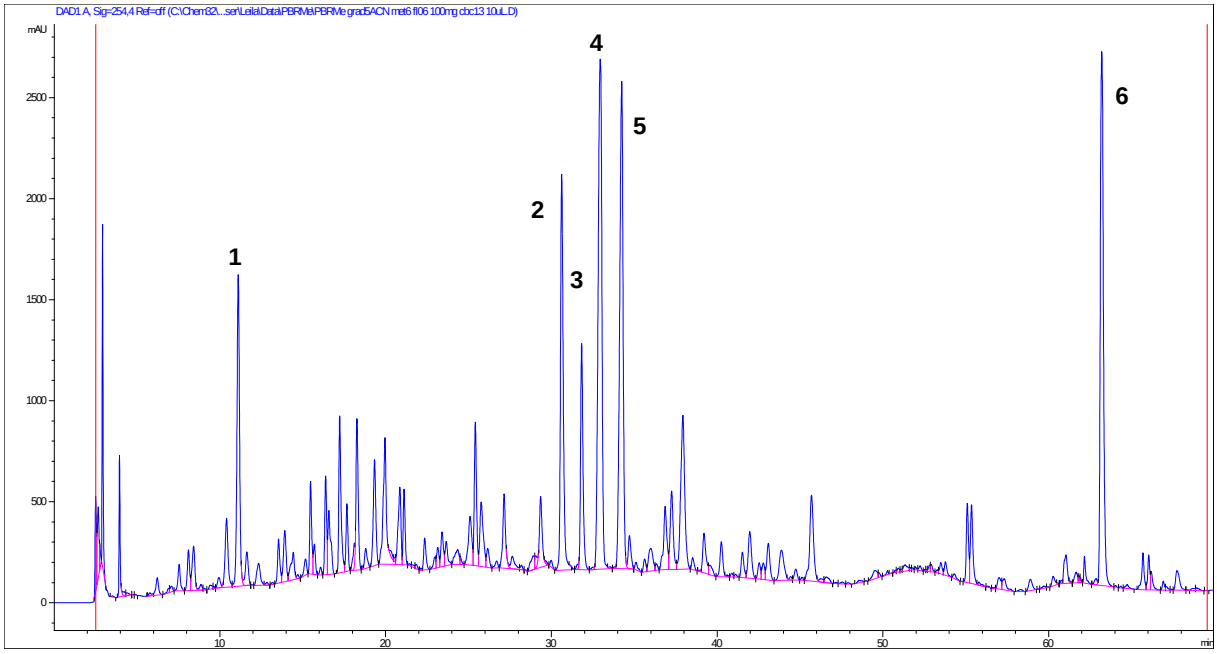

FIGURE 3.14 – Reversed-Phase HPLC Chromatogram at 254 nm using a gradient elution indicating the compounds collected from PBRMe.

TABLE 3.10 – Mass of the compounds isolated from the analytical reversed-phase HPLC purifications of PBRMe

Compounds	Mass (mg)
PBRMe 01	0.89
PBRMe 02 **(compound 30)**	2.91
PBRMe 03 **(compound 31)**	1.66
PBRMe 04	1.97
PBRMe 05	1.79
PBRMe 06	1.17

Thereafter, the gradient elution of this separation was adjusted aiming to perform the high-resolution inhibitory profile. The column and mobile phase was kept as the same used to isolate the compounds: a gradient elution constituted by acetonitrile-water (5:95) + 0.1% formic acid (eluent A) and acetonitrile-water (95:5) + 0.1% formic acid (eluent B). However, small changes were performed to the gradient elution, according to the following description: 0 min, 5% B; 15 min, 19% B; 44 min,

40% B; 46 min, 45% B; 50 min, 59% B; 55 min, 59% B; 58 min, 85% B, 65 min, 100% B; 70 min, 100% B. Thus, the eluent from 2 to 70 min was collected in 176 wells of a 96-well microplate (the last column of each microplate was reserved for blanks and controls), yielding a resolution of 2.58 data points/ min. It was injected 15 µL of a 100 mg/mL concentration solution of the extract, maintained the same flow rate elution as before. The plates were evaporated to dryness using a speed vacuum concentrator and the semi-high-resolution inhibition assay to α-glucosidase and PTP1B enzymes were performed according to the methodology described in item 3.3.4.2. After the construction of the biochromatogram, it was noticed the bioactive compounds were concentrated in the last part of the chromatogram in both bioassays, related to the overlapped smaller compounds. Despite several attempts developing a gradient elution, it was not possible to develop an analytical-scale HPLC base-line separation able to distinguish all minor compounds directly from the crude extract. Thus, a preparative-scale reversed-phase HPLC was used aiming to divide the extract in three main fractions: PBMRe 1 (collected from 0 to 22 min), PBRMe 2 (collected from 22 to 48 min) and PBRMe 3 (collected from 48 to 70 min).

The fraction 03 was analyzed in an analytical-scale HPLC and a gradient elution constituted by methanol-water (5:95) + 0.1% formic acid (eluent A) and methanol-water (95:5) + 0.1% formic acid (eluent B) was developed: 0 min, 60% B; 50 min, 100% B; 60 min, 100% B. This condition was also used to the microfractionation to further high-resolution inhibition assay. Thus, the eluent from 15.5 to 60 min was collected in 160 wells of a 96-well microplate, yielding a resolution of 3.59 data points/ min. It was injected 15 µL of a 30 mg/mL concentration solution of the fraction 3, maintained the flow rate elution at 0.6 mL/min. The PTP1B biochromatogram was subsequently constructed. Unfortunately neither the α-glucosidase biochromatogram, nor the isolation and identification of the bioactive compound could be performed during the abroad internship.

4 - RESULTS AND DISCUSSION

4.1 – ISOLATED COMPOUNDS

The phytochemical study of *P. glazioviana* yielded 22 new nortriterpenes with new chemical skeleton. Among these, compounds **2** and **3**, **8** and **9**, **12** and **13**, **18** and **19** comprise 4 pairs of diastereoisomers. From *P. bahiensis,* 02 new C,O-diglycosides anthones and 05 known anthraquinones were isolated. All structures are described below:

P. glazioviana

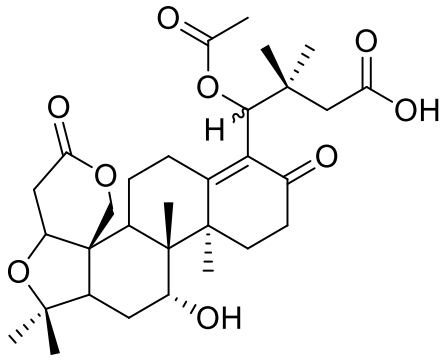

1

(Page 119)

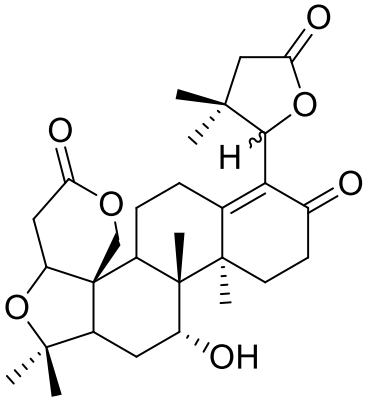

2

(Page 100)

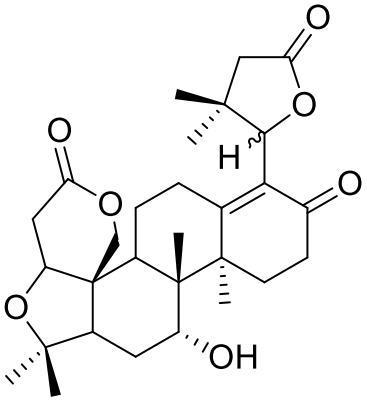

3

(Page 100)

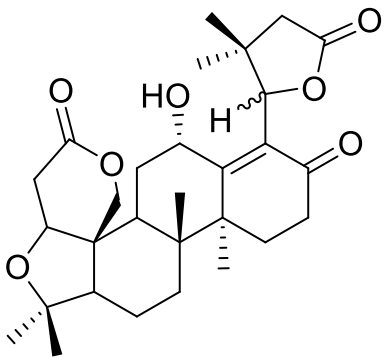

5

(Page 100)

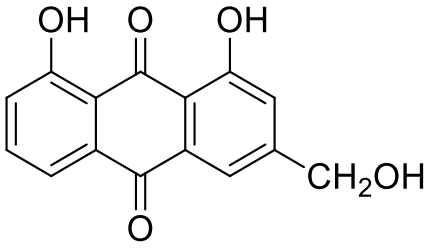

5a

(Page 163)

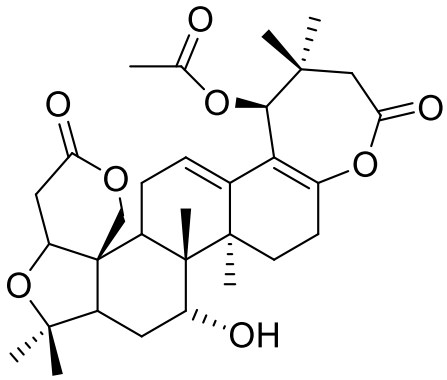

6

(Page 77)

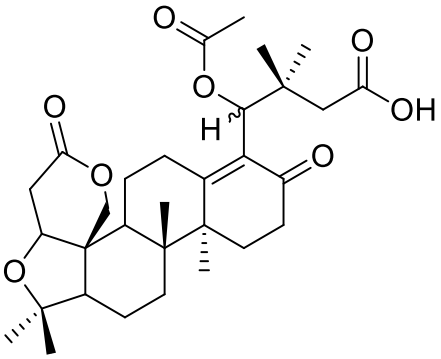

7

(Page 119)

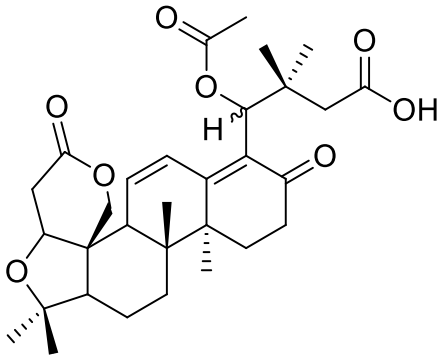

7a

(Page 119)

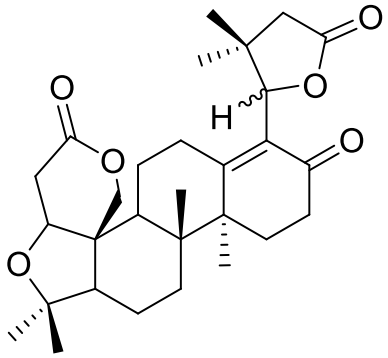

8

(Page 83)

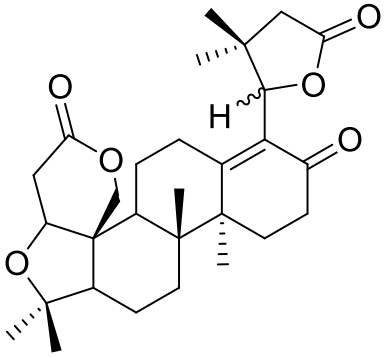

9

(Page 83)

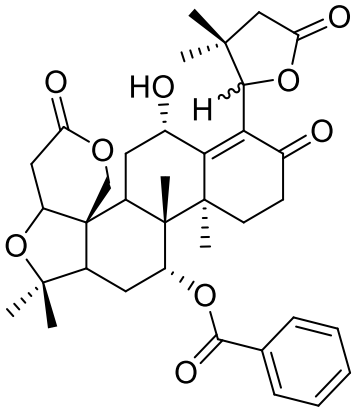

12

(Page 100)

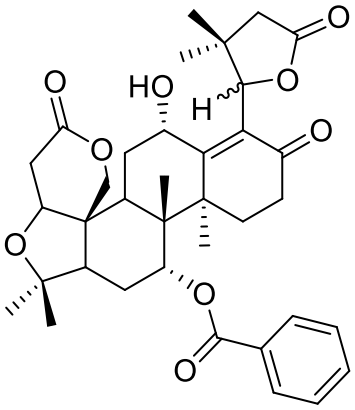

13

(Page 100)

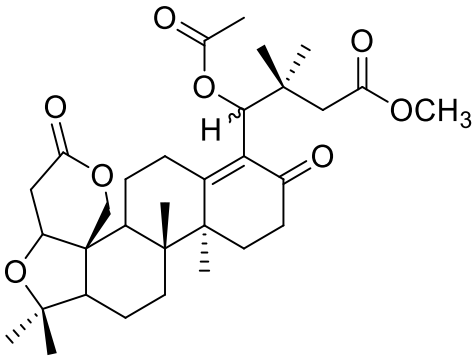

14

(Page 119)

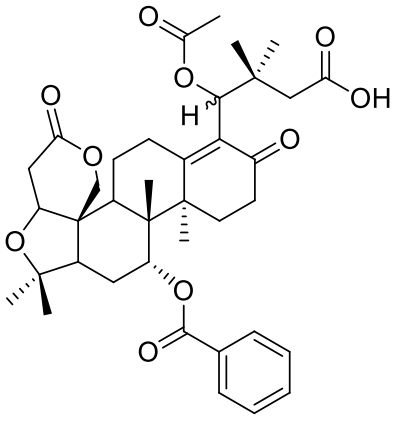

15

(Page 119)

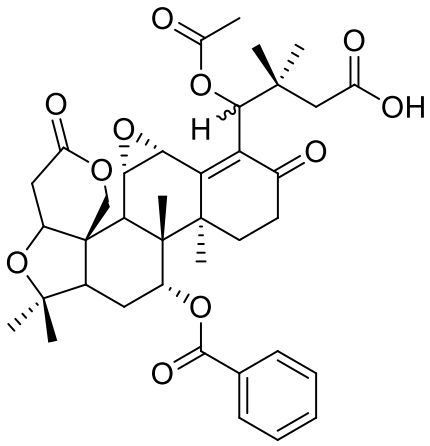

16

(Page 119)

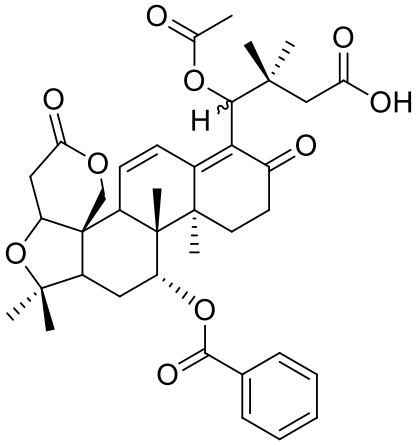

17

(Page 119)

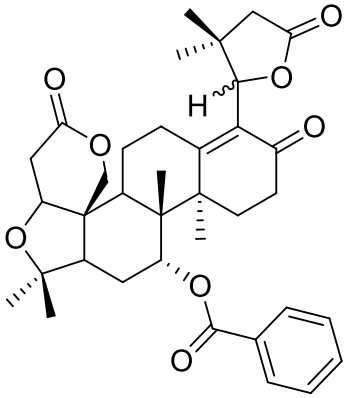

18

(Page 92)

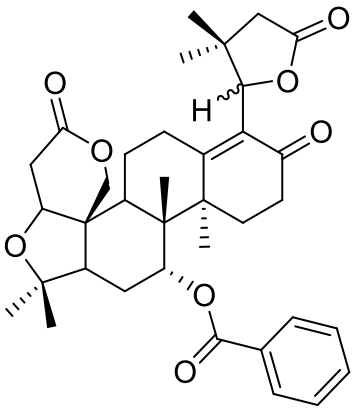

19

(Page 92)

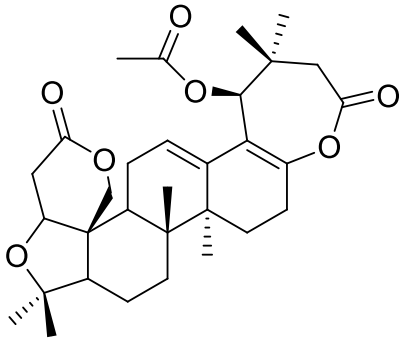

(20)

(Page 51)

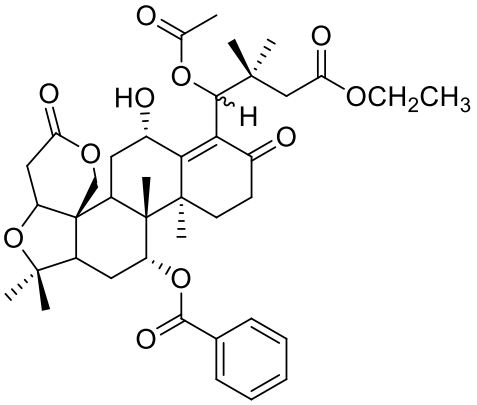

21

(Page 148)

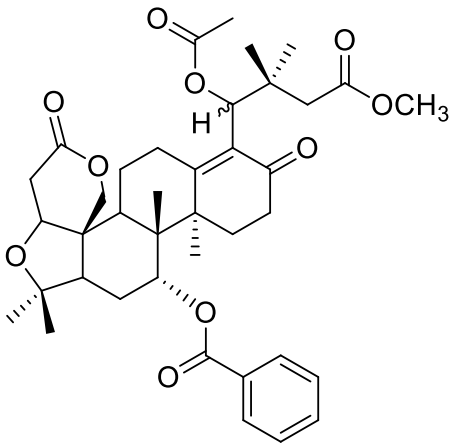

22

(Page 119)

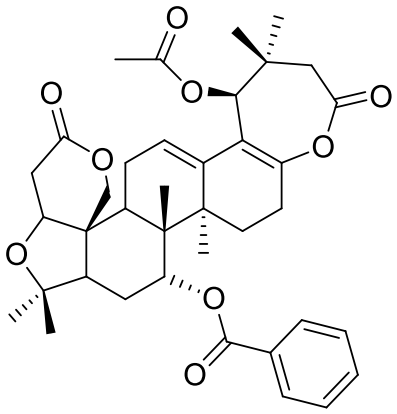

(23)

(Page 51)

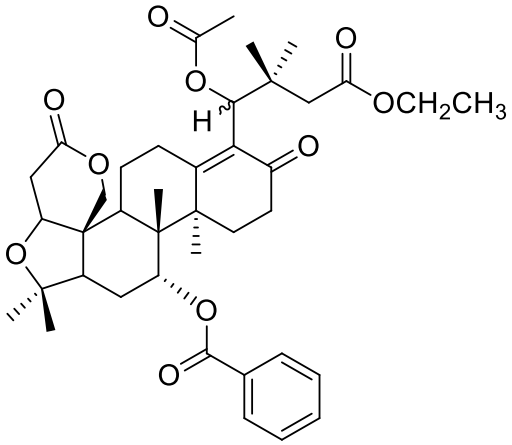

24

(Page 148)

P. bahiensis

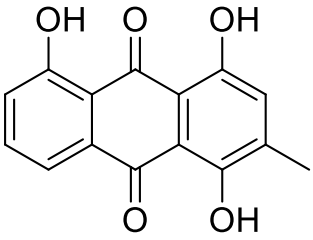

25

(Page 163)

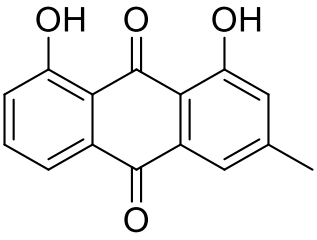

26

(Page 163)

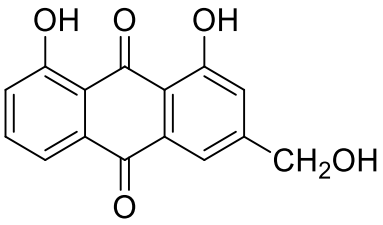

27

(Page 163)

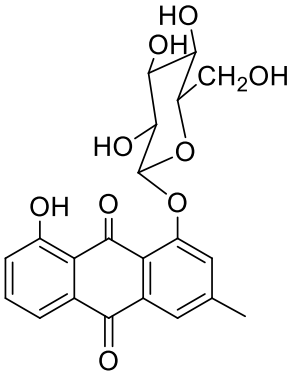

28

(Page 173)

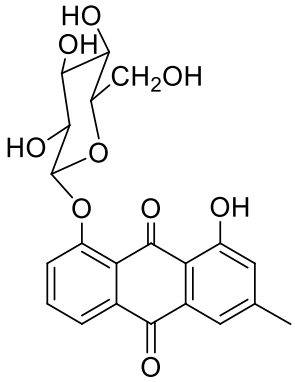

29

(Page 173)

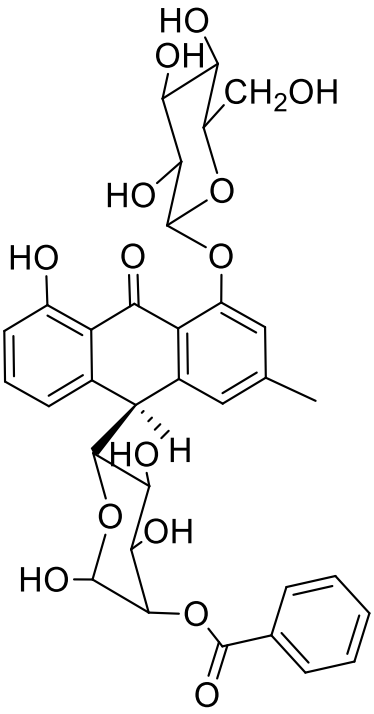

30

(Page 183)

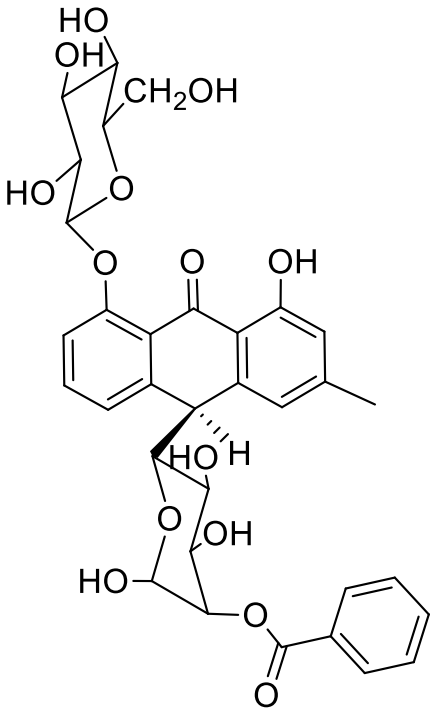

31

(Page 183)

4.1.1 – Nortriterpenes

The study of the dichloromethane partition from *P. glazioviana* disclosed 22 new nortriterpenes with new carbon skeleton, and one known anthraquinone (discussion page 163). Hereby, is presented the discussion to these new compounds:

4.1.1.1 – Nortriterpenes 23 and 20

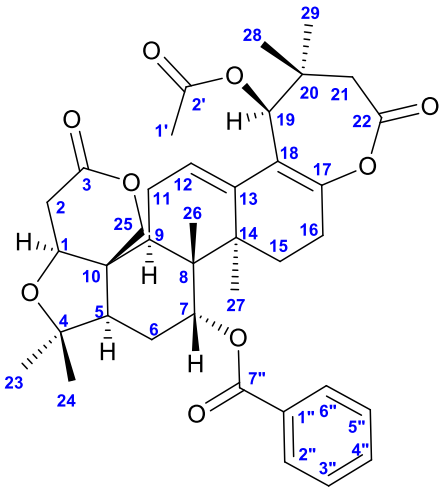

(23)

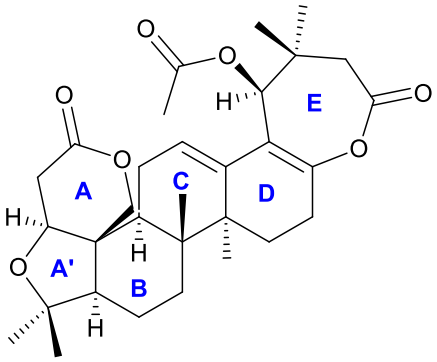

(20)

The nortriterpene **23** was isolated as a white wax, and had a molecular formula of $C_{38}H_{46}O_9$ as determined by HRESIMS ($[M+H]^+$ 647.3210, calcd. 647.3220), indicating an index of hydrogen deficiency of 16 (FIGURE 4.14). The optical rotation measured disclosed: $[\alpha]_{D:}^{26}$ + 43.53 (c. 0.76, MeOH).

The structure was established based on spectroscopic data from 1D ^{1}H NMR, ^{13}C NMR, and DEPT135 as well as 2D NMR experiments (COSY, HSQC, HMBC and NOESY, FIGURES 4.3 to 4.13). The structural assignment was also supported by Heteronuclear 2-Bond Correlation (H2BC) spectrum, an experiment which alleviates the problem of missing two-bond correlations in HMBC spectra once correlates almost exclusively protons and proton-bearing carbon spins separated by two covalent bonds and is independent of occasionally vanishing $^2J_{CH}$ coupling constants. H2BC also solves the problem of distinguishing two- and three-bond correlations in HSQC–TOCSY or HMBC (PETERSEN, 2006).

The UV spectrum of **23** was acquired from the HPLC-HRESIMS and showed the absorbances λ_{max} at 232 and 255 nm, in agreement with the conjugation of the double-bond system, resulted of the bathochromic shift and consequently an increase of the absorption intensity. The IR spectrum disclosed sp^2 and sp^3 C-H stretch vibrations in the range from 2900 to 3000 cm^{-1} beside that very characteristic to C=O stretching frequency as a strong bond at 1735 cm^{-1} resulted of the electron-withdrawing effects (inductive effects) from the esters functions. Moreover, vibrations in the range from 1100 to 1200 cm^{-1} due to C-O stretching vibrations and in the range at 1450 cm^{-1} due to C=C ring stretch absorption were also observed (FIGURE 4.18).

The ^{1}H NMR spectrum of **23** displayed two tertiary methyl groups at δ 1.11 and 1.15 (3H, s, H-24 and H-23, respectively), diastereotopic proton pairs corresponding to a methylene (δ 2.64, 1H, dd, *J* = 16.8 and 1.6 Hz, H2α and δ 2.95, 1H, dd, *J* = 16.8 and 3.7 Hz, H2β), an oxymethylene (δ 4.59, 1H, d, *J* = 13.3 Hz, H25α and δ 4.63, 1H, d, *J* = 13.3 Hz, H25β), an oxymethine at *δ* 4.21 (1H, dd, *J* = 3.7 and 1.6 Hz, H1), and a methine at *δ* 2.48 (1H, dd, *J* = 13.8 and 2.0 Hz, H5). These signals are very similar to the ^{1}H NMR signals observed for the A and A' rings of the well-known limonoid limonin (FIGURES 4.3 to 4.6, ZHANG, 2017). The presence of the A and A' rings was further supported by HMBC correlations from H-1 to the carbon at δ 45.4 (C-10), from H-1, H-2, and H-25 to the carbonyl group at δ 169.7 (C-3), as well as from H-23 and H-24 to each other carbon atoms and to the carbons at δ 80.7 (C-4) and δ 53.7 (C-5). The B, C and D-rings were subsequently identified based on combined use of COSY and HMBC spectra. Thus, the COSY spectrum showed three spin systems corresponding to the C-5 – C-6 – C-7, the C-9 – C-11 – C-12, and the C-15 – C-16 backbones (FIGURE 4.12). These spin systems were assembled based on HMBC correlations from H-7, H-9 and H-15β to the quaternary C-8 (δ 43.40), from H-7, H-12 and H-15β to the quarternary C-14 (δ 41.0), from H-11, H-12 and H-15α to the olefinic C-13 (δ 138.9), from H-12 and H-16 to C-18 (δ 118.1), and from H-15α and H-16 to C-17 (δ 148.9) – as seen from the HMBC correlations provided in TABLE 4.1 and FIGURE 4.9. HMBC correlations from H-26 and H-27 to C-8 and C-14, respectively, supports the position of these methyl groups, and the downfield shift of H-7 and HMBC correlations from H-7 and H-2''/H-6'' to the carbonyl group at δ 164.9 (C-7”) shows the presence of a benzoate group attached to C-7.

The highly substituted heptanolide ring system (E-ring) was established based on HMBC correlations from H-19 to the C-17 – C-18 double bond, to the quaternary C-20 (δ 43.9) and the two methyl groups attached to C-20 (δ 24.7 and 28.1, C-28 and C-29), and to C-2' (δ 169.2) of the acetate group. Furthermore, the H-21 methylene group was identified as intervening C-20 and C-22 based on HMBC correlation to these two carbon atoms (FIGURE 4.9). The complete assignments of all ^{1}H and ^{13}C NMR resonances are given in TABLE 4.1.

The correlations observed in the H2BC spectrum from H-1 to the C-2, H-5 and H-7 to the C-6 and H-9 and H-12 to the C-11 were useful confirming the proposed structure (FIGURE 4.1 and 4.11).

The stereospecific assignment of the hydrogens was obtained using the NOESY spectrum (FIGURE 4.13). Thus, NOEs between H-1 and H-5, H-9 and H-23 and between H-27 and H-9, H-15α, H-16, and H2''/H-6'', confirmed these hydrogens to be on the same side of the molecule, i.e., tentatively assigned to α. Likewise, NOEs between H-26 and H-6β, H-7, H-11β, H-15β and H-25 confirmed these hydrogens to be on the other side of the molecule, i.e. tentatively assigned to β. Thus, these NOEs established the relative stereochemistry of **23** as 1*S**,5*R**,7*R**,8*R**,9*S**,10*R**,14*R**. However, the relative configuration at C-19 could not be established to these stereocenters, since the only correlation on ring C observed between H-19 and H-12 does not corroborated to this establishment, due the flexibility of the E ring conformation.

Thus, vibrational circular dichroism (VCD) and DFT calculations experiments were performed in collaboration with Prof. Dr. João Batista M. Jr. and Prof. Dr. Fernando Martins dos Santos Jr. aiming the establishment of the absolute stereochemistry to all chiral centers. For this, density functional theory (DFT) calculations of IR and VCD spectra were performed to the lowest-energy conformations as well as their overlay, and further geometry optimized at the B3LYP/6-31G* level, as shown in FIGURE 4.15. The calculated [wB97XD/PCM($CHCl_3$)/6-311G**] IR and VCD spectra of both epimers (1*S*,5*R*,7*R*,8*R*,9*S*,10*R*,14*R*,19*S*) and (1*S*,5*R*,7*R*,8*R*,9*S*,10*R*,14*R*,19*R*), as well as those of their enantiomers, are shown in FIGURES 4.16 and 4.17. The two diastereoisomers were discriminated since some VCD bands with reversed signs, especially by the fundamentals 132 and 171 bands, resulted of the spatial arrangement of rings A and E combined with the opposite configuration for the chiral

center at C-19. These bands arise mainly from the C-O stretching vibration of the acetate group at C-19 coupled with CH_3 deformation modes on ring E (fundamental 132), as well as from the CH_2 twisting of ring A and the in-plane C-H bending of H-19 coupled with the CH_2 wagging of ring E (fundamental 171). Therefore, the excellent correlation between experimental and calculated IR/VCD data for compound **23** (FIGURE 4.16), led to the assignment of its absolute configuration as (1*S*,5*R*,7*R*,8*R*,9*S*,10*R*,14*R*,19*S*).

The nortriterpene **20** was elucidated on the basis of spectroscopic data from 1D ^{1}H NMR, ^{13}C NMR, and DEPT135, as well as 2D NMR experiments (COSY, HSQC, HMBC, H2BC, and NOESY, FIGURES 4.20 to 4.29) and had a molecular formula of $C_{31}H_{42}O_7$ as determined by HRESIMS ($[M+H]^+$ = 527.2998, calcd. 527.3008) indicating an index of hydrogen deficiency of 11 (FIGURE 4.30). The optical rotation measured disclosed: $[\alpha]_{D}^{26}$ + 63.93 (c. 0.41, MeOH). The UV spectrum to **20** was acquired from the HPLC-HRESIMS and showed the absorbances λ_{max} at 229 and 252 nm, in agreement with the conjugation of the double-bond system resulted of the bathochromic shift. The IR spectrum, likewise to compound **23**, disclosed sp^3 C-H stretch vibrations in the range from 2900 to 3000 cm^{-1} beside that very characteristic to the C=O stretching frequency as a strong bond at 1735 cm^{-1} resulted from the esters functions. Vibrations in the range from 1100 to 1200 cm^{-1} due to C-O stretching vibrations were also observed (FIGURE 4.31).

The ^{13}C NMR spectrum was identical to that observed for **23**, except for the absence of signals for the benzoate group as well as the disappearance of the oxymethine observed for C-7 in **23** and the appearance of an additional methylene signal for C-7 in **20** (FIGURE 4.23). This indicated that **20** has the same structure as **23**, except for the absence of the benzoate group, which is in agreement with the ^{2}J and ^{3}J HMBC correlations observed from H-5 at *δ* 1.71 to C-6 and C-7 at *δ* 18.3 and *δ* 33.6, respectively. The complete assignments of all ^{1}H and ^{13}C resonances was performed based on analysis of all 2D NMR spectra, and the assignments with all observed 2D correlations are given in TABLE 4.2. The absolute configuration of compound **20** is assigned (1*S*,5*R*,8*R*,9*S*,10*R*,14*R*,19*S*), assuming that the biosynthetic pathways to **23** and **20** are identical in this plant, and mainly due the high similarities of chemical shift, coupling constants and NOESY correlations in NMR spectrum to both compounds.

TABLE 4.1- ^{13}C and ^{1}H chemical shifts and full NOESY, COSY and HMBC correlations for compound **23** acquired in $CDCl_3$

C	δ_C	δ_H	NOESY	COSY	HMBC
1	80.6	4.21 dd (3.7, 1.6)	H-2α, H-2β, H-5, H-9, H-23	H-2α, H-2β	C-3, C-5, C-9, C-10, C-24, C-25
2	35.5	β: 2.95 dd (16.8, 3.7)	H-1, H-2α	H-1, H-2α	C-1, C-3, C-10, C-25
		α: 2.64 dd (16.8, 1.6)	H-1, H-2β, H-11α	H-1, H-2β	C-1, C-3, C-10
3	169.7				
4	80.7				
5	53.7	2.48 dd (14.4, 2.0)	H-2”, H-6”, H-1, H-6α, H-9, H-23	H-6α, H-6β	C-4, C-6, C-7, C-9, C-10, C-23, C-24, C-25
6	25.5	α: 1.97 td (14.4, 2.0)	H-6β, H-7, H-24, H-25α, H-25β, H-26	H-5, H-6β, H-7	C-5, C-10
		β: 1.72 dt (14.4, 2.6)	H-1’, H-5, H-6α, H-7, H-23, H-24	H-5, H-6α, H-7	C-4, C-5, C-7, C-8, C-10
7	74.7	5.36 t (2.6)	H- 6α, H-6β, H-15α, H-15β, H-26	H-6α, H-6β	C-4, C-5, C-6, C-8, C-9, C-26, C-7”
8	43.4				
9	42.4	2.82 dd (10.3, 7.8)	H-2”, H-6”, H-1, H-5, H-27	H-11α, H-11β	C-1, C-5, C-8, C-10, C-11, C-14, C-25, C-26
10	45.4				
11	26.1	β: 2.55 ddd (19.4, 10.3, 4.1)	H-11α, H-12, H-25α, H-25β, H-26	H-9, H-11β, H-12	C-9, C-10, C-12, C-13, C-17, C-18
		α: 2.43 ddd (19.4, 7.8, 4.1)	H-2α, H-11β, H-12	H-9, H-11α, H-12	C-8, C-12, C-13, C-17
12	116.8	5.77 br t (4.1)	H-11α, H-11β, H-19, H-29	H-11α, H-11β	C-9, C-11, C-13, C-14, C-17, C-18, C-27
13	138.9				
14	41.0				
15	25.8	β: 1.87 m	H-7, H-15α, H-16, H-26	H-15α, H-16	C-8, C-13, C-14, C-17, C-27
		α: 1.38 dt (12.8, 3.8)	H-7, H-15β, H-16, H-27	H-15β, H-16	C-13, C-14, C-17, C-27
16	24.9	2.23 *m*, 1H	H-15α, H-15β, H-27	H-15α, H-15β	C-14, C-15, C-17, C-18
17	148.9				
18	118.1				
19	73.3	5.28 s	H-1’, H-12, H-28, H-29		C-1’, C-2’, C-13, C-17, C-18, C-20, C-21, C-28, C-29
20	43.9				
21	43.8	β: 2.15 d (12.0)	H-21α, H-28, H-29	H-21α	C-19, C-20, C-22, C-28
		α: 2.31 d (12.0)	H-21β, H-27, H-29	H-21β	C-20, C-22, C-28, C-29
22	169.1				
23	30.6	1.15 s	H-2”, H-6”, H-1, H-5, H-6β		C-4, C-5, C-24
24	21.6	1.11 s	H-6α, H-6β, H-25α, H-25β		C-4, C-5, C-23
25	65.9	β: 4.63 d (13.3)	H-6α, H-11β, H-24, H-26	H-25α	C-1, C-3, C-5, C-9, C-10, C-26
		α: 4.59 d (13.3)	H-6α, H-11β, H-24, H-26	H-25β	
26	17.6	0.88 s	H-6α, H-7, H-11β, H-15β, H-25α, H-25β		C-7, C-8, C-9, C-14
27	24.8	1.23 s	H-2”, H-6”, H-9, H-15α, H-16, H-21α, H-29		C-8, C-13, C-14, C-15
28	24.7	1.14 s	H-19, H-21β, H-29		C-19, C-20, C-21, C-29
29	28.1	0.93 s	H-12, H-19, H-21α, H-21β, H-27, H-28		C-19, C-20, C-21, C-22, C-28
1´	20.8	2.01 s	H-6β, H-19		C-2’
2´	169.9				
1”	130.1				
2”/ 6”	129.6	8.02 XX’-system	H-3”, H-4”, H-5”, H-5, H-9, H-23, H-27	H-3”, H-5”	C-2”, C-4”, C-6”, C-7”
3”/ 5”	128.71	7.46 AA’-system	H-2”, H-6”	H-2”, H-4”, H-6”	C-1”, C-3”, C-4”,C-5”, C-7”
4”	133.55	7.59 tt (8.4, 1.2)	H-2”, H-6”	H-3”, H-5”	C-2”, C-6”
7”	164.99				

TABLE 4.2- ^{13}C and ^{1}H chemical shifts and full NOESY, COSY and HMBC correlations for compound **20** acquired in $CDCl_3$

C	δ_C	δ_H	NOESY	COSY	HMBC
1	80.3	4.05 dd (3.7, 1.6)	*	H-2α, H-2β	C-3, C-9, C-10, C-24, C-25
2	35.9	β: 2.93 dd (16.7, 3.7)	H-1, H-2α	H-1, H-2α	C-1, C-3, C-10, C-25
		α: 2.61 dd (16.7, 1.5)	H-1, H-2β, H-11α, H-25α	H-1, H-2β	C-1, C-3, C-10
3	170.2				
4	81.1				
5	60.8	1.71 br d (11.3)	H-1, H-9, H-23, H-27	H-6	C-4, C-6, C-7, C-9, C-10, C-23, C-24, C-25
6	18.3	1.62 m	H-23, H-24, H-25β,H-26	H-5, H-7	C-4, C-5, C-7, C-8, C-10
7	33.6	1.64 m	H-26, H-15α	H-6	C-5, C-6, C-8, C-14, C-26
8	39.5				
9	44.7	2.14 dd (11.4, 5.8)	H-1, H-5, H-27	H-11α, H-11β	C-1, C-5, C-8, C-10, C-11, C-14, C-25, C-26, C-27
10	45.3				
11	26.2	β: 2.40 m	H-11α, H-12, H-25α, H-26	H-9, H-11α, H-12	C-9, C-12, C-13, C-18
		α: 2.19 m	H-2α, H-11β, H-12	H-9, H-11β, H-12	C-8, C-9, C-12, C-13, C-18
12	118.4	5.95 br t (3.8)	H-11α, H-11β, H-19, H-29	H-11α, H-11β	C-9, C-11, C-13, C-14, C-17, C-18, C-27
13	136.9				
14	40.7				
15	26.8	β: 1.72 m	H-15α, H-16, H-26	H-15α, H-16	C-8, C-13, C-14, C-16, C-27
		α: 1.45 dt (12.8, 3.6)	H-7, H-15β, H-16, H-27	H-15β, H-16	C-8, C-13, C-14, C-16, C-17, C-27
16	25.4	2.31 dd (9.2, 3.6)	H-15α, H-15β, H-27	H-15α, H-15β	C-13, C-14, C-15, C-17, C-18
17	148.8				
18	119.2				
19	73.6	5.36 s	H-12, H-28, H-29		C-13, C-17, C-18, C-21, C-28, C-29, C-2′
20	44.2				
21	43.8	β: 2.21 d (12.1)	H-21α, H-28, H-29	H-21α	C-19, C-20, C-22, C-28
		α: 2.42 d (12.1)	H-21β, H-27, H-29	H-21β	C-20, C-22, C-28, C-29
22	169.3				
23	30.9	1.28 s	H-5, H-6, H-24		C-4, C-5, C-24
24	21.6	1.14 s	H-6, H-23, H-25β		C-4, C-5, C-23
25	66.1	β: 4.60 d (13.1)	H-6, H-24, H-26	H-25α	C-1, C-3, C-5, C-9, C-10, C-26
		α: 4.52 d (13.1)	H-2α, H-11β, H-26	H-25β	
26	17.3	0.80 s	H-6, H-7, H-11β, H-15β, H-25α, H-25β		C-7, C-8, C-9, C-14
27	21.0	1.13 s	H-5, H-9, H-15α, H-16, H-21α		C-8, C-13, C-14, C-15
28	24.7	1.15 s	H-19, H-21β, H-29		C-19, C-20, C-21, C-29
29	28.0	0.93 s	H-12, H-19, H-21α, H-21β,H-28		C-19, C-20, C-21, C-28
1′	20.8	2.04 s			C-19, C-2′
2′	170.0				

*Not observed correlation

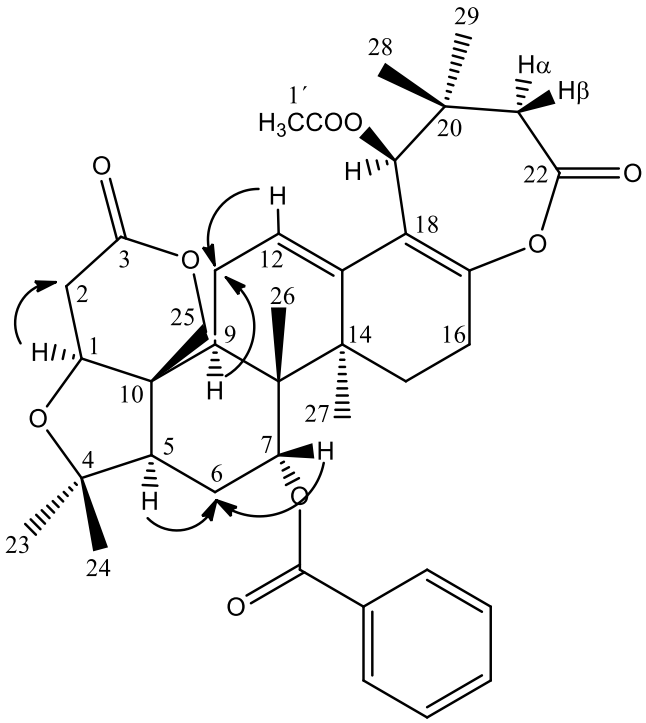

FIGURE 4.1 - Key correlations in the H2BC spectrum of the picraviane A (**23)**.

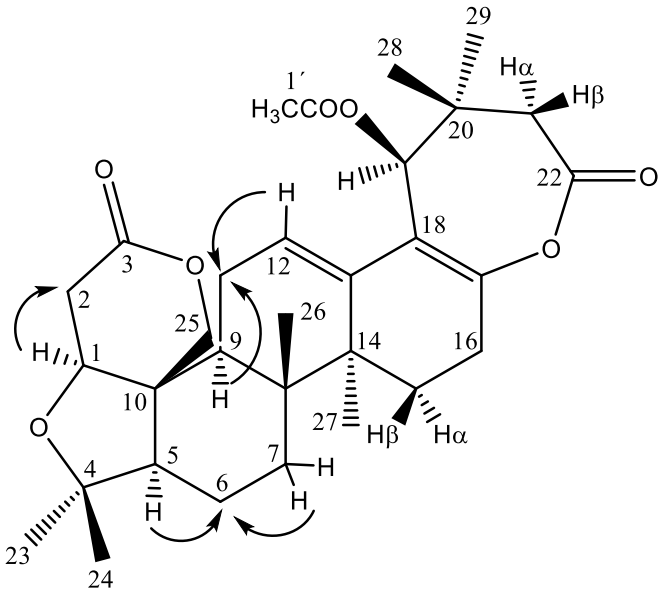

FIGURE 4.2 - Key correlations in the H2BC spectrum of the picraviane B (**20)**.

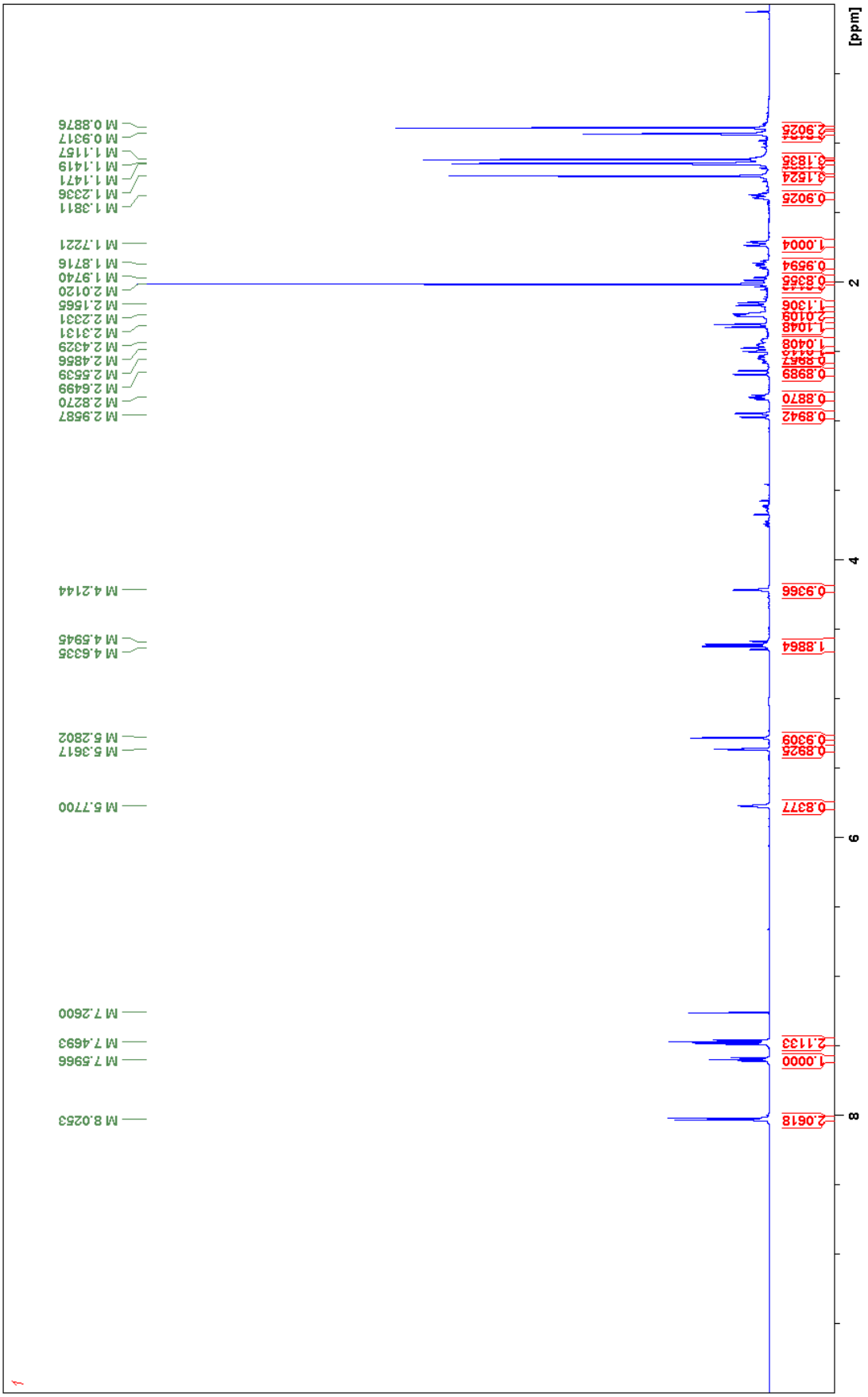

FIGURE 4.3 - ^{1}H NMR spectrum of Picraviane A (**23**) in $CDCl_3$ (600 MHz).

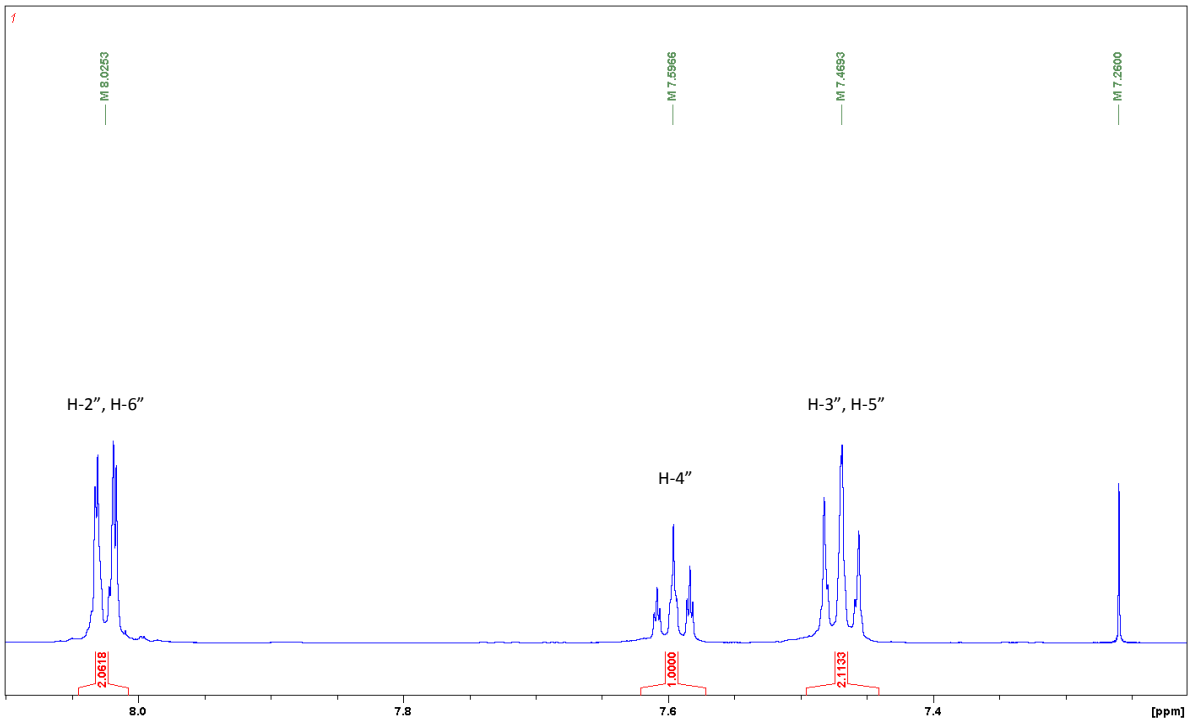

FIGURE 4.4- Expansion of the ^{1}H NMR spectrum of Picraviane A (**23**) in $CDCl_3$ (600 MHz).

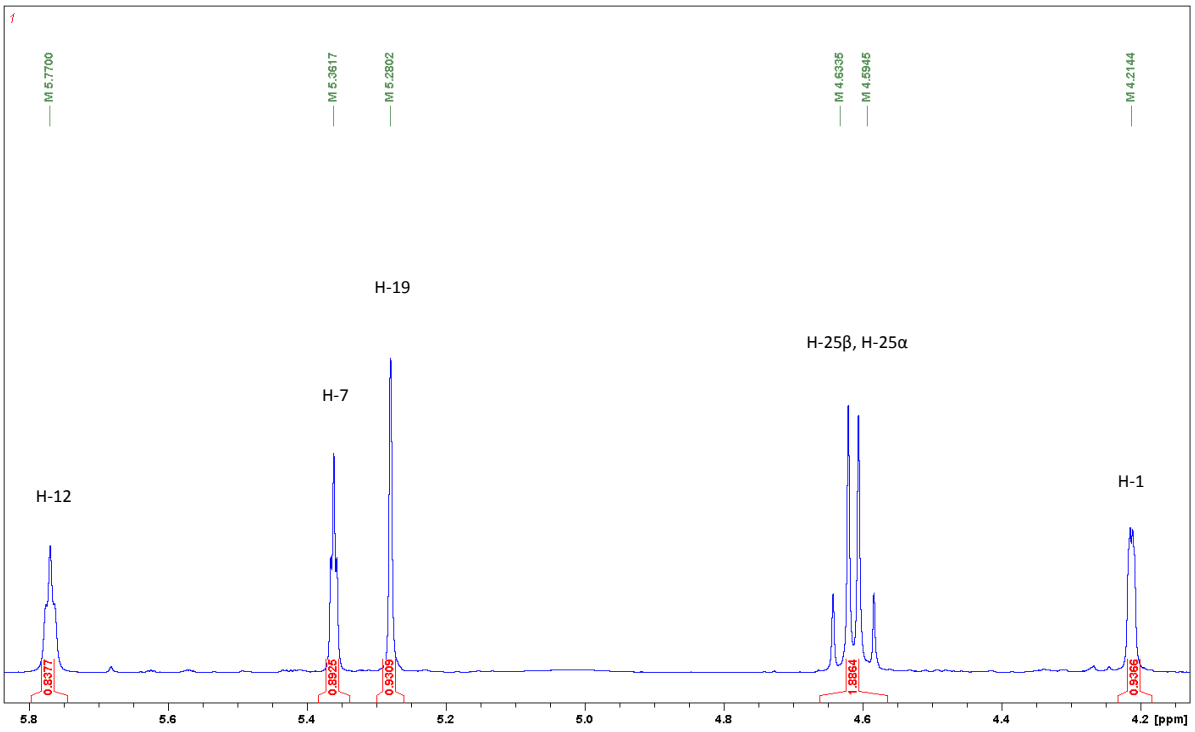

FIGURE 4.5 - Expansion of the ^{1}H NMR spectrum of Picraviane A (**23**) in $CDCl_3$ (600 MHz).

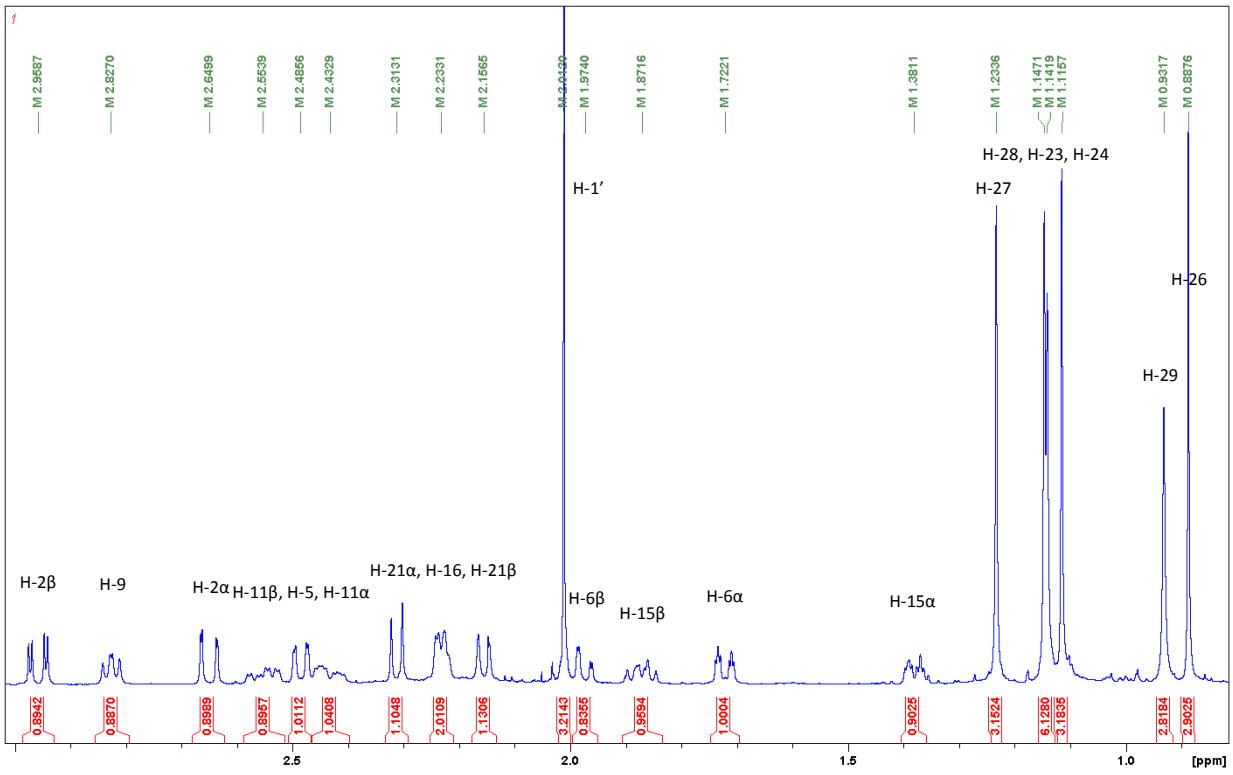

FIGURE 4.6 - Expansion of the ^{1}H NMR spectrum of Picraviane A (**23**) in $CDCl_3$ (600 MHz).

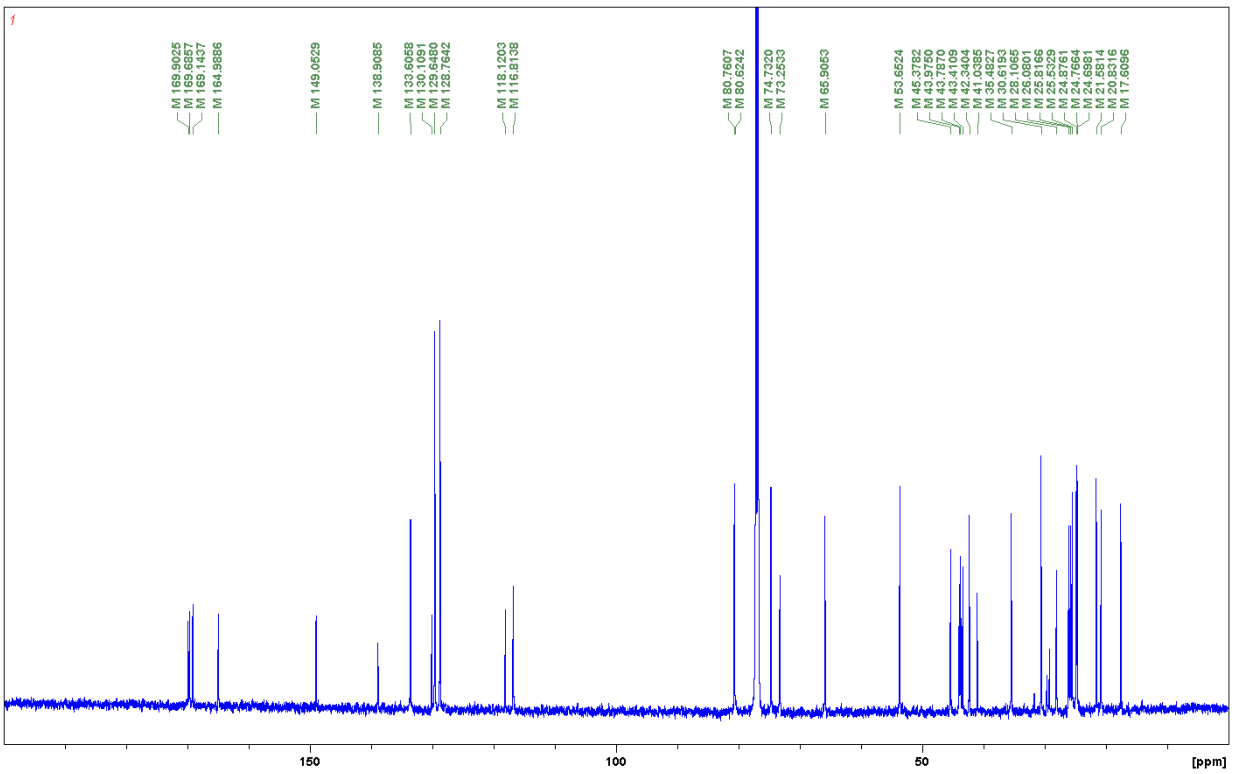

FIGURE 4.7 - ^{13}C NMR spectrum of Picraviane A (**23**) in $CDCl_3$ (150 MHz).

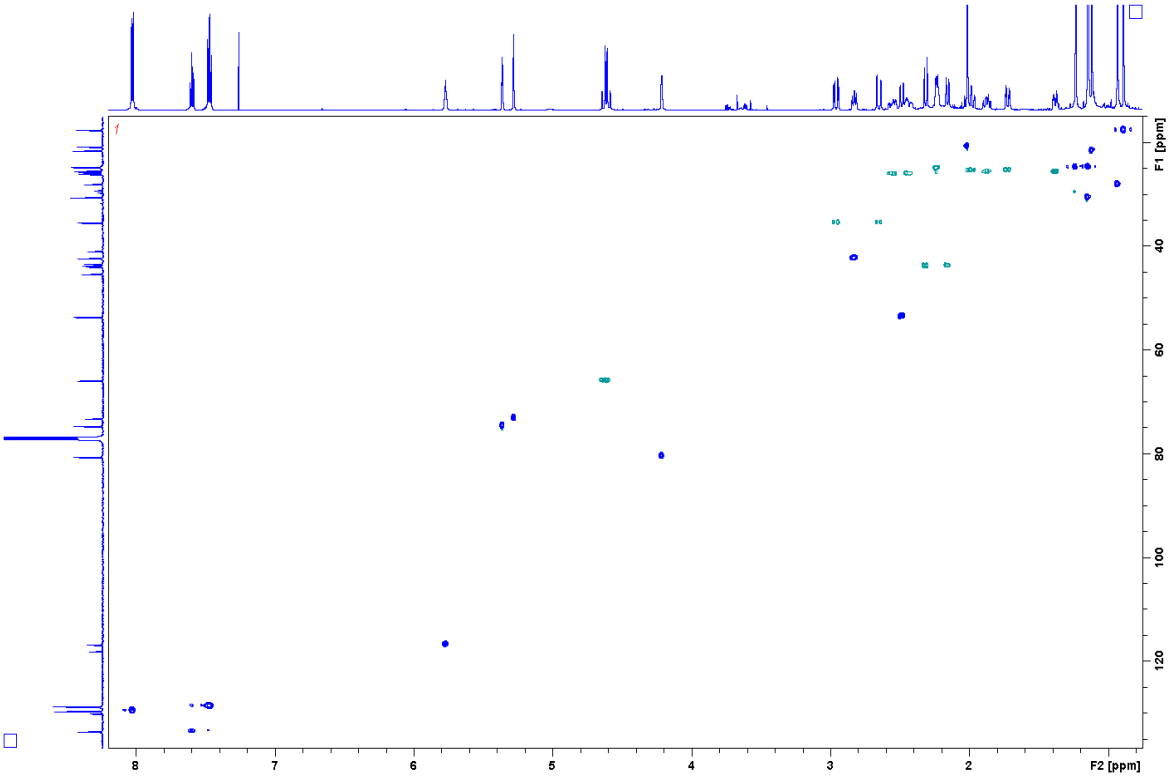

FIGURE 4.8 - HSQC spectrum of Picraviane A (**23**) in $CDCl_3$ (600 MHz).

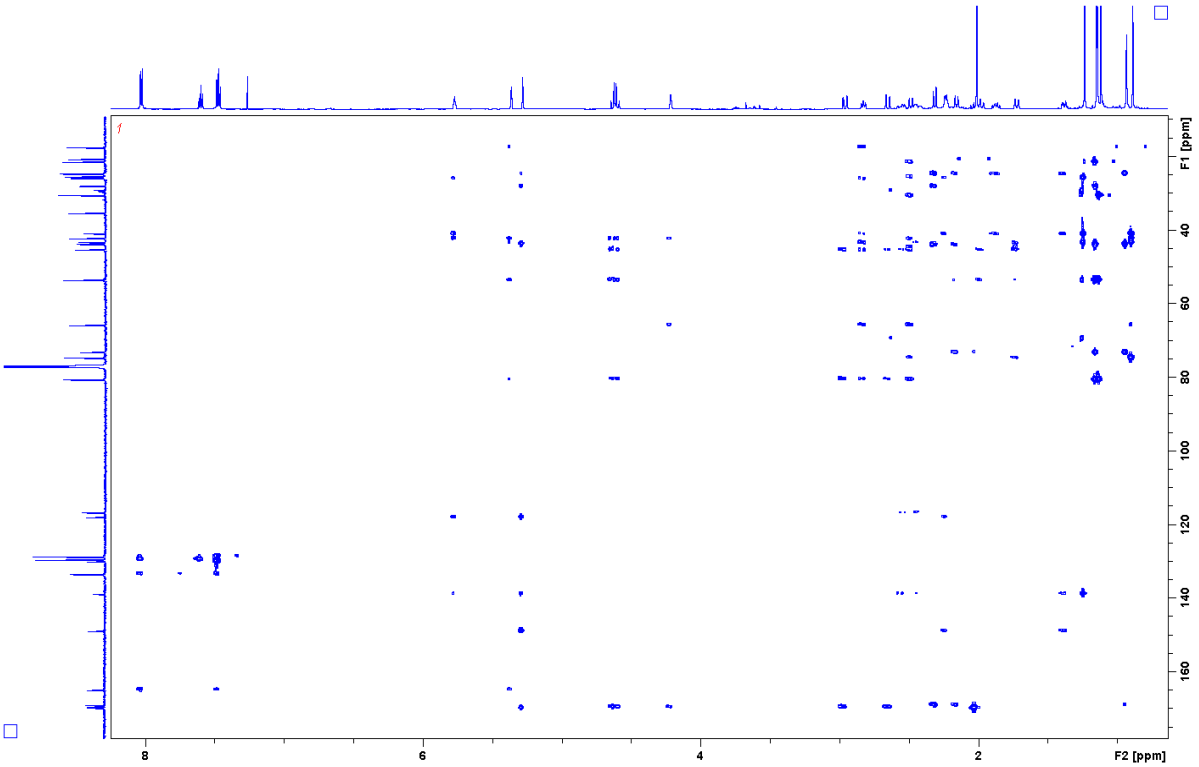

FIGURE 4.9 - HMBC spectrum of Picraviane A (**23**) in $CDCl_3$ (600 MHz).

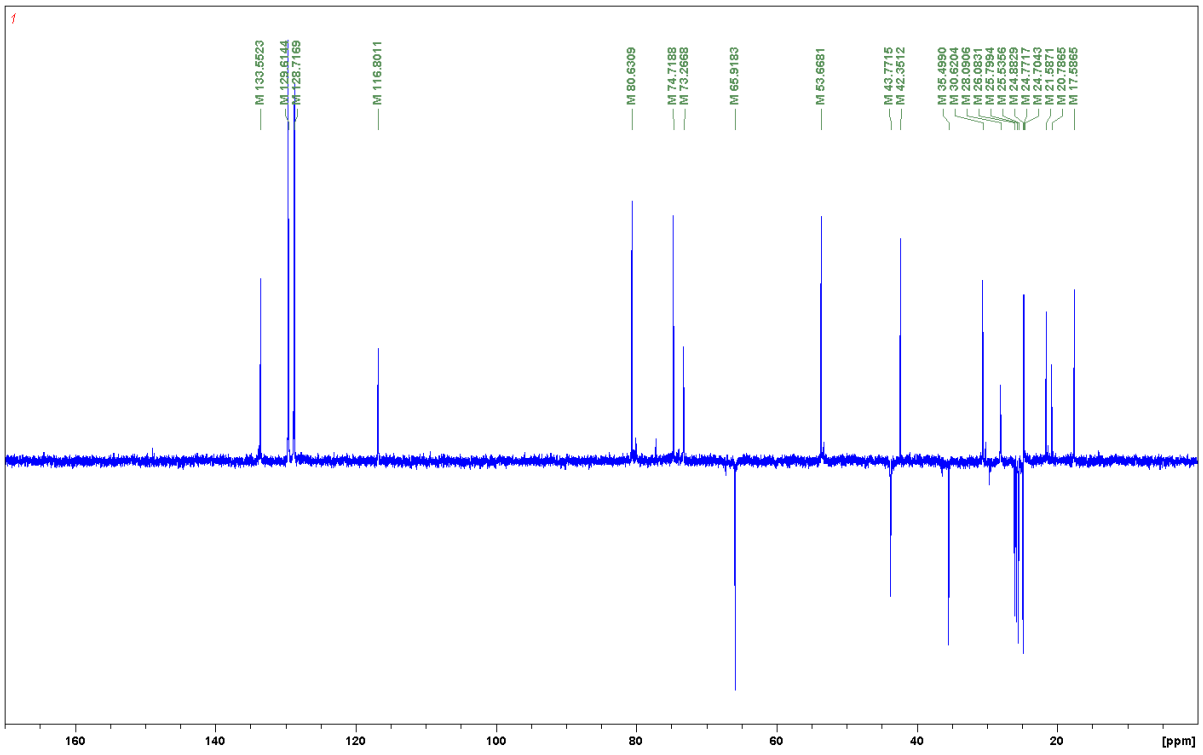

FIGURE 4.10 - DEPT135 spectrum of Picraviane A (**23**) in $CDCl_3$ (100 MHz).

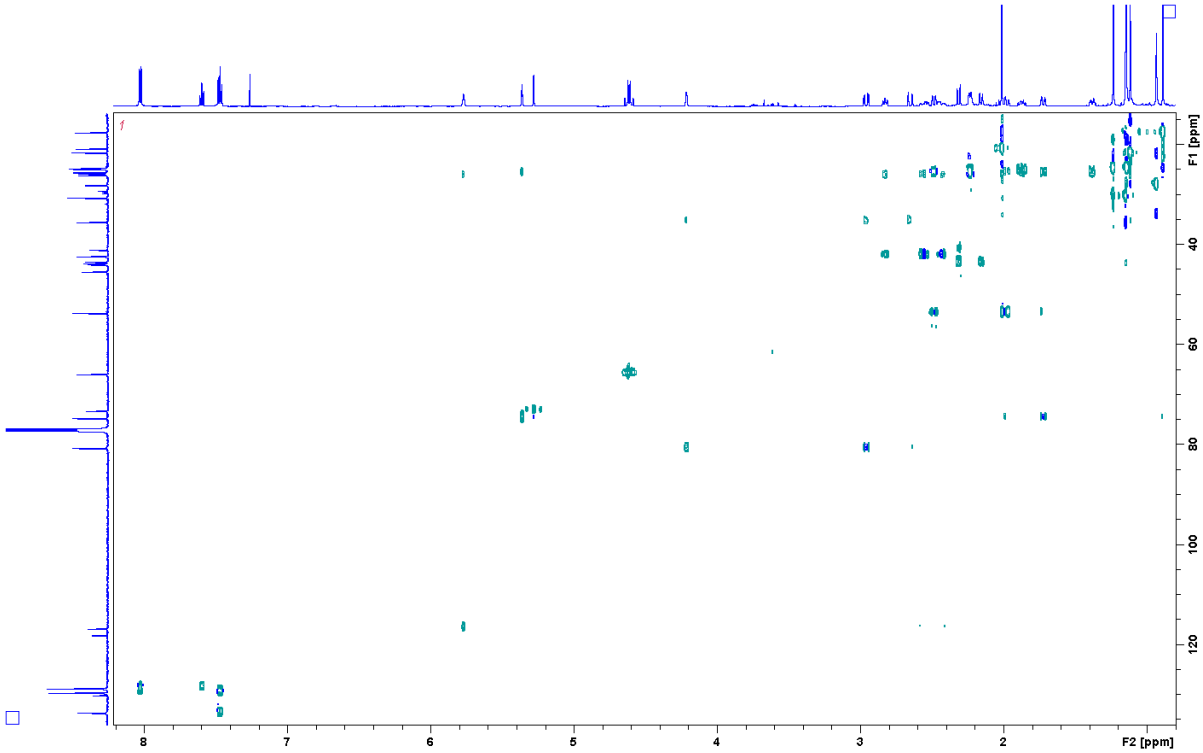

FIGURE 4.11 - H2BC spectrum of Picraviane A (**23**) in $CDCl_3$ (600 MHz).

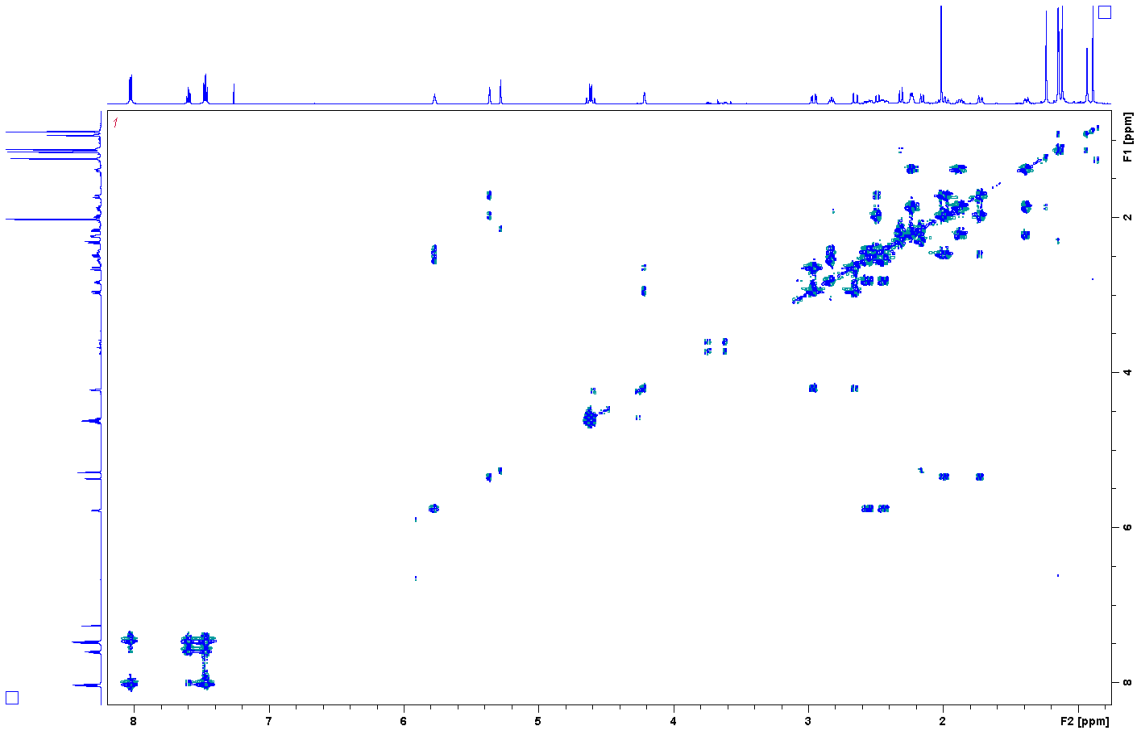

FIGURE 4.12 - ^{1}H-^{1}H COSY spectrum of Picraviane A (**23**) in $CDCl_3$ (600 MHz).

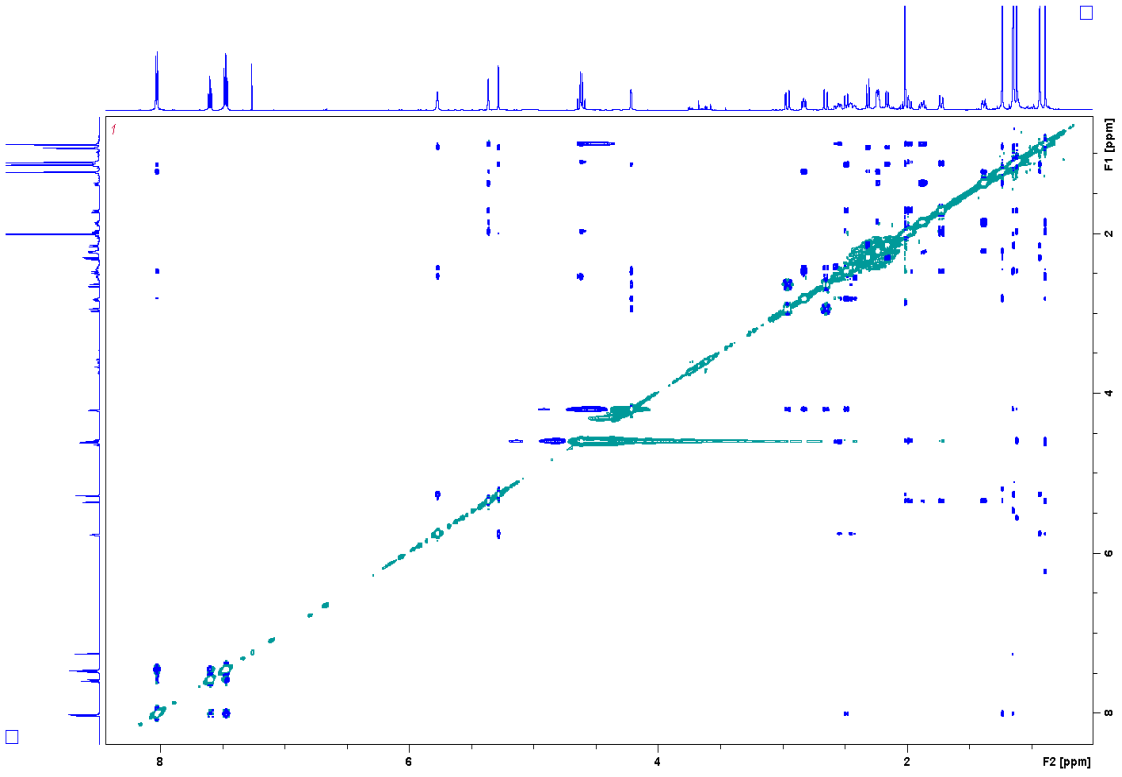

FIGURE 4.13 - NOESY spectrum of Picraviane A (**23**) in $CDCl_3$ (600 MHz).

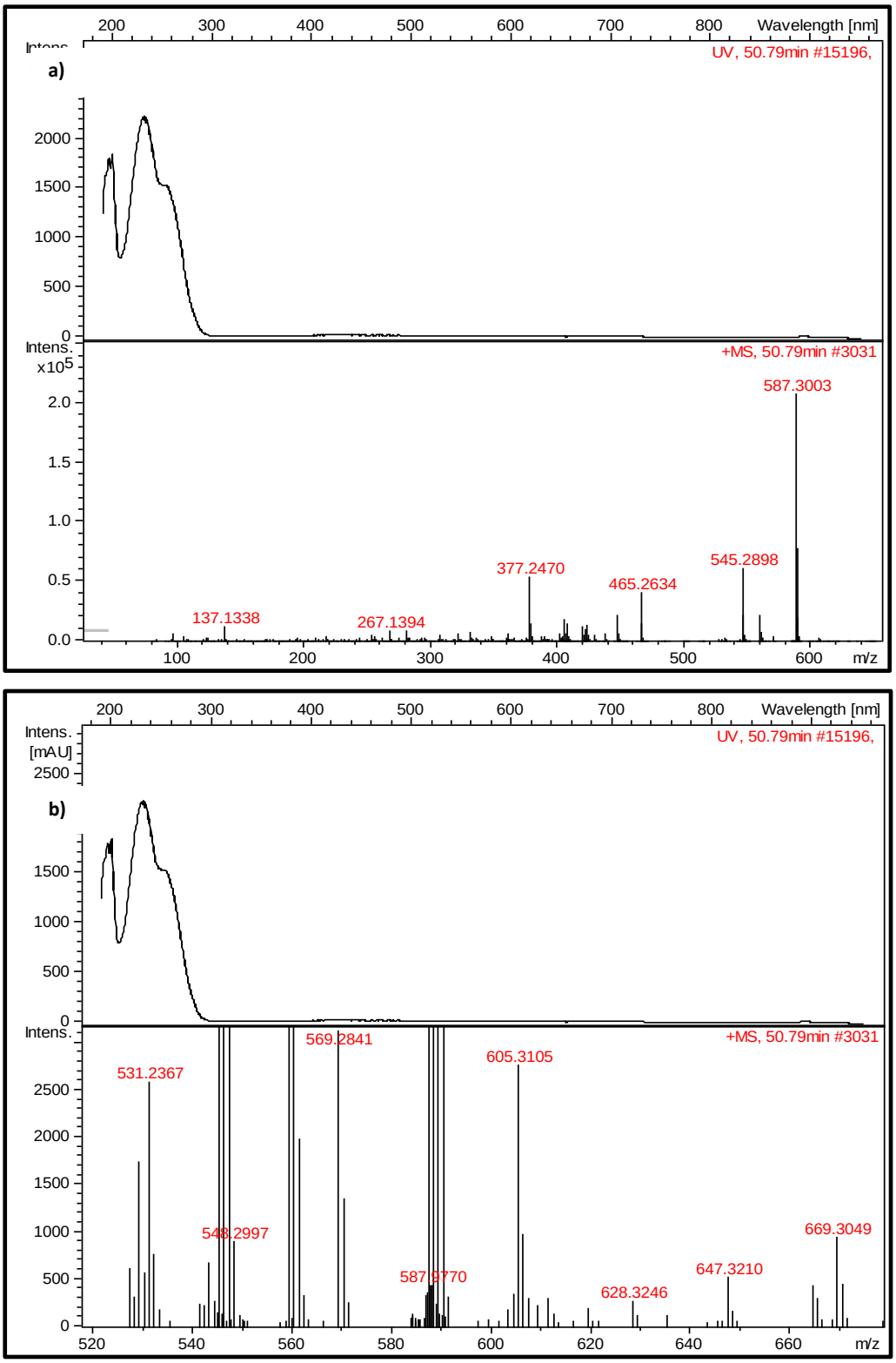

FIGURE 4.14 - HRESIMS spectrum of Picraviane A (**23**) indicating **a)** $[M+H-CH_3CO_2H]^+$ = 587.3003 and **b)** $[M+H]^+$ = 647.3210.

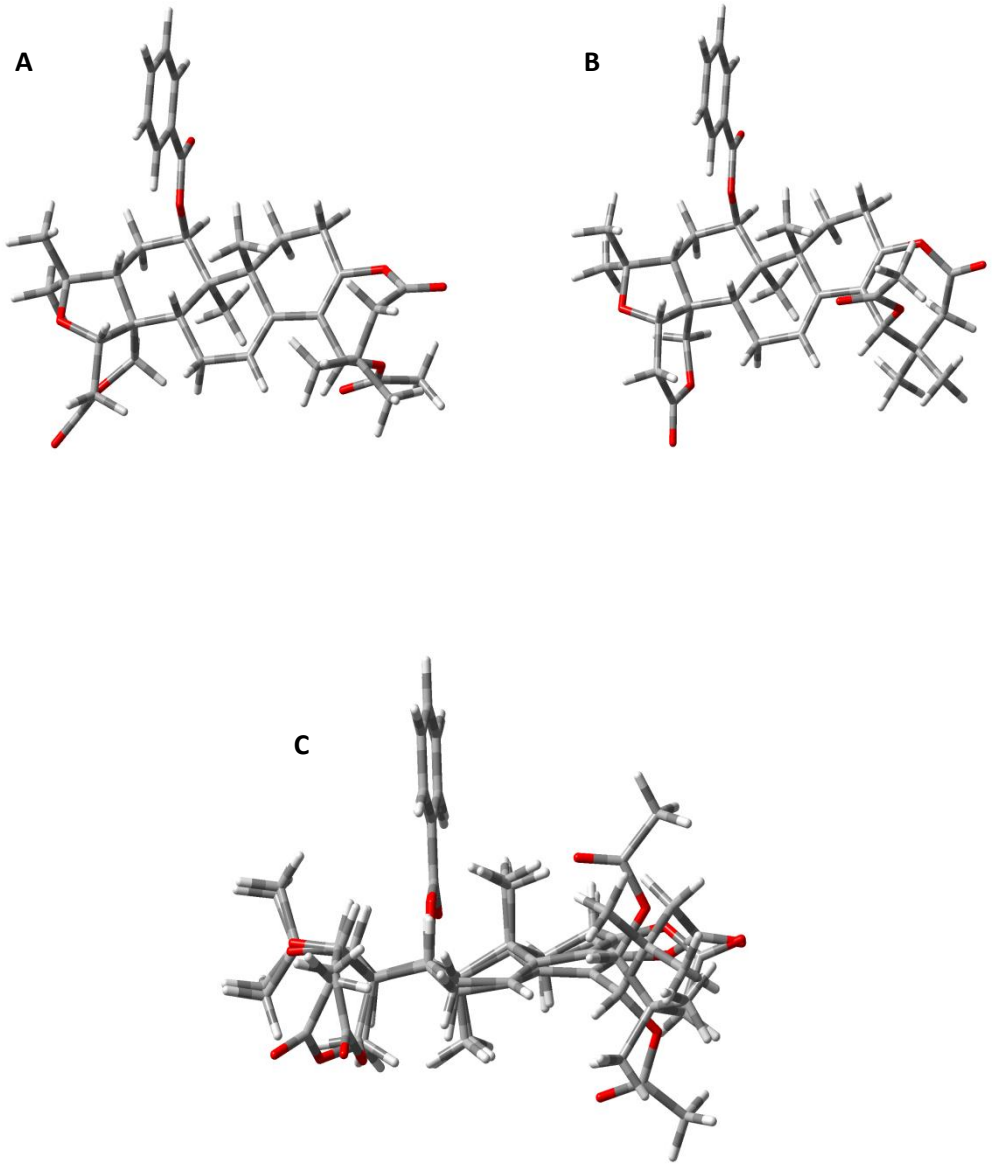

FIGURE 4.15 - Structures of the lowest-energy conformers identified for (1*S*,5*R*,7*R*,8*R*,9*S*,10*R*,14*R*,19*S*) (**A**), (1*S*,5*R*,7*R*,8*R*,9*S*,10*R*,14*R*,19*R*) (**B**) at the wB97XD/PCM($CHCl_3$)/6-311G** level and their overlay (**C**).

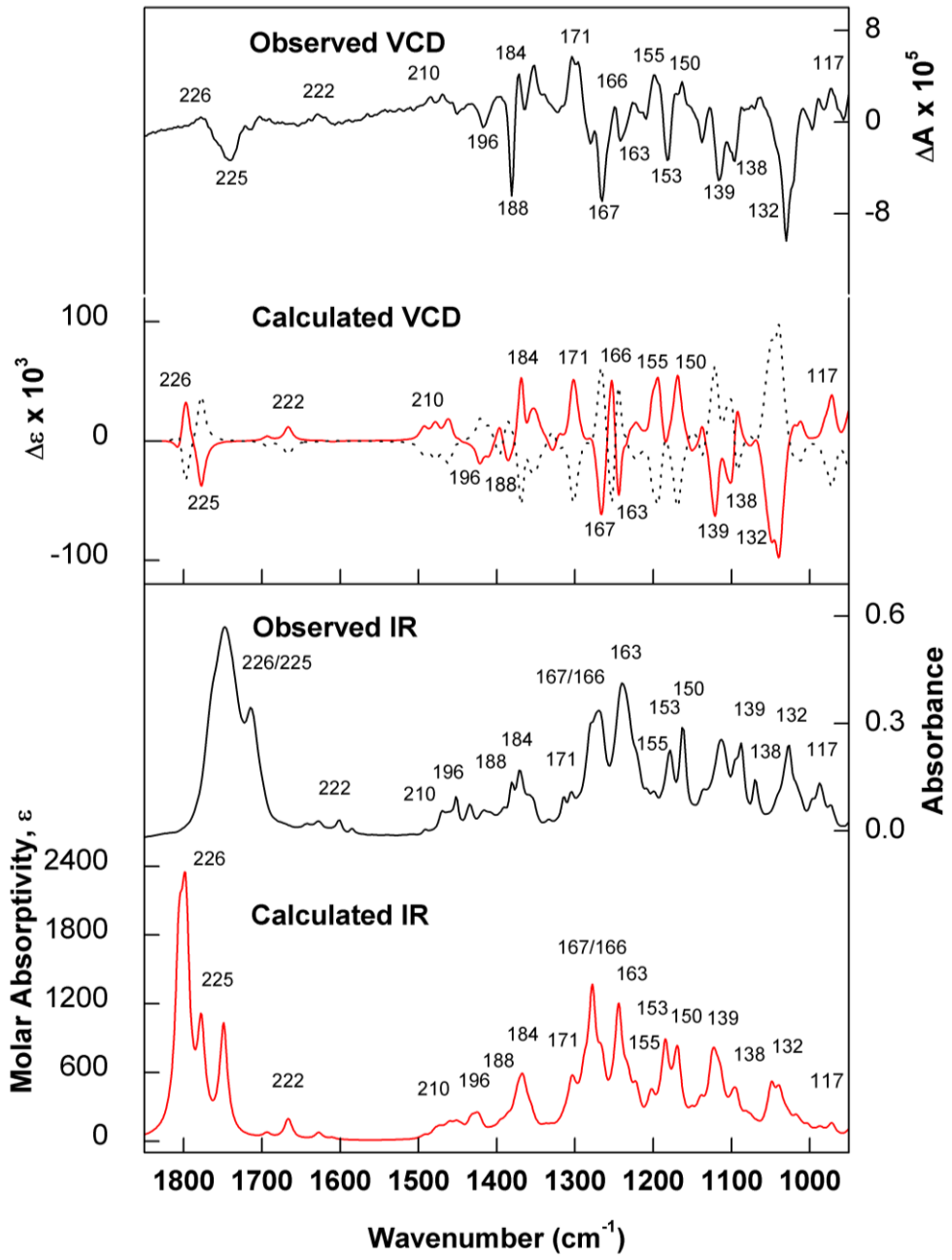

FIGURE 4.16 - Comparison of the observed IR and VCD spectra of Picraviane A (**23**) with the calculated [wB97XD/PCM($CHCl_3$)/6-311G**] IR and VCD spectra of the corresponding enantiomers (1*S*,5*R*,7*R*,8*R*,9*S*,10*R*,14*R*,19*S*) (solid) and (1*R*,5*S*,7*S*,8*S*,9*R*,10*S*,14*S*,19*R*) (dotted). Numbers represent selected vibrational modes.

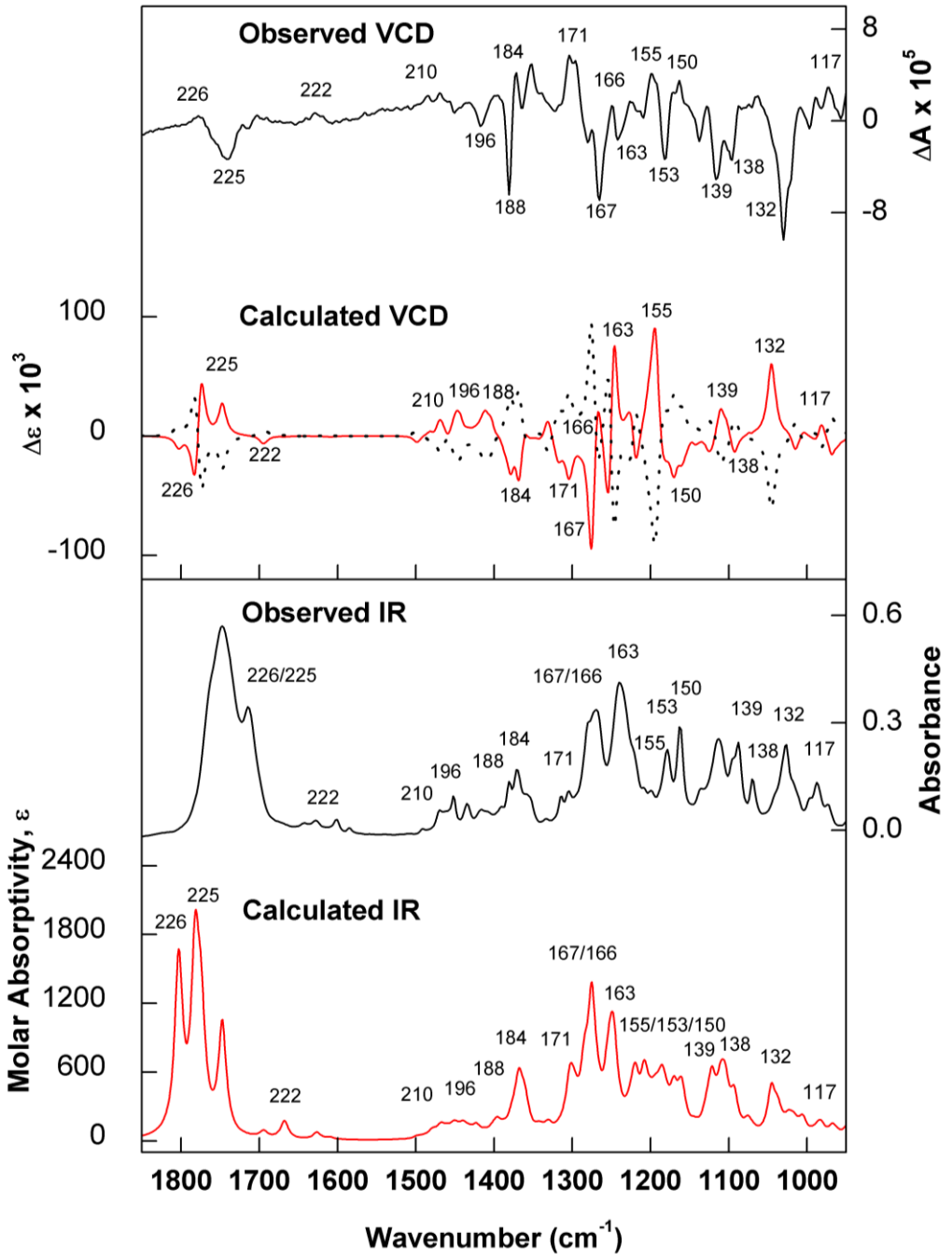

FIGURE 4.17 - Comparison of the observed IR and VCD spectra of Picraviane A (**23**) with the calculated **[**wB97XD/PCM($CHCl_3$)/6-311G**] IR and VCD spectra of the corresponding enantiomers (1*S*,5*R*,7*R*,8*R*,9*S*,10*R*,14*R*,19*R*) (solid) and (1*R*,5*S*,7*S*,8*S*,9*R*,10*S*,14*S*,19*S*) (dotted). Numbers represent selected vibrational modes.

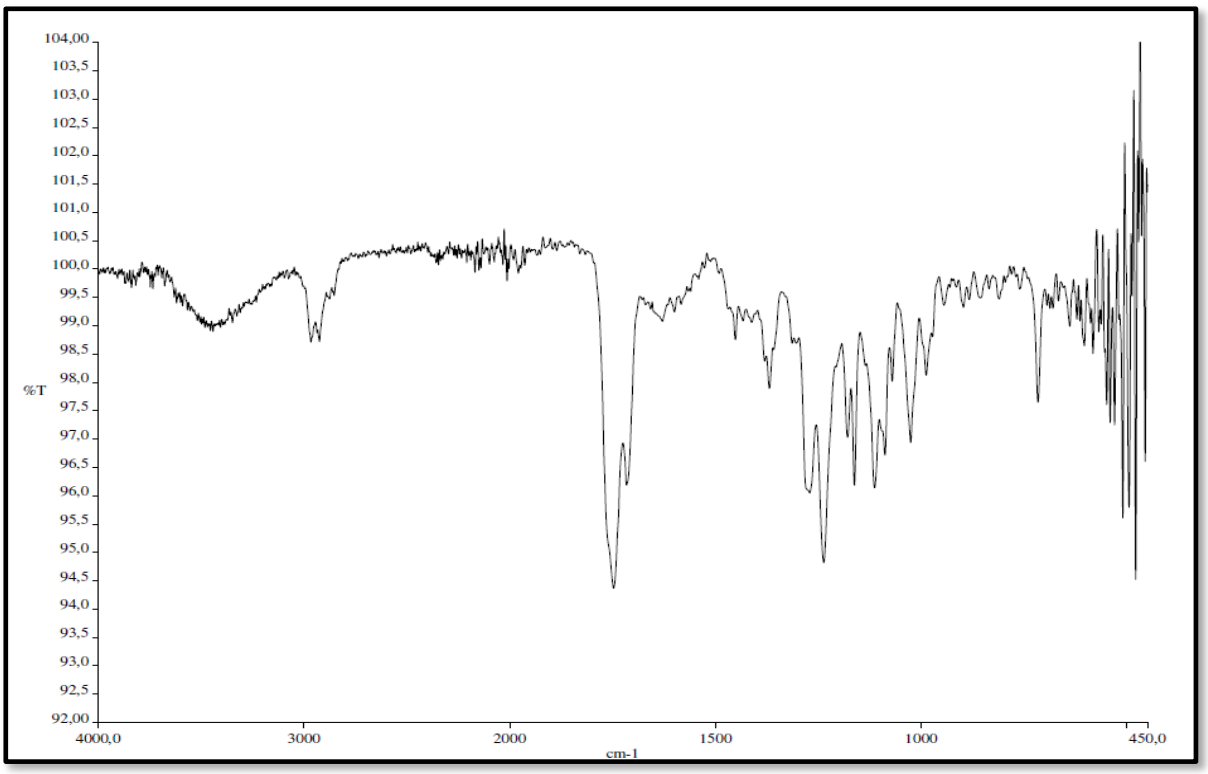

FIGURE 4.18 - Infrared spectrum of Picraviane A (**23**).

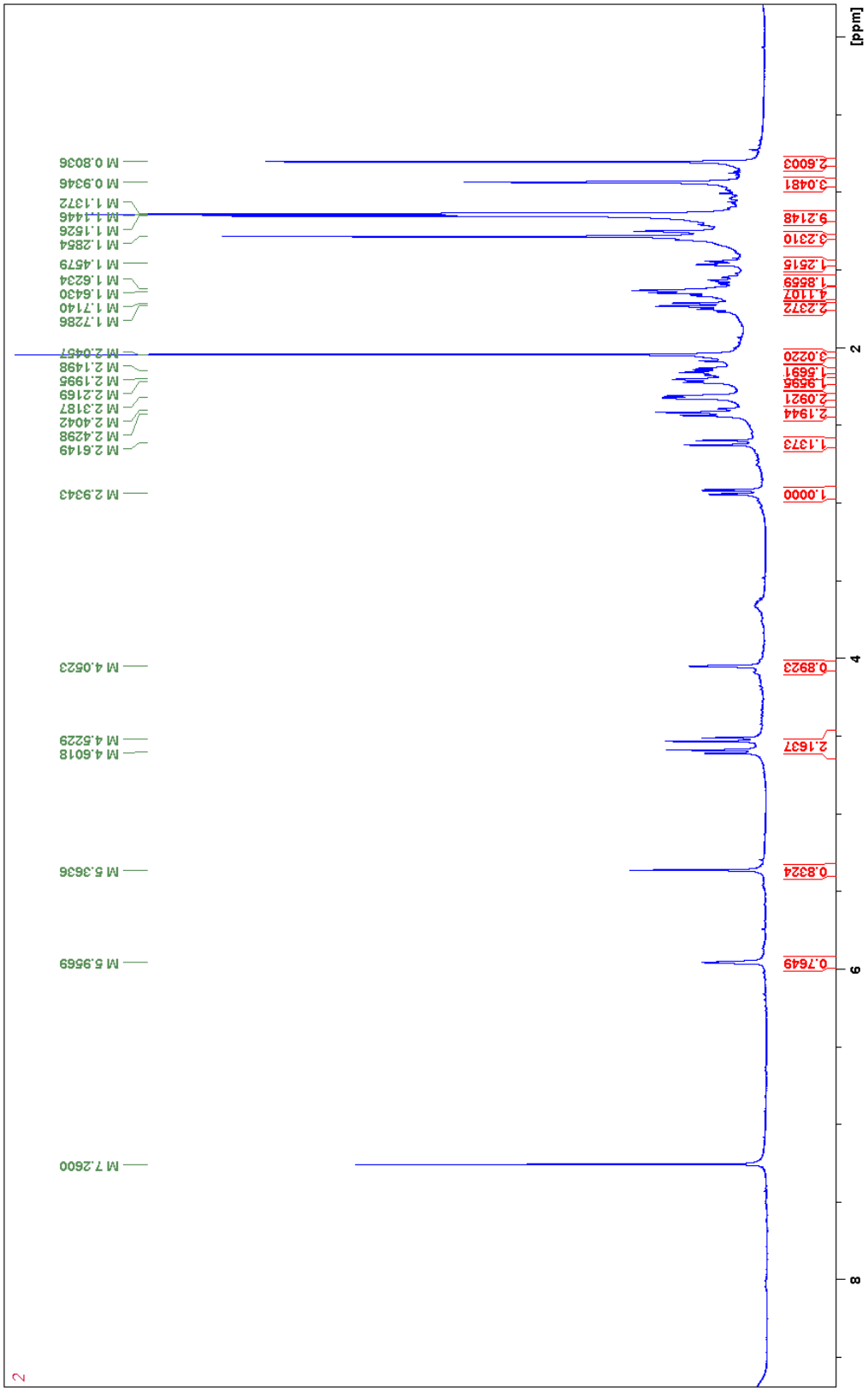

FIGURE 4.19 - ^{1}H NMR spectrum of Picraviane B (**20**) in $CDCl_3$ (600 MHz).

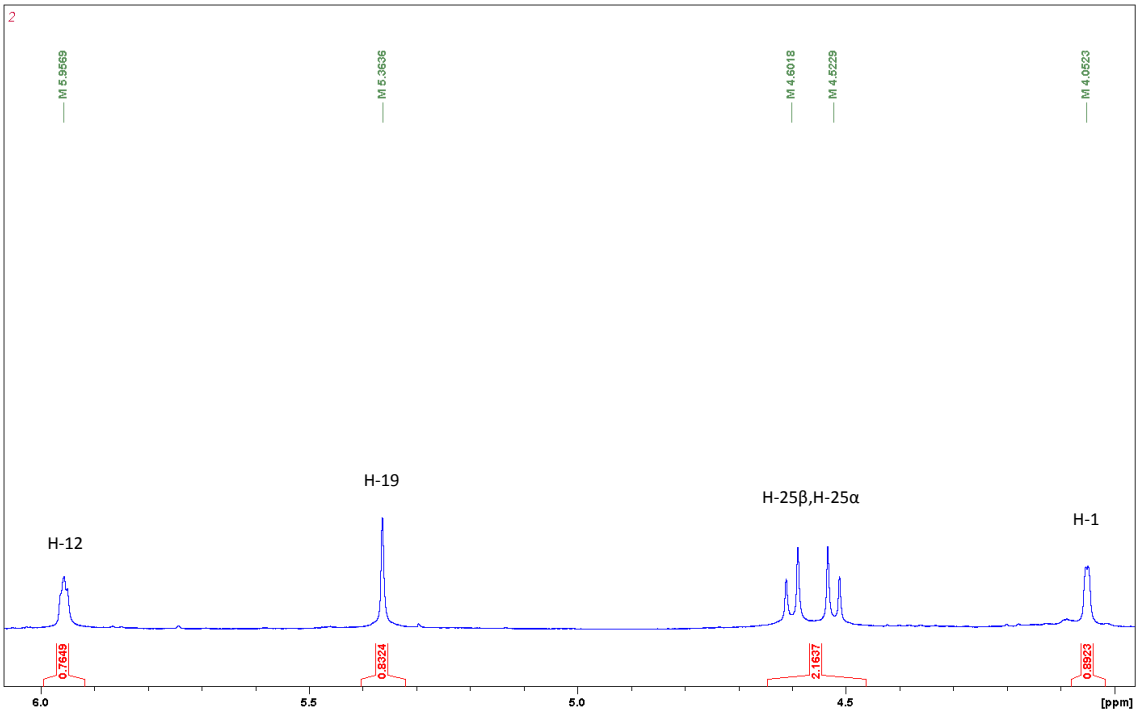

FIGURE 4.20 - Expansion of the ^{1}H NMR spectrum of Picraviane B (**20**) in $CDCl_3$ (600 MHz).

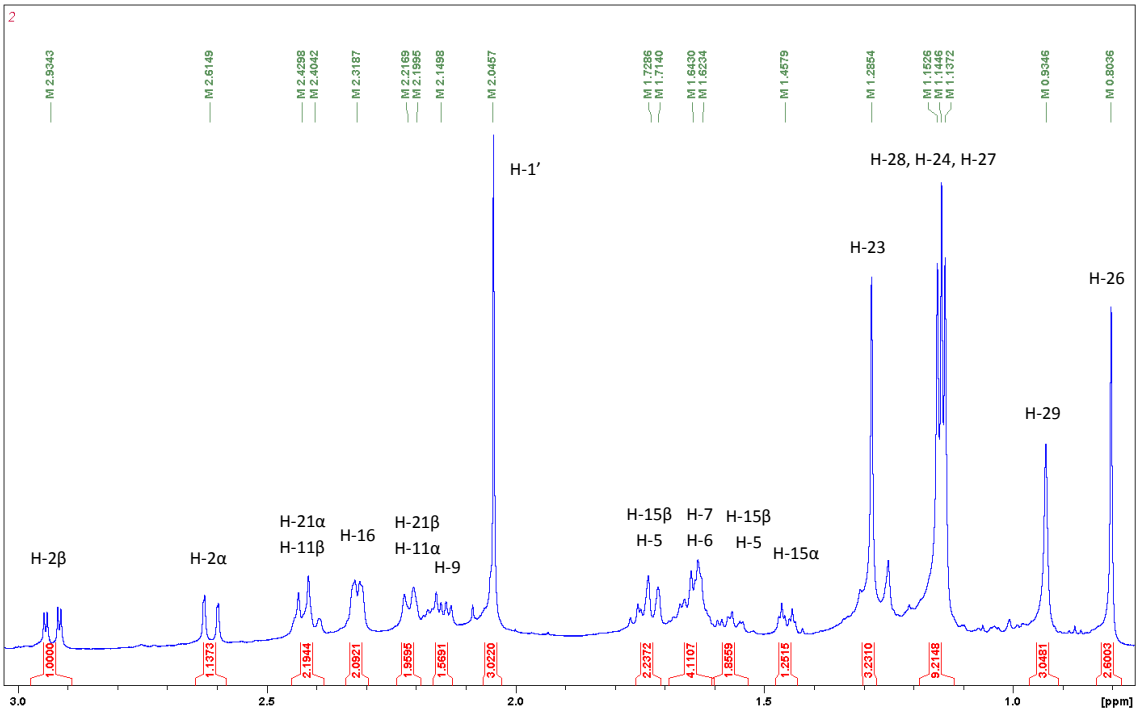

FIGURE 4.21- Expansion of the ^{1}H NMR spectrum of Picraviane B (**20**) in $CDCl_3$ (600 MHz).

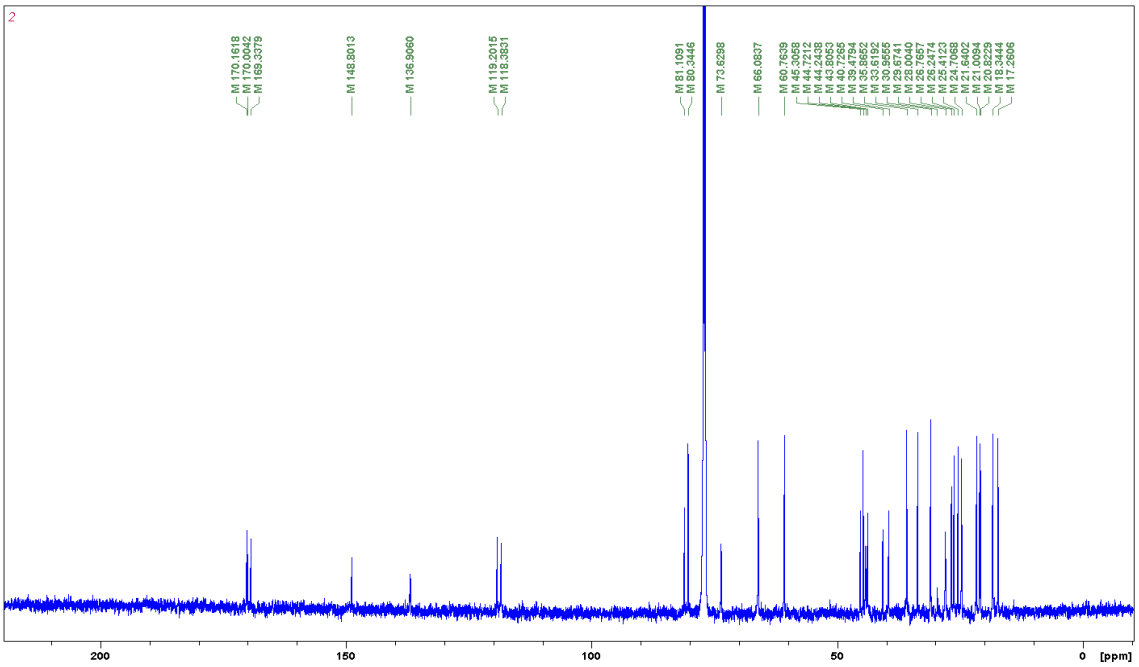

FIGURE 4.22 - ^{13}C NMR spectrum of Picraviane B (**20**) in $CDCl_3$ (150 MHz).

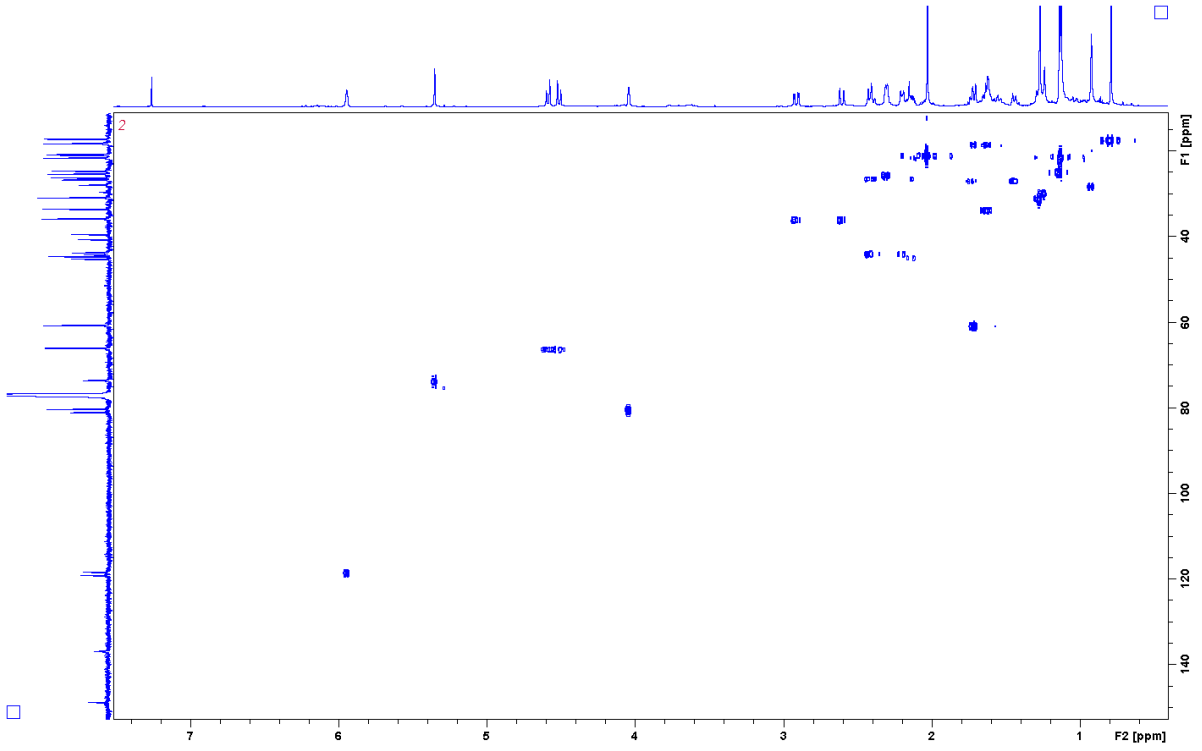

FIGURE 4.23 - HSQC spectrum of Picraviane B (**20**) in $CDCl_3$ (600 MHz).

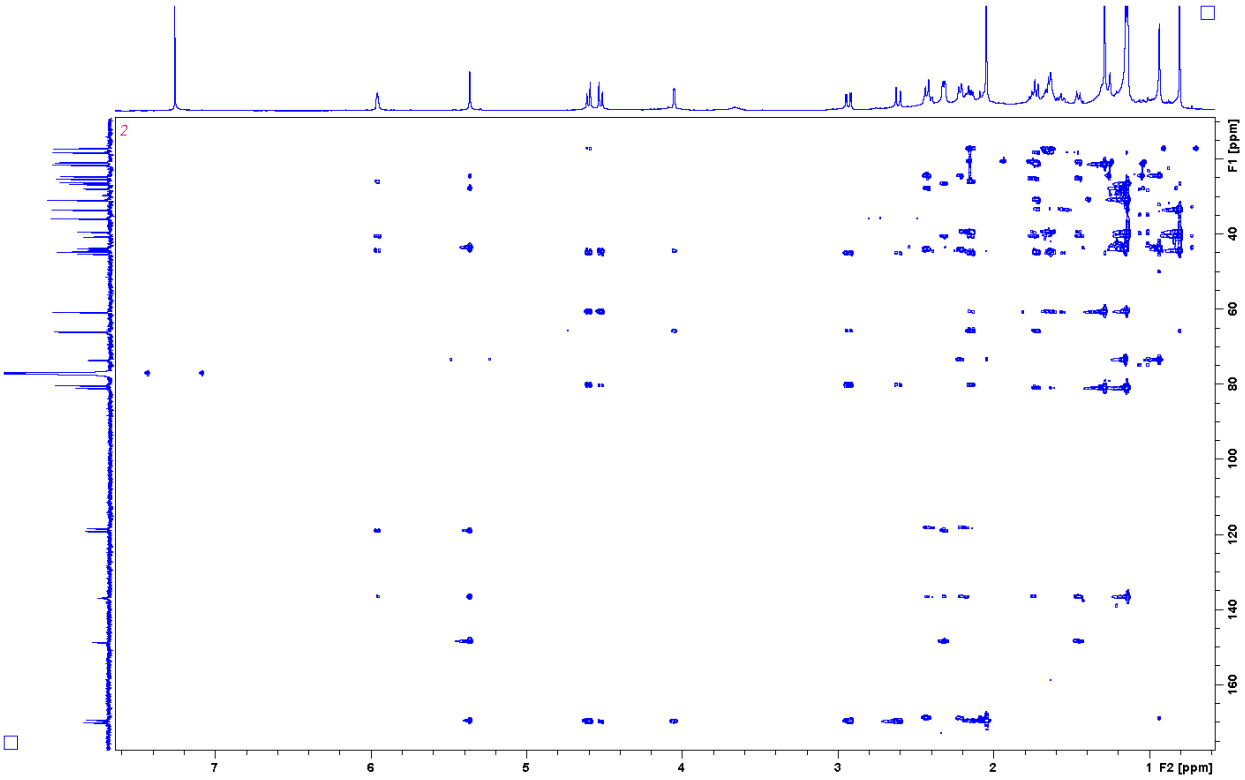

FIGURE 4.24 - HMBC spectrum of Picraviane B (**20**) in $CDCl_3$ (600 MHz).

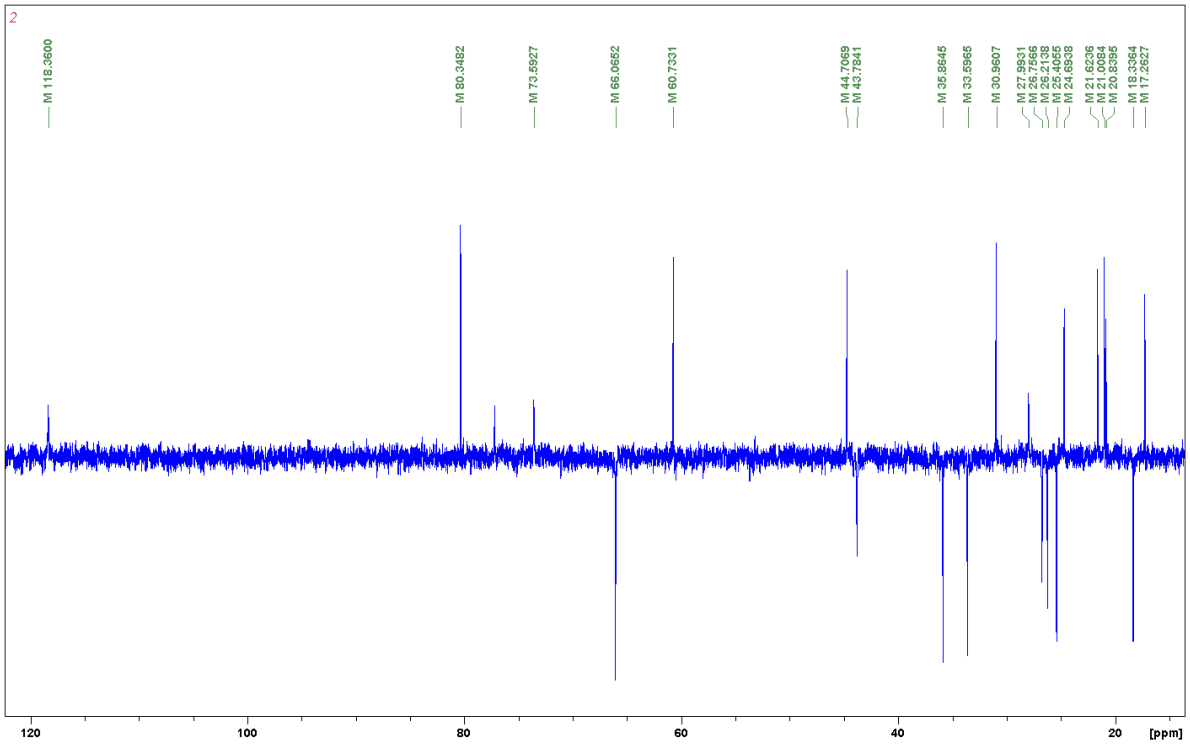

FIGURE 4.25 - DEPT135 spectrum of Picraviane B (**20**) in $CDCl_3$ (100 MHz).

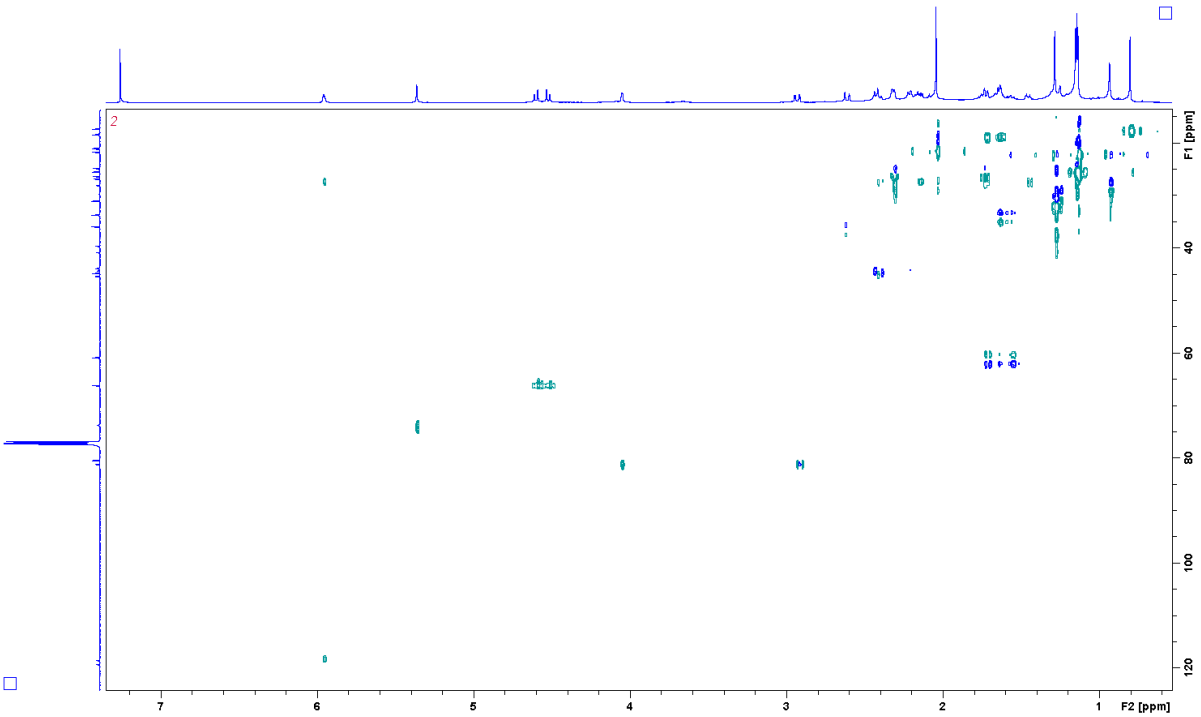

FIGURE 4.26 - H2BC spectrum of Picraviane B (**20**) in $CDCl_3$ (600 MHz).

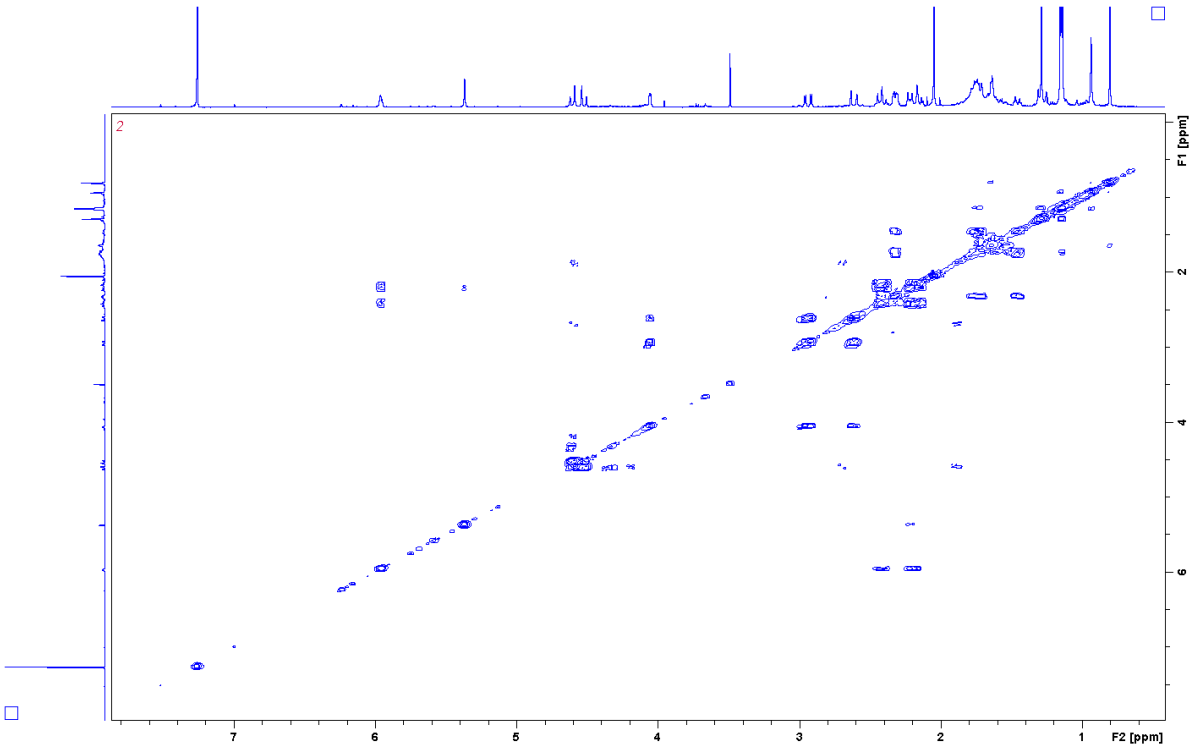

FIGURE 4.27 - ^{1}H-^{1}H COSY spectrum of Picraviane B (**20**) in $CDCl_3$ (400 MHz).

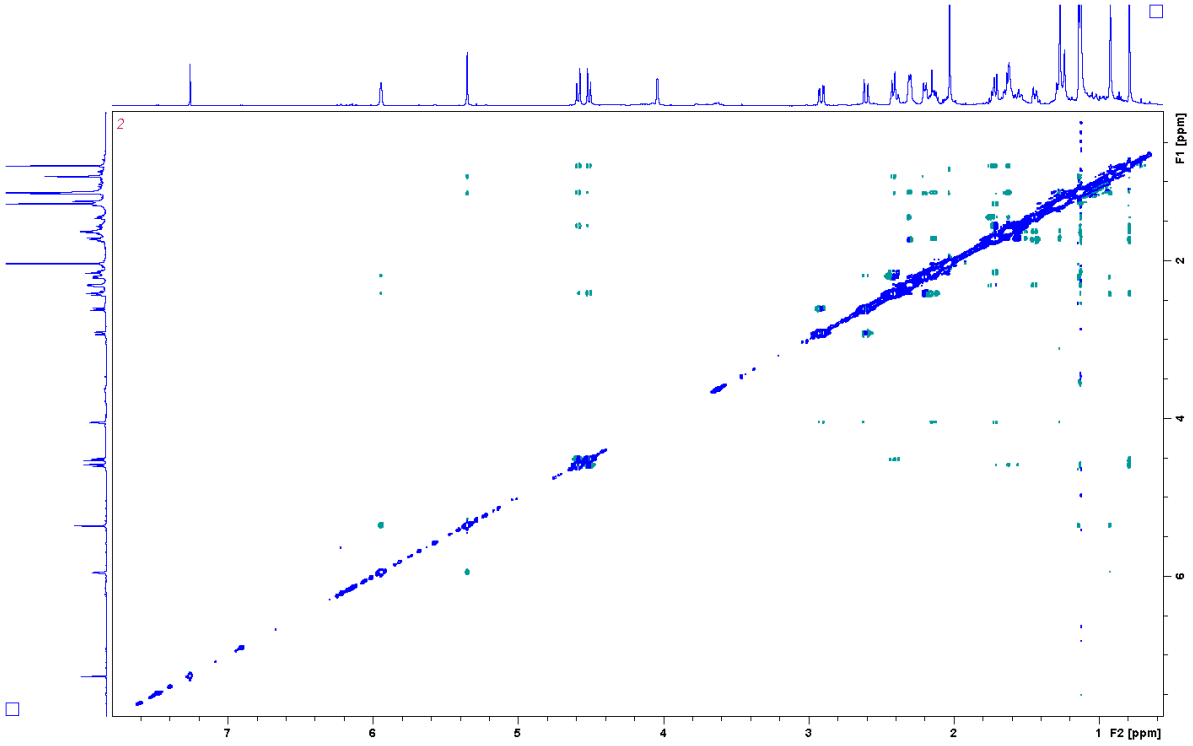

FIGURE 4.28 - NOESY spectrum of Picraviane B (**20**) in $CDCl_3$ (600 MHz).

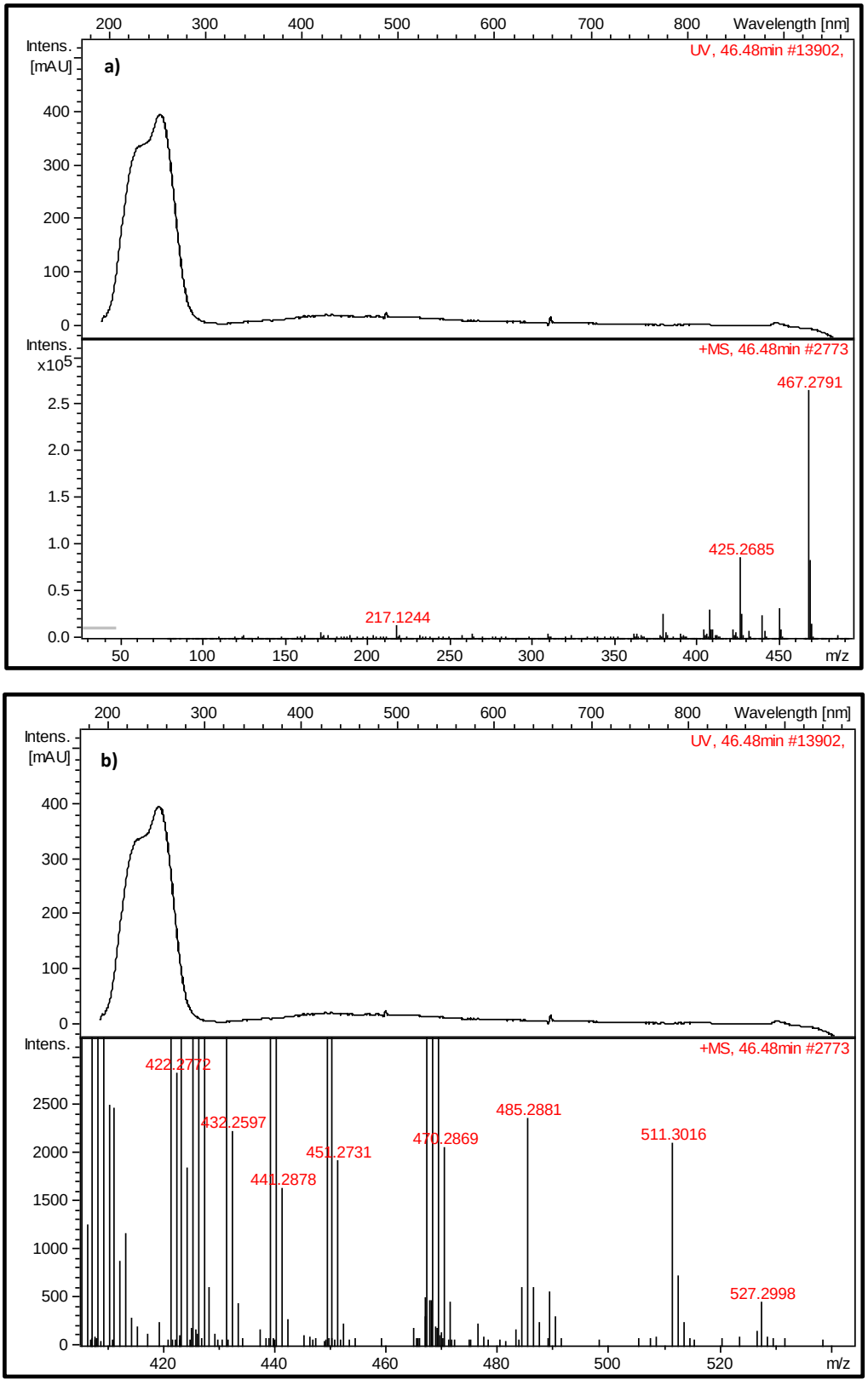

FIGURE 4.29 - HRESIMS spectrum of Picraviane B (**20**) indicating **a)** $[M+H-CH_3CO_2H]^+$ = 467.2791 and **b)** $[M+H]^+$ = 527.2998.

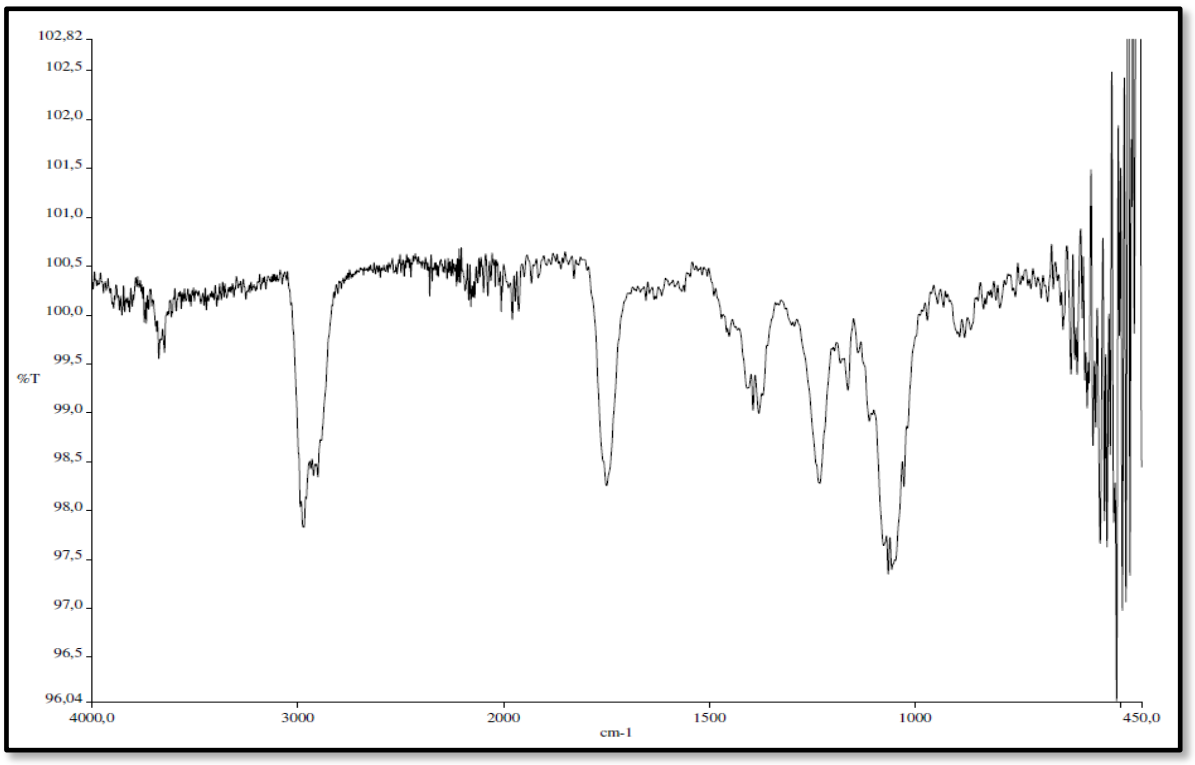

FIGURE 4.30 - Infrared spectrum of Picraviane A (**20**).

4.1.1.2 – Nortriterpene Picraviane C (06)

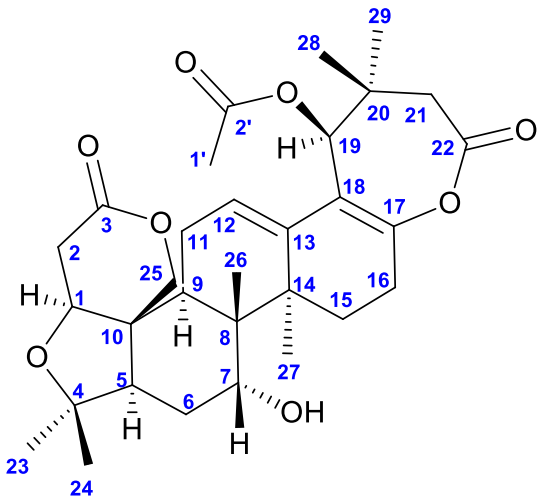

(06)

The nortriterpene Picraviane C (**06**) was elucidated on the basis of spectroscopic data from 1D ^{1}H NMR, ^{13}C NMR (FIGURES 4.31 to 4.33) as well as 2D NMR experiments (COSY, HSQC, HMBC and NOESY, see Supporting Information pages 242 and 243). Compound **06** had a molecular formula of $C_{31}H_{42}O_8$ as determined by HRESIMS ($[M+H]^+$ = 543.2917, calcd. 543.2957) indicating an index of hydrogen deficiency of 11 (FIGURES 4.34 and 4.35). The optical rotation measured disclosed: $[\alpha]_{D}^{26}$: + 43.54 (c. 0.092, MeOH).

The ^{13}C and NMR spectrum disclosed signals characteristics to the A and A' skeleton of the nortriterpene, as observed to compounds **20** and **23**, due the presence of the deshielded carbons at C-1 (δ 80.4) and C-4 (δ 80.7), the methylene at C-2 (δ 35.5) and the carbonyl at C-3 (δ 169.9). The presence of two diastereotopic protons at δ 2.93 and δ 2.59 coupling each other with 16.8 Hz (H-2α and H-2 β) and with a smaller coupling constant with the oxymethine proton H-1 at δ 4.10, observed in the ^{1}H NMR spectrum, also confirmed the A, A' limonin type backbone.

Moreover, the remaining signals observed in the ^{13}C NMR spectrum were very similar to those observed for **23** and **20**. However, the absence of aromatic signals in ^{1}H and ^{13}C NMR spectra and the appearance of a deshielded oxymethine proton observed in C-7 at δ 4.00 (integrating to 1) suggested the presence of a hydroxyl group. This indicated that **06** has the same structure as **23**, but instead of the presence of a benzoate group, there is a hydroxyl substituent placed at the same

position, which is also in agreement with the molecular mass (addition of 16 Da to compound **20**). The data spectra obtained from COSY confirmed the presence and position of the hydroxyl substituent at C-7 and the structure as a whole. Three spin systems corresponding to C-5 (*δ* 2.52), C-6 (*δ* 2.00; *δ* 1.48) and C-7 (*δ* 4.00) were observed in the spectrum, besides those corresponding to the C and D backbones: correlations among C-9 (*δ* 2.67), C-11 (*δ* 2.47; *δ* 2.37) and C-12 (*δ* 5.70) and correlations between C-15 (*δ* 1.87; *δ* 1.77) and C-16 (*δ* 2.45; *δ* 2.32). Likewise, ^{2}J and ^{3}J correlations were also observed in HMBC spectrum from H-5 at *δ* 2.52 to C-6 and C-7 (at *δ* 29.4 and *δ* 72.9, respectively), beyond those observed to the heptanolide E ring system and to the conjugated double bonds. The acetate unit at C-19, likewise to compounds **20** and **23**, showed correlations from H-19 (*δ* 5.29) to C-13 (δ 139.6), C-17 (δ 148.9) and C-18 (δ 118.4), to the quaternary C-20 (δ 44.0), to both methyl groups attached to C-20 (δ 24.7 and 28.2, corresponding C-28 and C-29, respectively), and to the carbonyl carbon at C-2' (δ 169.9). Furthermore, the methylene protons H-21 were identified as intervening C-20 and C-22 based on HMBC correlation to these two carbon atoms. The complete assignments of all ^{1}H and ^{13}C resonances are given in TABLE 4.3.

The UV spectrum to **06** was acquired from the HPLC-HRESIMS and showed absorbances at λ_{max} 230 and 255 nm, in agreement to compound **20** and to the conjugated double-bond system. Some mass fragments from the mass spectrum indicated the presence of both substituents due the losses observed at *m/*z [M+H-CH_3CO_2H]$^{+}$ = 483.2726 and [M+H-CH_3CO_2H-H_2O]$^{+}$ = 465.22617.

NOESY spectrum was used to the stereospecific assignment of the hydrogens, and the NOEs between H-1, H-5 and H-9 and between H-27 and H-9, confirmed these hydrogens to be on the same side of the molecule, assigned to α. Likewise, NOEs between H-26 and H-7 assigns to β. Then, the absolute configuration of compound **06** was assigned (1*S*,5*R*,8*R*,9*S*,10*R*,14*R*,19*S*), assuming the same biosynthetic pathways as **23** and **20**.

TABLE 4.3 - ^{13}C and ^{1}H NMR Data for Compound Picraviane C (**06**) acquired in $CDCl_3$

		06
C	δ_C	δ_H (*J* in Hz)
1	80.4	4.10 d (3.7)
2	35.5	α: 2.93 dd (16.8, 3.7)
		β: 2.59 dd (16.8, 1.4)
3	169.9	
4	80.7	
5	51.8	2.52 dd (13.8, 2.0)
6	29.4	α: 2.00 td (14.4, 2.0)
		β: 1.48 dt (14.4, 3.2)
7	72.9	4.00 br s
8	43.4	
9	41.1	2.67 t (10.1)
10	45.5	
11	25.9	β: 2.47 ddd (19.1, 10.1, 4.3)
		α: 2.37 ddd (19.1, 7.8, 4.3)
12	116.9	5.70 br t (4.3)
13	139.6	
14	41.4	
15	25.3	β: 1.87 td (12.9, 5.8)
		α: 1.77 dd (12.9, 5.4)
16	25.0	β: 2.45 m
		α: 2.32 dd (18.4, 5.4)
17	148.9	
18	118.4	
19	73.4	5.29 s
20	44.0	
21	43.9	β: 2.41 d (12.0)
		α: 2.21 d (12.0)
22	169.4	
23	30.5	1.31 s
24	21.9	1.15 s
25	66.0	β: 4.57 d (13.3)
		α: 4.53 d (13.3)
26	17.8	0.71 s
27	24.6	1.35 s
28	24.7	1.17 s
29	28.2	0.96 s
1´	20.8	2.03 s
2’	169.9	

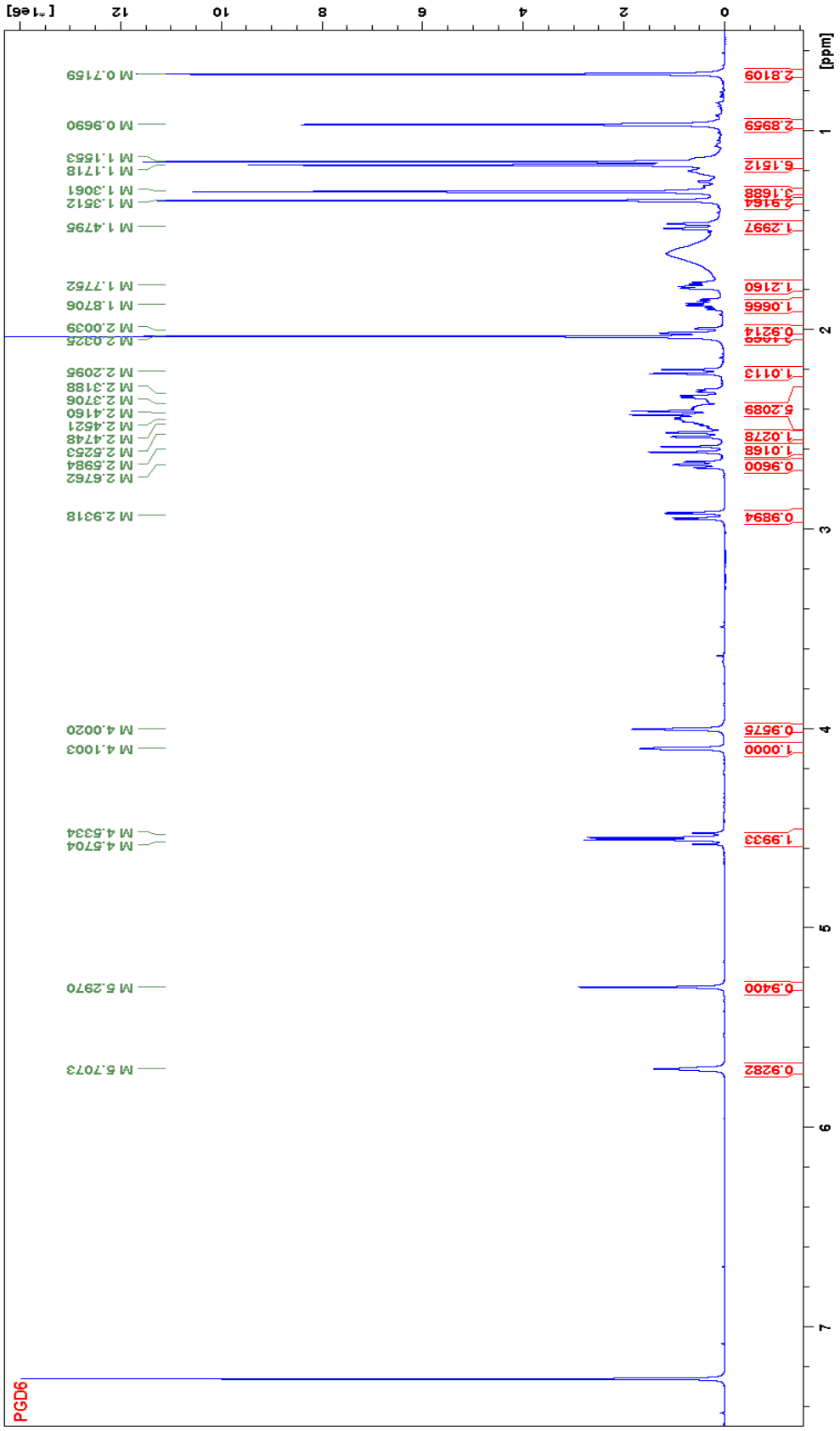

FIGURE 4.31 - ^{1}H NMR spectrum of Picraviane C (**06**) in $CDCl_3$ (600 MHz).

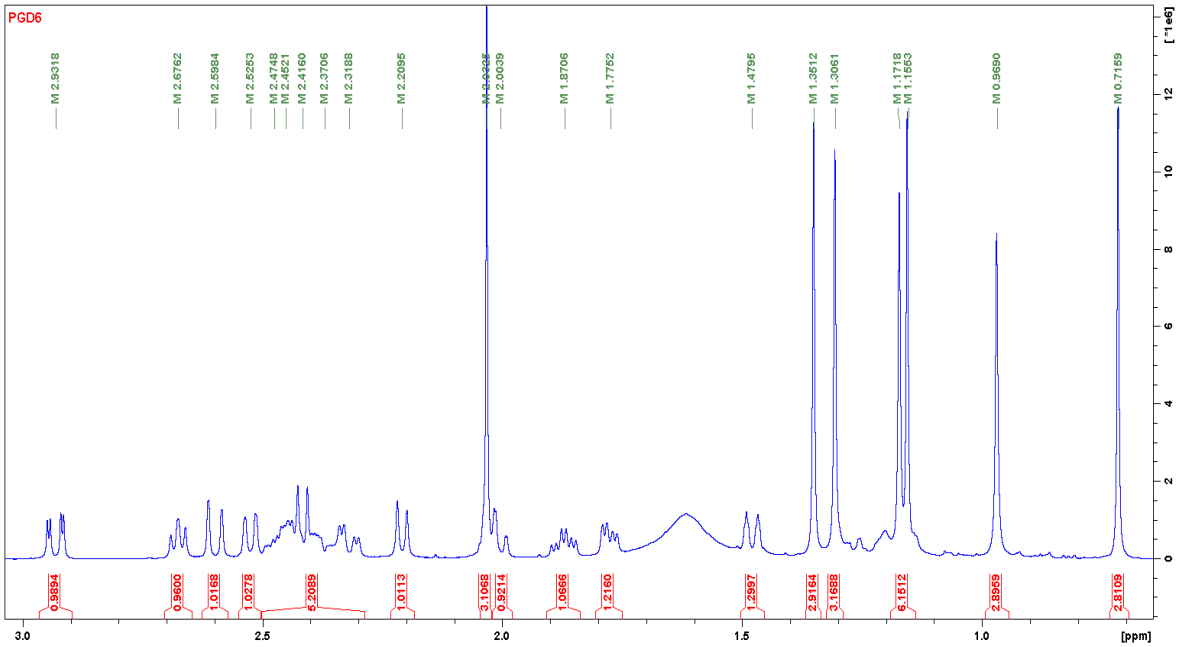

FIGURE 4.32 - Expansion of the ^{1}H NMR spectrum of Picraviane C (**06**) in $CDCl_3$ (600 MHz).

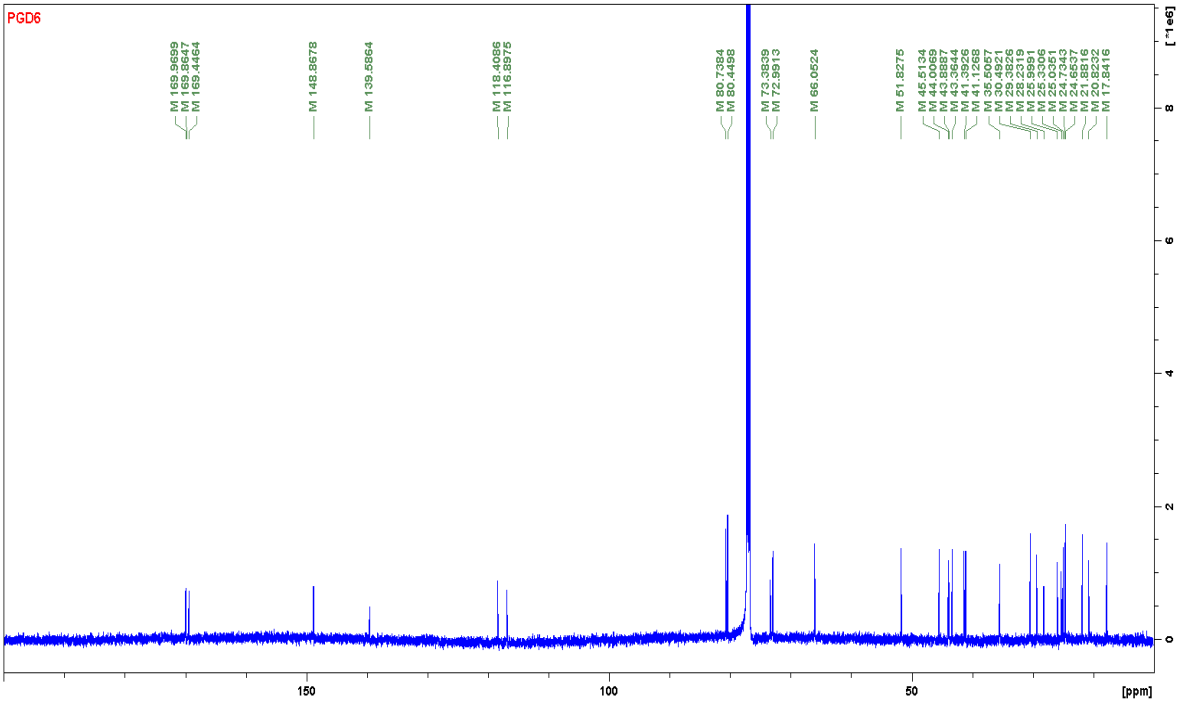

FIGURE 4.33 - ^{13}C NMR spectrum of Picraviane C (**06**) in $CDCl_3$ (150 MHz).

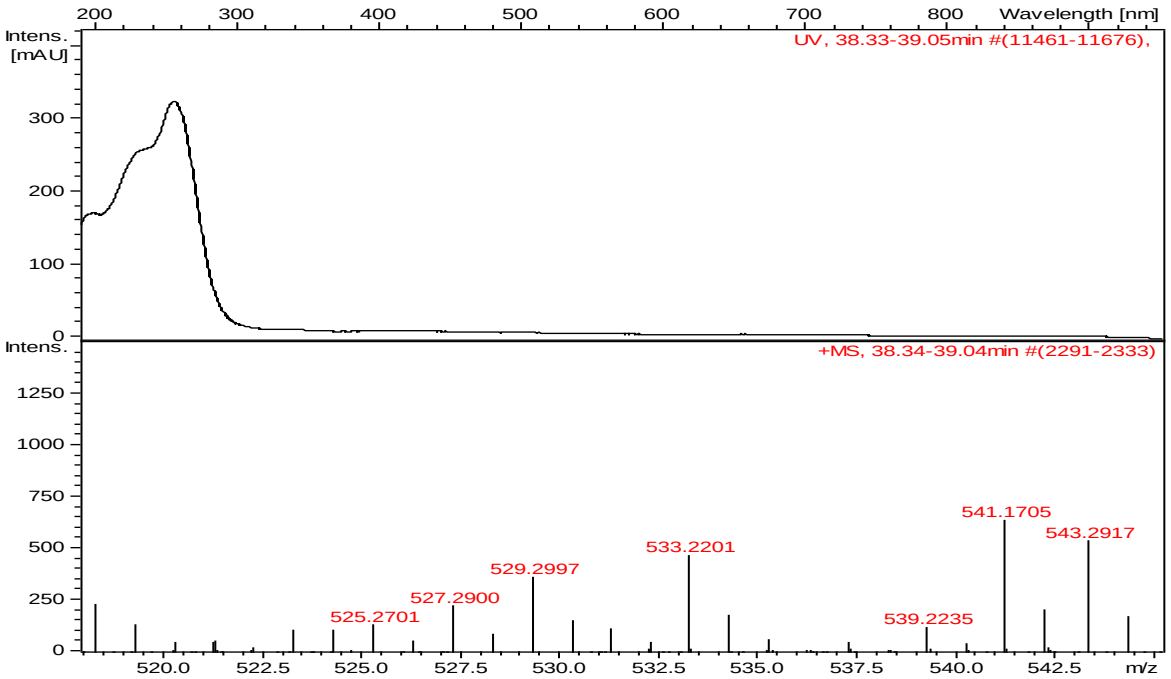

FIGURE 4.34 - HRESIMS spectrum of Picraviane C (**06**) indicating *m/z* $[M+H]^+$ = 543.2917.

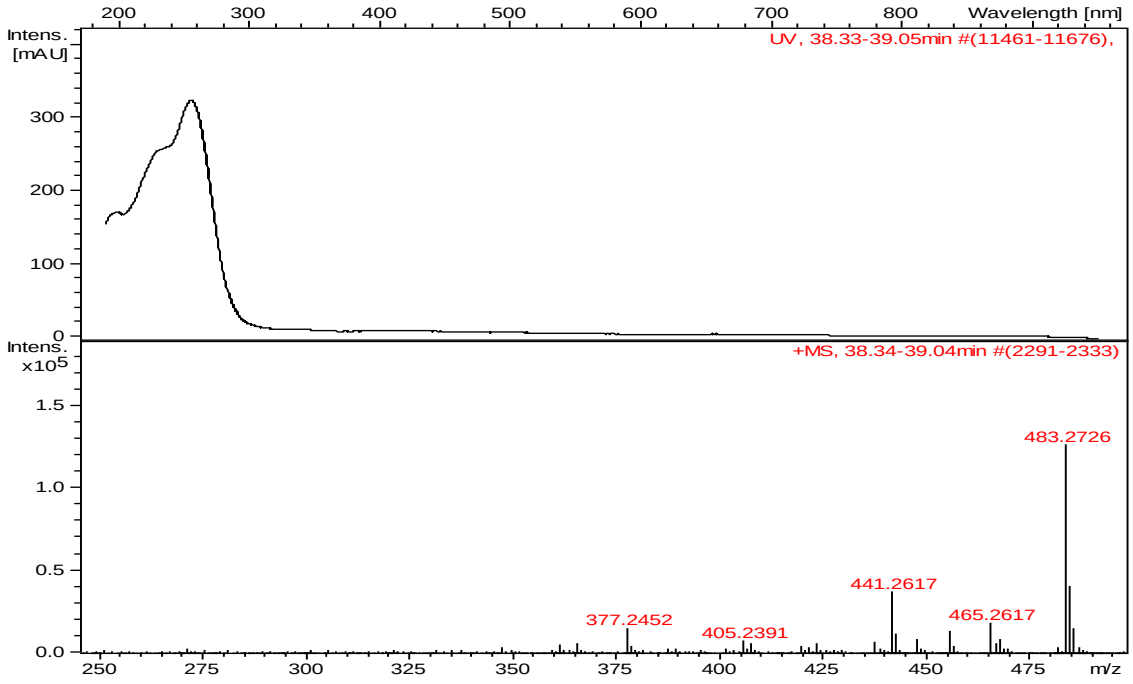

FIGURE 4.35- HRESIMS spectrum of Picraviane C (**06**) indicating *m/z* $[M+H-CH_3CO_2H]^+$ = 483.2726 and $[M+H-CH_3CO_2H-H_2O]^+$ = 465.22617.

4.1.1.3 – Nortriterpenes Picraviane D (08) and E (09)

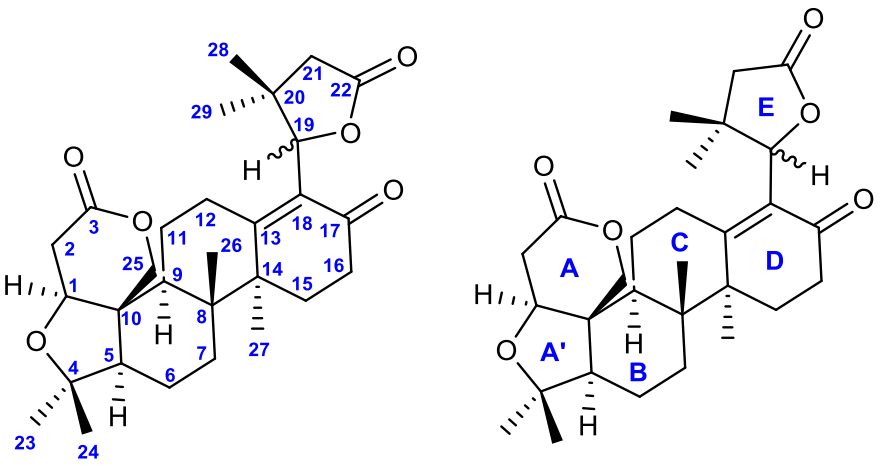

(8) (9)

Picravianes D and E (**08** and **09**) had both, the same molecular formula established to $C_{29}H_{40}O_6$ (10 degrees of unsaturation) indicating a pair of diastereoisomers, on the basis of HRESIMS at m/z $[M+H]^+$ = 485.2890 (calc. for 485.2898) and $[M+H]^+$ = 485.2886 (calc. for 485.2898, FIGURES 4.42 and 4.46) respectively, and were elucidated on the basis of spectroscopic data from 1D (^{1}H NMR, ^{13}C NMR, FIGURES 4.36 to 4.38 and 4.40 to 4.42) as well as 2D NMR experiments (COSY, HSQC, HMBC and NOESY, see Supporting Information pages 248 to 251). The optical rotation measured disclosed to compound **08**: $[\alpha]_{D:}^{25}$ - 41.66 (c. 0.048, MeOH) and to compound **09**: $[\alpha]_{D:}^{25}$ - 9.19 (c. 0.11, MeOH)

The UV spectrum to **08** and **09** were acquired from the HPLC-HRESIMS and showed absorbance at λ_{max} 250 nm to both compounds. The IR spectrum disclosed sp^3 C-H stretch vibrations at 2960 cm^{-1} in both compounds, C=O stretching frequency as a strong bond at 1757/ 1758 cm^{-1} resulted from the lactone functions and C=O stretch vibrations resulted of the conjugated ketone with a double bond at 1664/ 1677 cm^{-1} corresponding to compounds **08** and **09** respectively, besides vibrations in the range from 1100 to 1200 cm^{-1} observed in both compounds, due to C-O stretching vibrations (FIGURES 4.44 and 4.45).

The ^{13}C NMR spectrum resolved 29 carbon resonances corresponding to 6 methyl, 9 methylenes (one oxygenated), 4 methine (two oxygenated), and 10 quaternary (one oxygenated, two olefinic, and three carbonyl) carbons as

distinguished by HSQC spectrum. These information in association with the ^{1}H NMR and HMBC spectrum to both compounds were very similar to those found in Picraviane A (**23**) and B (**20**) as described above. The same biogenetic skeleton (A, A´and B rings) of the structure was established analyzing the ^{1}H NMR spectrum (coupling constants and multiplicity of the signals) as well as by HMBC correlations: from both methyl groups at H-23 and H-24 correlating each other, and with the quaternary oxygenated carbon at C-4; the diasterotopics hydrogens at H-2 (double doublets) coupling with C-1, C-3 and C-10; and from the two doublets at H-25 (coupling each other with a large constant at J= 12.9 Hz) to the oxymethine broad singlet (H-1). However, the absence of aromatic signals, as well as to the deshielded oxymethine proton discarded the presence of the monosubstituted ring or a hydroxyl group placed at C-7. The last moiety corresponding to the D and E rings were elucidated observing the shielded value found to the carbonyl carbon at δ 196.7 and δ 198.1 to the respective compounds **08** and **09,** which were very informative to establish the presence of a ketone function conjugated with a double bond in the D ring. The ^{1}H NMR and HSQC spectra disclosed one oxymethine proton (H-19), as a singlet at *δ* 5.12 (*δ* 86.1) and *δ* 5.21 (*δ* 85.6) to compounds **08** and **09**, respectively. The key correlations observed to this deshielded proton in HMBC spectrum were decisive for its positioning at H-19 closed to the enone functional group, and the absence of signals from to the acetate unit suggested the E ring closure in a five-membered ring to both compounds. Specifically, HMBC spectrum displayed correlations from H-19 to C-13, C17, C-18, C-20, C-22 and C-28 to compound **08** and to C-13, C-17, C-20, C-22 and C-28 to compound **09**, indicating the linkage between the D and E rings. In addition, were also observed correlations from the tertiary methyl group at C-27 to the olefinic carbon at C-13, and from the methylenic protons at C-16 to the olefinic carbon at C-18 and to the ketone unit at C-17, corroborating to this positioning. The value of the chemical shift to the methylene carbon at C-16 (*δ* 34.2, compound **08**) and (*δ* 35.5, compound **09**), more deshielded in relation to the value found to compounds **06**, **20**, and **23** (at the range of 25 ppm) corroborated to the presence of the ketone at C-17. The deshielded carbon at C-22 are also in agreement with the existence of a pentanolide E ring.

The COSY spectrum also contributed confirming the isolated proton at H-19 as well as to the methylene protons H-21 (only correlating each other), supporting the previous establishment of the E ring . In addition, three set of spin

systems were also observed corresponding to the remaining protons: C-1 (*δ* 4.05) and C-2 (*δ* 2.93; *δ* 2.64); C-5 (*δ* 1.72), C-6 (*δ* 1.65; *δ* 1.52) and C-7 (*δ* 1.60); besides correlations to the methine and methylene protons from the C ring excluding the existence of another double bond as observed to the previously described compounds: C-9 (*δ* 2.20), C-11 (*δ* 1.89; *δ* 1.72) and C-12 (*δ* 2.81; *δ* 2.23). The complete assignments of the ^{1}H and ^{13}C are given in TABLE 4.4.

The relative configuration of **08** and **09** were established by the analyses of their NOESY spectrum. The key NOESY correlations from the hydrogen H-5 with H-1, H-9 and H-23 as well as from the hydrogen H-9 with H-1, H-5 and H-27 observed in both compounds corroborated to the presumed positioning of these hydrogens as α. Consequently, the methyl group at C-26 was positioned to adopt a β-orientation. These analyses were consistent with the well-established stereocenters found to compound **23** resulted of the same biosynthetic pathway in this plant. However, the flexibility and easy twist of the E ring in the structure, did not allow the distinction of the relative stereochemistry to H-19. A preliminary analysis in the ^{1}H and ^{13}C NMR data of **09** suggests the proximity of the proton H-19 close to the ketone group and consequently, the methyl group in C-29 close to the double bond in C-13, turning the protons at C-29 to compound **09** deshielded in relation to **08,** due the anisotropy of the double bond (See TABLE 4.4). However, for a reliable definition and establishment of the absolute configuration to the stereocenter in C-19, as well to confirm all chiral centers in the structure, these compounds should be evaluated in a future work by (electronic/vibrational) circular dichroism, in association with calculations of the most stable conformer or through the use of X-ray experiments by the crystallization the compounds, allowing to distinguish both diastereomeric pair.

TABLE 4.4- ^{13}C and ^{1}H NMR Data for Compounds **08** and **09** acquired in $CDCl_3$

	08		**09**	
C	δ_C	δ_H (*J* in Hz)	δ_C	δ_H (*J* in Hz)
1	80.1	4.05 br s	79.9	4.05 br s
2	36.1	α: 2.93 dd (16.9, 3.4) β: 2.64 dd (16.9, 1.4)	36.1	α: 2.93 dd (16.8, 3.4) β: 2.65 dd (16.8, 1.8)
3	169.9	-	169.9	-
4	80.8	-	80.8	-
5	60.7	1.72 d (12.4)	60.8	1.72 d (12.4)
6	18.0	α: 1.65 dd (12.1, 2.5) β: 1.52 m	17.9	α: 1.64 dq (14.1, 2.5) β: 1.50 m
7	34.1	1.60 m	33.7	1.56 m
8	42.5	-	42.2	-
9	47.4	2.20 dd (13.1, 3.6)	47.1	2.17 dd (13.0, 3.8)
10	45.9	-	45.9	-
11	23.6	α: 1.72 m β: 1.89 qd (13.1, 5.1)	23.9	α: 1.77 m β: 1.81 qd (13.0, 5.1)
12	26.7	β: 2.81 dd (16.4, 4.0) α: 2.23 m	26.3	β: 2.74 dd (15.2, 3.8) α: 2.35 m
13	166.2	-	162.1	-
14	45.6	-	45.9	-
15	27.6	β: 2.15 td (14.3, 6.5) α: 1.58 m	29.3	β: 2.12 td (14.8, 4.2) α: 1.61 m
16	34.2	2.41 m	35.5	α: 2.50 td (15.2, 5.2) β: 2.33 d (15.2)
17	196.7	-	198.1	-
18	131.4	-	131.7	-
19	86.1	5.12 s	85.6	5.21 s
20	38.9	-	39.1	-
21	44.1	β: 2.30 d (17.3) α: 2.75 d (17.3)	43.6	β: 2.30 d (17.7) α: 2.90 d (17.7)
22	177.3	-	177.1	-
23	30.9	1.28 s	30.9	1.28 s
24	21.9	1.13 s	21.9	1.13 s
25	66.1	β: 4.54 d (12.9) α: 4.38 d (12.9)	66.0	β: 4.52 d (12.9) α: 4.37 d (12.9)
26	18.2	0.88 s	17.9	0.82 s
27	20.1	1.39 s	19.6	1.41 s
28	30.5	1.26 s	30.7	1.25 s
29	23.7	0.86 s	24.8	0.98 s

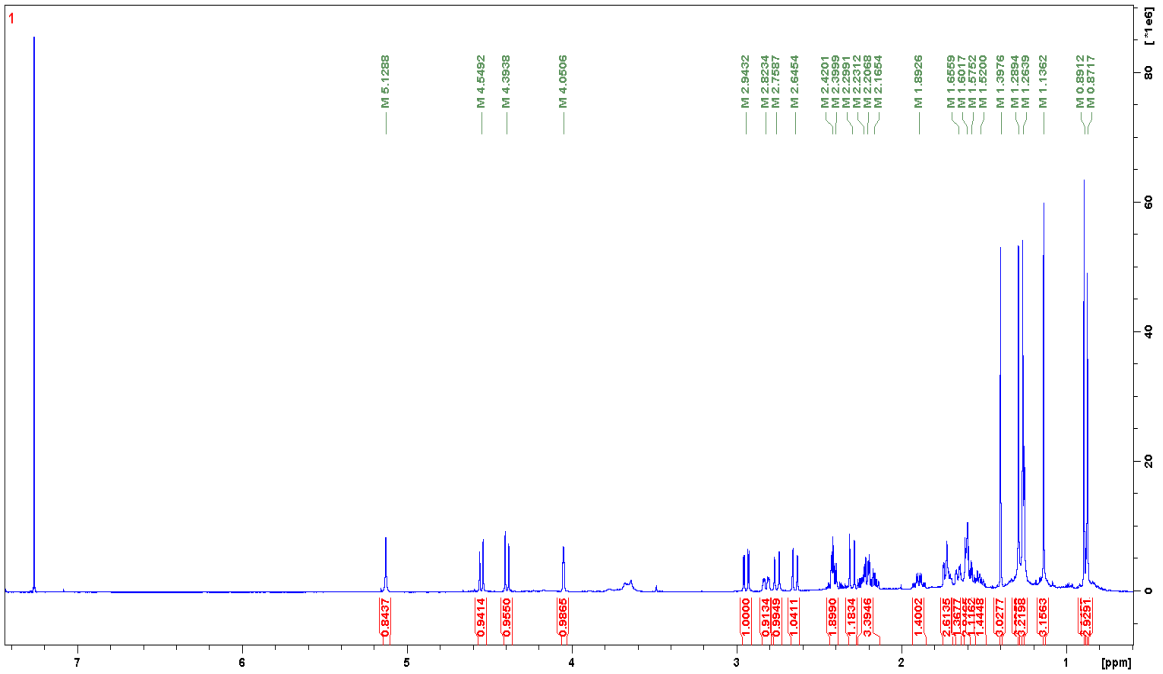

FIGURE 4.36 - ^{1}H NMR spectrum of Picraviane D (**08**) in $CDCl_3$ (600 MHz).

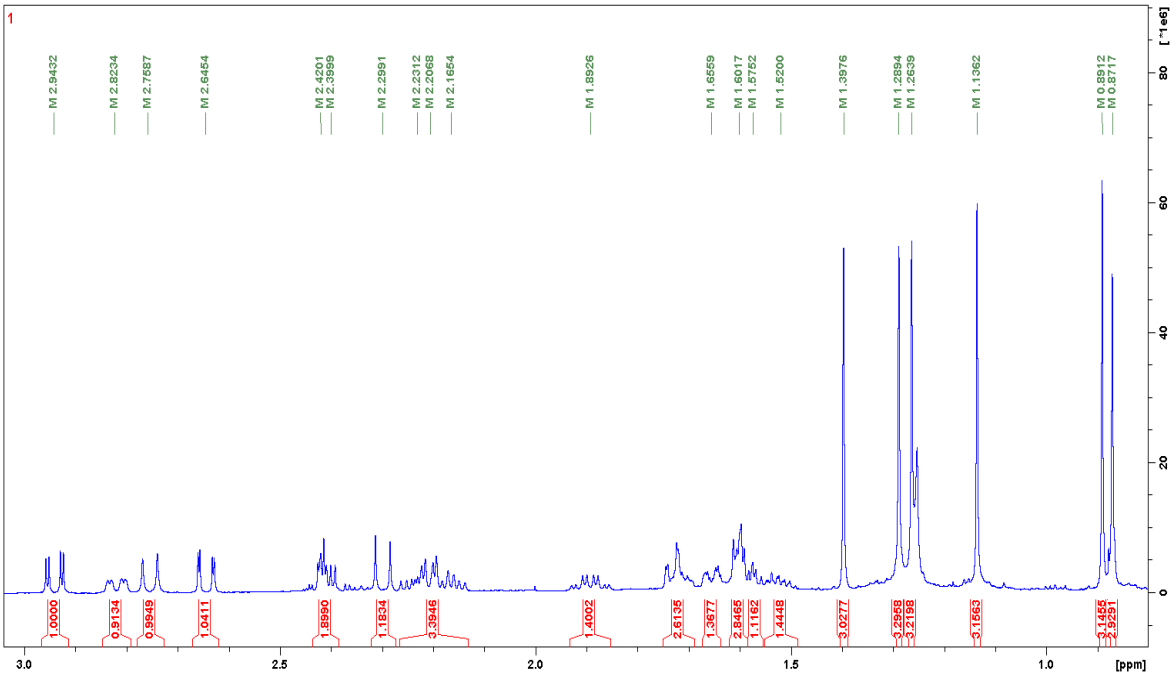

FIGURE 4.37- Expansion of the ^{1}H NMR spectrum of Picraviane D (**08**) in $CDCl_3$ (600 MHz).

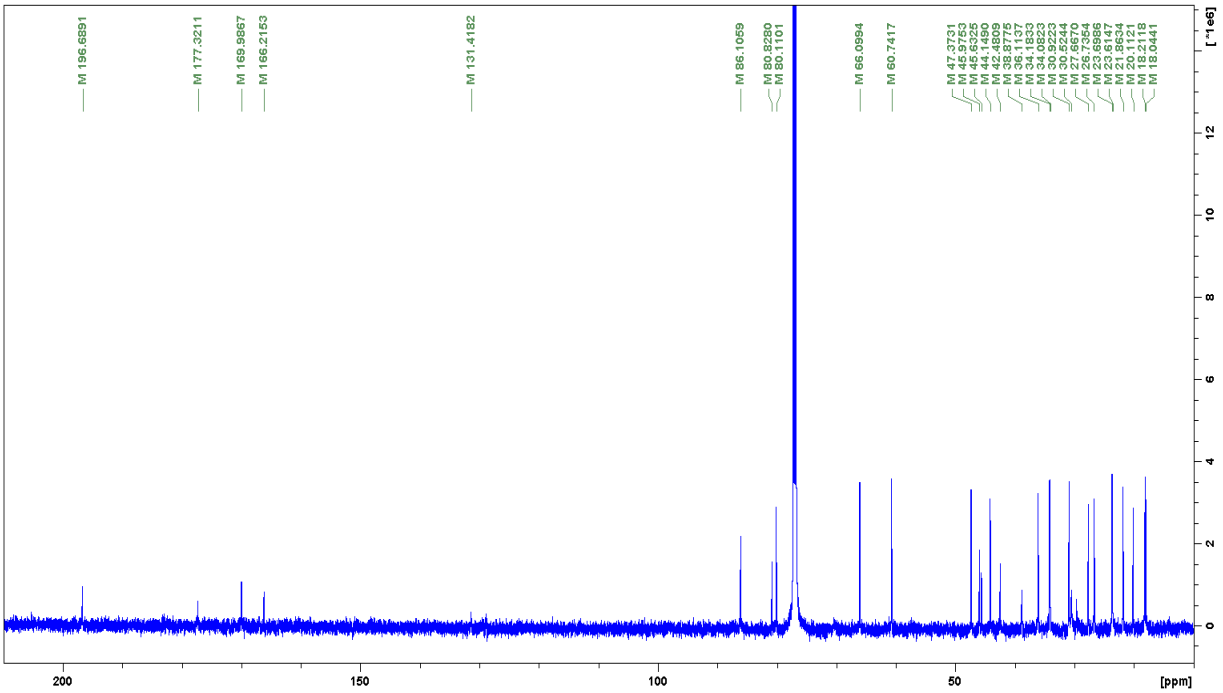

FIGURE 4.38 - ^{13}C NMR spectrum of Picraviane D (**08**) in $CDCl_3$ (150 MHz).

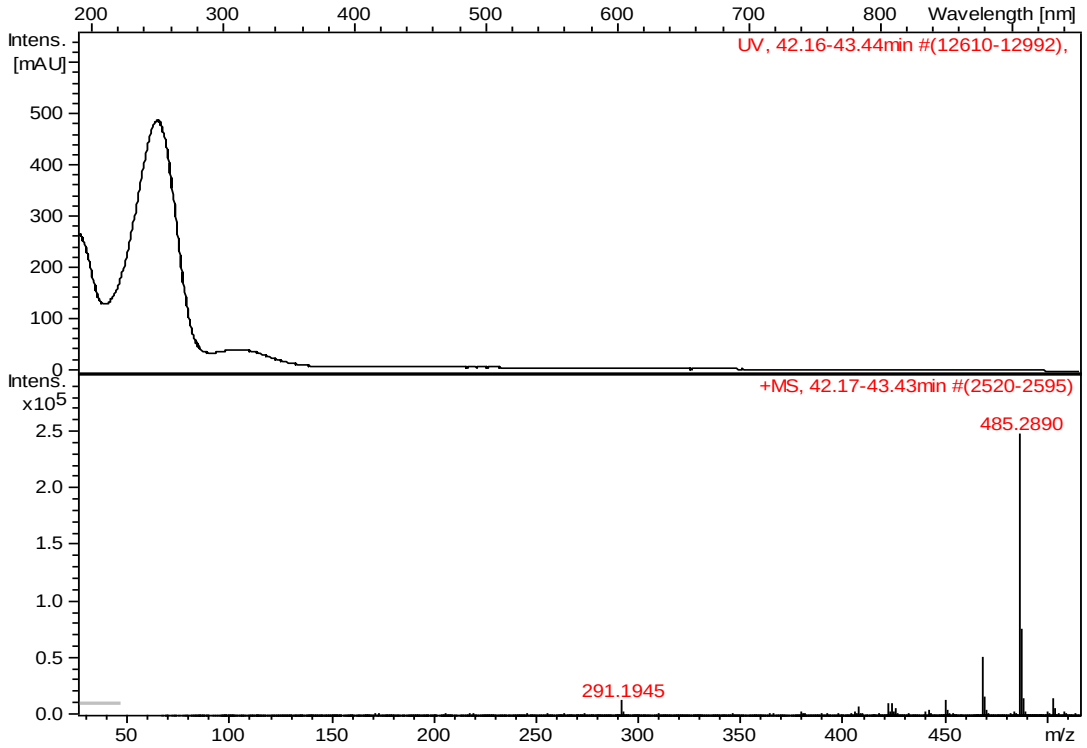

FIGURE 4.39 - HRESIMS spectrum of Picraviane D (**08**) indicating *m/z* $[M+H]^+$ = 485.2890.

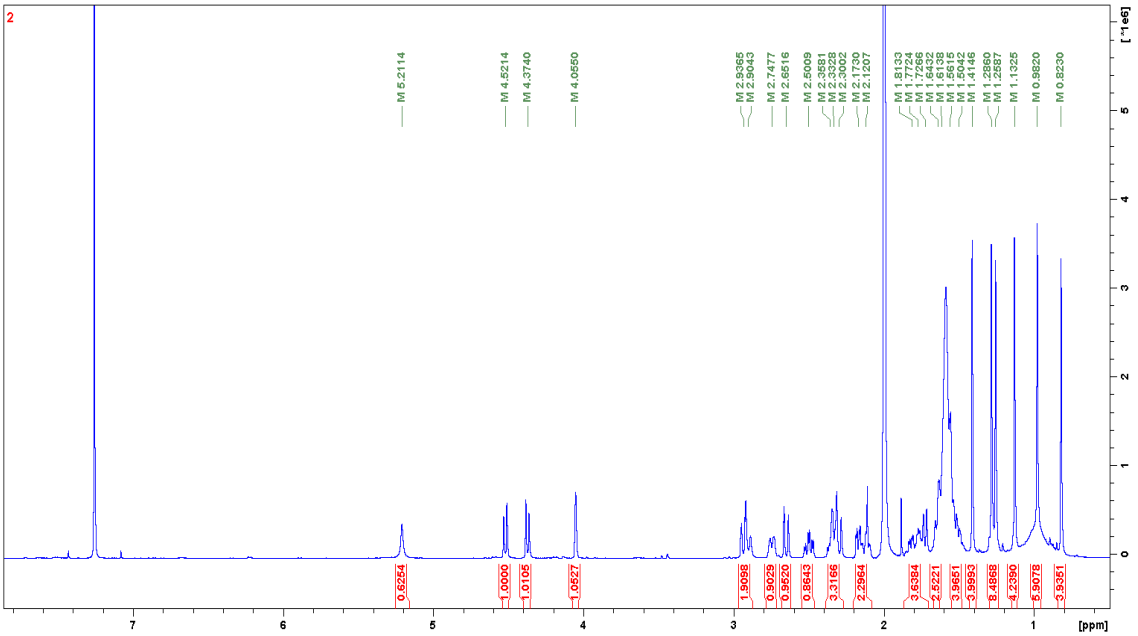

FIGURE 4.40 - ^{1}H NMR spectrum of Picraviane E (**09**) in $CDCl_3$ (600 MHz).

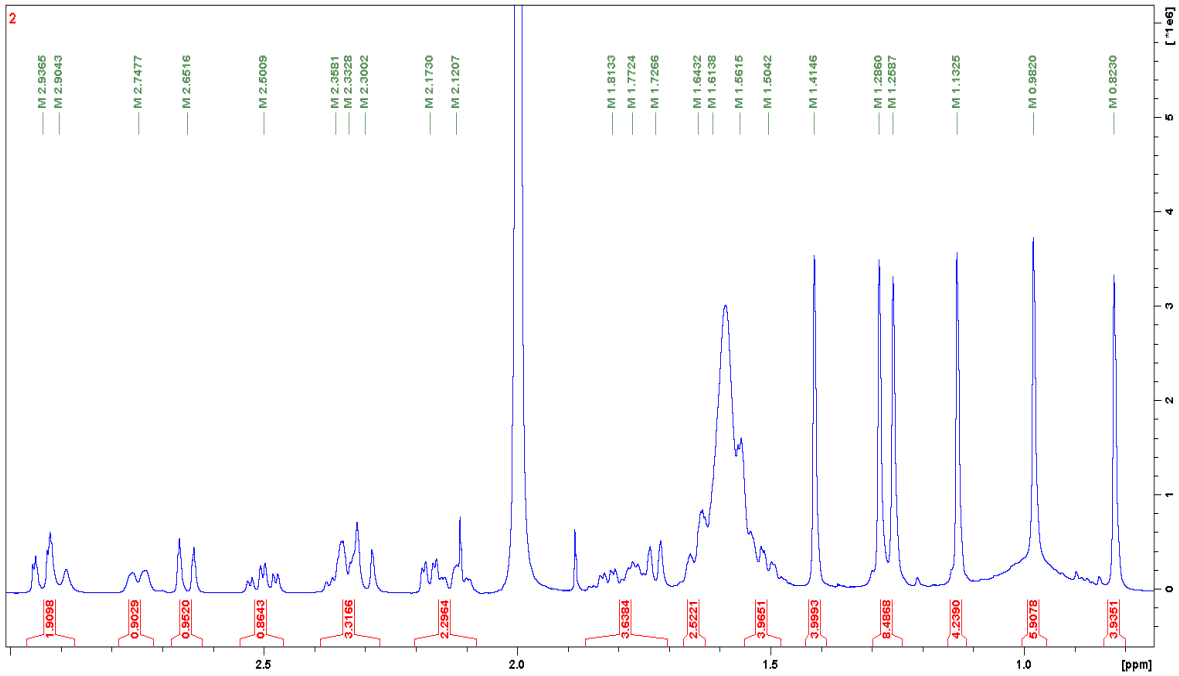

FIGURE 4.41- Expansion of the ^{1}H NMR spectrum of Picraviane E (**09**) in $CDCl_3$ (600 MHz).

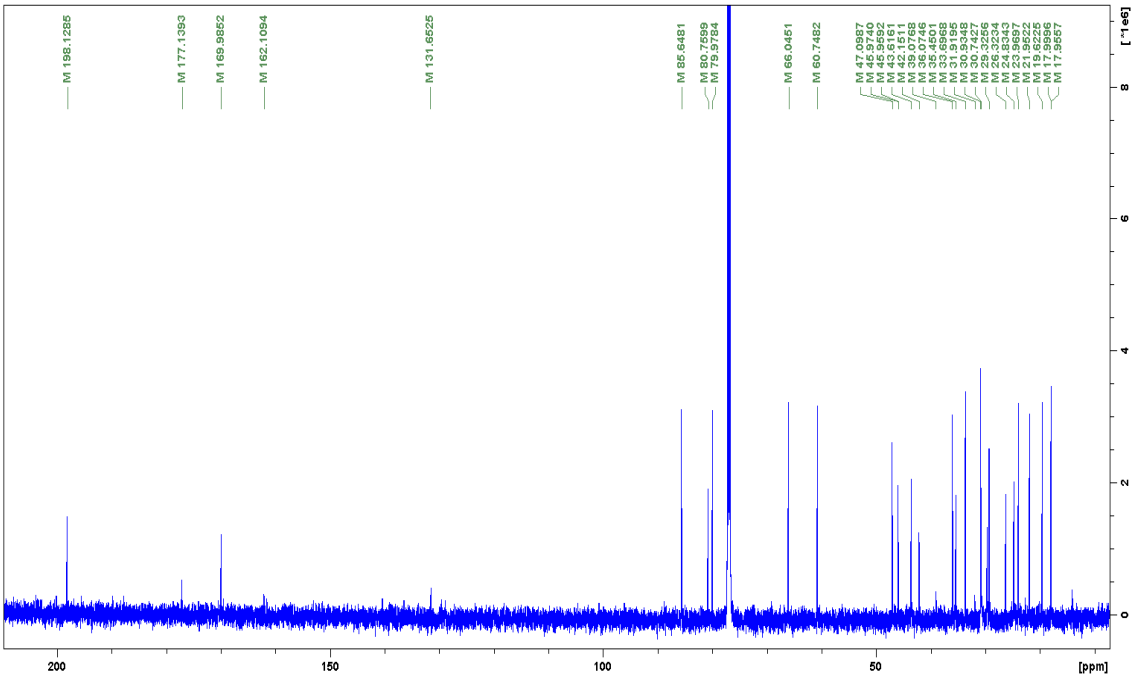

FIGURE 4.42 - ^{13}C NMR spectrum of Picraviane E (**09**) in $CDCl_3$ (150 MHz).

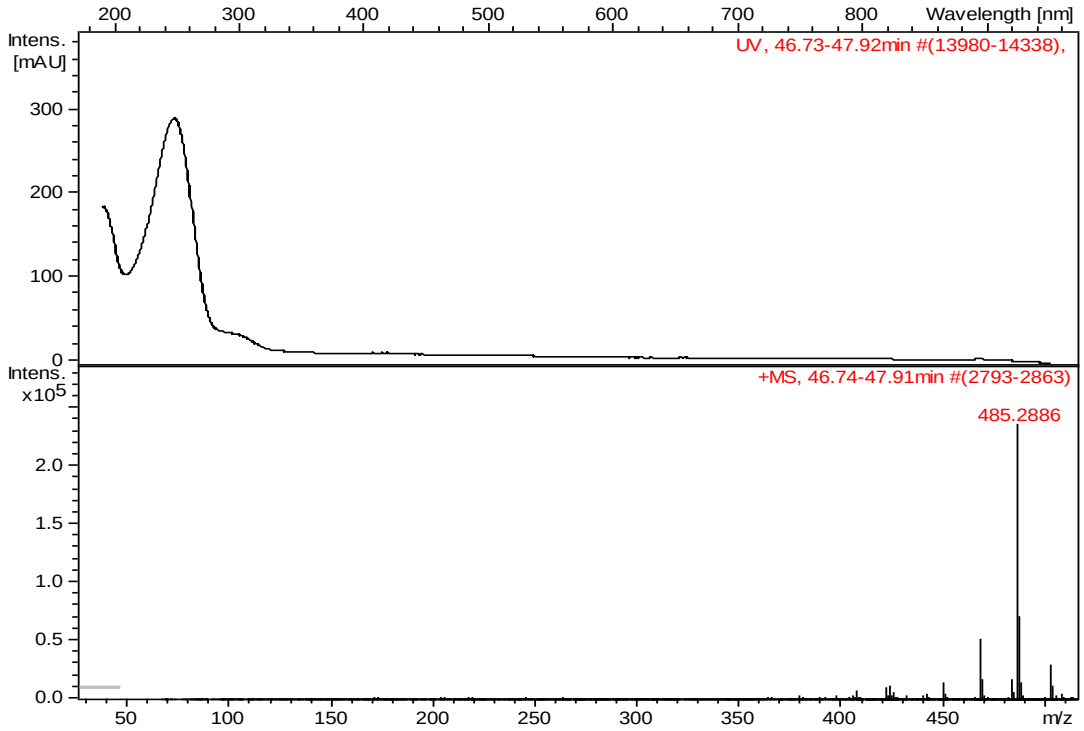

FIGURE 4.43 - HRESIMS spectrum of Picraviane E (**09**) indicating *m/z* $[M+H]^+$ = 485.2886.

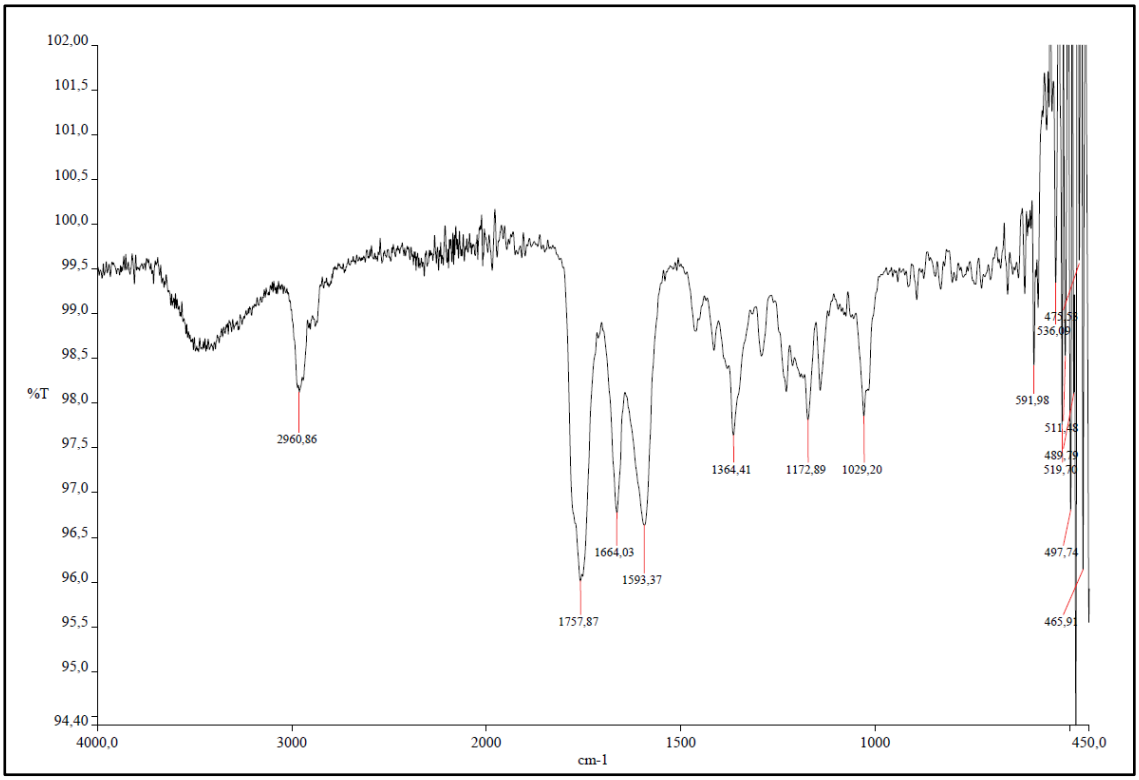

FIGURE 4.44 - Infrared spectrum of Picraviane D (**08**).

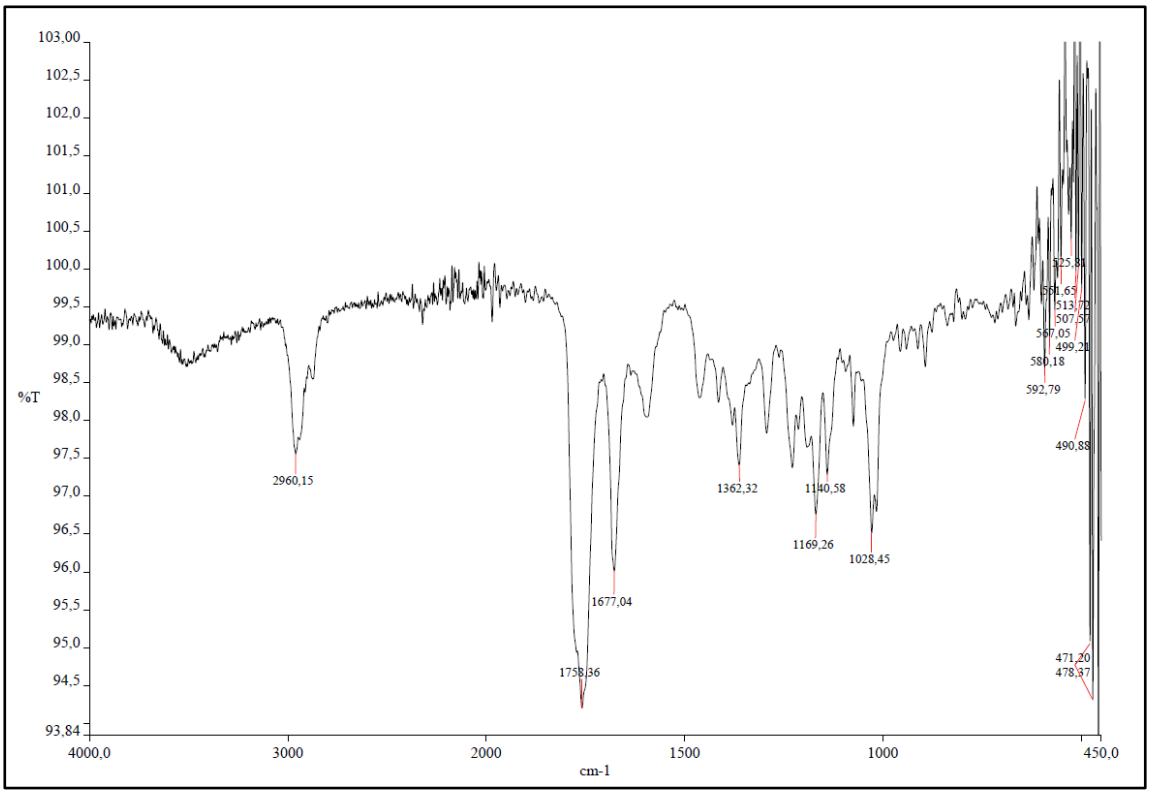

FIGURE 4.45 - Infrared spectrum of Picraviane E (**09**).

4.1.1.4 – Nortriterpenes Picraviane F (18) and G (19)

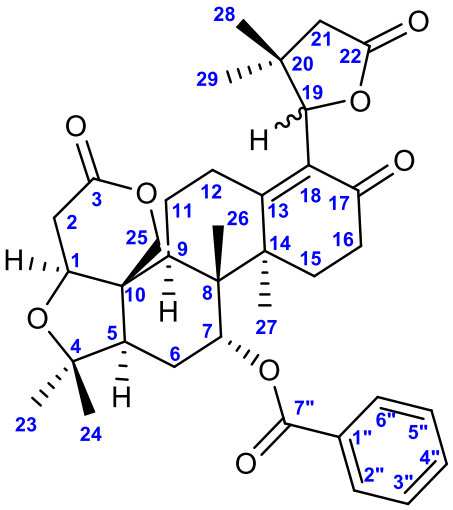

(18)

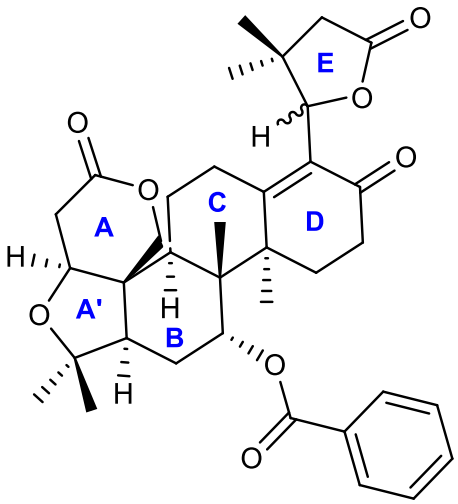

(19)

Picravianes F (**18)** and G (**19)** were assigned to have the same molecular formula as $C_{36}H_{44}O_8$ (15 degrees of unsaturation) on the basis of HRESIMS data at m/z $[M+H]^+$ = 605.3100 (calc. for 605.3109, compound 18) and $[M+H]^+$ = 605.3099 (calc. for 605.3109, compound 19), which was consistent to be another pair of diastereoisomers (FIGURES 4.52 and 4.56). They were elucidated on the basis of spectroscopic data from 1D ^{1}H NMR, ^{13}C NMR (FIGURES 4.46 to 4.48 and 4.50 to 4.52) as well as 2D NMR experiments (COSY, HSQC, HMBC and NOESY, see Supporting Information pages 264 to 267). The optical rotation measured disclosed to compound **18**: $[\alpha]_D^{25}$: - 56.38 (c. 0.32, MeOH) and to compound **19**: $[\alpha]_D^{25}$: - 66.48 (c. 0.19, MeOH).

The UV spectrum to **18** and **19** were acquired from the HPLC-HRESIMS and showed absorbances at λ_{max} 197 and 237 nm in both compounds. The IR spectrum disclosed sp^3 C-H stretch vibrations at 2969 cm^{-1} in both compounds, C=O stretching frequency as a strong bond at 1752/ 1751 cm^{-1} resulted from the lactones and esters functions, and C=O stretch vibrations resulted of the conjugated ketone with a double bond at 1666/ 1676 cm^{-1} (corresponding to compounds **18** and **19** respectively), besides vibrations in the range from 1100 to 1200 cm^{-1} due to C-O stretching vibrations observed in both compounds, and an out

of plane (oop) bending at 716 and 717 cm^{-1} due =C-H of aromatic rings (compounds **18** and **19**, respectively) (FIGURES 4.54 and 4.55).

The NMR data of **18** and **19** showed high similarities with those of **08** and **09**, except for the presence of a benzoate unit, which is consistent with their molecular formula. The aromatic signals in the range at *δ* 7.50 – 8.04 in the HMBC spectrum showed correlations with the carbonyl carbon at *δ* 164.8, as the same way as the oxymethine proton at *δ* 5.30 in both compounds, allowing the positioning of the benzoate group at C-7.

The ^{1}H NMR and HSQC spectra disclosed one oxymethine proton, as a singlet at *δ* 5.08 (*δ* 85.9) and *δ* 5.24 (*δ* 85.4) to compounds **18** and **19**, respectively, corresponding to H-19. Likewise to compounds **08** and **09**, the key HMBC correlations observed from H-19 to the carbons C13, C-17, C-18 and C-22 indicated the presence the five-membered ring and confirmed the positioned of the enone function as observed to **08** and **09**. The COSY spectrum displayed the spin system such as: H-1 and H-2; H-5, H-6 and H-7, and H-9, H-11 and H-12, enclosing the establishment of the structure.

The relative configuration of the stereocenters to both compounds followed the same pattern as observed before to compounds **08** and **09**. Therefore, the hydrogen H-5 was determined to assume an α spatial position due correlations with those of the aromatic ring H-2'' and H-6" and with H-1, H-6α, H-9 and H-23 in both compounds. The hydrogen H-7, consequently, due the correlations observed to the methyl group at C-26 indicated adopting the β-orientation. Similarly to the compounds described above, **19** also presented a more deshielded proton at C-29 than **18,** which indicates **19** assuming the same configuration than compound **09**. Further experiments should be acquired to determinate the absolute stereochemistry and to distinguish the diastereomeric pair. The complete assignments of the ^{1}H and ^{13}C are given in TABLE 4.5.

TABLE 4.5- ^{13}C and ^{1}H NMR Data for Picraviane F (**18**) and G (**19**) acquired in $CDCl_3$

	18		**19**	
C	δ_C	δ_H (*J* in Hz)	δ_C	δ_H (*J* in Hz)
1	80.5	4.23 br t (3.5)	80.4	4.24 br t (3.5)
2	35.9	α: 2.99 dd (17.0, 3.5) β: 2.70 dd (17.0, 2.2)	35.8	α: 2.99 dd (17.0, 3.5) β: 2.71 dd (17.0, 2.2)
3	169.6	-	169.6	-
4	80.4	-	80.3	-
5	53.4	2.50 dd (13.8, 1.6)	53.5	2.49 dd (13.7, 1.8)
6	24.9	α: 1.93 td (14.8, 1.6) β: 1.74 dt (14.8, 3.5)	24.9	α: 1.92 m β: 1.74 dt (14.8, 3.5)
7	75.2	5.30 t (3.5)	75.0	5.30 t (3.5)
8	45.5	-	45.3	-
9	44.6	2.76 dd (12.9, 4.5)	44.4	2.74 dd (12.9, 4.9)
10	45.7	-	45.8	-
11	23.2	β: 2.00 m α: 1.83 m	23.5	1.89 m
12	26.0	β: 2.83 dd (16.4, 4.9) α: 2.29 m	25.8	β: 2.80 dd (15.6, 4.7) α: 2.39 m
13	166.4	-	162.5	-
14	45.8	-	46.1	-
15	27.7	β: 2.30 m α: 1.57 m	29.2	β: 2.25 td (16.0, 4.1) α: 1.61 m
16	33.9	2.35 m	34.9	β: 2.28 dt (15.3, 3.8) α: 2.42 td (15.3, 5.4)
17	196.5	-	197.8	-
18	130.0	-	130.2	-
19	85.9	5.08 s	85.4	5.24 br s
20	38.9	-	39.4	-
21	44.1	β: 2.29 m α: 2.71 d (17.4)	43.6	β: 2.32 d (17.3) α: 2.86 d (17.3)
22	177.2	-	176.9	-
23	30.6	1.15 s	30.6	1.14 s
24	21.8	1.11 s	21.9	1.11 s
25	65.9	β: 4.58 d (12.9) α: 4.50 d (12.9)	65.8	β: 4.56 d (12.9) α: 4.48 d (12.9)
26	18.2	0.95 s	18.1	0.88 s
27	24.6	1.55 s	24.2	1.59 s
28	30.5	1.26 s	30.5	1.24 s
29	23.6	0.84 s	24.7	0.97 s
1”	129.8	-	129.9	-
2”/ 6”	129.6	8.04 XX'-system	129.7	8.04 XX'-system
3”/ 5”	128.8	7.50 AA'-system	128.9	7.50 AA'-system
4”	133.8	7.63 tt (8.2, 1.4)	133.8	7.63 tt (8.1, 1.5)
7”	164.8	-	164.8	-

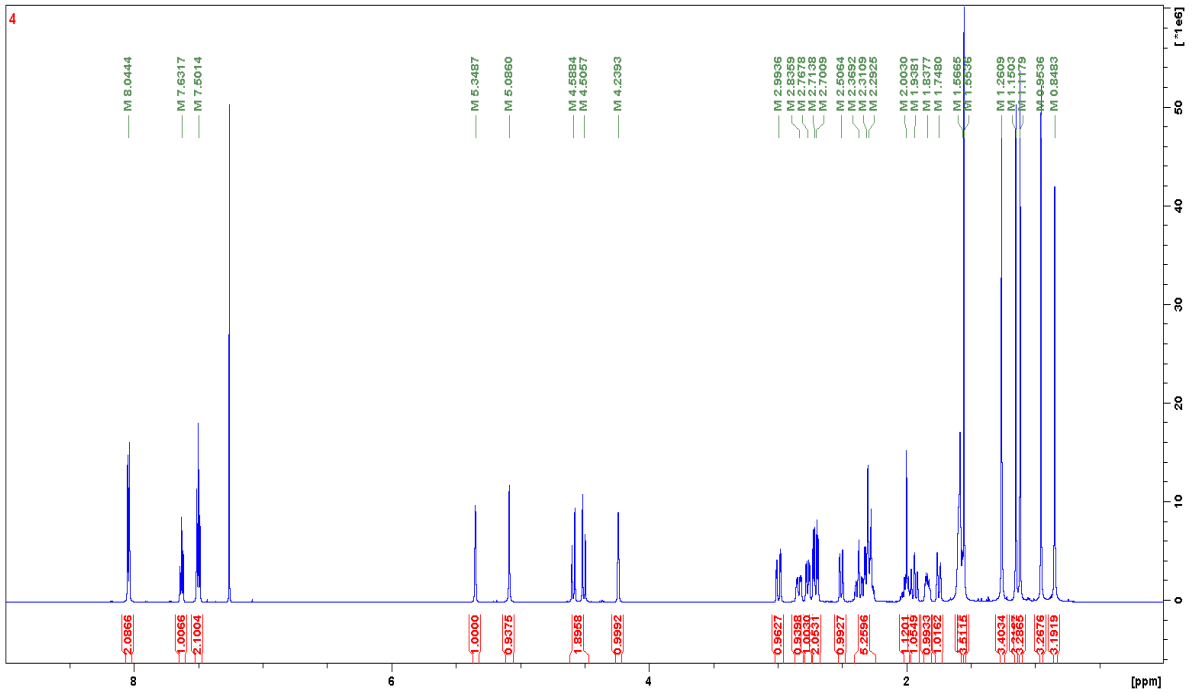

FIGURE 4.46 - ^{1}H NMR spectrum of Picraviane F (**18**) in $CDCl_3$ (600 MHz).

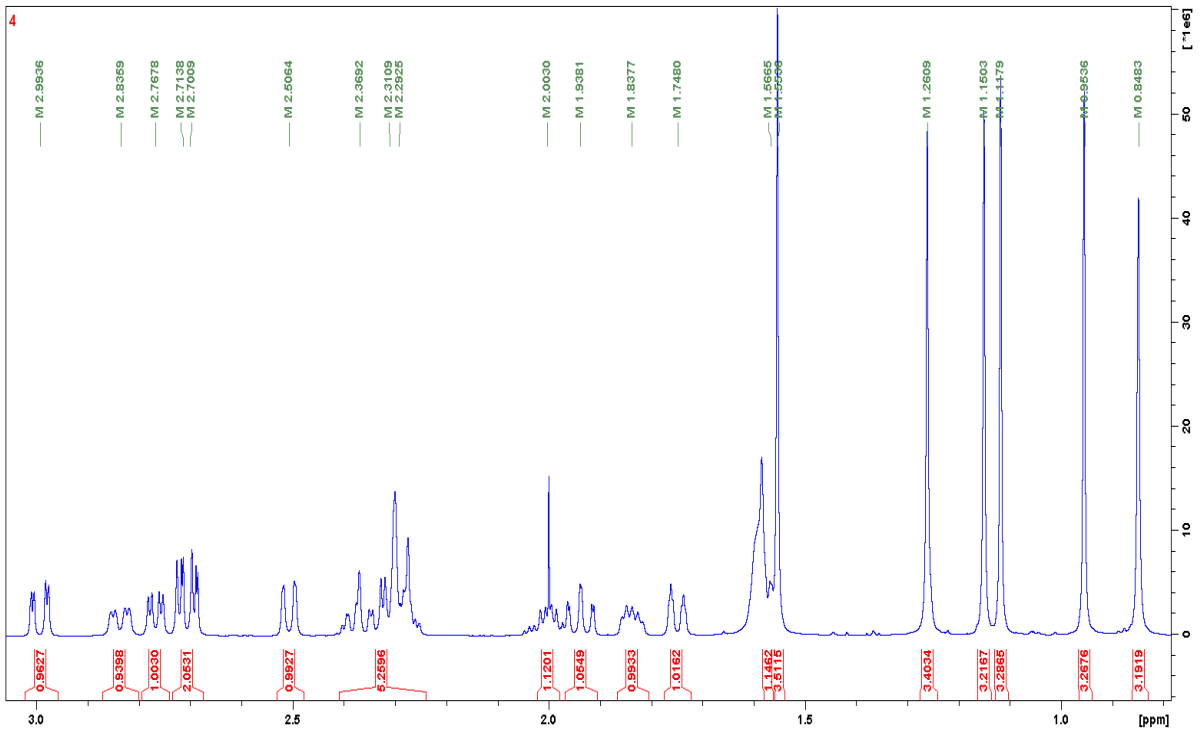

FIGURE 4.47 - Expansion of the ^{1}H NMR spectrum of Picraviane F (**18**) in $CDCl_3$ (600 MHz).

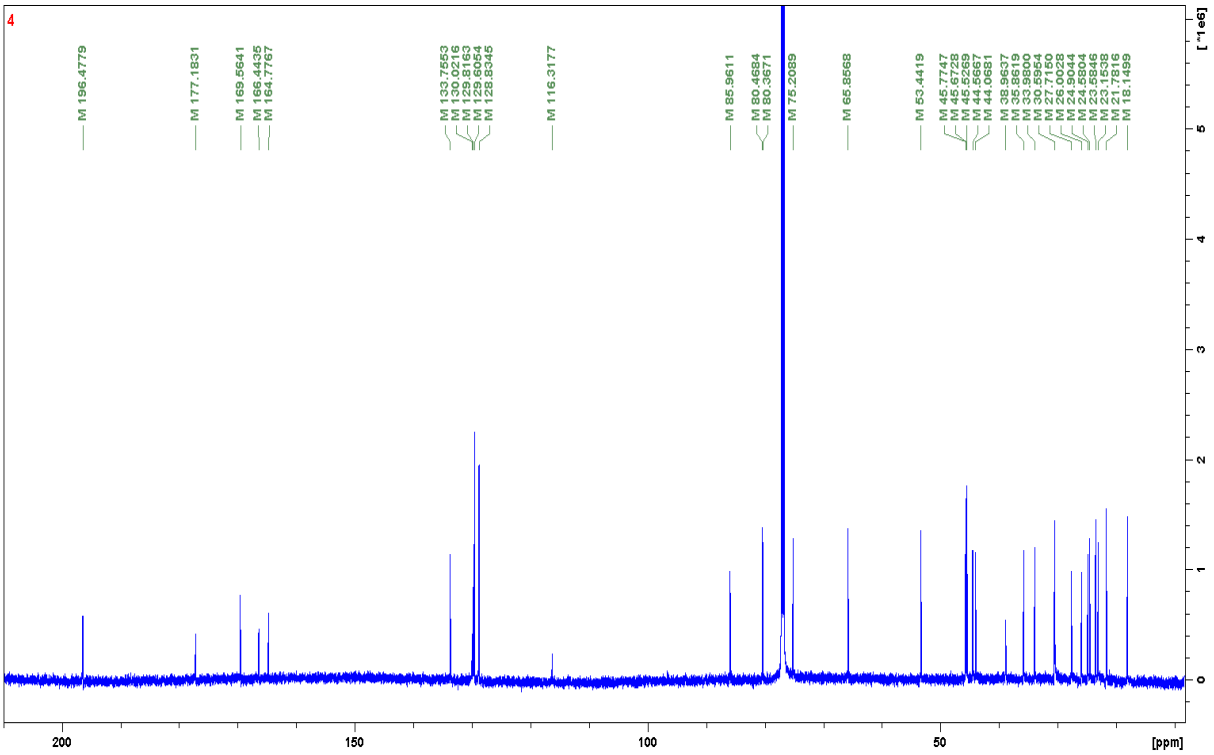

FIGURE 4.48 - ^{13}C NMR spectrum of Picraviane F (**18**) in $CDCl_3$ (150 MHz).

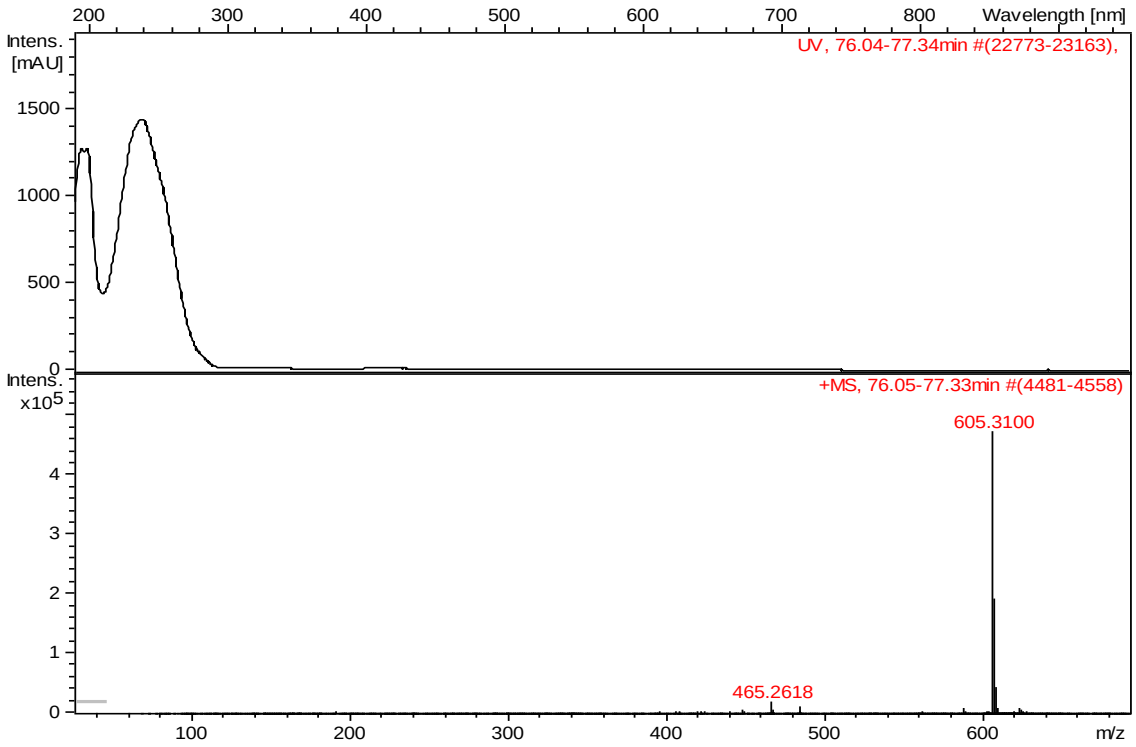

FIGURE 4.49- HRESIMS spectrum of Picraviane F (**18**) indicating *m/z* $[M+H]^+$ = 605.3100.

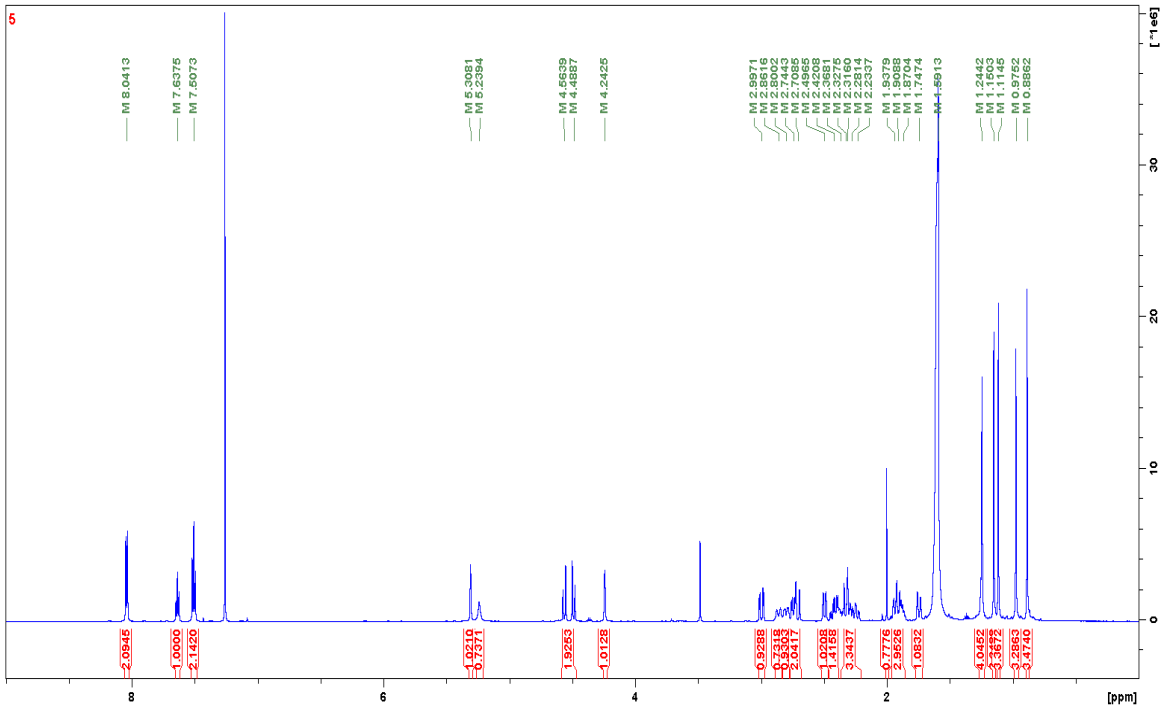

FIGURE 4.50 - ^{1}H NMR spectrum of Picraviane G (**19**) in $CDCl_3$ (600 MHz).

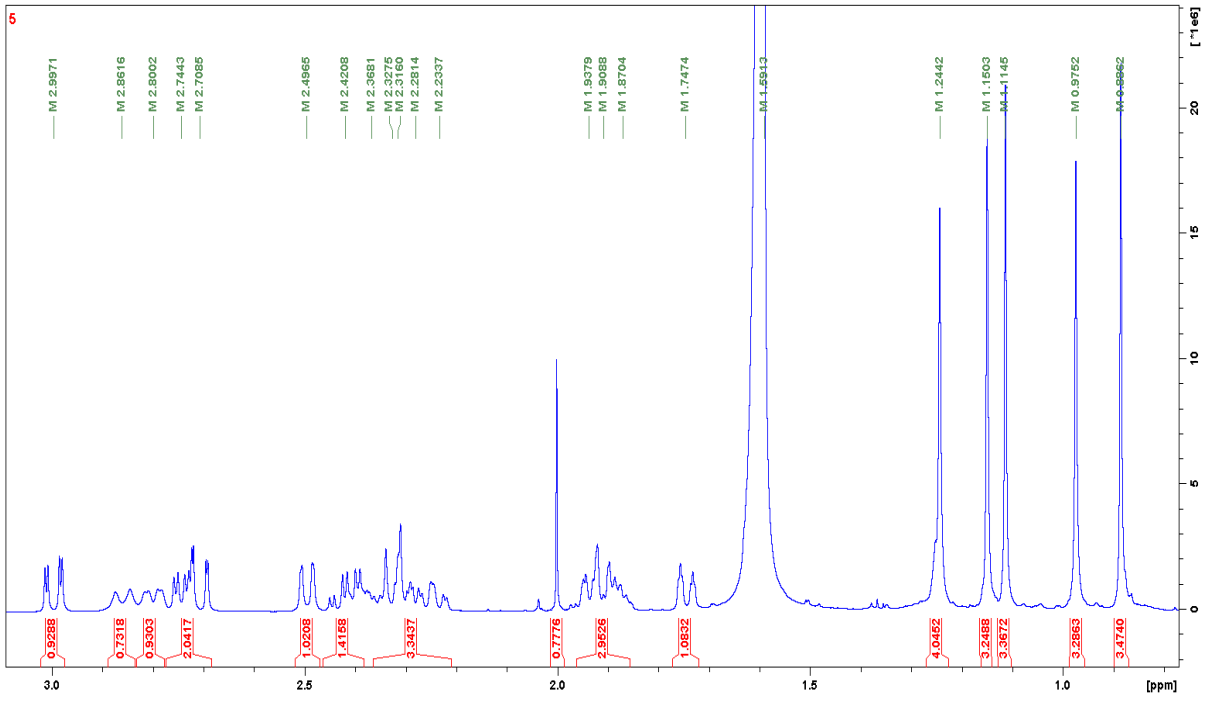

FIGURE 4.51 - Expansion of the ^{1}H NMR spectrum of Picraviane G (**19**) in $CDCl_3$ (600 MHz).

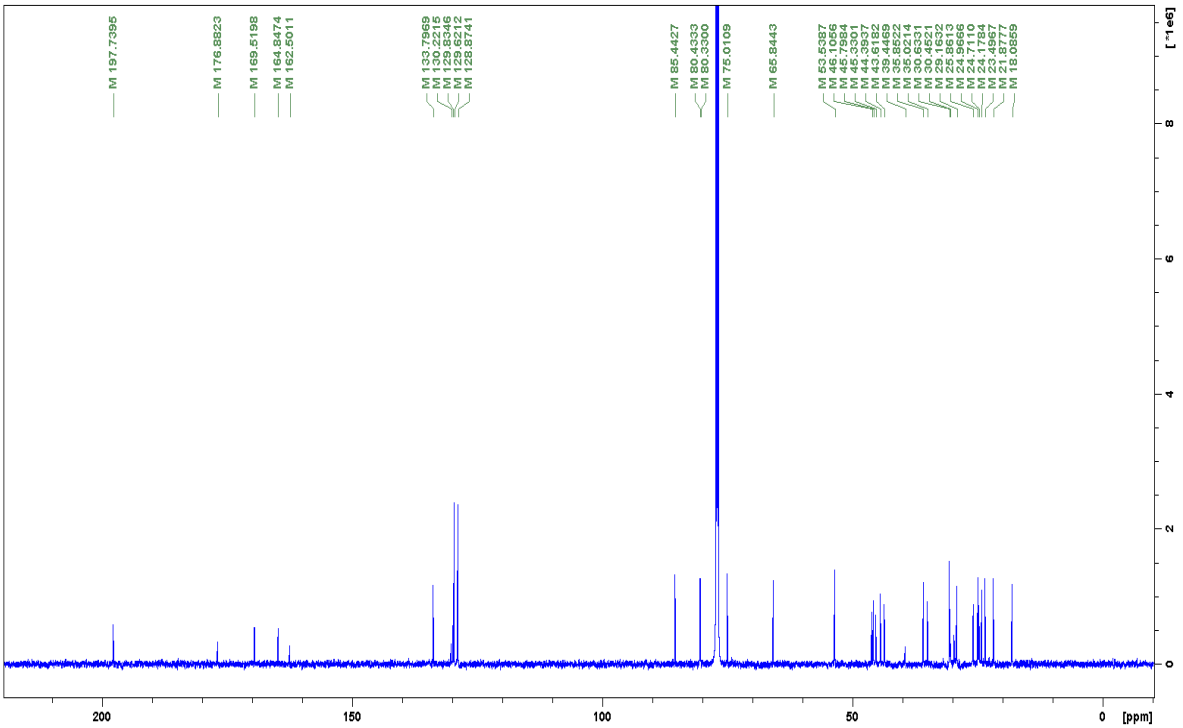

FIGURE 4.52 - ^{13}C NMR spectrum of Picraviane G (**19**) in $CDCl_3$ (150 MHz).

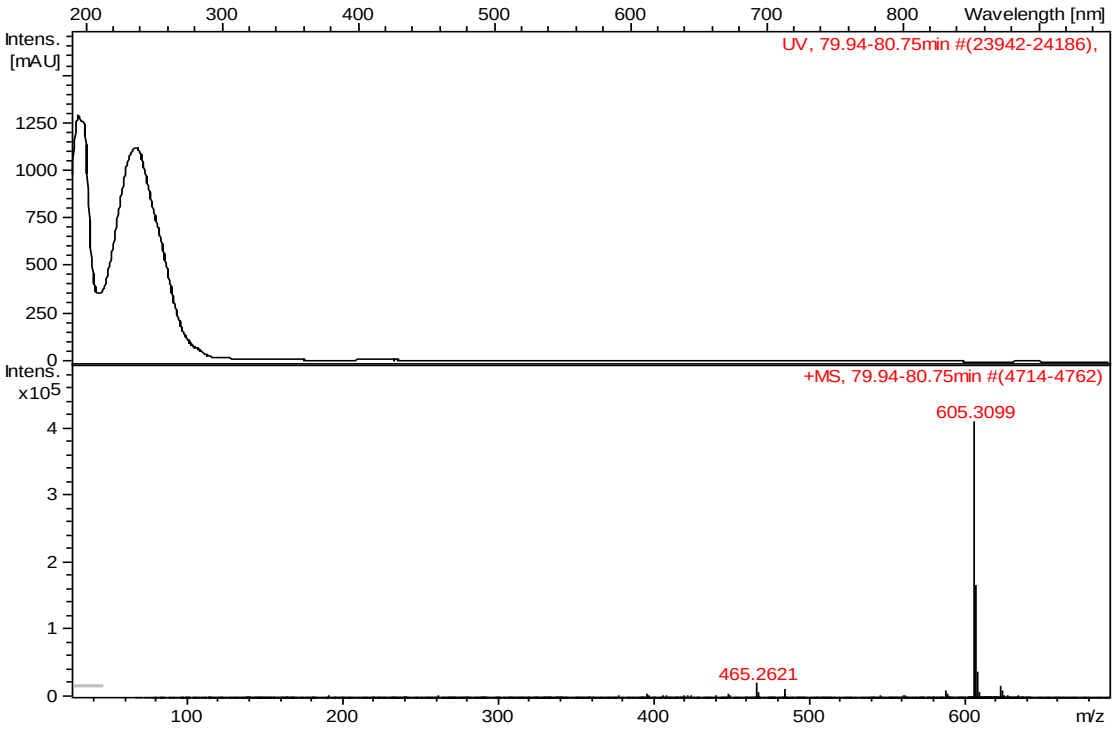

FIGURE 4.53 - HRESIMS spectrum of Picraviane G (**19**) indicating *m/z* $[M+H]^+$ = 605.3099.

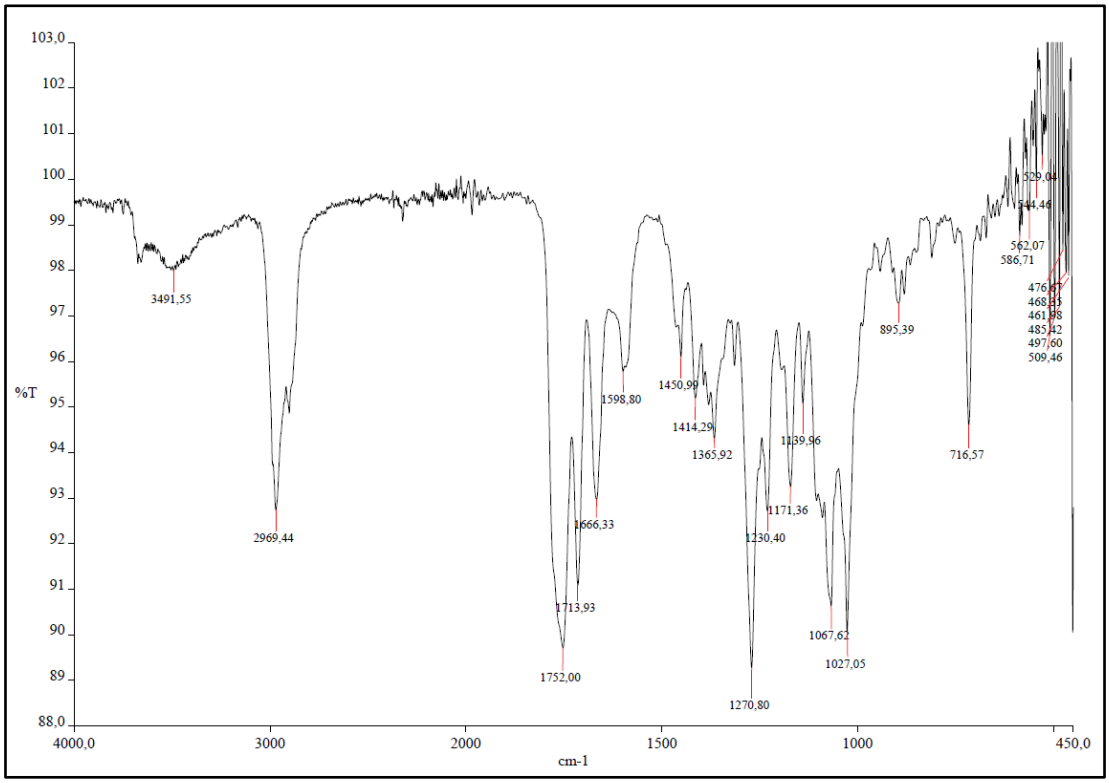

FIGURE 4.54 - Infrared spectrum of Picraviane F (**18**).

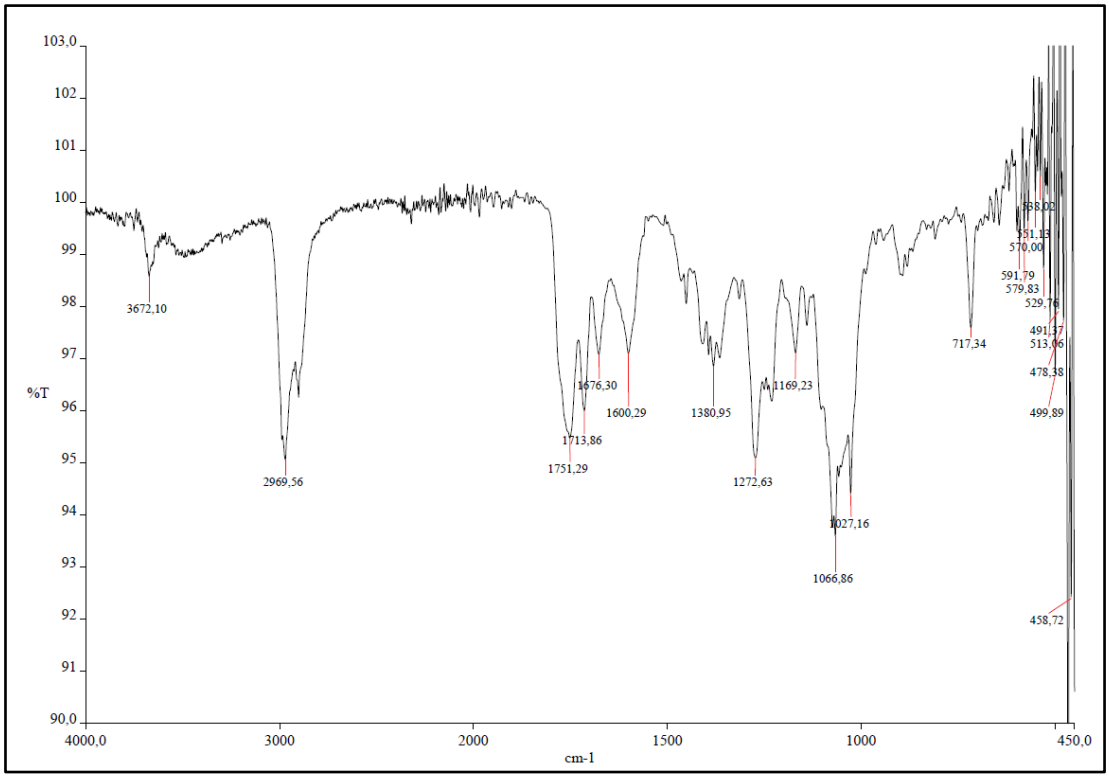

FIGURE 4.55 - Infrared spectrum of Picraviane G (**19**).

4.1.1.5 – Nortriterpenes Picravianes H (02), I (03), J (05), K (12) and L (13)

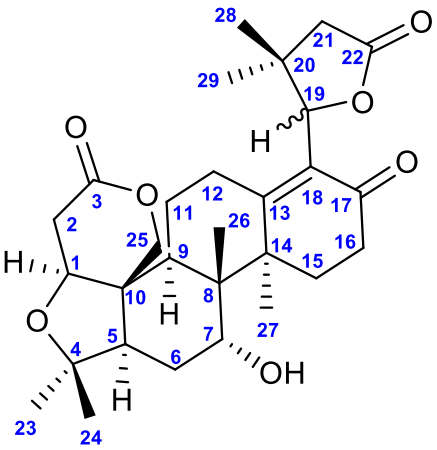

(02)

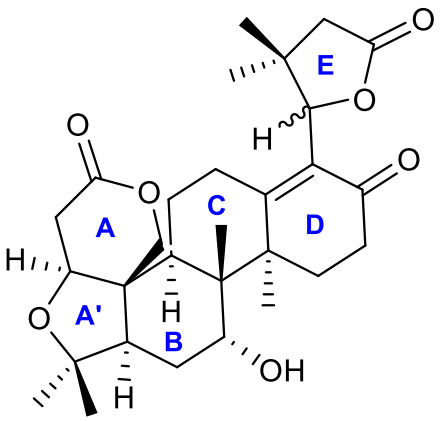

(03)

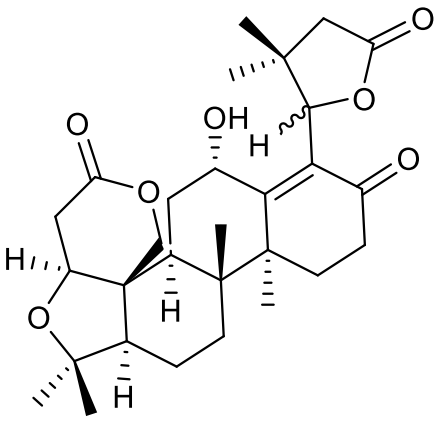

(05)

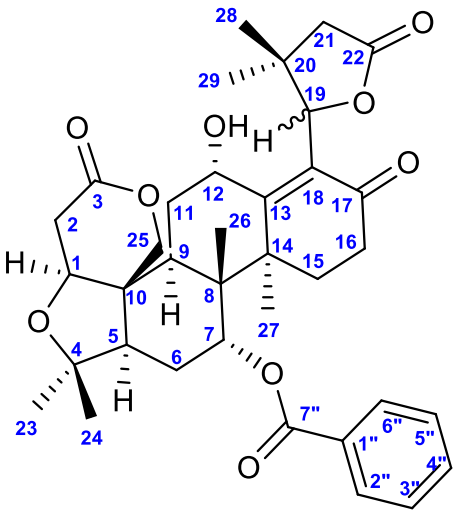

(12)

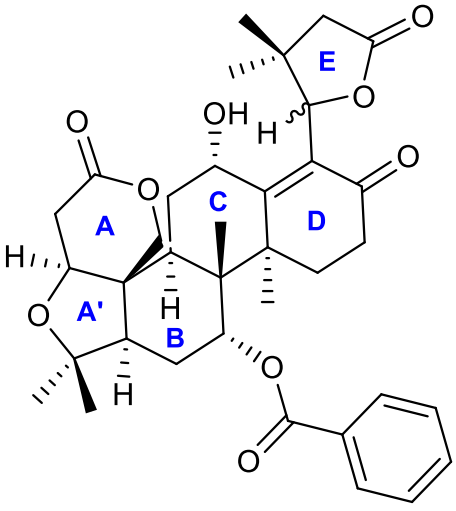

(13)

Picravianes H (**02**), I (**03**), J (**05**), K (**12**) and L (**13**) were elucidated on the basis of spectroscopic data from 1D ^{1}H NMR, ^{13}C NMR as well as 2D NMR experiments (COSY, HSQC, HMBC and NOESY, see Supporting Information pages 236 to 241 and 252 to 255). Due the high similarities of their structures, according with the compounds described above, these structures will be discussed together.

Picravianes H (**02**) and I (**03**), K (**12**) and L (**13**) presented as two pairs of diastereoisomers, based on the HRESIMS data:

- Compound **02**: m/z $[M+H]^+$ = 501.2836 (calc. for 501.2852), molecular formula as $C_{29}H_{40}O_7$ (10 degrees of unsaturation, FIGURE 4.59);
- Compound **03**: m/z $[M+H]^+$ = 501.2839 (calc. for 501.2852), molecular formula as $C_{29}H_{40}O_7$ (10 degrees of unsaturation, FIGURE 4.63);
- Compound **12**: m/z $[M+H]^+$ = 621.3051 (calc. for 621.3063), molecular formula as $C_{36}H_{44}O_9$ (15 degrees of unsaturation, FIGURE 4.73);
- Compound **13**: m/z $[M+H]^+$ = 621.3056 (calc. for 621.3063), molecular formula as $C_{36}H_{44}O_9$ (15 degrees of unsaturation, FIGURE 4.77).
- To compound **05**, the HRESIMS data indicated m/z $[M+Na]^+$ = 523.2657 (calc. for 523.2671), m/z $[M+H]^+$ = 501.2825 (calc. for 501.2852), molecular formula as $C_{29}H_{40}O_7$ (10 degrees of unsaturation), however the base peak to this compound corresponded to the fragment m/z $[M+H]^+$ = 483.2735, indicating the loss of a water molecule (FIGURES 4.67 and 4.68).

Due the low amount isolated to these five compounds, the measured of the optical rotation were not acquired to all of them. The infrared, however, was acquired to all these compounds, but since the signals of the methanol (the solvent used to solubilize the samples) appeared in the spectrum, these analyses should be repeated.

The UV spectrum was acquired from the HPLC-HRESIMS and showed to compounds **02** and **03** and **05** the absorbance at λ_{max} 246 nm. To compounds **12** and **13**, disclosed absorbances at λ_{max} 194 and 232 nm.

The ^{1}H and ^{13}C NMR data to the five compounds presented signals characteristics to the A', A, B, C, D and to the pentanolide E backbone of the nortriterpenes: signals belonging to the carbonyl groups, including the conjugated ketone, to the quaternary carbon at δ 80 ppm (C-4), besides those to the diastereotopic proton pairs, to oxymethylene, oxymethines and methyl groups were in agreement to the compounds **08**, **09**, **18** and **19**, as discussed previously. The

difference from each compound was analyzed comparing each HRMS spectrum and NMR data. Thus, the diastereoisomers **02** and **03**, **12** and **13** showed a downfield shift to H-7. Further analyses indicated the presence of the benzoate unit in **12** and **13 (**due the presence of aromatic signals in the ^{1}H NMR spectrum at δ 7.50 to 8.10 ppm), and correlations in HMBC spectrum from H-7 to the carbonyl carbon at δ 164.9 ppm and to the C-5 at δ 53 ppm established the benzoate unit at C-7. However, the absence of the benzoate group clearly observed in the ^{1}H NMR spectrum and a more shielded value to H-7 for **02** and **03** in relation to **12** and **13** suggested the existence of a hydroxyl group at this position (C-7). Otherwise, compound **05** did not present any oxymethine hydrogen that would indicate a substituent at C-7 (no carbon at the range of δ 70 - 75 was observed in the HSQC spectrum). Thus, correlations in COSY spectrum indicated the three spin systems corresponding to the C-5 – C-6 – C-7, and the HSQC experiment showed C-7 as a methylene (δ 1.69 and 1.63 with δ 34.3).

Compounds **05**, **12** and **13** disclosed an additional deshielded oxymethine proton with chemical shift at δ 4.89 (δ 64.9, compound **05**); δ 4.80 (δ 64.0, compound **12**) and δ 4.92 (δ 64.3, compound **13**), suggesting the presence of a hydroxyl substituent. HMBC experiment allowed the establishment of this proton at the position at C-12, due the correlations observed from H-12 to C-9, C-13 and C-18. Spin system to H-9 – H-11 – H-12 was also observed through the COSY experiment, enclosing the structural elucidation to these compounds.

The presence of hydroxyl group in each nortriterpene was also noticed by the elimination of a water molecule in all mass spectra. Elimination of benzoic acid, in addition, was observed to compounds **12** and **13** (FIGURES 4.59; 4.63; 4.68; 4.73 and 4.78).

The relative configuration to the stereocenters in H-1, H-5, H-9, H-26 and H-27 in all compounds has followed the same pattern as already discussed above. However, the hydrogen H-12 in compounds **05**, **12** and **13** was determined to assume a β spatial position since this proton presents a key correlation with the methyl group at C-26, strongly observed in **13** and weaker in **05** and **12**. Moreover, the ^{1}H NMR spectrum indicated a ^{3}J in H-9 with the same coupling constant than H-11α, and a ^{3}J in H-12 coupling with the same constant to H-11β, supporting this establishment (TABLE 4.7 and 4.8).

Compound **02** presented a deshielded chemical shift to the carbon C-13, whereas compound **03** showed the methyl protons in C-29 more deshielded. This

observation suggests compound **02** having the same configuration to H-19 as compounds **08** and **18**, and compound **03**, on the other hand, should present the configuration to H-19 as compounds **09** and **19**. The same occurs to compounds **12** and **13**. However, in this case, compound **13** presents the most deshielded value to C-13. When the proton in H-19 is close to the ketone group (C-17) in **13**, the arrangement of the atoms favors the lactone function of the pentanolide E ring next to C-12, justifying the slightly more deshielded proton in H-12 to compound **13** than to compound **12**. The correlations in NOESY spectrum from H-12 to H-19 in **12** and absence of this correlation in **13** contribute to this observation. The stereochemistry to H-19 in compound **05**, however, should be the same as to compound **13**, due the similar chemical shift found in ^{13}C NMR spectrum. The absolute stereochemistry to all compounds should be evaluated in a next future, allowing to confirm all these previous establishment.

The complete assignments of the ^{1}H and ^{13}C to compounds **02** and **03**, **05**, **12** and **13** are given in TABLE 4.6; 4.7 and 4.8, respectively. Compounds **02**, **05** and **12** presented high level of impurities after acquiring the ^{1}H NMR spectrum. Further analyses indicated the compound **05** mixed with the anthraquinone aloe-emodin. Although all 2D NMR experiments have been acquired to these compounds mixed with their respective impurities, the nortriterpenes **02** and **05** were subjected to successive injections in the analytical HPLC aiming their purifications. The ^{1}H NMR after these processes are currently underway. However, some collections from the PGD partition in semi-preparative scale during the isolation of all compounds (as described in section 3.5.1.4) also resulted in a pure nortriterpene **12** (FIGURE 4.70). The 2D NMR experiments, however, had already been acquired from the compound **12** with impurities, and due the long time needed to the acquisition of these experiments, the spectra were not repeated. ^{1}H and ^{13}C NMR spectra to these five compounds are shown in FIGURES 4.56 - 4.58 (compound **02**); 4.60 – 4.62 (compound **03**); 4.64 – 4.66 (compound **05**); 4.69 – 4.72 (compound **12**) and 4.74 – 4.76 (compound **13**).

TABLE 4.6- ^{13}C and ^{1}H NMR Data for Picravianes H (**02**) and I (**03**) acquired in $CDCl_3$

	02		**03**	
C	δ_C	δ_H (*J* in Hz)	δ_C	δ_H (*J* in Hz)
1	80.3	4.11 t (3.5)	80.2	4.11 t (3.5)
2	35.8	α: 2.95 dd (17.0, 3.5) β: 2.64 dd (17.0, 2.0)	35.9	α: 2.95 dd (17.0, 3.5) β: 2.65 dd (17.0, 2.0)
3	169.8	-	169.8	-
4	80.4	-	80.3	-
5	51.5	2.57 dd (13.8, 2.1)	51.6	2.57 m
6	28.9	α: 1.96 td (14.1, 2.1) β: 1.46 dt (14.1, 2.6)	29.0	α: 1.94 td (14.4, 2.2) β: 1.44 dt (14.4, 2.7)
7	73.5	4.02 t (2.6)	73.3	3.98 br s
8	45.5	-	45.3	-
9	43.0	2.61 dd (13.5, 4.7)	42.8	2.58 m
10	45.8	-	45.8	-
11	22.9	β: 1.93 dd (13.1, 6.1) α: 1.76 dt (13.1, 6.3)	23.3	β: 1.86 dd (13.1, 6.1) α: 1.80 dt (13.1, 6.3)
12	25.8	β: 2.75 m α: 2.28 m	25.7	β: 2.72 dd (15.7, 5.5) α: 2.40 m
13	167.7	-	163.6	-
14	46.10	-	46.5	-
15	27.1	β: 2.25 dd (14.8, 5.3) α: 2.02 m	28.7	β: 2.23 td (13.6, 4.5) α: 2.10 ddd (13.6, 5.7, 2.9)
16	34.2	β: 2.41 ddd (15.3, 5.3, 2.9) α: 2.47 dd (15.3, 5.6)	35.2	β: 2.35 ddd (15.0, 4.5, 2.9) α: 2.59 m
17	197.0	-	198.4	-
18	129.7	-	129.8	-
19	86.2	5.05 s	85.6	5.23 s
20	38.7	-	39.4	-
21	44.1	β: 2.27 d (17.2) α: 2.75 d (17.2)	43.7	β: 2.31 d (17.3) α: 2.87 d (17.3)
22	177.5	-	177.0	-
23	30.4	1.29 s	30.5	1.30 s
24	22.1	1.14 s	22.2	1.14 s
25	66.0	β: 4.52 d (12.9) α: 4.43 d (12.9)	65.9	β: 4.49 d (12.9) α: 4.42 d (12.9)
26	18.1	0.76 s	18.1	0.70 s
27	23.9	1.66 s	23.6	1.69 s
28	30.7	1.26 s	30.5	1.24 s
29	23.6	0.86 s	23.7	0.97 s
OH	-	*	-	*

TABLE 4.7- ^{13}C and ^{1}H NMR Data for Picraviane J (**05**) acquired in $CDCl_3$

		05
C	δ_C	δ_H (*J* in Hz)
1	79.9	4.12 t (3.4)
2	36.1	α: 2.95 dd (17.0, 3.4) β: 2.69 dd (17.0, 2.0)
3	170.3	-
4	80.6	-
5	60.7	1.78 d (13.5)
6	18.16	α: 1.66 m β: 1.52 dd (12.2, 3.1)
7	34.3	α: 1.69 m β: 1.63 m
8	41.7	-
9	41.8	2.52 dd (13.5, 4.1)
10	45.6	-
11	30.6	α: 1.82 dd (14.6, 4.1) β: 2.03 td (14.6, 4.9)
12	64.9	4.89 dd (4.9, 1.6)
13	165.8	-
14	45.4	-
15	29.1	β: 2.17 td (14.8, 4.8) α: 1.64 m
16	34.3	β: 2.59 dd (15.1, 5.5) α: 2.49 ddd (15.1, 4.8, 2.9)
17	198.3	-
18	130.9	-
19	84.9	5.53 s
20	40.5	-
21	44.4	2.55 br s
22	175.7	-
23	30.9	1.29 s
24	21.9	1.14 s
25	66.1	β: 4.57 d (12.7) α: 4.38 d (12.7)
26	19.4	0.88 s
27	22.1	1.59 s
28	28.3	1.24 s
29	24.0	0.97 s
OH	-	*

TABLE 4.8- ^{13}C and ^{1}H NMR Data for Picraviane K **(12)** and L **(13)** acquired in $CDCl_3$

	12		**13**	
C	δ_C	δ_H (*J* in Hz)	δ_C	δ_H (*J* in Hz)
1	80.2	4.27 t (3.1)	80.3	4.29 t (3.1)
2	35.6	α: 2.98 dd (17.4, 3.1) β: 2.79 dd (17.4, 2.5)	35.7	α: 2.98 dd (17.2, 3.1) β: 2.75 dd (17.2, 2.2)
3	169.8	-	169.6	-
4	80.0	-	80.1	-
5	53.3	2.55 dd (13.5, 1.9)	53.3	2.56 dd (13.6, 1.9)
6	25.1	α: 1.87 td (14.6, 1.9) β: 1.72 dt (14.6, 3.5)	25.1	α: 1.90 td (14.6, 1.9) β: 1.73 dt (14.6, 3.3)
7	75.1	5.33 t (2.5)	75.3	5.38 t (2.6)
8	44.9	-	44.9	-
9	39.7	3.00 dd (13.5, 4.2)	40.0	3.01 dd (13.5, 4.4)
10	45.4	-	45.4	-
11	31.7	α: 1.99 dd (14.1, 4.2) β: 2.13 td (14.1, 4.9)	30.8	α: 1.97 dd (14.9, 4.4) β: 2.16 td (14.9, 5.6)
12	64.0	4.8 d (4.9)	64.3	4.92 d (5.6)
13	160.9	-	166.0	-
14	45.6	-	45.8	-
15	30.5	β: 2.25 m α: 1.59 ddd (12.9, 5.3, 2.5)	29.0	β: 2.30 dd (13.7, 4.4) α: 1.63 ddd (13.7, 5.4, 2.8)
16	35.3	β: 2.26 m α: 2.50 td (16.2, 5.3)	34.1	β: 2.45 ddd (16.2, 4.4, 3.1) α: 2.50 dd (16.2, 5.4)
17	199.1	-	198.1	-
18	132.7	-	130.0	-
19	85.4	5.16 s	85.0	5.45 s
20	38.7	-	40.6	-
21	43.2	β: 2.26 d (17.5) α: 2.95 d (17.5)	44.4	2.54 br s
22	177.5	-	175.2	-
23	30.6	1.14 s	30.6	1.14 s
24	22.1	1.12 s	21.9	1.12 s
25	66.1	β: 4.60 d (12.7) α: 4.49 d (12.7)	65.9	β: 4.61 d (12.8) α: 4.51 d (12.8)
26	18.8	0.88 s	19.2	0.97 s
27	25.5	1.76 s	25.6	1.74 s
28	31.2	1.29 s	28.1	1.26 s
29	25.2	0.95 s	24.1	0.94 s
1”	129.7	-	129.8	-
2”/ 6”	129.6	8.04 XX'-system	129.7	8.06 XX'-system
3”/ 5”	128.8	7.50 AA'-system	128.8	7.50 AA'-system
4”	133.8	7.63 tt (8.1, 1.5)	133.8	7.63 t (8.0)
7”	164.8	-	164.9	-
OH	-	*	-	*

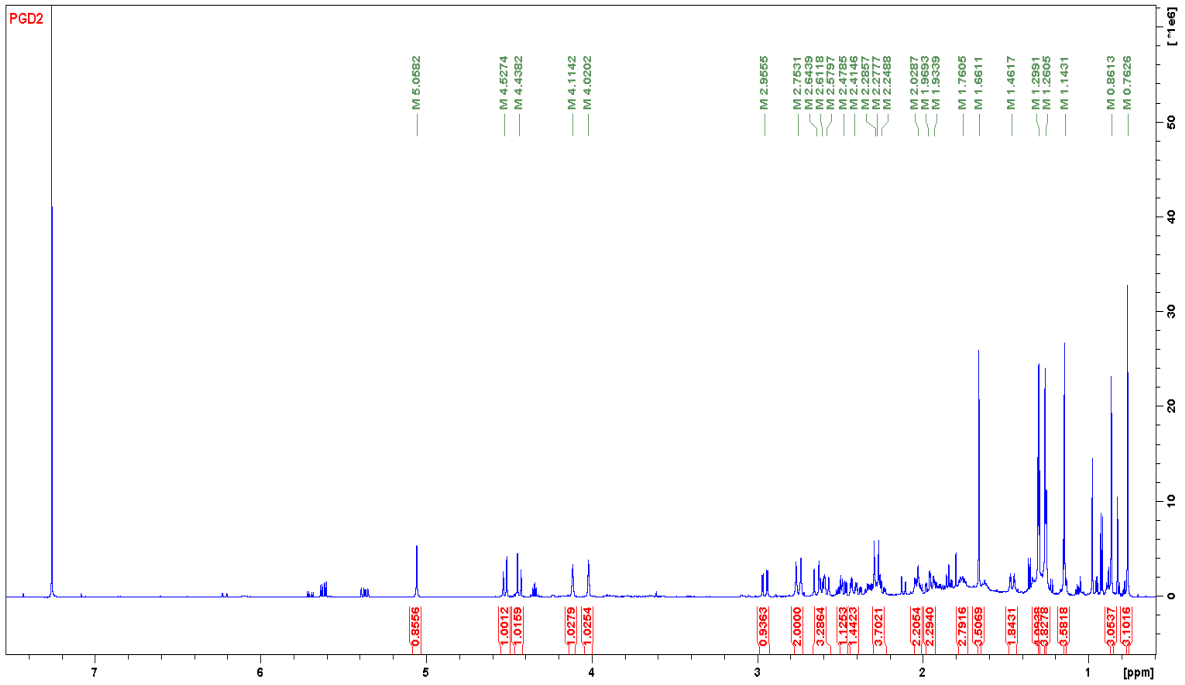

FIGURE 4.56 - ^{1}H NMR spectrum of Picraviane H (**02**) in $CDCl_3$ (600 MHz).

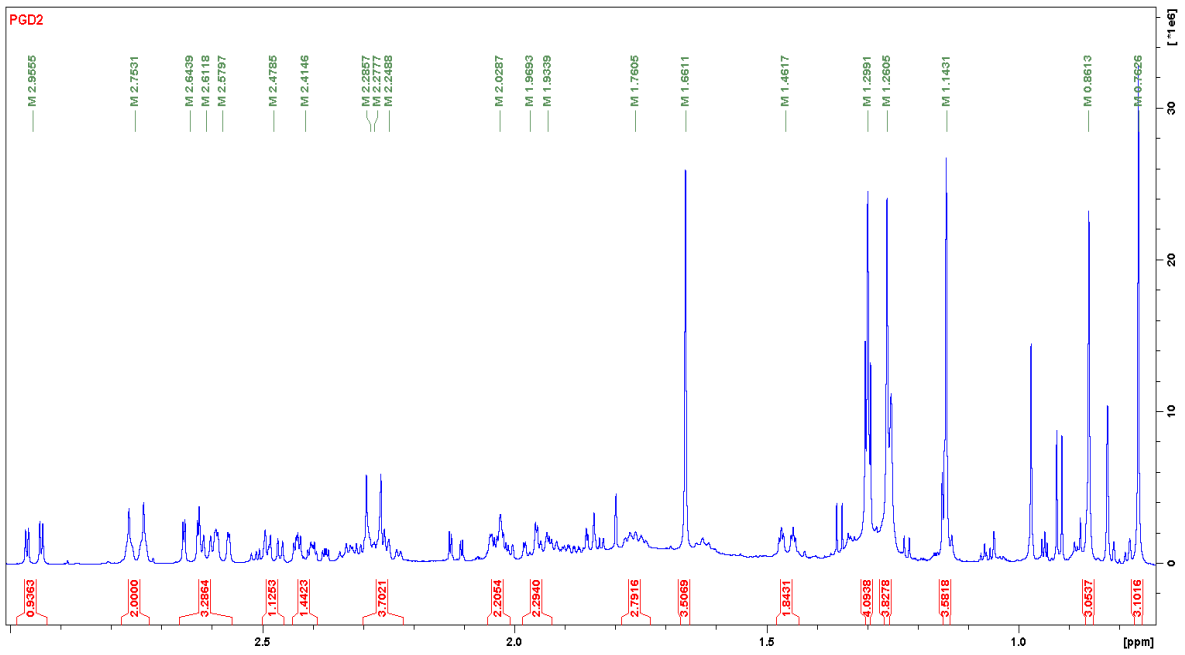

FIGURE 4.57 - Expansion of the ^{1}H NMR spectrum of Picraviane H (**02**) in $CDCl_3$ (600 MHz).

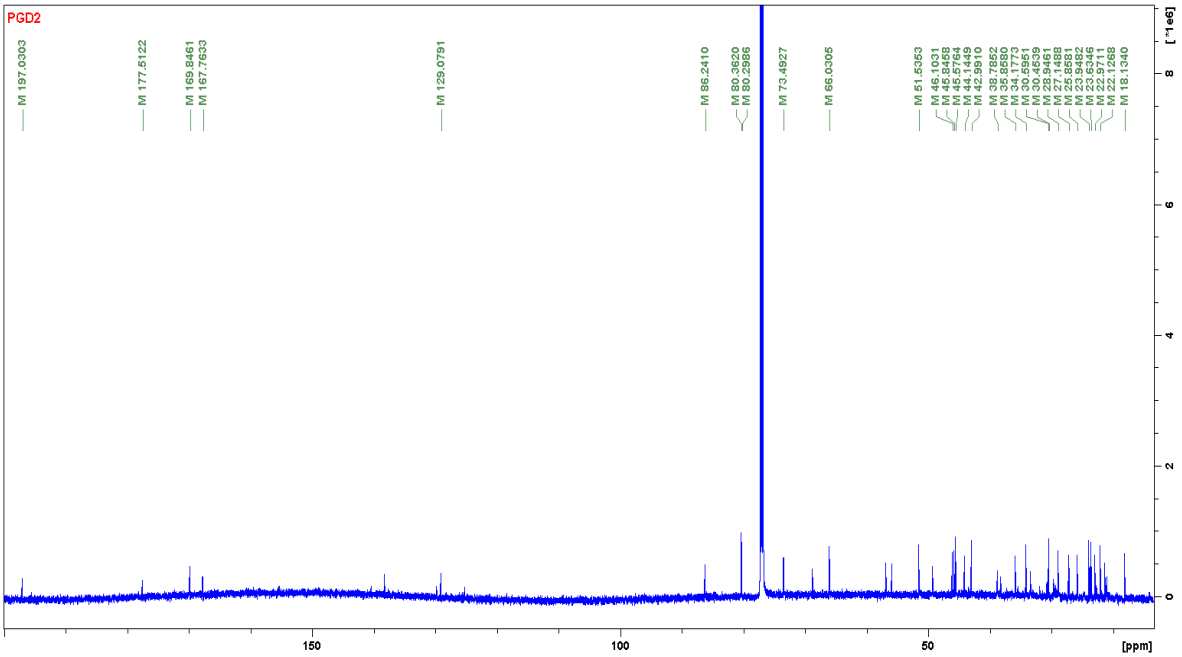

FIGURE 4.58 - ^{13}C NMR spectrum of Picraviane H (**02**) in $CDCl_3$ (150 MHz).

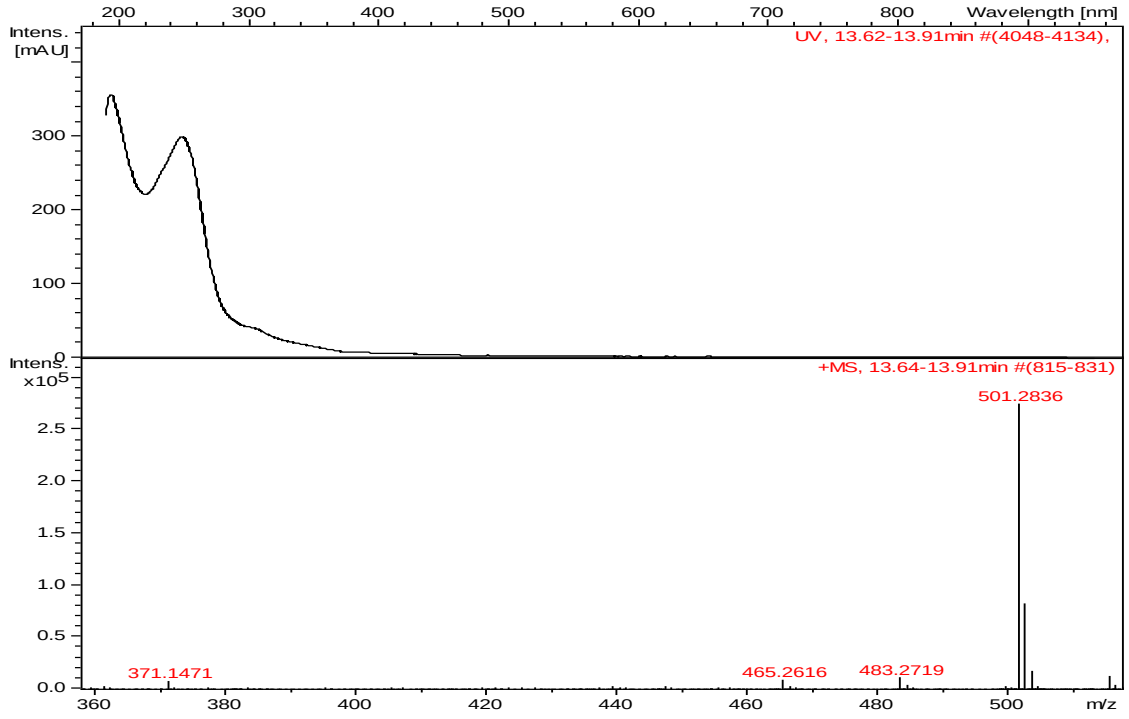

FIGURE 4.59 - HRESIMS spectrum of Picraviane H (**02**) indicating *m/z* $[M+H]^+$ = 501.2836 and $[M+H-H_2O]^+$ = 483.2719.

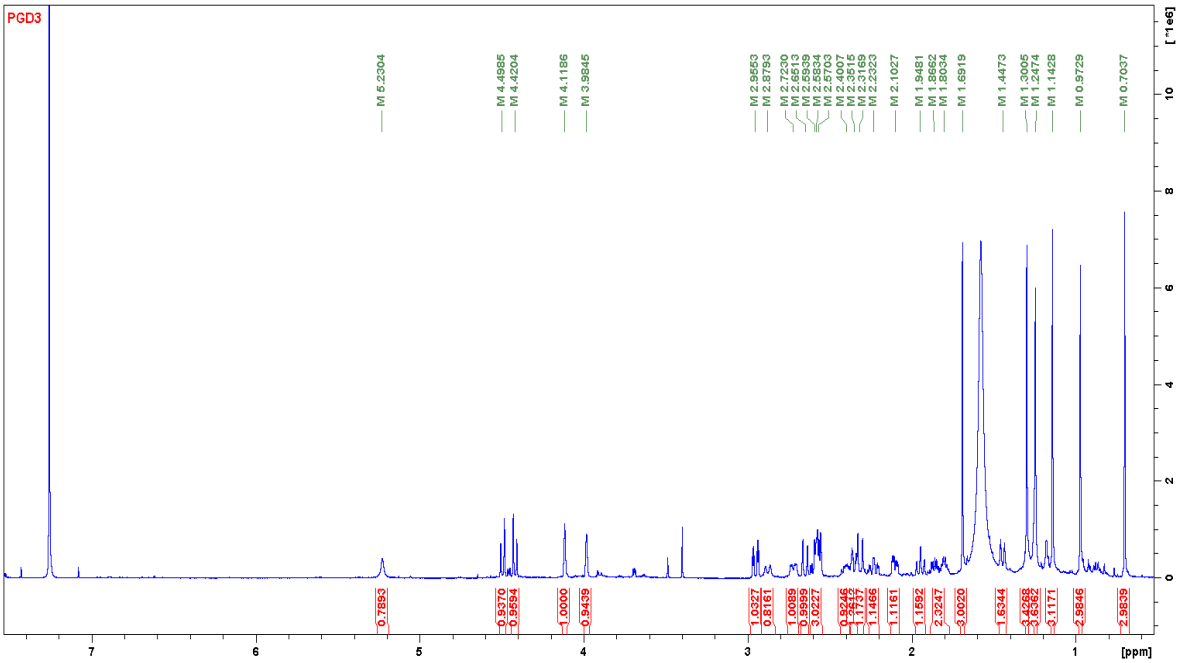

FIGURE 4.60 - ^{1}H NMR spectrum of Picraviane I (**03**) in $CDCl_3$ (600 MHz).

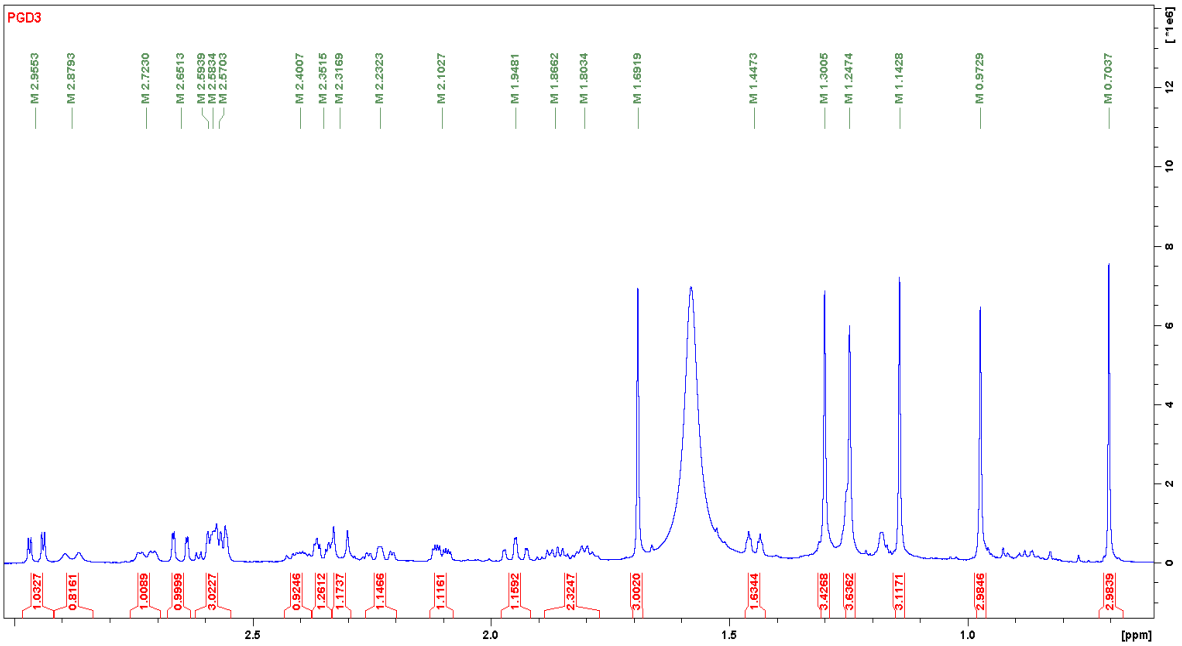

FIGURE 4.61 - Expansion of the ^{1}H NMR spectrum of Picraviane I (**03**) in $CDCl_3$ (600 MHz).

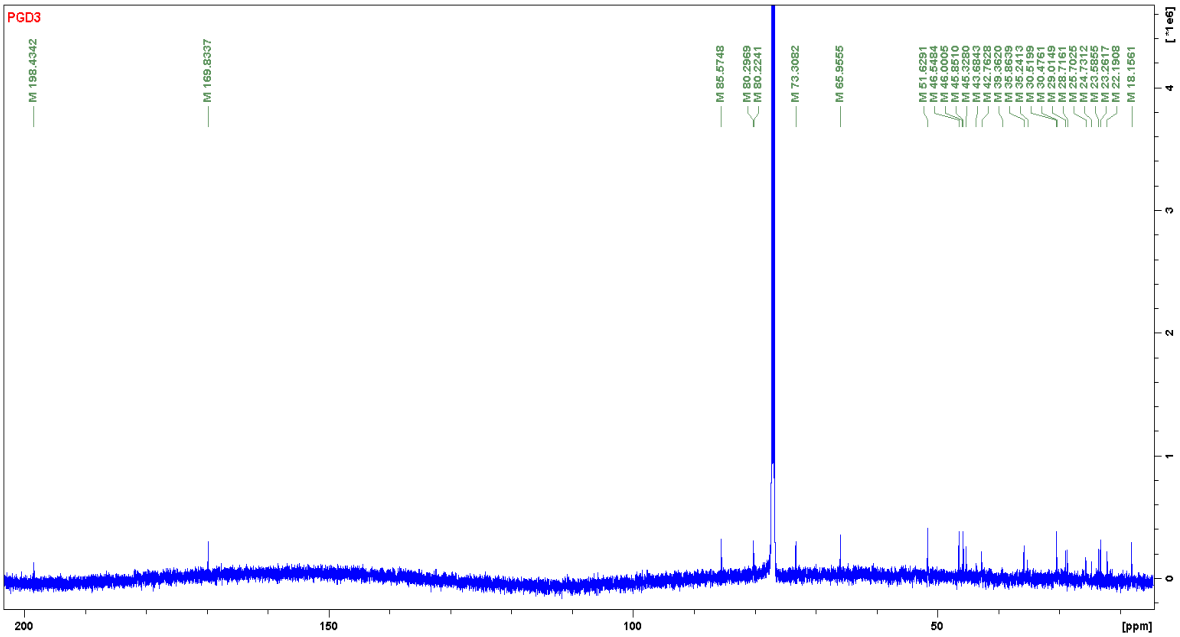

FIGURE 4.62 - ^{13}C NMR spectrum of Picraviane I (**03**) in $CDCl_3$ (150 MHz).

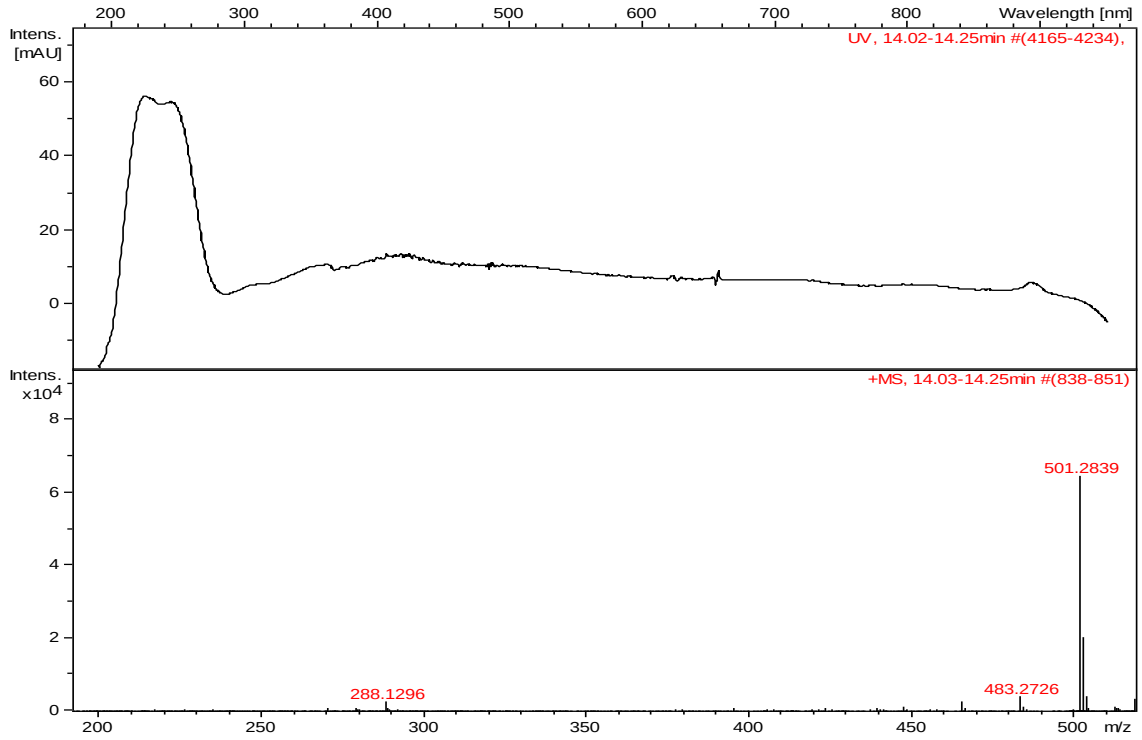

FIGURE 4.63 - HRESIMS spectrum of Picraviane I (**03**) indicating *m/z* $[M+H]^+$ = 501.2839 and $[M+H-H_2O]^+$ = 483.2726.

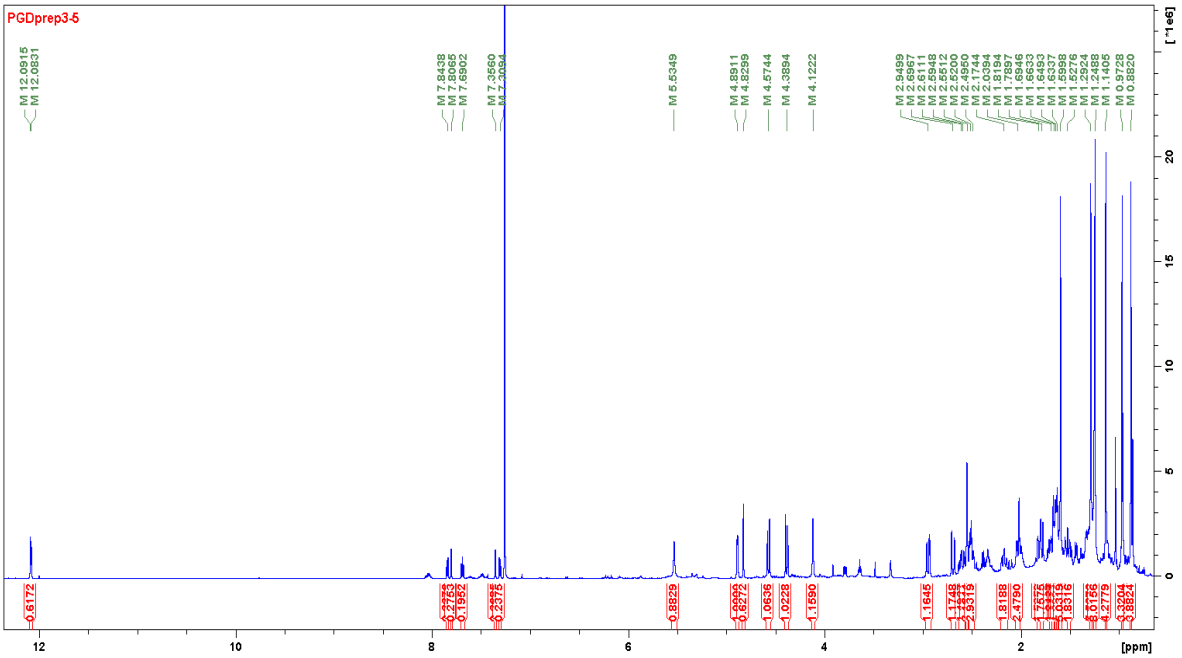

FIGURE 4.64 - ^{1}H NMR spectrum of Picraviane J (**05**) in $CDCl_3$ (600 MHz).

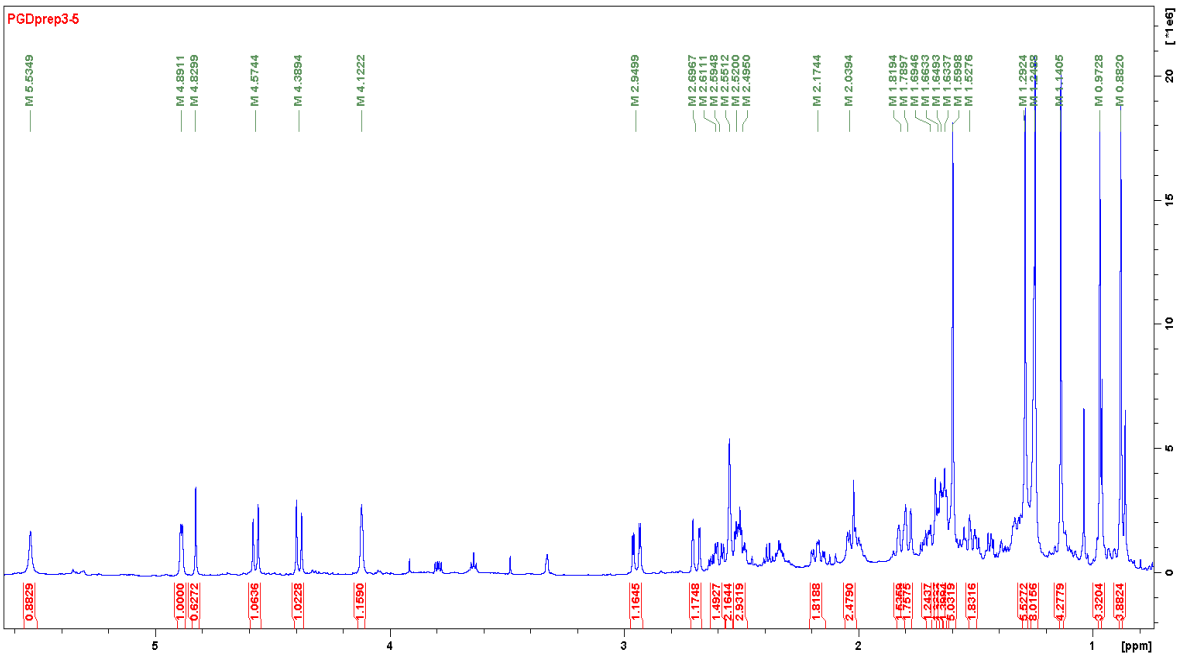

FIGURE 4.65 - Expansion of the ^{1}H NMR spectrum of Picraviane J (**05**) in $CDCl_3$ (600 MHz).

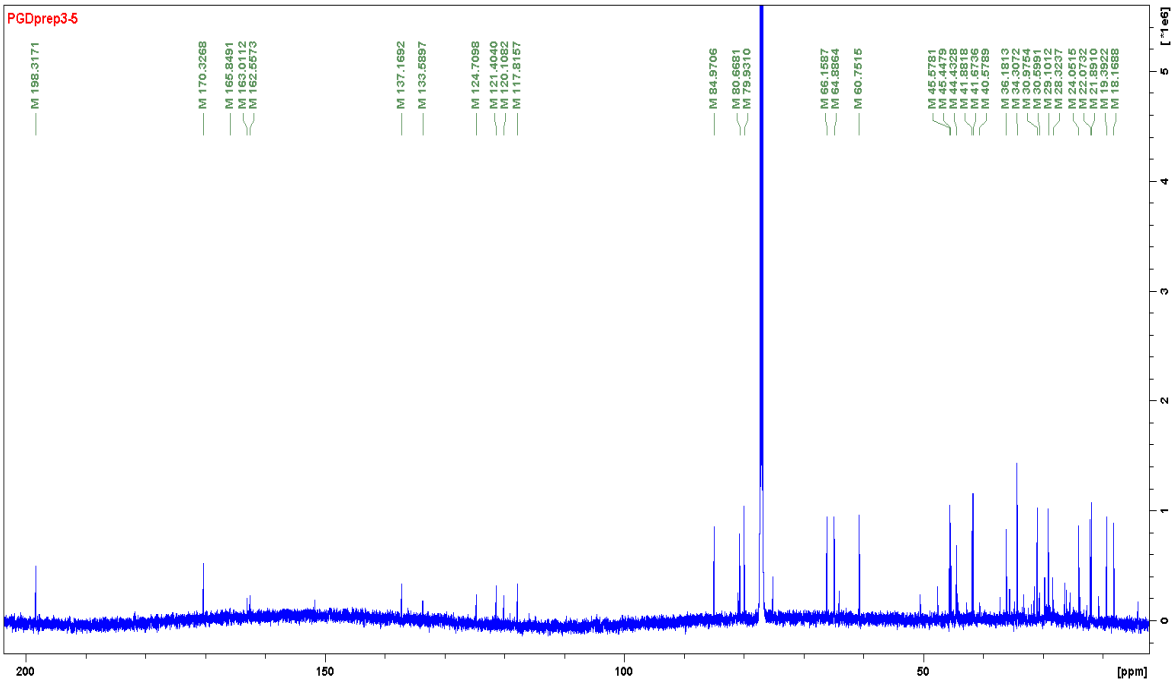

FIGURE 4.66 - ^{13}C NMR spectrum of Picraviane J (**05**) in $CDCl_3$ (150 MHz).

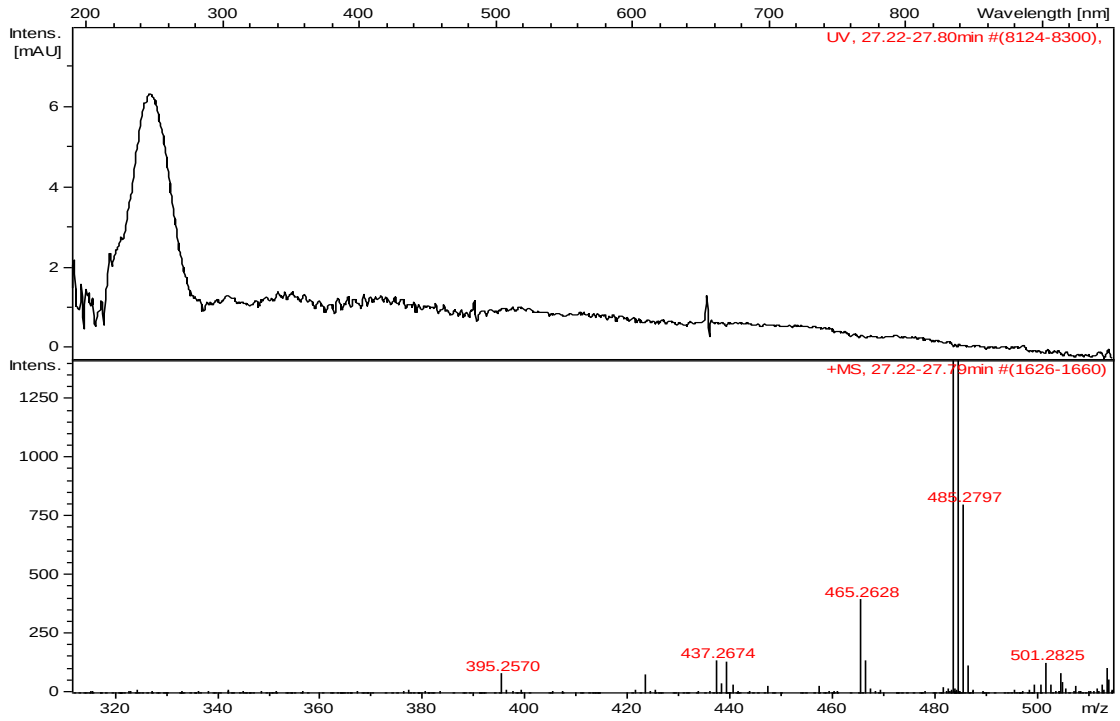

FIGURE 4.67- HRESIMS spectrum of Picraviane J (**05**) indicating *m/z* $[M+H]^+$ = 501.2825.

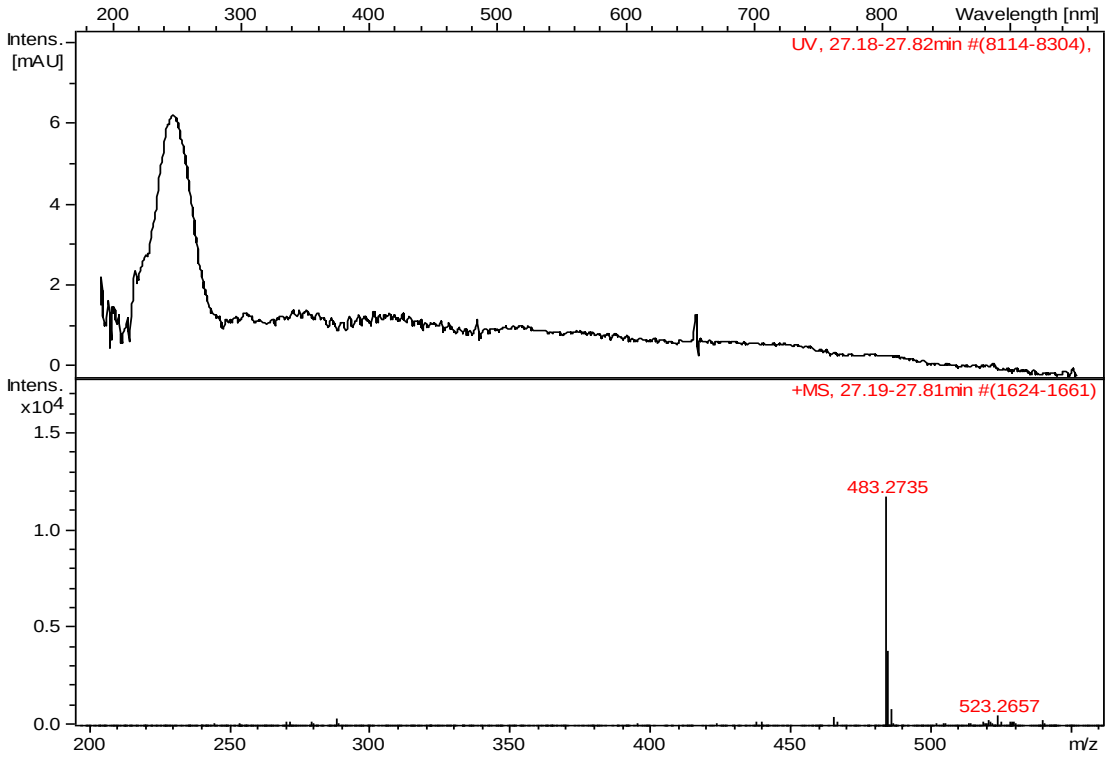

FIGURE 4.68- HRESIMS spectrum of Picraviane J (**05**) indicating *m/z* $[M+Na]^+$ = 523.2657 and *m/z* $[M+H-H_2O]^+$ = 483.2735.

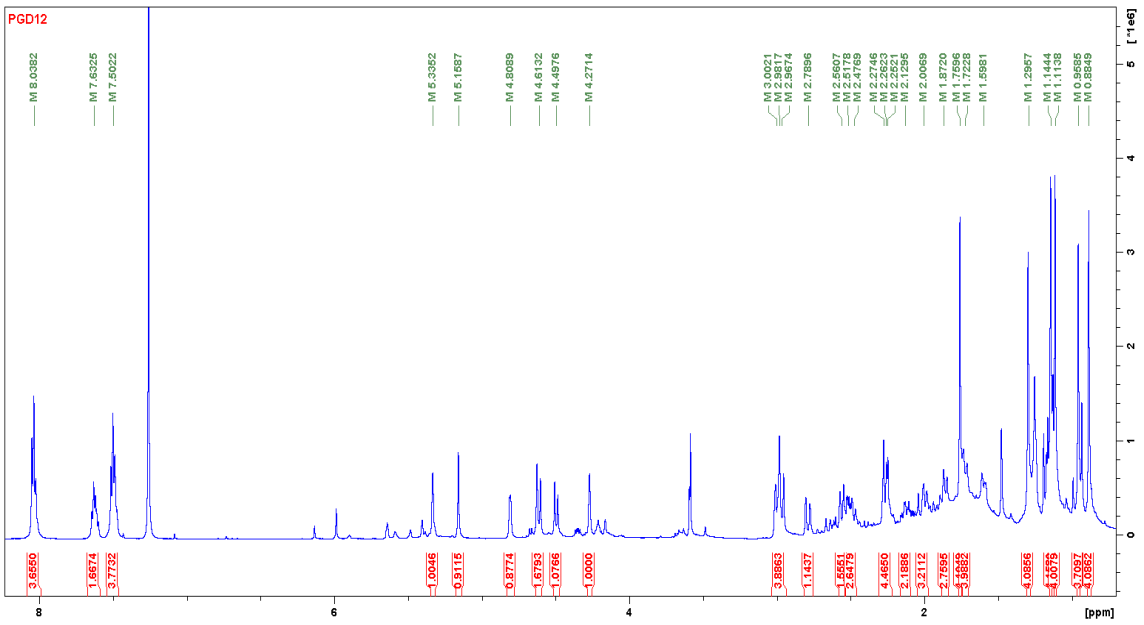

FIGURE 4.69 - ^1H NMR spectrum of Picraviane K (**12**) in $CDCl_3$ (600 MHz).

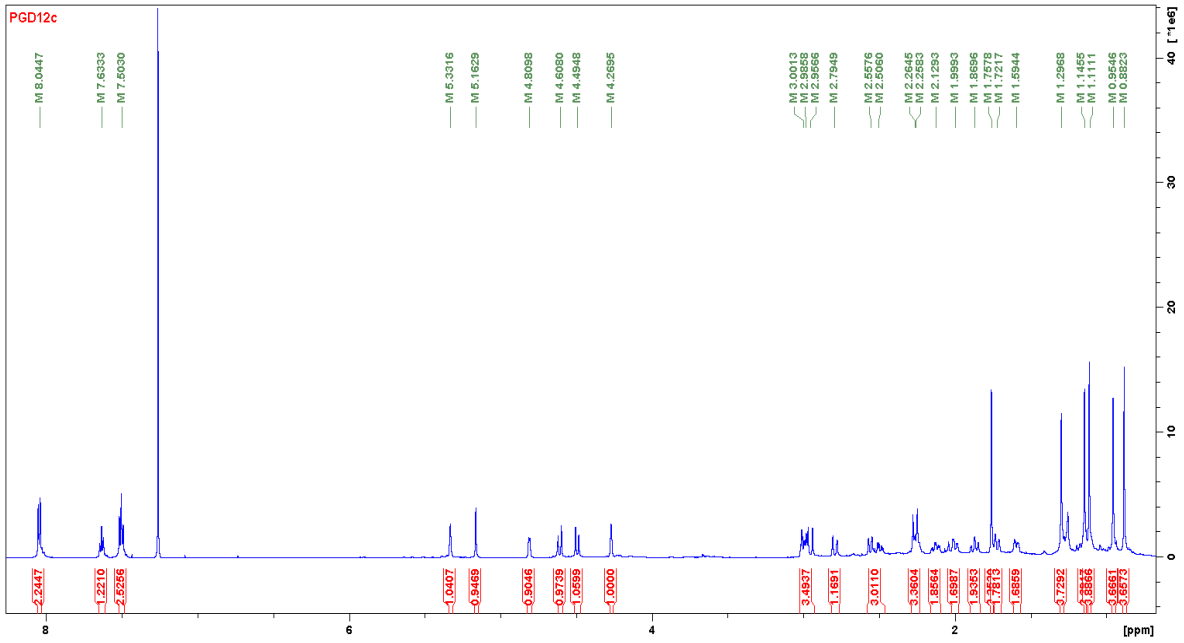

FIGURE 4.70 - ^{1}H NMR spectrum of Picraviane K (**12**) in $CDCl_3$ (600 MHz).

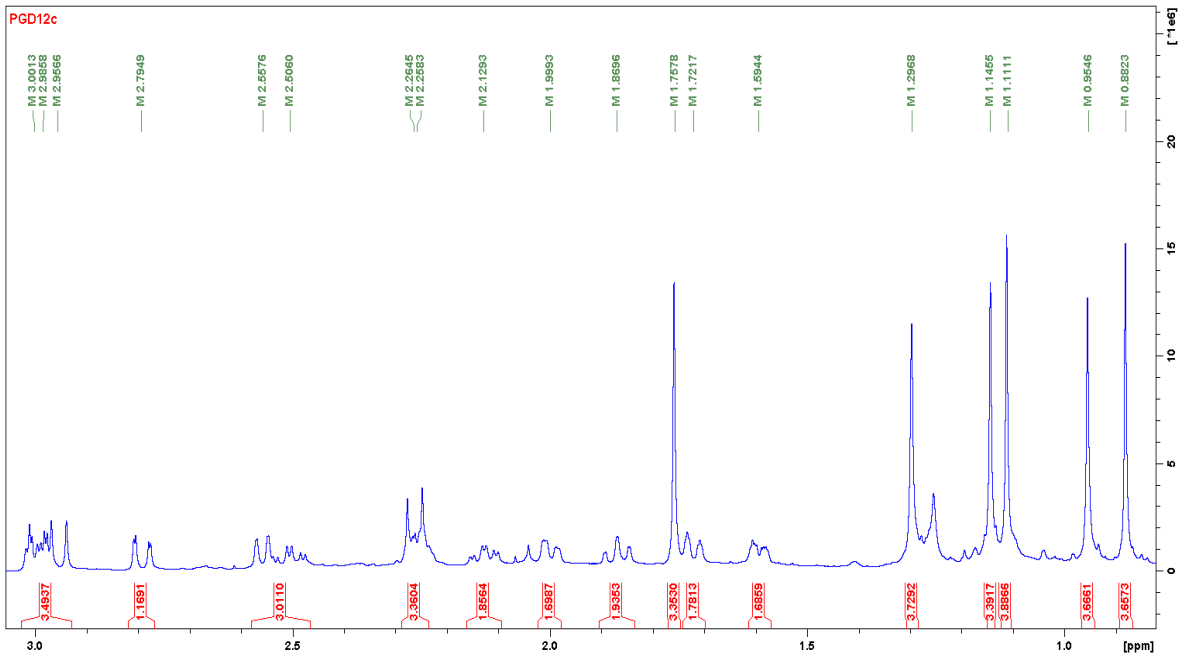

FIGURE 4.71- Expansion of the ^{1}H NMR spectrum of Picraviane K (**12**) in $CDCl_3$ (600 MHz).

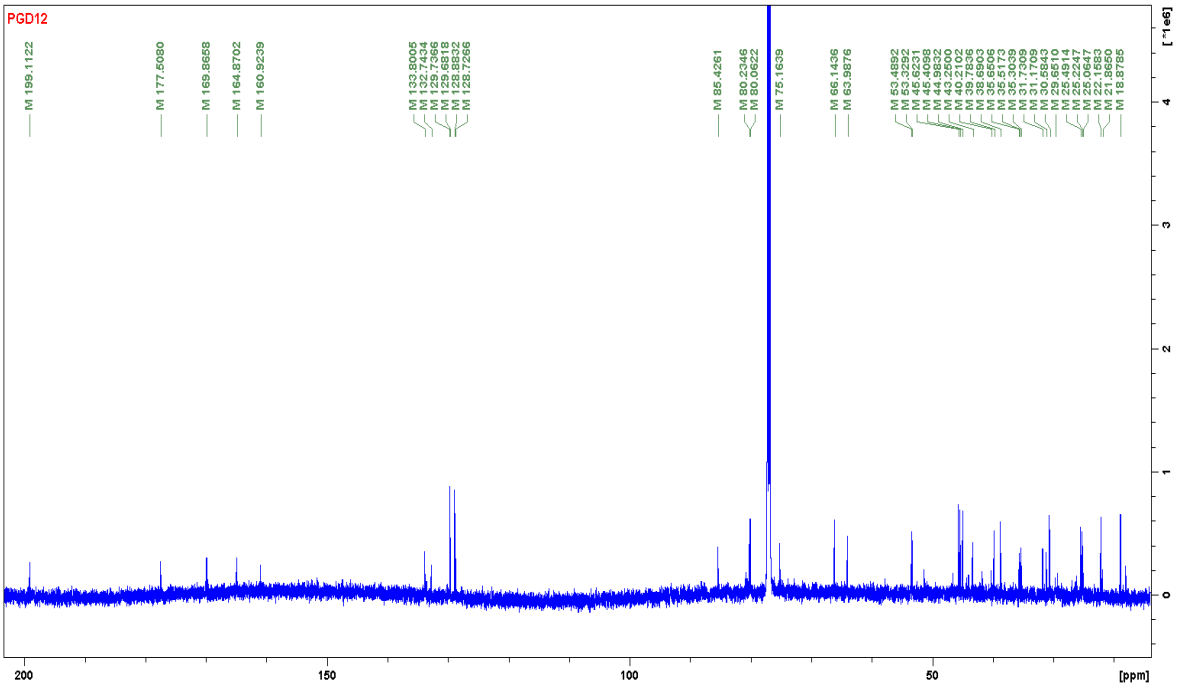

FIGURE 4.72 - ^{13}C NMR spectrum of Picraviane K (**12**) in $CDCl_3$ (150 MHz).

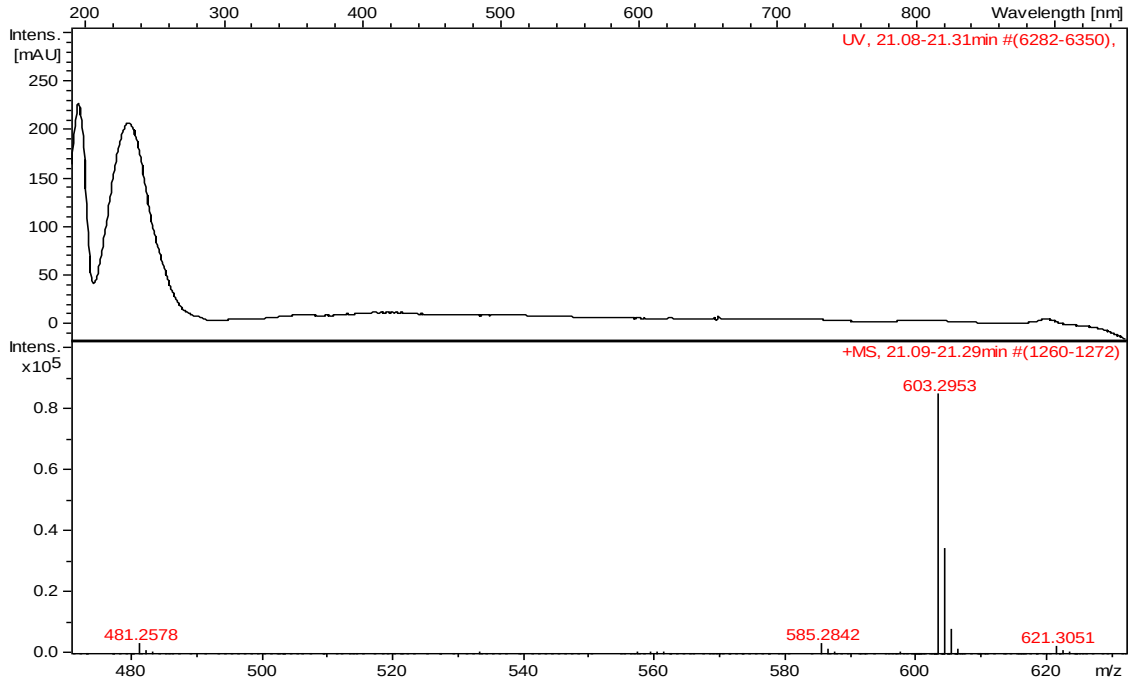

FIGURE 4.73- HRESIMS spectrum of Picraviane K (**12**) indicating *m/z* $[M+H]^+$ = 621.3051; $[M+H-H2O]^+$ = 603.2953 and $[M+H-H2O- C_6H_5CO_2H]^+$ = 481.2598.

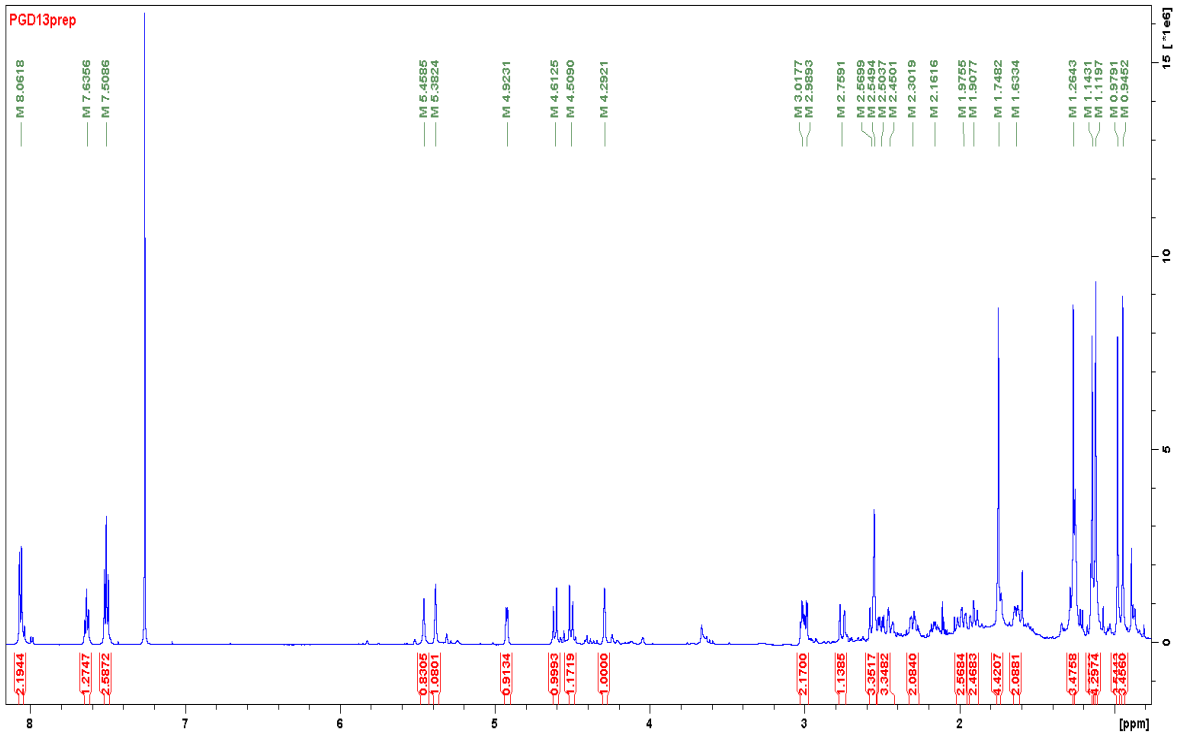

FIGURE 4.74 - ^{1}H NMR spectrum of Picraviane L (**13**) in $CDCl_3$ (600 MHz).

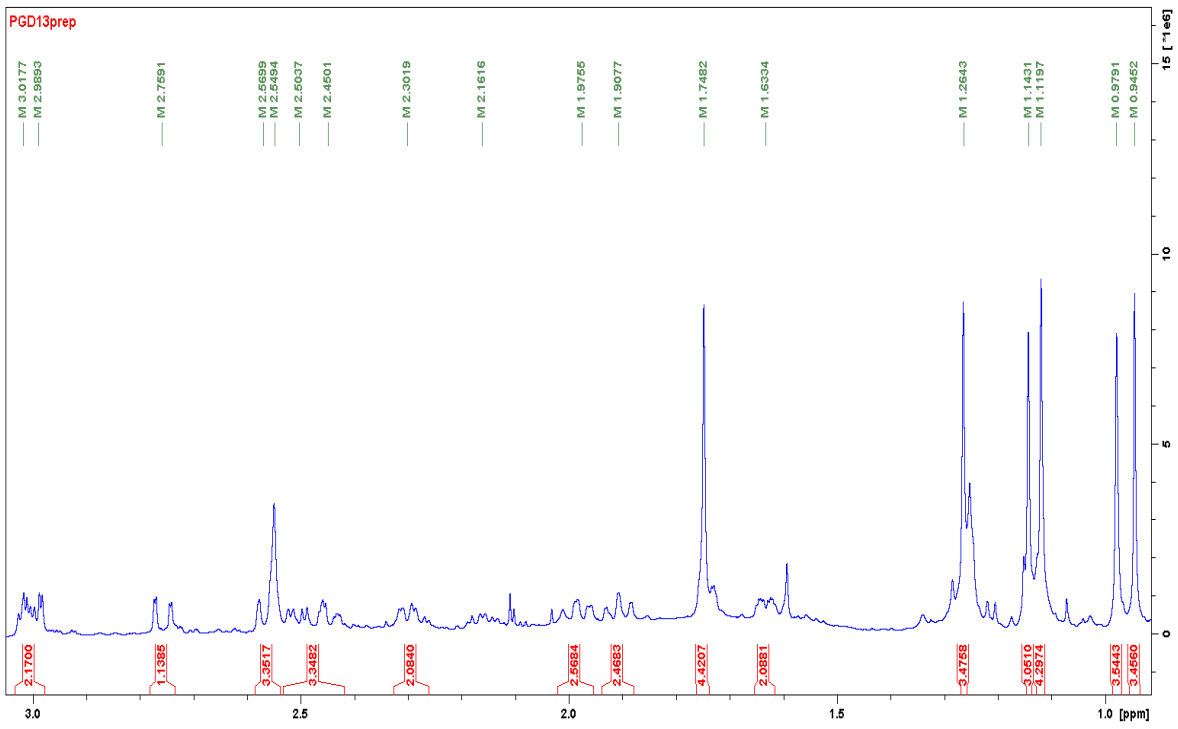

FIGURE 4.75 - Expansion of the ^{1}H NMR spectrum of Picraviane L (**13**) in $CDCl_3$ (600 MHz).

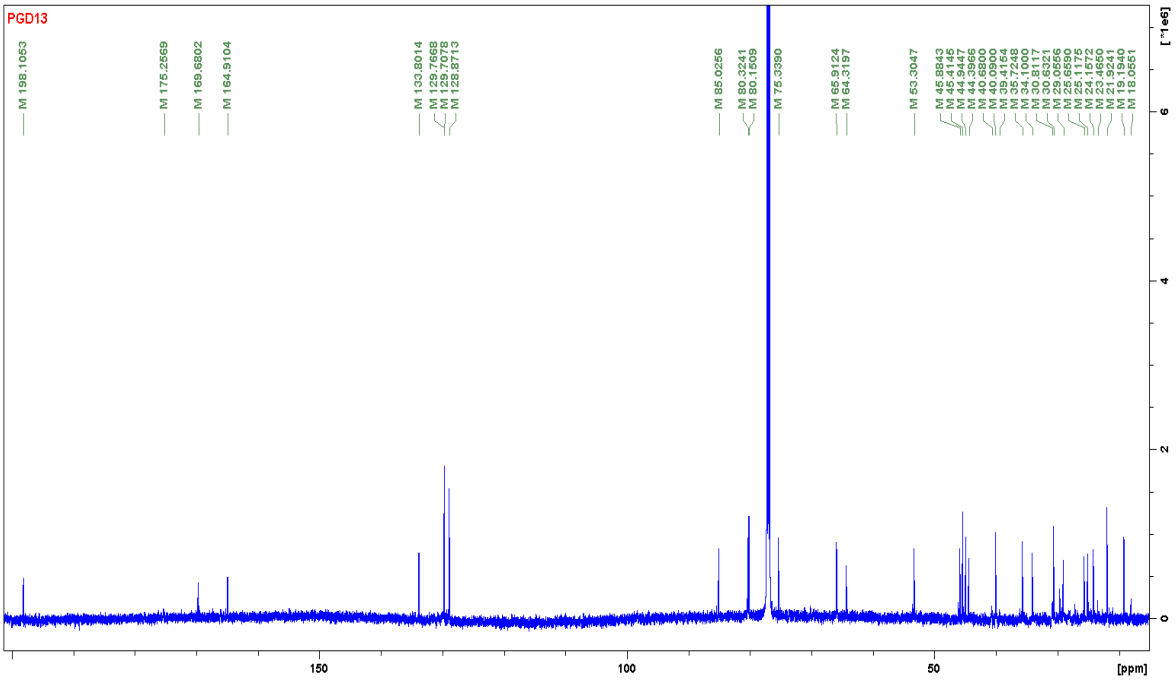

FIGURE 4.76 - ^{13}C NMR spectrum of Picraviane L (**13**) in $CDCl_3$ (150 MHz).

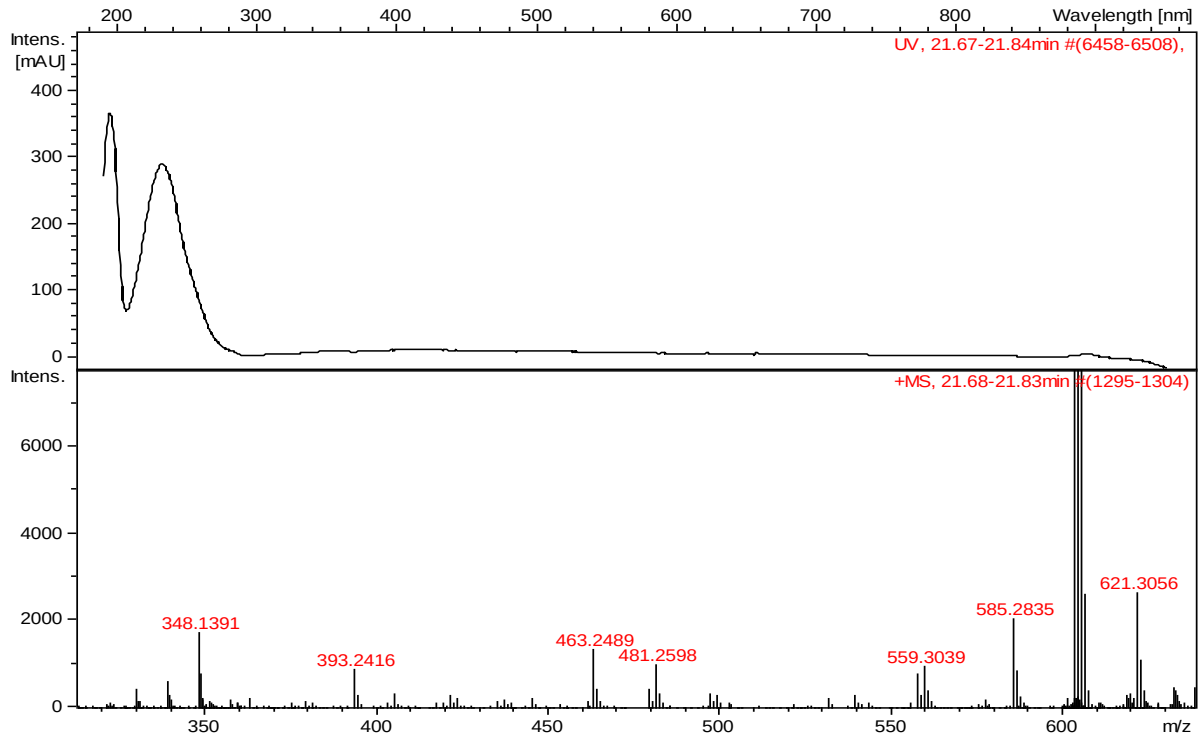

FIGURE 4.77 - HRESIMS spectrum of Picraviane L (**13**) indicating *m/z* $[M+H]^+$ = 621.3056 and $[M+H-H2O- C_6H_5CO_2H]^+$ = 481.2598.

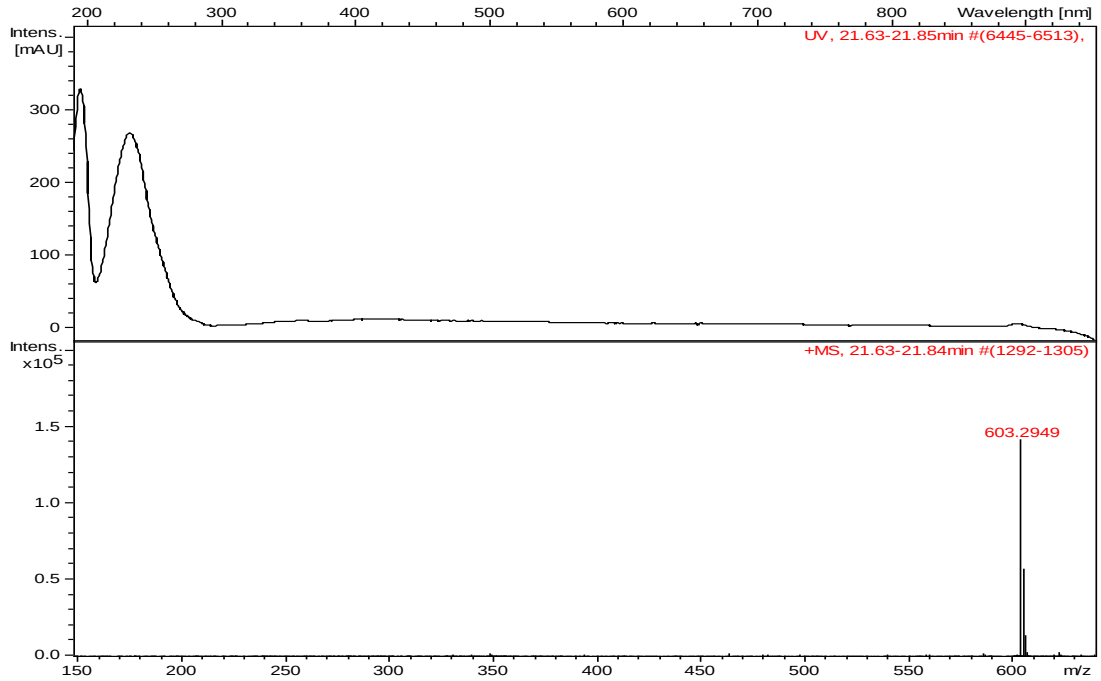

FIGURE 4.78 - HRESIMS spectrum of Picraviane L (**13**) indicating *m/*z $[M+H-H_2O]^+$ = 603.2949.

4.1.1.6 – Nortriterpenes Picravianes M (01), N (07), O (07a), P (14), Q (15), R (16), S (17) and T (22)

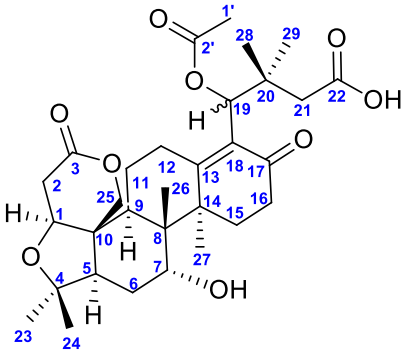

1

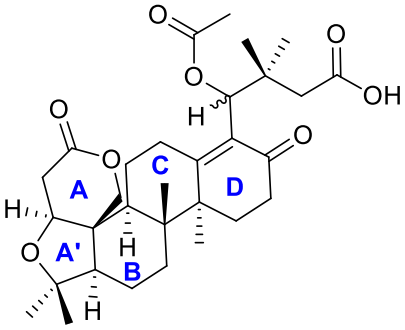

7

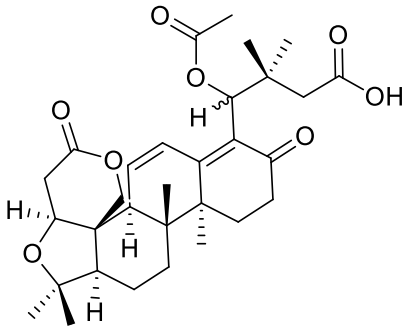

7a

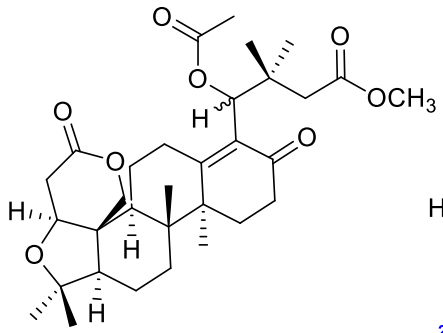

14

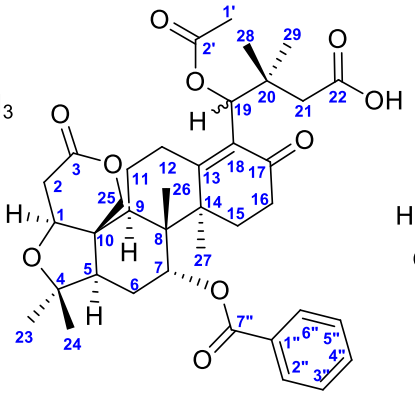

15

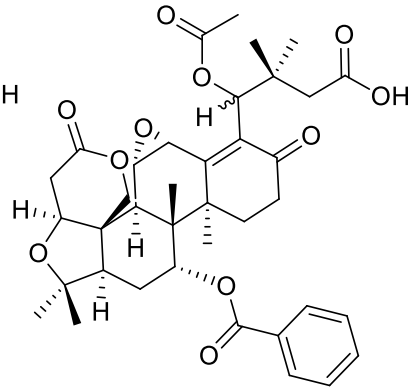

16

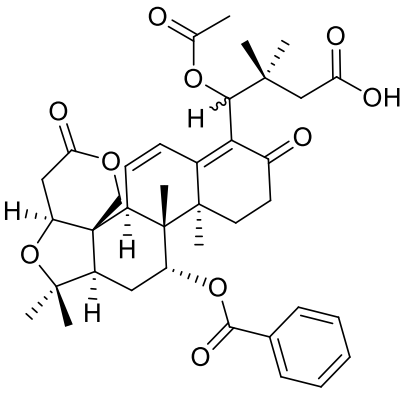

17

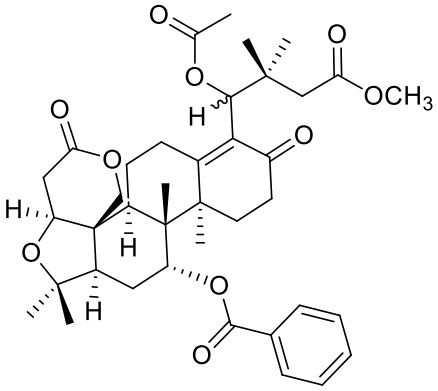

22

Picravianes M (**01**), N (**07**), O (**07a**), P (**14**), Q (**15**), R (**16**), S (**17**) and T (**22**) were elucidated on the basis of spectroscopic data from 1D ^{1}H NMR, ^{13}C NMR as well as 2D NMR experiments (COSY, HSQC, HMBC, NOESY and ROESY, see Supporting Information pages 234, 235, 244 to 247, 256 to 263 and 270 to 271). Likewise to compounds discussed above, the structures showed high similarities in their chemical backbone and among all compounds already described. Therefore, they will be discussed together, highlighting the main difference from each other.

The measure of the optical rotation disclosed the following values:

- Compound **07**: $[\alpha]_{\mathbf{D}}^{\mathbf{25}}$: - 38.58 (c. 0.13, MeOH);
- Compound **14**: $[\alpha]_{\mathbf{D}}^{\mathbf{25}}$: - 31.39 (c. 0.16, MeOH);
- Compound **15**: $[\alpha]_{\mathbf{D}}^{\mathbf{25}}$: - 57.62 (c. 0.24, MeOH);
- Compound **16**: $[\alpha]_{\mathbf{D}}^{\mathbf{25}}$: - 17.09 (c. 0.12, MeOH);
- Compound **17**: $[\alpha]_{\mathbf{D}}^{\mathbf{25}}$: - 83.68 (c. 0.18, MeOH);
- Compound **22**: $[\alpha]_{\mathbf{D}}^{\mathbf{25}}$: - 43.94 (c. 0.16, MeOH).

Due the low amount isolated for compounds **01**, and **07a**, the measured of the optical rotation were not acquired. The infrared spectra acquired to these compounds also need to be repeated, once the spectra presented signals from to the methanol (solvent used to solubilize the samples).

The UV spectrum acquired from the HPLC-HRESIMS disclosed the following absorbances:

- Compound **01** at λ_{max} 194nm and 249 nm;
- Compound **07** at λ_{max} 249 nm;
- Compound **07a** at λ_{max} 196nm and 291 nm;
- Compound **14** at λ_{max} 245 nm.
- Compounds **15** and **16** at λ_{max} 195nm and 235 nm;
- Compound **17** at λ_{max} 196nm, 231 and 288 nm
- Compound **22** at λ_{max} 200nm and 238.

The values are in agreement with the structures proposed since both compounds that present an extension of the conjugated double bond are also those that presented the highest value of the ultraviolet absorbance (compounds **07a** and **17**).

The HRESIMS data for each compound is indicated below:

- Compound **01** m/z $[M+H]^+$ = 561.3044 (calc. for 561.3063), molecular formula as $C_{31}H_{44}O_9$ (10 degrees of unsaturation) and a base peak corresponding to the fragment m/z $[M+H\text{-}CH_3CO_2H]^+$ = 501.2837 (FIGURE 4.81);
- Compound **07**: m/z $[M+H]^+$ = 545.3096 (calc. for 545.3114), molecular formula as $C_{31}H_{44}O_8$ (10 degrees of unsaturation) and a base peak corresponding to the fragment m/z $[M+H\text{-}CH_3CO_2H]^+$ = 485.2892 (FIGURE 4.85);
- Compound **07a**: m/z $[M+H]^+$ = 543.29387 (calc. for 543.2952), molecular formula as $C_{31}H_{42}O_8$ (11 degrees of unsaturation) and a base peak corresponding to the fragment m/z $[M+H\text{-}CH_3CO_2H]^+$ = 483.2735 FIGURES 4.89 and 4.90);
- Compound **14**: m/z $[M+H]^+$ = 559.3237 (calc. for 559.3270), molecular formula as $C_{32}H_{46}O_8$ (10 degrees of unsaturation) and a base peak corresponding to the fragment m/z $[M+H\text{-}CH_3CO_2H]^+$ = 499.3036 (FIGURE 4.94);
- Compound **15**: m/z $[M+H]^+$ = 665.3327 (calc. for 665.3325), molecular formula as $C_{38}H_{48}O_{10}$ (15 degrees of unsaturation) and a base peak corresponding to the fragment m/z $[M+H\text{-}CH_3CO_2H]^+$ = 605.3119 (FIGURE 4.98);
- Compound **16**: m/z $[M+H]^+$ = 679.3114 (calc. for 679.3118), molecular formula as $C_{38}H_{46}O_{11}$ (16 degrees of unsaturation) and a base peak corresponding to the fragment m/z $[M+H\text{-}CH_3CO_2H]^+$ = 619.2885 (FIGURES 4.102 and 4.103);
- Compound **17**: m/z $[M+H]^+$ = 663.3140 (calc. for 663.3169), molecular formula as $C_{38}H_{46}O_{10}$ (16 degrees of unsaturation) and a base peak corresponding to the fragment m/z $[M+H\text{-}CH_3CO_2H]^+$ = 603.2942 (FIGURE 4.107);
- Compound **22**: m/z $[M+H]^+$ = 679.3464 (calc. for 679.3477), molecular formula as $C_{39}H_{50}O_{10}$ (15 degrees of unsaturation) and a base peak corresponding to the fragment m/z $[M+H\text{-}CH_3CO_2H]^+$ = 619.3277 (FIGURE 4.111).

Thus, the discussion to the structure elucidation to the compounds presented below considers firstly, the opening of the pentanolide E system. Afterwards, is presented the discussion about the difference in the backbone for each structure.

The analysis of the mass data showed the base peak corresponding to the fragment losing 60 Da in all compounds, indicating the presence of the acetate unit in all structures. The shielded chemical shift found to the carbonyl carbon C-17 at the range of δ 196 -198 ppm in all compounds (observed by ^{13}C NMR spectrum and/or HMBC correlations) has suggested a conjugated ketone with a double bond,

excluding the possibility to have an heptanolide E ring as observed to compounds **06**, **20** and **23**. The HMBC spectrum to compounds **01**, **07**, **14**, **15**, **16**, **22**, presented correlations from the oxymethine proton H-19 to the carbonyl carbon from the acetate unit (C-2'), supporting the presence and localization of this functional group at C-19. Moreover, further correlations in the HMBC spectrum from H-19 to the carbons C-13, C-17 and C-18 collaborate to the right positioning of this proton close to the enone system in these structures and suggests the opening of the five membered E ring in a carboxylic acid termination (compounds **01**, **07, 15** and **16**) and an ester termination to **14** and **22** due the large singlet at δ 3.66 (δ 51.41) integrating for three protons (in both compounds) that also correlates with C-22 at δ 172.10 (compound **14**) and δ 172.05 (compound **22**) in HMBC spectrum.

The loss of a water molecule $[M+H-CH_3CO_2H-H_2O]^+$ as well as a methanol molecule $[M+H-CH_3CO_2H-CH_3OH]^+$ in the mass spectrum supports the carboxylic acid and ester termination proposed. Moreover, the opening of the pentanolide E system is also in agreement due the absence of correlation in HMBC spectrum from the H-19 to the carbonyl carbon at C-22 (as observed to the compounds presenting the pentanolide E-ring).

Although to compounds **07a** and **17** no correlations were observed from H-19, the presence of acetate unit was clearly observed in the ^{1}H NMR spectrum and confirmed by HRMS data. The positioning of this unit was established according to the analyses of all signals in the whole structure and consequently placed at C-19. These features allowed to stablish the remaining compounds **07a** and **17** also having the opening of the pentanolide E ring.

Once the opened E ring system to all structures has established, the following discussions are given focusing on the B and C rings and the substituents presented for each compound: Thus, the downfield shift to the oxymethine hydrogen at H-7 correlating to the carbonyl carbon in the range of δ 164 ppm in HMBC spectrum, beside the aromatic signals observed in the ^{1}H NMR spectrum from δ 7.50 to 8.10 ppm established the benzoate substituent to **15**, **16**, **17** and **22**. The HMBC correlations from H-7 to C-5 and to the methyl group in C-26 support the positioning of this unit. However, the absence of the benzoate group clearly seen in the ^{1}H NMR spectrum for **01** and the presence of the oxymethine proton at δ 3.98 ppm (δ 73.1 ppm) in association with the spin system to H-5 (δ 2.56) – H-6 (δ 1.96; 1.45) – H-7 (δ 3.98) in COSY spectrum established the positioning of a hydroxyl group at the same

position (C-7). Otherwise, these set of signals and correlations were not seen to compounds **07**, **07a** and **14**, suggesting C-7 as a methylene. The HSQC analyses for each one confirmed this observation: (δ 33.9, compound **07**); (δ 32.4, compound **07a**) and (δ 34.0, compound **14**).

In addition to the mentioned substituents, compounds **07a** and **17** presented an extension of the double bond at C-11 – C-12, whereas compound **16** showed the presence of an epoxide ring replacing this double bond. Since these compounds presented as the most challenging to structural elucidation owing the lack of important signals and correlations in the NMR spectrum, further details and discussions to compounds **17, 07a** and **16** are presented below.

Compound **17** was firstly isolated after trapping using the HPLC-HRMS-SPE/NMR platform, and yielded 0.5 mg of the pure compound. The ^{1}H NMR spectrum displayed two deshielded signals at δ 7.12 ppm (*br s,* H-12) and δ 6.14 ppm (*br d*, 9.2 Hz, H-11) corresponding to the carbons at δ 129.2 ppm and δ 133.3 ppm, respectively, after analyses of the HSQC spectrum. These correlations excluded the possibility of these broad signals being hydroxyl groups, especially due the doublet with large constant ^{3}J observed to H-11 indicating a cis coupling with H-12. The COSY experiment, however, was decisive to establish their position in the structure, allowing connecting these hydrogens in a spin system as H-9 – H-11 – H-12. However, no correlations in HMBC spectrum were observed to H-12, to the oxymethine proton H-19 at δ 5.96 ppm (as mentioned above), and to the methylene protons H-21 at δ 2.33 ppm. Few correlations, on the other hand, were observed to H-11, specifically to the quaternary carbons C-8 and C-13. Thus, aiming to improve the quality of the acquired data and observing those important correlations in the structure, another experiment duplicating the time of acquisition (increasing the number of scans) was performed. However, due the prolonged time of the sample solubilized in $CDCl_3$ after acquisition of all experiments, some decomposition processes was observed occurring to the sample (the same issue also occurred to other compounds, see section 3.5.1.3). Consequently, this compound was isolated again by semi-preparative HPLC, yielding in 1.75 mg of the pure compound. The HMBC spectrum was repeated again with more amount of sample, adjusting the window of acquisition (spectral width and O1P parameters) and also changing the value of the coupling constant CNST 13 to $^{n}J_{C,H}$ = 4 and 12 Hz, beside also acquiring using the default 8 Hz. Unfortunately, even after all these attempts was not possible

to find those specific correlations to the signals mentioned above. These events however, were not a limitation for the full characterization of the structure. The association of all 1D and 2D NMR data, HRMS and UV absorbances supported very well the structure proposed.

Thus, correlations observed in COSY and HMBC spectrum, as mentioned above, established the connectivity between B and C rings. The presence of the ketone was observed in the ^{13}C NMR spectrum at δ 196.5 and supported by the correlations from H-15 and H-16 to C-17 in HMBC. The presence of the benzoate and acetate units as discussed above, were placed at C-7 and C-19, respectively. Moreover, correlations in HMBC has established the C, D, and the opened E system: from the pairs of the methyl groups C-28 and C-29 to the carbons C-19, C-20 and C-21; from each H-9, H-11, H-15 and C-27 to the olefinic carbon at C-13; besides the weak correlation observed from H-19 to C-1' (methyl group from the acetate unit) in HMBC. These results are in agreement with value of the molecular mass found in HRMS and the number of unsaturation index of the formula (16). To conclude, keys correlation in NOESY spectrum from the oxymethine proton H-19 (δ 5.96 ppm) to H-12 (δ 7.12 ppm), H-21 (δ 2.33 ppm) and to the methyl groups H-28 and H-29 (δ 1.04 and 1.08 ppm) were useful supporting the structural elucidation.

The NMR data to compound **07a** was identical to that observed for **17**, except for the absence of signals for the benzoate group as well as the disappearance of the oxymethine proton at C-7 in **17** and the appearance of an additional methylene signal. The ^{1}H NMR spectrum also displayed two deshielded signals at δ 7.09 ppm (*br s,* H-12) and δ 6.10 ppm (*br s*, H-11) corresponding to the carbon at δ 128.6 ppm and δ 133.9 ppm, respectively, by analyses of the HSQC spectrum. An oxymethine proton at δ 6.13 ppm (*br s*, H-19) correlating to the carbon δ 75.6 ppm by HSQC was observed to be overlapped with H-11. None of these signals presented correlations in HMBC spectrum, as reported to compound **17**. However, the structural elucidation was taken on basis to the 1D and 2D NMR spectrum, comparing with those acquired to compound **17**. The HRMS had also an important role supporting the structural proposal. Thus, compound **07a** was suggested to have the same structure as **17**, except for the absence of the benzoate group, which is in agreement with the ^{2}J and ^{3}J HMBC correlations observed from H-5 at *δ* 1.79 to C-6 and C-7 at *δ* 18.1 and *δ* 32.4, respectively.

Compound **16** presented as the most challenging for structural elucidation. The absence of important correlations in HMBC spectrum, very poor ^{13}C NMR spectrum, and extremely broad signals in ^{1}H NMR brought a huge limitation for distinguishing which kind of skeleton belonged to the structure. After isolation of more amount to this compound by semi-preparative HPLC (yield of 1.58 mg), the experiments were acquired again, and better results were achieved after acquisition of a good ^{13}C NMR and HMBC spectrum, which exclude the possibility to have an heptanolide E ring by the confirmation of the presence of a enone system: correlations from H-19 (*δ* 6.14) to C-13 (*δ* 157.2), C-17 (*δ* 195.4) and C-18 (*δ* 137.9) in HMBC spectrum were finally observed. Thus, ^{1}H NMR spectrum disclosed five oxymethine protons. Among these five, three of them were established to benzoate and acetate units (placed at C-7 and C-19 as the description above), and the third relates to the connections between the A and A' rings (C-1). The remaining two oxymethine protons at *δ* 4.34 (*δ* 52.0, C-12) and *δ* 3.63 (*δ* 55.5, C-11) showed correlations each other by COSY spectrum whereas the correlations from H-11 with the proton at *δ* 3.00 (*δ* 44.3, C-9) allowed the assignment of the system H-9 – H-11 – H-12 establishing the connection between B and C ring. Consequently, by the molecular formula $C_{36}H_{46}O_{11}$ and unsaturation index defined to 16, H-11 and H-12 were established to an epoxide ring, enclosing the structure elucidation to this compound.

Compounds **7**, **7a**, **15** and **16** presented several noises after acquisition of their NOESY spectrum (See Supporting Information pages 274 to 275). These compounds also presented very broad signals in the ^{1}H NMR spectrum. Thus, the ROESY experiment was performed to these compounds. Keys correlation in NOESY/ ROESY spectra to all compounds resembled to the relative stereochemistry found in **23** and have followed the same pattern as to the other structures already discussed: H-1 correlating to H-5 and H-9; H-9 correlating to H-5 and H-27 – has established these hydrogens to assume an α orientation. Correlations from H-7 to the methyl group at C-26 (referring to compounds **1**, **15**, **16**, **17** and **22**) assuming consequently, a β orientation. Compound **16** also showed correlations from H-11 and H-12 with H-26, suggesting these hydrogens assuming a β orientation. Further analyses from electronic/vibrational or X-ray experiments should be acquired aiming to confirm all these chiral centers.

The complete assignments of the ^{1}H and ^{13}C to the compounds **01** and **07**; **07a** and **14**; **15** and **16**; and **17** and **22** are given in TABLES 4.9, 4.10, 4.11 and 4.12, respectively. ^{1}H and ^{13}C NMR spectra are shown in FIGURES 4.79 - 4.80 (compound **01**); 4.82 – 4.84 (compound **07**); 4.86 – 4.88 (compound **07a**); 4.91 – 4.93 (compound **14**); 4.95 – 4.97 (compound **15**); 4.99 – 4.101 (compound **16**); 4.104 – 4.106 (compound **17**) and 4.108 – 4.110 (compound **22**).

TABLE 4.9 - ^{13}C and ^{1}H NMR Data for Picravianes M (**01**) and N (**07**) acquired in $CDCl_3$

	01		**07**	
C	δ_C	δ_H (*J* in Hz)	δ_C	δ_H (*J* in Hz)
1	80.2	4.11 br s	80.1	4.05 br s
2	35.7	α: 2.95 dd (17.0, 3.6) β: 2.64 d (17.0)	36.2	α: 2.93 dd (16.8, 3.6) β: 2.64 d (16.8)
3	169.6	-	170.2	-
4	80.3	-	80.9	-
5	51.4	2.56 m	60.7	1.72 d (12.4)
6	28.8	α: 1.96 t (14.4) β: 1.45 d (14.4)	18.0	α: 1.64 m β: 1.53 m
7	73.2	3.98 s	33.9	1.55 m
8	45.1	-	42.1	-
9	42.6	2.58 m	47.0	2.20 d (12.9)
10	45.5	-	45.9	-
11	22.7	β: 1.77 m α: 1.72 m	23.5	β:1.78 dd (4.9, 12.9) α: 1.68 m
12	26.1	β: 3.20 dd (16.8, 4.4) α: 2.18 m	26.9	β: 3.28 d (15.5) α: 2.12 m
13	165.6	-	165.2	-
14	46.6	-	46.1	-
15	27.3	β: 2.14 m α: 2.05 m	27.8	β: 2.04 m α: 1.57 m
16	33.6	β: 2.57 m α: 2.43 m	33.9	2.45 m
17	197.3	-	197.1	-
18	129.5	-	131.3	-
19	76.4	5.75 s	75.7	5.84 s
20	37.7	-	37.8	-
21	43.4	β: 2.32 d (13.5) α: 2.38 d (13.5)	44.7	β: 2.32 d (13.4) α: 2.39 d (13.4)
22	173.6	-	174.4	-
23	30.4	1.29 s	30.9	1.28 s
24	21.8	1.14 s	21.7	1.13 s
25	65.7	β: 4.49 d (12.9) α: 4.43 d (12.9)	66.0	β: 4.52 d (12.7) α: 4.39 d (12.7)
26	17.9	0.75 s	18.1	0.87 s
27	23.4	1.60 s	19.4	1.34 s
28	23.9	1.08 s	24.0	1.15 s
29	23.5	1.15 s	24.1	1.07s
1´	20.2	2.01 s	20.5	2.01 s
2’	169.1	-	169.8	-
OH	-	*	-	*

Carbon assigned based on HMBC and HSQC experiments to Compound **01**
* Not detected signals

TABLE 4.10 - ^{13}C and ^{1}H NMR Data for Picravianes O (**07a**) and P (**14**) acquired in $CDCl_3$

	7a		**14**	
C	δ_C	δ_H (*J* in Hz)	δ_C	δ_H (*J* in Hz)
1	79.7	4.13 br s	80.1	4.04 br s
2	36.5	α: 3.04 d (16.3) β: 2.78 d (16.3)	36.1	α: 2.94 dd (16.8, 3.5) β: 2.63 d (16.8)
3	170.0	-	170.1	-
4	80.7	-	80.9	-
5	60.2	1.79 d (12.8)	60.7	1.72 d (12.4)
6	18.1	α: 1.71 d (12.8) β: 1.60 m	18.0	α: 1.64 m β: 1.53 m
7	32.4	1.54 m α: 1.48 d (12.2)	34.0	1.55 m
8	42.6	-	42.1	-
9	51.5	2.64 br s	47.0	2.19 d (12.9)
10	45.1	-	45.8	-
11	133.9	6.10 br s	23.5	β:1.77 dd (4.3, 12.9) α: 1.68 m
12	128.6	7.09 br s	26.8	β: 3.27 d (14.8) α: 2.12 m
13	156.9	-	163.9	-
14	43.6	-	46.1	-
15	25.7	β: 2.06 m α: 1.56 m	27.9	β: 2.04 m α: 1.57 m
16	33.2	β: 2.58 m α:2.53 m	33.9	2.45 m
17	196.8	-	196.5	-
18	*	-	131.3	-
19	75.6	6.13 br s	76.4	5.82 s
20	38.9	-	38.1	-
21	44.3	2.31 m	43.9	β: 2.31 d (13.1) α: 2.36 m
22	*	-	172.1	-
23	30.5	1.29 s	30.9	1.28 s
24	21.5	1.13 s	21.7	1.13 s
25	67.5	β: 4.57 d (12.8) α: 4.19 d (12.8)	66.0	β: 4.52 d (12.9) α: 4.39 d (12.9)
26	17.0	0.83 s	18.1	0.87 s
27	17.7	1.15 s	19.4	1.34 s
28	24.3	0.99 s	24.0	1.03 s
29	24.4	1.05 s	23.7	1.11 s
1′	20.8	2.03 s	20.5	2.01 s
2′	169.5	-	169.3	-
OCH_3	-	-	51.4	3.66 s
OH	-	*	-	-

* Not detected signals

TABLE 4.11- ^{13}C and ^{1}H NMR Data for Picravianes Q (**15**), R (**16**) acquired in $CDCl_3$

	15		**16**	
C	δ_C	δ_H (*J* in Hz)	δ_C	δ_H (*J* in Hz)
1	80.5	4.23 s	80.3	4.43 s
2	35.9	β: 2.98 d (16.4) α: 2.70 d (16.4)	35.8	β: 3.09 d (16.7) α: 2.91 d (16.7)
3	169.8	-	169.5	-
4	80.5	-	80.3	-
5	53.5	2.48 d (13.0)	52.9	2.44 d (14.0)
6	24.8	α: 1.93 t (14.1) β: 1.73 d (14.1)	24.7	α: 2.04 m β: 1.77 d (12.4)
7	75.2	5.30 s	73.5	5.23 s
8	45.2	-	45.3	-
9	44.4	2.74 d (12.4)	44.3	3.00 br s
10	45.7	-	45.1	-
11	23.0	β: 1.86 d (12.4) α: 1.80 m	55.5	3.63 br s
12	26.3	β: 3.26 d (14.0) α: 2.16 m	52.0	4.34 br s
13	164.5	-	157.2	-
14	46.3	-	43.2	-
15	28.1	β: 2.18 m α: 1.54 m	27.6	β: 2.20 m α: 1.45 m
16	33.6	2.35 m	33.1	2.51 m
17	196.7	-	195.4	-
18	130.0	-	137.9	-
19	76.3	5.78 br s	74.9	6.14 br s
20	37.9	-	37.9	-
21	44.2	2.32 m	44.8	2.30 m
22	176.3	-	176.5	-
23	30.6	1.12 s	30.3	1.14 s
24	21.6	1.09 s	21.4	1.12 s
25	65.8	β: 4.55 d (12.8) α: 4.50 d (12.8)	66.8	β: 4.66 d (12.8) α: 4.53 d (12.8)
26	18.1	0.92 s	19.3	1.03 s
27	24.2	1.48 s	23.5	1.42 s
28	23.9	1.12 s	24.7	1.10 s
29	24.2	1.04 s	24.6	0.98 s
1´	20.3	1.98 s	20.8	2.02 s
2’	169.4	-	169.7	-
1”	129.8	-	129.5	-
2”/ 6”	129.6	8.03 XX'-system	129.6	8.00 XX'-system
3”/ 5”	128.8	7.61 AA'-system	128.9	7.61 AA'-system
4”	133.7	7.48 t (8.5)	133.9	7.48 t (8.7)
7”	164.8	-	164.8	-
OH	-	*	-	*

* Not detected signals

TABLE 4.12 - ^{13}C and ^{1}H NMR Data for Picravianes S (**17**) and T (**22**) acquired in $CDCl_3$

	17		**22**	
C	δ_C	δ_H (*J* in Hz)	δ_C	δ_H (*J* in Hz)
1	80.1	4.35 d (3.5)	80.5	4.23 br s
2	36.5	β: 3.11 dd (16.7, 3.5) α: 2.85 dd (16.7, 1.2)	35.9	α: 2.99 dd (16.9, 3.3) β: 2.69 d (16.9)
3	169.7	-	169.6	-
4	80.4	-	80.6	-
5	53.2	2.51 dd (13.9, 2.1)	53.52	2.49 d (13.5)
6	24.9	α: 2.07 td (15.2, 2.1) β: 1.80 dt (15.2, 3.4)	24.9	α: 1.93 t (15.1) β: 1.75 d (15.1)
7	74.0	5.32 s	75.2	5.30 s
8	44.9	-	45.2	-
9	48.9	3.24 br s (3.6)	44.4	2.74 d (10.9)
10	45.3	-	45.7	-
11	133.3	6.14 br d (9.2)	23.1	β:1.87 d (12.6) α: 1.80 m
12	129.2	7.12 br s	26.2	β: 3.26 d (15.4) α: 2.17 m
13	156.6	-	163.7	-
14	44.5	-	46.3	-
15	25.5	β: 2.18 dt (13.5, 8.9) α: 1.54 dt (13.5, 4.8)	28.1	β: 2.18 m α: 1.55 m
16	33.0	2.47 m	33.7	2.37 m
17	196.5	-	196.3	-
18	131.1	-	130.2	-
19	75.7	5.96 br s	76.6	5.72 s
20	38.9	-	38.0	-
21	44.1	2.33 m	43.9	β: 2.31 d (13.3) α: 2.37 m
22	176.5	-	172.1	-
23	30.2	1.16 s	30.6	1.14 s
24	21.3	1.12 s	21.7	1.10 s
25	67.3	β: 4.60 d (13.1) α: 4.25 d (13.1)	65.8	β: 4.56 d (13.3) α: 4.51 d (13.3)
26	18.0	0.93 s	18.2	0.93 s
27	20.8	1.37 s	24.2	1.49 s
28	24.4	1.04 s	23.9	1.04 s
29	24.3	1.08 s	23.7	1.11 s
1´	20.8	2.03 s	20.4	2.00 s
2’	169.5	-	169.2	-
1”	129.7	-	129.9	-
2”/ 6”	129.6	8.04 XX'-system	129.6	8.04 XX'-system
3”/ 5”	128.9	7.50 AA'-system	128.8	7.49 AA'-system
4”	133.8	7.64 tt (8.1, 1.2)	133.8	7.63 t (8.2)
7”	164.9	-	164.8	-
OCH_3	-	-	51.4	3.66 s
OH	-	*	-	-

* Not detected signal

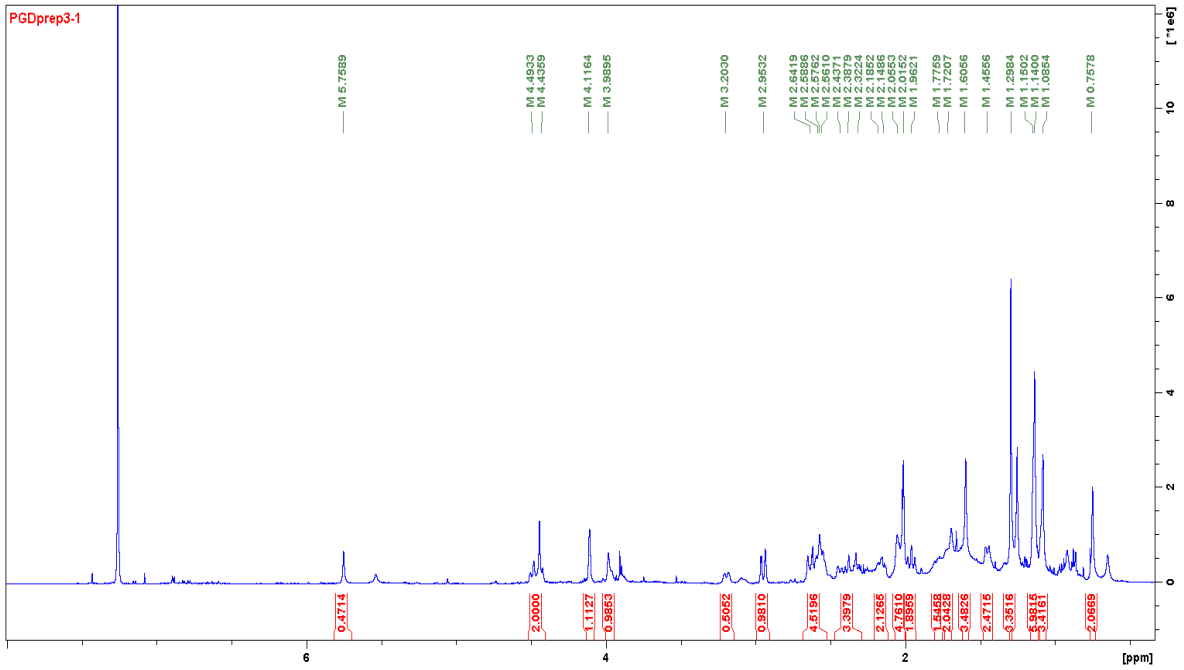

FIGURE 4.79 - ^{1}H NMR spectrum of Picraviane M (**01**) in $CDCl_3$ (600 MHz).

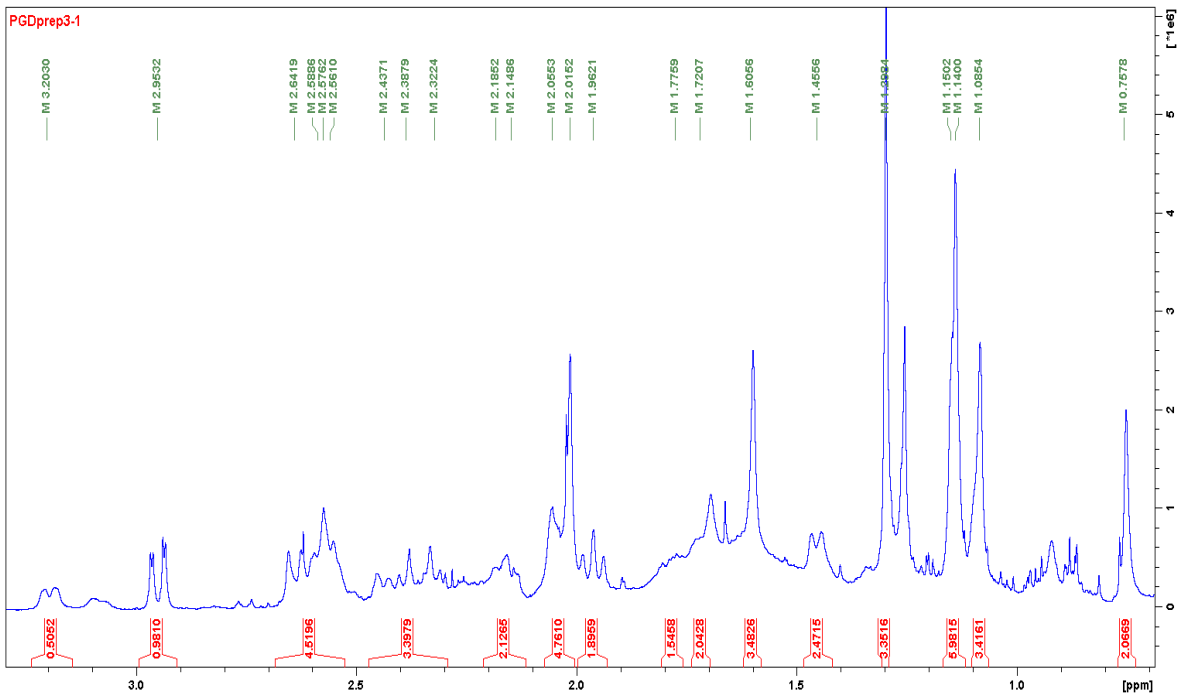

FIGURE 4.80 - Expansion of the ^{1}H NMR spectrum of Picraviane M (**01**) in $CDCl_3$ (600 MHz).

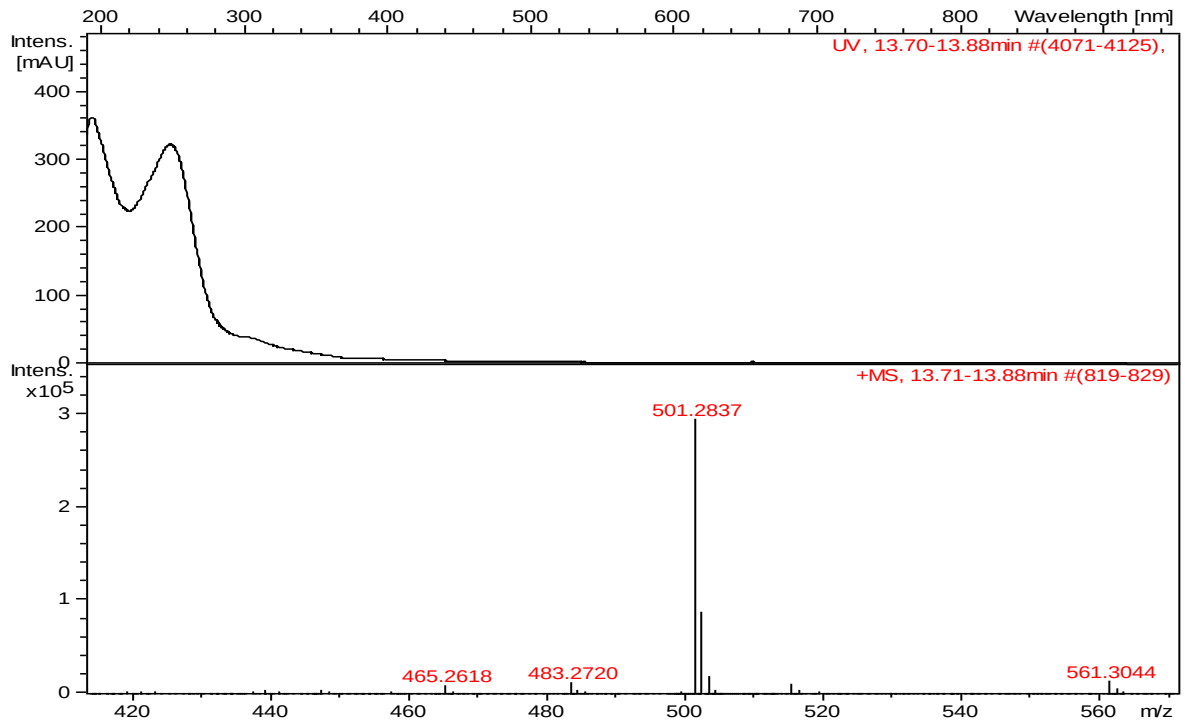

FIGURE 4.81 - HRESIMS spectrum of Picraviane M (**01**) indicating *m/z* $[M+H]^+$ = 561.3044; $[M+H\text{-}CH_3CO_2H]^+$ = 501.2837 and $[M+H\text{-}H_2O]^+$ = 483.2720.

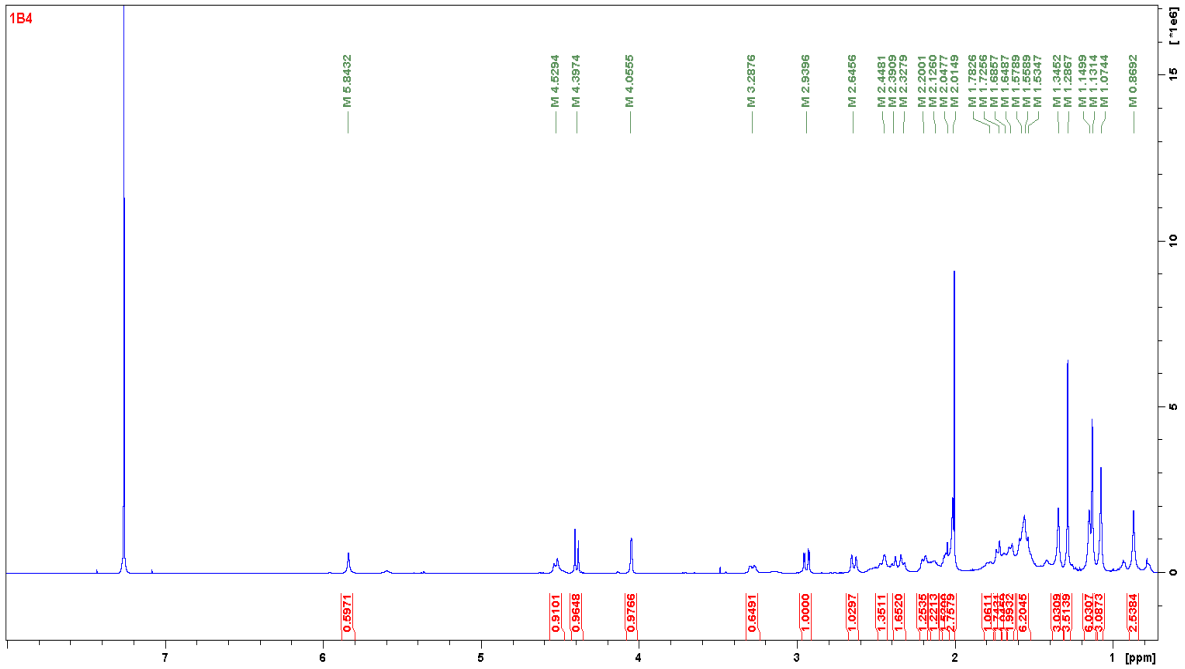

FIGURE 4.82 - ^1H NMR spectrum of Picraviane N (**07**) in $CDCl_3$ (600 MHz).

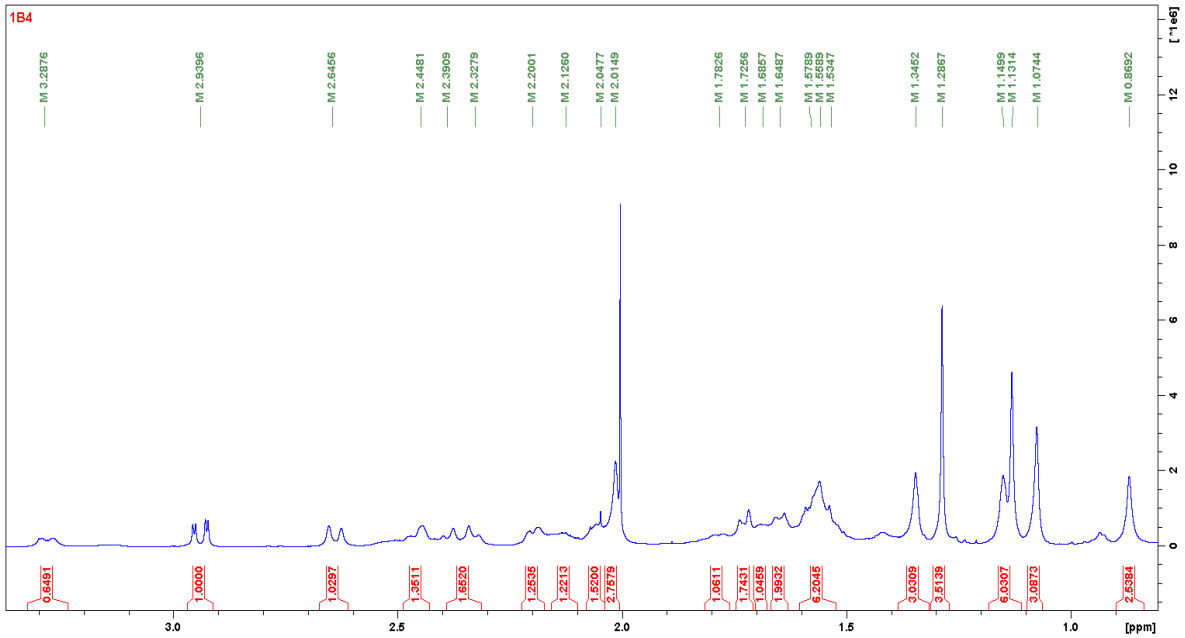

FIGURE 4.83 - Expansion of the ^{1}H NMR spectrum of Picraviane N (**07**) in $CDCl_3$ (600 MHz).

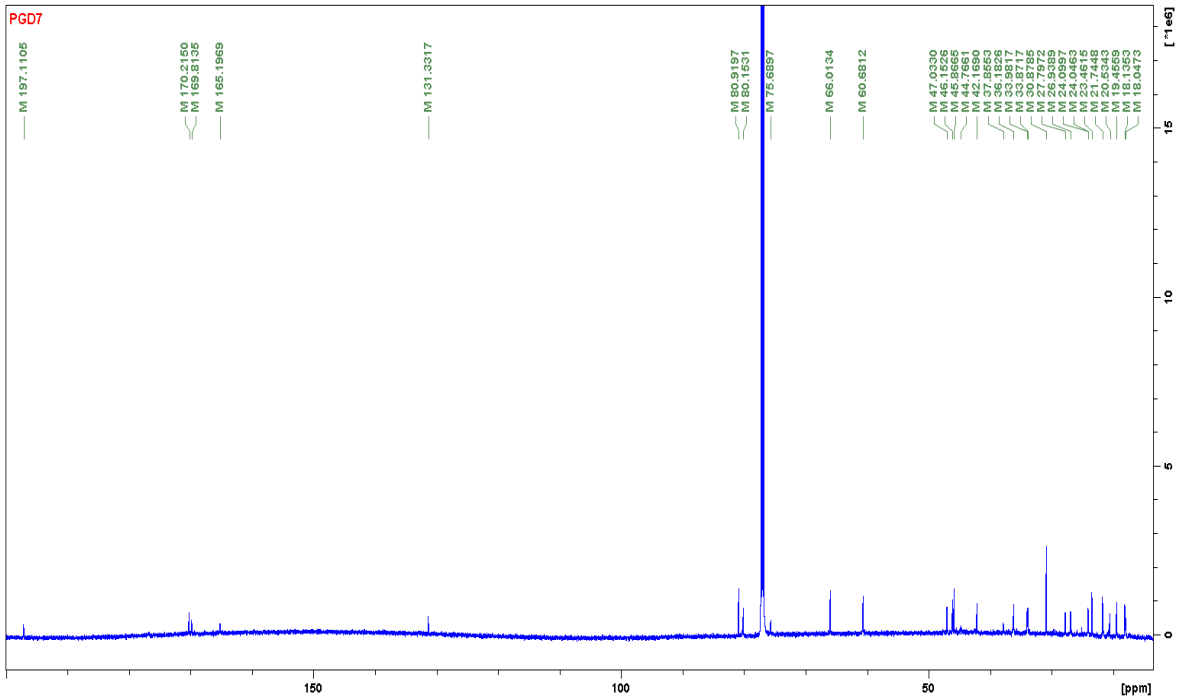

FIGURE 4.84 - ^{13}C NMR spectrum of Picraviane N (**07**) in $CDCl_3$ (150 MHz).

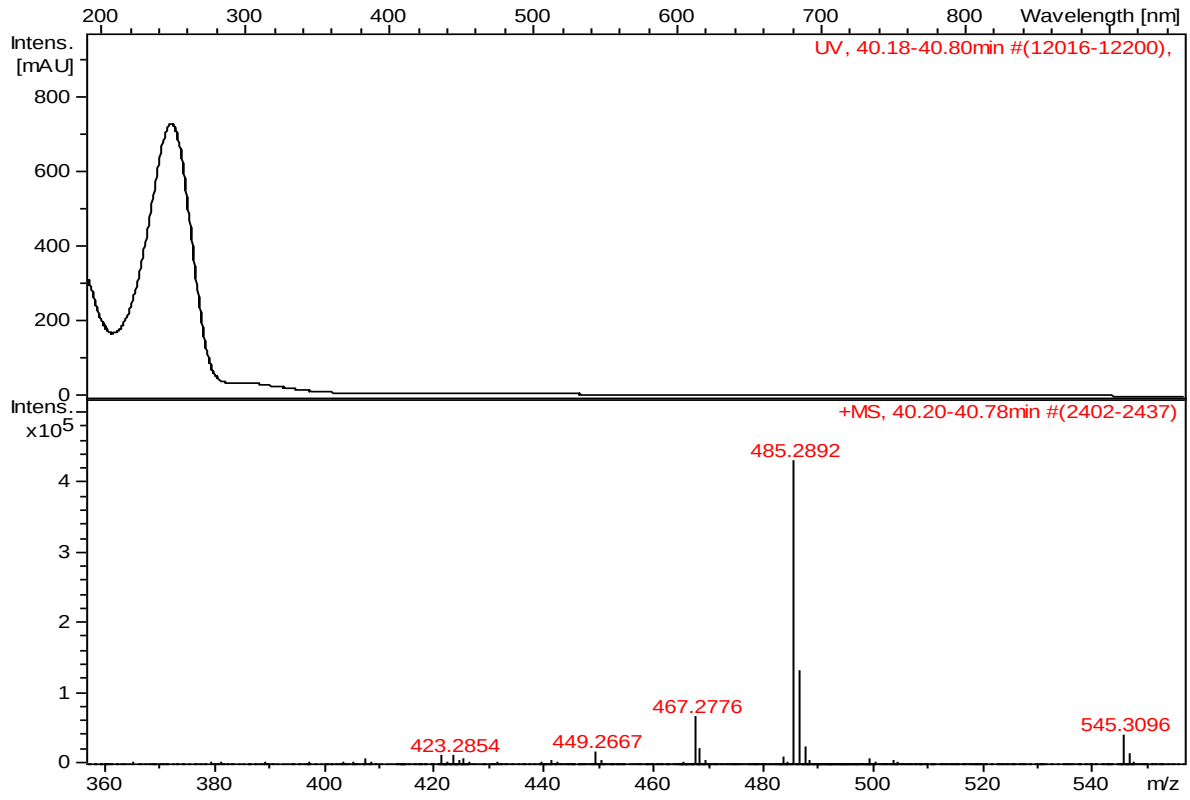

FIGURE 4.85 - HRESIMS spectrum of Picraviane N (**07**) indicating *m/z* $[M+H]^+$ = 545.3096; $[M+H\text{-}CH_3CO_2H]^+$ = 485.2892 and $[M+H\text{-}CH_3CO_2H\text{-}H_2O]^+$ = 467.2776

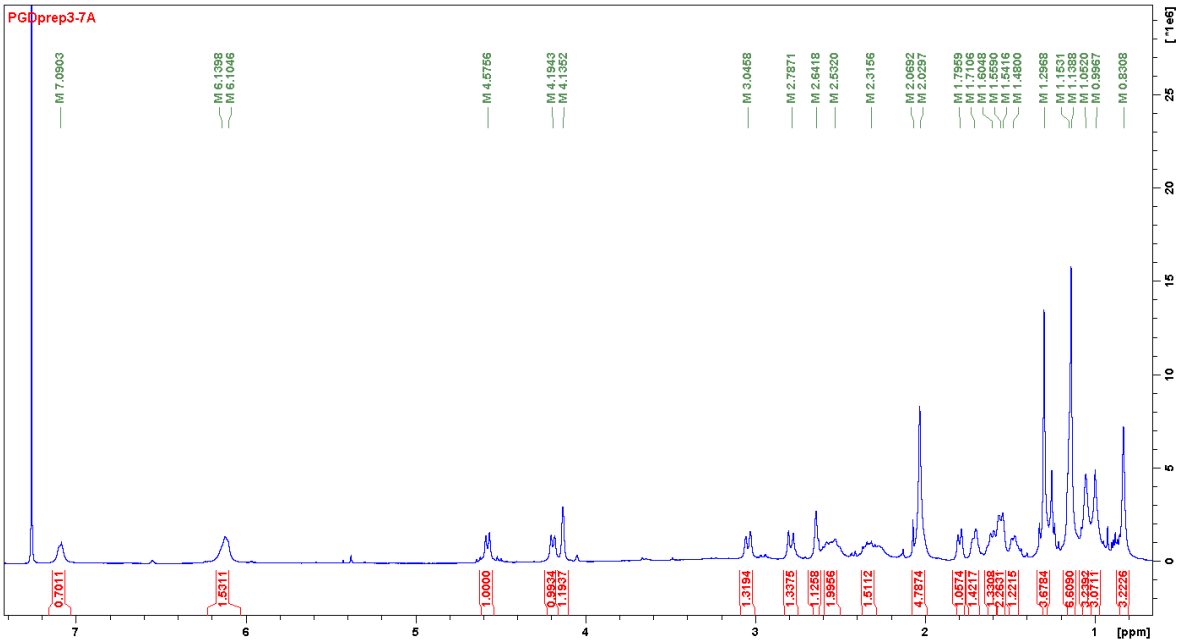

FIGURE 4.86 - ^1H NMR spectrum of Picraviane O (**7a**) in $CDCl_3$ (600 MHz).

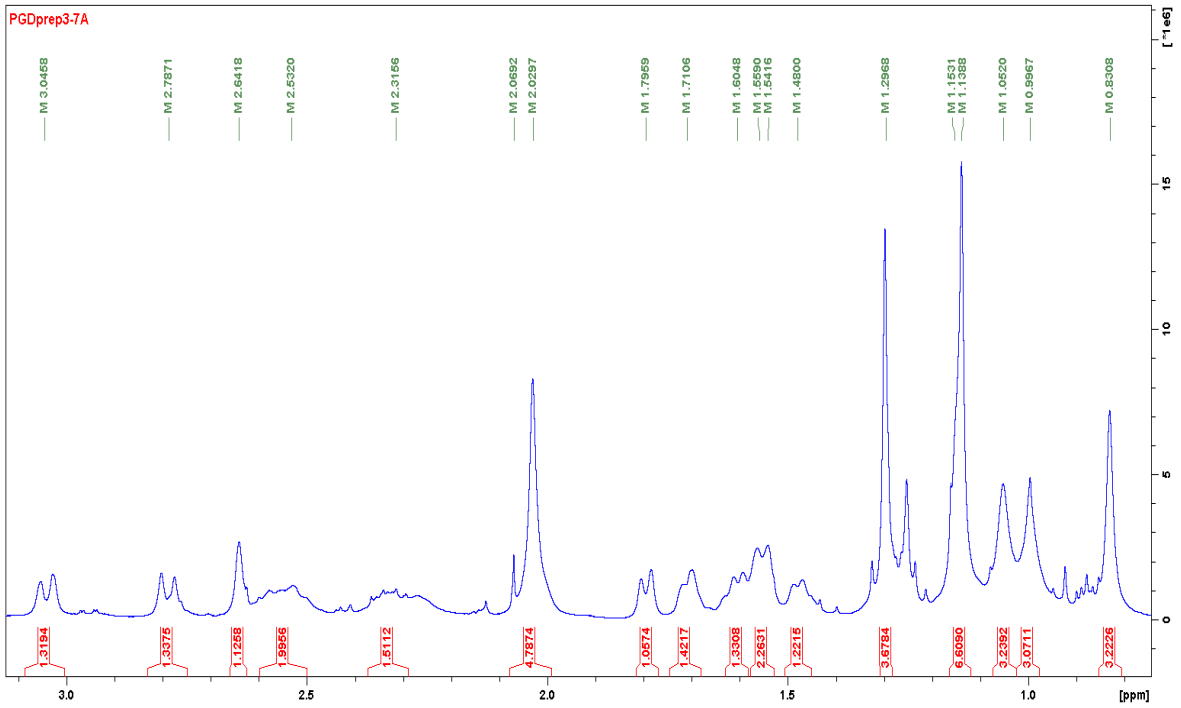

FIGURE 4.87 - Expansion of the ^{1}H NMR spectrum of Picraviane O (**7a**) in $CDCl_3$ (600 MHz).

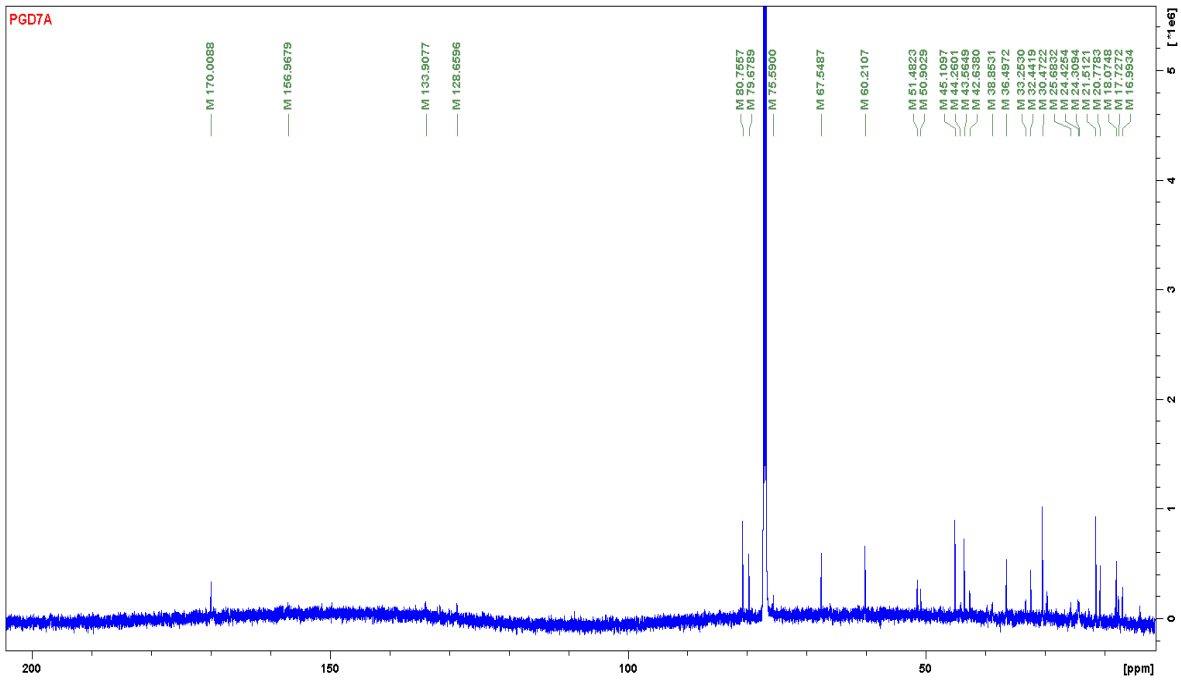

FIGURE 4.88 - ^{13}C NMR spectrum of Picraviane O (**7a**) in $CDCl_3$ (150 MHz).

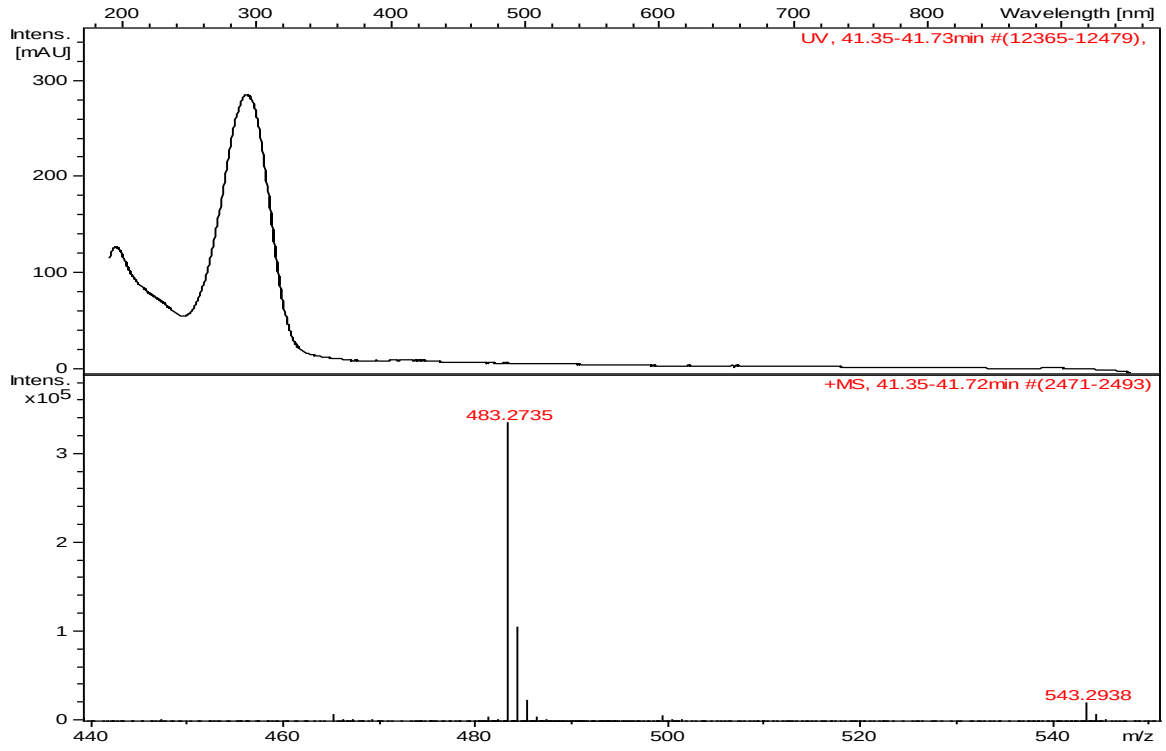

FIGURE 4.89 - HRESIMS spectrum of Picraviane O (**07a**) indicating *m/*z $[M+H]^+$ = 543.2938 and $[M+H\text{-}CH_3CO_2H]^+$ = 483.2735.

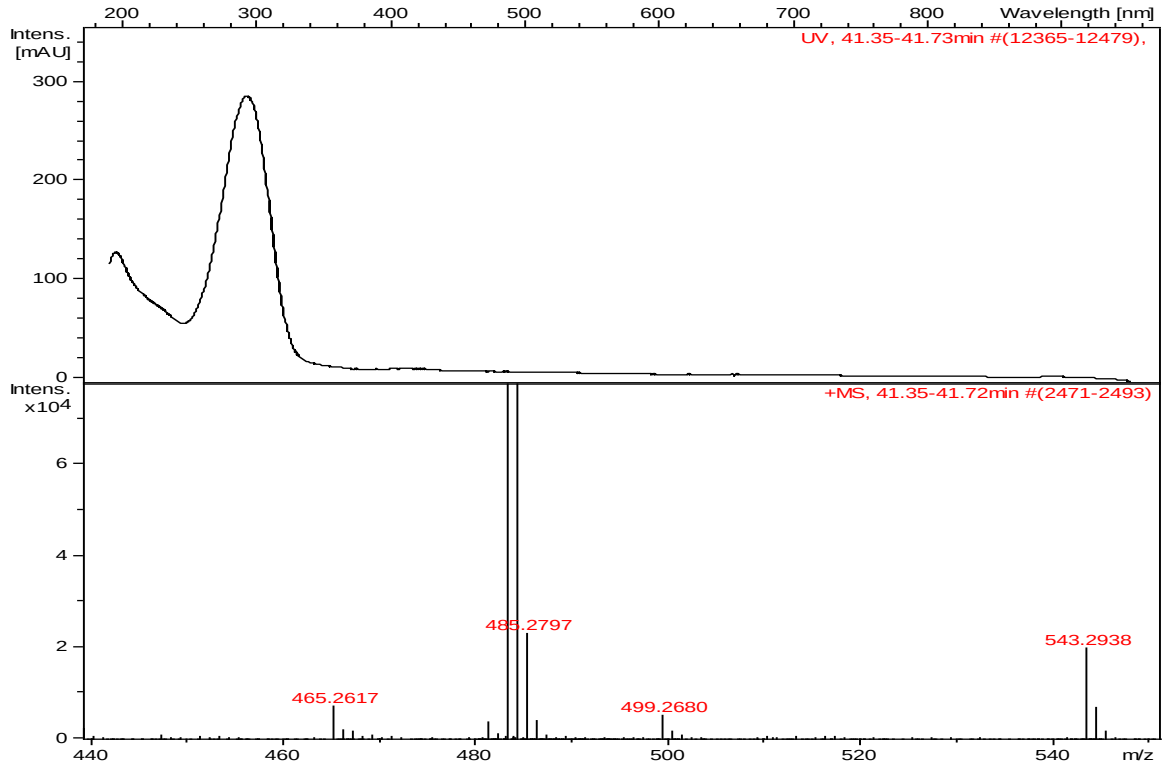

FIGURE 4.90 - HRESIMS spectrum of Picraviane O (**07a**) indicating *m/*z $[M+H]^+$ = 543.2938; and $[M+H\text{-}CH_3CO_2H\text{-}H_2O]^+$ = 465.2617.

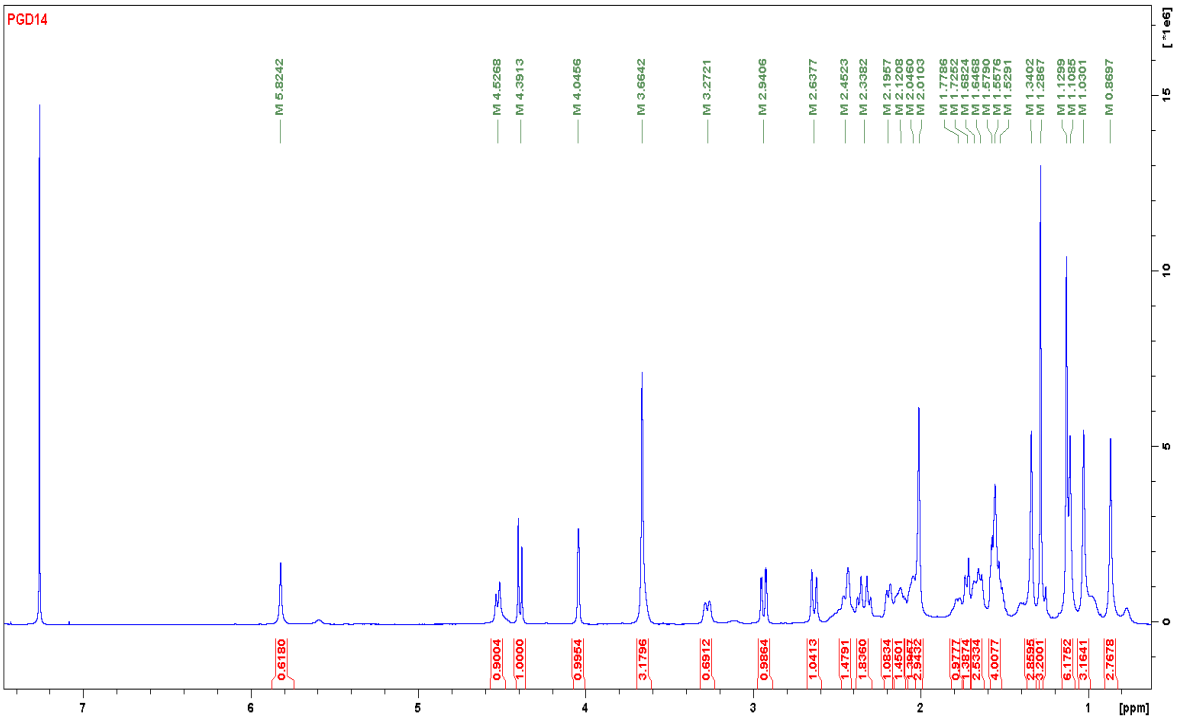

FIGURE 4.91 - ^{1}H NMR spectrum of Picraviane P (**14**) in $CDCl_3$ (600 MHz).

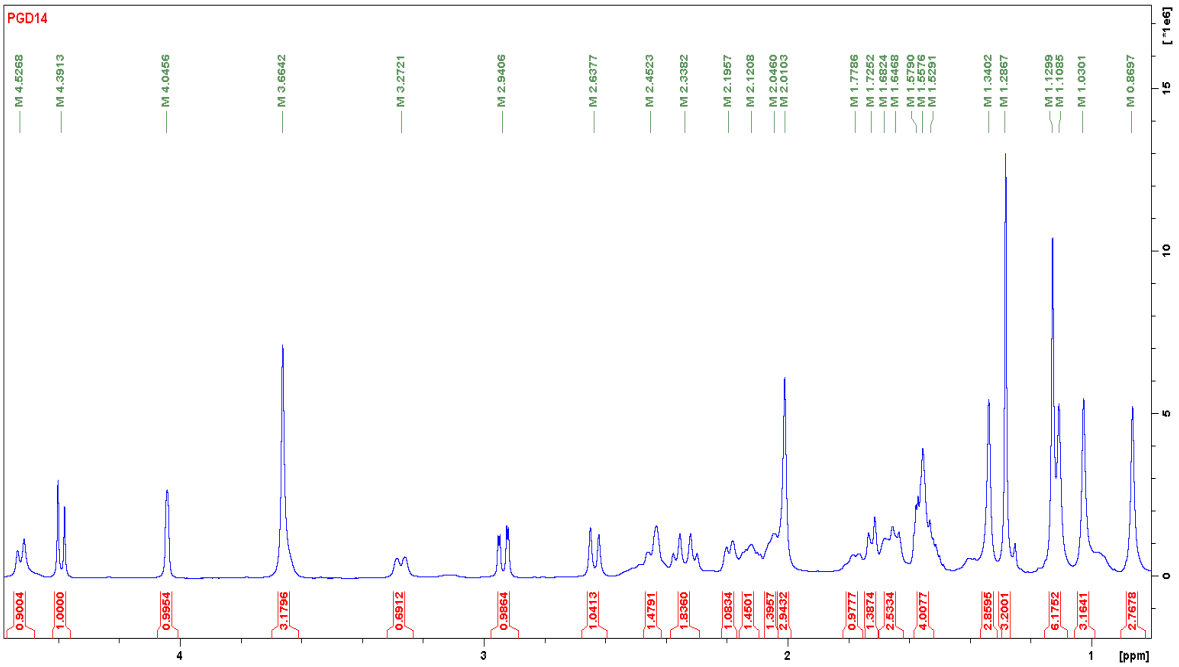

FIGURE 4.92 - Expansion of the ^{1}H NMR spectrum of Picraviane P (**14**) in $CDCl_3$ (600 MHz).

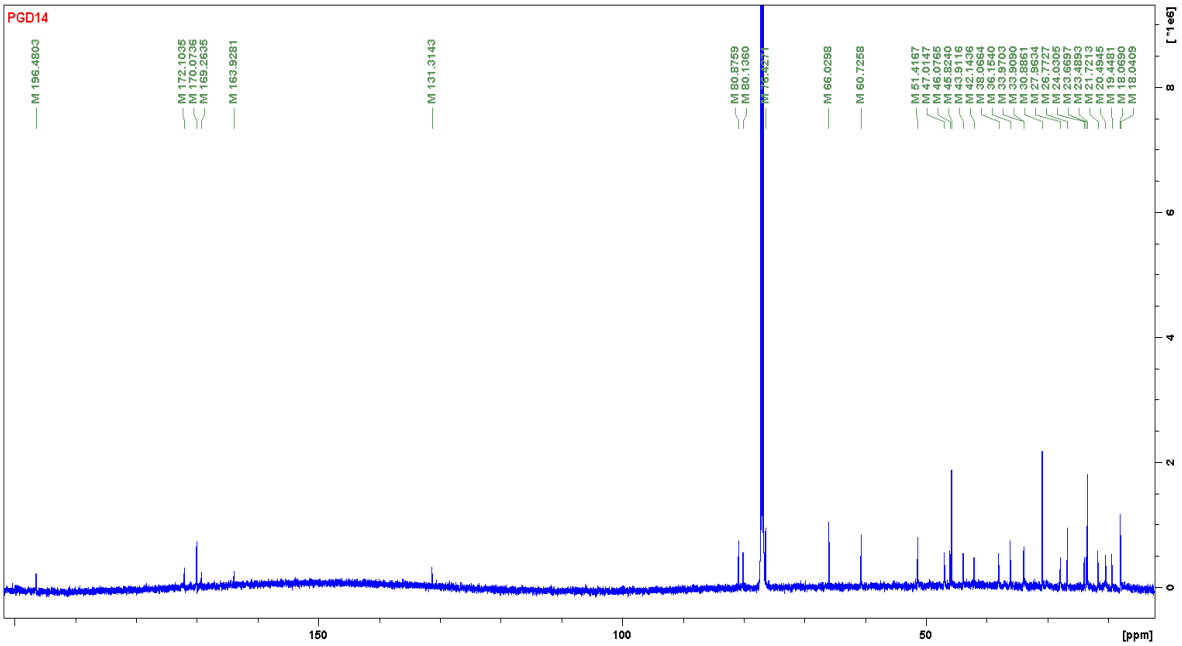

FIGURE 4.93 - ^{13}C NMR spectrum of Picraviane P (**14**) in $CDCl_3$ (150 MHz).

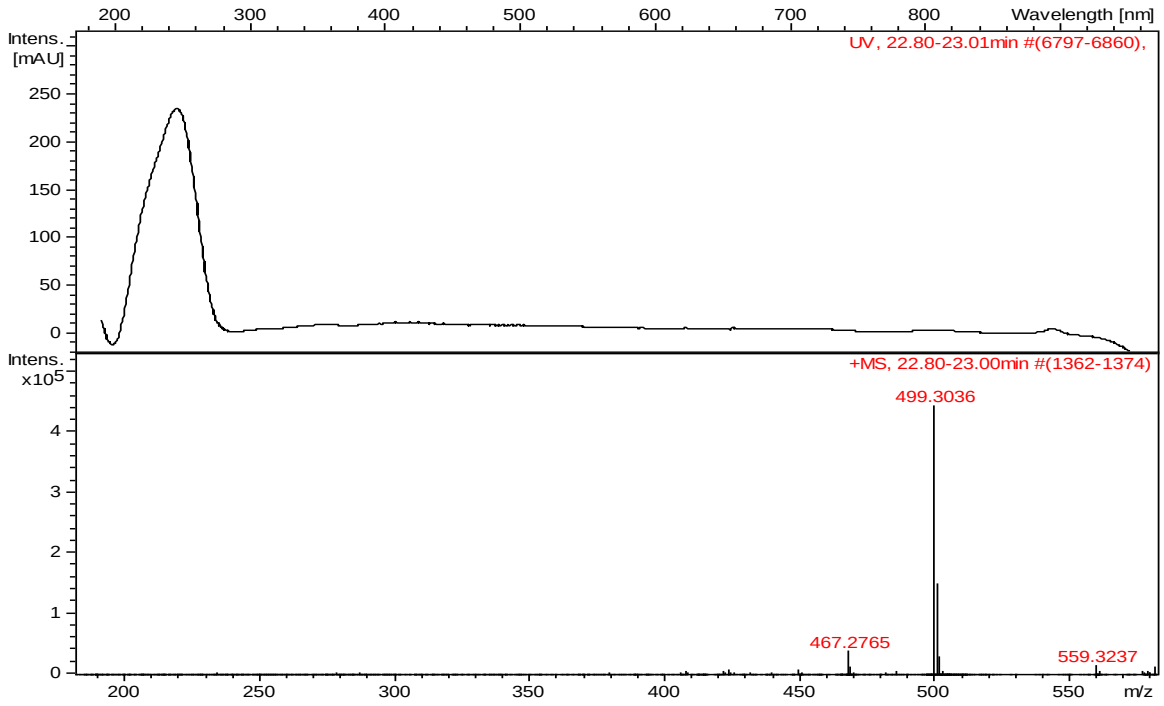

FIGURE 4.94 - HRESIMS spectrum of Picraviane P (**14**) indicating *m/z* $[M+H]^+$ = 559.3237, $[M+H\text{-}CH_3CO_2H]^+$ = 499.3036 and $[M+H\text{-}CH_3CO_2H\text{-}CH_3OH]^+$ = 467.2766.

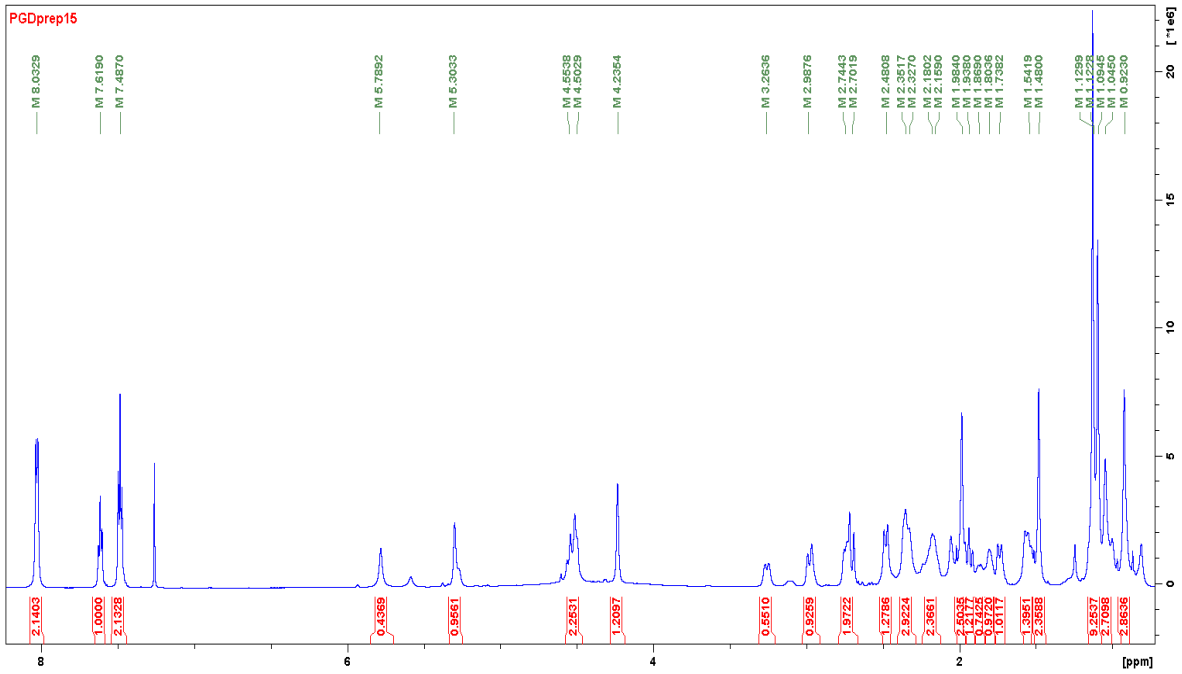

FIGURE 4.95 - ^{1}H NMR spectrum of Picraviane Q (**15**) in $CDCl_3$ (600 MHz).

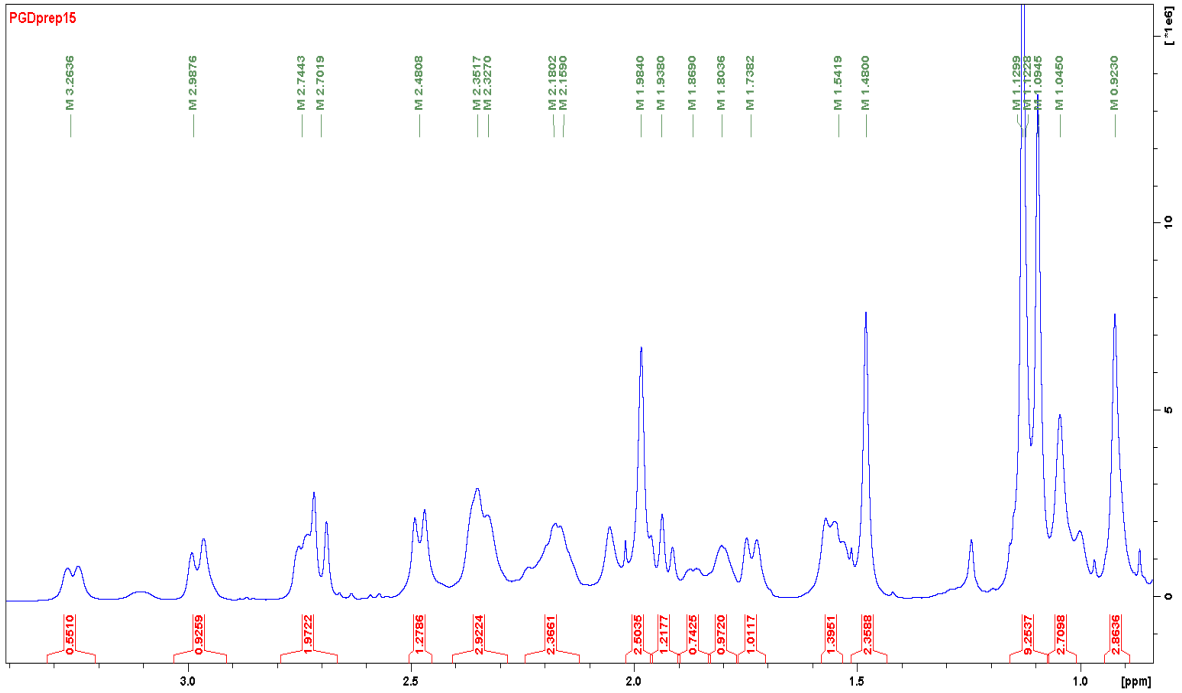

FIGURE 4.96 - Expansion of the ^{1}H NMR spectrum of Picraviane Q (**15**) in $CDCl_3$ (600 MHz).

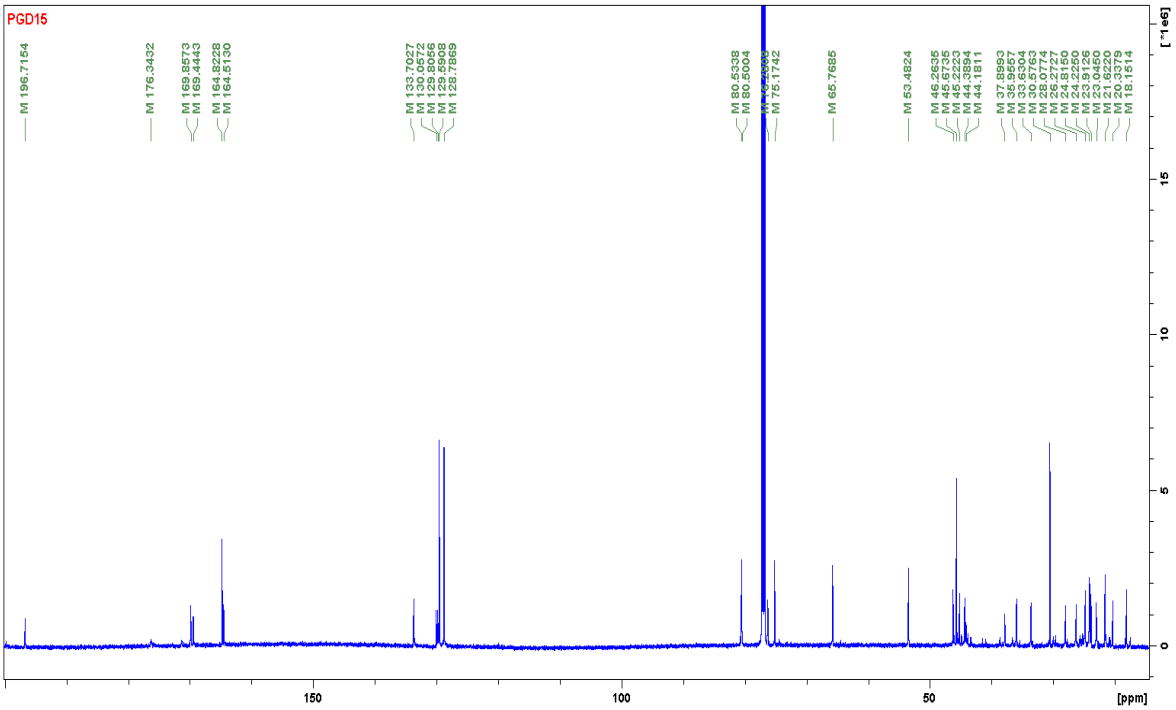

FIGURE 4.97 - ^{13}C NMR spectrum of Picraviane Q (**15**) in $CDCl_3$ (150 MHz).

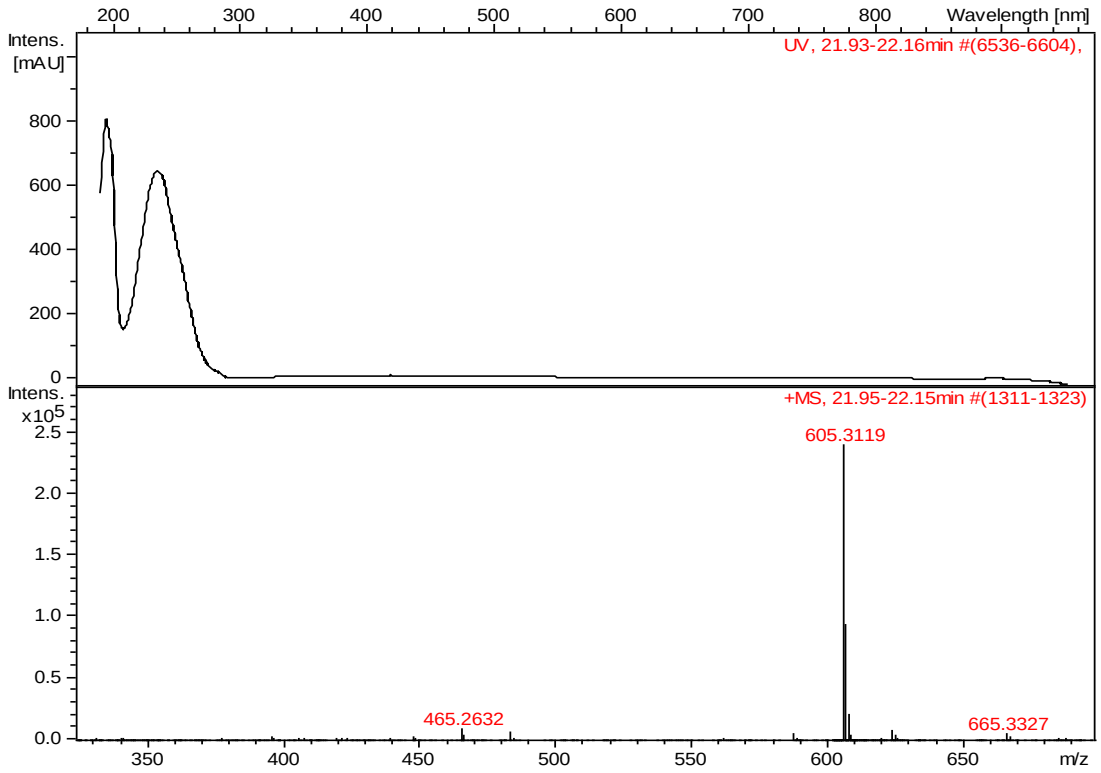

FIGURE 4.98 - HRESIMS spectrum of Picraviane Q (**15**) indicating *m/z* $[M+H]^+$ = 665.3327 and $[M+H\text{-}CH_3CO_2H]^+$ = 605.3119.

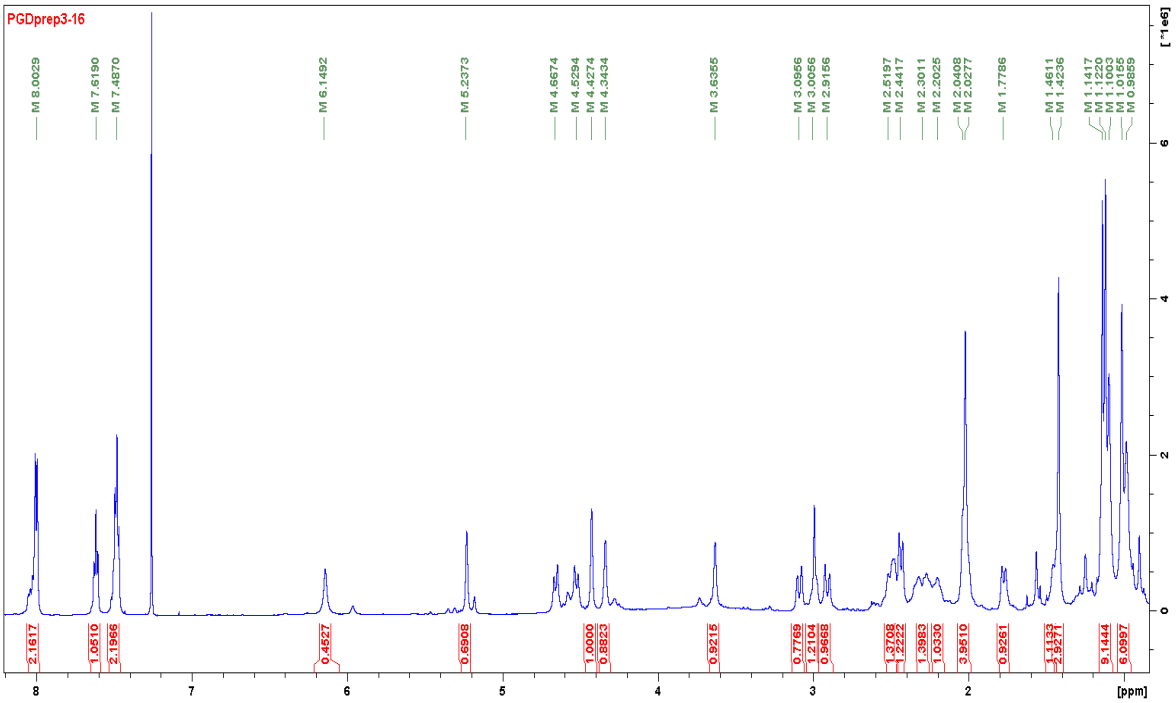

FIGURE 4.99 - ^{1}H NMR spectrum of Picraviane R (**16**) in $CDCl_3$ (600 MHz).

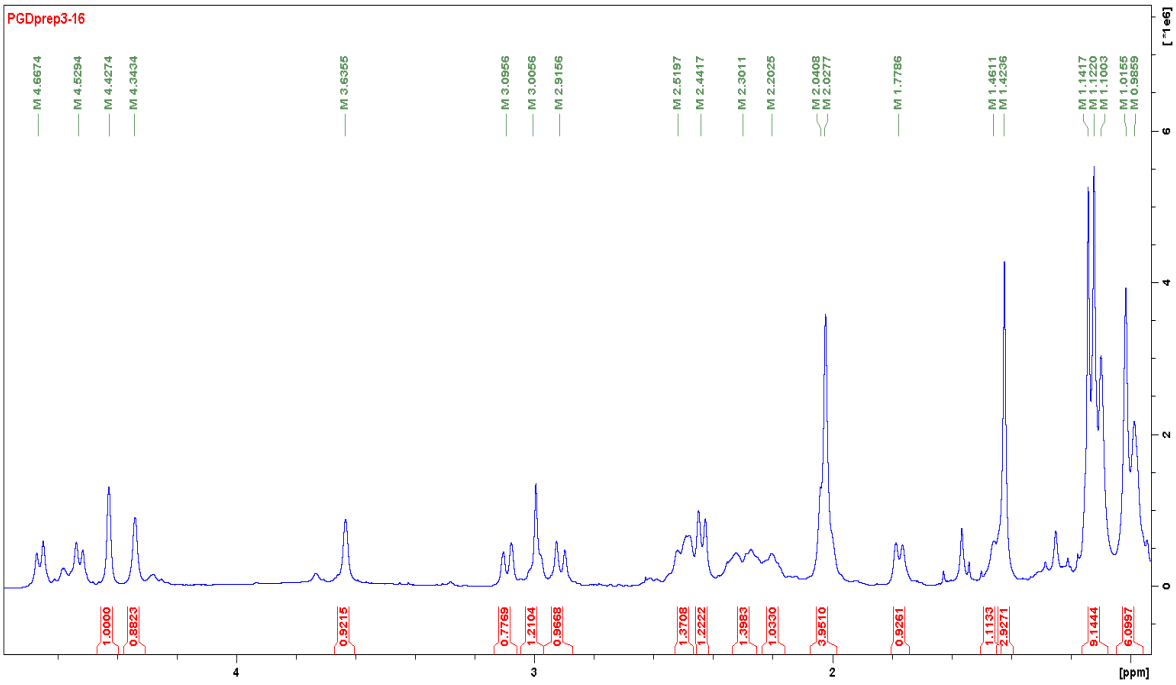

FIGURE 4.100 - Expansion of the ^{1}H NMR spectrum of Picraviane R (**16**) in $CDCl_3$ (600 MHz).

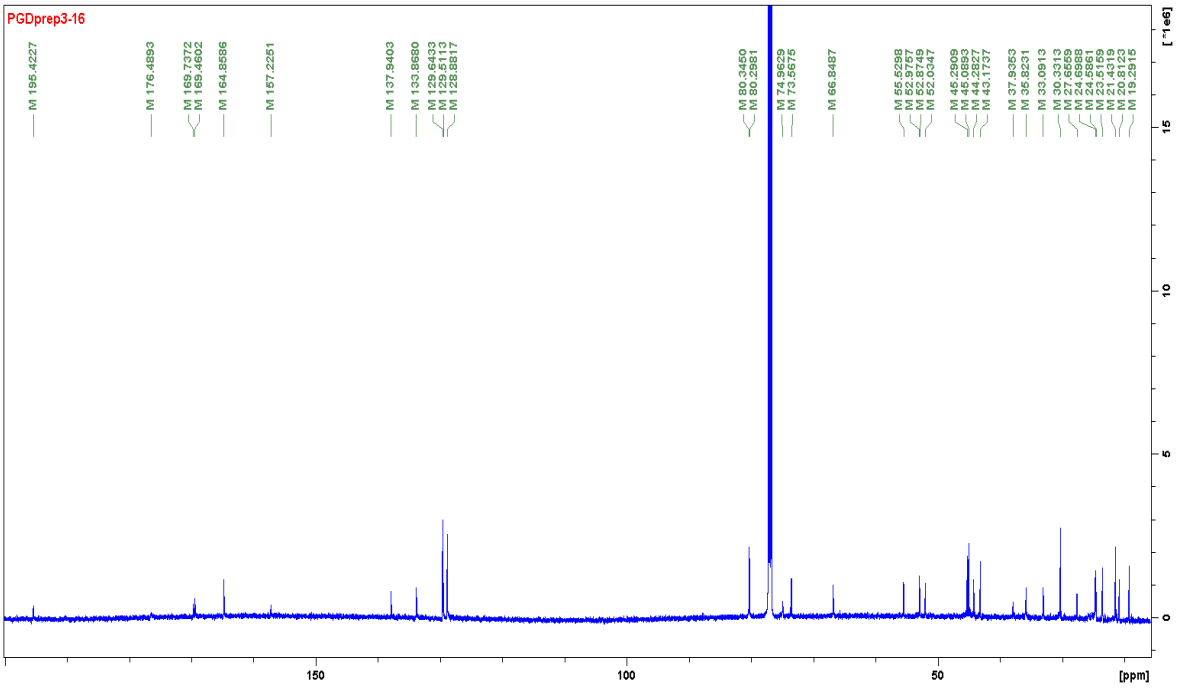

FIGURE 4.101 - ^{13}C NMR spectrum of Picraviane R (**16**) in $CDCl_3$ (150 MHz).

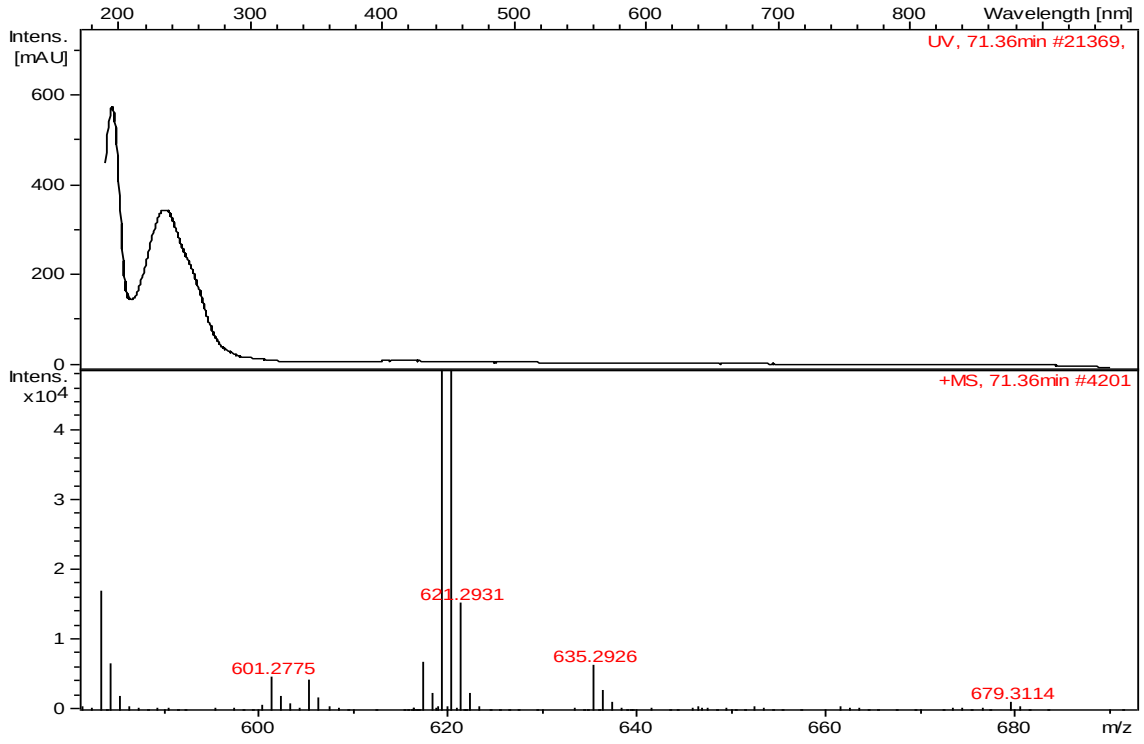

FIGURE 4.102 - HRESIMS spectrum of Picraviane R (**16**) indicating *m/z* $[M+H]^+$ = 679.3114; $[M+H\text{-}CH_3CO_2H\text{-}H_2O]^+$ = 601.2775.

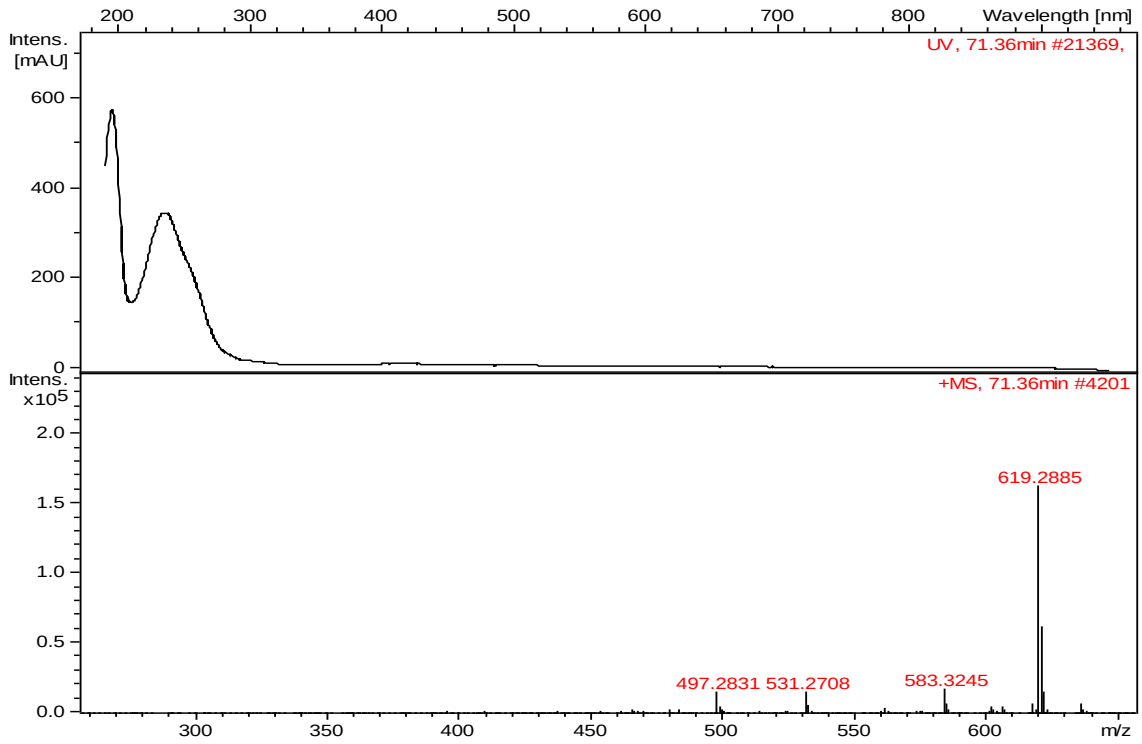

FIGURE 4.103 - HRESIMS spectrum of Picraviane R (**16**) indicating *m/z* [M+H-CH_3CO_2H]$^+$ = 619.2885.

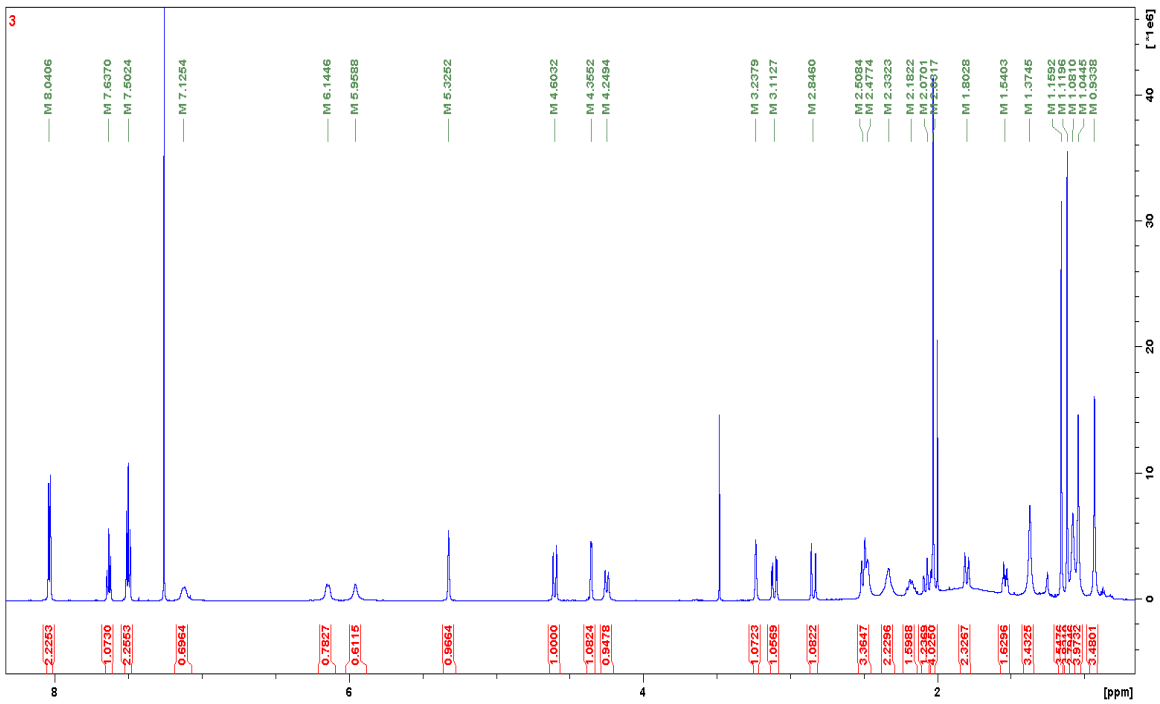

FIGURE 4.104 - ^{1}H NMR spectrum of Picraviane S (**17**) in $CDCl_3$ (600 MHz).

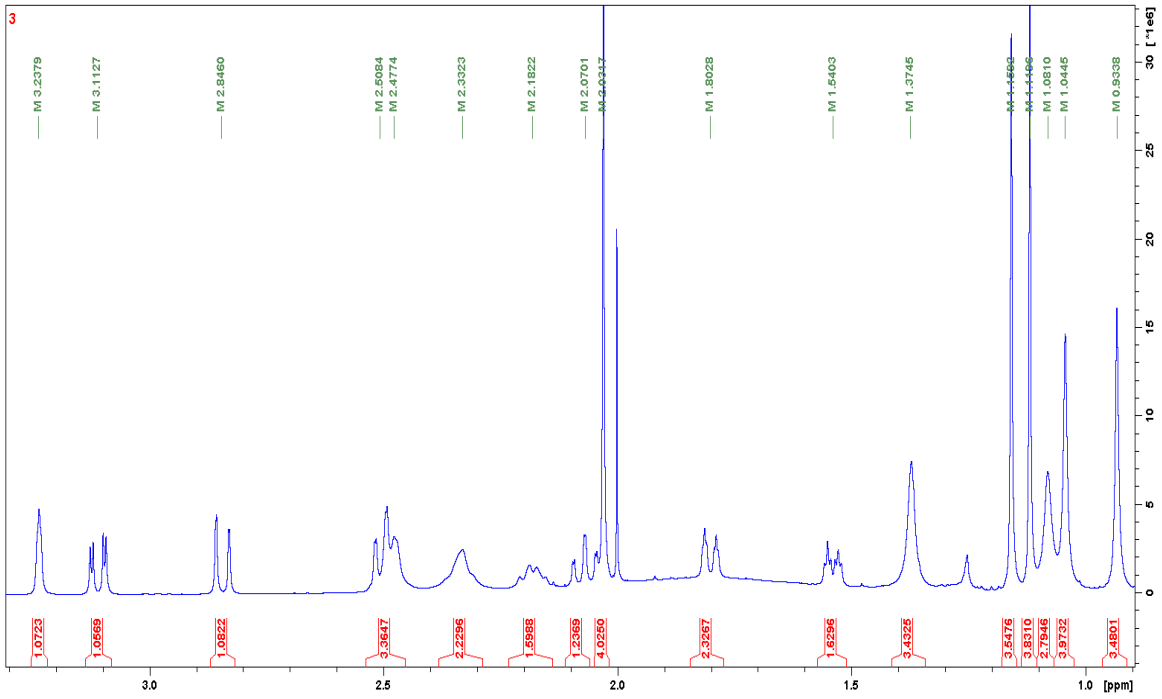

FIGURE 4.105 - Expansion of the ^{1}H NMR spectrum of Picraviane S (**17**) in $CDCl_3$ (600 MHz).

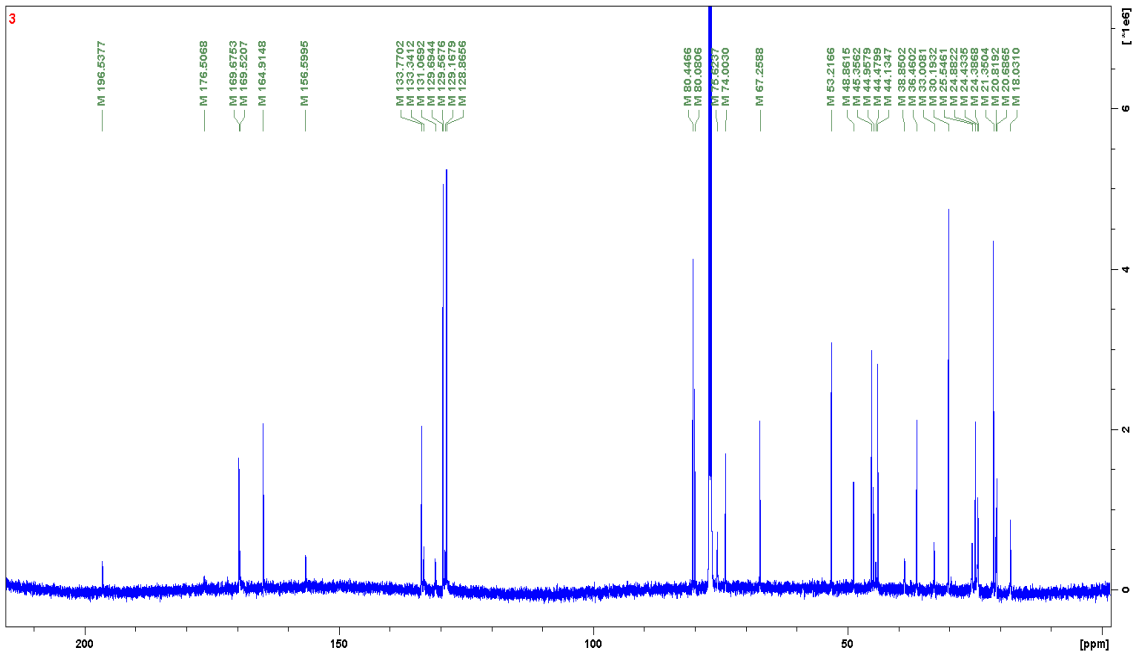

FIGURE 4.106 - ^{13}C NMR spectrum of Picraviane S (**17**) in $CDCl_3$ (150 MHz).

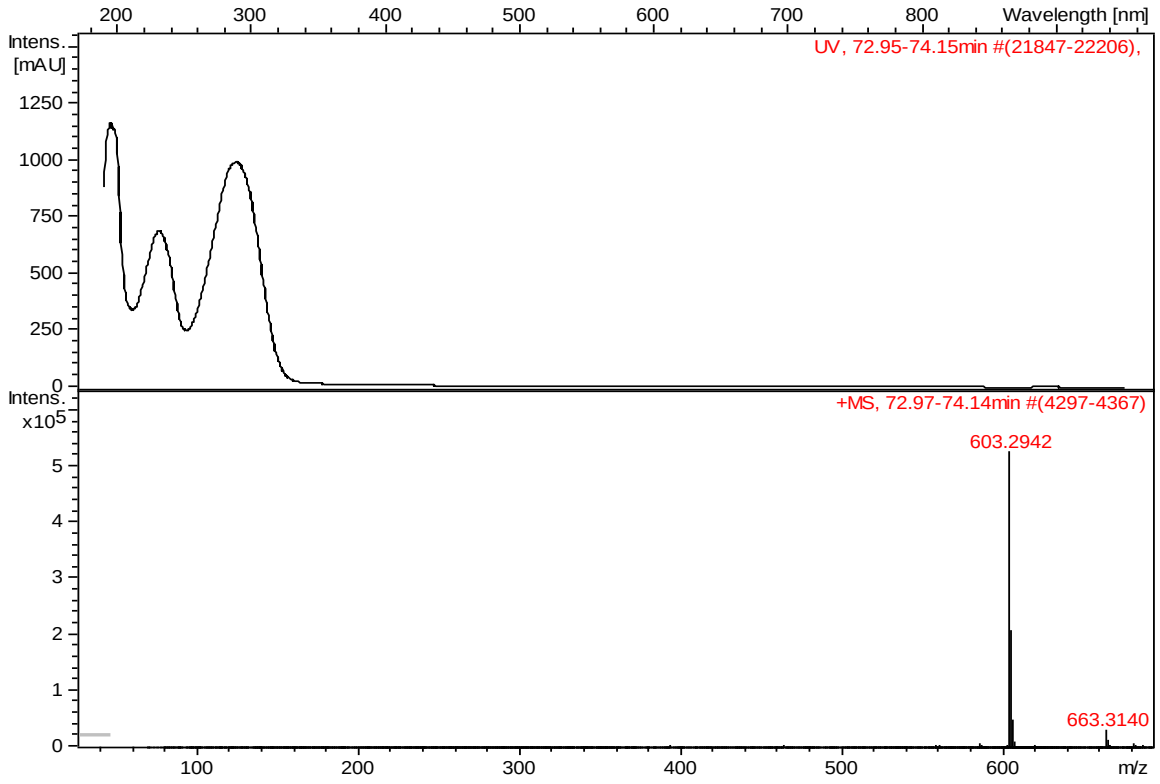

FIGURE 4.107 - HRESIMS spectrum of Picraviane S (**17**) indicating *m/z* $[M+H]^+$ = 663.3140 and $[M+H\text{-}CH_3CO_2H]^+$ = 603.2942.

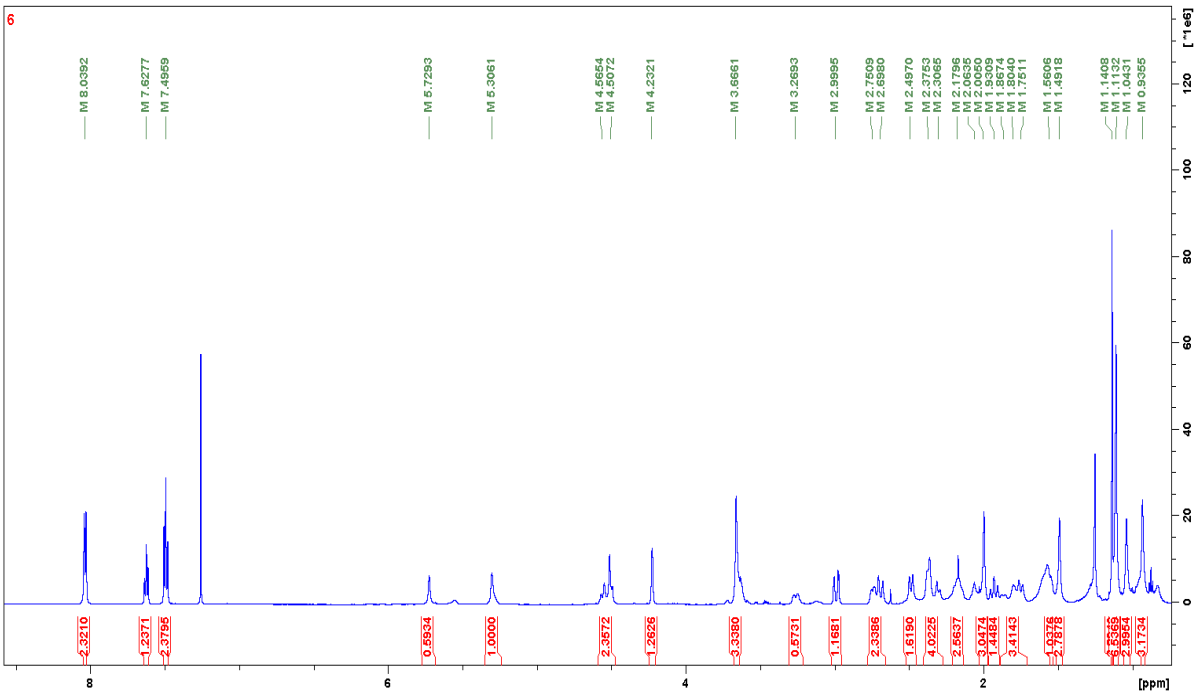

FIGURE 4.108 - ^1H NMR spectrum of Picraviane T (**22**) in $CDCl_3$ (600 MHz).

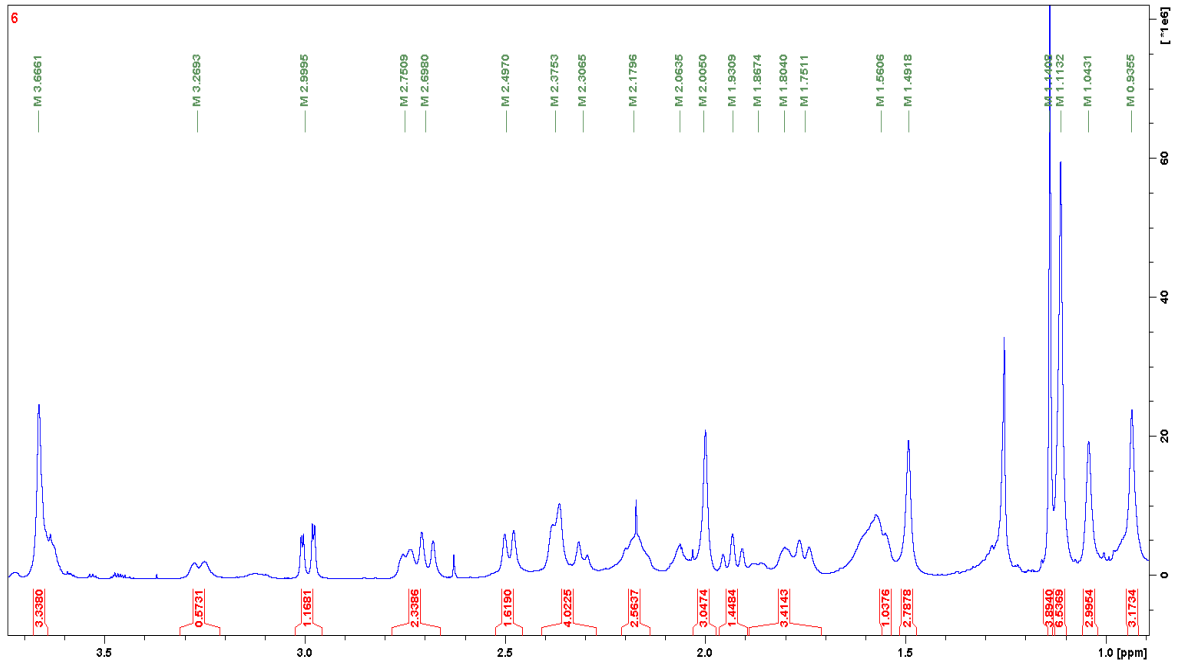

FIGURE 4.109 - Expansion of the ^{1}H NMR spectrum of Picraviane T (**22**) in $CDCl_3$ (600 MHz).

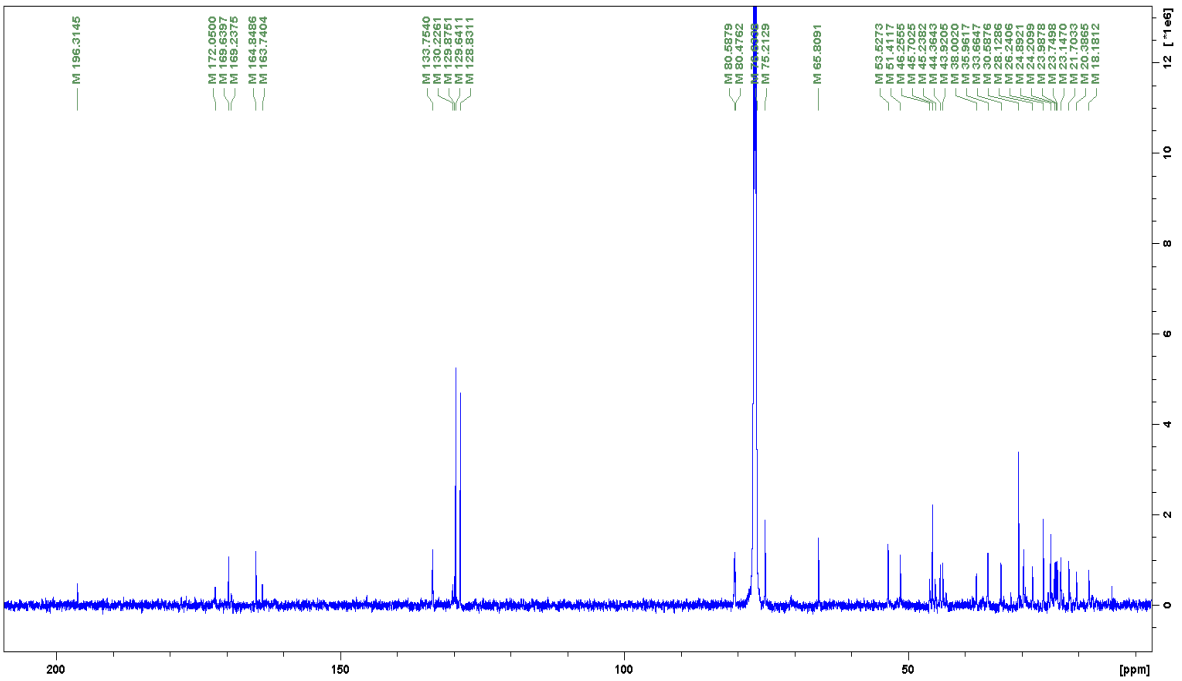

FIGURE 4.110 - ^{13}C NMR spectrum of Picraviane T (**22**) in $CDCl_3$ (150 MHz).

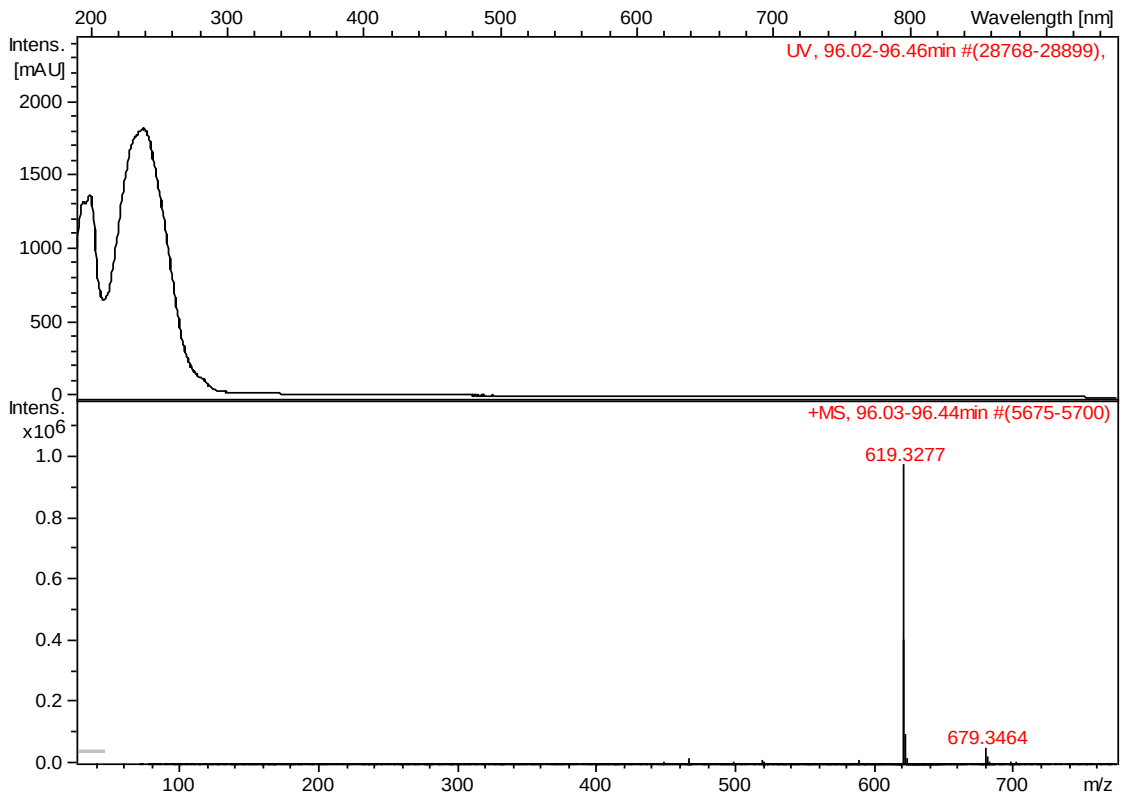

FIGURE 4.111 - HRESIMS spectrum of Picraviane T (**22**) indicating *m/z* $[M+H]^+$ = 679.3464 and $[M+H\text{-}CH_3CO_2H]^+$ = 619.3277.

4.1.1.7 – Nortriterpenes Picravianes U (21) and V (24)

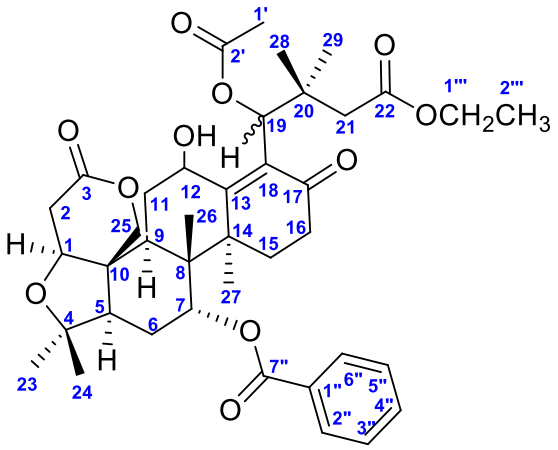

21

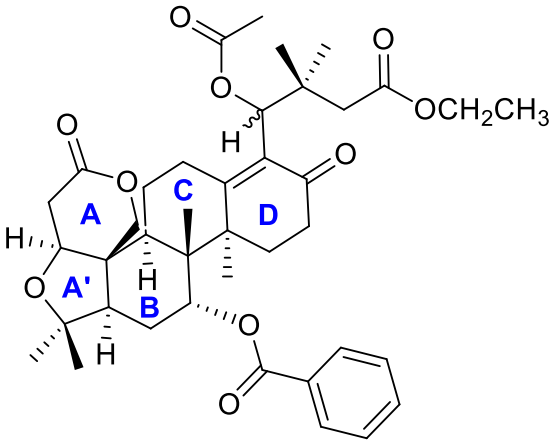

24

Picraviane U (**21**) and V (**24**) were elucidated on the basis of spectroscopic data from 1D ^{1}H NMR, ^{13}C NMR as well as 2D NMR experiments (COSY, HSQC, HMBC, NOESY and ROESY, see Supporting Information pages 268 to 269 and 272 to 273).

Due the low amount isolated for compounds **21**, and **24**, the measured of the optical rotation were not acquired. The infrared acquired to these compounds also needs to be repeated, once the spectrum presented signals from the methanol (solvent used to solubilize the samples). The UV spectrum was acquired from the HPLC-HRESIMS and disclosed the absorbances at λ_{max} 195nm and 231 nm in both compounds.

The HRESIMS data for each compound is indicated below:

- Compound **21** m/z $[M+H]^+$ = 709.3557 (calc. for 709.3587), molecular formula as $C_{40}H_{53}O_{11}$ (15 degrees of unsaturation) and a base peak corresponding to the fragment m/z $[M+H-H_2O]^+$ = 691.3439 (FIGURES 4.115 and 4.116);
- Compound **24**: m/z $[M+H]^+$ = 693.3610 (calc. for 693.3652), molecular formula as $C_{40}H_{53}O_{10}$ (15 degrees of unsaturation) and a base peak corresponding to the fragment m/z $[M+H-CH_3CO_2H]^+$ = 663.3408 (FIGURES 4.120 and 4.121);

Likewise to compounds discussed in section 4.1.1.6, both compounds presented the opening of the E ring. The mass spectrum showed the loss of the acetic acid in both compounds, and correlations in the HMBC spectrum from H-19 at *δ* 6.05 (compound **21**) and *δ* 5.74 (compound **24**) with the carbons C-13, C-17 and

C-18 collaborated to the positioning of this proton close to the enone system in both structures, in agreement with the opening of the five membered E ring.

A deshielded quadruplet at *δ* 4.13 (*δ* 60.4) coupling with a triplet at *δ* 1.26 (*δ* 14.2) with 7.3 Hz through the ^{1}H NMR spectrum and correlating with a carbonyl carbon at *δ* 171.3 (C-22) observed in the HMBC spectrum to compound **21** indicated an ethyl ester terminated E backbone in the structure. The same signals were observed in compound **24** at *δ* 4.13 (*δ* 60.3) - although the broad signal observed in the ^{1}H NMR spectrum limited the definition of the multiplicity - and a triplet at *δ* 1.25 (*δ* 14.3). Besides, the loss of an ethanol molecule in the mass spectrum to both compounds was in agreement with this establishment.

Compounds **21** and **24** showed the presence of the benzoate unit, very clearly observed by the ^{1}H NMR and placed at the C-7 position due correlations of the oxymethine proton at *δ* 5.38 (Compound **21**) and *δ* 5.30 (compound **24**) to the carbon C-5 at *δ* 53.3 (compound **21**) and *δ* 53.5 (compound **24**) in HMBC spectrum, beside the set of spin system H-5 – H-6 – H-7 observed by the COSY spectrum.

The remaining oxymethine proton was observed to compound **21** at *δ* 5.22 (*δ* 66.2). The value of the chemical shift to its the carbon and proton, beyond the loss of a water molecule in the mass spectrum, and keys correlations observed in HMBC spectrum from this proton to the carbon at *δ* 39.9 (C-9) and to the olefinic carbon at *δ* 133.0 (C-18) have established a hydroxyl group at the position C-12.

The NOESY spectra in both compounds indicate the same relative stereochemistry to the stereocenters C-1, C-5, C-9, C-7, C-26 and C-27 according to all previous discussions. The H-19 could not be established due the flexibility of the structure, and H-12 showed the same pattern of correlations in NOESY than compound **12**, indicating the relative stereochemistry to this proton assuming a β orientation.

The full assignments of the ^{1}H and ^{13}C to the compounds **21** and **24** are shown in TABLE 4.13. ^{1}H and ^{13}C NMR and HRMS spectra to compound **21** are presented in FIGURES 4.112 to 4.116. ^{1}H and DEPTQ NMR and HRMS spectra to compound **24** are presented in FIGURES 4.117 to 4.121. A proposal of mass fragmentation is presented in FIGURE 4.122 to compound **24**.

TABLE 4.13 - ^{13}C and ^{1}H NMR Data for Picraviane U (**21**) and V (**24**) acquired in $CDCl_3$

	21		**24**	
C	δ_C	δ_H (*J* in Hz)	δ_C	δ_H (*J* in Hz)
1	80.5	4.28 br t (3.1)	80.6	4.23 br t (3.5)
2	35.9	α: 3.01 dd (17.2, 3.1) β: 2.76 dd (17.2, 1.7)	35.9	α: 2.99 dd (16.9, 3.5) β: 2.69 d (16.9)
3	169.7	-	169.6	-
4	80.3	-	80.5	-
5	53.3	2.57 d (13.1)	53.5	2.49 d (13.5)
6	25.1	α: 1.91 td (14.3, 2.5) β: 1.74 dt (14.3, 3.2)	24.9	α: 1.93 t (14.6) β: 1.75 d (14.6)
7	75.4	5.38 br t (3.2)	75.2	5.30 s
8	45.7	-	44.2	-
9	39.9	2.98 dd (13.1, 4.0)	44.3	2.75 dd (12.9, 4.6)
10	45.3	-	45.7	-
11	30.8	2.11 m 1.89 m	23.2	β:1.87 dd (12.8, 4.8) α: 1.80 m
12	66.2	5.22 d (3.6)	26.2	β: 3.27 dd (16.4, 4.8) α: 2.18 m
13	162.2	-	163.7	-
14	45.7	-	46.0	-
15	29.1	β: 2.20 td (13.5, 5.4) α: 1.58 m	28.1	β: 2.18 m α: 1.56 m
16	33.4	2.46 dd (13.5, 4.6)	33.7	2.37 d (8.5)
17	196.3	-	196.4	-
18	133.1	-	130.2	-
19	75.6	6.05 s	76.5	5.74 s
20	38.6	-	38.0	-
21	44.2	α: 2.31 d (13.2) β: 2.27 d (13.2)	44.1	2.32 d (9.3)
22	171.3	-	171.5	-
23	30.6	1.14 s	30.6	1.14 s
24	21.9	1.12 s	21.7	1.10 s
25	66.0	β: 4.63 d (12.7) α: 4.52 d (12.7)	65.8	β: 4.56 d (12.4) α: 4.50 d (12.4)
26	18.9	0.98 s	18.2	0.93 s
27	26.0	1.66 s	24.2	1.49 s
28	23.9	1.04 s	23.9	1.05 s
29	24.1	0.98 s	23.8	1.11 s
1´	21.3	2.09 s	20.4	2.00 s
2’	170.2	-	169.1	-
1”	129.8	-	129.9	-
2”/ 6”	129.7	8.06 XX'-system	129.6	8.04 XX'-system
3”/ 5”	128.9	7.50 AA'-system	128.8	7.49 AA'-system
4”	133.8	7.63 t (7.3)	133.7	7.63 tt (8.1, 1.1)
7”	164.9	-	164.8	-
1’’’	60.4	4.13 q (7.3)	60.3	4.13 m
2’’’	14.2	1.26 t (7.3)	14.3	1.25 t (7.3)
OH	-	*	-	-

* Not detected signals

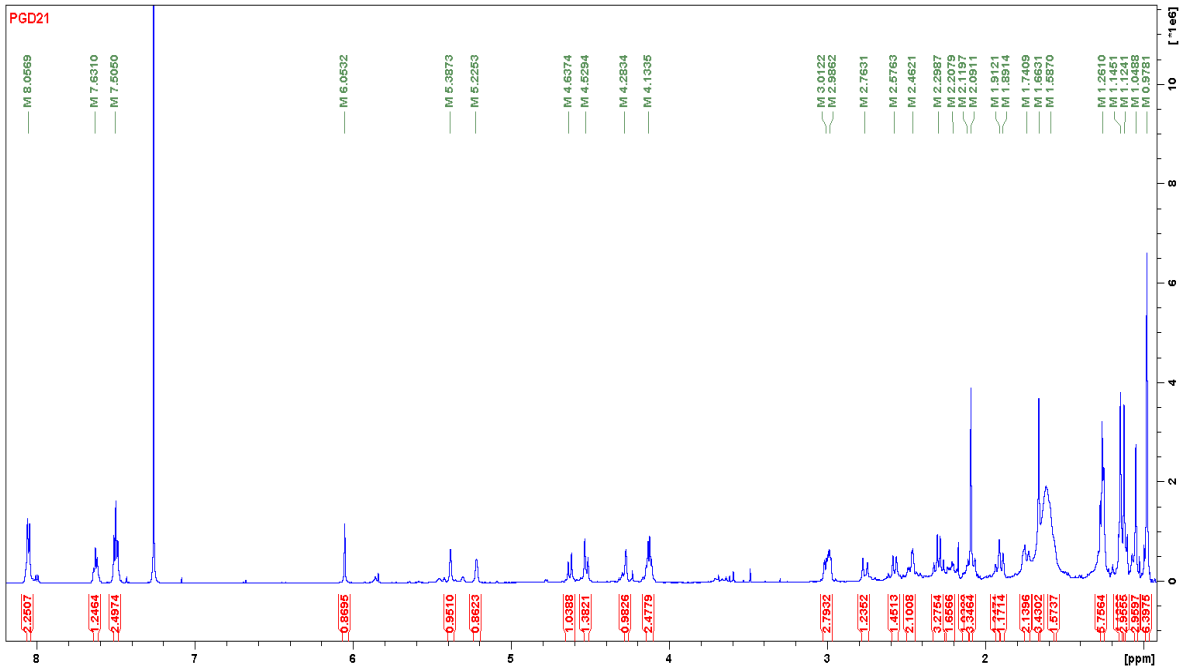

FIGURE 4.112 - ^{1}H NMR spectrum of Picraviane U (**21**) in $CDCl_3$ (600 MHz).

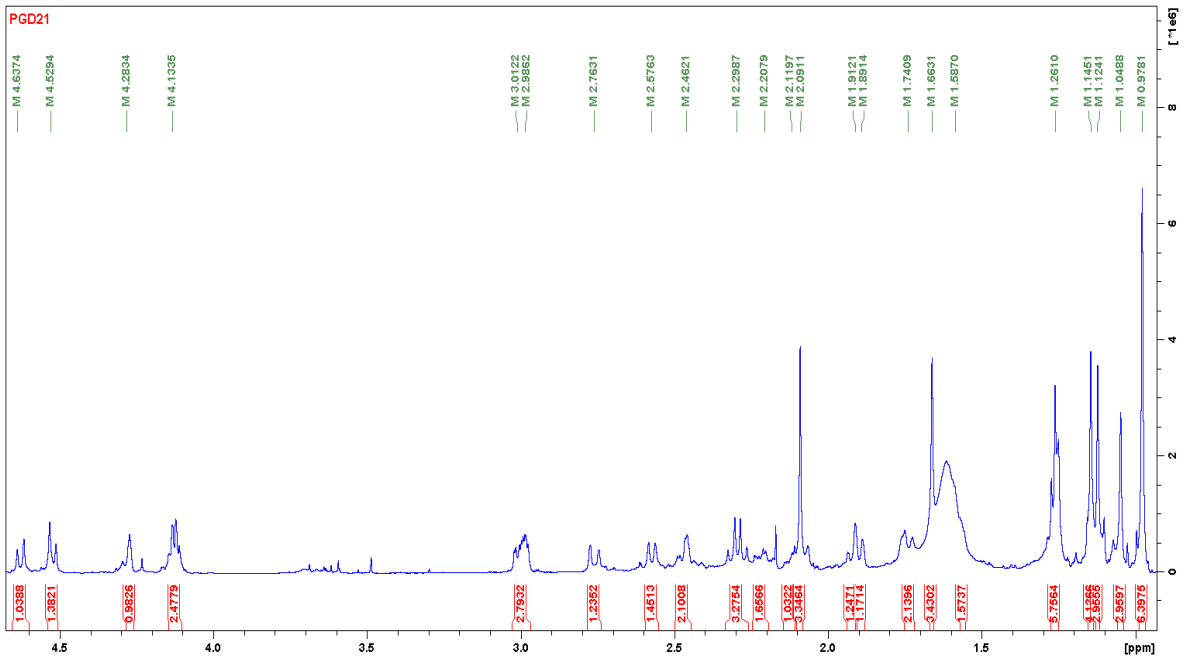

FIGURE 4.113 - Expansion of the ^{1}H NMR spectrum of Picraviane U (**21**) in $CDCl_3$ (600 MHz).

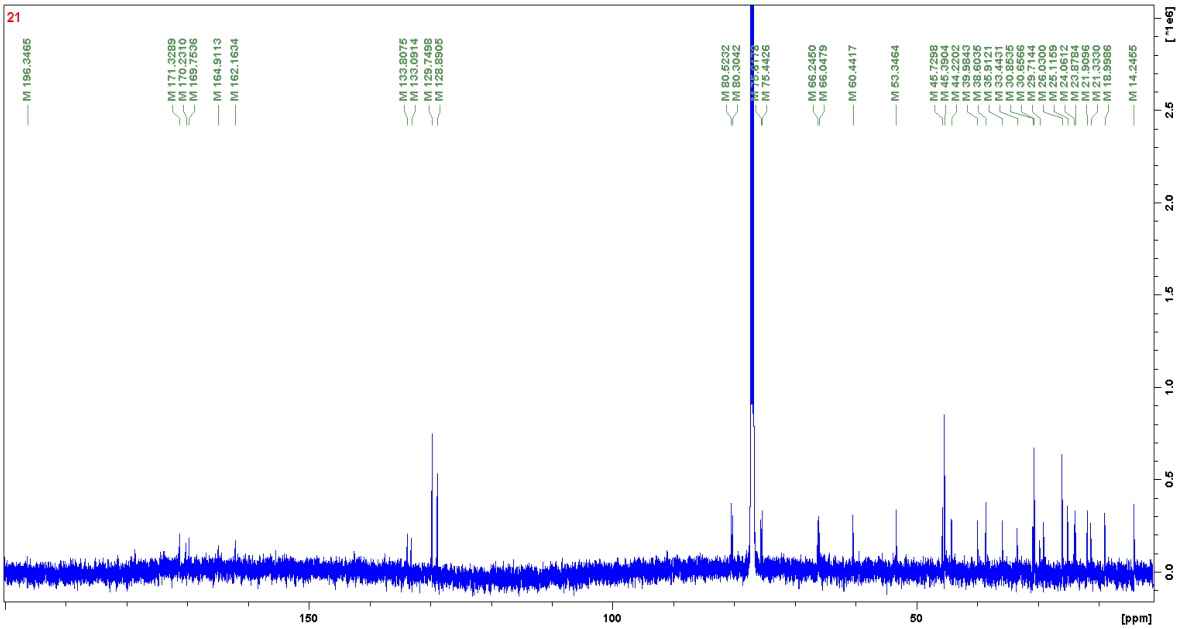

FIGURE 4.114 - ^{13}C NMR spectrum of Picraviane U (**21**) in $CDCl_3$ (150 MHz).

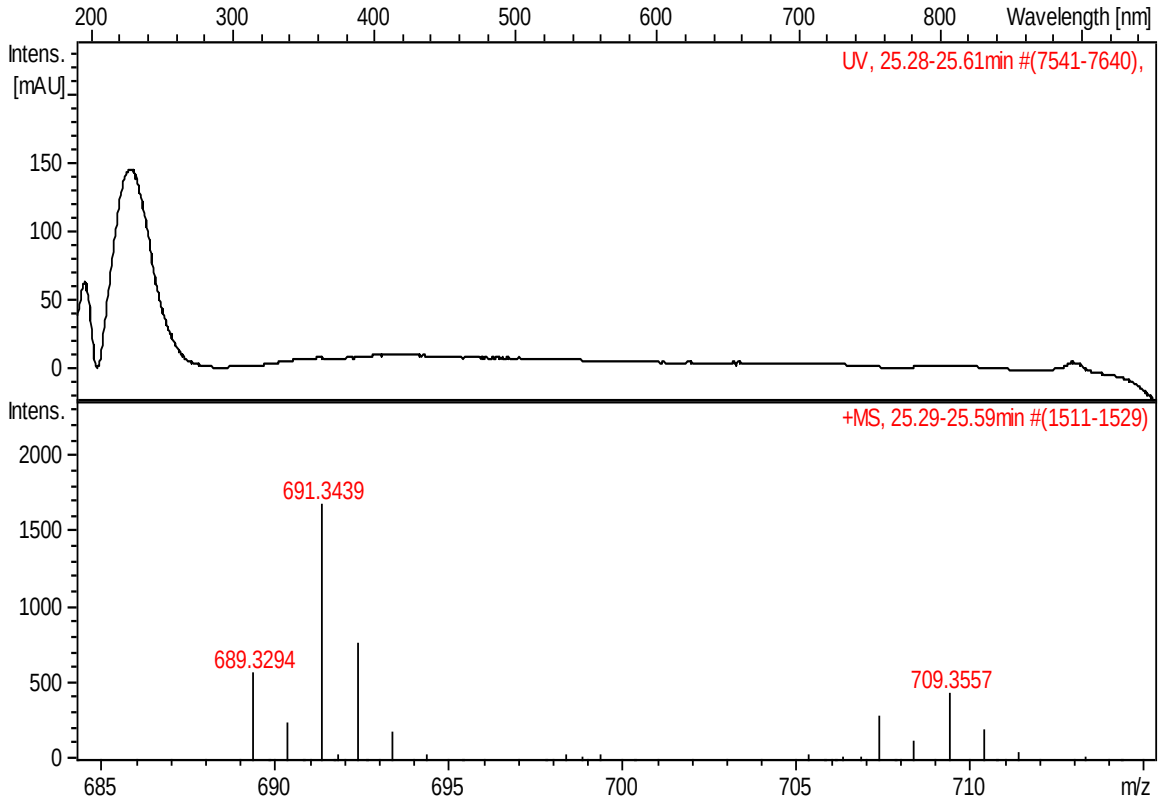

FIGURE 4.115 - HRESIMS spectrum of Picraviane U (**21**) indicating *m/z* $[M+H]^+$ = 709.3557 and $[M+H-H_2O]^+$ = 691.3439.

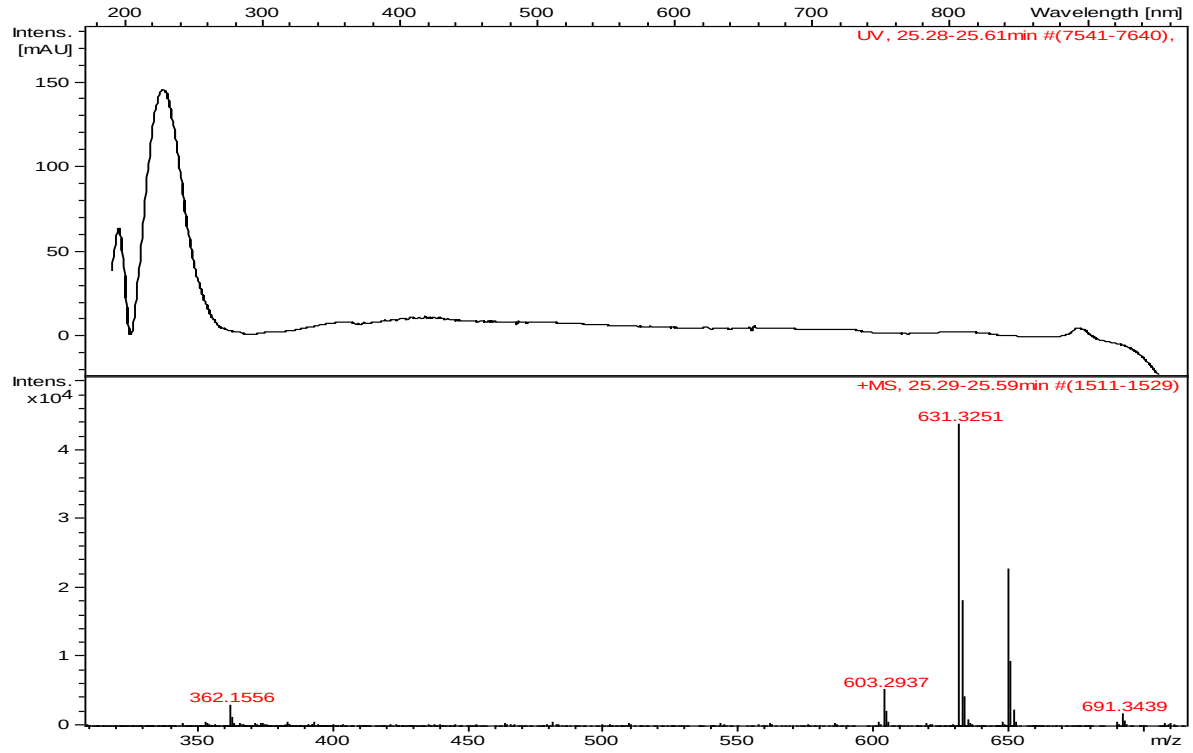

FIGURE 4.116 - HRESIMS spectrum of Picraviane U (**21**) indicating *m/z* $[M+H-H_2O-CH_3CO_2H]^+$ = 631.3251.

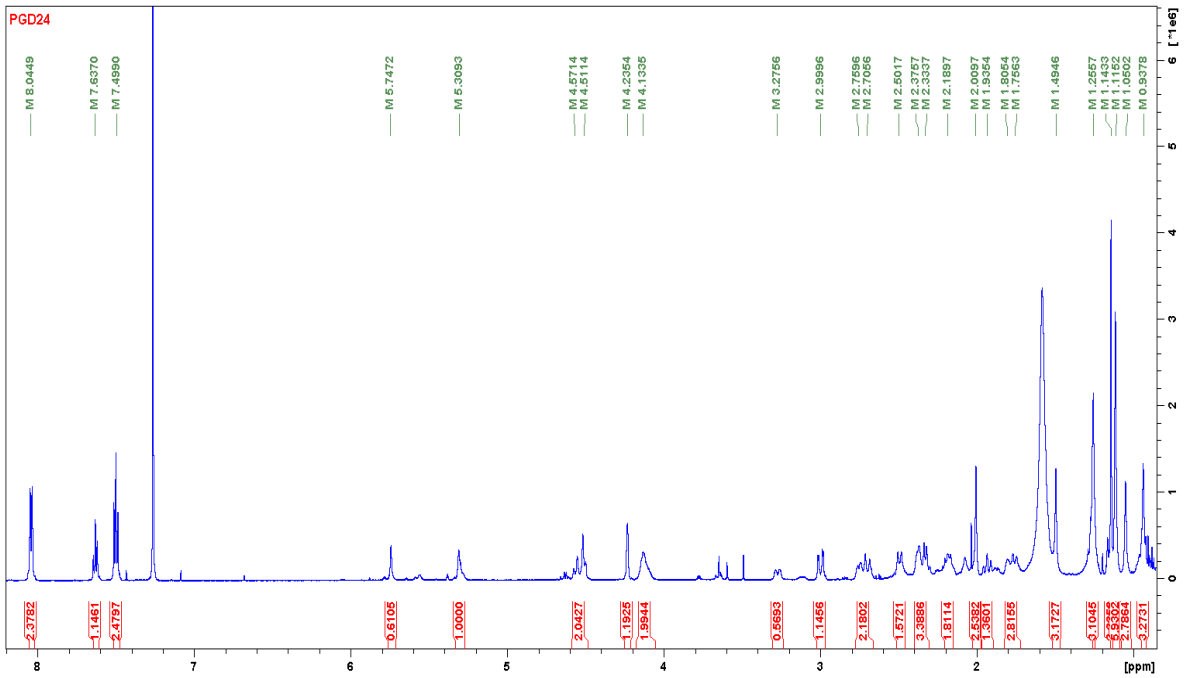

FIGURE 4.117- ^1H NMR spectrum of Picraviane V (**24**) in $CDCl_3$ (600 MHz).

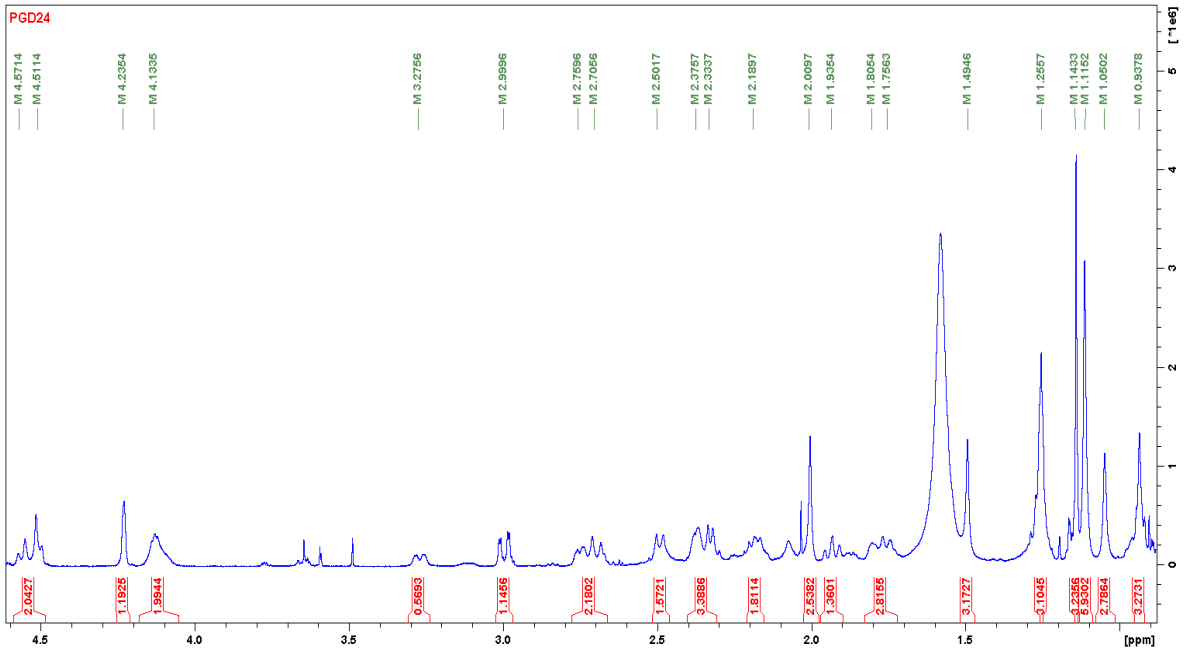

FIGURE 4.118 - Expansion of the ^{1}H NMR spectrum of Picraviane V (**24**) in $CDCl_3$ (600 MHz).

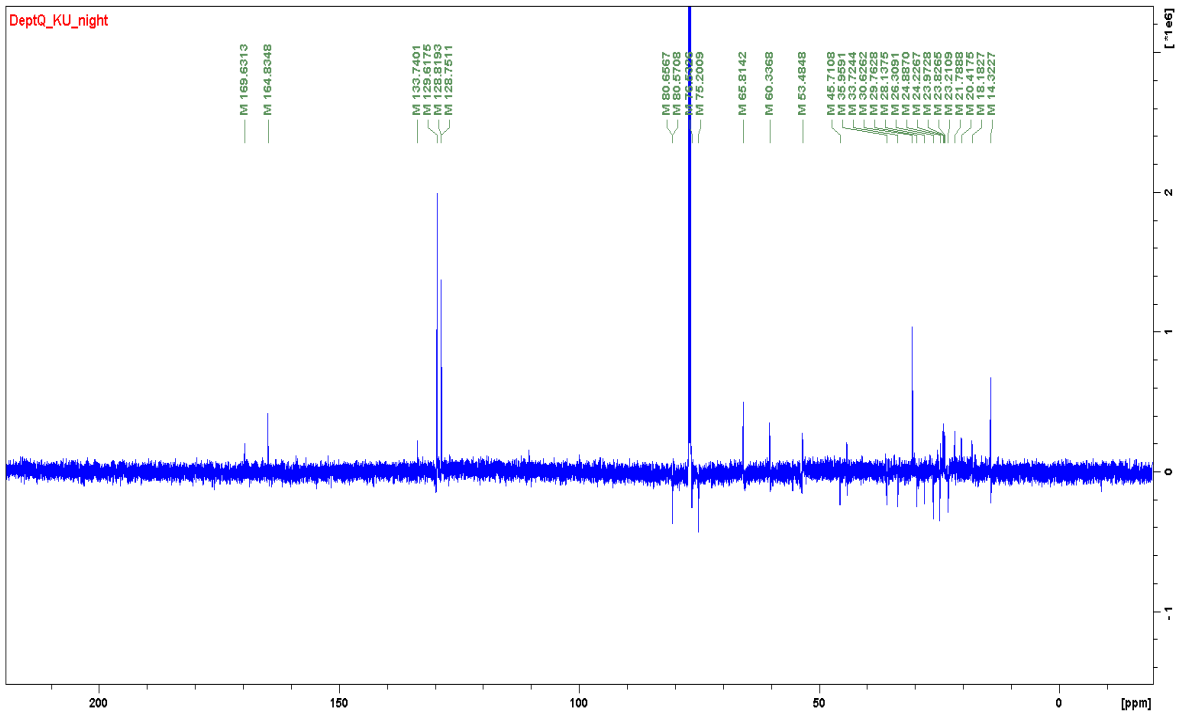

FIGURE 4.119 - DEPTQ NMR spectrum of Picraviane V (**24**) in $CDCl_3$ (150 MHz).

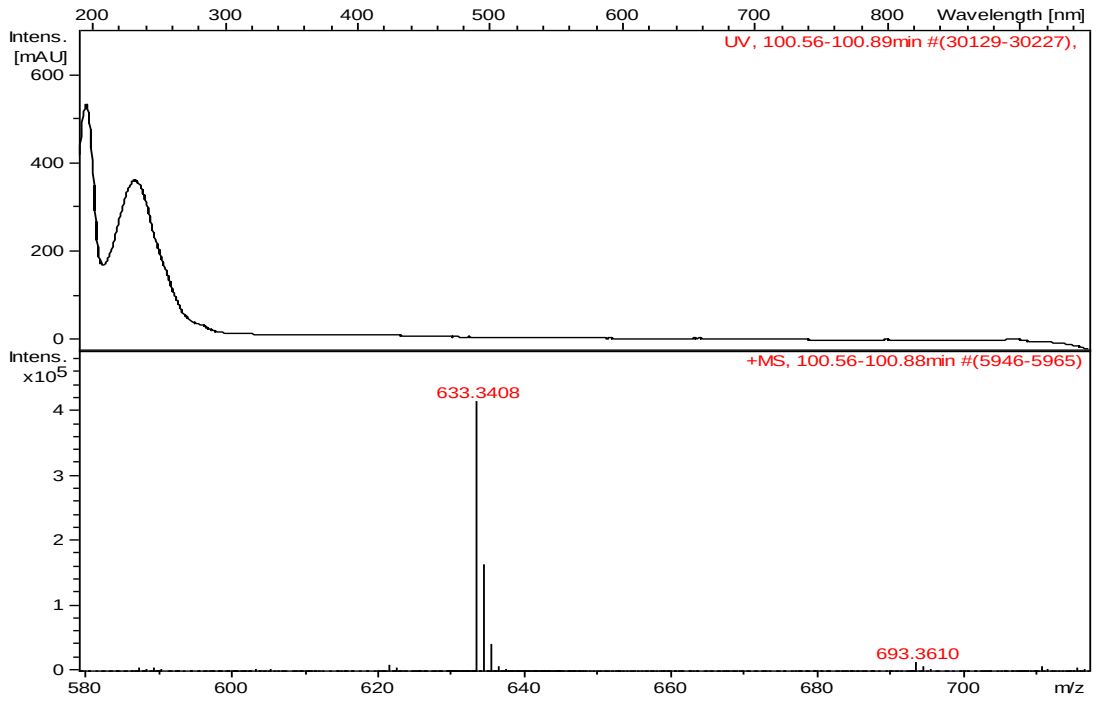

FIGURE 4.120 - HRESIMS spectrum of Picraviane V (**24**) indicating *m/*z $[M+H]^+$ = 693.3610 and $[M+H\text{-}CH_3CO_2H]^+$ = 633.3408.

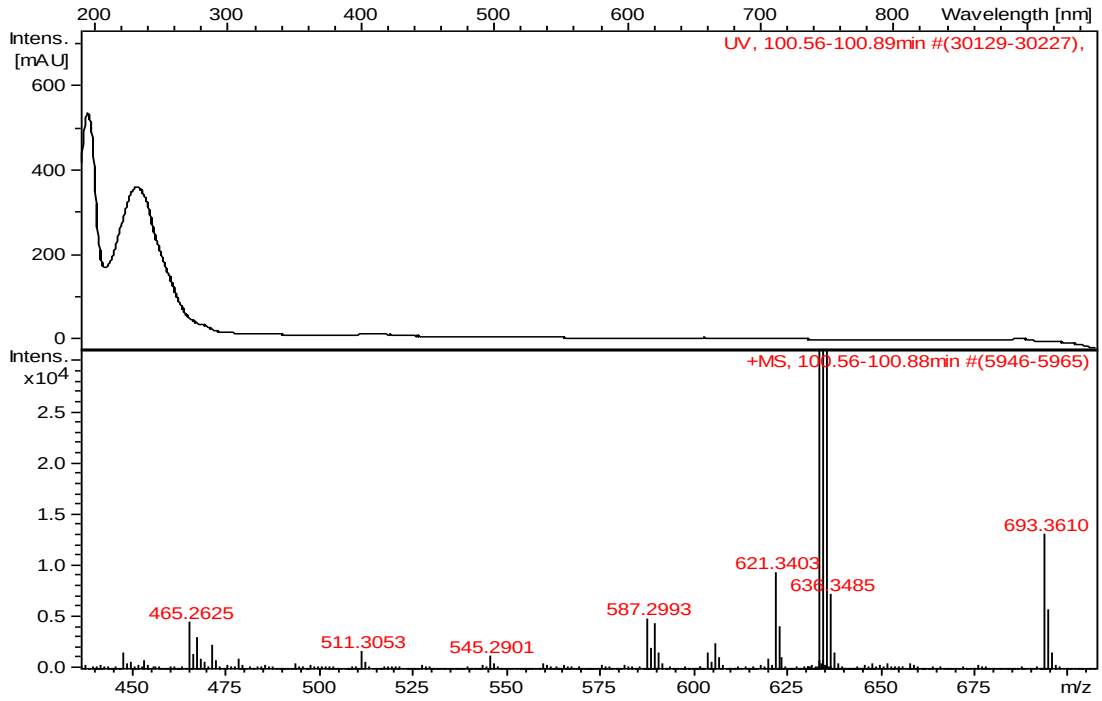

FIGURE 4.121 - HRESIMS spectrum of Picraviane V (**24**) indicating *m/*z $[M+H]^+$ = 693.3610; $[M+H\text{-}CH_3CO_2H\text{-}CH_3CH_2OH]^+$ = 587.2993 and $[M+H\text{-}CH_3CO_2H\text{-}CH_3CH_2OH\text{-}C_6H_5CO_2H]^+$ = 465.2625.

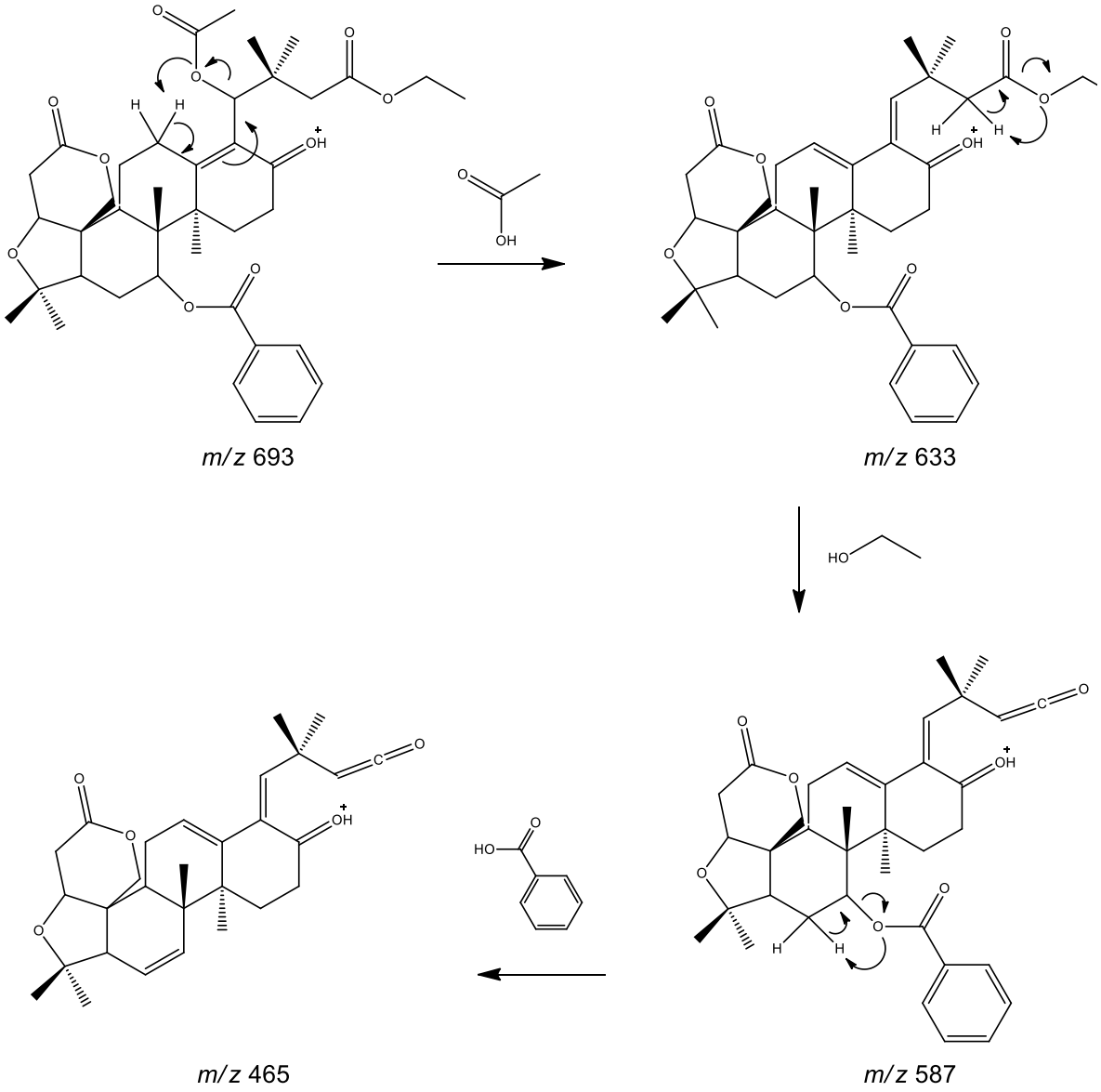

FIGURE 4.122 - Fragmentation proposal for Picraviane V (**24**).

4.1.1.8 – Biosynthetic Proposal – Modified Triterpenoids

Triterpenoids skeletons may be subjected to a variety of structural modification. Limonoids (tetranortriterpenoids) are considered degraded triterpenoids which the biosynthetic pathway is related to precursors of the euphol or tirucallol type, as shown in FIGURE 4.123 (DEWICK, 2003). These secondary metabolites are found mainly in plants of the Rutaceae, Meliaceae and Simaroubaceae families, into the Rutales order. The same biosynthetic precursor is proposed to provide another class of secondary metabolites known as quassinoids, other degraded triterpenoids produced in many plants of Simaroubaceae family (DEWICK, 2003).

The genus *Picramnia* however, also belonging to Rutales order, was removed from the Simaroubaceae family considering the morphological classification and supported by the absence of quassinoids in its species (as described in the introduction of this present work, section 1.3). However, a positioning based in the absence of secondary metabolites is limited to the species studied, and always brings up the questioning if these compounds can be found in a future investigation. Therefore, the isolation of new nortriterpenes in a specie of *Picramnia* presented in this work, contributes not only to the chemosystematics of this genus, but also supports its positioning into the Picramniaceae family, once a new proposal of the biosynthetic pathway is suggested to lead the formation of this new class of degraded terpenoids (nortriterpenes).

Thus, the isolation of oleanolic acid in some *Picramnia* species, as well the observation of oleanolic acid in crude ethanol extract of *P. glazioviana* ($C_{30}H_{47}O_3$, $[M\text{-}H]^-$ = 455.3518, calcd. 455.3531; FIGURE 4.124) suggested the plausible biogenetic pathway of **6**, **20** and **23** as illustrated in FIGURE 4.125 (BALDERRAMA, 2001; JACOBS, 2003). Primarily, the A and A' rings common in some limonoids can be formed by the oxidation of C-1 and C-25 in the intermediates **A** and **B**, followed by two intramolecular cyclization and consequently loss of two molecules of water (**C**). The decarboxylation together dehydration in ring D supports the 29 carbon atoms for the nortriterpenes (**D**-**F**). An allylic oxidation suggests the formation of the intermediary F, which converts to G by a Baeyer-Villiger oxidation, possessing the main skeleton of **06**, **20** and **23**. Finally, the nortriterpenes **06**, **20** and **23** are formed by further oxidations at C-19 and C-7 and esterifications.

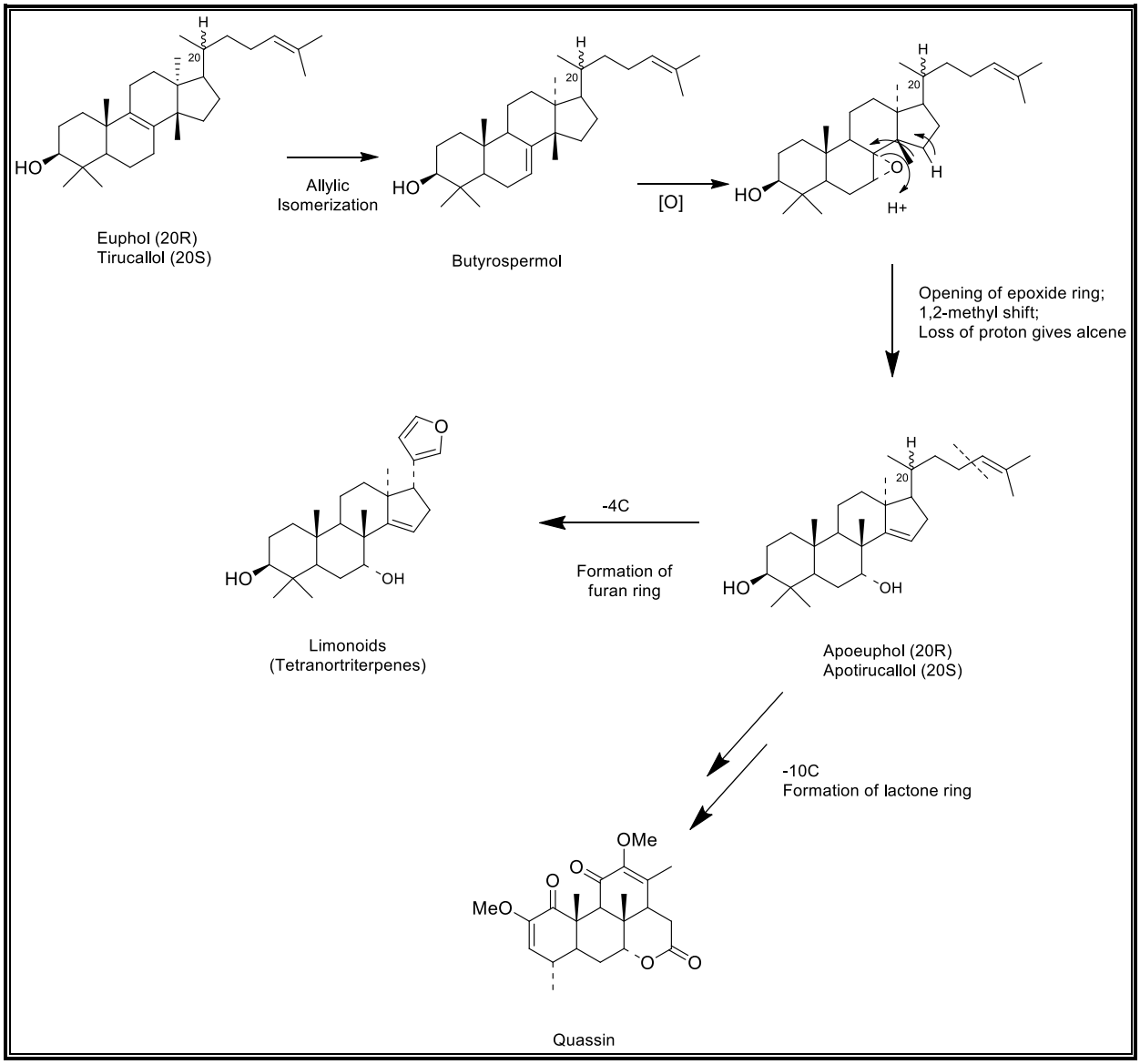

FIGURE 4.123 – Biosynthetic pathway to the degraded triterpenes in Rutales (DEWICK, 2003).

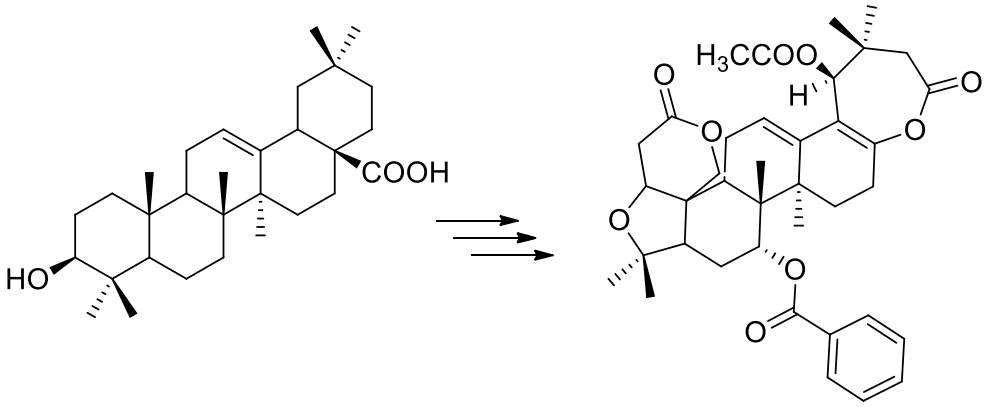

Oleanolic acid (**23**)

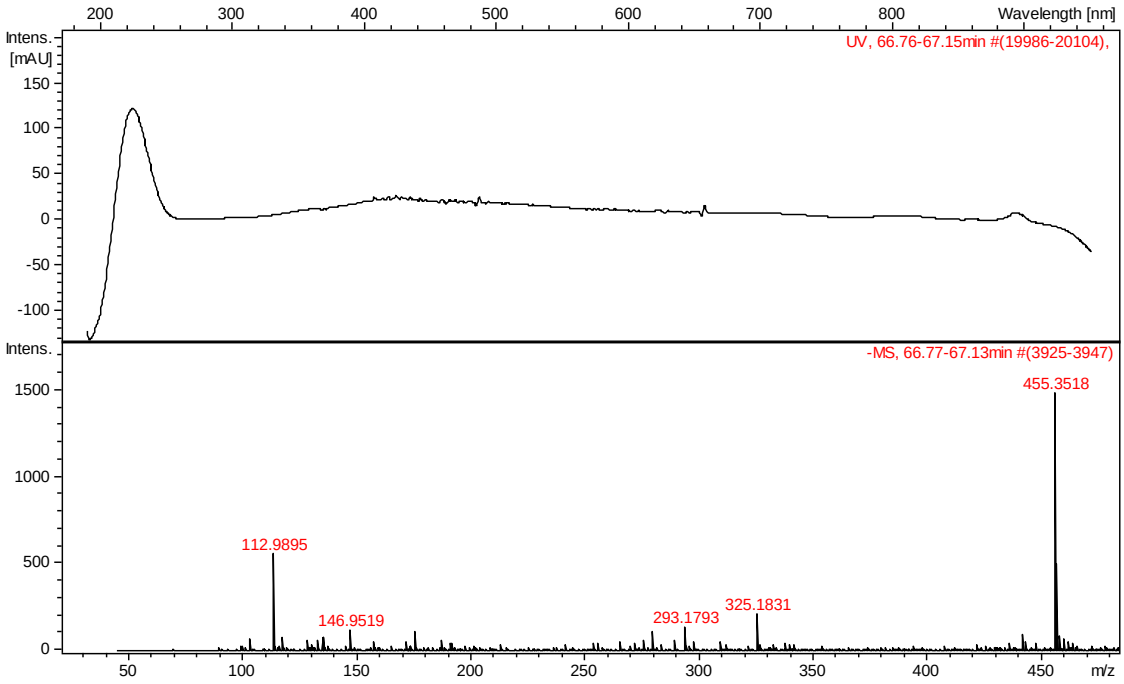

FIGURE 4.124 - HRESIMS extracted ion spectrum of $[M-H]^-$ = 455.3518 ($C_{30}H_{47}O_3$, negative mode) indicating the presence of the biossynthetic precursor oleanolic acid in the ethanolic extract of *P. glazioviana*.

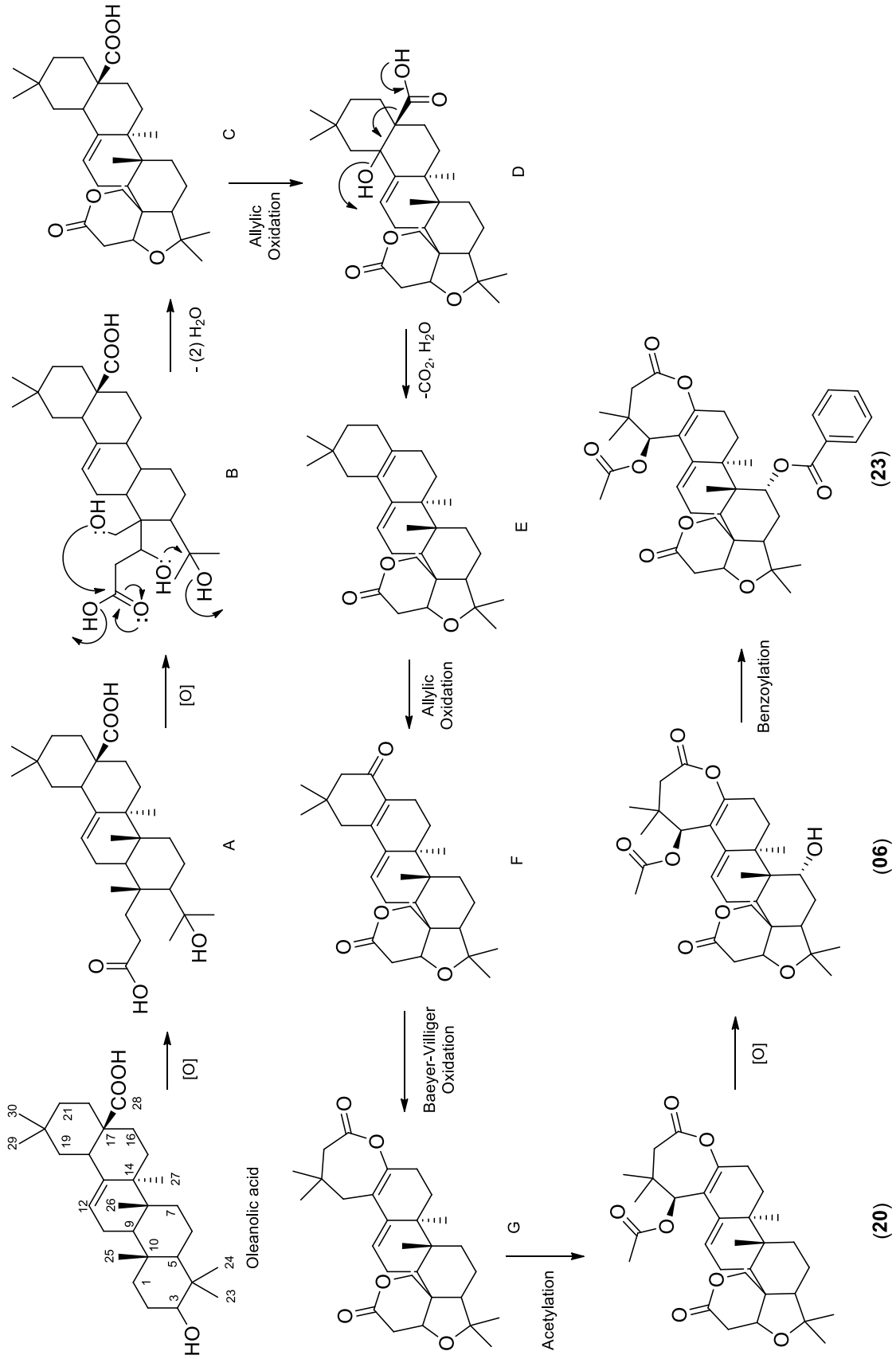

FIGURE 4.125 - Plausible Biogenetic Pathway of Compounds **23**, **20** and **06.**

The remaining compounds isolated present an unprecedented E ring modifications. Although four pairs of distereoisomers were isolated, the stereospecific hydroxylation in plant would lead the formation of only one isomer from each pair of diastereoisomers, while the second one would be involved in the opening and closing reactions of the γ–lactone ring during the extraction procedures. Hereby is presented a plausible biogenetic pathway for them. Biogenetically, the main skeleton (intermediary **G**, Figure 4.125) is followed by an allylic hydroxylation at the carbon C-19 (intermediary **H**). The stereospecificity hydroxylation at C-19, followed by an intramolecular nucleophilic cyclization at the carbonyl carbon C-22 would lead the formation of a γ–lactone in **08** or **09**. Compounds **18** and **19** are formed by further oxidations and sterifications processes. Oxidations at the carbon C-7 and allylic oxidation at C-12 from **08** and **09** lead to compounds **02** and **03** and **05**. Compounds **18** and **19** woud be the precursors of **12** and **13** through allylic oxidation in C-12.

An allylic oxidation at C-12 from Picraviane B (**20**) would lead the formation of the intermediary **I**. Thus, a nucleophilic attack at the carbonyl carbon C-22 by hydroxyl groups from external water molecules followed by the rearrangement of the double bonds would lead the rupture of the E ring and formation of the compound **07a**. This same mechanism involving the nucleophilic attack at C-22 by external water molecules can also be proposed to the formation of compound **07** from the Picraviane B (**20**), that converts to compound **01** (by oxidation at C-7) and to compound **14** through an enzymatic methylation.

In a similar way, from Picraviane A (**23**), a nucleophilic attack at the carbonyl carbon C-22 by hydroxyl groups and rearrangement of the double bonds lead to compound **15**, followed by an enzymatic methylation to obtain the compound **22**. Still from Picraviane **A (23)**, the intermediary **J** is reached by an allylic oxidation at C-12, followed by another nucleophilic attack at C-22 obtaining compound **17**. Thus, the epoxidation in **17** can be proposed by a mono-oxygenase involving cytochrome P-450 (which NADPH features as hydrogen donor) resulting, finally to the compound **16** (FIGURE 4.126, DEWICK, 2003).

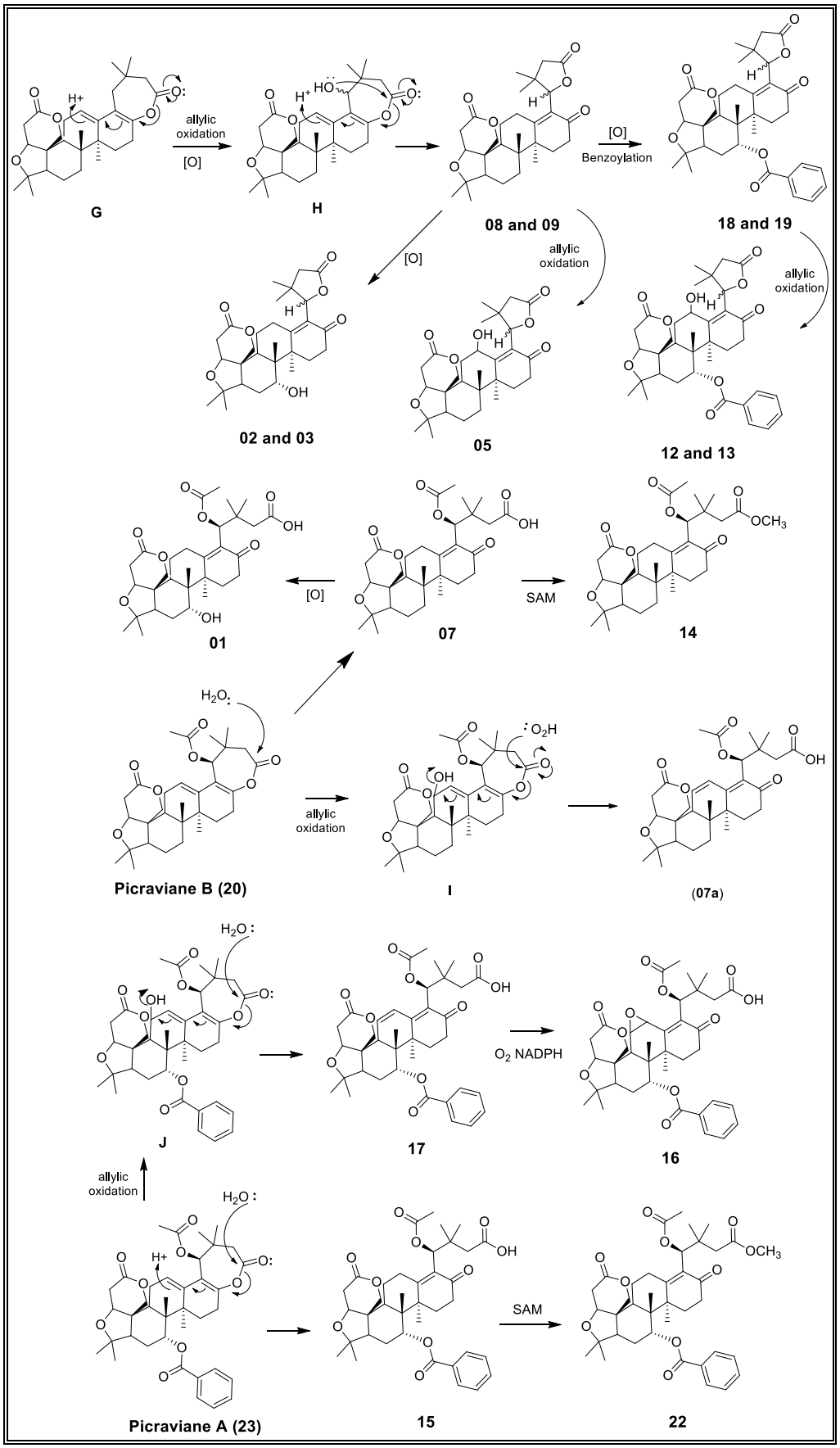

FIGURE 4.126 - Plausible Biogenetic Pathway to the remaining isolated compounds from *P. glazioviana*.

4.1.2 – Anthraquinones

The study of the methanol extract from the stem of *P. bahiensis* (PBCMe) disclosed 03 known anthraquinones and 02 known glycosides anthraquinones. Hereby, is presented the discussion to these compounds:

4.1.2.1 – Anthraquinones 25, 26 and 27

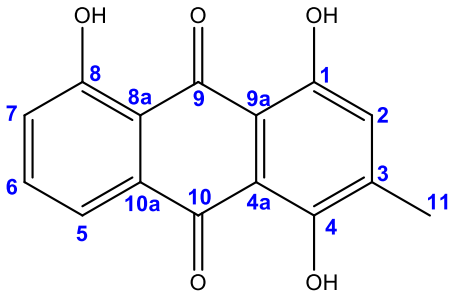

(25)

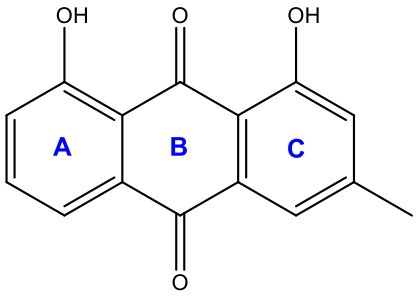

(26)

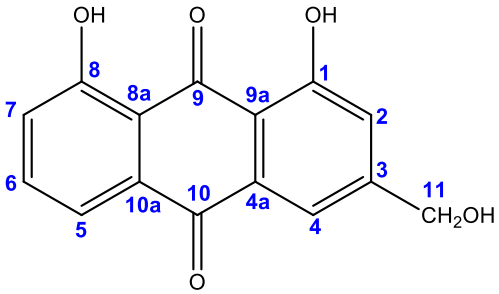

(27)

The discussion to the isolated anthraquinones is presented below as the following sequence: compound **26**, **27** and then to compound **25**.

The anthraquinone **26** was isolated as an intense orange color and identified through analyses of ^{1}H and ^{13}C NMR spectrum and GC-MS experiments as the compound chrysophanol. The NMR data was compared with data acquired from literature (RODRIGUEZ-GAMBOA, 2011).

The ^{1}H NMR spectrum disclosed two signals consisting a chelated hydroxyl at δ 12.01 and δ 12.12, besides a methyl at δ 2.46 and five aromatic protons. The substitution pattern in the anthracene backbone of the anthraquinone **26**

was defined according with the chemical shifts and multiplicity of the aromatic protons. Thus, the ring C was assembled due the presence of the proton H-4, a broad doublet (1.7 Hz), peri to the carbonyl group at *δ* 7.65 and the proton H-2, a doublet of quartet (observed due the coupling W ^4J with the methyl group, 1.7 and 0.8 Hz) peri carbinol at *δ* 7.10. In the ring A, the aromatic protons appears at *δ* 7.82 (dd, *J* = 7.5; 1.2 Hz, 1H), *δ* 7.67 (dd, 8.3; 7.5, 1H) and *δ* 7.28 (dd, *J* = 8.3; 1.2 Hz, 1H).

The ^{13}C NMR spectrum displayed 15 carbons. Among of them, a methyl group at *δ* 22.2 and two carbonyl carbons at *δ* 192.5 (C-9) and *δ* 182.0 (C10) were observed, confirming the anthracene skeleton of the anthraquinone. The assignments of the ^{1}H and ^{13}C resonances to the compound **26** are shown in TABLE 4.14. The ^{1}H and ^{13}C NMR spectra are presented in FIGURES 4.129 to 4.131.

TABLE 4.14 –^{1}H and ^{13}C NMR Data for Compounds **26** (acquired in $CDCl_3$, 400 MHz) compared with the compound chrysophanol (acquired in $CDCl_3$, 200 MHz)

	δ_H (ppm), *J* (Hz)		δ_C (ppm)	
H/C	**26**	RODRIGUEZ-GAMBOA, 2001	**26**	RODRIGUEZ.-GAMBOA, 2001
2	7.10 (dq, 1.7; 0.8)	7.10 (dq, 1.6 e 0.8)	124.4	124.4
4	7.65 (br d, 1.7)	7.66 (br d, 1.6)	119.9	119.9
5	7.82 (dd, 7.5; 1.2)	7.82 (dd, 7.6 e 1.3)	121.3	121.3
6	7.67 (dd, 8.3; 7.5)	7.67 (br t, 7.6)	136,9	136.9
7	7.28 (dd, 8.3 e 1.2)	7.28 (dd, 8.3 e 1.3)	124.6	124.6
CH_3	2.46 (t, 0.8)	2.47 (t, 0.8)	22.2	21.7
1-OH	12.01[a] (s)	12.02[a]	--	--
8-OH	12.12[a] (s)	12.13[a]	--	--

[a] Signals may be switched.

Compound **26** was also analyzed by GC-MS. The mass spectrum disclosed a very intense molecular ion peak at m/z 254, also being the base peak, since fragmentation of the aromatic rings requires a great deal of energy. The molecular formula was established being $C_{15}H_{10}O_4$, according to the compound chrysophanol. The mass spectrum acquired and its respective comparison with the database of the instrument is shown in FIGURE 4.127.

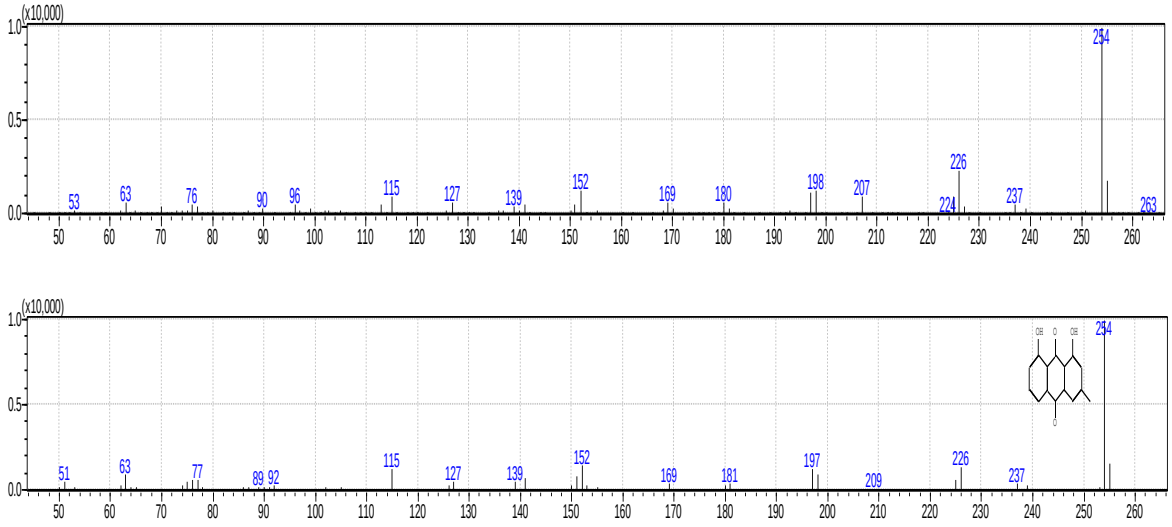

FIGURE 4.127 - Mass spectrum of compound **26** (chrysophanol).

The anthraquinone **27** was isolated as yellow solid and identified through analyses of 1D and 2D NMR spectrum as the compound aloe-emodin. The NMR data was compared with data acquired from the literature (VIEIRA, 1995). This compound was also identified from *P. glazioviana* (compound **5a**), isolated together with the nortriterpene **05**.

The ^{1}H NMR spectrum of compound **27** showed very similar to compound **26**. The substitution pattern to the rings A and C of the anthracene skeleton was identical to the chrysophanol: three aromatic signals featuring the trisubstituted ring A: *δ* 7.84 (dd, *J* = 7.5; 1.2 Hz, 1H), *δ* 7.69 (dd, *J* = 8.4; 7.5, 1H) and *δ* 7.31 (dd, *J* = 8.4; 1.2 Hz, 1H); two aromatic signals featuring the ring C: *δ* 7.35 (dt, *J* = 1.5; 0.8 Hz, 1H) and *δ* 7.80 (dt, *J* = 1.5; 0.8 Hz, 1H). Besides, it was also noticed a hydroxymethylene signal at *δ* 4.83 (br s, 2H), substituting the methyl group at C-11 as observed in compound **26**. The HSQC spectrum showed the following

correlations to these set of signals: *δ* 7.84 / 120.0; *δ* 7.69 / 137.1; *δ* 7.31 / 124.7; *δ* 7.35 / 121.4; *δ* 7.80 / 117.7 and *δ* 4.83 / 64.1.

Although the ^{13}C NMR spectrum showed the absence of carbonyl carbon at C-9, and very weak carbon at C-10 (*δ* 181.7), two signals consisting a chelated hydroxyl at *δ* 12.08 and *δ* 12.09 were observed through the ^{1}H NMR spectrum, confirming the carbonyl at C-9. Moreover, the absence of signal around *δ* 4.60 as singlet, excludes the possibility of having protons at C-10, common in anthrones. This establishment can also be confirmed by the coupling pattern of the protons H-2 and H-4 as a doublet of triplet, indicating the coupling with the methylene proton at C-11. By the ^{13}C NMR spectrum, the absence of some carbon around *δ* 75.0 excludes the possibility of having a hydroxyl substituent at C-10, characteristic of oxanthrones.

The assignments of the ^{1}H and ^{13}C resonances to the compound **27** are shown in TABLE 4.15. The ^{1}H, ^{13}C NMR and HSQC spectra are presented in FIGURES 4.132 to 4.134.

TABLE4.15 –^{1}H and ^{13}C NMR Data for Compounds **27** (acquired in $CDCl_3$, 400 MHz) compared with the compound aloe-emodin (acquired in DMSO-d_6 and $CDCl_3$, 400 MHz)

	δ_H (ppm), *J* (Hz)		δ_C (ppm)	
H/C	**27**	VIEIRA, 1995	**27**	VIEIRA, 1995
2	7.35 (dt, 1.5; 0.8)	7.35 (br s)	121.4	123.9
4	7.80 (dt, 1.5; 0.8)	7.79 (br s)	117.7	119.3
5	7.84 (dd, 7.5; 1.2)	7.81 (d, 8.8)	120.0	120.7
6	7.69 (dd, 8.4; 7.5)	7.06 (t, 8.8)	137.1	136.5
7	7.31 (dd, 8.4 e 1.2)	7.30 (d, 8.8)	124.7	123.9
11	4.83 (br s)	4.74 (d, 0.8)	64.1	62.6
1-OH	12.08[a] (s)	12.06[a]	--	--
8-OH	12.09[a] (s)	12.11[a]	--	--

[a] Signals may be switched.

The anthraquinone **25** was isolated as red solid. Due the small amount (0.5 mg) obtained, the compound was only analyzed by ^{1}H NMR spectrum and GC-MS. The mass spectrum acquired from the GC-MS analysis displayed the molecular ion peak at m/z 270, corresponding to the molecular formula as $C_{15}H_{10}O_{5.}$ The mass spectrum acquired and its respective comparison with the database of the instrument is shown in FIGURE 4.128.

The comparison with the database of the instrument indicated to be the compound emodin. However, after obtaining the ^{1}H NMR spectrum, it was possible to observe signals belonging to the ring A, identical as those observed to compound **27**: δ 7.89 (dd, J = 7.5; 1.1 Hz, 1H), δ 7.69 (t, J = 8.4, 1H) and δ 7.30 (dd, J = 8.4; 1.1 Hz, 1H). Consequently, a mistakenly establishment of compound **25** by GC-MS considering only the molecular weight and comparison with the database of the instrument showed to be hasty and not reliable. The data from ^{1}H NMR indicated a trisubstituted A ring to compound **25**, and consequently, placing the hydroxyl group at the ring C. Although the acquisition of the NMR spectrum was performed with a short width, limiting the observation of the chelated protons relevant to the confirmation of the structure, the correct positioning of the hydroxyl group on C ring could be established considering the value of the chemical shift to its proton. Thus, since protons peri to the carbonyl group present a deshielded chemical shift, the shielded proton observed at δ 7.16 (br s, 1H) was established at H-2. The NMR data compared with the data from literature allowed the identification of **25** as the compound islandicin (TIETZE, 2007).

Islandicin is an anthraquinone pigment produced by *Penicillium islandicum* (DEWICK, 2003). This compound has also been isolated from several species of plants, as for example from species of *Cassia* (Fabaceae), from *Bulbine abyssinica* (Asphodelaceae) and from *Ventilago leiocarpa* (Rhamnaceae, JIBRIL, 2017; LIN, 2001; MANIKANDASELVI, 2016; WANJOHI, 2005). However, this is the first report of isolation of this compound in species of Picramniaceae family. The assignments of the ^{1}H resonances to the compound **27** are shown in TABLE 4.16. The ^{1}H spectrum and expansion are presented in FIGURES 4.135 and 4.136.

TABLE 4.16 – ^{1}H NMR Data for Compounds **25** (acquired in $CDCl_3$, 600 MHz) compared with the compound islandicin (acquired in $CDCl_3$, 300 MHz).

	δ_H (ppm), *J* (Hz)	
H/C	**25**	TIETZE, 2007
2	7.16 (br s)	7.15 (br s)
5	7.89 (dd, 7.5; 1.1)	7.88 (dd, 7.6; 1.1)
6	7.69 (t, 8.4)	7.69 (t, 8.3)
7	7.30 (dd, 8.4 e 1.1)	7.30 (dd, 8.4 e 1.0)
CH_3	2.38 (d, 0.9 Hz)	2.38 (d, 0.6 Hz)

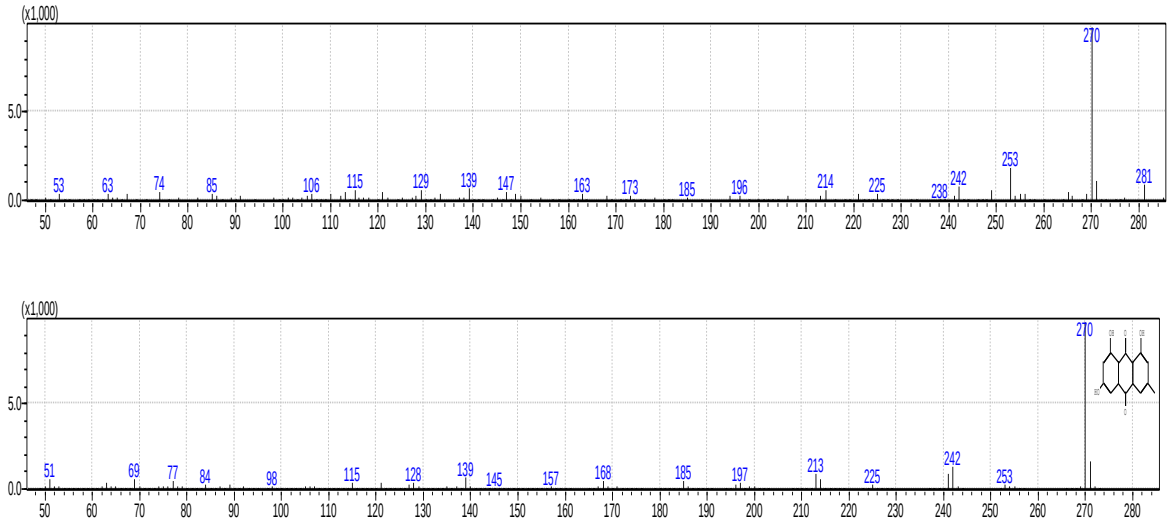

FIGURE 4.128 - Mass spectrum of compound **25** (islandicin) in comparison with the compound emodin indicated by the database.

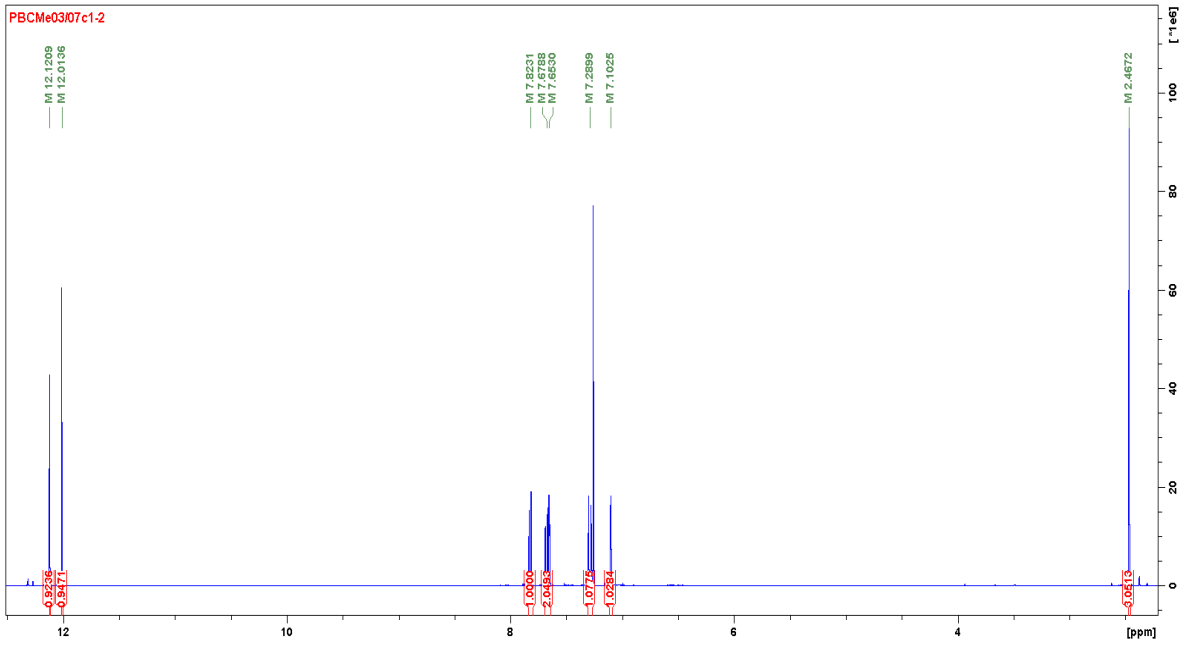

FIGURE 4.129 - ^{1}H NMR spectrum of compound **26** in $CDCl_3$ (400 MHz).

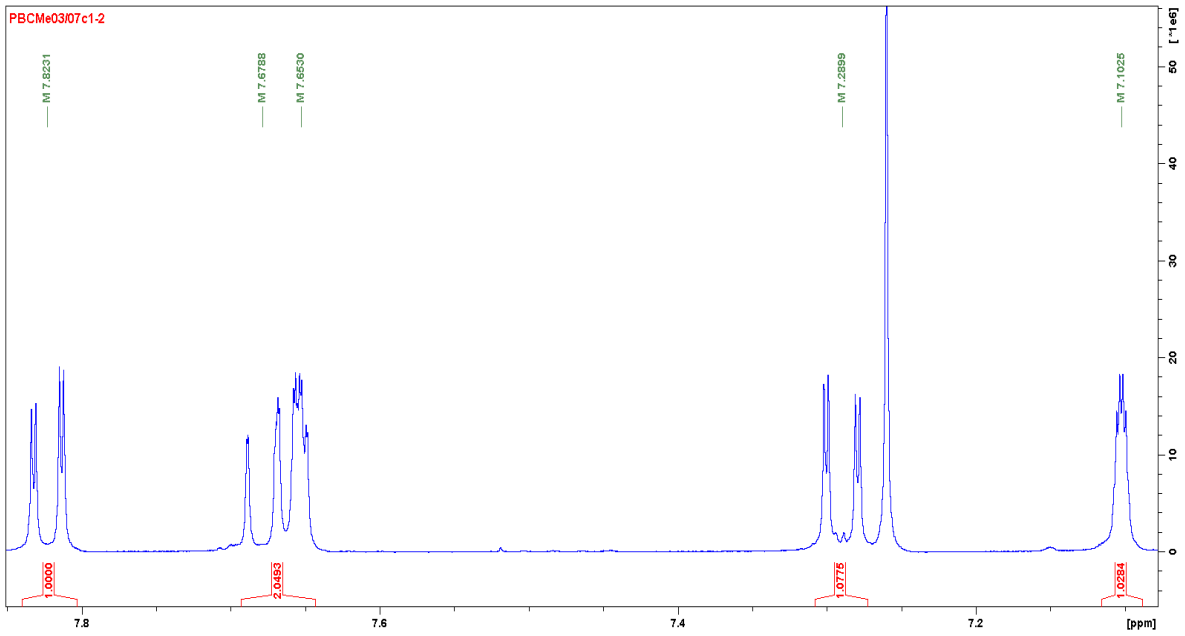

FIGURE 4.130 - Expansion of the ^{1}H NMR spectrum of compound **26** in $CDCl_3$ (400 MHz).

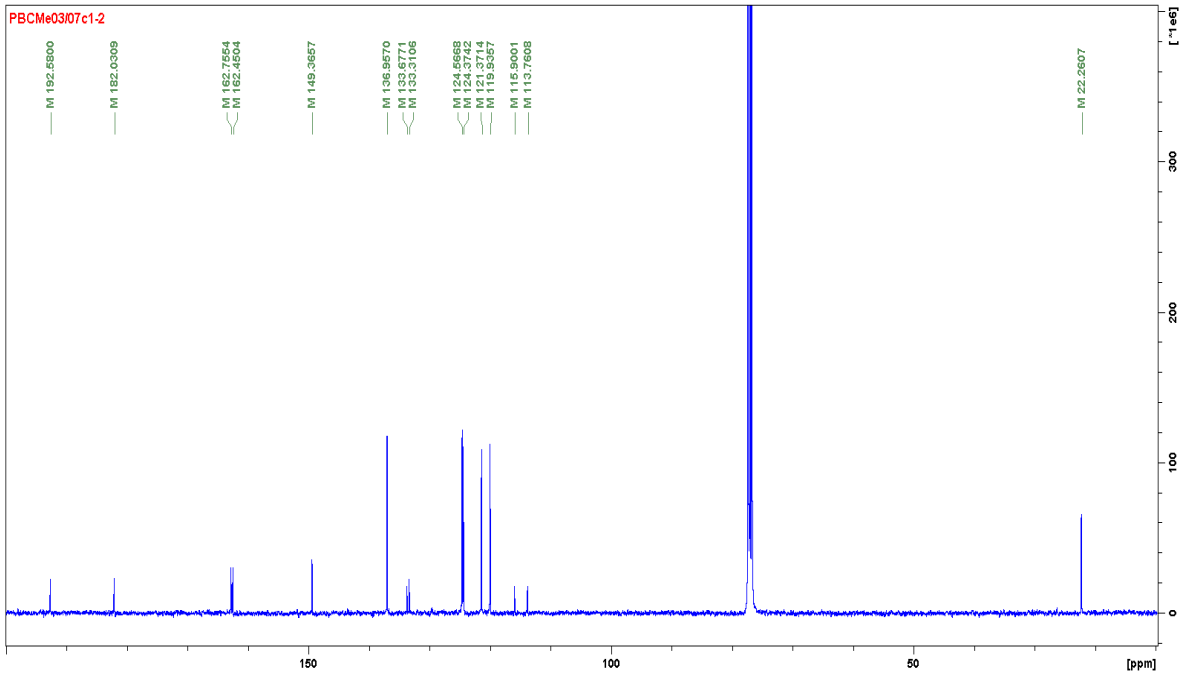

FIGURE 4.131- ^{13}C NMR spectrum of compound **26** in $CDCl_3$ (100 MHz).

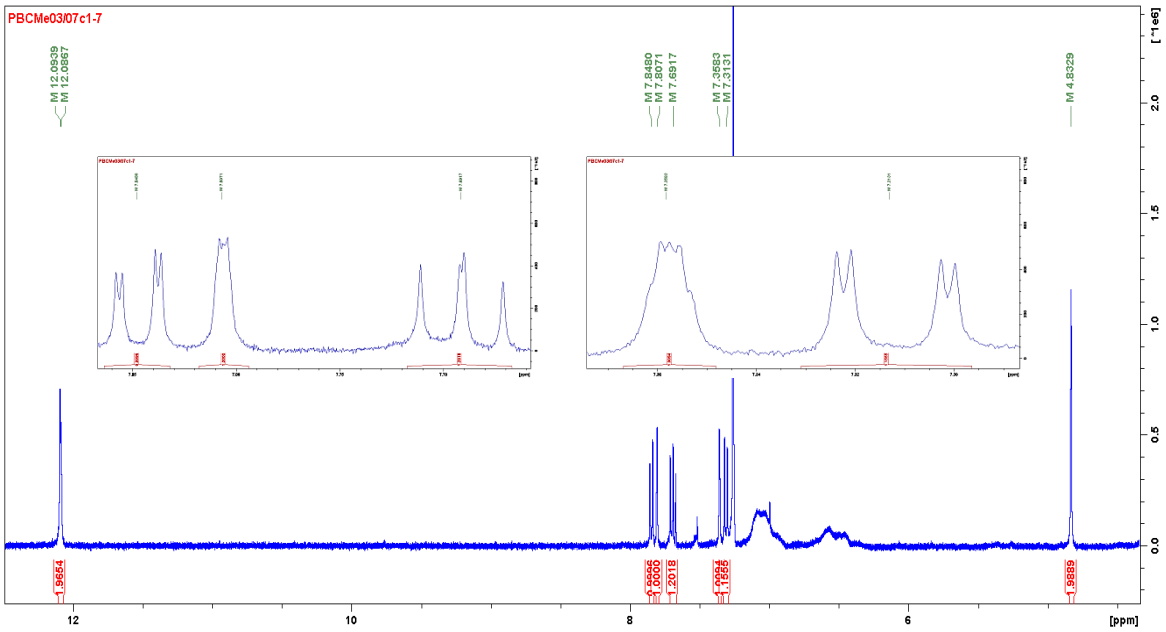

FIGURE 4.132 - ^{1}H NMR spectrum and expansion of the aromatic region to compound **27** in $CDCl_3$ (400 MHz).

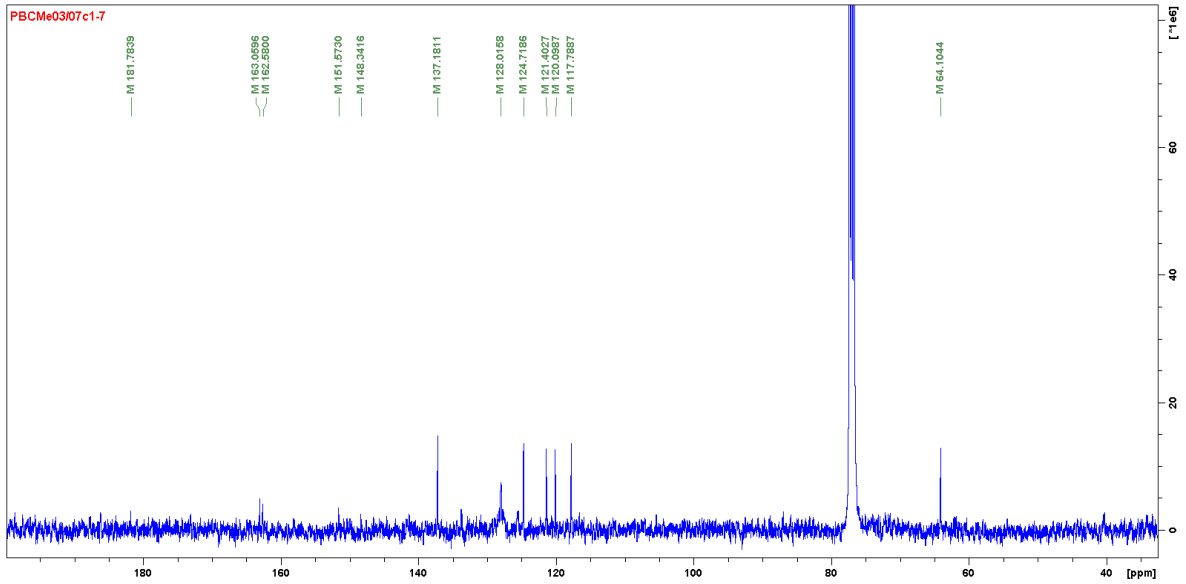

FIGURE 4.133 - ^{13}C NMR spectrum of compound **27** in $CDCl_3$ (100 MHz).

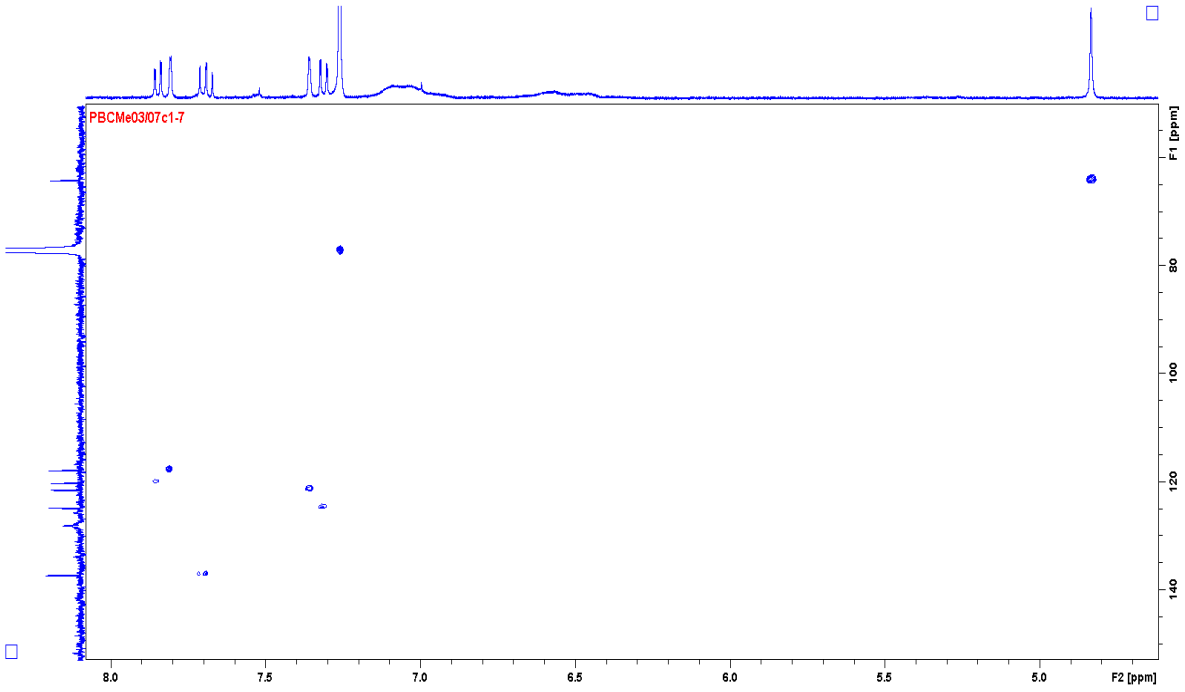

FIGURE 4.134 - HSQC spectrum of compound **27** in $CDCl_3$ (400 MHz).

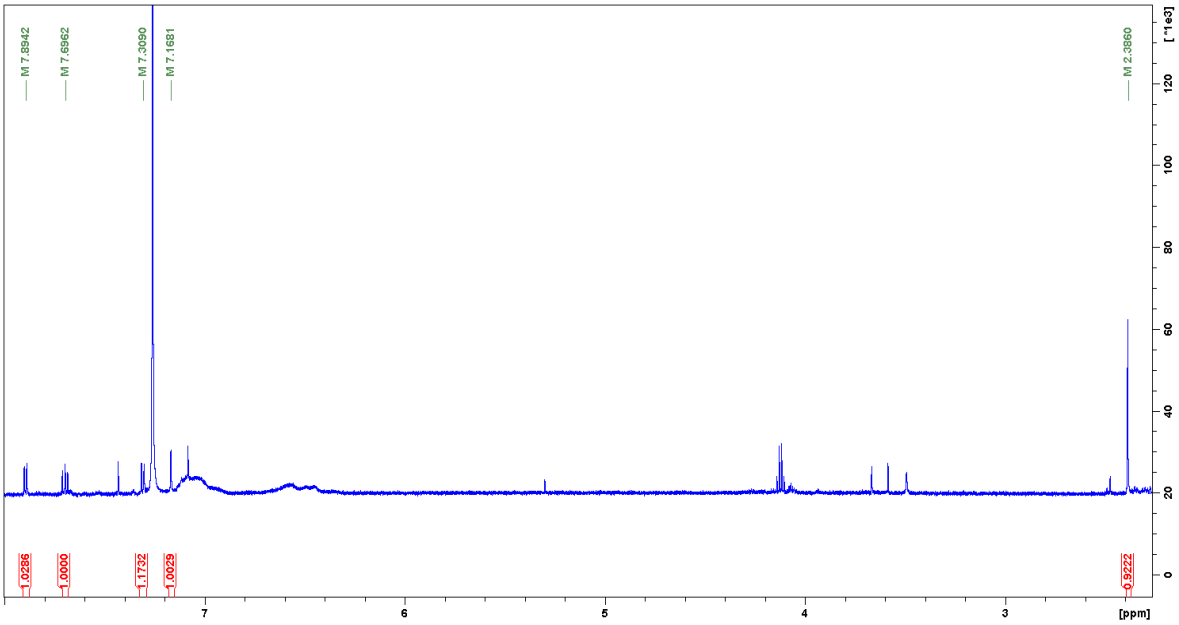

FIGURE 4.135 - ^{1}H NMR spectrum of compound **25** in $CDCl_3$ (600 MHz).

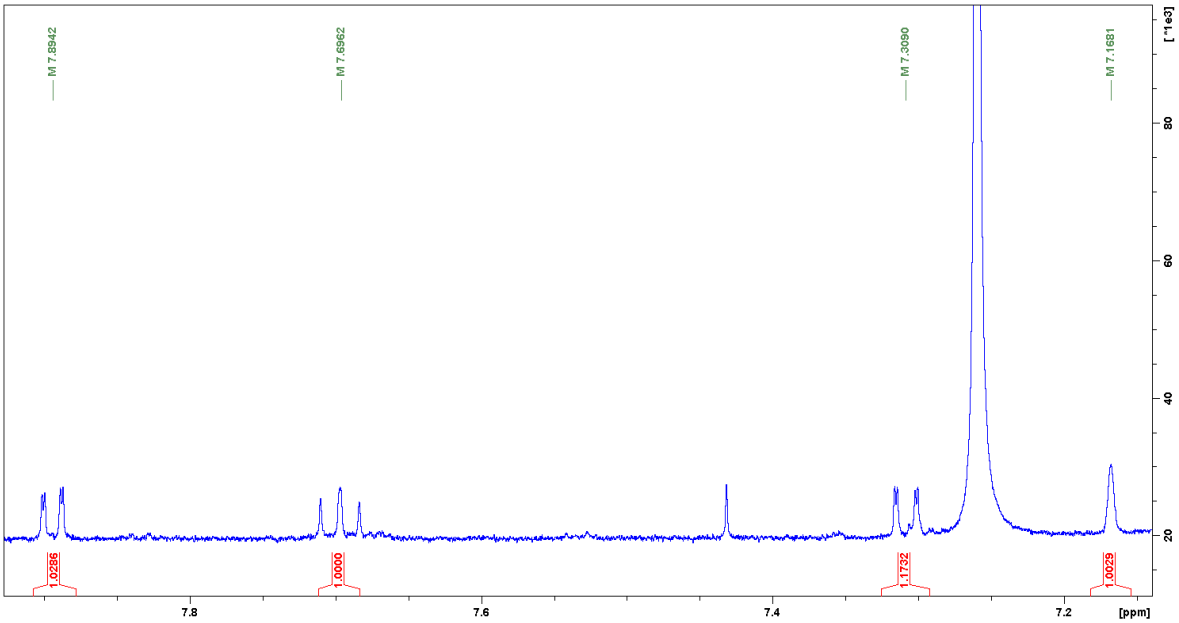

FIGURE 4.136 - Expansion of the ^{1}H NMR spectrum of compound **25** in $CDCl_3$ (600 MHz).

4.1.2.2 – Anthraquinones 28 and 29

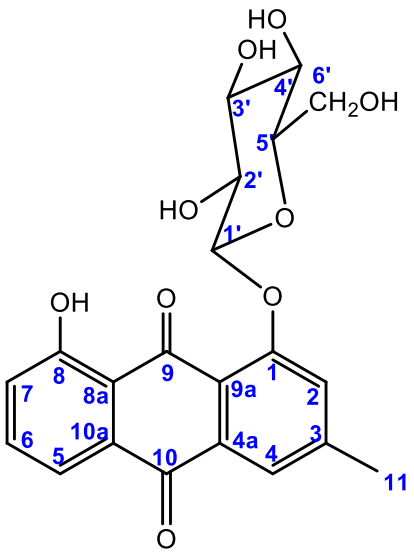

(28)

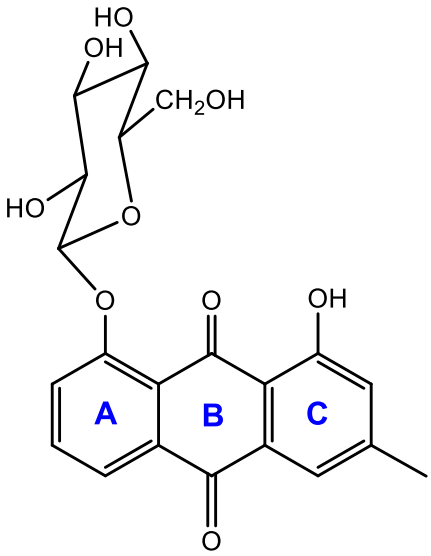

(29)

The anthraquinones **28** and **29** were isolated as orange powder and identified through analyses of 1D and 2D NMR spectrum and HRESIMS data. The NMR data was compared with data acquired from literature (VIEIRA, 1995).

The ^{1}H NMR spectrum of compound **28** and **29** showed very similar to compound **26**. The substitution pattern to the rings A and C of the anthracene skeleton was identical to the chrysophanol (FIGURES 4.139 and 4.143):

- Compound **28**: three aromatic signals featuring the trisubstituted ring A: *δ* 7.72 (d, *J* = 7.5 Hz, 1H), *δ* 7.68 (t, *J* = 8.2 Hz, 1H) and *δ* 7.29 (d, *J* = 8.2 Hz, 1H); two aromatic signals featuring the ring C: *δ* 7.60 (s, 1H) and *δ* 7.83 (s, 1H) and a methyl group at *δ* 2.50 (s, 3H).
- Compound **29**: three aromatic signals featuring the trisubstituted ring A: *δ* 8.02 (dd, *J* = 7.3; 1.5 Hz, 1H), *δ* 7.82 (dd, *J* = 8.5; 7.3 Hz, 1H) and *δ* 7.79 (dd, *J* = 8.5; 1.5 Hz, 1H); two aromatic signals featuring the ring C: *δ* 7.15 (dq, *J* = 1.7; 0.8 Hz, 1H) and *δ* 7.60 (d, *J* = 1.7 Hz, 1H) and a methyl group at *δ* 2.45 (br d, *J* = 0.8 Hz, 3H).

Moreover, the ^{1}H NMR spectrum displayed signals indicating a glucose unit present in both compounds due signals at the range of *δ* 3.0 -4.0, beside the

very characteristic anomeric proton at *δ* 5.08 (d, 7.8 Hz, compound **28**) and *δ* 5.09 (d, 7.6 Hz, compound **29**). The similarity of ^{1}H NMR spectrum and ^{13}C NMR data for **28** and **29** (acquired from HSQC and HMBC experiments) established both these compounds as positional isomers, distinguishing each other by the position of the glucose unit.

The HRESIMS data and UV spectrum for each compound also confirmed they are positional isomers (FIGURES 4.137 and 4.138):

- Compound **28:** $[M+H]^+$ = 417.1190, molecular formula as $C_{21}H_{21}O_9$ (12 degrees of unsaturation) and a base peak corresponding to chrysophanol backbone: $[M+H\text{-glucose}]^+$ = 255.0659; UV absorptions at: 223, 260 and 412 nm, according with the high extension of the conjugated double bond.
- Compound **29:** $[M+H]^+$ = 417.1229, molecular formula as $C_{21}H_{21}O_9$ (12 degrees of unsaturation) and a base peak corresponding to chrysophanol backbone: $[M+H\text{-glucose}]^+$ = 255.0656; UV absorptions at: 221, 258 and 410 nm, according with the high extension of the conjugated double bond.

Therefore, the glucose unit was established analyzing the HMBC and NOESY spectrum. Thus correlation between H-5 and H-4 to the carbonyl at *δ* 183 excluded the presence of the glucose at C-10 in both compounds. Moreover, it was observed correlations from the anomeric proton H-1' at *δ* 5.09 to the carbon C-1 at *δ* 160.0 (in HMBC spectrum, FIGURE 4.141) and to the proton H-2 at *δ* 7.60 (through NOESY spectrum, FIGURE 4.142) in compound **28**, justifying the positioning of the glucose unit at C-1. Likewise, compound **29** presented correlations from the anomeric proton H-1' at *δ* 5.08 to the carbon C-8 at *δ* 159.7 (in HMBC spectrum, FIGURE 4.145) and to the proton H-7 *δ* 7.79 (through NOESY spectrum, FIGURE 4.146), confirming the position of the glucoside at C-8.

Consequently, compounds **28** and **29** could be identified as the known compounds respectively, pulmatin (1,8-dihydroxy-3-methyl-anthraquinone-1-O-β-D-glucoside) and chrysophanein (1,8-dihydroxy-3-methyl-anthraquinone-8-O-β-D-glucoside). Although VIEIRA, 1995 have related the isolation of these compounds from *P. glazioviana*, this is the first report relating the isolation of these compounds from *P. bahiensis*.

The assignments of the ^{1}H and ^{13}C resonances to the compound **28** **a**nd **29** are shown in TABLE 4.17 and 4.18.

TABLE 4.17 –^{1}H and ^{13}C NMR Data for Compounds **28** (acquired in MeOD, 600 MHz) compared with the compound pulmatin (acquired in DMSO-d_6 and $CDCl_3$, 400 MHz)

	δ_H (ppm), *J* (Hz)		δ_C (ppm)	
H/C	**28**	VIEIRA, 1995	**28**	VIEIRA, 1995
1	---	---	160.0	159.6
2	7.60 (s)	7.58 (q, 8.0)	125.0	124.3
3	---	---	149.4	148.8
4	7.83 (s)	7.79 (q, *)	123.4	122.8
5	7.72 (d, 7.5)	7.71 (d, 8.0)	119.5	119.3
6	7.68 (t, 8.2)	7.71 (t, 8.0)	137.0	136.9
7	7.29 (d, 8.2)	7.31 (d, 8.0)	125.2	125.1
8	---	---	163.4	162.7
9	---	---	*	189.2
10	---	---	183.5	183.1
8a	---	---	118.2	117.8
4a	---	---	*	119.8
10a	---	---	134.2	135.7
9a	---	---	120.5	133.7
11	2.50 (s)	2.50 (s)	21.9	22.0
1’	5.08 (d, 7.8)	5.12 (d, 7.6)	103.3	102.5
2’	3.68 (t, 7.8)	3.35 (dd, 8.8 e 7.6)	74.6	74.4
3’	3.54 (t, 10.2)	3.22 (t, 9.2)	77.4	77.3
4’	3.44 (t, 10.2)	3.6 (dd, 12.0 e 2.0)	71.1	70.7
5’	3.56 (dt, 10.2; 2.1)	3.27 (m)	78.4	78.3
6’	3.95 (dd, 12,1; 2.1)	3.41 (dd, 5.6 e 12.0)	62.4	61.9
	3.73 (dd, 12.1; 6.2)			

Carbon assigned based on HMBC and HSQC experiments
* Not detected signals

TABLE 4.18 –^{1}H and ^{13}C NMR Data for Compounds **29** (acquired in MeOD, 600 MHz) compared with the compound chrysophanein (acquired in DMSO-d_6 and MeOD, 400 MHz)

	δ_H (ppm), *J* (Hz)		δ_C (ppm)	
H/C	**29**	VIEIRA, 1995	**29**	VIEIRA, 1995
1	---	---	*	159.4
2	7.15 (dq, 1.7, 0.8)	6.94 (br s)	125.1	123.9
3	---	---	149.3	148.9
4	7.60 (d, 1.7)	7.32 (br s)	120.7	120.5
5	8.02 (dd, 7.3, 1.5)	7.71 (dd, 7.6, 1.2)	122.6	122.0
6	7.82 (dd, 8.5, 7.3)	7.61 (t, 7.6)	136.7	136.8
7	7.79 (dd, 8.5, 1.5)	7.51 (dd, 7.6, 1.2)	124.8	124.9
8	---	---	159.7	162.8
9	---	---	*	188.9
10	---	---	183.4	183.9
8a	---	---	122.8	115.8
4a	---	---	*	*
10a	---	---	136.4	136.0
9a	---	---	115.9	133.4
11	2.45 (br t, 0.8)	2.21 (s)	21.77	22.0
1’	5.09 (d, 7.6)	4.90 (d, 7.6)	103.4	102.4
2’	3.69 (dd, 9.2, 7.9)	3.35 (dd, 8.8 e 7.6)	74.6	74.4
3’	3.53 (t, 9.0)	3.22 (t, 9.2)	77.4	77.3
4’	3.46 (dd, 9.7, 9.0)	3.6 (dd, 12.0 e 2.0)	71.0	70.7
5’	3.54 (dd, 9.7, 2.3)	3.27 (m)	78.4	78.3
6’	3.94 (dd, 12,1; 2.3)	3.41 (dd, 5.6 e 12.0)	62.3	61.9
	3.75 (dd, 12.1; 5.9)			

Carbon assigned based on HMBC and HSQC experiments
* Not detected signals

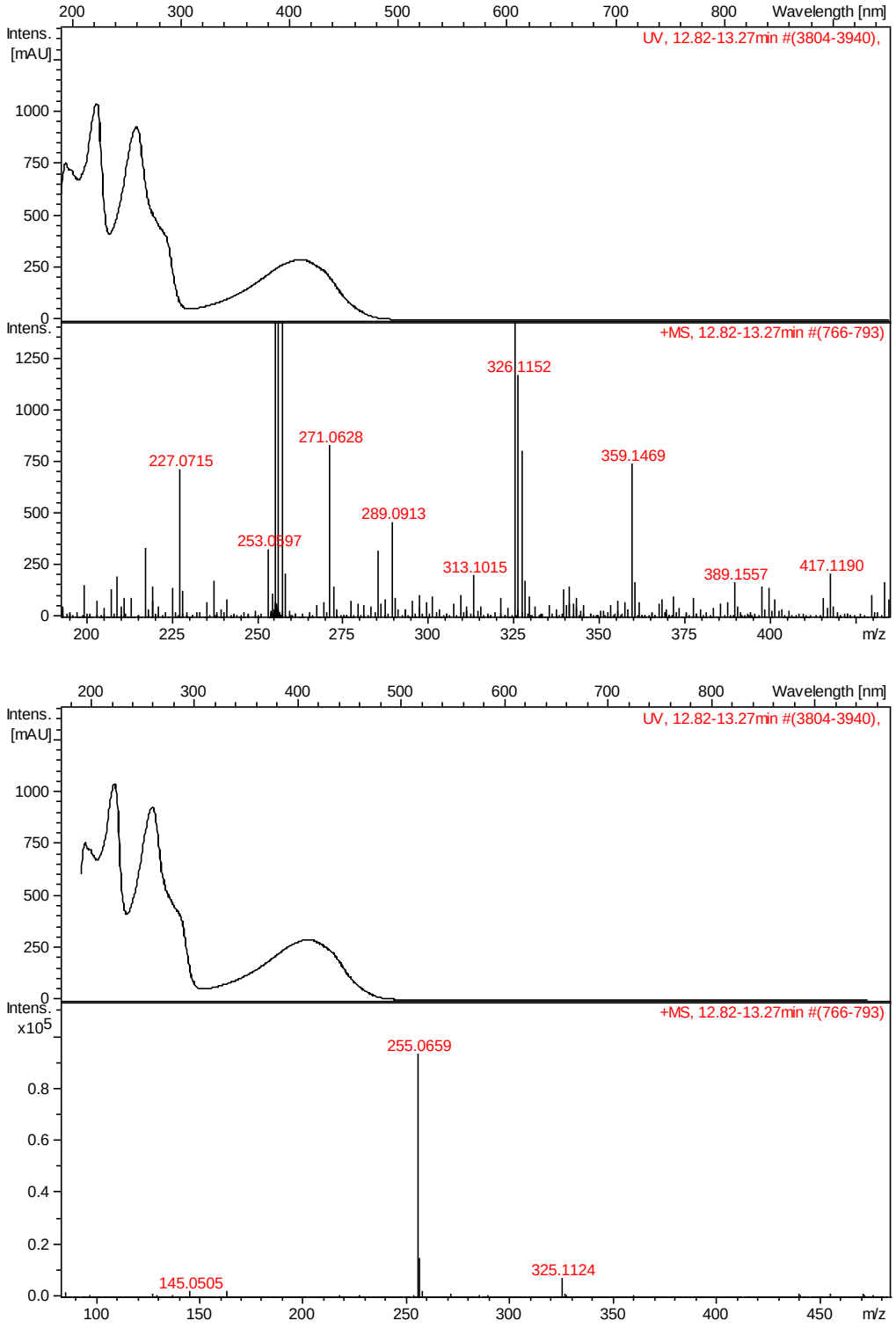

FIGURE 4.137 - HRESIMS spectrum of compound **28** (pulmatin) indicating *m/z* $[M+H]^+$ = 417.1190 and $[M+H\text{-glucose}]^+$ = 255.0659.

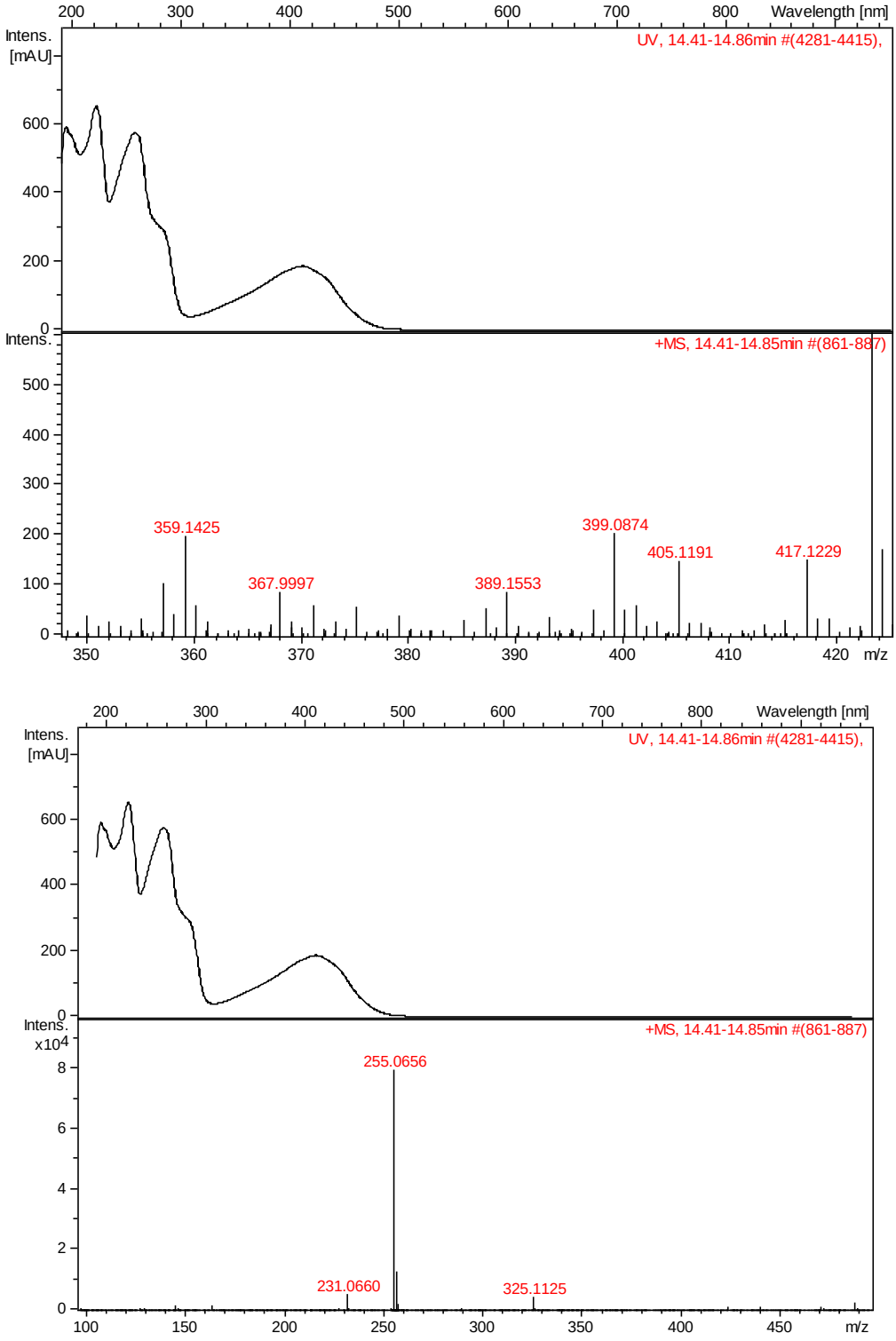

FIGURE 4.138 - HRESIMS spectrum of compound **29** (chrysophanein) indicating *m/z* $[M+H]^+$ = 417.1229 and $[M+H\text{-glucose}]^+$ = 255.0656.

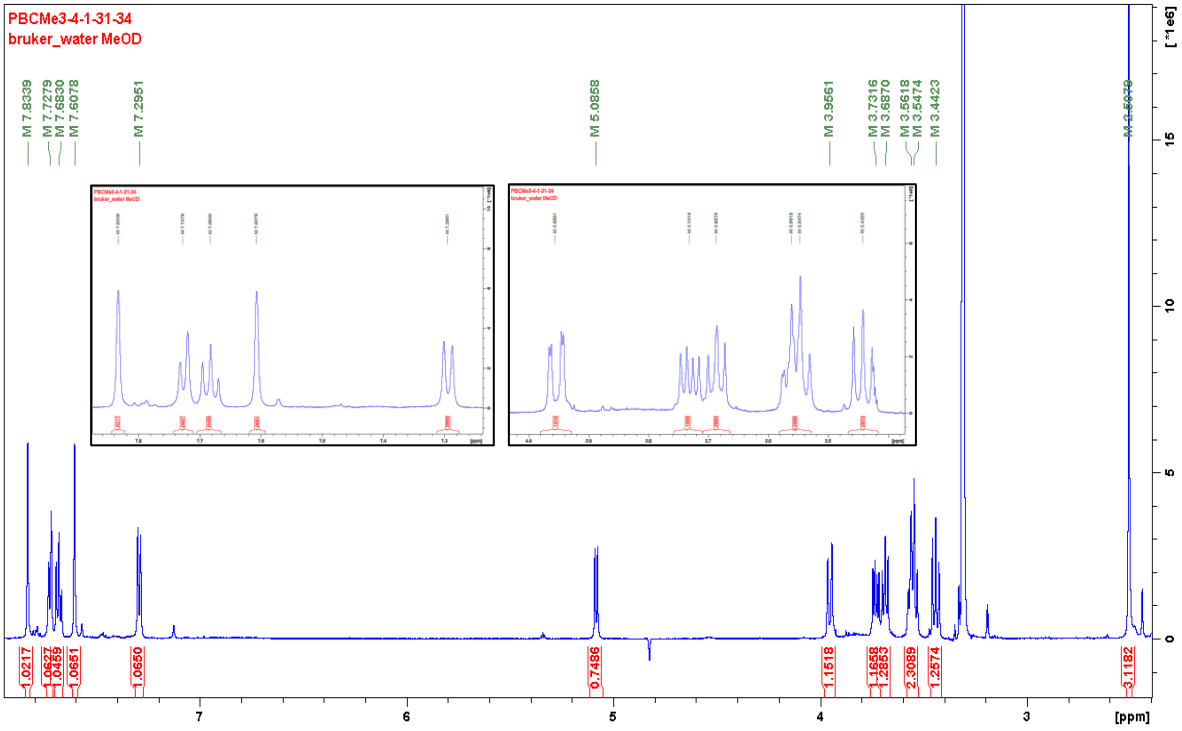

FIGURE 4.139 - ^{1}H NMR spectrum and expansions to compound **28** in MeOD (600 MHz).

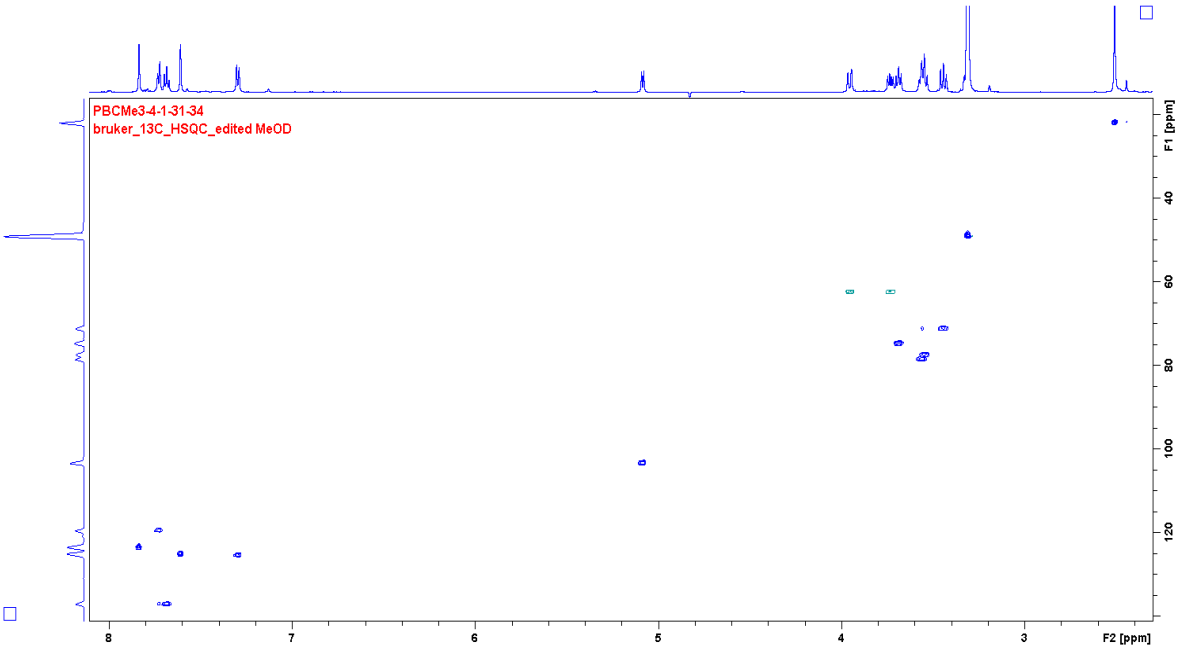

FIGURE 4.140 - HSQC spectrum to compound **28** in MeOD (600 MHz).

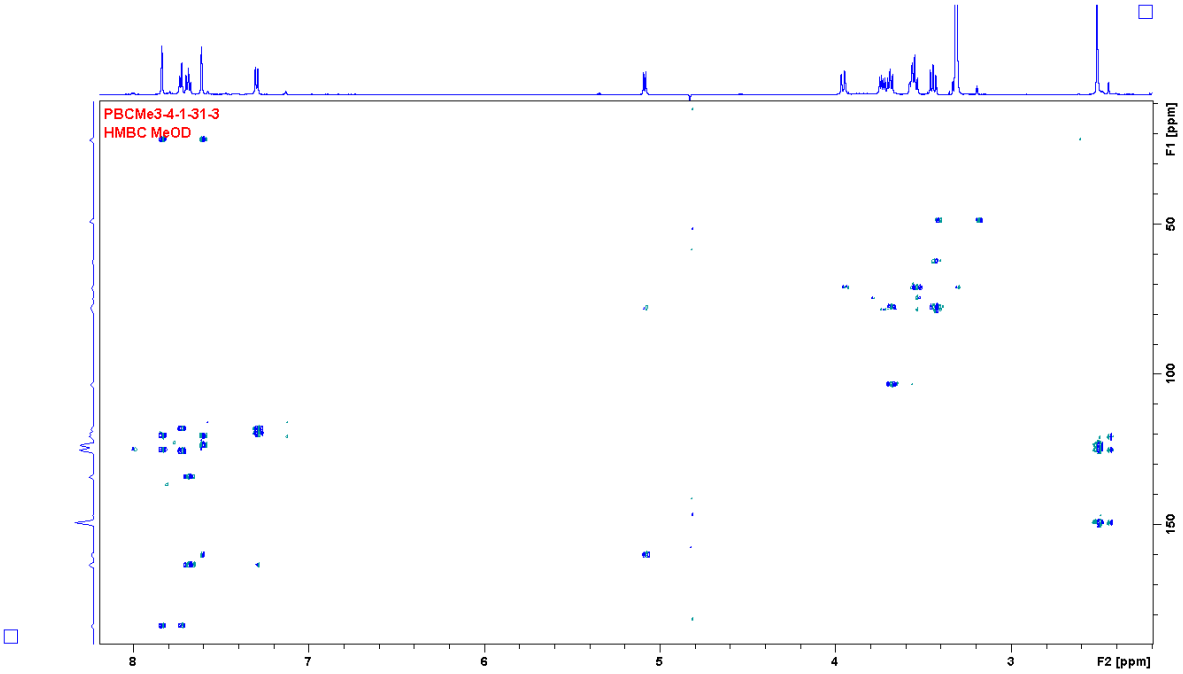

FIGURE 4.141 - HMBC spectrum to compound **28** in MeOD (600 MHz).

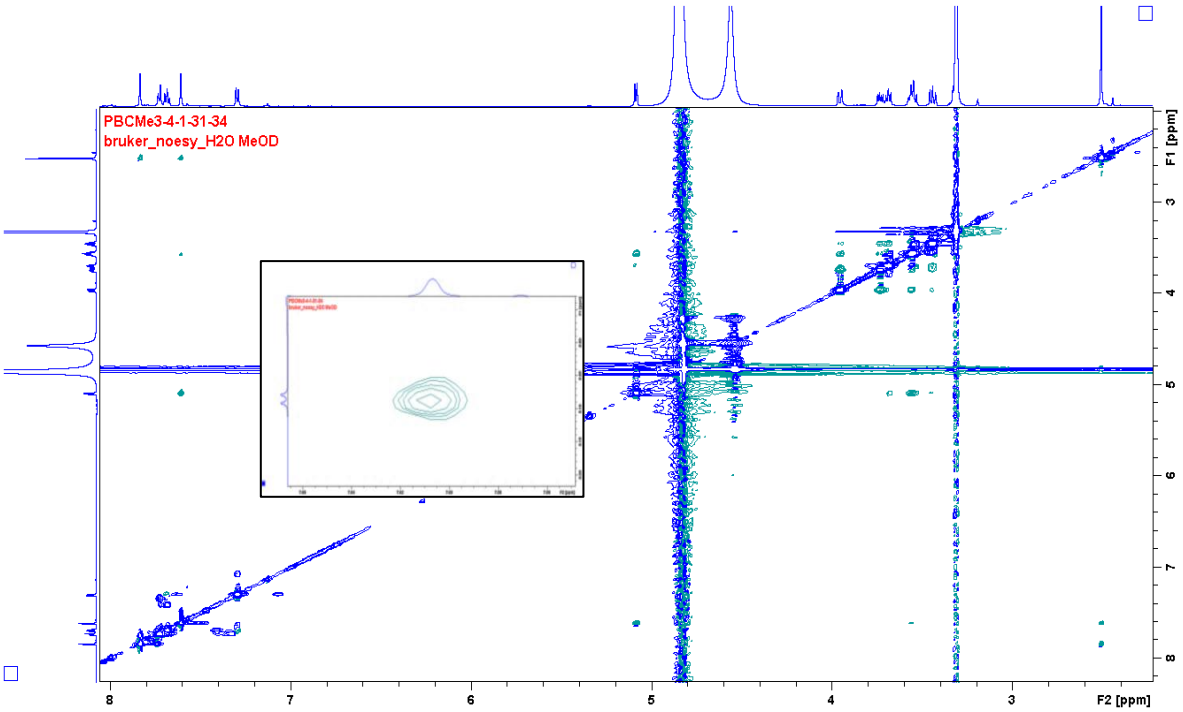

FIGURE 4.142 - NOESY spectrum and expansion indicating the correlation H-1'(*δ* 5.08) - H-2 (*δ* 7.60) to compound **28** in MeOD (600 MHz).

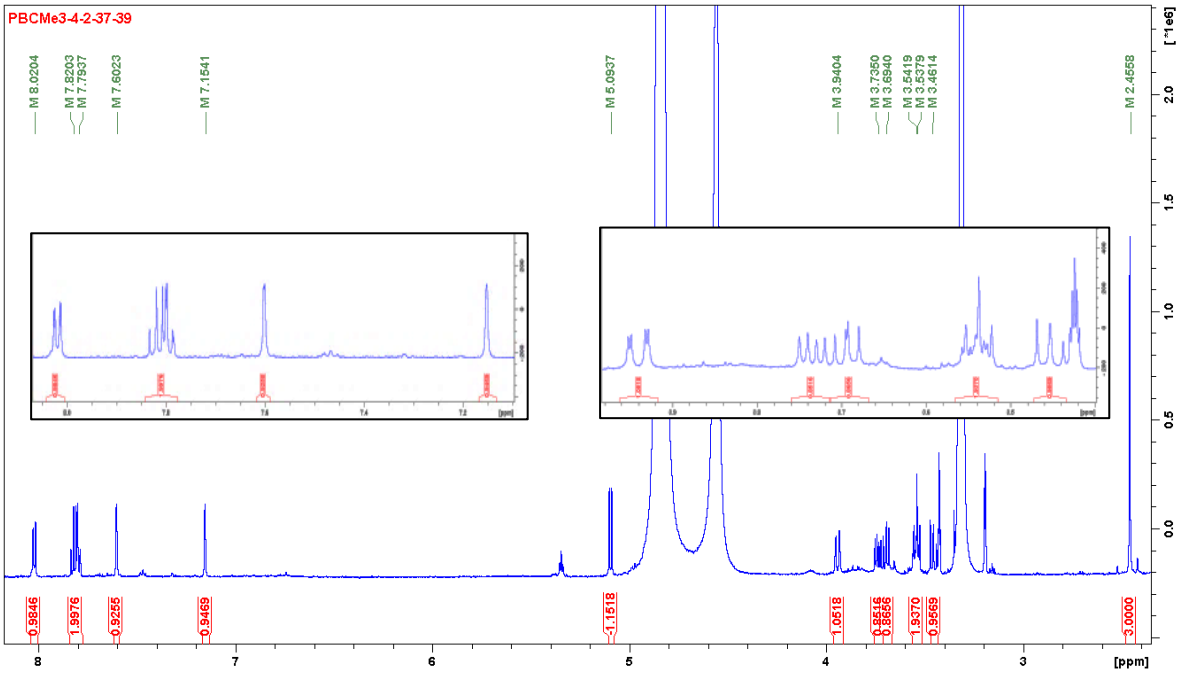

FIGURE 4.143 - ^{1}H NMR spectrum and expansions to compound **29** in MeOD (600 MHz).

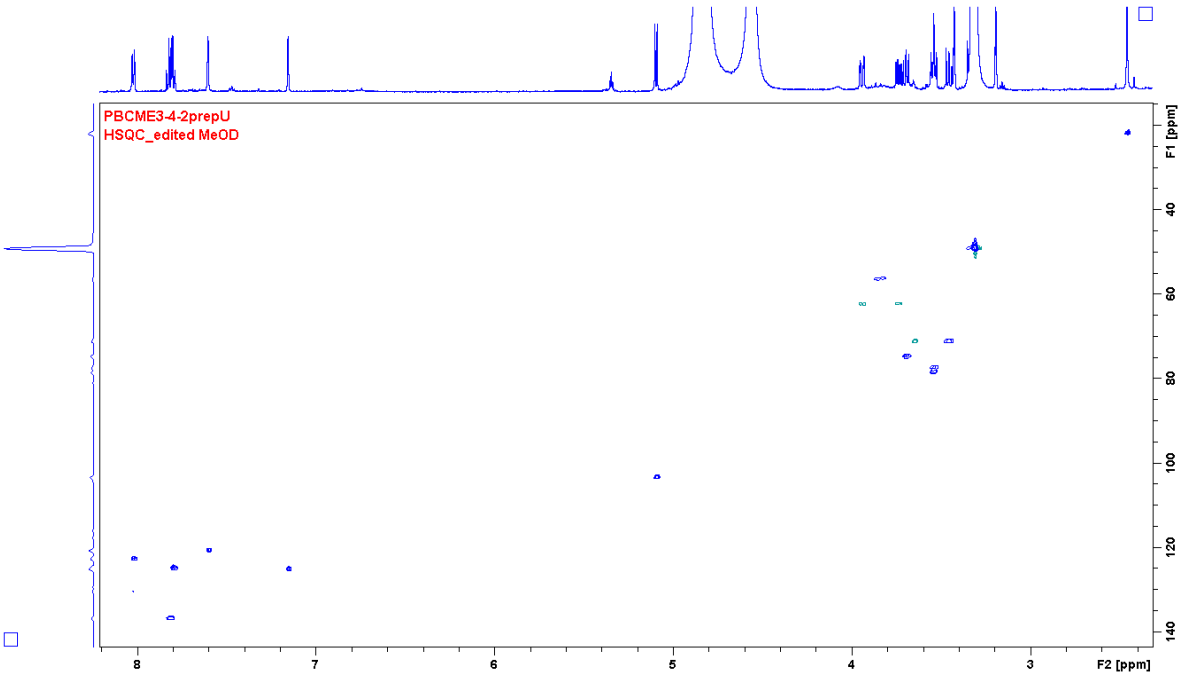

FIGURE 4.144 - HSQC spectrum to compound **29** in MeOD (600 MHz).

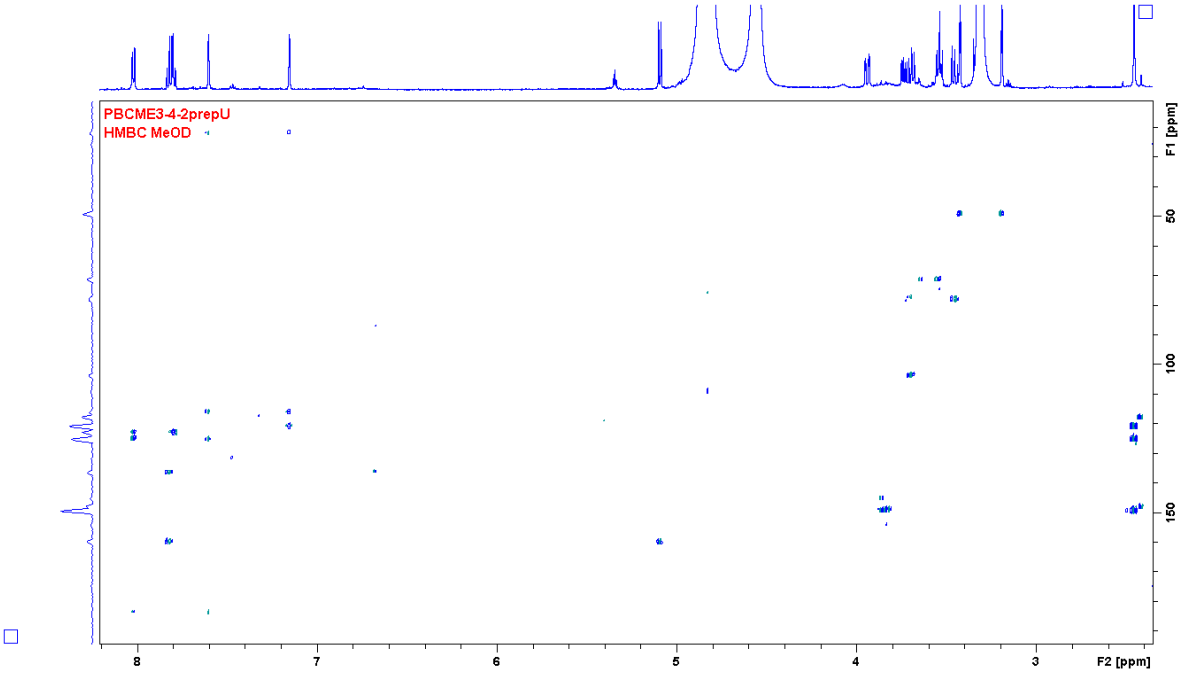

FIGURE 4.145 - HMBC spectrum to compound **29** in MeOD (600 MHz).

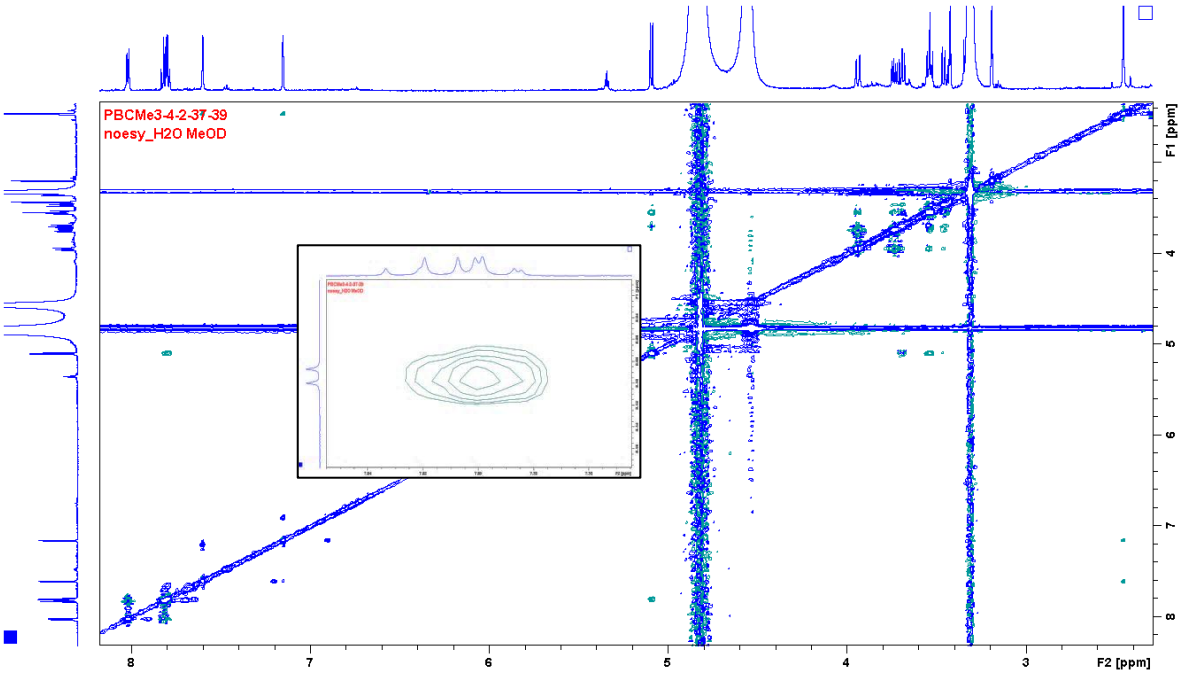

FIGURE 4.146 - NOESY spectrum and expansion indicating the correlation H-1'(*δ* 5.09) - H-7 (*δ* 7.79) to compound **29** in MeOD (600 MHz).

4.1.3 – Anthrones

The study of the methanol extract from the roots of *P. bahiensis* (PBRMe) disclosed two new C,O-diglycosides anthones. Hereby, is presented the discussion to these new compounds:

4.1.3.1 – Anthrones 30 and 31

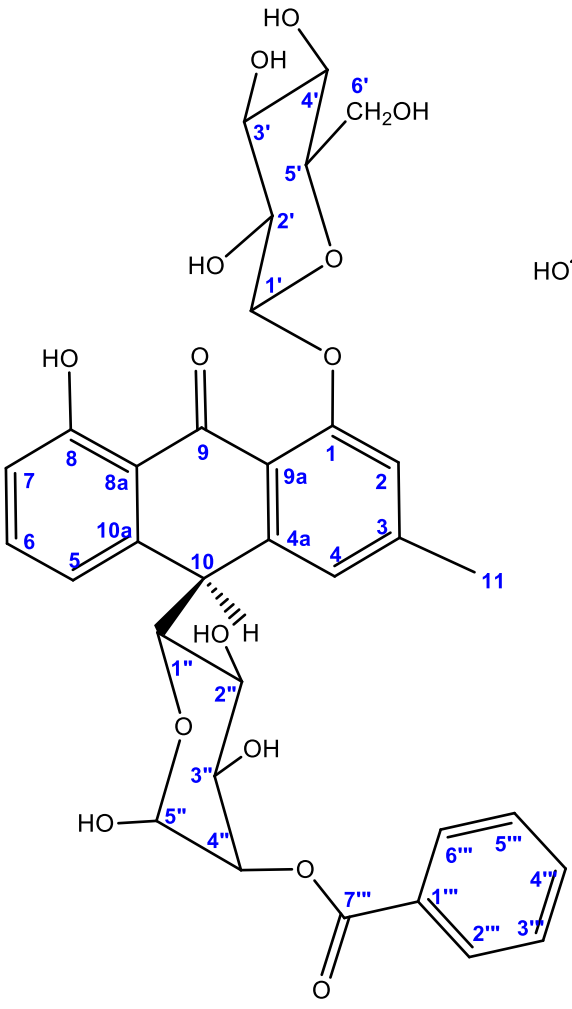

(30)

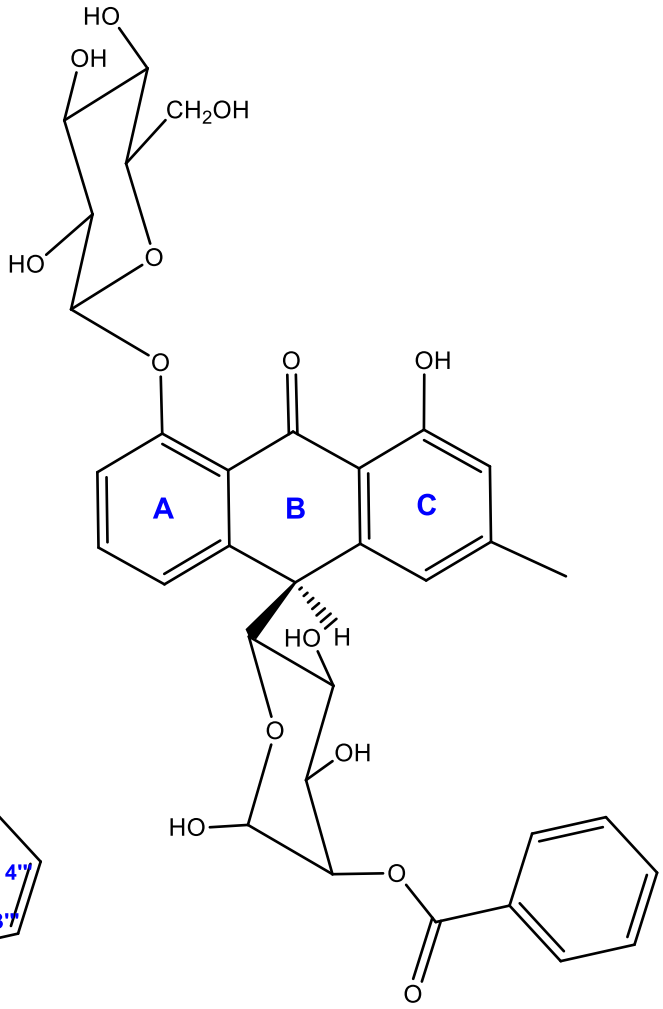

(31)

The anthones **30** and **31** were isolated as orange powder and identified through analyses of 1D and 2D (HSQC, HMBC, COSY and NOESY) NMR spectrum besides HRESIMS analyses. The ^{1}H NMR spectrum of compound **30** and **31** showed very similar to compound **26**. The substitution pattern to the rings A and C of the anthracene skeleton was similar to the chrysophanol (FIGURES 4.151 and 4.156):

- Compound **30**: three aromatic signals featuring the trisubstituted ring A: *δ* 7.54 (dd, *J* = 8.4; 7.5 Hz, 1H), *δ* 7.12 (d, *J* = 7.5 Hz, 1H) and *δ* 7.00 (dd, *J* = 8.4; 1.0 Hz, 1H); two aromatic signals featuring the meta substitution on ring C: *δ* 7.20 (br s, 1H) and *δ* 7.15 (br s, 1H) and a methyl group at *δ* 2.43 (s, 3H).
- Compound **31**: three aromatic signals featuring the trisubstituted ring A: *δ* 7.59 (dd, *J* = 8.3; 7.5 Hz, 1H), *δ* 7.37 (dd, *J* = 8.3; 0.9 Hz, 1H) and *δ* 7.30 (d, *J* = 7.5 Hz, 1H); two aromatic signals featuring the meta substitution on ring C: *δ* 6.97 (br s, 1H) and *δ* 6.84 (br s, 1H) and a methyl group at *δ* 2.44 (s, 3H).

Moreover, likewise to compounds **28** and **29**, the ^{1}H NMR spectrum to **30** and **31,** in association with the values of the coupling constants *J* and the values of ^{13}C obtained from HSQC spectrum (FIGURES 4.152 and 4.157), displayed signals indicating a glucose unit present in both compounds: signals at the range of *δ* 3.0 - 4.0 (*δ* 62 – 78), including the diastereotopic protons at *δ* 3.94/ 3.75 (*δ* 62.3, compound **30**) and at *δ* 3.93/ 3.74 (*δ* 62.3, compound **31**).

The presence of the very characteristic anomeric protons observed at *δ* 4.86 (d, 7.7 Hz, *δ* 104.5) in both compounds confirmed the glucose unit, and the its positioning was established analyzing the HMBC and NOESY spectrum: correlations from H-1' to the carbon C-1 at *δ* 159.1 (in HMBC spectrum, FIGURES 4.148 and 4.153) and to the proton H-2 at *δ* 7.20 (through NOESY spectrum, FIGURE 4.155) in compound **30**, established the positioning of the glucose unit at C-1. Likewise, compound **31** presented correlations from the anomeric proton H-1' to the carbon C-8 at *δ* 158.8 (in HMBC spectrum, FIGURES 4.148 and 4.158) and to the proton H-7 *δ* 7.37 (through NOESY spectrum, FIGURE 4.160), confirming the position of the glucoside at C-8.

A doublet at *δ* 4.65 (*δ* 45.3, compound **30**) and *δ* 4.62 (*δ* 45.2, compound **31**) indicated a methine proton at C-10, common to anthrones, and further correlations observed from H-5 and H-4 to C-10 in HMBC spectrum confirming this establishment, excluding the possibility of having a carbonyl carbon at C-10, as found to anthraquinones. Moreover, further aromatic signals observed in the ^{1}H NMR

spectrum presented a coupling pattern typically of a monosubstituted ring, and correlations from these aromatic protons to a carbonyl carbon at *δ* 166.9 (compound **30**) and *δ* 166.8 (compound **31**) in HMBC spectrum suggested the presence of a benzoate unit in both compounds (FIGURE 4.148).

The presence of a second glycosyl moiety was proposed due the remaining carbinol protons at the range of *δ* 3.7 - 5.1 (*δ* 69 – 93) observed in ^{1}H NMR and HSQC spectra. Thus, the anomeric proton appeared as a double doublet at *δ* 4.04 coupling with H-10 with a small *J*, and the HMBC spectrum disclosed correlations from this anomeric proton to C-4a and C-10a, in both compounds, establishing the positioning of the glycosyl moiety at C-10. Still in HMBC spectrum, correlations from H-4” at *δ* 5.05 with the carbonyl carbon at C-7”’ [*δ* 166.9 (**30**) and 166.8 (**31**)] suggested the benzoate unit as a substituent belonging to this second glycosyl moiety, and the COSY experiment was crucial and helpful for the establishment of its right positioning: the oxymethine proton at *δ* 4.76 (d, 1.9 Hz, H-5”) showed correlations only with the proton at *δ* 5.05 (dd, 3.1; 1.9 Hz, H-4”) whereas a spin system correlation among H-1” - H-2” - H-3” and among H-3” - H-4” - H-5” were observed. The shielded chemical shift found to H-4” at *δ* 74.6 (compound **30**) and *δ* 74.5 (compound **31**) and the multiplicity of this signal comparing with that found to RODRIGUEZ-GAMBOA, 1999 also contributed to the positioning of the benzoate unit at C-4” (FIGURE 4.147 and 4.148).

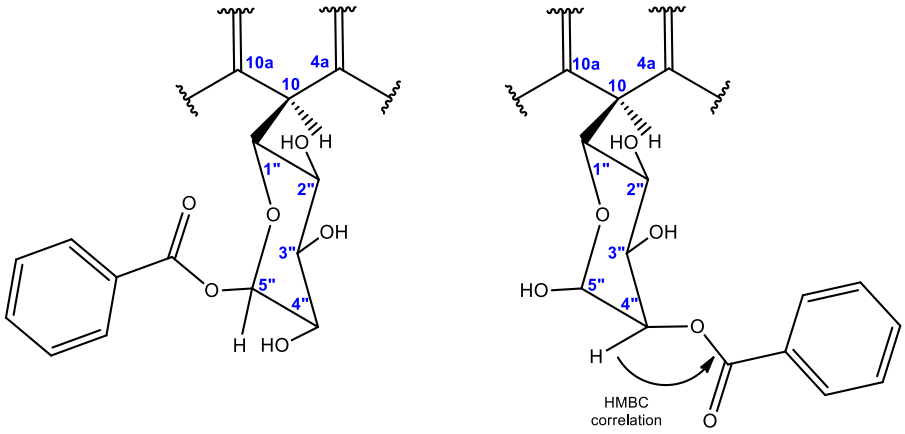

H-5"
δ 5.76 (d, 1.5)
δ 96.1

(Picramnioside D)

H-4"
δ 5.05 (dd, 3.1; 1.9)
δ 74.6

(Compound 30)

FIGURE 4.147 - Distinction of the positioning of the benzoate unit in the glycoside moiety through NMR data analyses.

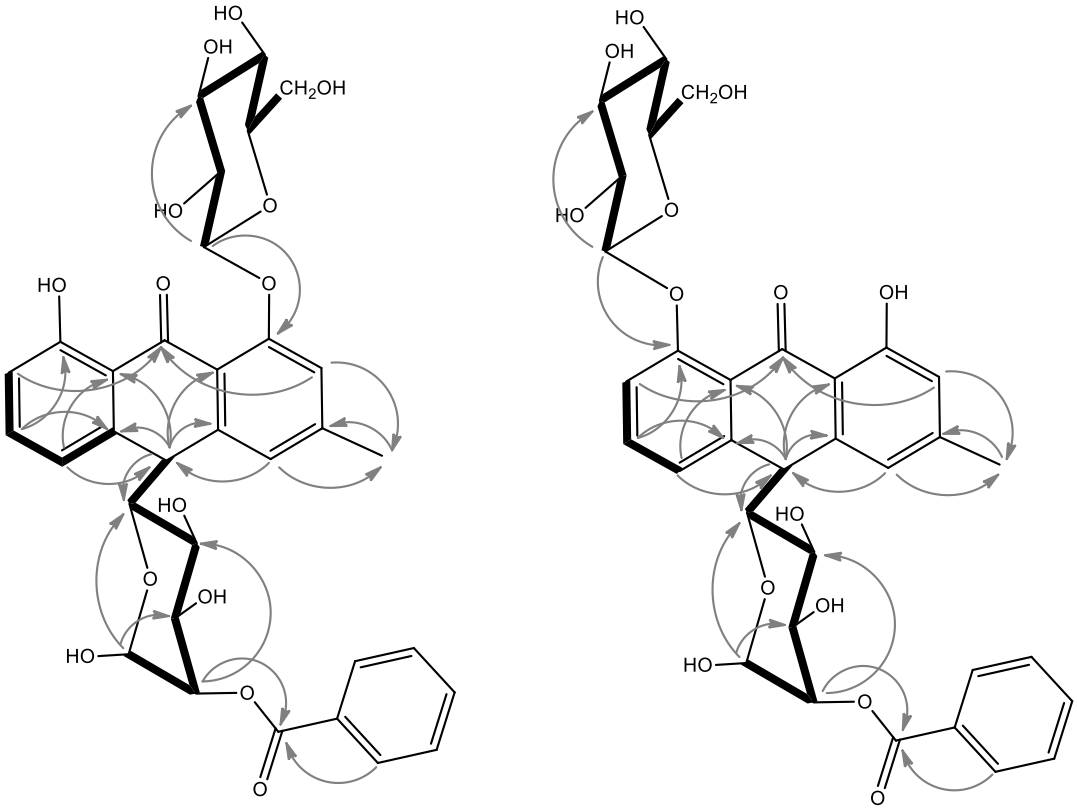

(30) **(31)**

FIGURE 4.148 - COSY spin systems (bold) and key HMBC correlations (grey arrows) used for structure elucidation of **30** and **31**. Arrows point from H to C.

The HRESIMS data and UV spectrum for each compound disclosed the following data, as described below:

- Compound **30:** $[M+H]^+$ = 655.1998 (calc. for 655.2027), molecular formula as $C_{33}H_{34}O_{14}$ (17 degrees of unsaturation) and base peak corresponding to $[M+H\text{-glucose-}C_6H_5CO_2H\text{-}H_2O]^+$ = 353.1016; UV absorptions at: 228, 268, 296 and 330 nm, according to the high conjugation of the double bond (FIGURE 4.149)
- Compound **31:** $[M+H]^+$ = 655.2019 (calc. for 655.2027), molecular formula as $C_{33}H_{34}O_{14}$ (17 degrees of unsaturation) and base peak corresponding to $[M+H\text{-glucose-}C_6H_5CO_2H\text{-}H_2O]^+$ = 353.1015; UV absorptions at: 228, 268, 296 and 330 nm, according to the high conjugation of the double bond (FIGURE 4.150)

The relative configuration at C-10 in both compounds was established comparing the value of the chemical shift found to the methyl group at the ring C. According to RODRIGUEZ-GAMBOA, 2001, a shielded value of C-11 around δ 1.84 has suggested C-10 as 10S. Likewise, all compounds isolated that had the absolute configuration in C-10 determined as 10R showed the chemical shift to C-11 around δ 2.3 - δ 2.4 (HERNANDEZ-MEDEL, 1996, 1998, 1999, RODRIGUEZ-GAMBOA, 2001). Therefore, the values found to compounds **30** and **31** could establish the configuration of C-10 as 10R. This proposal, however, should be confirmed by further experiments (circular dichroism or X-ray crystallographic analysis).

Then, the high similarities found to **30** and **31** in all NMR spectrum (very similar chemical shift to protons and carbons, as well as very similar coupling constant pattern) besides the same HRMS spectra allowed to establish these compounds as positional isomers, presenting the same preferential conformation in their glycosides, and distinguishing each other only by the positioning of the glucose moiety at C-1 (compound **30**) or C-8 (compound **31**).

The assignments of the ^1H and ^{13}C resonances to the compound **30** and **31** are shown in TABLE 4.19.

TABLE 4.19 –^{1}H and ^{13}C NMR Data for Compounds **30** and **31** (acquired in MeOD, 600 MHz)

	δ_H (ppm), *J* (Hz)		δ_C (ppm)	
H/C	**30**	**31**	**30**	**31**
1	---	---	159.1	161.8
2	7.20 (br s)	6.84 (br s)	118.2	116.8
3	---	---	147.6	146.7
4	7.15 (br s)	6.97 (br s)	124.0	122.0
5	7.12 (d, 7.5)	7.30 (d, 7.5)	120.9	123.4
6	7.54 (dd, 8.4, 7.5)	7.59 (dd, 8.3, 7.5)	134.8	135.5
7	7.00 (dd, 8.4, 1.0)	7.37 (dd, 8.3, 0.9)	116.7	117.5
8	---	---	161.7	158.8
9	---	---	192.0	191.8
10	4.65 (d, 2.4)	4.62 (d, 2.3)	45.3	45.2
8a	---	---	121.4	124.5
4a	---	---	147.3	141.3
10a	---	---	141.4	147.4
9a	---	---	122.3	119.2
11	2.43 (s)	2.44 (s)	21.7	21.9
1’	4.86 (d, 7.7)	4.86 (d, 7.7)	104.5	104.5
2’	3.59 (dd, 9.4, 7.7)	3.60 (dd, 9.3, 7.7)	74.6	74.6
3’	3.51 (t, 10.1)	3.50 (t, 9.3)	77.0	77.0
4’	3.41 (dd, 10.1, 9.6)	3.43 (t, 9.3)	71.1	71.0
5’	3.49 (dd, 9.6, 2.1)	3.49 (dd, 5.8, 2.3)	78.4	78.4
6’	3.94 (dd, 12,2; 2.1)	3.93 (dd, 12,1; 2.3)	62.3	62.3
	3.75 (dd, 12.2; 6.2)	3.74 (dd, 12.1; 5.8)		
1”	4.04 (dd, 9.8, 2.4)	4.04 (dd, 9.9, 2.3)	77.8	77.8
2”	3.69 (t, 9.6)	3.72 (t, 9.9)	69.1	69.0
3”	4.02 (dd, 9.6, 3.1)	4.02 (dd, 9.9, 3.1)	70.4	70.4
4”	5.05 (dd, 3.1, 1.9)	5.05 (dd, 3.1, 1.9)	74.6	74.5
5”	4.76 (d, 1.9)	4.76 (d, 1.9)	92.6	92.6
1’”	---	---	130.5	130.9
2’”/6’”	7.45 XX'-system	7.47 XX'-system	130.2	130.1
3’”/5’”	7.40 AA'-system	7.41 AA'-system	129.1	129.0
4’”	7.57 (tt, 7.4, 1.4)	7.59 (tt, 7.5, 8.3)	133.9	134.0
7’”	---	---	166.9	166.8

Carbon assigned based on HMBC and HSQC experiments

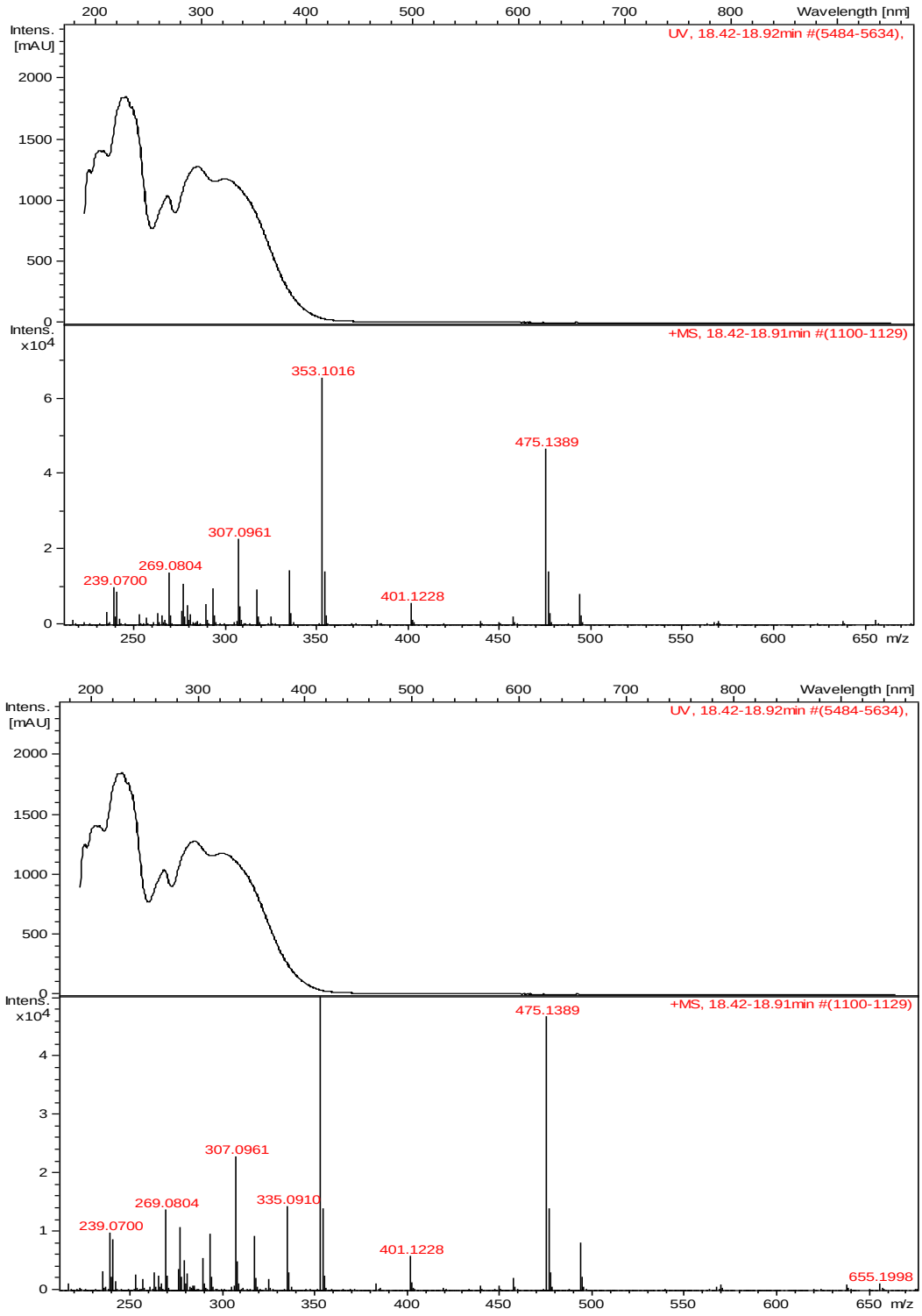

FIGURE 4.149 - HRESIMS spectrum of compound **30** indicating *m/z* $[M+H]^+$ = 655.1998 and $[M+H\text{-glucose-}C_6H_5CO_2H\text{-}H_2O]^+$ = 353.1016.

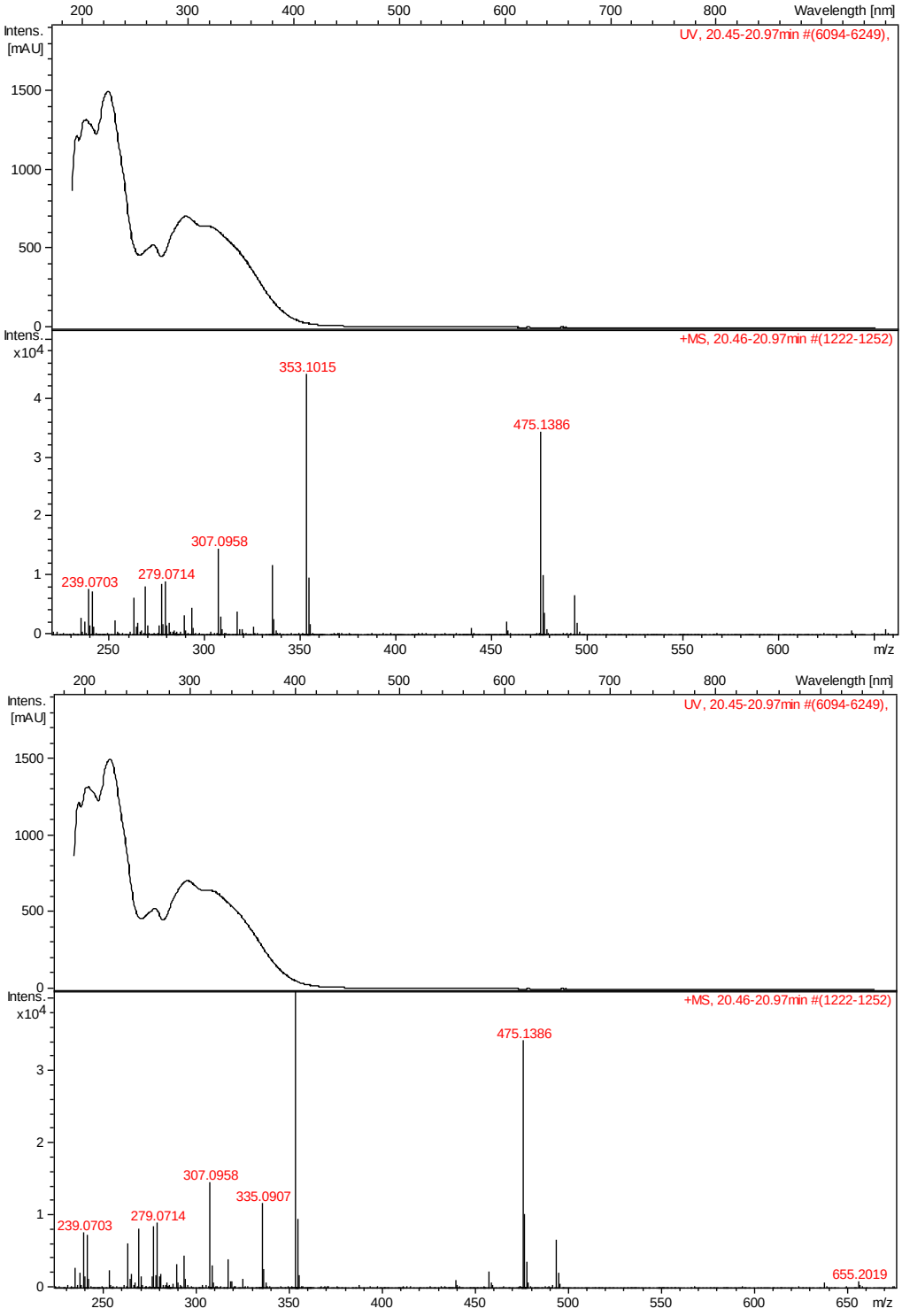

FIGURE 4.150 - HRESIMS spectrum of compound **31** indicating *m/z* $[M+H]^+$ = 655.2019 and $[M+H\text{-glucose-}C_6H_5CO_2H\text{-}H_2O]^+$ = 353.1015.

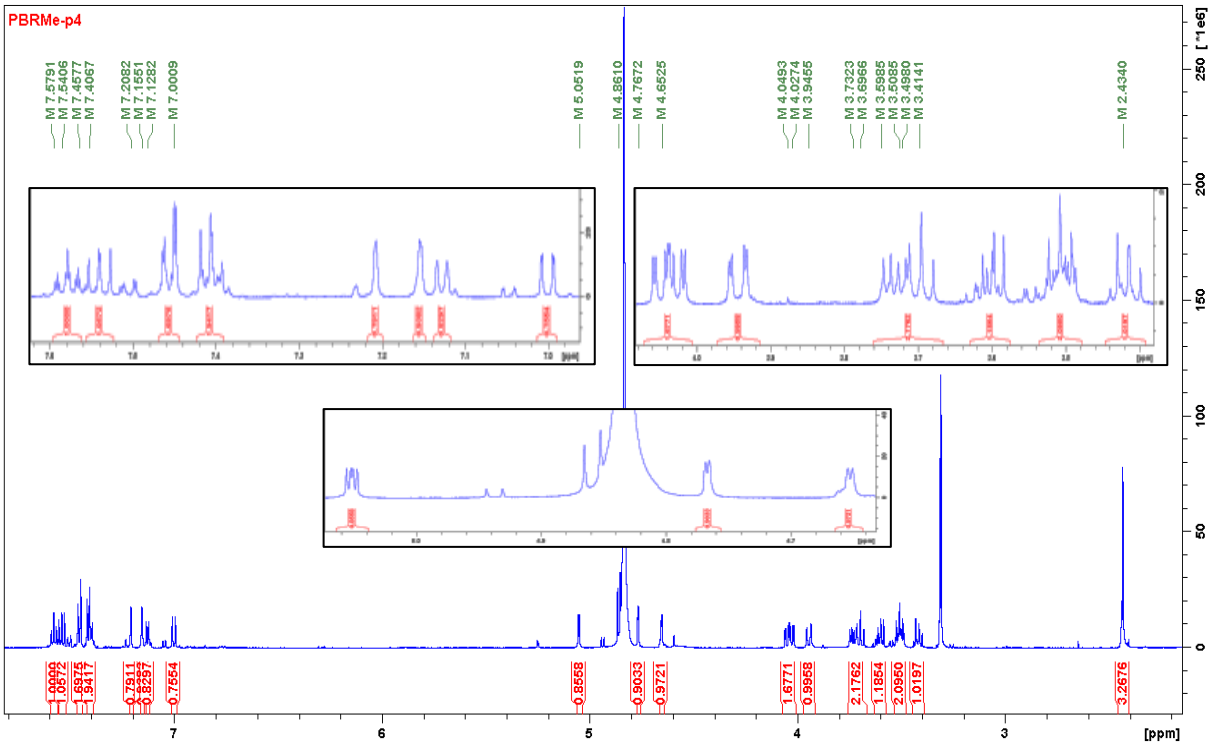

FIGURE 4.151 - ^{1}H NMR spectrum and expansions to compound **30** in MeOD (600 MHz).

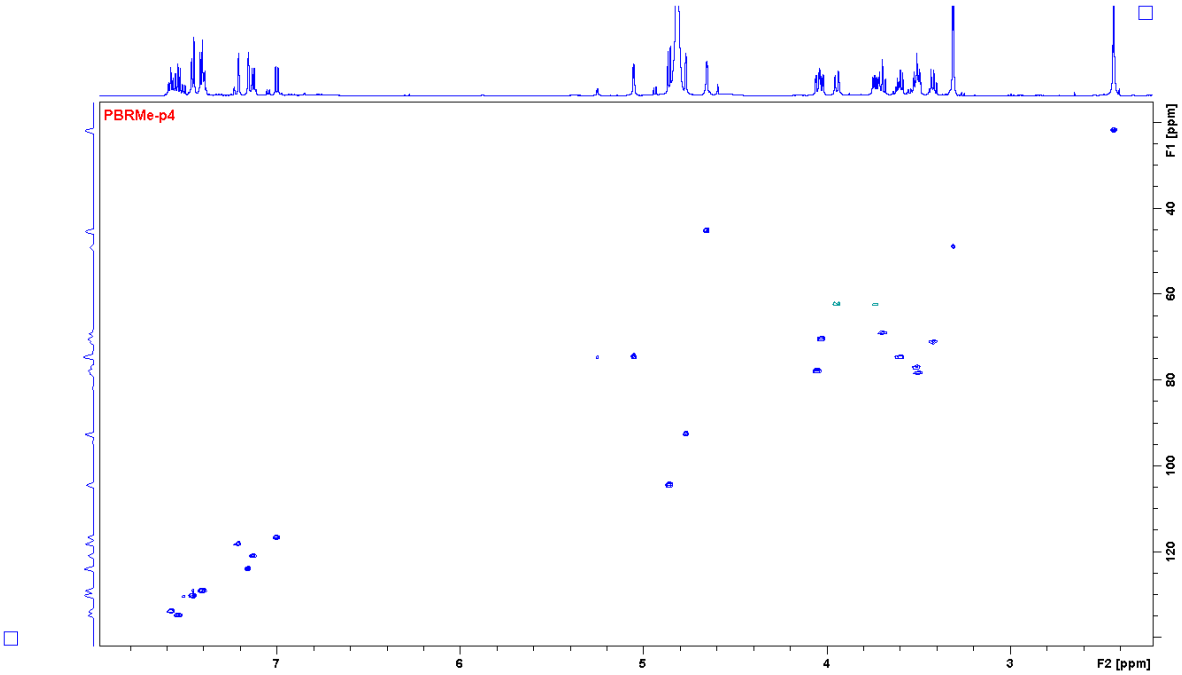

FIGURE 4.152 - HSQC spectrum to compound **30** in MeOD (600 MHz).

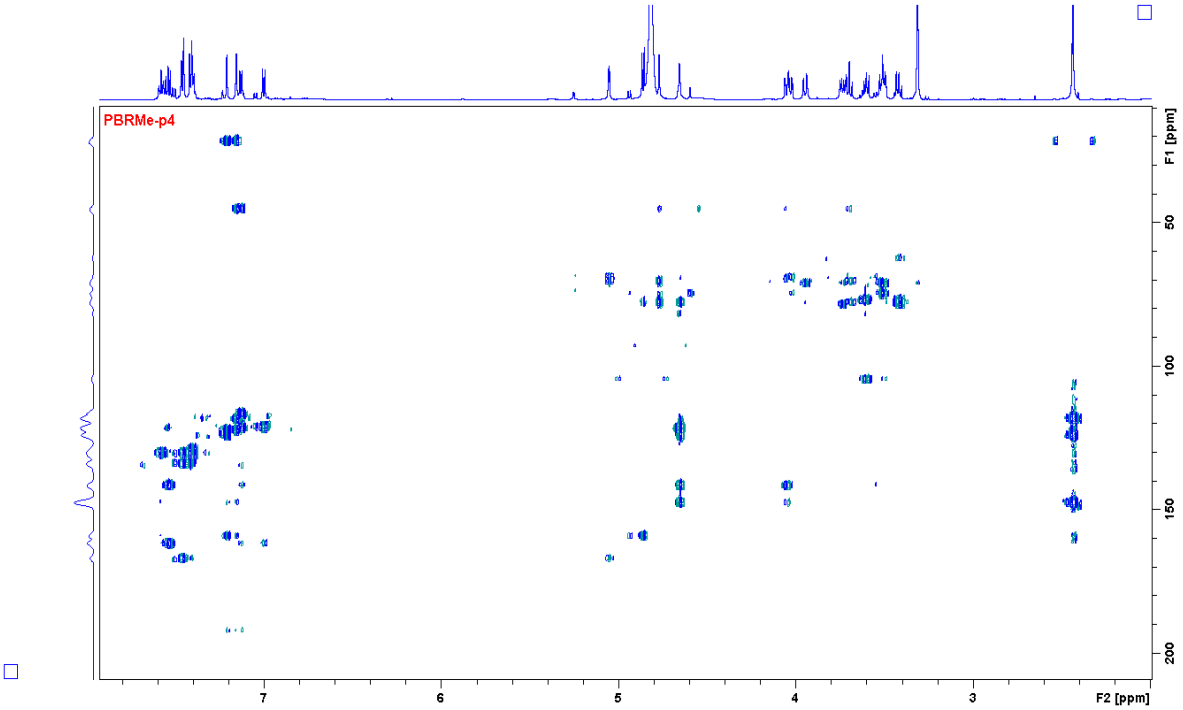

FIGURE 4.153 - HMBC spectrum to compound **30** in MeOD (600 MHz).

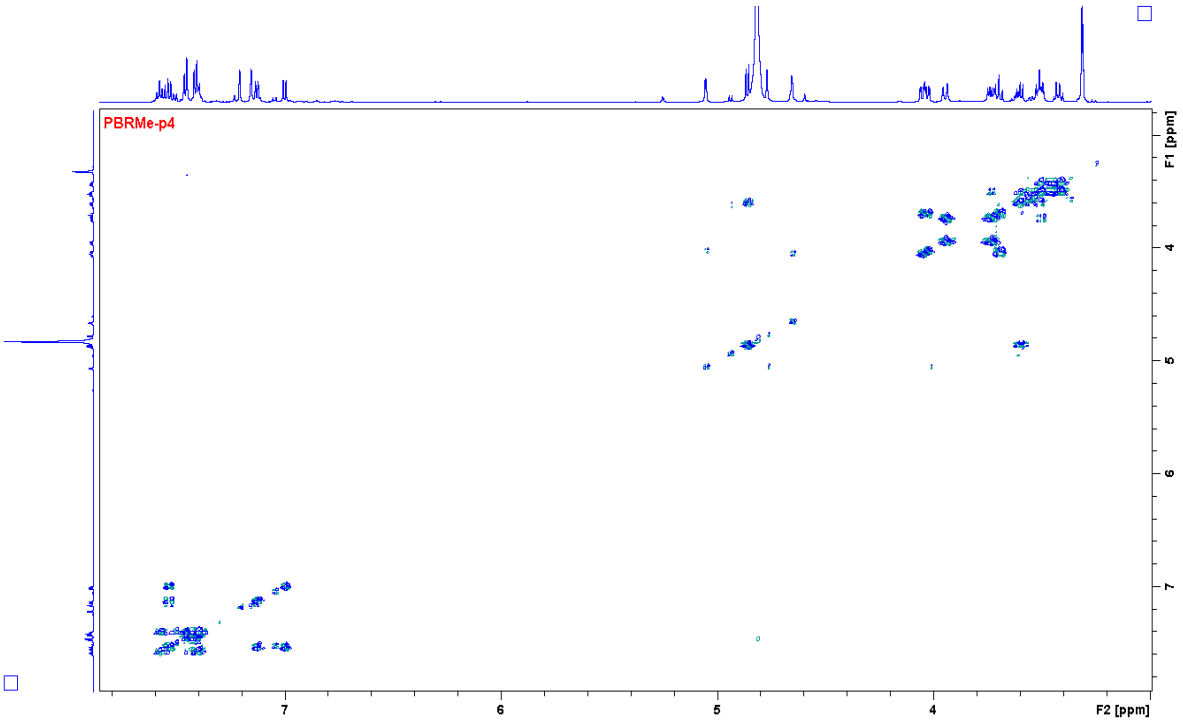

FIGURE 4.154 - COSY spectrum to compound **30** in MeOD (600 MHz).

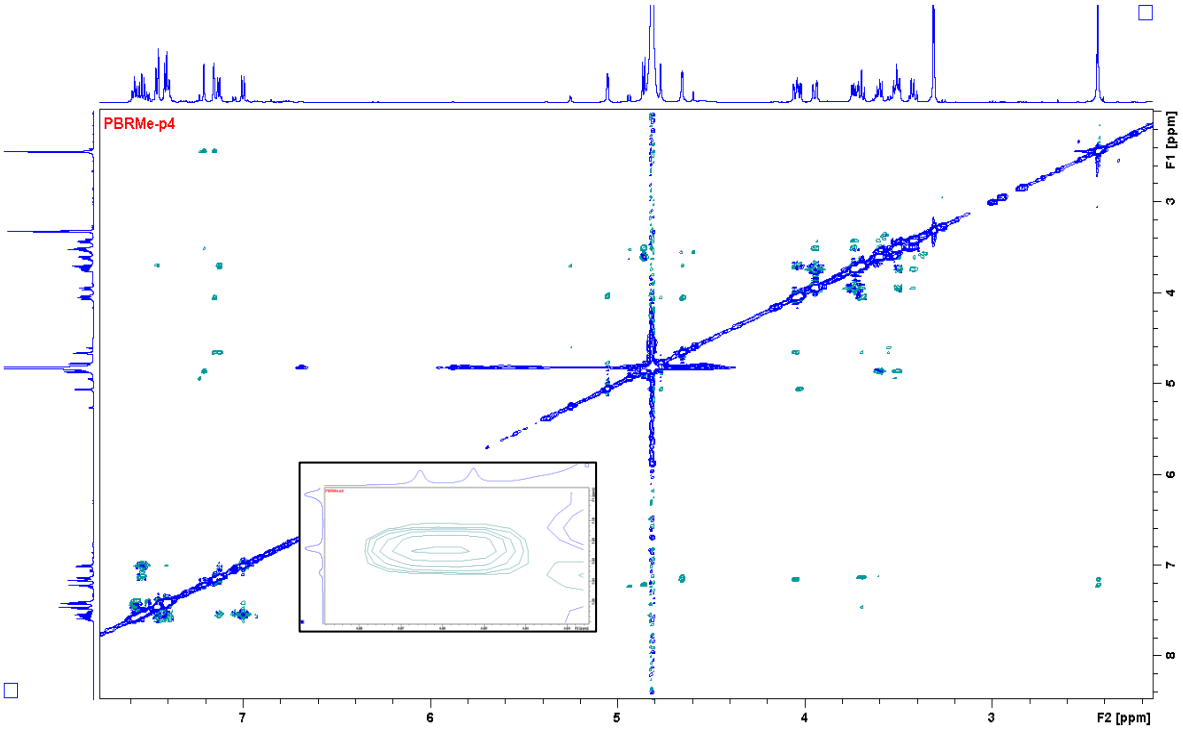

FIGURE 4.155 - NOESY spectrum and expansion indicating the correlation H-1'(*δ* 4.86) - H-2 (*δ* 6.84) to compound **30** in MeOD (600 MHz).

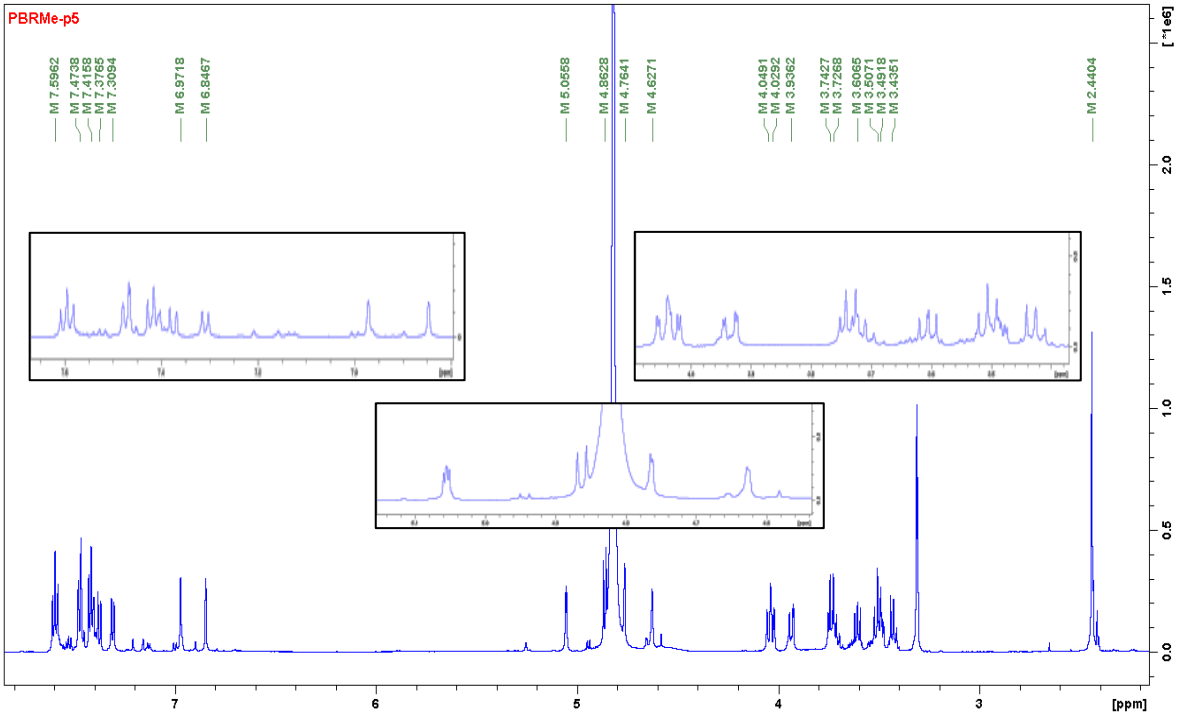

FIGURE 4.156 - ^{1}H NMR spectrum and expansions to compound **31** in MeOD (600 MHz).

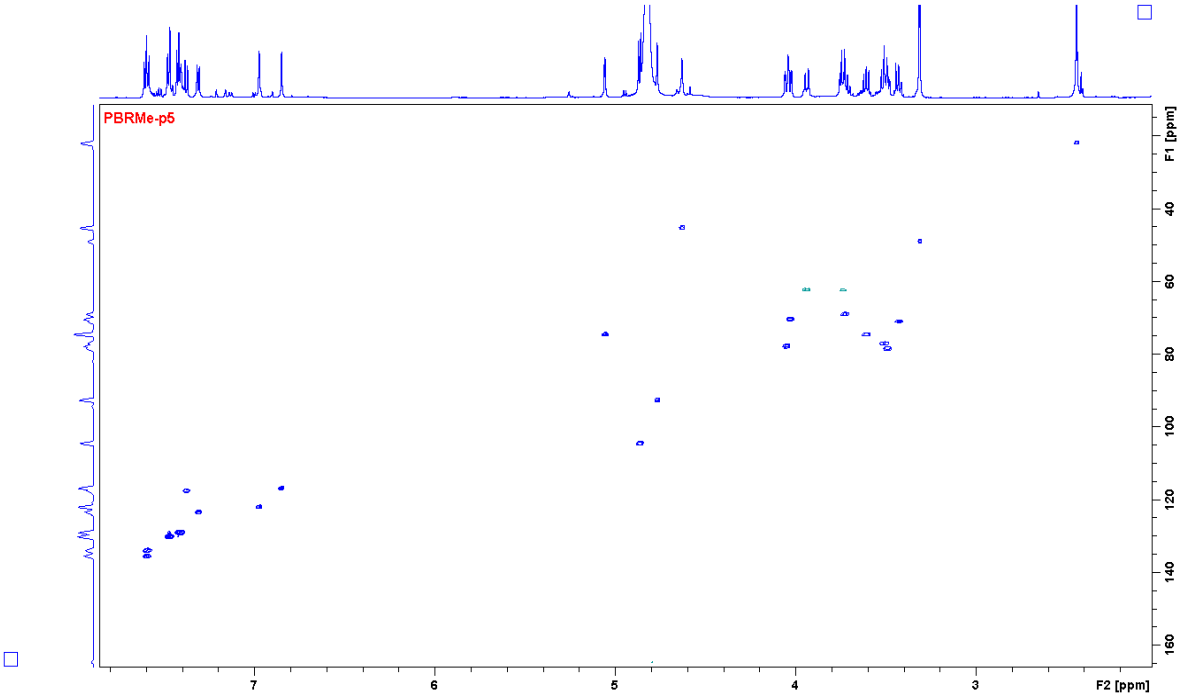

FIGURE 4.157 - HSQC spectrum to compound **31** in MeOD (600 MHz).

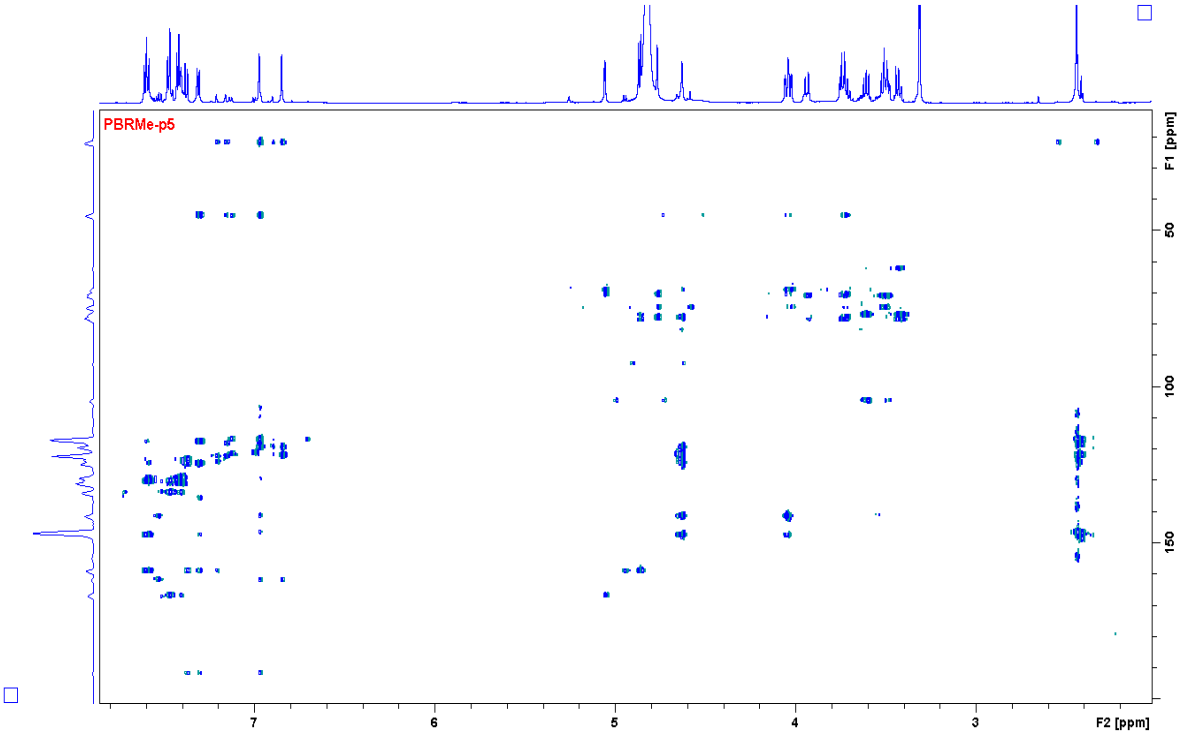

FIGURE 4.158 - HMBC spectrum to compound **31** in MeOD (600 MHz).

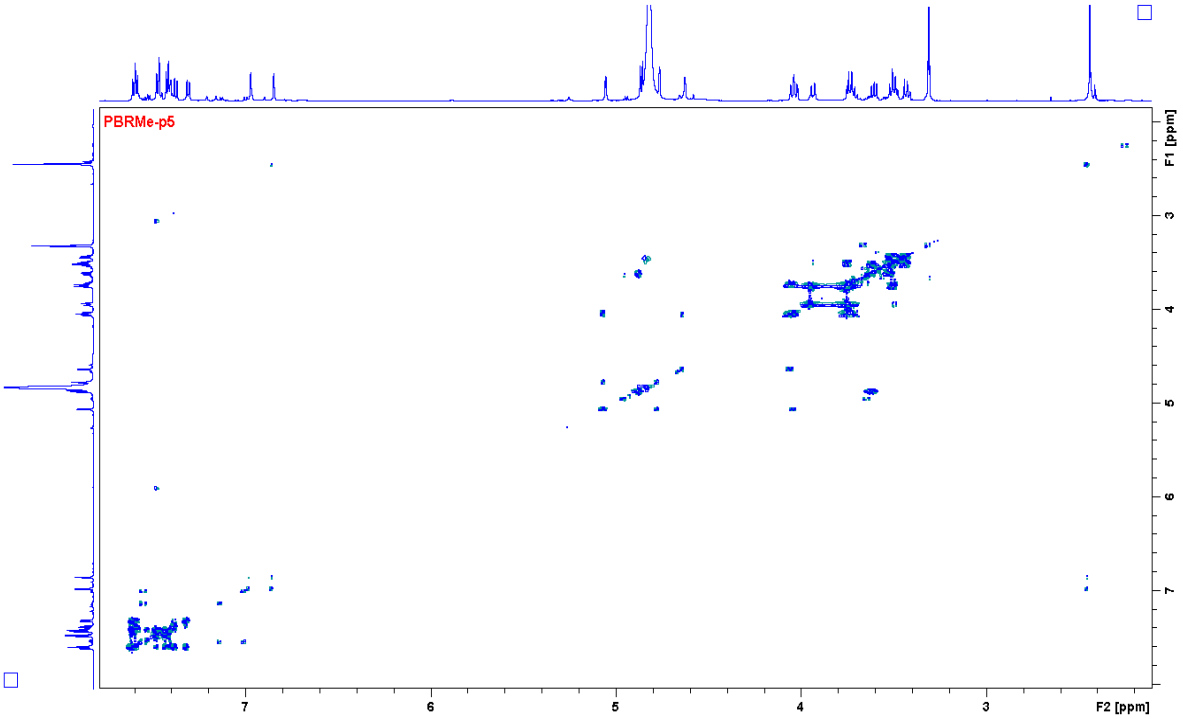

FIGURE 4.159 - COSY spectrum to compound **31** in MeOD (600 MHz).

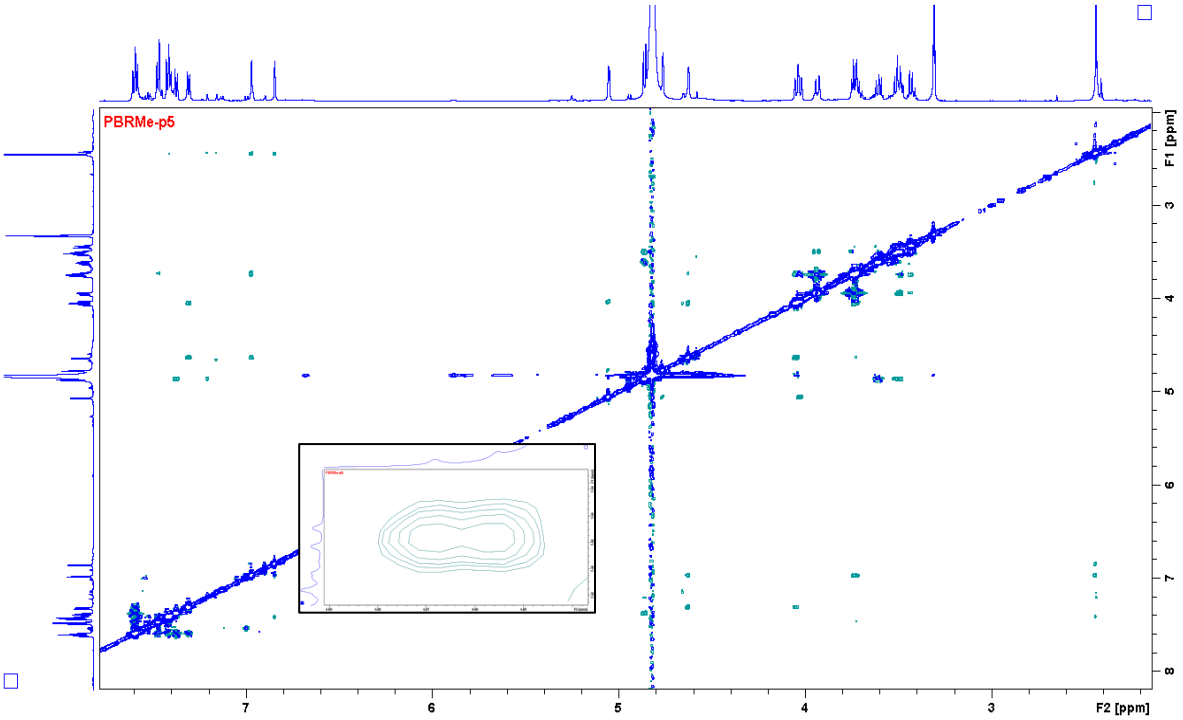

FIGURE 4.160 - NOESY spectrum and expansion indicating the correlation H-1'(*δ* 4.86) - H-7 (*δ* 7.37) to compound **31** in MeOD (600 MHz).

4.2 – BIOLOGICAL ACTIVITIES

4.2.1- Insecticide activity against *A. sexdens rubropilosa*

4.2.1.1- *Picramnia glazioviana*

4.2.1.1.1- Crude extract

The crude extract from *P. glazioviana* was submitted to the toxicity test (by ingestion) with the leaf-cutting ants according to the methodology described in item 3.4.1. In order to analyze the obtained result, the survival curves from the ants submitted to the treatment by ingestion of the extract incorporated into the diet were plotted, comparing with the curve obtained from the control containing only pure diet, after a period of 25 days of experiment, and using the "log-rank" test. The obtained result is presented in FIGURE 4.161 and TABLE 4.20

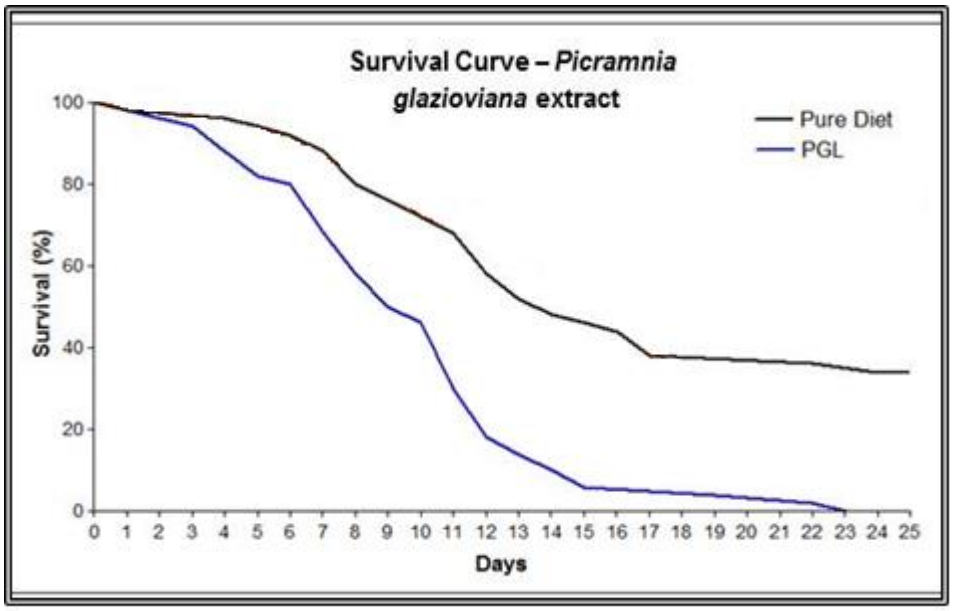

FIGURE 4.161 – Survival curve of *A. sexdens rubropilosa* workers submitted to the ingestion treatment with leaves extract from *P. glazioviana*.

TABLE 4.20 - Cumulative mortality and median survival (Md) of *A. sexdens rubropilosa* workers submitted to the bioassay of incorporation in artificial diet the extract from leaves of *P. glazioviana*

Treatment	**Cumulative % of mortality per day**										**Md** *
	1	**2**	**3**	**6**	**8**	**10**	**14**	**17**	**21**	**25**	
Pure Diet	2	2	2	8	20	24	52	60	60	64	14***a***
***P. glazioviana* leaves extract**	2	2	6	20	42	54	90	94	96	100	9,5***b***

* Different letters in relation to the control indicate a significant difference according to the "log rank" test ($p < 0.05$).

Thus, from the result observed above, the ethanol extract from leaves of *P. glazioviana* showed a toxic activity to the workers of *A. sexdens rubropilosa*. Comparing with the control, there was 50% of mortality of ants in 9 days of experiments, reaching 100% of dead ants at the end of the 25 days of experiments. This result, very promising, motivated the fractionation of this extract for continuous study. Thereafter, the extract was partitioned with solvent of different polarities.

4.2.1.1.2- Fractions obtained from Liquid-Liquid Partition

After partitioning the leaves ethanolic extract from *P. glazioviana*, the hexane, dichloromethane, ethyl acetate and hydroalcoholic phases were submitted to evaluate their respectives activities against leaf-cutting ants, by the ingestion test according to the methodology described in item 3.4.1. The obtained results are shown in FIGURE 4.162 and TABLE 4.21.

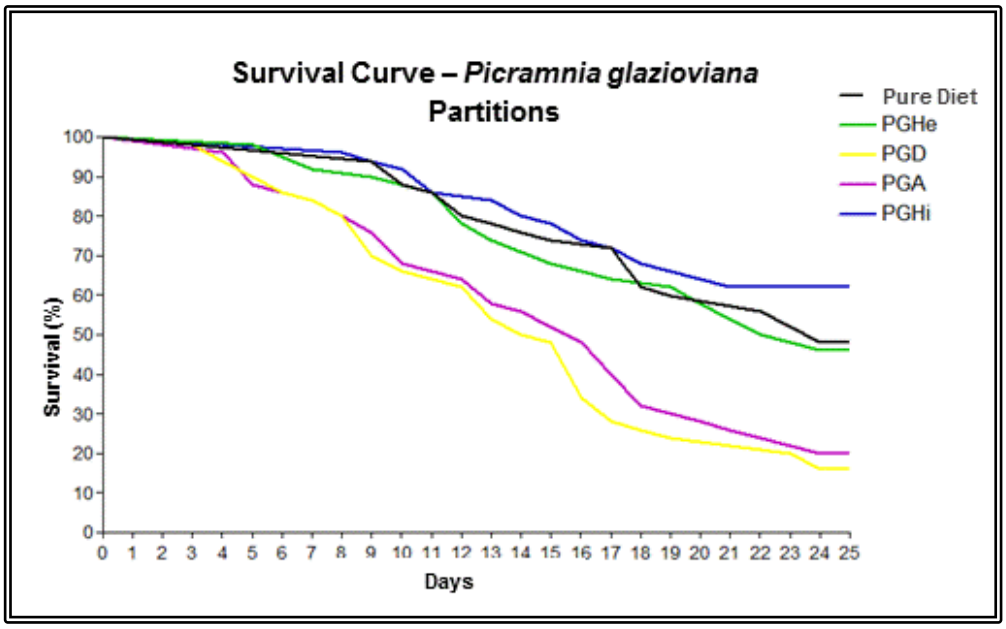

FIGURE 4.162 – Survival curve of *A. sexdens rubropilosa* workers submitted to the ingestion treatment with the partitions extracts from the ethanolic extract of *P. glazioviana*.

TABLE 4.21 - Cumulative mortality and median survival (Md) of *A. sexdens rubropilosa* workers submitted to the bioassay of incorporation in artificial diet the partitions of *P. glazioviana*

Treatment	Cumulative % of mortality per day										Md *
	1	2	3	6	8	10	14	17	21	25	
Pure Diet	0	0	2	2	2	12	24	28	40	52	24***a***
PGHe	0	0	0	2	8	10	26	36	46	54	22,5***a***
PGD	0	0	2	14	20	34	50	72	76	84	15***b***
PGA	0	0	0	12	20	32	44	60	74	80	16***b***
PGHi	0	0	0	2	4	8	20	28	38	38	>25***a***

* Different letters in relation to the control indicate a significant difference according to the "log rank" test ($p < 0.05$).

Thus, from the results observed above, the dichloromethane phase (PGD) and ethyl acetate phase (PGA) from the ethanol extract of leaves from *P. glazioviana* showed a toxic activity to the workers of *A. sexdens rubropilosa*. Comparing with the control, there was 50% of mortality of ants in 15 days of experiments to PGD, and in 16 days to PGA. The hydroalcoholic and hexane phases, however, showed very similar survival curve as observed to the control with the pure diet, presenting no significant activity. The results obtained from these bioassays motivated further fractionations for isolation the pure constituents in these partitions. For this, PGD was selected to the initial studies, and once this study resulted in plenty of new compounds, which some specific experiments are still needed to complete the full structural elucidation, the bioassay with the pure compounds were not performed until this present moment.

4.2.1.2- *Picramnia bahiensis*

4.2.1.2.1- Crude extracts

All crude extracts from stem, leaves and roots of *P. bahiensis* were sent to the Social Insects Study Center (CEIS), Unesp - Rio Claro by the student Rodrigo O. S. Kitamura under the supervision of Prof. Dr. Odair Correa Bueno to evaluate the insecticide activity on the workers of *A. sexdens rubropilosa* according to methodology described in item 3.4.1. The survival curves from the ants submitted to the treatment by ingestion of the extracts incorporated into the diet were plotted, comparing with the curve obtained from the control containing only pure diet, after a period of 25 days of experiment, and using the "log-rank" test. The results obtained are shown in FIGURES 4.163 - 4.165 and in TABLES 4.22 – 4.24.

Thus, from the leaves extracts, the methanol (PBFMe) and dichloromethane (PBFD) extracts showed a greater activity. The methanol extract presented a lethal action of 50% of the workers in 4 days of experiments, and the dichloromethane extract, a lethal action of 50% of the workers in 8 days of experiment. The hexane extract (PBFHe), on the other hand, did not present toxic potential against the workers of *A. sexdens rubropilosa*, which the survival curve showed very similar to the control of the pure diet.

Likewise for the stem extracts, a greater insecticidal potential was observed to the methanol (PBCMe) and dichloromethane (PBCD) extracts. A mortality of 50% of workers of *A. sexdens rubropilosa* was observed after 5 days of experiment for dichloromethane extract, and 6 days for the methanolic. However, no significant activity was observed to the hexane extract (PBCHe), showing very close similarity as the control using the pure diet.

From the roots, all extracts present an excellent activity, showing a lethal action of 50% of the workers in 4 and 4,5 days of experiments to hexane+ dichloromethane (PBRHe+D) and methanol (PBRMe) extracts, respectively.

These results showed excellent activity to all structures analyzed of *P. bahiensis*, indicating this plant as a potential source for insecticide compounds. The significant activity observed brought the motivation for continuing studies, and once RODRIGO, 2013 only studied the hexane/dichloromethane (PBRHe+D) extract from roots of *P. bahiensis* during his PhD, the intial studies to this work focused on the methanol extract from stem.

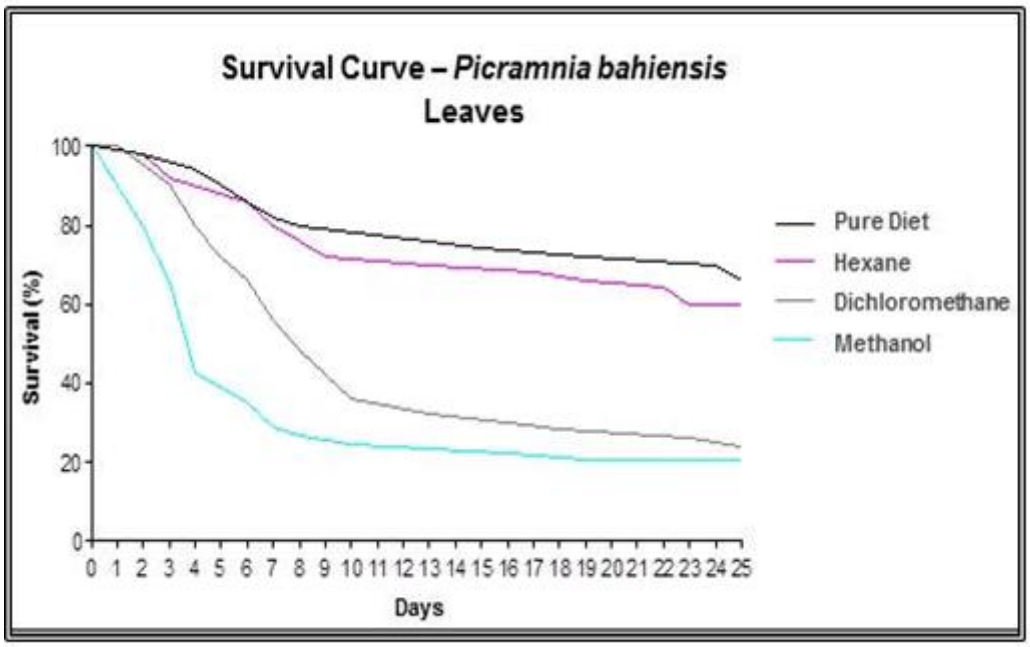

FIGURE 4.163 – Survival curve of *A. sexdens rubropilosa* workers submitted to the ingestion treatment with the leaves extracts of *P. bahiensis* (KITAMURA, 2013).

TABLE 4.22 - Cumulative mortality and median survival (Md) of *A. sexdens rubropilosa* workers submitted to the bioassay of incorporation in artificial diet the leaves extracts of *P. bahiensis*

Treatment	Cumulative % of mortality per day										Md*
	1	2	3	6	8	10	14	17	21	25	
Pure Diet	0	2	2	14	20	20	24	26	28	34	>25[a]
PBFHe	0	2	8	14	24	28	30	32	34	40	>25[a]
PBFD	0	0	10	34	52	64	68	70	72	74	8***b***
PBFMe	2	22	36	66	74	76	76	78	80	80	4***b***

* Different letters in relation to the control indicate a significant difference according to the "log rank" test ($p < 0.05$).

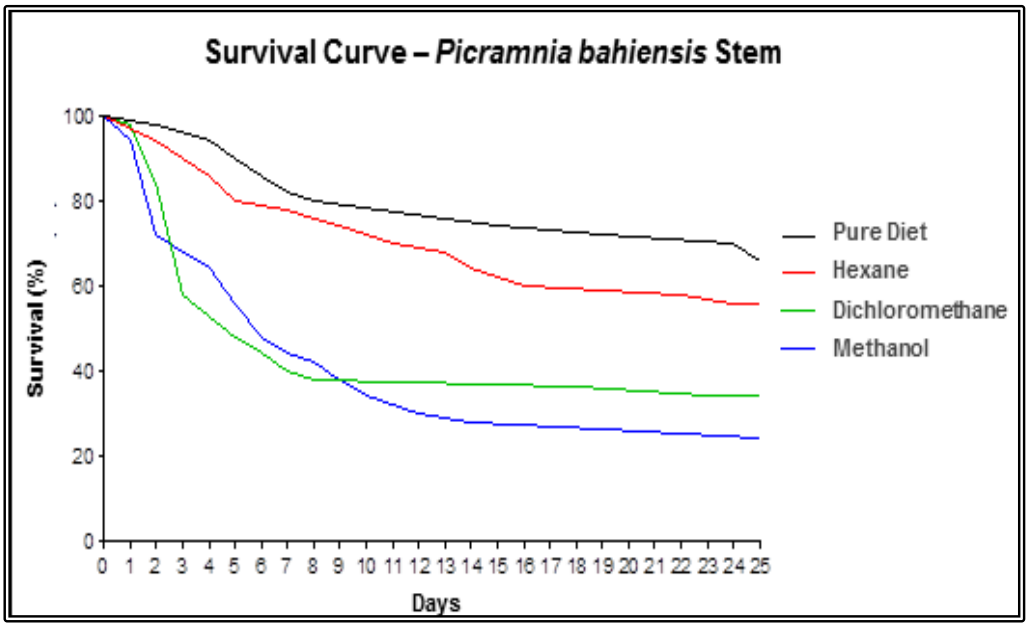

FIGURE 4.164 – Survival curve of *A. sexdens rubropilosa* workers submitted to the ingestion treatment with the stem extracts of *P. bahiensis* (KITAMURA, 2013).

TABLE 4.23 - Cumulative mortality and median survival (Md) of *A. sexdens rubropilosa* workers submitted to the bioassay of incorporation in artificial diet the stem extracts of *P. bahiensis*

Treatment	Cumulative % of mortality per day										Md*
	1	2	3	6	8	10	14	17	21	25	
Pure Diet	0	2	2	14	20	20	24	26	28	34	>25[a]
PBCHe	0	6	6	20	24	26	36	40	40	44	>25[a]
PBCD	2	16	42	70	76	76	76	76	78	80	5***b***
PBCMe	6	28	32	52	58	66	72	72	74	76	6***b***

* Different letters in relation to the control indicate a significant difference according to the "log rank" test ($p < 0.05$).

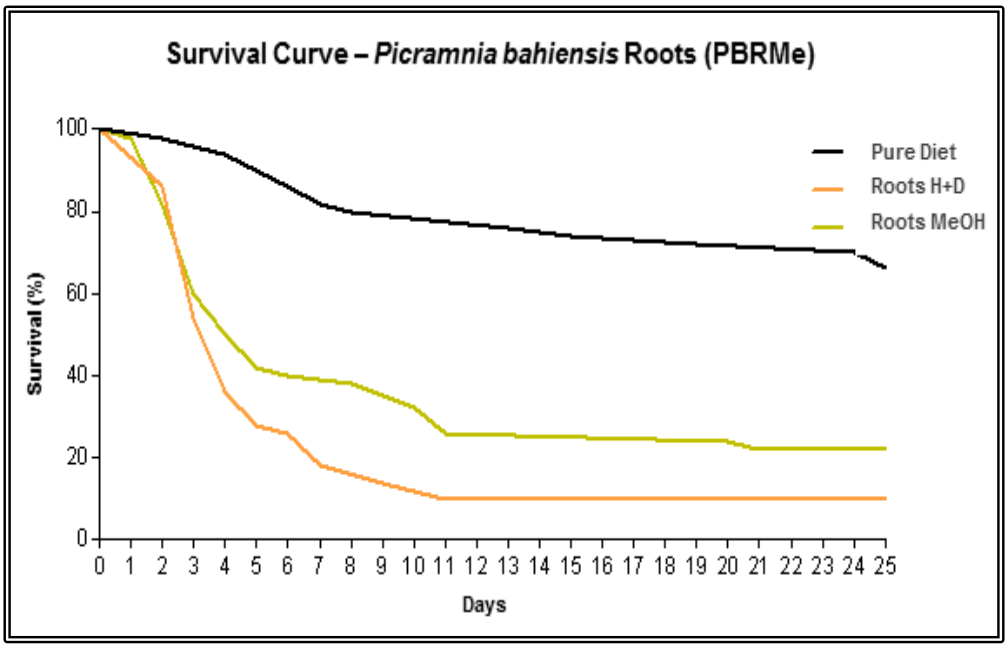

FIGURE 4.165 – Survival curve of *A. sexdens rubropilosa* workers submitted to the ingestion treatment with the roots extracts of *P. bahiensis* (KITAMURA, 2013).

TABLE 4.24 - Cumulative mortality and median survival (Md) of *A. sexdens rubropilosa* workers submitted to the bioassay of incorporation in artificial diet the roots extracts of *P. bahiensis*

Treatment	Cumulative % of mortality per day										Md*
	1	2	3	6	8	10	14	17	21	25	
Pure Diet	0	2	2	14	20	20	24	26	28	34	>25***a***
PPRHe+D	0	14	46	74	82	86	90	90	90	90	4***b***
PBRMe	2	18	40	60	62	68	74	74	78	80	4,5***b***

* Different letters in relation to the control indicate a significant difference according to the "log rank" test ($p < 0.05$).

4.2.1.2.2- Fractions from PBCMe

The group PBCMe 03 and its respective fractions were sent to evaluate their insecticidal activity. The assay was performed at concentrations of 1 and 2 mg/mL for the group PBCMe 03 and at 1 mg/mL for the fractions obtained from this group. The survival curves from the ants submitted to the treatment were plotted, comparing with the curve obtained from the control containing only pure diet, after a period of 25 days of experiment, and using the "log-rank" test. The obtained result is presented in FIGURE 4.166 and TABLE 4.25.

The PBCMe group 03 and its fractions showed excellent insecticidal activity, justifying the continuous study with these samples and isolation of the compounds. The group PBCMe 03, in both concentrations analyzed, showed an average mortality of the ants with only three days of experiments, reaching 100% of mortality in 11 days of experiments when the lowest concentration of 1mg/mL was tested. From this group, as presented in experimental section, it was isolated three anthraquinones (chrysophanol, aloe-emodin and islandicin). The literature indicate the potential insecticide to the compound chrysophanol against *A. sexdens rubropilosa*, presenting an average mortality in 05 days of experiment, justifying the high insecticidal activity found to the group PBCMe 03 (RODRIGO, 2013).

The fractions obtained from the group PBCMe 03 were also very active, especially the fraction PBCMe 03/05 that showed a median mortality in three days of experiments, reaching 100% mortality in 15 days.

Further studies with the fractions PBCMe 03/04 and PBCMe 03/05 indicated the presence of the same major compounds in both fractions (compounds **28** and **29**). However, the activity observed to the fraction PBCMe 03/05 was even more pronounced than to the group PBCMe 03/04. Once the group PBCMe 03/05 also showed the presence of two minor compounds from analysis of the HPLC chromatogram (section 3.5.2.4), it is an indicative that the greater activity observed to this fraction can be related with these minor constituents, showing the importance of continuous studies to identification and future assays to these compounds. Moreover, the isolated compounds **28** and **29** will be sent to evaluate their activities in a near future, contributing to the establishment of structure-activity to these isomers.

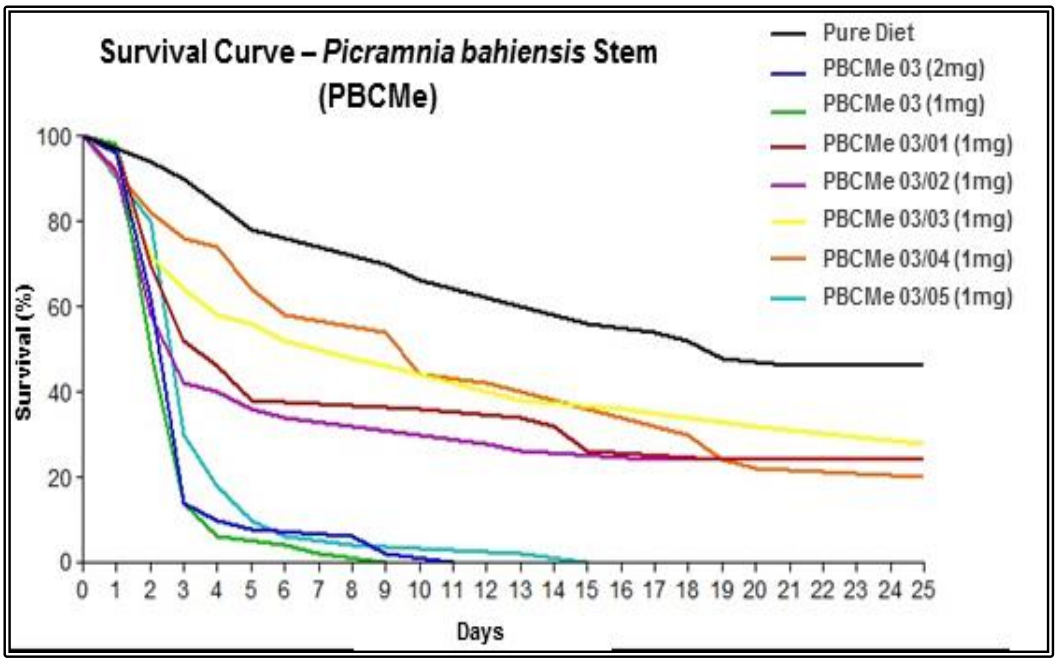

FIGURE 4.166 – Survival curve of *A. sexdens rubropilosa* workers submitted to the ingestion treatment with the fractions of *P. bahiensis*.

TABLE 4.25 - Cumulative mortality and median survival (Md) of *A. sexdens rubropilosa* workers submitted to the bioassay of incorporation in artificial diet the fractions of *P. bahiensis*

Treatment	Cumulative % of mortality per day										Md *
	1	2	3	6	8	10	14	17	21	25	
Pure Diet	0	6	10	22	28	34	42	46	54	54	>19***a***
PBCMe 03 (1mg)	4	38	86	92	94	98	100	100	100	100	3,0***b***
PBCMe 03 (2mg)	2	50	86	96	98	100	100	100	100	100	2,5***b***
PBCMe 03/01 (1mg)	2	30	48	62	62	64	64	74	76	76	4,0***b***
PBCMe 03/02 (1mg)	8	42	58	66	66	70	74	76	76	76	3,0***b***
PBCMe 03/03 (1mg)	8	28	36	48	52	54	62	64	64	72	7,5***b***
PBCMe 03/04 (1mg)	0	18	24	42	42	56	62	68	78	78	10***b***
PBCMe 03/05 (1mg)	0	20	70	94	96	96	98	100	100	100	3,0***b***

* Different letters in relation to the control indicate a significant difference according to the "log rank" test ($p < 0.05$).

4.2.2- Fungicide activity against *L. gongylophorus*

4.2.2.1- *Picramnia glazioviana*

4.2.2.1.1- Crude extracts

The ethanol extract from the leaves of *P. glazioviana* was submitted to the in vitro assay with the symbiotic fungus of leaf-cutting ants, *L. gongylophorus*. The bioassay was carried out at the Department of Chemistry, Laboratory of Bioassays, UFSCar, under coordination of Ms. Dorai Periotto Zandonai, according to the methodology described in item 3.4.2. The sample was incorporated into the culture medium at the final concentration of 1 mg/mL and the inhibition of mycelial growth for the extract was evaluated in an interval of 30 days. The result of the fungicide bioassay is shown in FIGURE 4.167.

The bioassay acquired from the leaves ethanol extract of *P. glazioviana* was quite satisfactory, showing an inhibition of the mycelial growth of the symbiont fungus of 53% comparing to the control. Thus, from this result, in association with that obtained from the insecticide assay, the partitioning of this extract was performed aiming the evaluation of the fungicide activity to its respective phases.

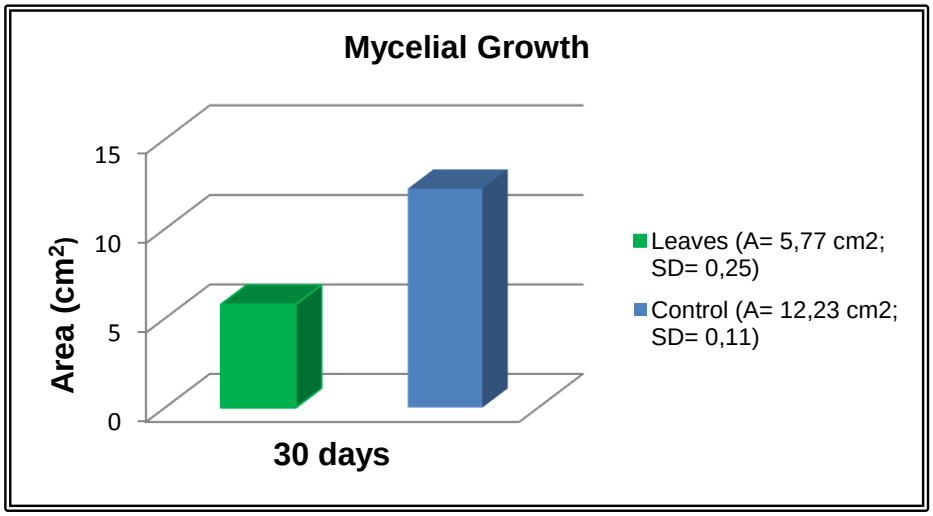

FIGURE 4.167 – Inhibition of the mycelial growth of *L. gongylophorus* submitted to the in vitro assay with ethanol extract of *P. glazioviana*.

4.2.2.1.2- Fractions obtained from Liquid-Liquid Partition

After the partitioning the leaves ethanol extract of *P. glazioviana*, the obtained phases in hexane (PGHe), dichloromethane (PGD), ethyl acetate (PGA) and hydroalcoholic (PGHi) were submitted to the in vitro assay with the fungus *L. gongylophorus*, according to the methodology described in item 3.4.2. The samples were incorporated into the culture medium at the final concentration of 1 mg/mL and the inhibition of mycelial growth was evaluated at a 30 days interval. The result of the fungicidal assay to each phases is shown in FIGURES 4.168 and 4.169.

Although the satisfactory inhibition obtained to the ethanol extract, the same activity was not observed to the phases obtained from the partitioning of this extract. The inhibition of the mycelial growth of the symbiont fungus for the PGHe, PGD and PGA phases were, respectively, 14%, 32% and 30%. The hydroalcoholic

phase (PGHi) showed no inhibition; instead, this phase stimulated the growth of the symbiotic fungus at 9%.

These results indicate that may have had synergism between the phases, justifying the result observed to the extract. In addition, after analyses of all results, there is an indication the constituents of *P. glazioviana* present an insecticidal characteristic more relevant than the fungicide.

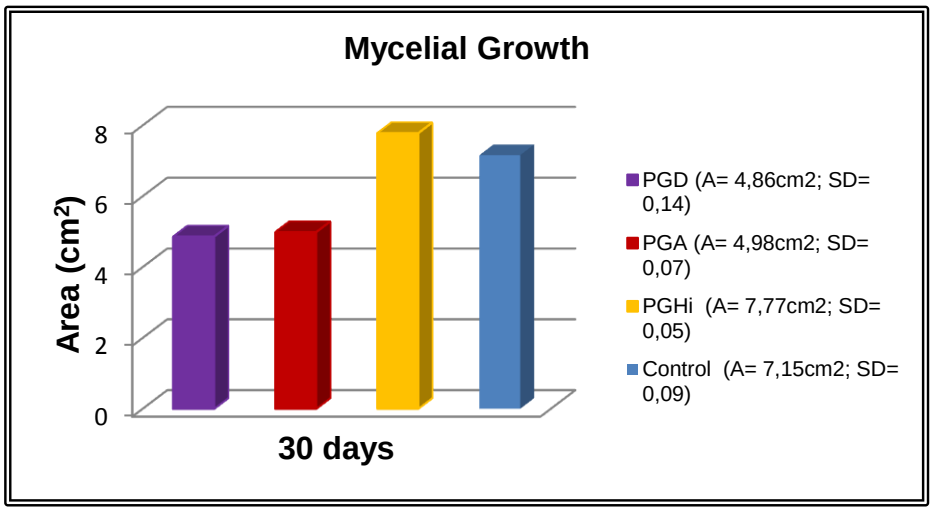

FIGURE 4.168 – Inhibition of the mycelial growth of *L. gongylophorus* submitted to the in vitro assay with the fractions PGD, PGA and PGHi of *P. glazioviana*.

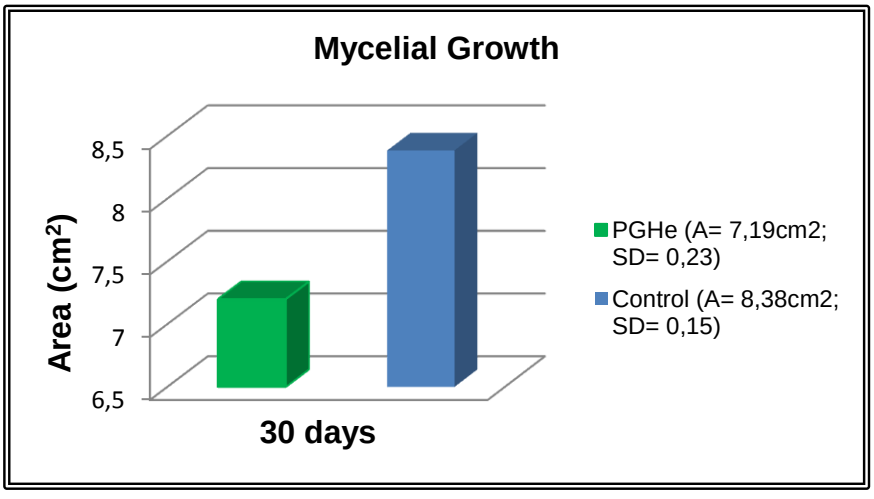

FIGURE 4.169 – Inhibition of the mycelial growth of *L. gongylophorus* submitted to the in vitro assay with the fractions PGD, PGA and PGHi of *P. glazioviana*.

4.2.2.2- *Picramnia bahiensis*

4.2.2.2.1- Crude extracts

The leaves and stem extracts of *P. bahiensis* were submitted to the in vitro assay with the symbiotic fungus of the leaf-cutting ants, *L. gongylophorus*, according to methodology described in item 3.4.2. It was analyzed the fungicidal potential to the hexane (PBFHe), dichloromethane (PBFD) and methanol (PBFMe) extracts from leaves and to the hexane (PBCHe), dichloromethane (PBCD) and methanol (PBCMe) extracts from stem. The samples were incorporated into the culture medium at the final concentration of 1 mg/mL and the inhibition of mycelial growth for these extracts was evaluated at a 30 days interval. The results of the fungicidal assays are shown in the following figure (FIGURE 4.170).

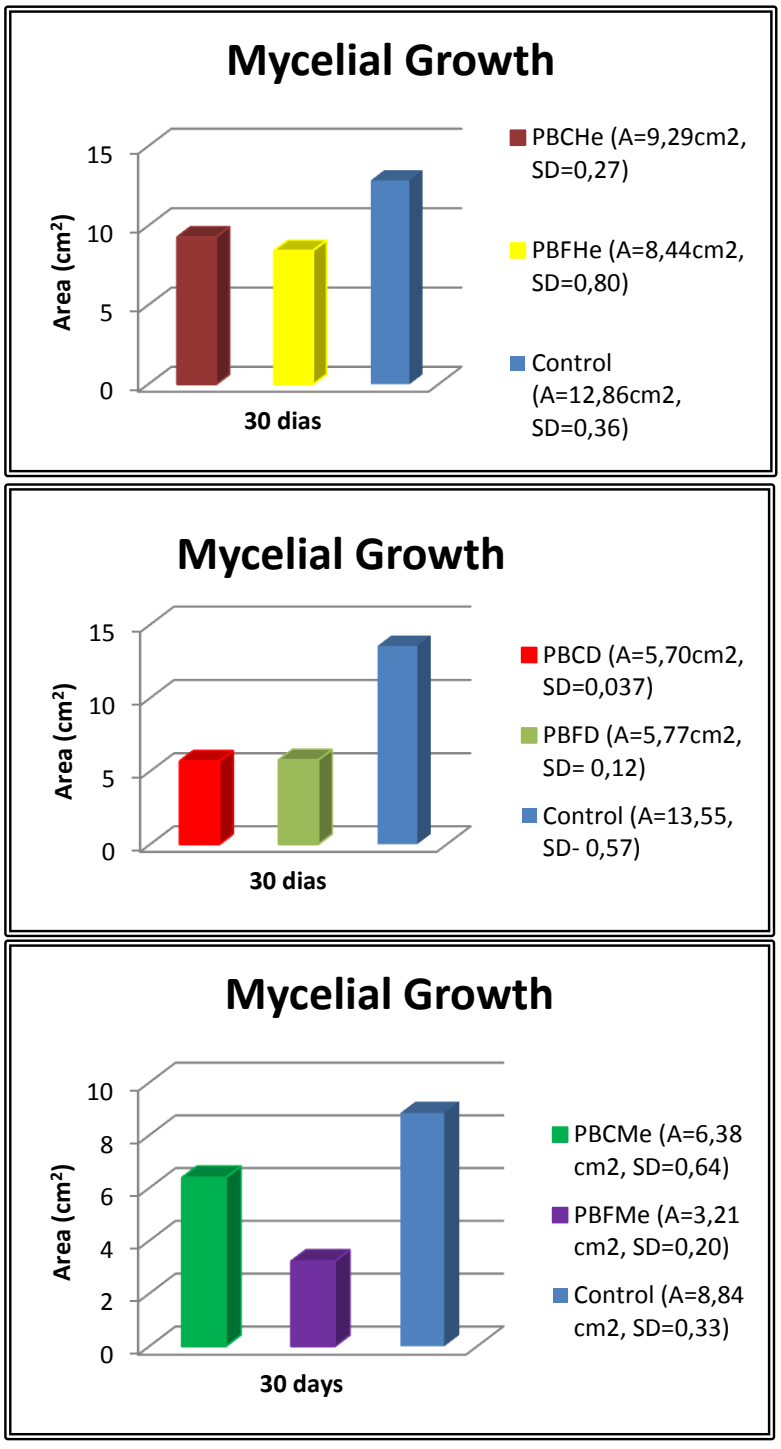

FIGURE 4.170 – Inhibition of the mycelial growth of *L. gongylophorus* submitted to the in vitro assay with the extracts of *P. bahiensis*.

The analysis of the results acquired from the extracts of leaves and stem of *P. bahiensis* were quite satisfactory. The mycelial growth inhibition of symbiont fungus for PBFHe and PBCHe extracts was 34% and 28%, respectively. The dichloromethane from leaves (PBFD) and stem (PBCD) extracts of *P. bahiensis* showed a higher inhibition, at 57%. To the most polar extracts, the activity was 64% inhibition to the methanol extract from leaves (PBFMe) and 28% of inhibition to the metanol extract from stem (PBCMe) of *P. bahiensis*.

Thus, from these assays it was possible to conclude the fungicidal constituents present a character of medium to high polarity, since the activities were not seen to the hexane extracts. In addition, despite the potential fungicide observed for PBFMe, the phytochemical study with the PBCMe extract was mainly based on the very promising insecticidal activity observed, since these results were performed after the beginning of the phytochemical study with this extract. Moreover, the higher amount PBCMe extract would facilitate the several processes of purifications, which motivated the choice of study.

4.2.2.2.2- Fractions of PBCMe extract

The group PBCMe 03 of *P. bahiensis* was submitted to the in vitro assay with the symbiotic fungus of the leaf-cutting ants, *L. gongylophorus*, according to the described methodology in item 3.4.2. The sample was incorporated into the culture medium in two final concentrations: 0.5 mg/mL (PBCMe 03a) and 1.0 mg/mL (PBCMe 03b). The fractions from the fractionation of the group PBCMe 03 were incorporated into the culture medium at the final concentration of 0.5 mg/mL. The inhibition of the mycelial growth for these samples was evaluated at a 30 days of interval. The results obtained from fungicide assay are shown in FIGURE 4.171.

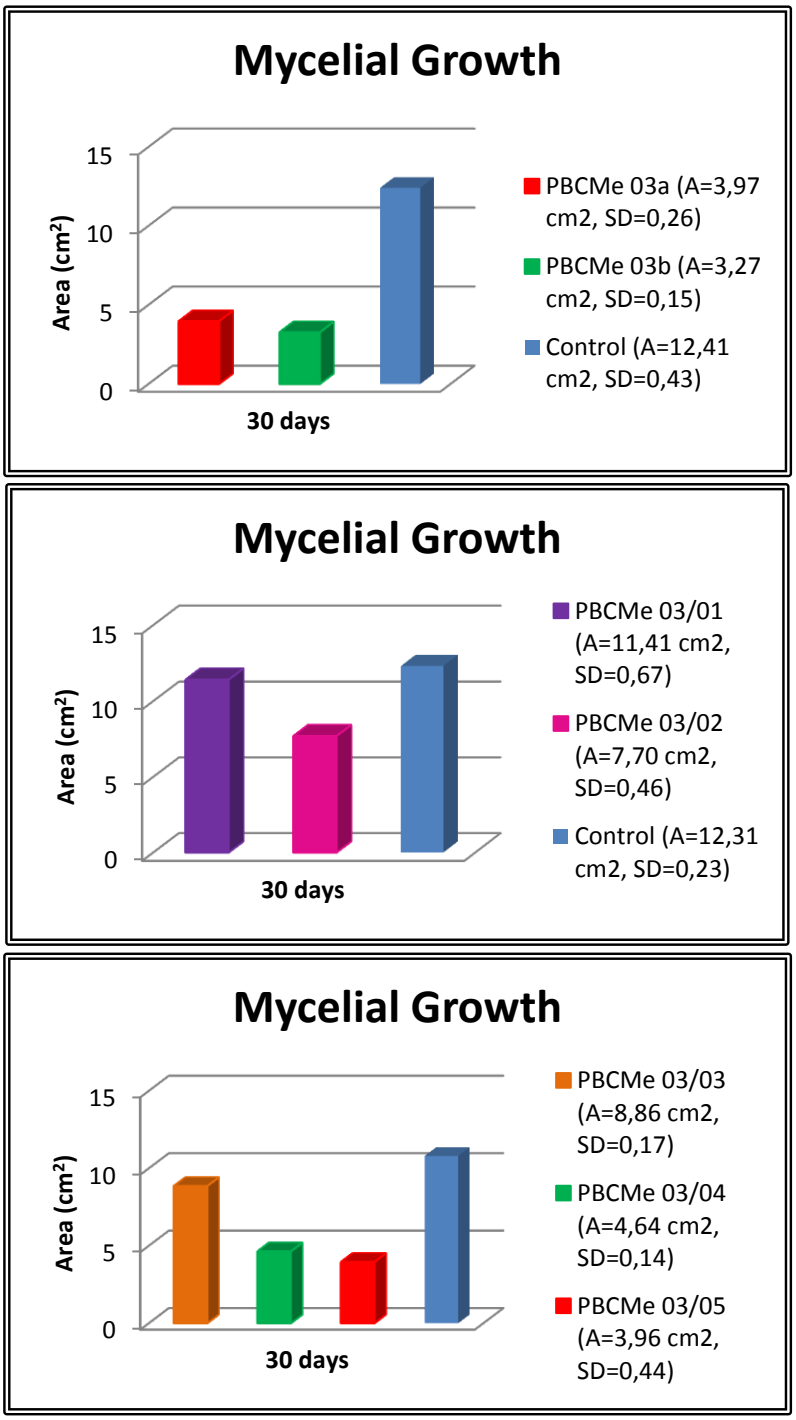

FIGURE 4.171 – Inhibition of the mycelial growth of *L. gongylophorus* submitted to the in vitro assay with the group PBCMe 03 and its respectives fractions of *P. bahiensis*.

The analysis of the PBCMe 03 bioassay was very promising in both concentrations analyzed. The inhibition of mycelial growth of the symbiont fungus for this group was 68%, and 74% at the concentration of 0.5 mg/mL and 1.0 mg/mL, respectively. These results also suggest the biological activity is not proportionally dependent of the concentration. Although the higher inhibition observed when the concentration of 1.0 mg/mL was used, the sample tested at the lowest concentration (0.5 mg/mL) nevertheless also presented a great result of inhibition for the symbiotic fungus.

Another important detail was also observed from this assay. The assay performed to the PBCMe extract, as described above, showed only 28% of inhibition of the symbiotic fungus. However, the assay performed with the group PBCMe 03 indicated there was a higher concentration of the active compounds present in this fraction (PBCMe 03), after the fractionation processes.

To the fractions obtained from the group PBCMe 03, as observed in the graphs above, the most active were the last PBCMe 03/04 and PCMe 03/05 fractions. There was an inhibition of the mycelial growth of the symbiont fungus of 57% for PBCMe 03/04 and of 63% for PBCMe 03/5 against 7%, 37% and 18% for the groups PBCMe 03/01, PBCMe 03/02 and PBCMe 03/03, respectively. These results have shown very promising and are in agreement to the data observed in the ^{1}H NMR spectrum, once the purification procedures resulted in the isolation of the glycosides anthraquinones for the groups PBCMe 03/04 and PBCMe 03/5, and characteristics signals of sugars observed to the initial groups.

The potential fungicide of some glycosides anthaquinones against the symbiotic fungus *L. gongylophorus* has already reported by RODRIGUEZ-GAMBOA, 2000. From this work, the two positional isomers 1-β-D-O-glucopyranosyl emodin and 8-β-D-O-glucopyranosyl emodin presented 70% of inhibition of the fungus *L. gongylophorus*. These compounds are very similar to the isolated compounds **28** and **29**, having only an additional hydroxyl group at the position C-6. Once the fractions which resulted in the isolation of the compounds **28** and **29** were very active, there is strong evidence the bioassay with these pure compounds can also present a great bioactivity. Thus, the evaluation of the activity to pure compounds will contributed for this understanding.

4.2.3- High-Resolution Bioassays

4.2.3.1- *Picramnia glazioviana*

The extracts from *P. glazioviana* were evaluated their antidiabetic potential through the construction of the IC_{50} curve and thereafter their biochromatogram were performed. Crude extracts can be considered as having a significant inhibitory effect if the IC_{50} value is below 50 µg/mL (TRINH, 2016). Based on this criterion, the study of ethanol extract from *P. glazioviana* displayed an inhibitory concentration value (IC_{50}) of 27.3 µg/mL towards α-glucosidase. The dichloromethane (PGD) and ethyl acetate partition (PGA) were also evaluated their antidiabetic potential, and displayed an IC_{50} value of 38.4 µg/mL and 15.1 µg/mL, respectively (FIGURES 4.172). Thus, the biochromatogram was constructed to the most active phase (PGA). However, the biochromatogram performed to this partition showed a large broad peak from 20 to 50 min, making the distinction of the active peaks not possible (FIGURE 4.173). Furthermore, previous studies with PGA partition allowed the isolation of some known flavonoids (not described in this present work), and the good value found to this partition is in agreement with the presence of these compounds, since flavonoids are very known of presenting antidiabetic activity (LIU, 2015; SILVA, 2016). However, these secondary metabolites are much studied and not attractive for the isolation of new compounds. Moreover, since the study with PGD partition demonstrated the presence of new compounds with new skeleton, the aim of this work focused on the searching for the activity to these new constituents. Thus, the PGD partition was also submitted to evaluate the antidiabetic potential with the enzyme PTP1B. The result obtained from this assay displayed an inhibitory concentration value (IC_{50}) of 31.1 µg/mL towards PTP1B (FIGURE 4.174). Thereafter, the PGD partition was subjected to high-resolution α-glucosidase and PTP1B profiling. However, after the construction of their respective biochromatograms (FIGURES 4.175 and 4.176) no active compounds could be pinpointed from the PTP1B high-resolution biochromatogram, and some discrete peaks, indicating a very low activity correlated to compounds **4**, **5** or **5a** and **6** could be observed from the α-glucosidase high-resolution bioassay. Thus, the antibacterial activity to *S. aureus* was evaluated to this partition through the high-resolution

bioassay and subsequent construction of the biochromatogram. The IC_{50} to this partition was not performed, once the solubility of the extract in 85% of water and 15% of DMSO (according to the methodology established in the group) was a limiting factor. The results acquired from high-resolution bioassay, however, indicated the active region of the chromatogram, allowing to suggest the compounds **04**, **05** or **05a** and **06** as the responsible to the observed activity (FIGURE 4.177).

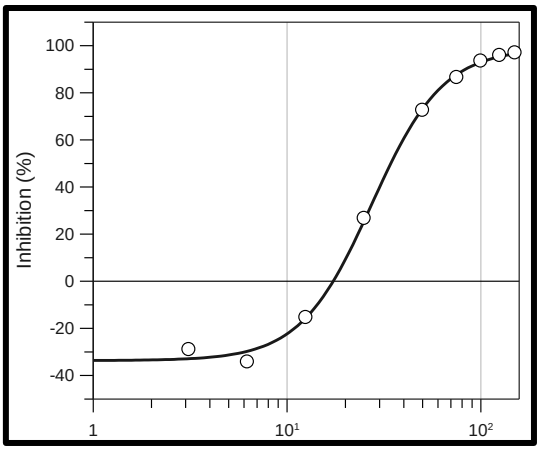

PG
IC_{50} = 27.3 µg/mL

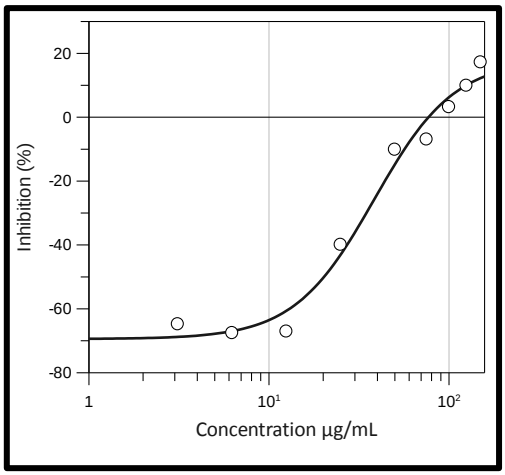

PGD
IC_{50} = 38.4 µg/mL

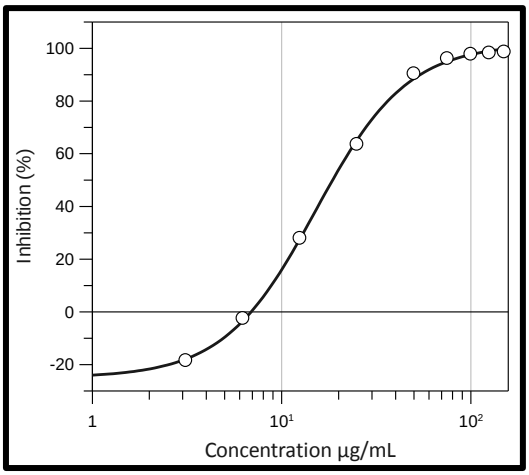

PGA
IC_{50} = 15.1 µg/mL

FIGURE 4.172 – Dose-response curve to PG, PGD and PGA from *P. glazioviana* in α-glucosidase assay. Each poin represents the average of triplicate measurements.

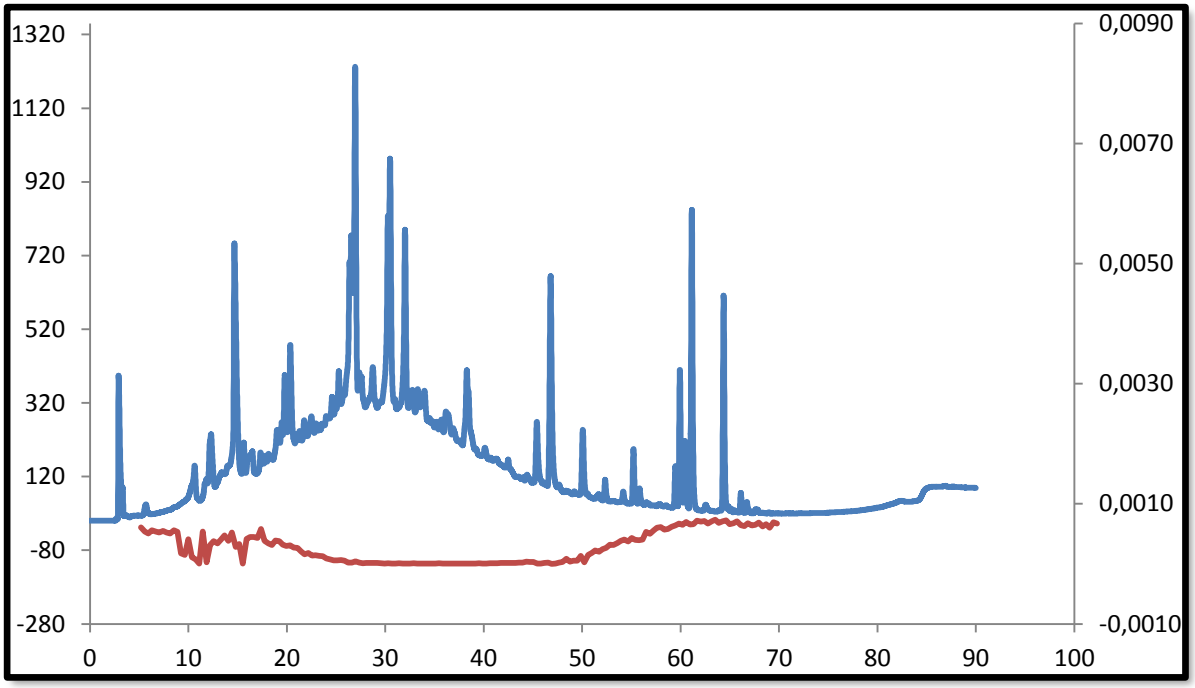

FIGURE 4.173 - α-glucosidase high-resolution bioassay to PGA from *P. glazioviana*. (Blue color indicates the UV chromatogram at 254 nm; Red color represents the biochromatogram).

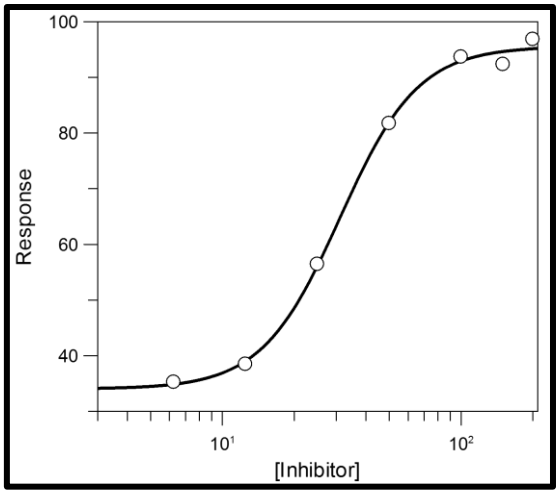

PGD
IC_{50} = 31.1 µg/mL

FIGURE 4.174 – Dose-response curve to PGD partition from *P. glazioviana* in PTP1B assay. Each poin represents the average of triplicate measurements.

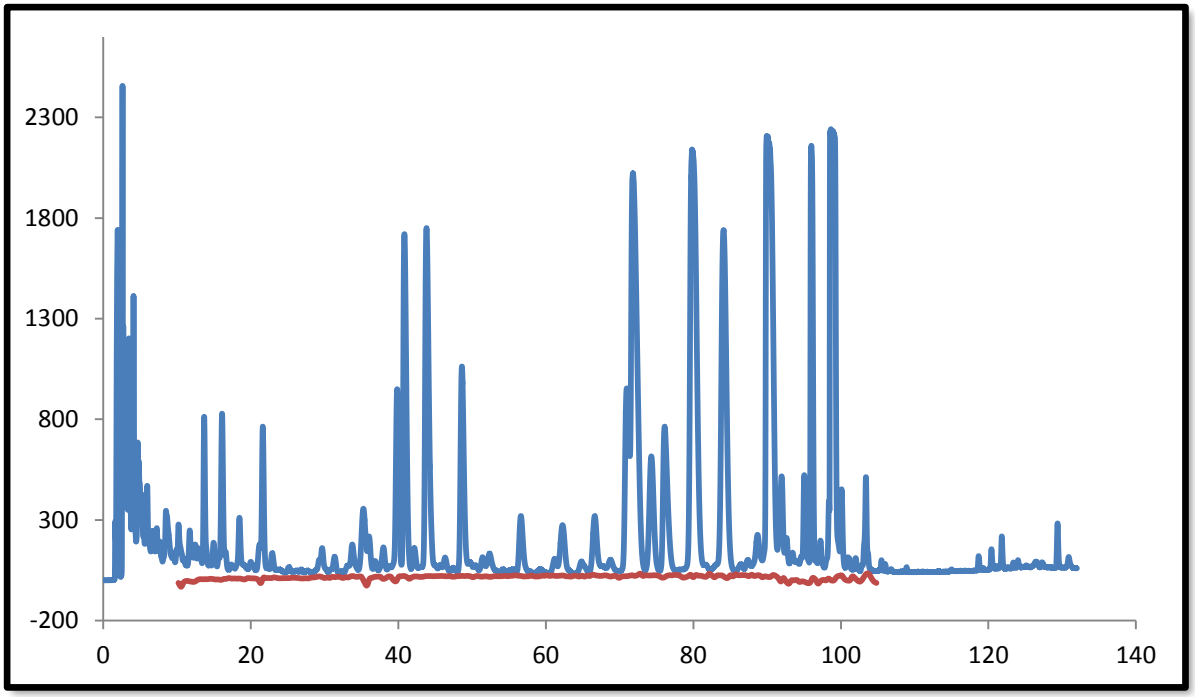

FIGURE 4.175 - α-glucosidase high-resolution bioassay to PGD from *P. glazioviana*. (Blue color indicates the UV chromatogram at 254 nm; Red color represents the biochromatogram).

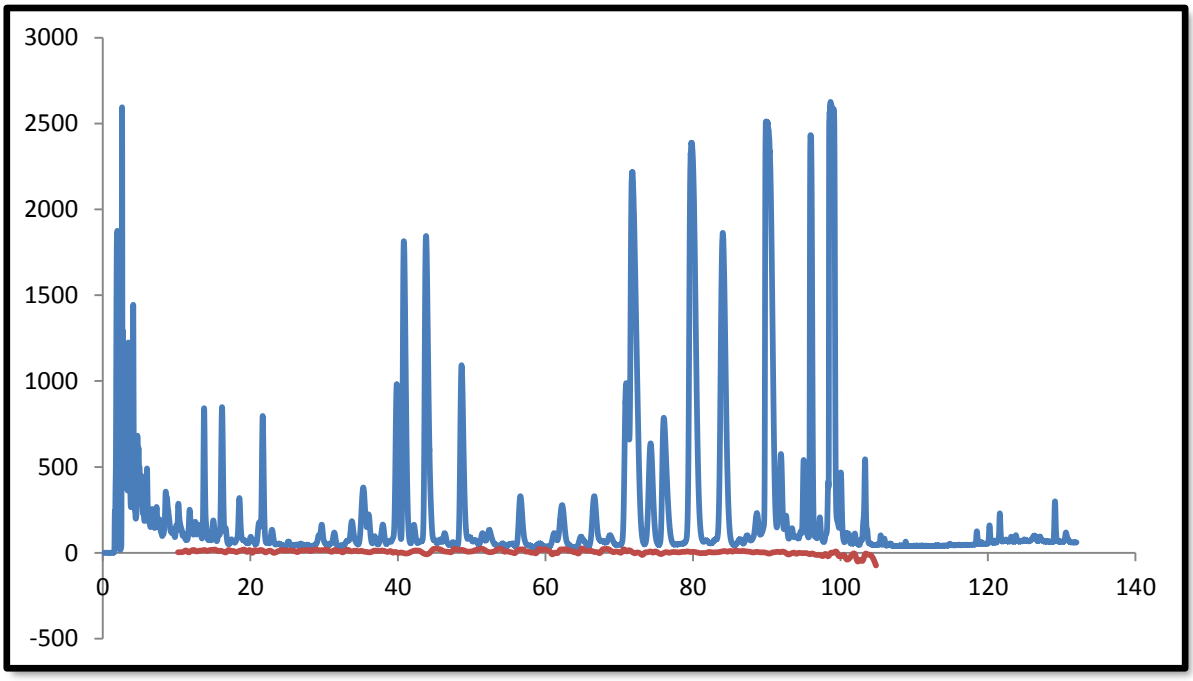

FIGURE 4.176 – PTP1B high-resolution bioassay to PGD of *P. glazioviana*. (Blue color indicates the UV chromatogram at 254 nm; Red color represents the biochromatogram).

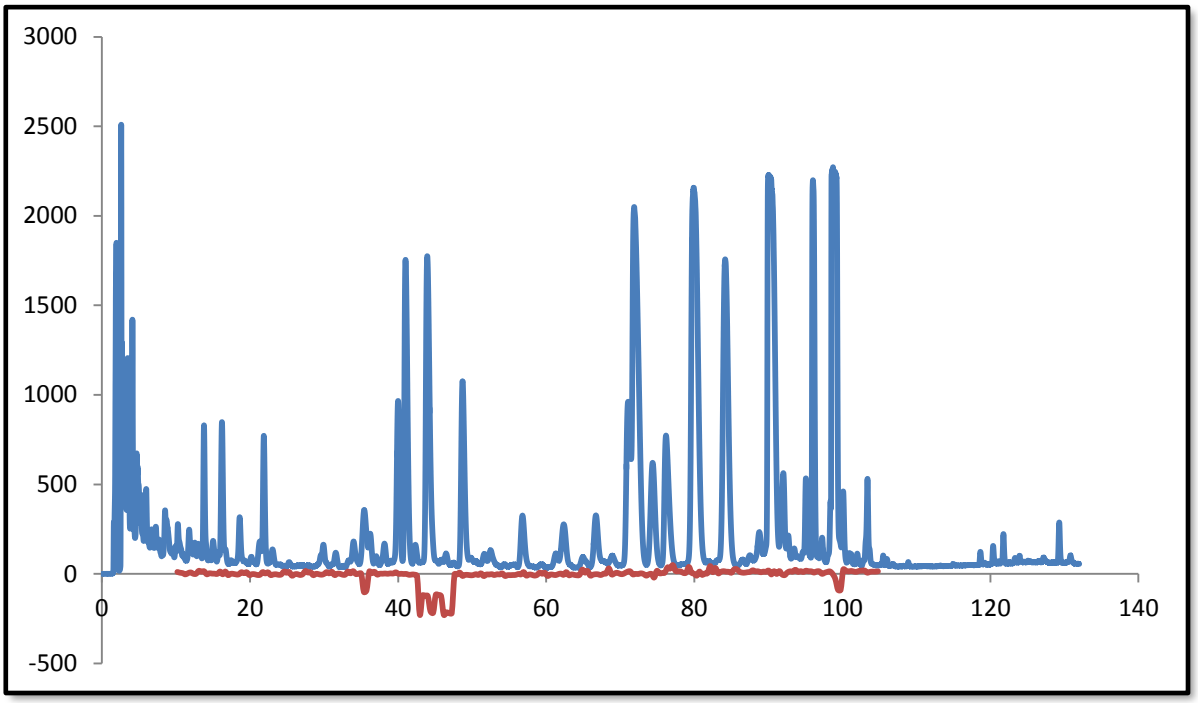

FIGURE 4.177 - Antibacterial high-resolution bioassay to PGD of *P. glazioviana* . (Blue color indicates the UV chromatogram at 254 nm; Red color represents the biochromatogram indicating the active compounds).

4.2.3.2 – *Picramnia bahiensis*

The extracts from *P. bahiensis* were evaluated their antidiabetic potential through the construction of the IC_{50} curve. It was evaluated the potential antidiabetic to the methanol extract from roots (PBRMe) and stem (PBCMe), in α-glucosidase assay. Thus, the dose-response curve to PBRMe and PBCMe displayed an inhibitory concentration value (IC_{50}) of 43.5 µg/mL and 43.3 µg/mL, respectively, towards α-glucosidase (FIGURE 4.178). Once both extracts displayed a very similar inhibitory activity, the PBRMe extract was chosen for the following procedures since this extract showed less complex in relation of its constituents than PBCMe (after analyses of the HPLC chromatogram). Thereafter, the PTP1B assay was also evaluated to PBRMe, but due the high standard error observed in the IC_{50} curve, this response was not disclosed to this work.

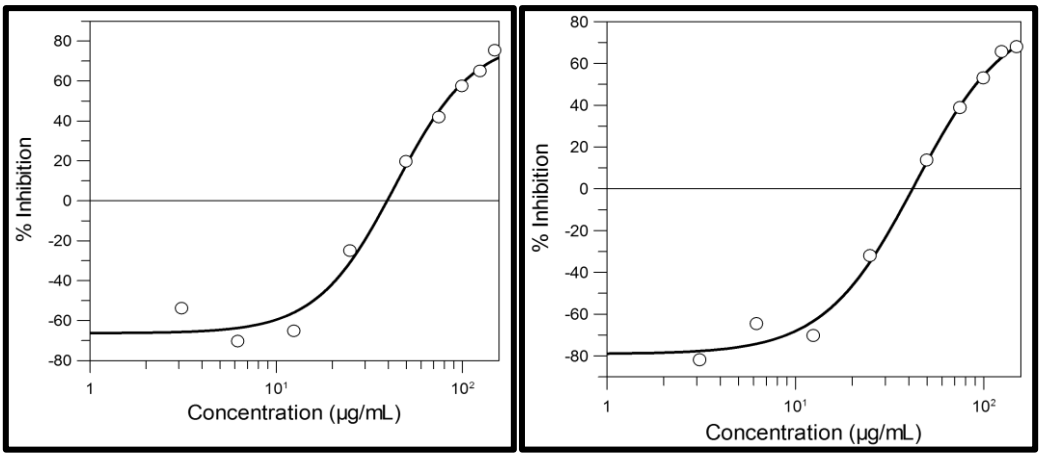

PBRMe
IC_{50} = 43.5 µg/mL

PBCMe
IC_{50} = 43.3 µg/mL

FIGURE 4.178 – Dose-response curve to PBRMe and PBCMe extracts from *P. bahiensis* in α-glucosidase assay. Each poin represents the average of triplicate measurements.

Thus, the dual high-resolution α-glucosidase and PTP1B profiling were performed to PBRMe (FIGURES 4.179 and 4.180). The analyses of the results allowed to correlate the bioactive constituents present at the end of the HPLC chromatogram, in both assays. Thus, semi-preparative fractionation was performed, aiming the separation this extract in three main parts (PBRMe 01, 02 and 03) and evaluating the assay to the active fraction.

Consequently, the PTP1B high-resolution bioassay to PBCMe 03 (the active fraction) was performed allowing to pinpoint the active compound present in this extract, after the construction of its biochromatogram (FIGURE 4.181). The high-resolution α-glucosidase profiling to PBCMe 03 as well as, the identification of the bioactive compound could not be performed until this present moment. However, this is the first report about the antidiabetic profile in plants of the family Picramniaceae, and this work can base future studies on the searching for antidiabetic constituents from *Picramnia* species.

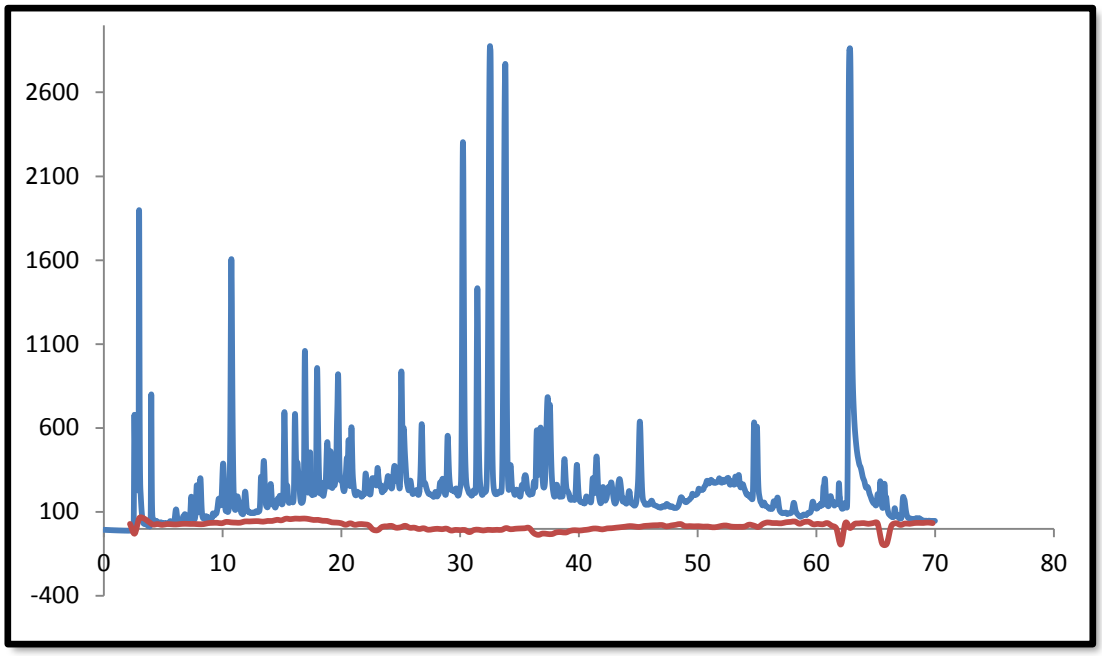

FIGURE 4.179 - α-glucosidase high-resolution bioassay to PBRMe of *P. bahiensis*.

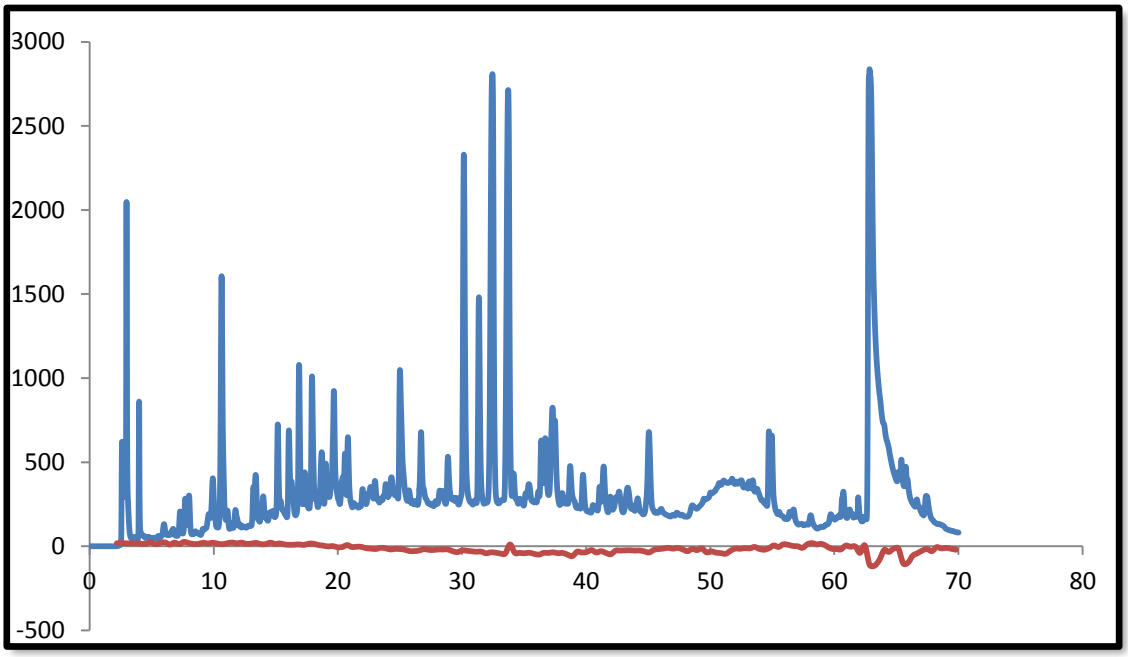

FIGURE 4.180 – PTP1B high-resolution bioassay to PBRMe of *P. bahiensis*.

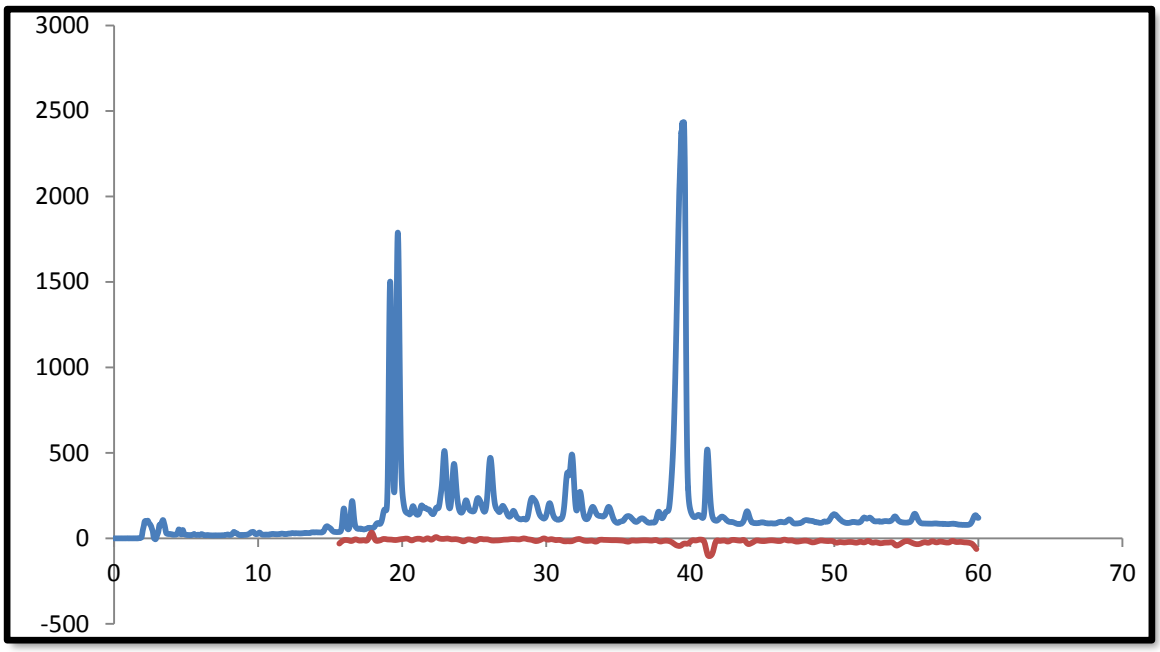

FIGURE 4.181 - PTP1B high-resolution bioassay to PBRMe 03 of *P. bahiensis*.

5 - CONCLUSION

The phytochemical study of *Picramnia* species in the literature allowed the isolation of several secondary metabolites with important biological activities. Anthraquinones, anthrones, coumarins, and triterpenes have already been reported in this genus.

In this present work, the phytochemical study of *Picramnia bahiensis* resulted in the isolation of two new C,O-diglycosides anthrones and five known anthraquinones. Moreover, compound **25** (islandicin) was isolated for the first time in species of Picramniaceae family. In addition, *Picramnia glazioviana* allowed the isolation of 22 new highly oxygenated nortriterpenes that presented a new chemical skeleton. This is the first time nortriterpenes are isolated in the Picramniaceae family, and the presence of these constituents with new skeleton are extremely important for the knowledge and contribution to the chemosystematics of this plant. Furthermore, the biosynthetic pathway proposed for the formation of these compounds has suggested the oleanolic acid as precursor, instead of the already suggested euphol as directly precursor to limonoids and quassinoids in Rutales. These results point to the need of futures investigations in this field, to prove a new biosynthetic pathway and precursors, besides to contribute with to the positioning of *Picramnia* species in the Picramniaceae family, once this positioning has been based on morphological classification and absence of the quassinoids.

In relation to the bioactivity evaluation of both these species of *Picramnia*, this work reports the potential insecticide, fungicide, antidiabetic, and antibacterial for their extracts and fractions.

In a specific approach, ethanol extract from leaves of *P. glazioviana*, as well as the PGD and PGA partitions showed a toxic activity to the workers of *A. sexdens rubropilosa.* On the other hand, the inhibition of the mycelial growth of the symbiont fungus was very discrete in this specie.

All vegetal structures of *Picramnia bahiensis* presented an excellent insecticide activity, highlighting the dichloromethane and methanol extracts (KITAMURA, 2013). The fractions from PBCMe also displayed great activity, highlighting the group PBCMe 03, and the fraction PBCMe 03/05. Since the anthraquinone **28** and **29** were isolated from these groups, there is a strong

indicative these compounds can show good insecticide activity. The compound chrysophanol, isolated from PBCMe 03 was also suggested to have contributed to the activity observed, since this compound showed a potential insecticide against leaf-cutting ants in previous studies in literature. The fungicide assay was promising to the extracts dichloromethane from leaves and stem, as well as to the methanol extract from leaves of *P. bahiensis*. The methanol extract from stem showed a discrete inhibition of the mycelial growth of the symbiont fungus. However, a concentration of the constituents to the group PBCMe 03 can explain the greater activity observed to this group. The fractions PBCMe 03/04 and PBCMe 03/05 also showed good fungicide potential, and these results can lead to the discovery of the fungicide activity to the compounds **28** and **29**, since other glycosides anthraquinones have already presented this potential in literature.

Moreover, this work presented for the first time the evaluation of species of *Picramnia* owning an antidiabetic potential. The extracts of PBRMe, PBCMe, PG, PGD and PGA presented good inhibitory concentration value (IC_{50}) to α-glucosidase. The high-resolution α-glucosidase and PTP1B profiling to the extract PBRMe allowed pinpointing the presence of antidiabetic constituents at the end of the HPLC chromatogram, indicating an apolar character of the bioactive constituents. The evaluation of the high-resolution PTP1B profiling to the group PBRMe 03 could pinpoint one main constituent as the compound responsible to this activity. Although the α-glucosidase high-resolution profiling and the identification of this active compound could not be performed until this current moment, this work showed the importance of considering species of *Picramnia* owning an antidiabetic potential, and can lead to future investigations under this perspective.

The dual high-resolution α-glucosidase and PTP1B profiling to the PGD partition was also evaluated. After the construction of the biochromatogram referring to each assay, no active compounds could be observed from the PTP1B biochromatogram, and very discrete compounds could be suggested from the α-glucosidase assay. On the other hand, the high-resolution bioachromatogram was performed to evaluate the antibacterial potential of these new compounds from PGD partition, and the results acquired from this assay allowed pinpointing the active compounds against *Staphylococcus aureus* directly from the complex matriz. This result is very promising to the discovery of new natural products with important

biological activities, and the high-resolution bioassays have proved to be an efficient and fast technology to pinpoint the active constituents from a crude extract.

The analysis performed in the HPLC-HRMS-SPE/NMR showed this technique as a powerful tool to isolation of the constituents in crude extracts. The trapping and isolation of the nortriterpenes from PGD presented high degree of purity allowing the acquisition of excellent NMR spectra in few days. This technique has proved its importance to the chemistry of natural products since it allows the reduction in time of analyses, and consummation of organic solvents, besides providing a fast and efficient information about the metabolites presented in a complex matrix.

However, when the analyzed compounds are new in literature, requiring further experiments for establishment of the full structural characterization, HPLC processes on preparative scale are still a good choice for isolation of higher amounts.

Decomposition processes of the nortriterpenes were also observed during the acquisition of the NMR spectra in deuterated chloroform, limiting the time these compounds can be solubilized in this solvent. It is highly recommended to dry the samples solubilized in deuterated chloroform in a maximum of 4 or 5 days, to avoid any degradation. It is also recommended to freeze the sample in case of necessity to keep it a long time in this solvent.

6 – BIBLIOGRAPHIC REFERENCES

BALDERRAMA, L., BRACA, A., GARCIA, E., MELGAREJO, M., PIZZA, C., De TOMMASI, N. "Triterpenes and anthraquinones from *Picramnia sellowii* Planchon in Hook (Simaroubaceae)". *Biochem. System. Ecol.* **29**: 331-333, 2001.

BOARETTO, M.A. & FORTI, M.C. "Perspectivas no controle de formigas cortadeiras". *Série Técnica, IPEF* **11**: 31-46, 1997.

BOULOGNE, I.; PETI, P.; OZIER-LAFONTAINE, H.; DESFONTAINES, L.; LORANGER-MERCIRIS, G. "Insecticidal and antifungal chemicals produced by plants: a review". *Environ. Chem. Lett.*, **10**: 325-347, 2012.

BUENO, O.C.; MORINI, M.S.C.; PAGNOCCA, F.C.; HEBLING, M.J.A. & SILVA, O.A. "Sobrevivência de operárias de *Atta sexdens rubropilosa* Forel (Hymenoptera: Formicidae) isoladas do formigueiro e alimentadas com dietas artificiais". *An. Soc. Entomol. Bras.* **26**: 107-113, 1997.

CHAMBERS, H.F. "The changing epidemiology of *Staphylococcus aureus*?". *Emerg. Infec. Dis.* **7**: 178-182, 2001.

DE-BRITTO, J.S.; FORTI, L.C.; DE-OLIVEIRA, M.C.; ZANETTI, R.; WILCKEN, C.F.; ZANUNCIO, J.C.; LOECK, A.E.; CADALTO, N.; NAGAMOTO, N.S.; LEMES, P.G.; CAMARGO, R.S. "Use of alternatives to PFOS, its salts and PFOSF for the control of leaf-cutting ants *Atta* and *Acromyrmex*". *Int. J. Res. Environ. Stud*. **3**: 11-92, 2016.

DEWICK, P. M. "Medicinal Natural Products. A Biosynthetic Approach". Second Edition. *John Wiley & Sons*, LTD. 2003.

DIAZ, F.; CHAI, H.B.; MI, Q.; SU, B.N.; VIGO, J.S.; GRAHAM, J.G.; CABIESES, F.; FARNSWORTH, N.R.; CORDELL, G.A.; PEZZUTTO, J.M.; SWANSON, S.M. & KINGHORN, A.D. "Anthrone and oxanthrone C-glycosides from *Picramnia latifolia* collected in Peru". *J. Nat. Prod.* **67**: 352-356, 2004.

FERNANDO E.S. & QUINN, C.J. "Picramniaceae, a new family, and recircumscription of Simaroubaceae". *Taxon*, **44**: 177-181, 1995.

FORIM, M.R.; MATOS, A.P.; SILVA, M.F.G.F.; CASS, Q.B.; VIEIRA, P.C.; FERNANDES, J.B. "Uso de clae no controle de qualidade em produtos comerciais de nim: reprodutibilidade da ação inseticida". *Quím. Nova*, **33**: 1082-1087, 2010.

GYAWALI, R. ; IBRAHIM, S.A. "Natural products as antimicrobial agents". *Food Control.* **46**: 412-429, 2014.

GROSSO, C. ; JAGER, A.K. ; STAERK, D. "Coupling of a High-resolution Monoamine Oxidase-A Inhibitor Assay and HPLC–SPE–NMR for Advanced Bioactivity Profiling of Plant Extracts". *Phytochem*. *Anal*. **24** : 141-147, 2013.

HERNANDEZ-MEDEL, M.D.R.; LOPEZ-MARQUEZ, O.; SANTILLAN, R. & TRIGOS, A. "Mayoside, an oxanthrone from *Picramnia hirsute"*. *Phytochemistry* **43**: 279-281, 1996.

HERNANDEZ-MEDEL, M.D.R.; GARCIA-SALMONES, I.; SANTILLAN, R. & TRIGOS, A. "An anthrone from *Picramnia antidesma"*. *Phytochemistry* **49**: 2599-2601, 1998.

HERNANDEZ-MEDEL, M.D.R.; RAMIREZ-CORZAS, C. O., RIVERA-DOMINGUEZ, M. N., RAMIREZ-MENDEZ, J., SANTILLAN, R., ROJAS-LIMA, S. "Diastereomeric C-glycosyloxanthrones from *Picramnia antidesma*". *Phytochemistry*, **50**: 1379-1383, 1999.

ILHA, C.; LUTINSKY, J.A.; PEREIRA, D.V.M.; GARCIA, F.R.M. "Riqueza de formigas (Hymenoptera: Formicidae) da Bacia Sanga Caramuru, município de Chapecó- SC". *Biotemas*, **22**: 95-105, 2009.

INTERNATIONAL DIABETES FEDERATION. *IDF Diabetes Atlas, 8th edn*. Brussels, Belgium: International Diabetes Federation, 2017. Online Version at http://www.diabetesatlas.org (acessed 18.01.18).

JACOBS, H. "Comparative phytochemistry of *Picramnia* and *Alvaradoa*, genera of the newly established family Picramniaceae". *Biochem Syst. Ecol.* **31**: 773-783, 2003.

JIBRIL, S., SIRAT, H. M., BASAR, N. "Bioassay-Guided Isolation of Antioxidants and α-Glucosidase Inhibitors from the Root of *Cassia sieberiana* DC (Fabaceae)". *Rec. Nat. Prod*, **11**: 406-410, 2017.

KITAMURA, R.O.S. "Estudo fitoquímico biomonitorado em *Picramnia bahiensis* e *Thyrsodium schomburgkianum* – Inseticidas, fungicidas e microencapsulação". PhD Thesis, Chemistry Department, Federal University of São Carlos, 2013.

LIN, L.C., CHOU, C.J., KUO, Y.C. "Cytotoxic Principles from *Ventilago leiocarpa*". *J. Nat. Prod.*, **64**: 674-676, 2001.

LIU, B.; KONGSTAD, K.T.; QINGLEI, S.; NYBERG, N.T.; JAGER, A.K.; STAERK, D. "Dual High-Resolution α-glucosidase and radical scavenging profiling combined with HPLC-HRMS-SPE-NMR for identification of minor and major constituents directly from the crude extract of *Pueraria lobata"*. *J. Nat. Prod*. **78**: 294-300, 2015.

LIU, Y.; STAERK, D.; NIELSEN, M.N.; NYBERG, N.; JAGER, A.K. "High-resolution hyaluronidase inhibition profiling combined with HPLC–HRMS–SPE–NMR for identification of anti-necrosis constituents in Chinese plants used to treat snakebite". *Phytochemistry,* **119**: 62-69, 2015.

LOGACHEVA, M.D.; SHIPUNOV, A.B. "Phylogenomic analysis of *Picramnia*, *Alvaradoa*, and *Leitneria* supports the independent Picramniales". *J. Syst. Evol*. **9999**: 1-6, 2017.

LOWY, F.D. "*Staphylococcus aureus* infections". *N. Eng. J. Med.* **339**: 520-532, 1998.

MAHADY, G.B.; HUANG, Y.; DOYLE, B.J.; LOCKLEAR, T. "Natural products as antibacterial agents". *Stud. Nat. Prod. Chem*. **35**: 423-444, 2008.

MANIKANDASELVI, S., VADIVEL, V., BRINDHA, P. “Review on nutraceutical potential of Cassia occidentalis L.–An Indian Traditional Medicinal and Food Plant”. *Int. J. Pharm. Sci. Rev. Res.* **37**: 141-146, 2016.

MARINHO, C.G.S.; DELLA-LUCIA, T.M.C.; PICANÇO, M.C. “Fatores que dificultam o controle das formigas cortadeiras”. *Bahia Agríc*. **7**: 18-21, 2006.

MARTINELLI, L.A.; NAYLOR, R.; VITOUSEK, P.M.; MOUTINHO, P. “Agriculture in Brazil: impacts, costs, and opportunities for a sustainable future”. *Curr. Opin. Env. Sust.* **2**: 431-438, 2010.

MARTÍNEZ, M.L.; POSER, G.V.; HENRIQUES, A.; GATTUSO, M.; ROSSINI, C. “Simaroubaceae and Picramniaceae as potential sources of botanical pesticides”. *Ind. Crops Prod*. **44**: 600-602, 2013.

MIYASHIRA, C.H. “Influência da cafeína na sobrevivência de saúvas *Atta sexdens rubropilosa* (Hymenoptera: Fomicidae) e no crescimento *in vitro* de seu fungo mutualista”. Masters Dissertation. Botanic Department, Bioscience Institute – USP. 2007.

NEWMAN, D.J. The influence of Brazilian biodiversity on searching for human use pharmaceuticals”. *J. Braz. Chem. Soc*. **28**: 402-414, 2017.

OLIVEIRA, C.M., AUAD, A.M.; MENDES, S.M.; FRIZZAS, M.R. “Crop losses and the economic impact of insect pests on Brazilian agriculture”. *Crop Prot*. **56**: 50-54, 2014.

PACHECO, A.G.; ALCÂNTARA, A.F.C.; ABREU, V.G.C.; CORRÊA, G.M. “Relationships between chemical structure and activity of triterpenes against gram-positive and gram-negative bacteria”. *Biochemistry, Genetics and Molecular Biology*, *A Search for Antibacterial Agents.* In Tech, Chapter **1**, 2012.

PAULI, G.F.; CHEN, S.; FRIESEN, J.B.; McALPINE, J.B.; JAKI, B.U.; “Analysis and purification of bioactive natural products: The AnaPurNa study”. *J. Nat. Prod*. **75**: 1243-1255, 2012.

PETERSEN, B. O., VINOGRADOV, E., KAY, W., WURTZ, P., NYBERG, N. T., DUUS, J. Ø., SORENSEN, O. W. “H2BC: a new technique for NMR analysis of complex carbohydrates”. *Carbohydr. Res.*, **341**: 550-556, 2006.

PHIFER, S.S.; LEE, D.; SEO, E.K.; KIM, N.C.; GRAF, T.N.; KROLL, D.J.; NAVARRO, H.A.; IZYDORE, R.A.; JUMNEZ, F.; GARCIA, R.; ROSE, W.C.; FAIRCHILD, C.R.; WILD, R.; SOEJARTO, D.D.; FARNSWORTH, N.R.; KINGHORN, A.D.; OBERLIES, N.H.; WALL, M.E. & WANI, M.C. “Alvaradoins E-N, antitumor and cytotoxic anthracenone C-glycosides from the leaves of *Alvaradoa haitiensis”*. *J. Nat. Prod.* **70**: 954-961, 2007.

PIRANI, J.R.; DEVECCHI, M.F. “Flora das cangas da Serra dos Carajás, Pará, Brasil: Picramniaceae”. *Rodriguésia*. **67**: 1447-1449, 2016.

REIS FILHO, W.; IEDE, E.T.; NICKELE, M.A.; CALDATO, M.; FERREIRA, A.C. “Reconhecimento dos danos causados por formigas cortadeiras do gênero *Acromyrmex* em plantios iniciais de *Pinus taeda* no Sul do Brasil”. *Comunicado Técnico 189 – Embrapa*, p 1-4, 2007.

RIBEIRO, M.L.; LOURENCETTI, C.; POLESE, L.; NAVICKIENE, S.; OLIVEIRA, L. C. "Pesticidas, usos e riscos para o meio-ambiente". *Holos Environ.*, **8**: 53-71, 2008.

ROBLEDO, S.M; CARDONA, W.; LIGARDO, K.; HENAO, J.; ARBELÁEZ, N.; MONTOYA, A.; ALZATE, F.; PÉREZ, J.M.; ARANGO, V.; VÉLEZ, I.D.; SÁEZ, J. "Antileishmanial effect of 5,3'-hydroxy-7,4'-dimethoxyflavanone of *Picramnia gracilis* Tul. (Picramniaceae) fruit: in vitro and in vivo studies". *Adv. Pharmacol. Sci*. **2015**: 1-8, 2015.

RODRIGUEZ-GAMBOA, T.; FERNANDES, J.B.; RODRIGUES FO., E.; SILVA, M.F.G.F. DA; VIEIRA, P.C.; CASTRO C., O. "Two New Anthrones and One Oxanthrone from *Picramnia teapensis". Phytochemistry*, **51**: 583-586, 1999.

RODRIGUEZ-GAMBOA, T.; VICTOR, S.R.; FERNANDES, J.B.; RODRIGUES FO., E.; DA SILVA, M.F.G.F.; VIEIRA, P.C.; PAGNOCCA, F.C.; BUENO, O.C.; HEBLING, M.J.A.; CASTRO C., O. "Anthrone and oxanthrone C,*O*-diglycosides from *Picramnia teapensis". Phytochemistry,* **55**: 837-841, 2000.

RODRIGUEZ-GAMBOA, T.P. "Estudo Químico de *Picramnia teapensis*, *Picramnia latifolia* e *Ipomoea batatas* em associação ao controle de formigas cortadeiras *Atta sexdens* e seu fungo simbionte *Leucoagaricus gongylophorus*". PhD Thesis, Chemistry DepartmentFederal University of São Carlos, 2001.

RODRIGUEZ-GAMBOA, T.; FERNANDES, J.B.; RODRIGUES FO., E.; DA SILVA, M.F.G.F.; VIEIRA, P.C.; BARRIOS Ch., M.; CASTRO-CASTILLO, O.; VICTOR, S.R.; PAGNOCCA, F.C.; BUENO, O.C.; HEBLING. M.J.A. "Triterpene Benzoates from the Bark of *Picramnia teapensis* (Simaroubaceae)". *J. Braz. Chem. Soc.,* **12**: 386-390, 2001.

SCHMIDT, J. S., LAURIDSEN, M. B., DRAGSTED, L. O., NIELSEN, J., STAERK, D. "Development of a bioassay-coupled HPLC-SPE-ttNMR platform for identification of α-glucosidase inhibitors in apple peel (Malus× domestica Borkh.)". *Food Chem.*, **135:** 1692-1699, 2012.

SCHIOTT, M.; ROGOWSKA-WRZESINSKA, A.; ROEPSTORFF, P.; BOOMSMA, J.J. "Leaf-cutting ant fungi produce cell wall degrading pectinase complexes reminiscent of phytopathogenic fungi". *BMC Biology*. **8**: 156-168, 2010.

SILVA-FILHO, M.C.; FALCO, M.C. "Interação planta-inseto. Adaptação dos insetos aos inibidores de proteinases produzidos pelas plantas". *Biotecnol. Ciênc. Desenvolv.* **2**: 38-42, 2000.

SOLIS, P.N.; RAVELO, A.G.; GONZALEZ, A.G.; GUPTA, M.P.; PHILLIPSON, J.D. "Bioactive anthraquinone glycosides from *Picramnia antidesma* ssp. *fessonia"*. *Phytochemistry* **38**: 477-480, 1995.

SPELLBERG, B.; GUIDOS, R.; GILBERT, D.; BRADLEY, J.; BOUCHER, H.W.; SCHELD, W.M.; BARTLETT, J.G.; EDWARDS JR, J. "The epidemic of antibiotic-resistant infections: A call to action for the medical community from the Infectious Diseases Society of America". *Clin. Infec. Dis*. **46**: 155-164, 2008.

TAHTAH, Y.; WUBSHET, S.G.; KONGSTAD, K.T.; HESKES, A.M., PATERAKI, I.; MOLLER, B.L.; JAGER, A.K.; STAERK, D. "High-resolution PTP1B inhibition profiling combined with high-performance liquid chromatography–high-resolution mass

spectrometry–solid-phase extraction–nuclear magnetic resonance spectroscopy: proof-of-concept and antidiabetic constituents in crude extract of *Eremophila lucida*". *Fitoterapia*. **110**: 52-58, 2016.

TIETZE, L. F., GERICKE, K. M., SCHUBERTH, I. "Synthesis of highly functionalized anthraquinones and evaluation of their antitumor activity". *Eur. J. Org. Chem.*, **2007**: 4563-4577, 2007.

TRINH, B.T.D, STAERK, D. JÄGER, A.K. "Screening for potential α-glucosidase and α-amylase inhibitory constituents from selected Vietnamese plants used to treat type 2 diabetes". *J. Ethnopharm*. **186**: 189-195, 2016.

TONG, S.Y.C.; DAVIS, J.S.; EICHENBERGER, E.; HOLLAND, T.H.; FOWLER JR, V.G. *Staphylococcus aureus* infections: epidemiology, pathophysiology, clinical manifestations, and management". *Clin. Microbiol. Rev*. **28**: 603-661, 2015.

THOMAS, W.W. "*Nothotalisia*, a new genus of Picramniaceae from Tropical America". *Brittonia* **63**: 51-61, 2011.

VIEGAS-JÚNIOR, C. "Terpenos com atividade: uma alternativa para o controle químico de insetos". *Quim. Nov*a, **26**: 390-400, 2003.

VIEIRA, I.J.C. "Uma Contribuição à química da família Simaroubaceae". PhD Thesis, Chemistry DepartmentFederal University of São Carlos, 1995.

WANJOHI, J. M., YENESEW, A., MIDIWO, J. O., HEYDENREICH, M., PETER, M. G., DREYER, M., REICHERT, M., BRINGMANN, G. "Three dimeric anthracene derivatives from the fruits of *Bulbine abyssinica*". *Tetrahedron*, **61**: 2667-2674, 2005.

WEI, Y.; LIU, Q.; YU, J.; FENG, Q.; ZHAO, L.; SONG, H.; WANG, W. "Antibacterial mode of action of 1,8-dihydroxy-anthraquinone from *Porphyra haitanensis* against *Staphylococcus aureus*". *Nat. Prod. Res*. **29**: 976-979, 2015.

WUBSHET, S.G.; TAHTAH, Y.; HESKES, A.M.; KONGSTAD, K.T.; PATERAKI, I.; HAMBERGER, B.; MOLLER, B.L.; STAERK, D. "Identification of PTP1B and α-glucosidase inhibitory serrulatanes from *Eremophila spp*. by combined use of dual high-resolution PTP1B and α-glucosidase inhibition profiling and HPLC-HRMS-SPE-NMR". *J. Nat. Prod*. **79**: 1063-1072, 2016.

ZARBIN, P.H.G; RODRIGUES, M.A.C.M.; LIMA, E.R. "Feromônios de insetos: tecnologia e desafios para uma agricultura competitiva no Brasil". *Quim. Nova*, **32**: 722-731, 2009.

ZHANG, Y., XU, H. "Recent progress in the chemistry and biology of limonoids. *RSC Adv.*, **7***:* 35191-35220, 2017.

Supporting Information

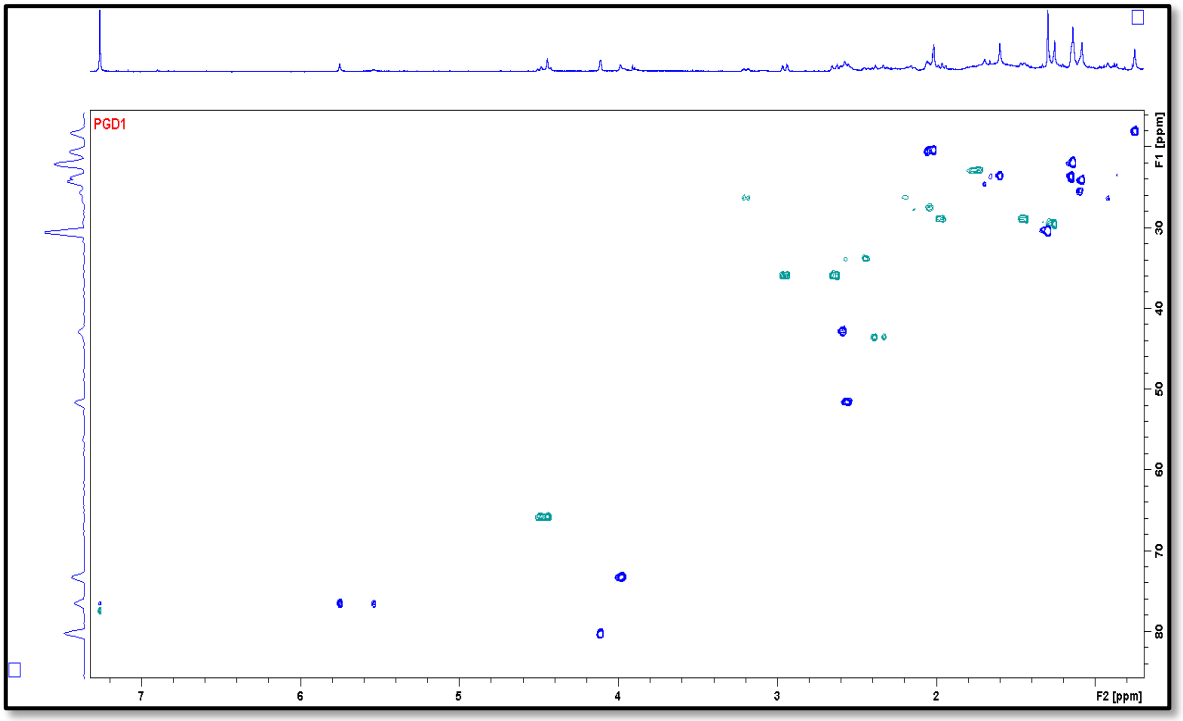

Figure S1: HSQC spectrum of Picraviane M (**01**) in $CDCl_3$ (600 MHz).

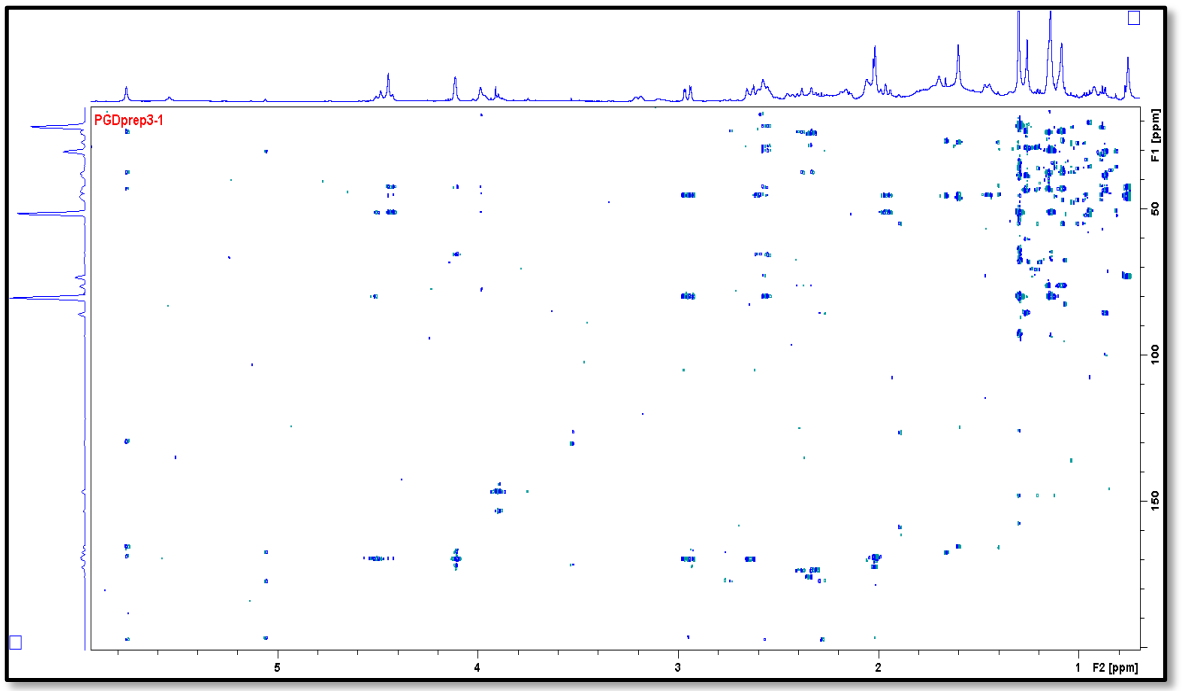

Figure S2: HMBC spectrum of Picraviane M (**01**) in $CDCl_3$ (600 MHz).

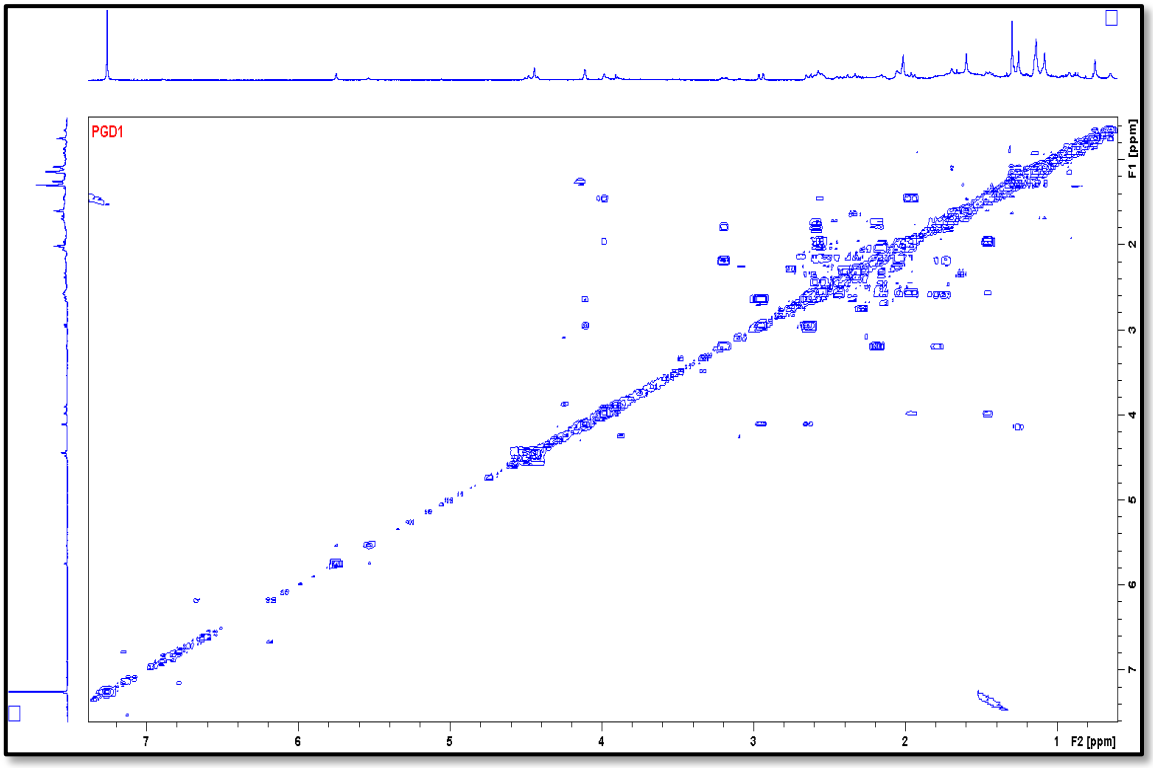

Figure S3: ^{1}H-^{1}H COSY spectrum of Picraviane M (**01**) in $CDCl_3$ (600 MHz).

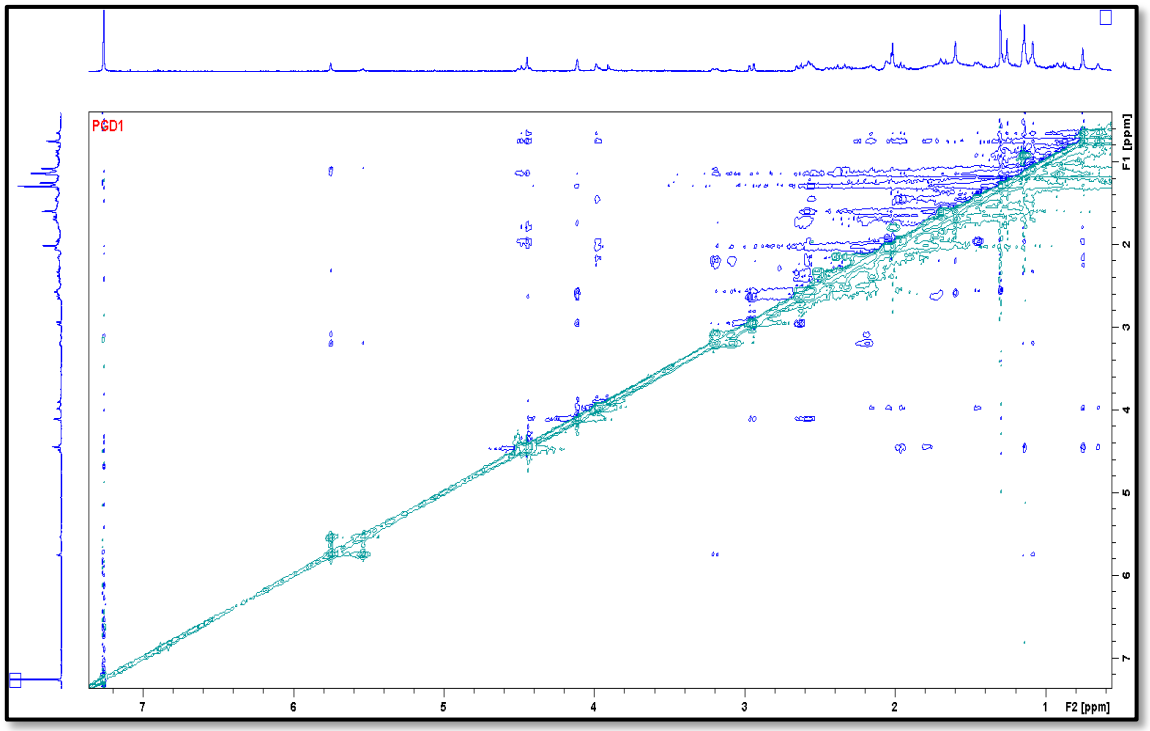

Figure S4: ROESY spectrum of Picraviane M (**01**) in $CDCl_3$ (600 MHz).

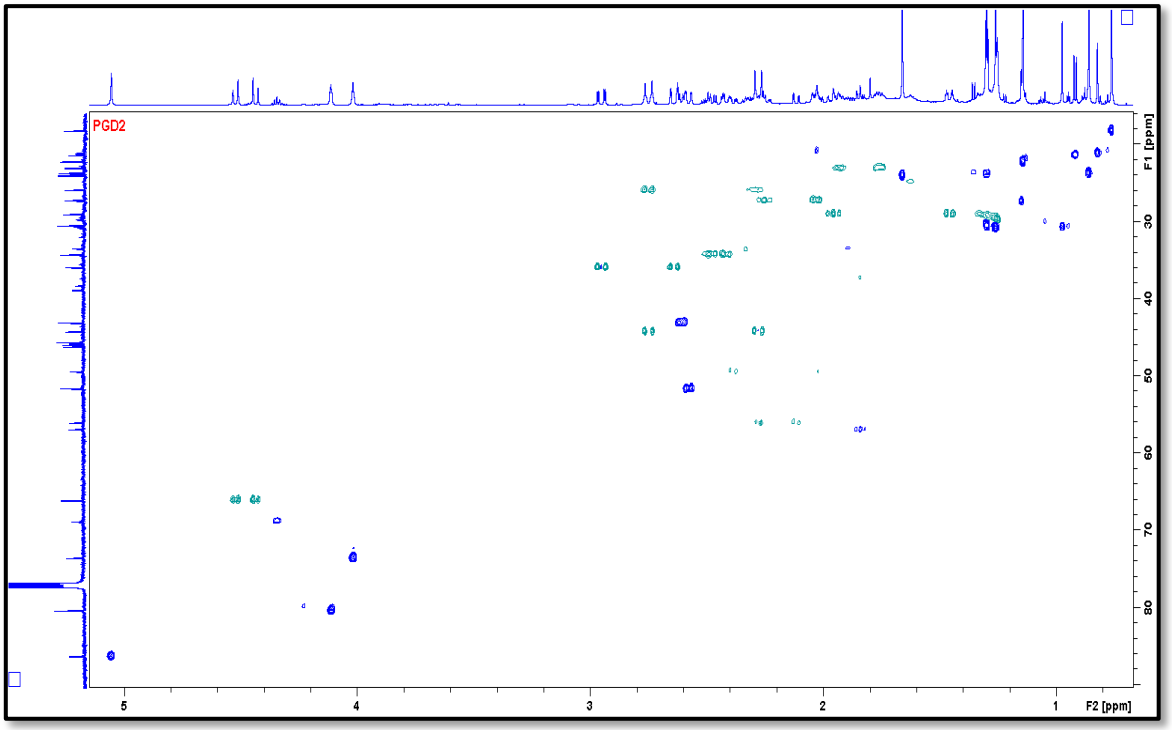

Figure S5: HSQC spectrum of Picraviane H (**02**) in $CDCl_3$ (600 MHz).

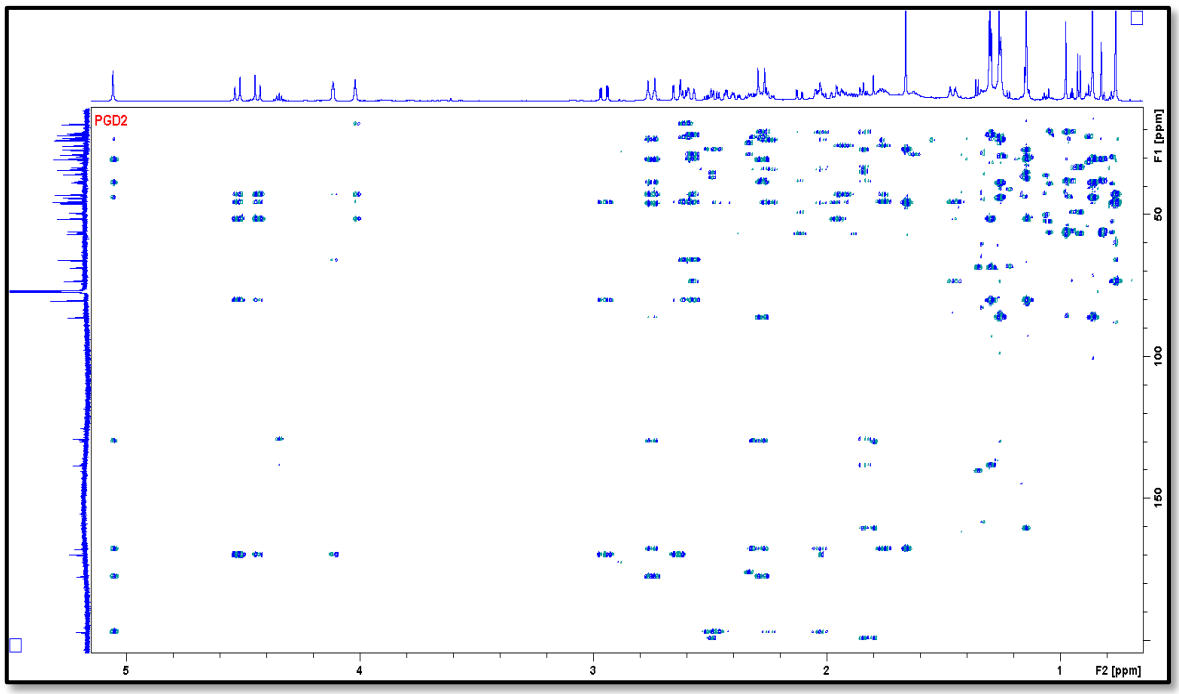

Figure S6: HMBC spectrum of Picraviane H (**02**) in $CDCl_3$ (600 MHz).

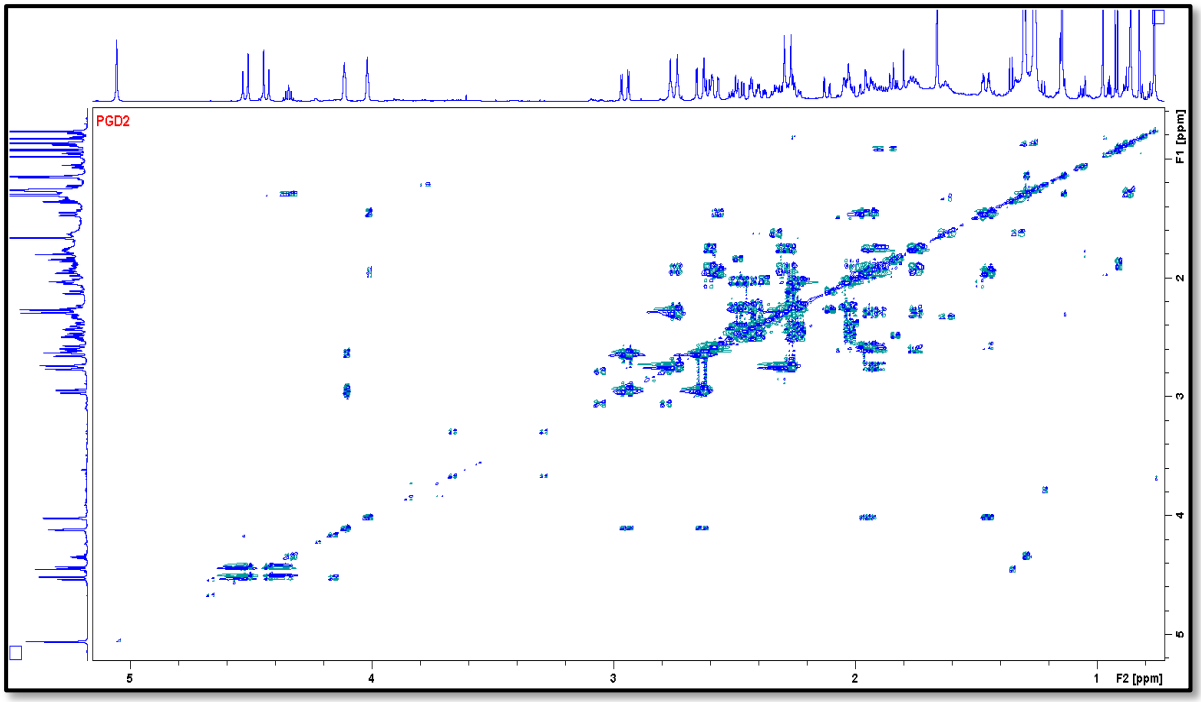

Figure S7: ^{1}H-^{1}H COSY spectrum of Picraviane H (**02**) in $CDCl_3$ (600 MHz).

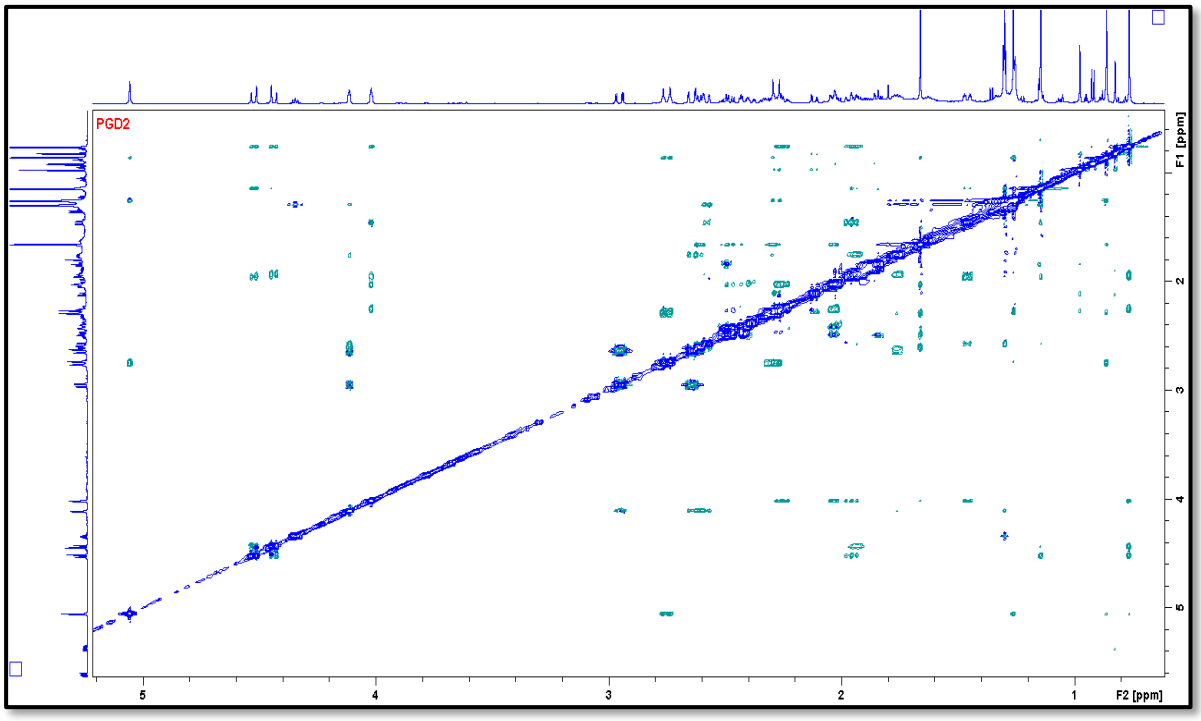

Figure S8: NOESY spectrum of Picraviane H (**02**) in $CDCl_3$ (600 MHz).

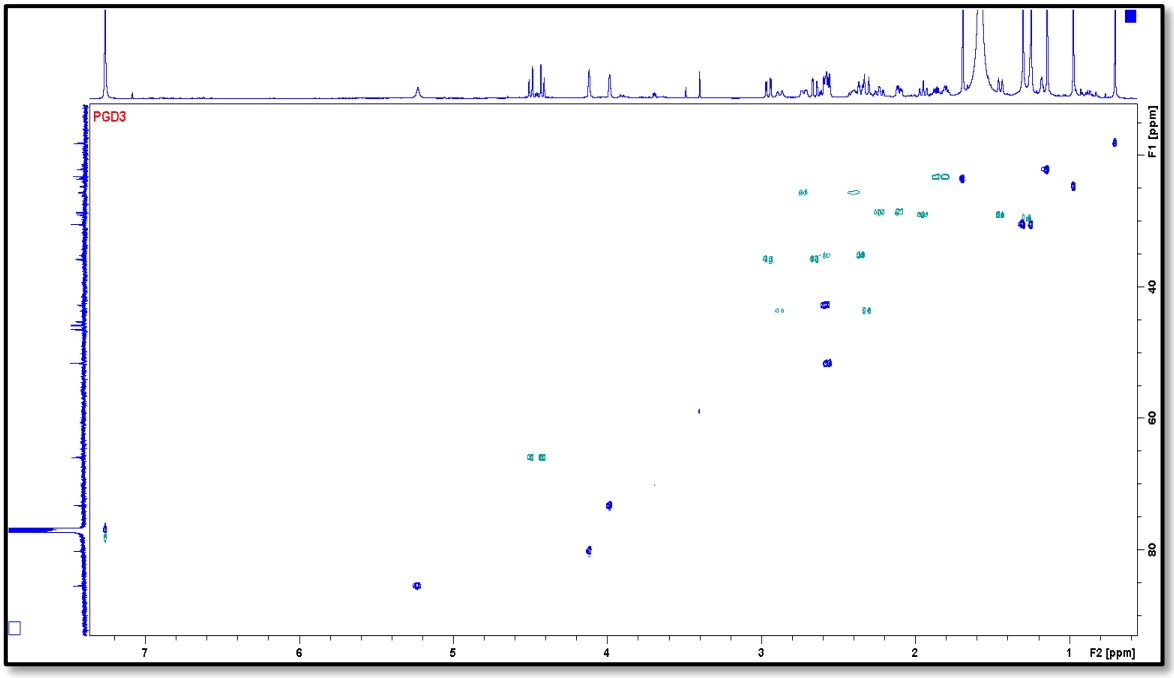

Figure S9: HSQC spectrum of Picraviane I (**03**) in $CDCl_3$ (600 MHz).

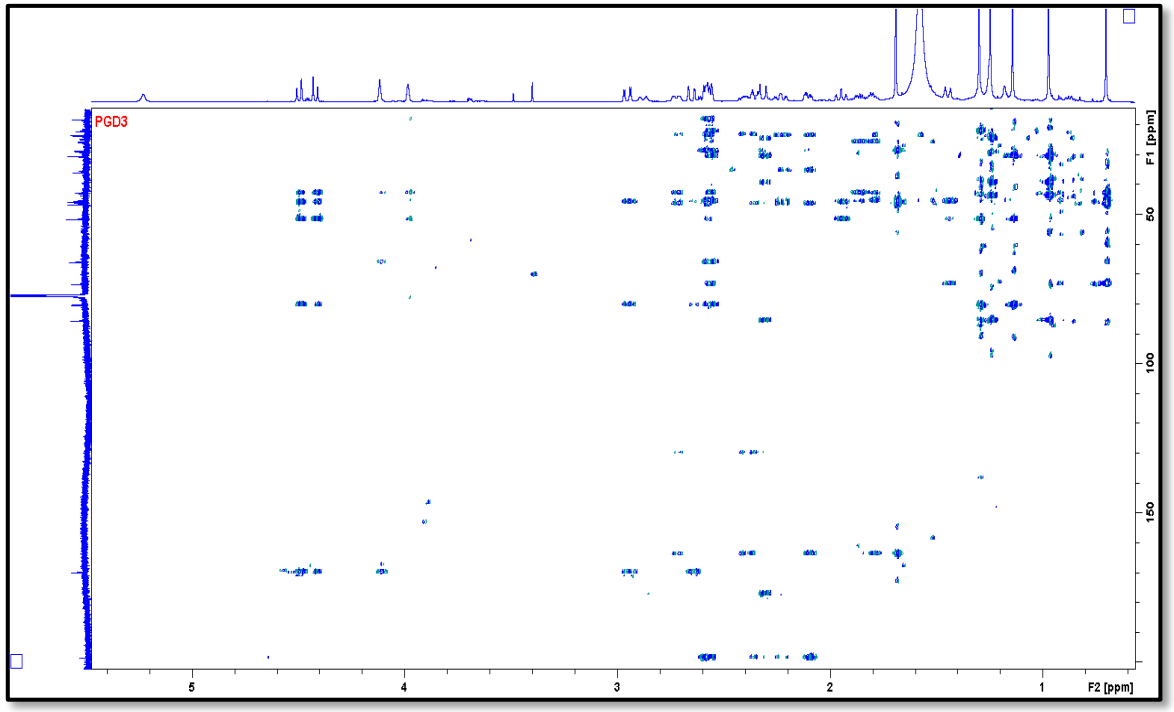

Figure S10: HMBC spectrum of Picraviane I (**03**) in $CDCl_3$ (600 MHz).

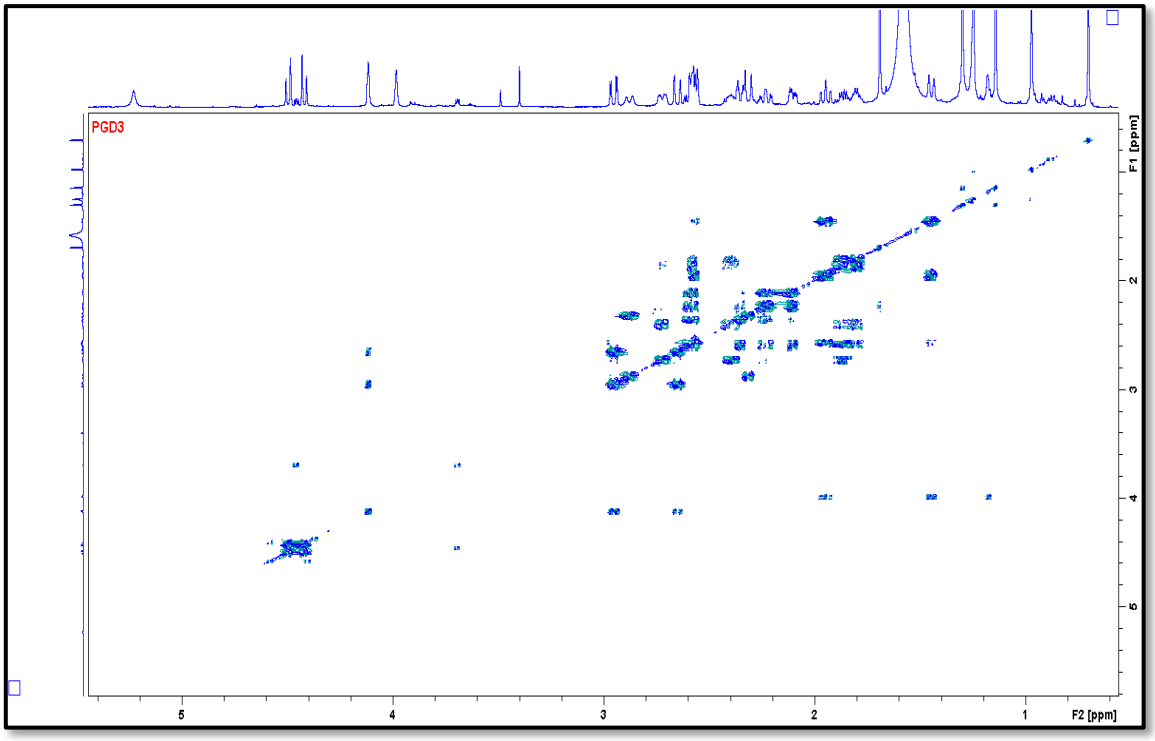

Figure S11: ^{1}H-^{1}H COSY spectrum of Picraviane I (**03**) in $CDCl_3$ (600 MHz).

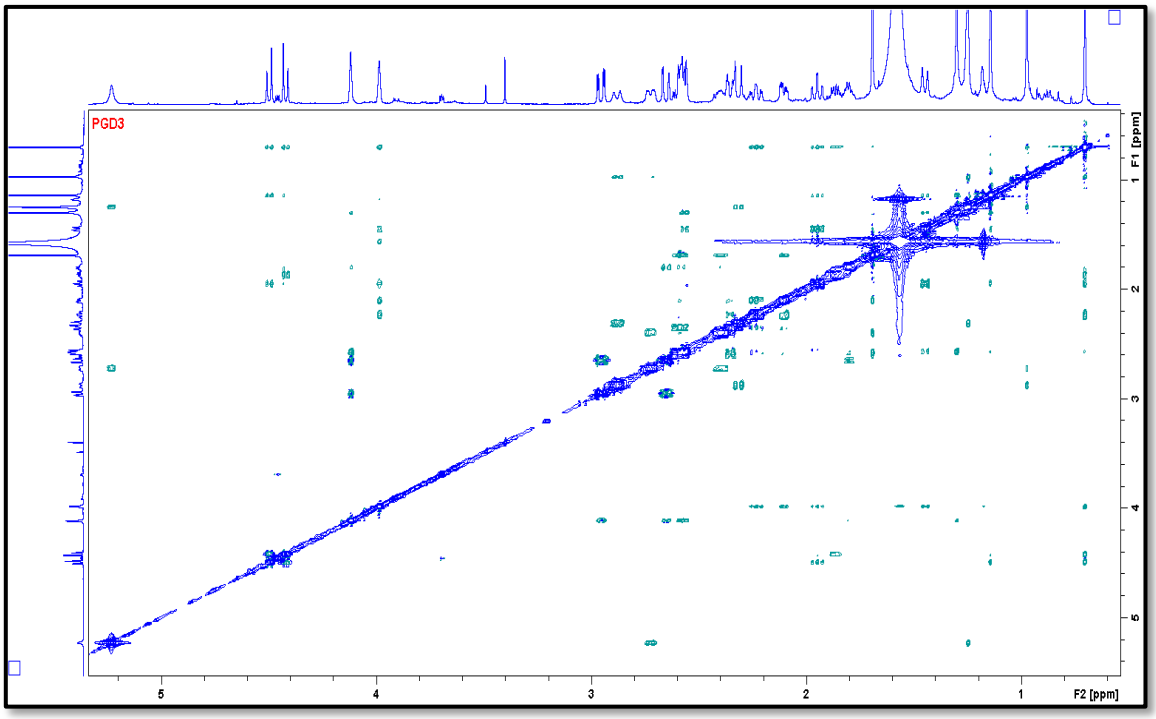

Figure S12: NOESY spectrum of Picraviane I (**03**) in $CDCl_3$ (600 MHz).

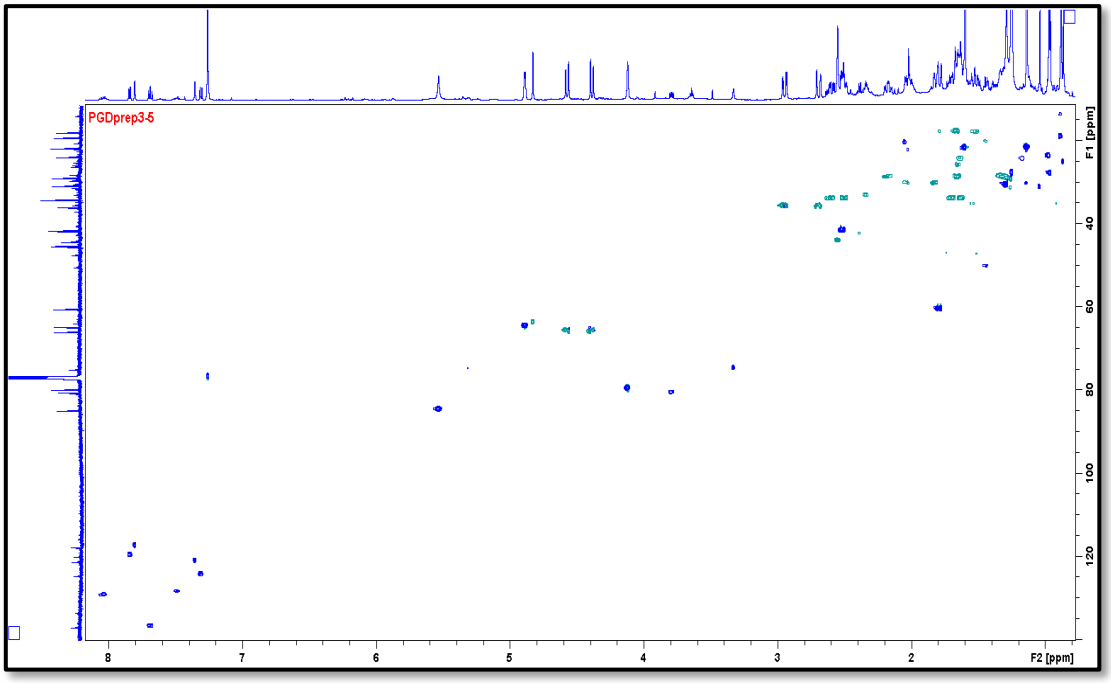

Figure S13: HSQC spectrum of Picraviane J (**05**) in $CDCl_3$ (600 MHz).

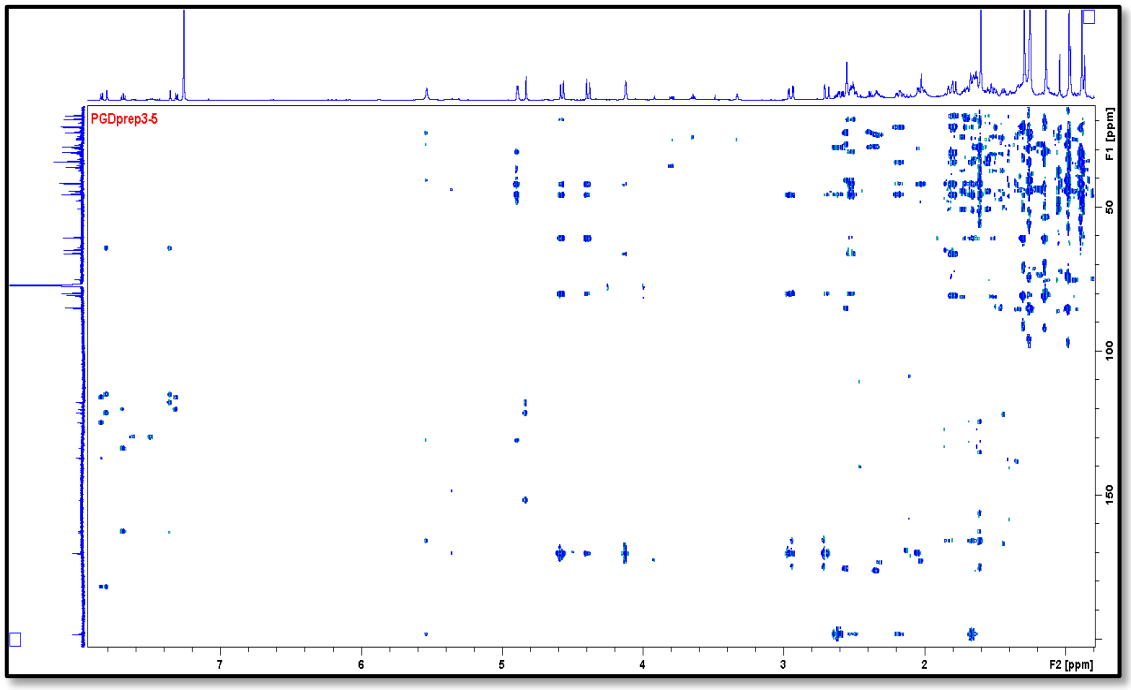

Figure S14: HMBC spectrum of Picraviane J (**05**) in $CDCl_3$ (600 MHz).

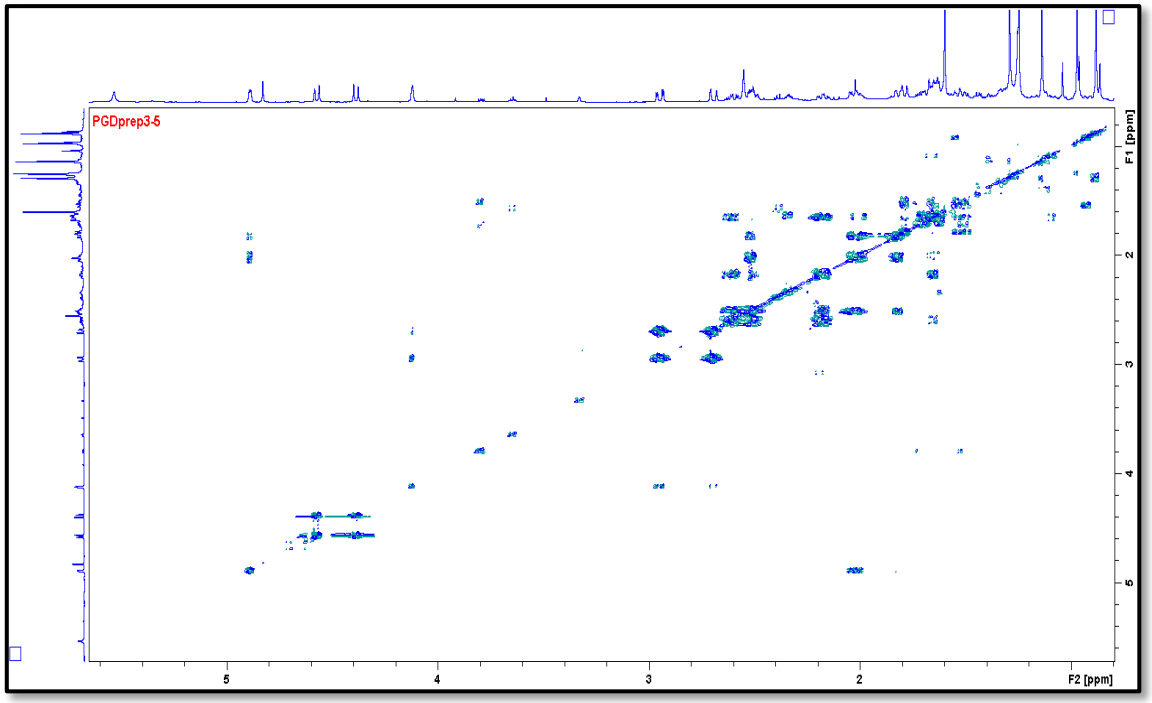

Figure S15: ^{1}H-^{1}H COSY spectrum of Picraviane J (**05**) in $CDCl_3$ (600 MHz).

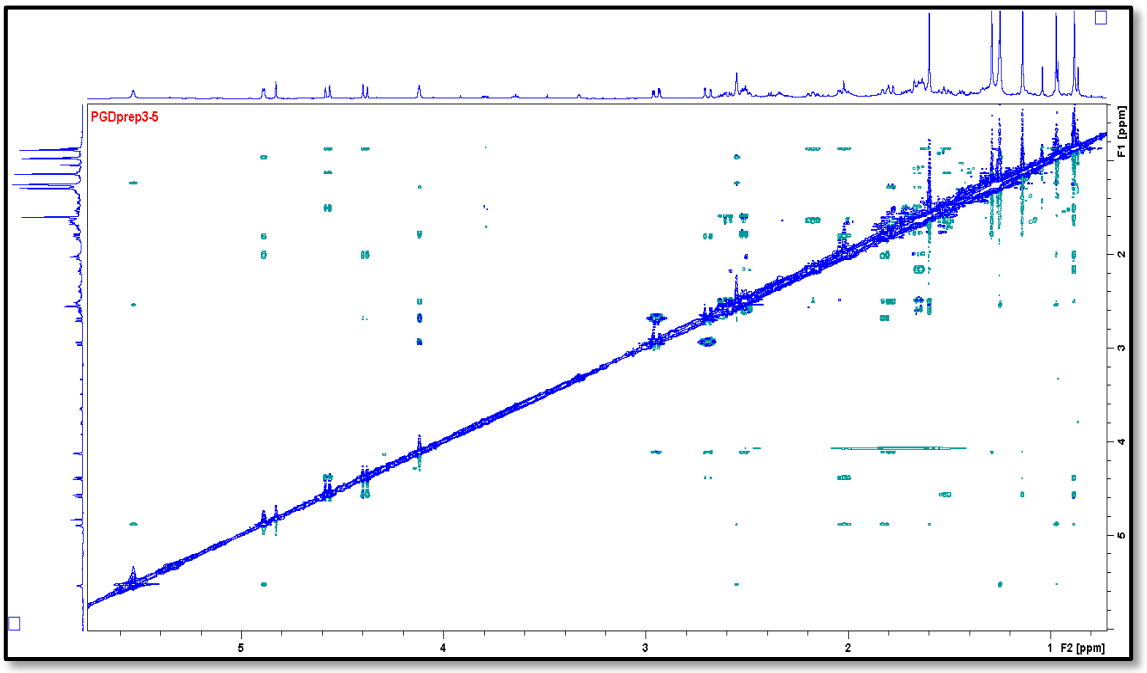

Figure S16: NOESY spectrum of Picraviane J (**05**) in $CDCl_3$ (600 MHz).

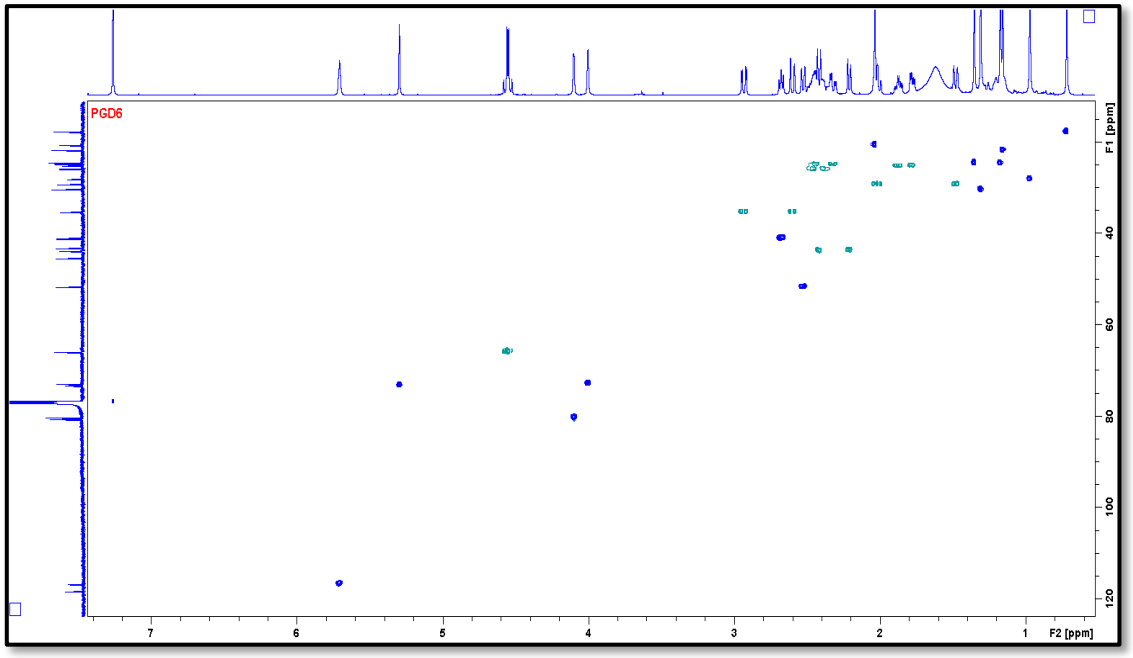

Figure S17: HSQC spectrum of Picraviane C (**06**) in $CDCl_3$ (600 MHz).

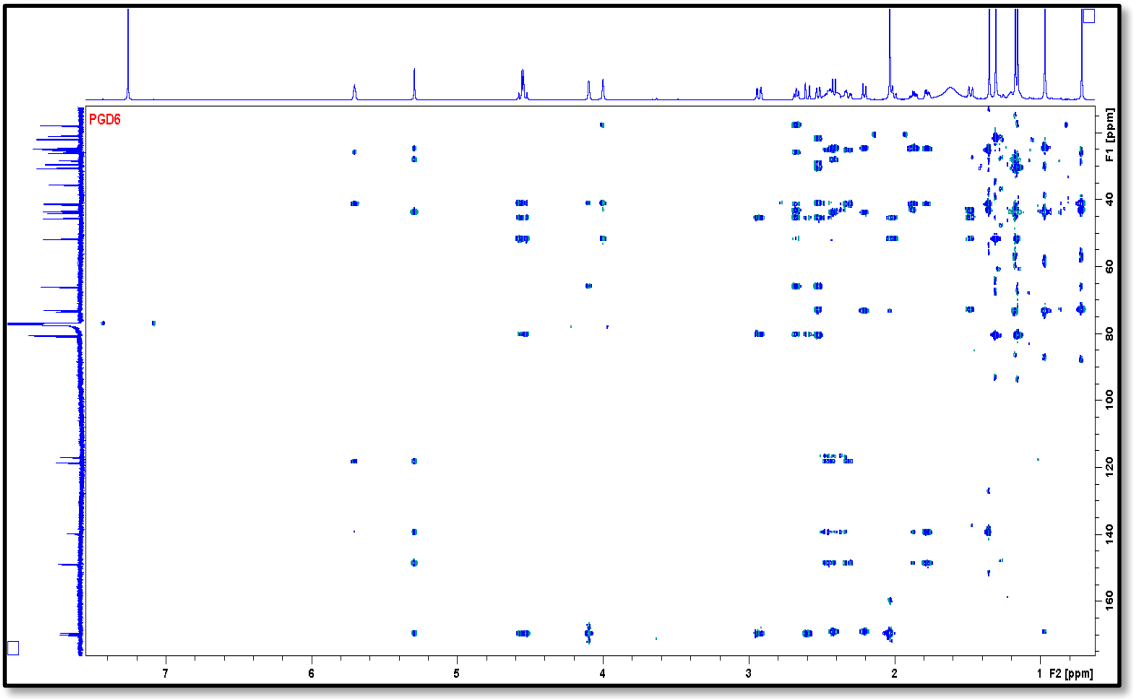

Figure S18: HMBC spectrum of Picraviane C (**06**) in $CDCl_3$ (600 MHz).

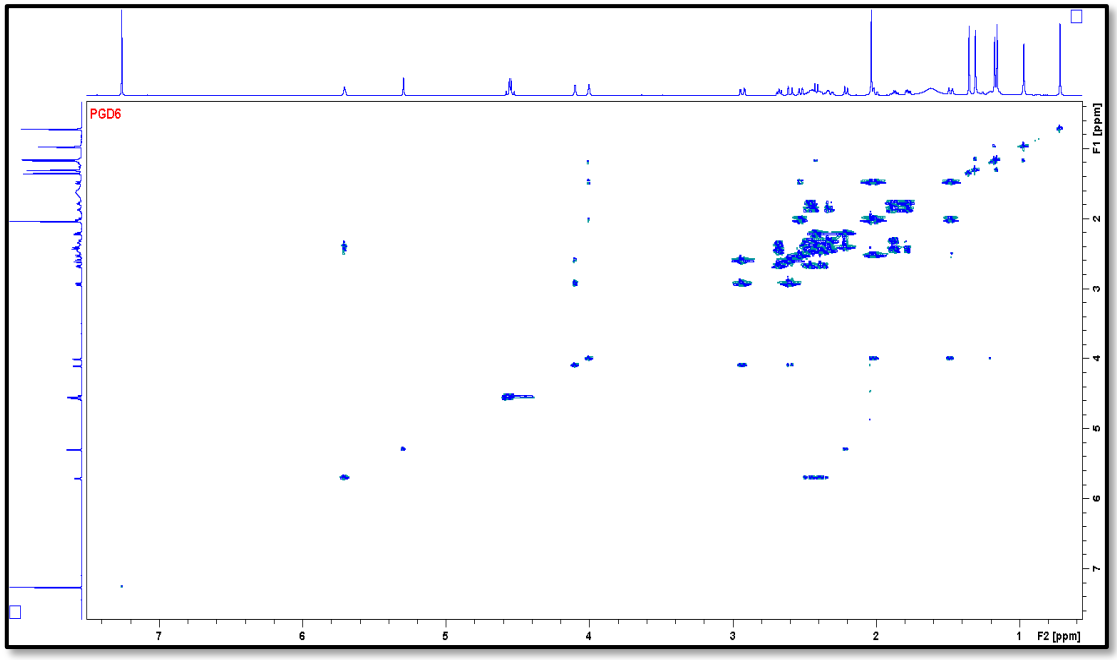

Figure S19: ^{1}H-^{1}H COSY spectrum of Picraviane C (**06**) in $CDCl_3$ (600 MHz).

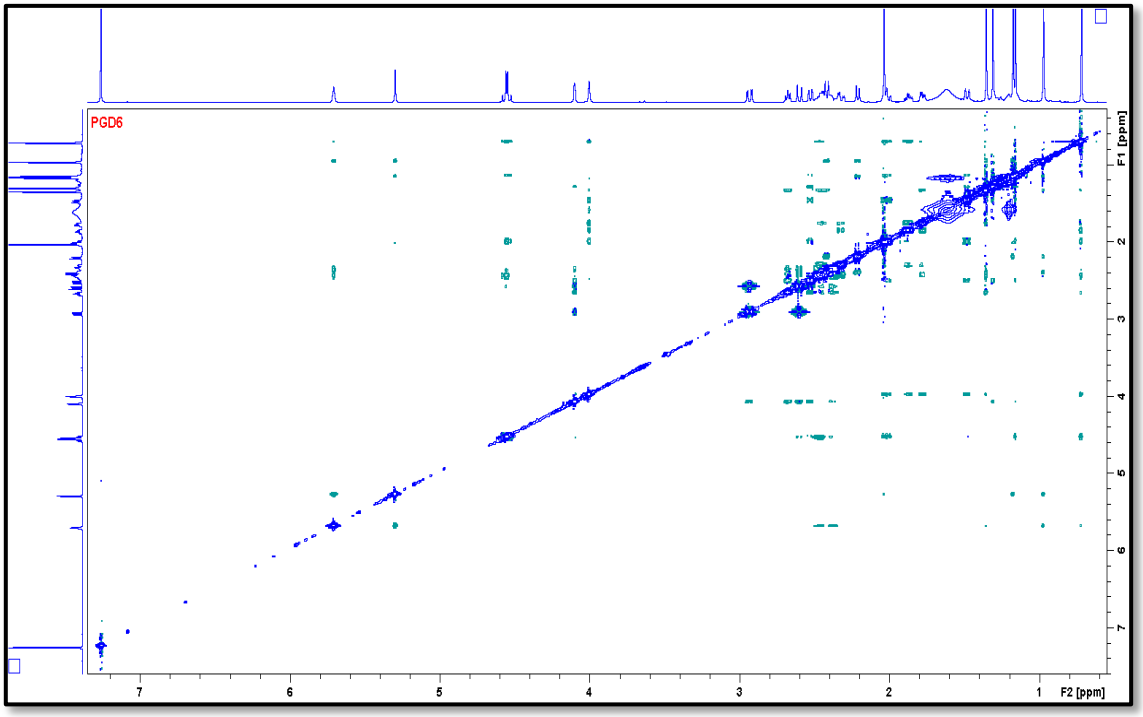

Figure S20: NOESY spectrum of Picraviane C (**06**) in $CDCl_3$ (600 MHz).

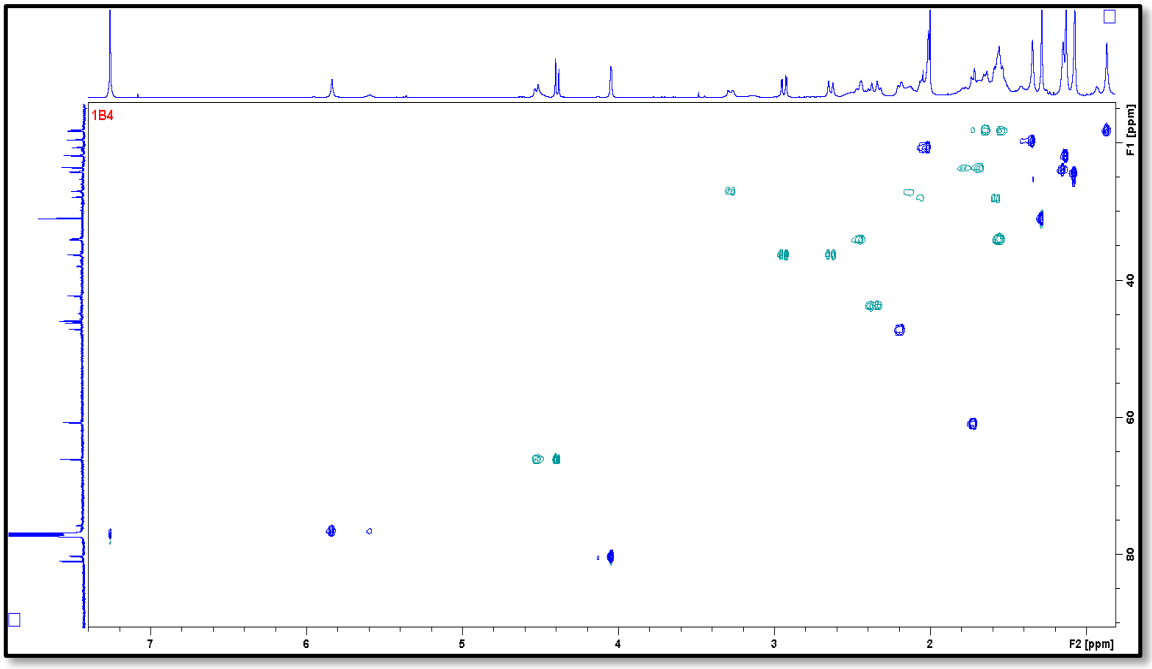

Figure S21: HSQC spectrum of Picraviane N (**07**) in $CDCl_3$ (600 MHz).

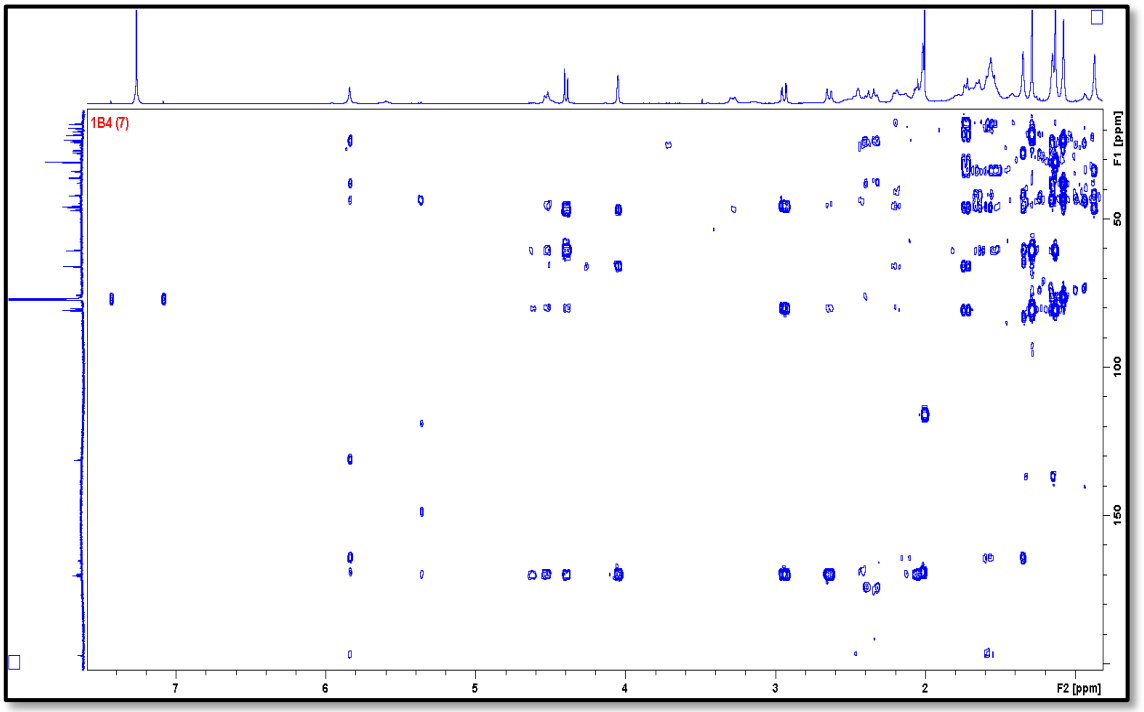

Figure S22: HMBC spectrum of Picraviane N (**07**) in $CDCl_3$ (600 MHz).

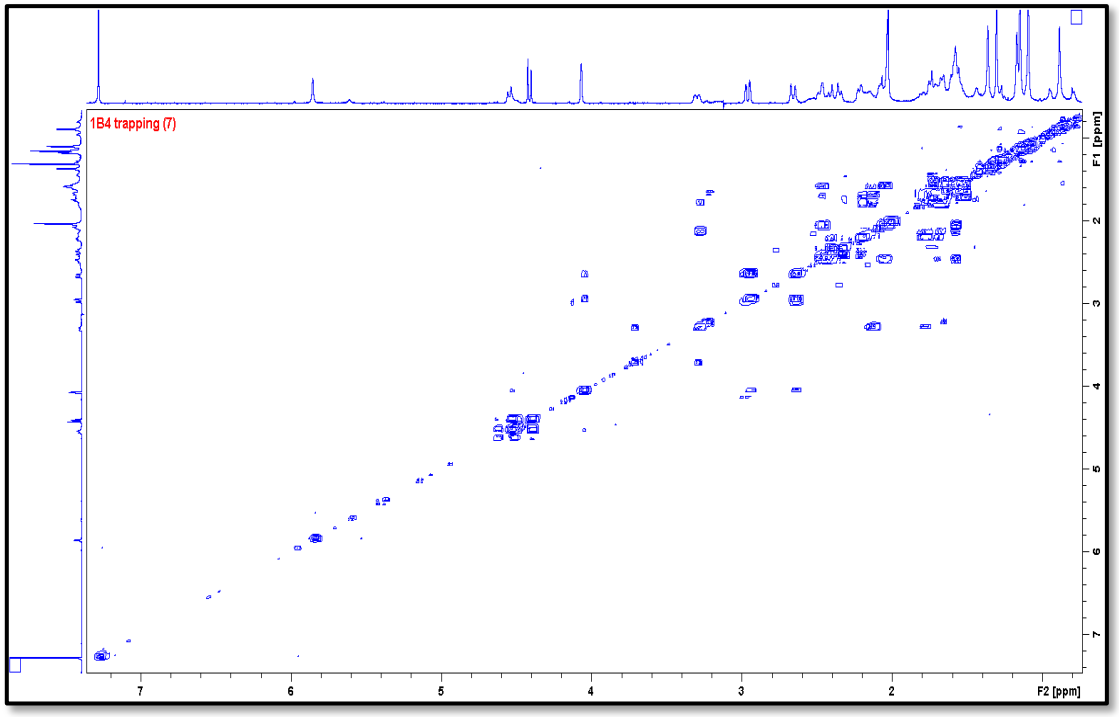

Figure S23: ^{1}H-^{1}H COSY spectrum of Picraviane N (**07**) in $CDCl_3$ (600 MHz).

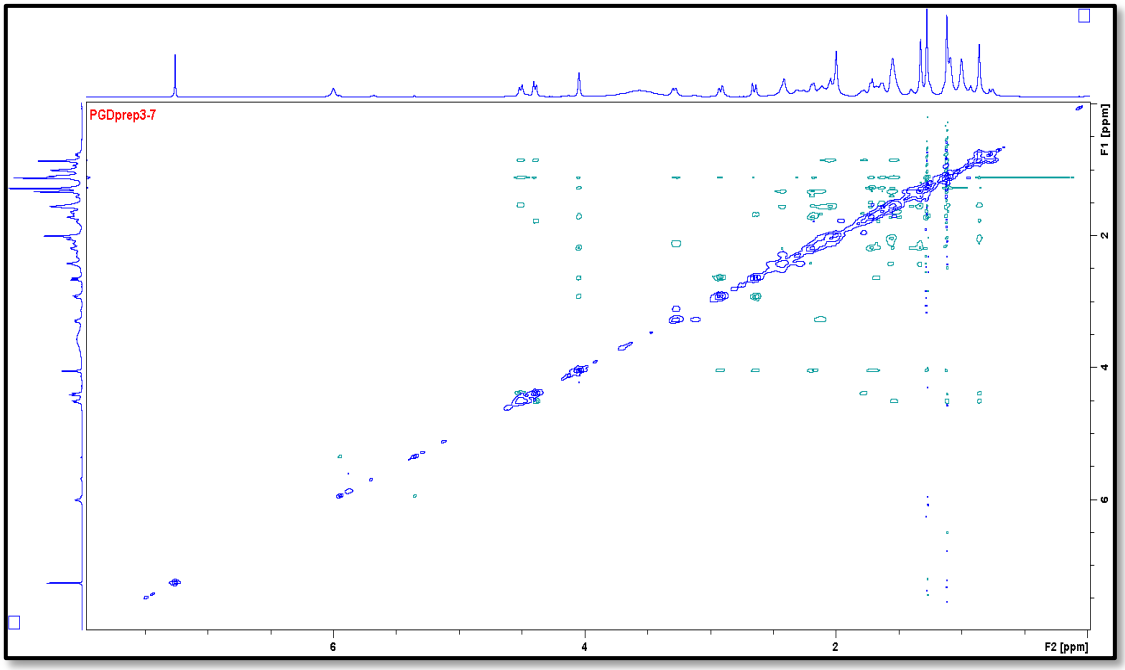

Figure S24: ROESY spectrum of Picraviane N (**07**) in $CDCl_3$ (600 MHz).

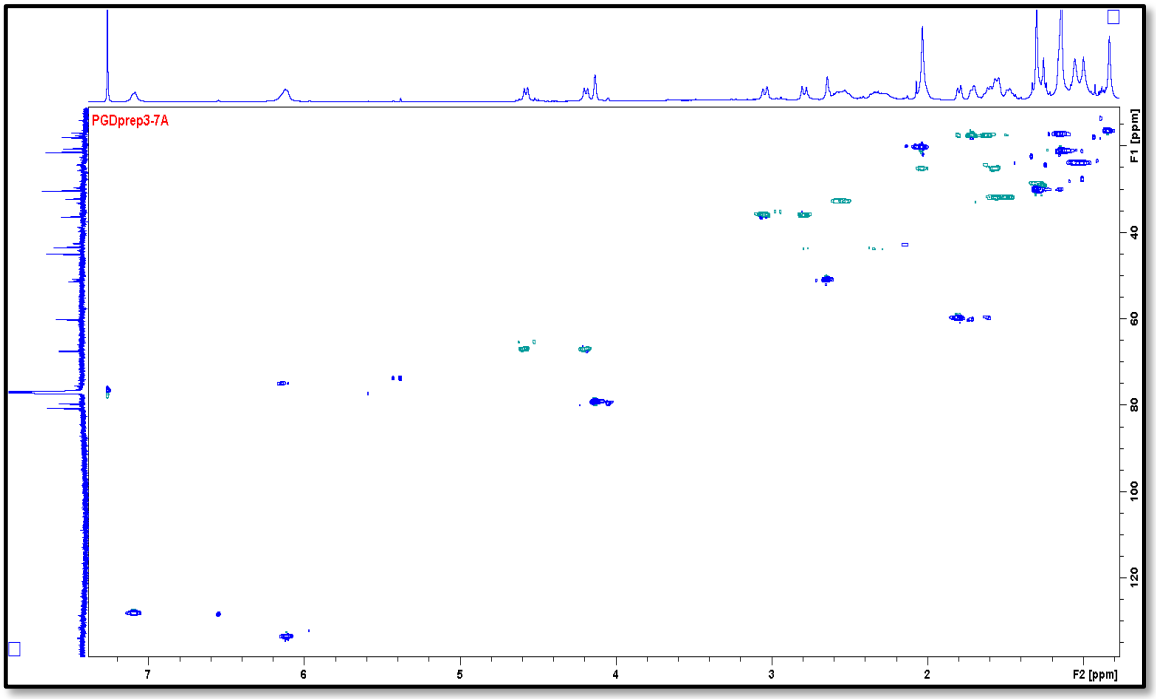

Figure S25: HSQC spectrum of Picraviane O (**07a**) in $CDCl_3$ (600 MHz).

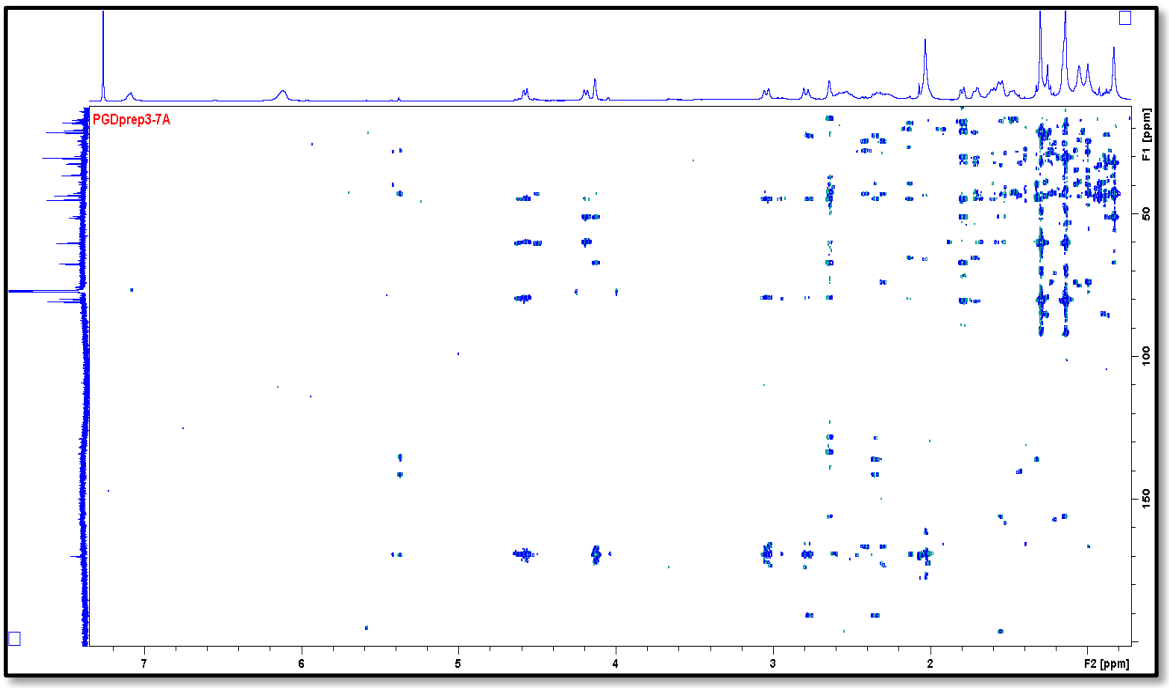

Figure S26: HMBC spectrum of Picraviane O (**07a**) in $CDCl_3$ (600 MHz).

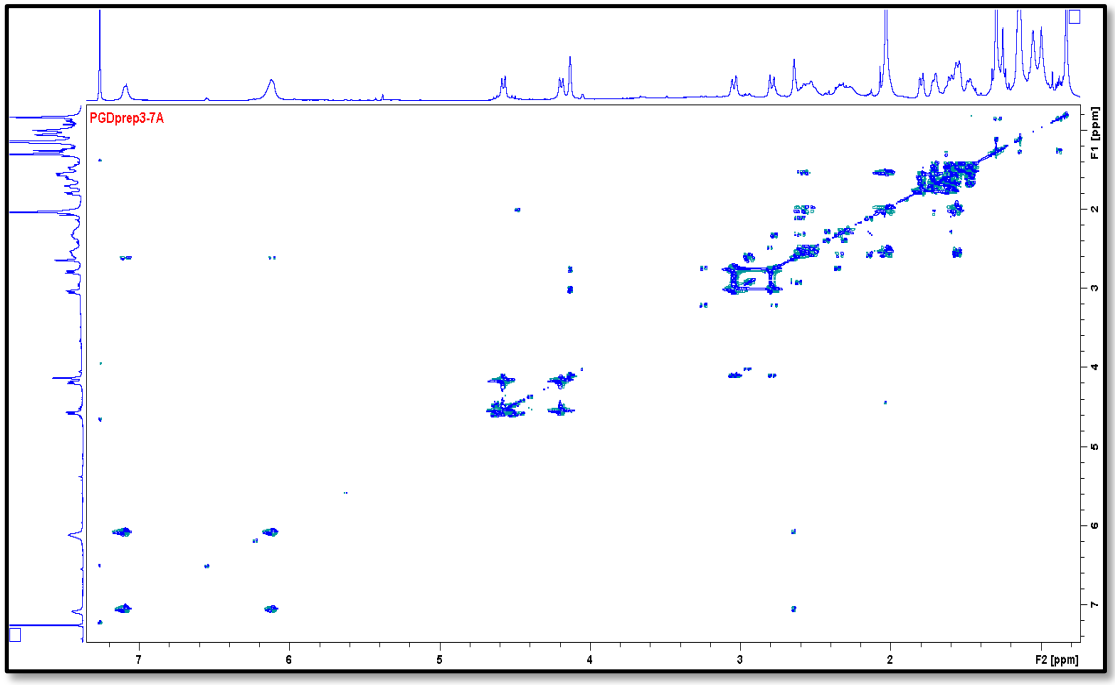

Figure S27: ^{1}H-^{1}H COSY spectrum of Picraviane O (**07a**) in $CDCl_3$ (600 MHz).

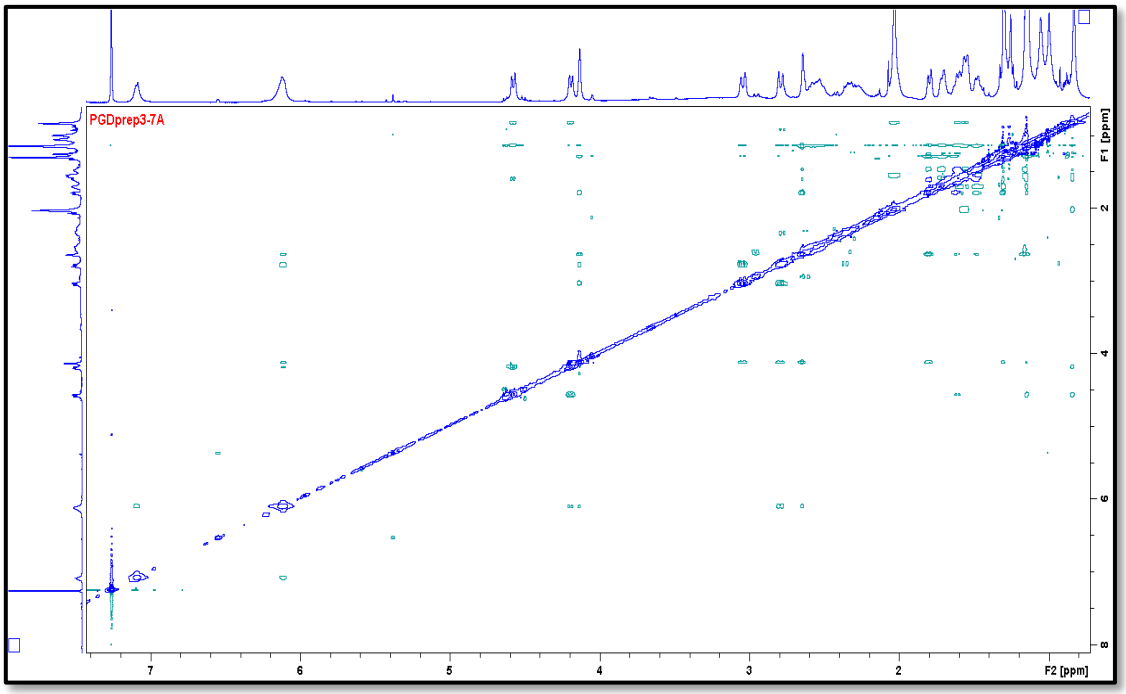

Figure S28: ROESY spectrum of Picraviane O (**07a**) in $CDCl_3$ (600 MHz).

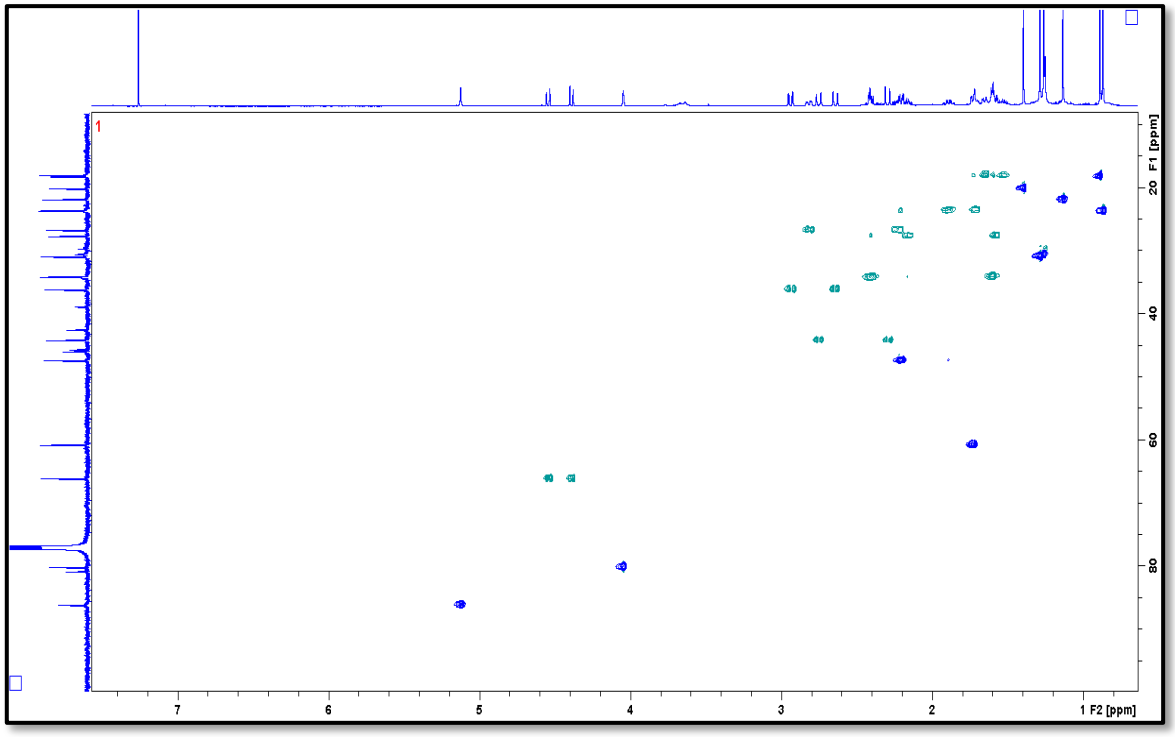

Figure S29: HSQC spectrum of Picraviane D (**08**) in $CDCl_3$ (600 MHz).

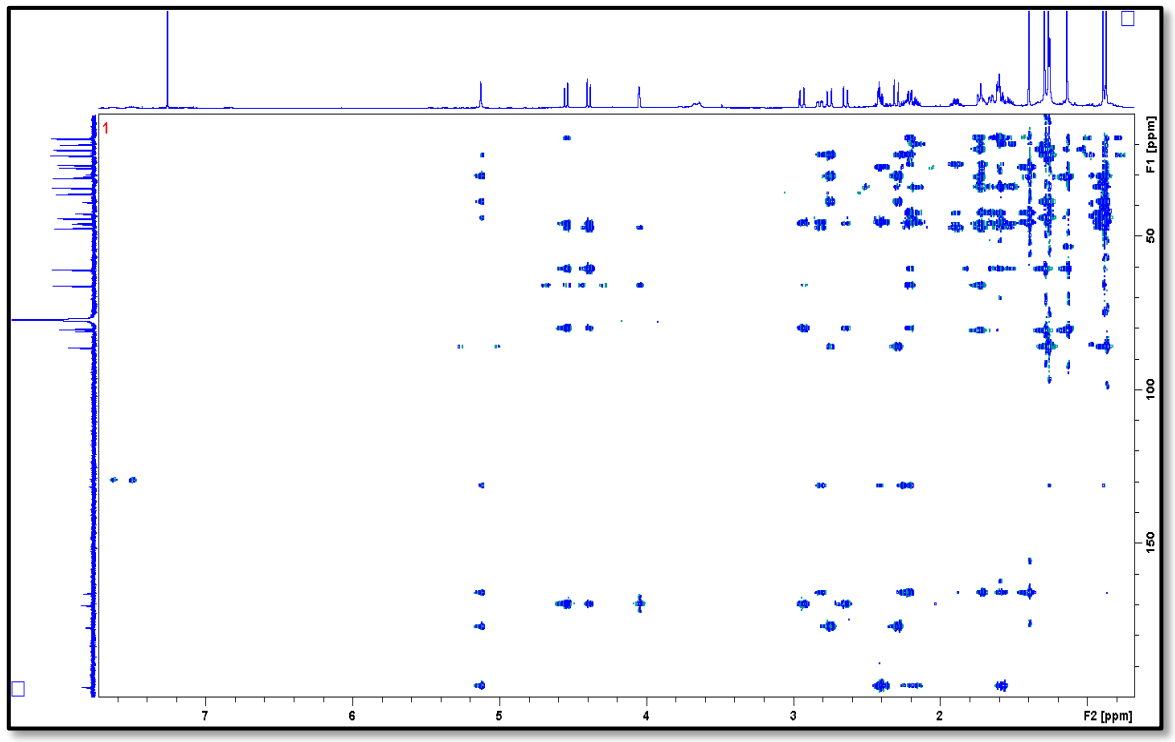

Figure S30: HMBC spectrum of Picraviane D (**08**) in $CDCl_3$ (600 MHz).

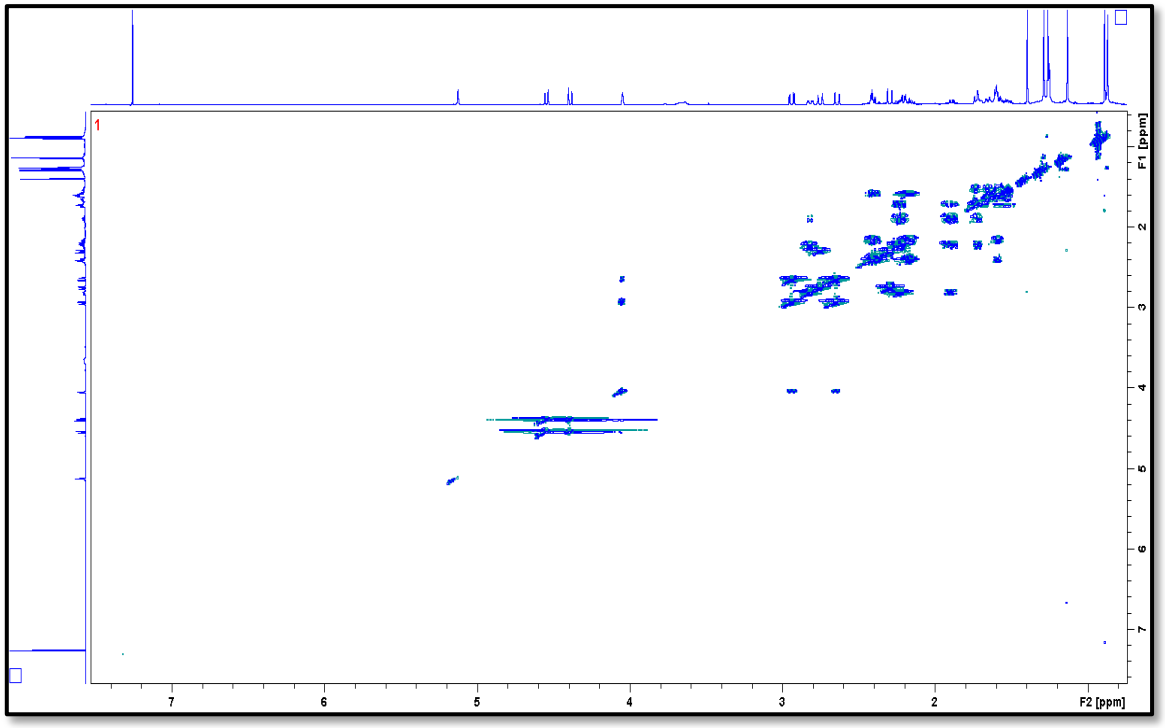

Figure S31: ^{1}H-^{1}H COSY spectrum of Picraviane D (**08**) in $CDCl_3$ (600 MHz).

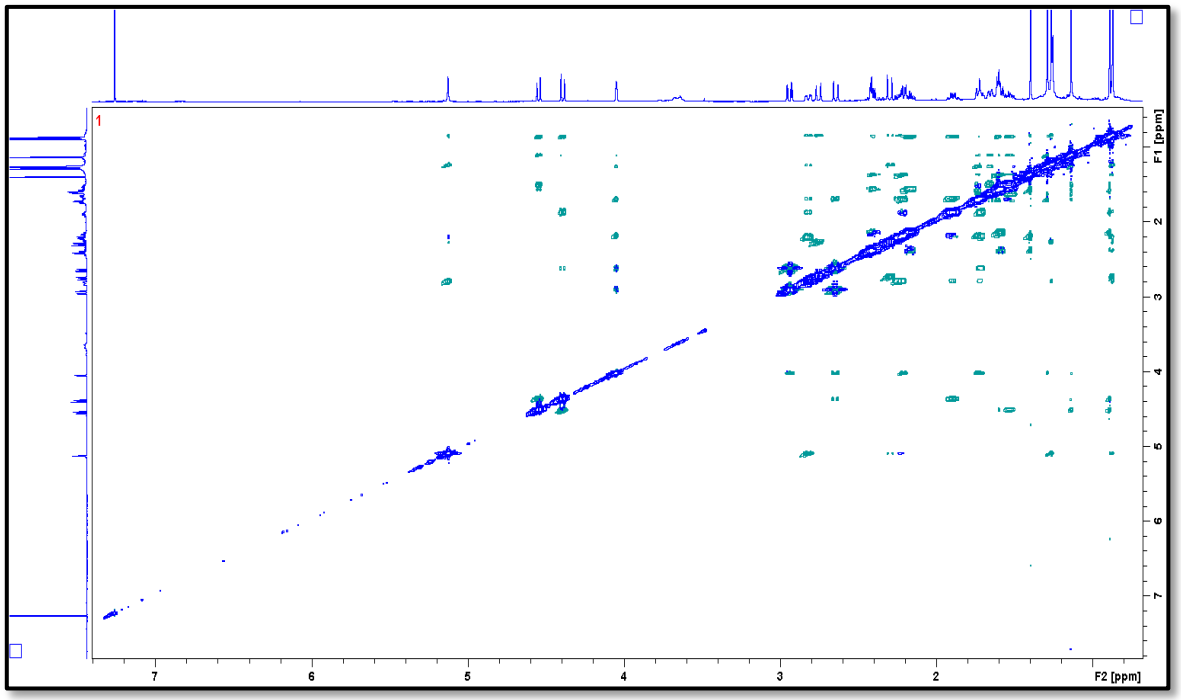

Figure S32: NOESY spectrum of Picraviane D (**08**) in $CDCl_3$ (600 MHz).

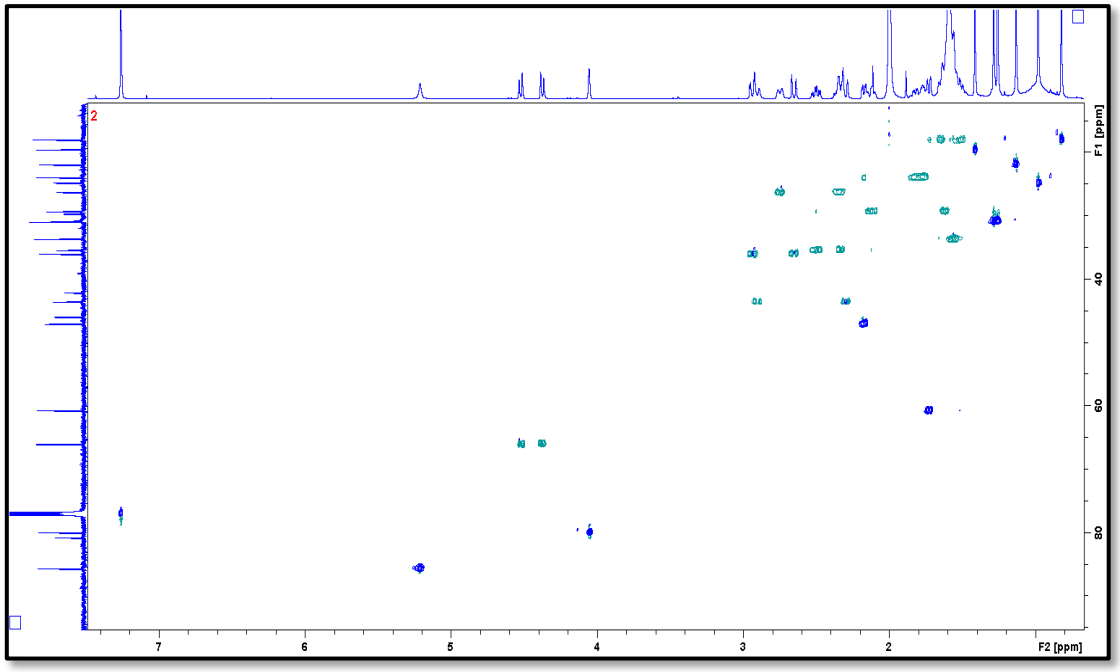

Figure S33: HSQC spectrum of Picraviane E (**09**) in $CDCl_3$ (600 MHz).

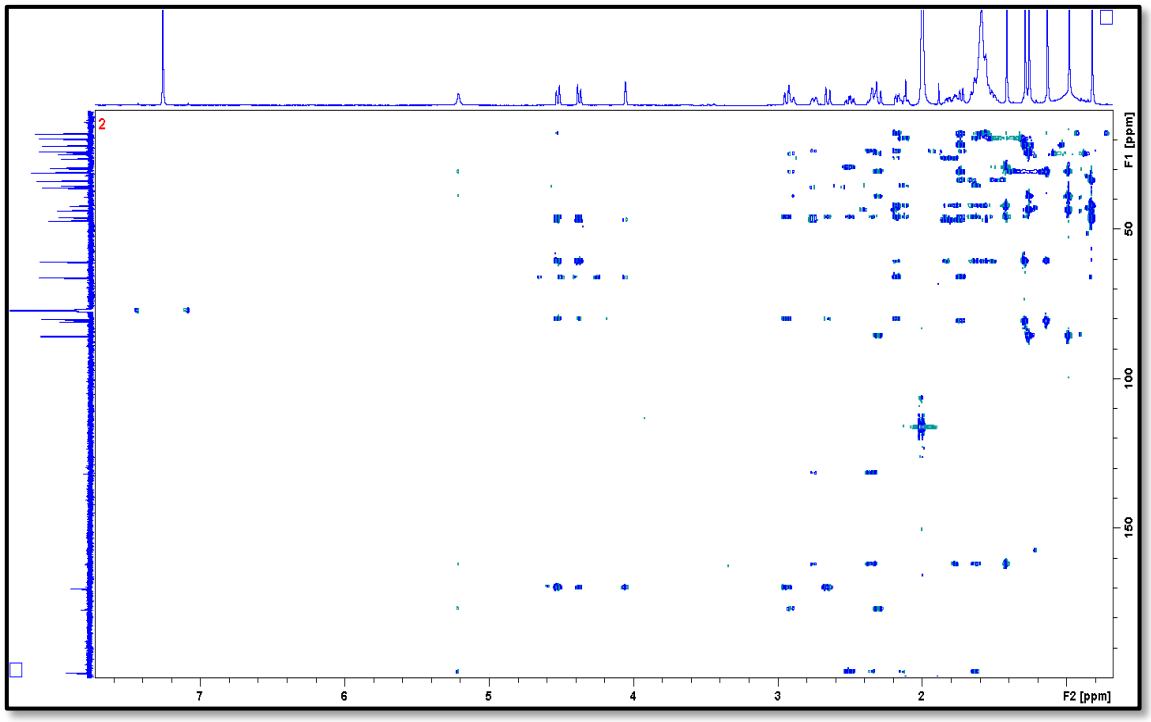

Figure S34: HMBC spectrum of Picraviane E (**09**) in $CDCl_3$ (600 MHz).

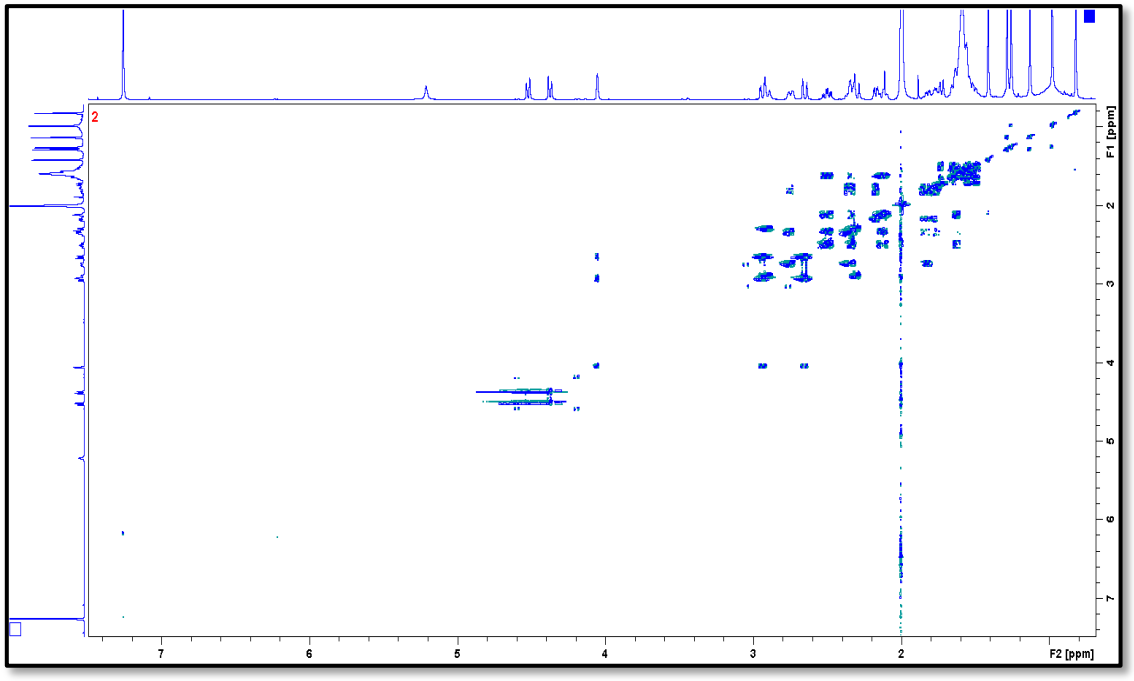

Figure S35: ^{1}H-^{1}H COSY spectrum of Picraviane E (**09**) in $CDCl_3$ (600 MHz).

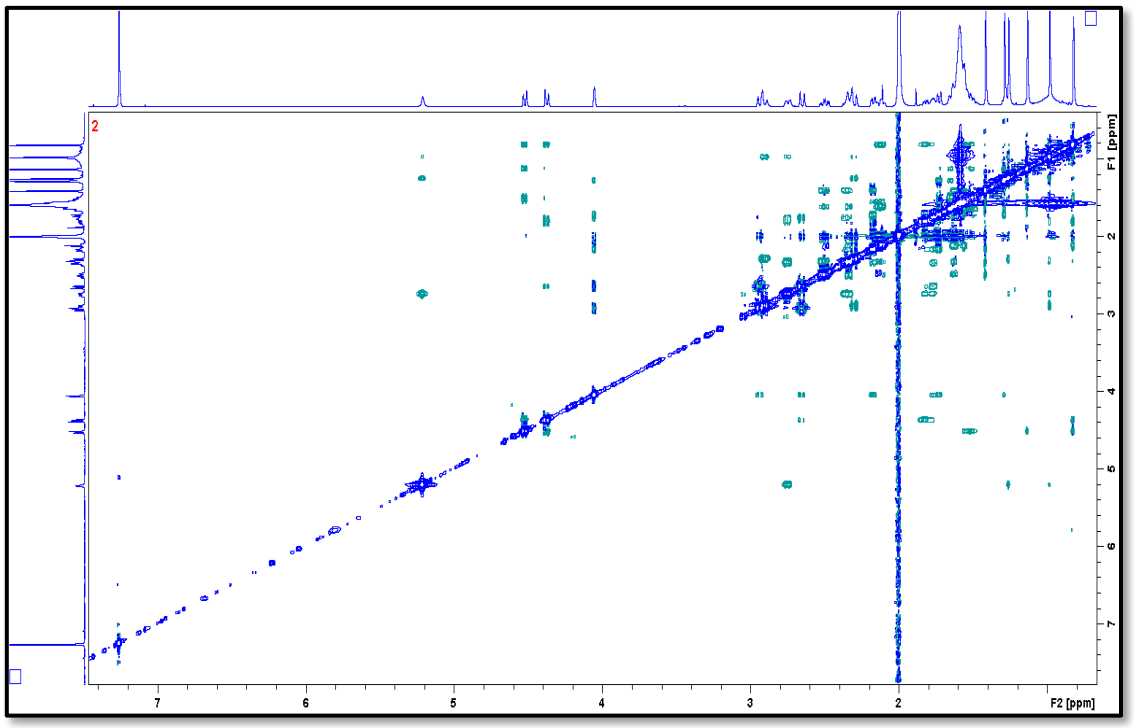

Figure S36: NOESY spectrum of Picraviane E (**09**) in $CDCl_3$ (600 MHz).

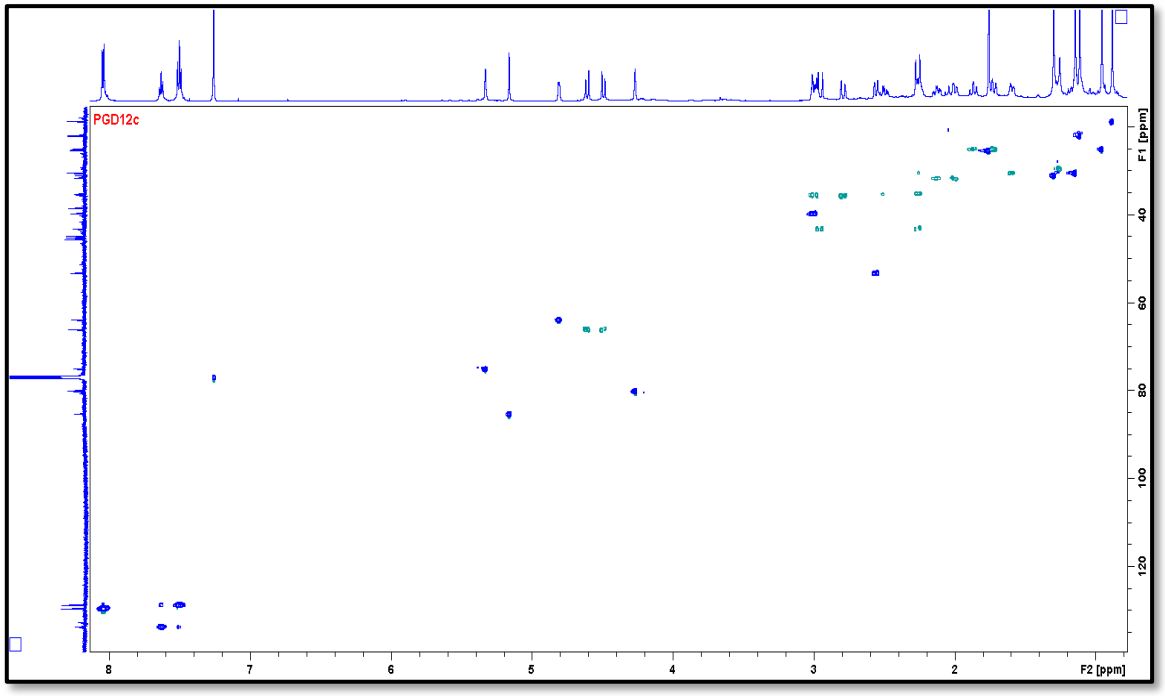

Figure S37: HSQC spectrum of Picraviane K (**12**) in $CDCl_3$ (600 MHz).

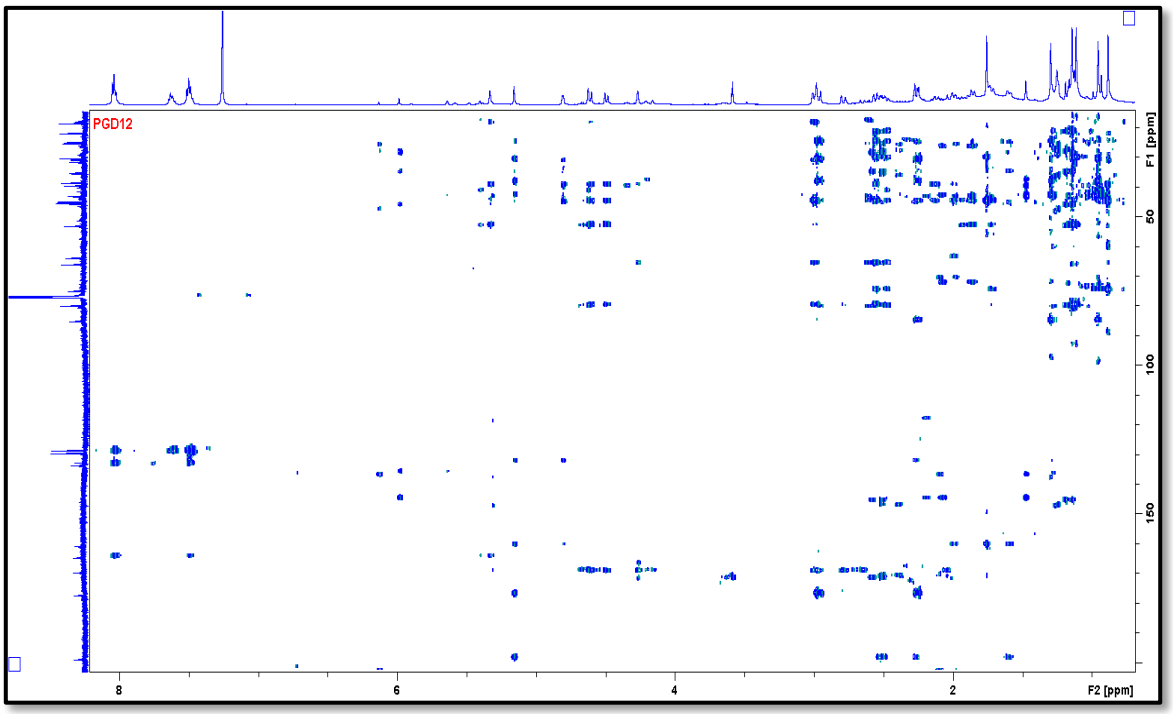

Figure S38: HMBC spectrum of Picraviane K (**12**) in $CDCl_3$ (600 MHz).

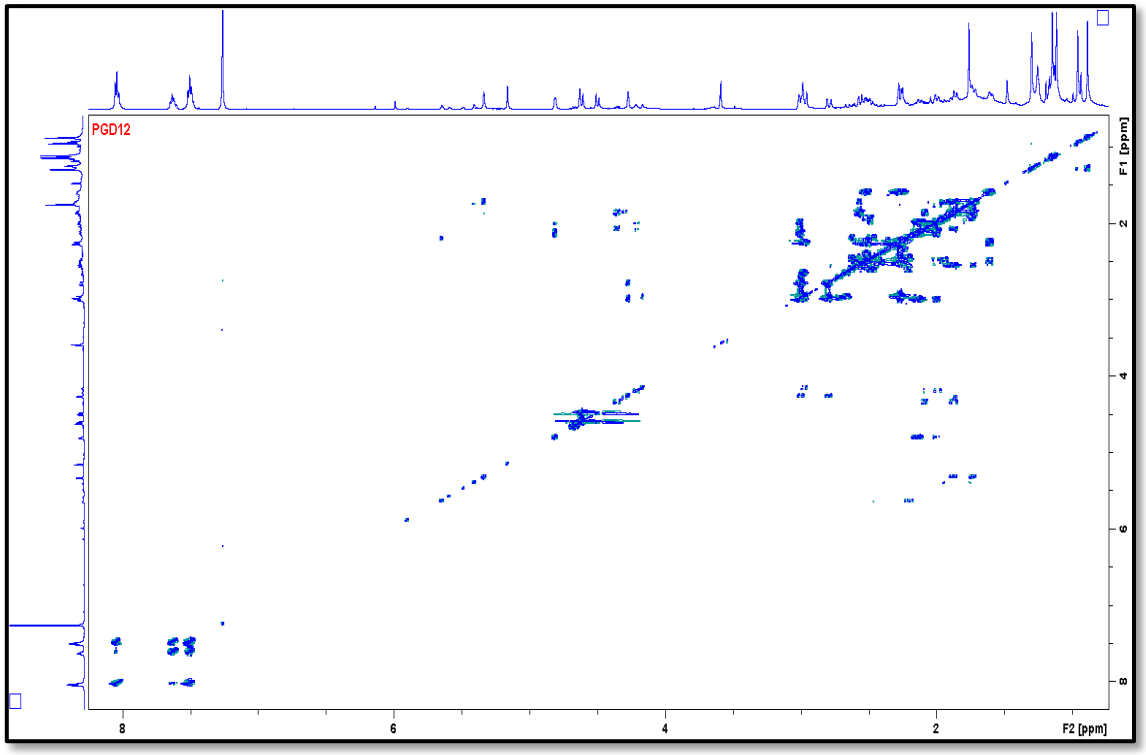

Figure S39: ^{1}H-^{1}H COSY spectrum of Picraviane K (**12**) in $CDCl_3$ (600 MHz).

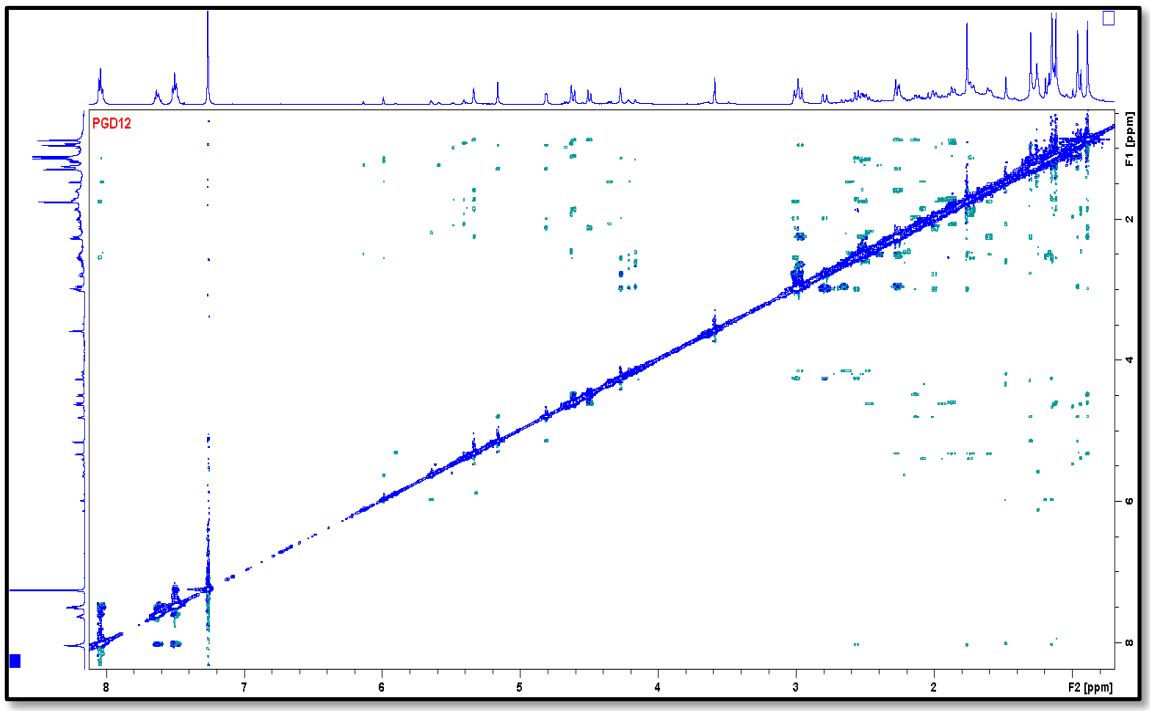

Figure S40: NOESY spectrum of Picraviane K (**12**) in $CDCl_3$ (600 MHz).

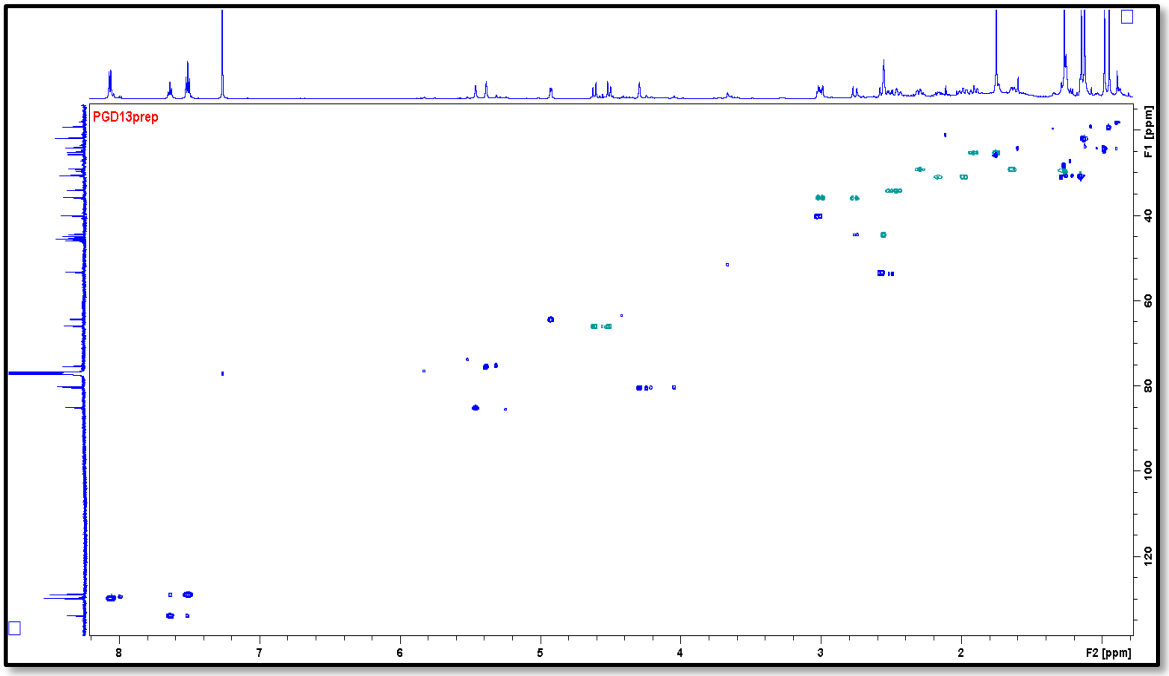

Figure S41: HSQC spectrum of Picraviane L (**13**) in $CDCl_3$ (600 MHz).

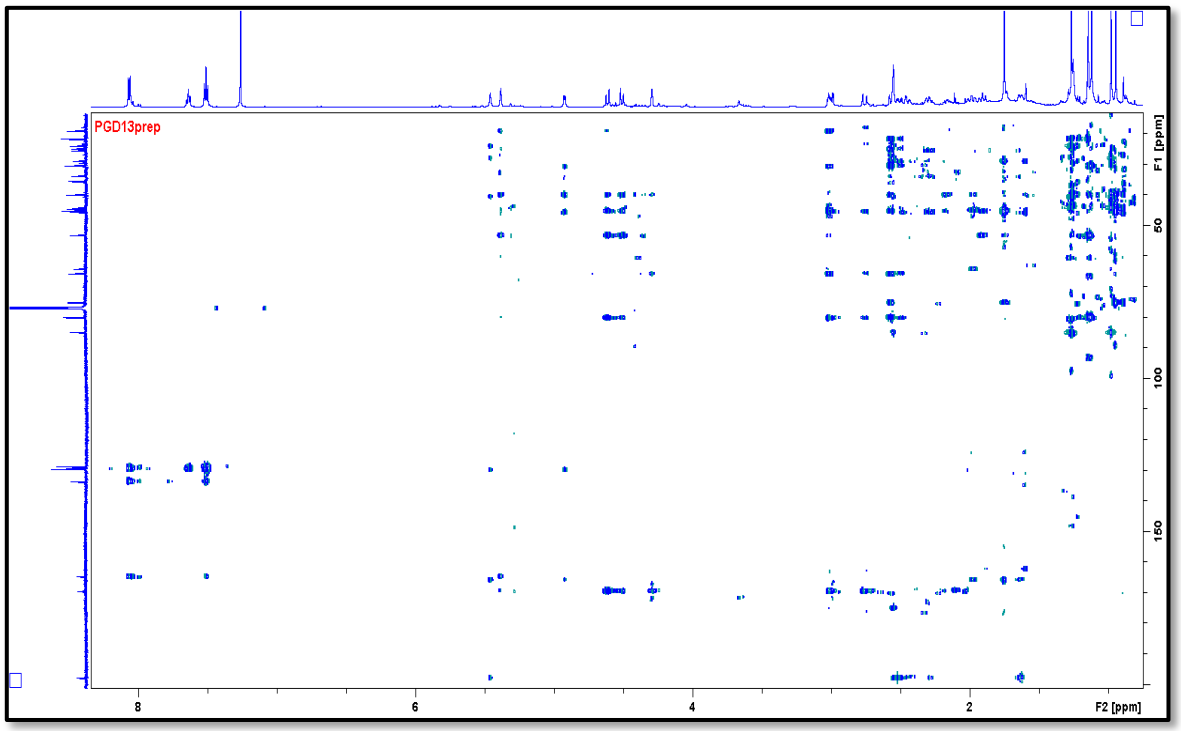

Figure S42: HMBC spectrum of Picraviane L (**13**) in $CDCl_3$ (600 MHz).

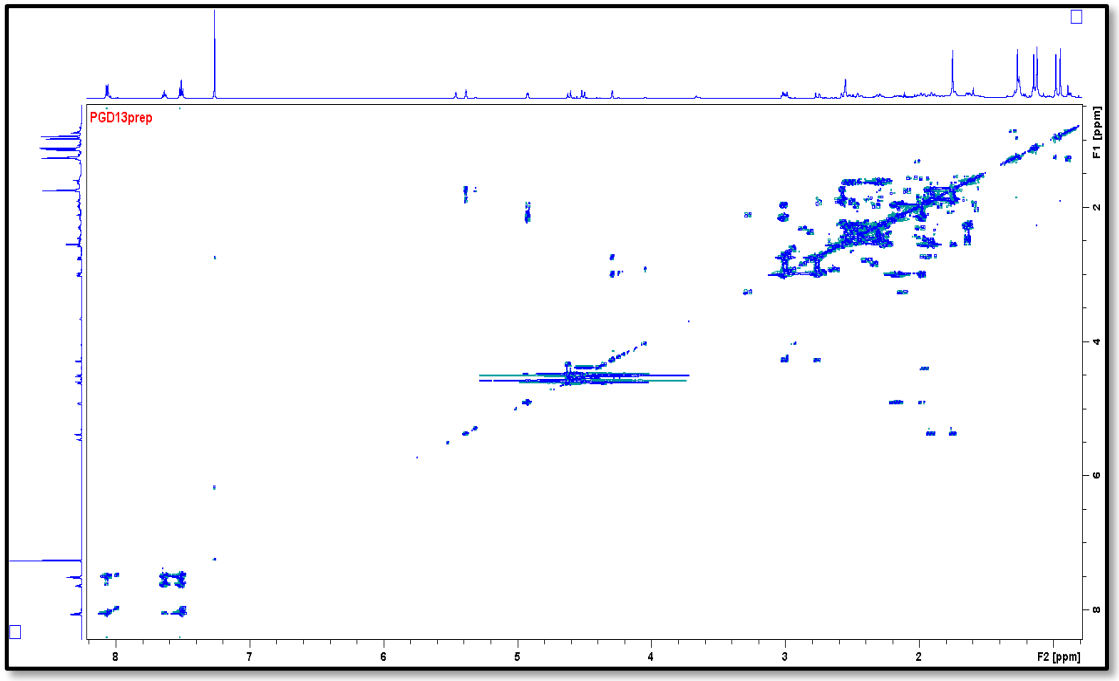

Figure S43: ^{1}H-^{1}H COSY spectrum of Picraviane L (**13**) in $CDCl_3$ (600 MHz).

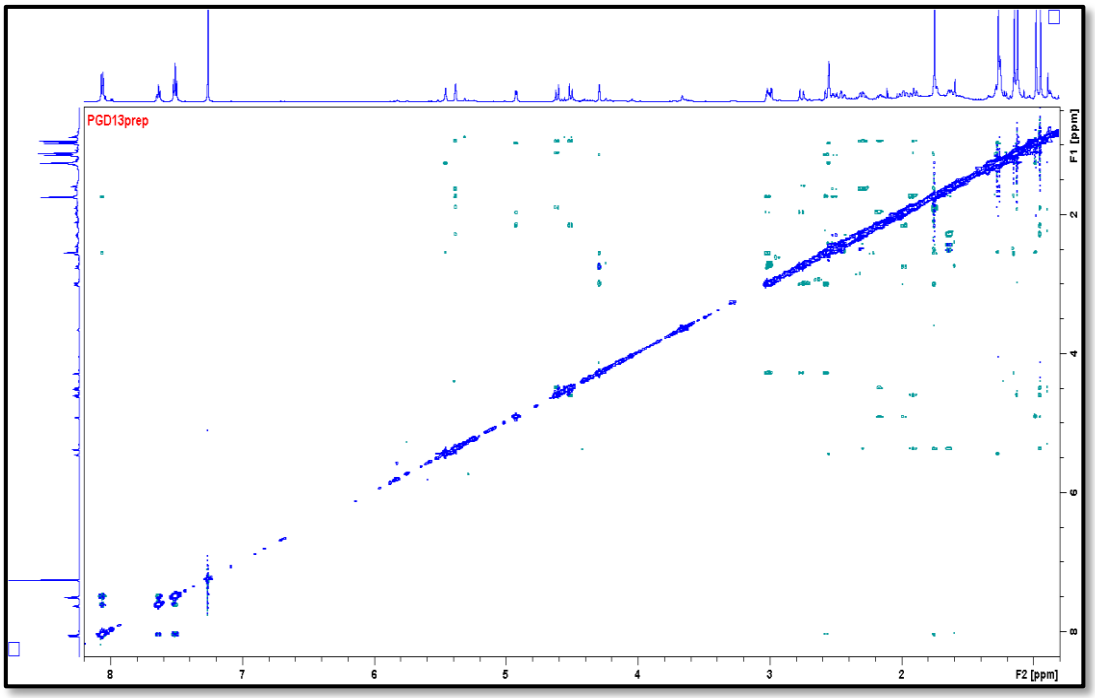

Figure S44: NOESY spectrum of Picraviane L (**13**) in $CDCl_3$ (600 MHz).

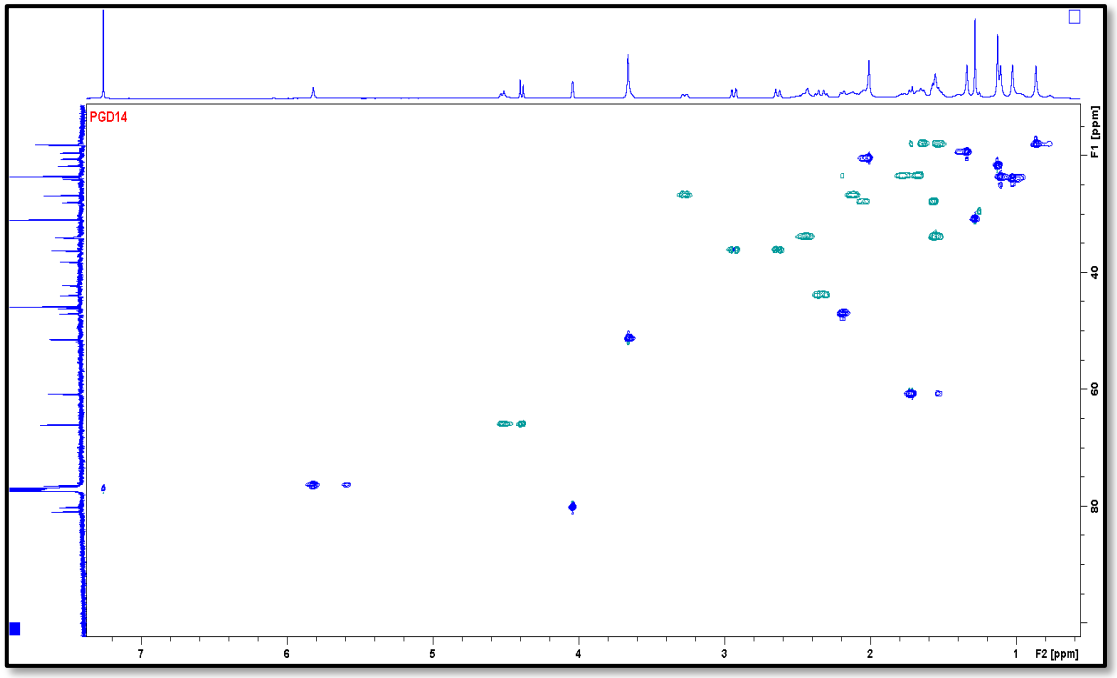

Figure S45: HSQC spectrum of Picraviane P (**14**) in $CDCl_3$ (600 MHz).

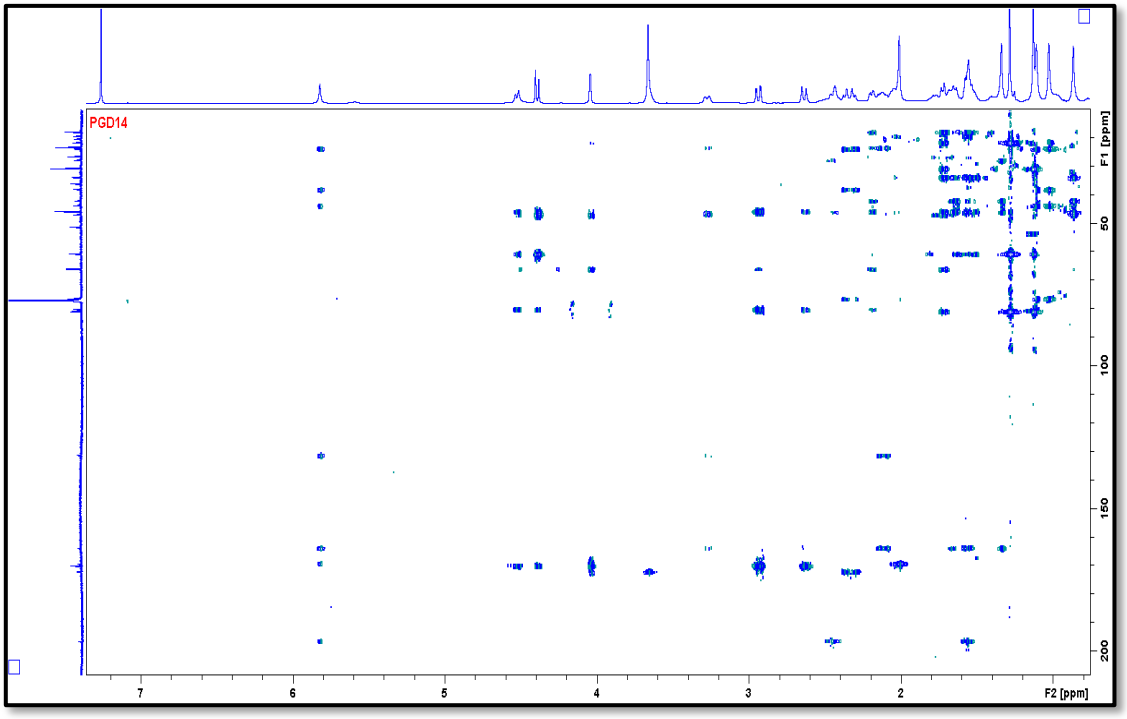

Figure S46: HMBC spectrum of Picraviane P (**14**) in $CDCl_3$ (600 MHz).

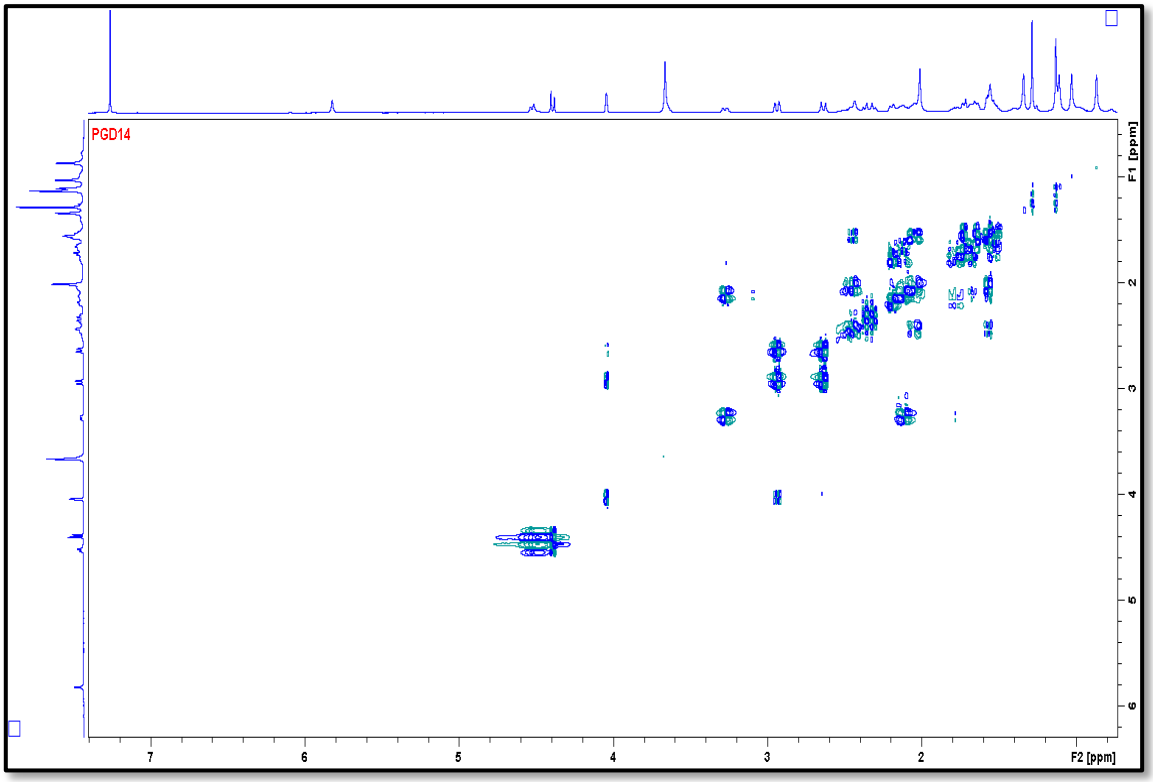

Figure S47: ^{1}H-^{1}H COSY spectrum of Picraviane P (**14**) in $CDCl_3$ (600 MHz).

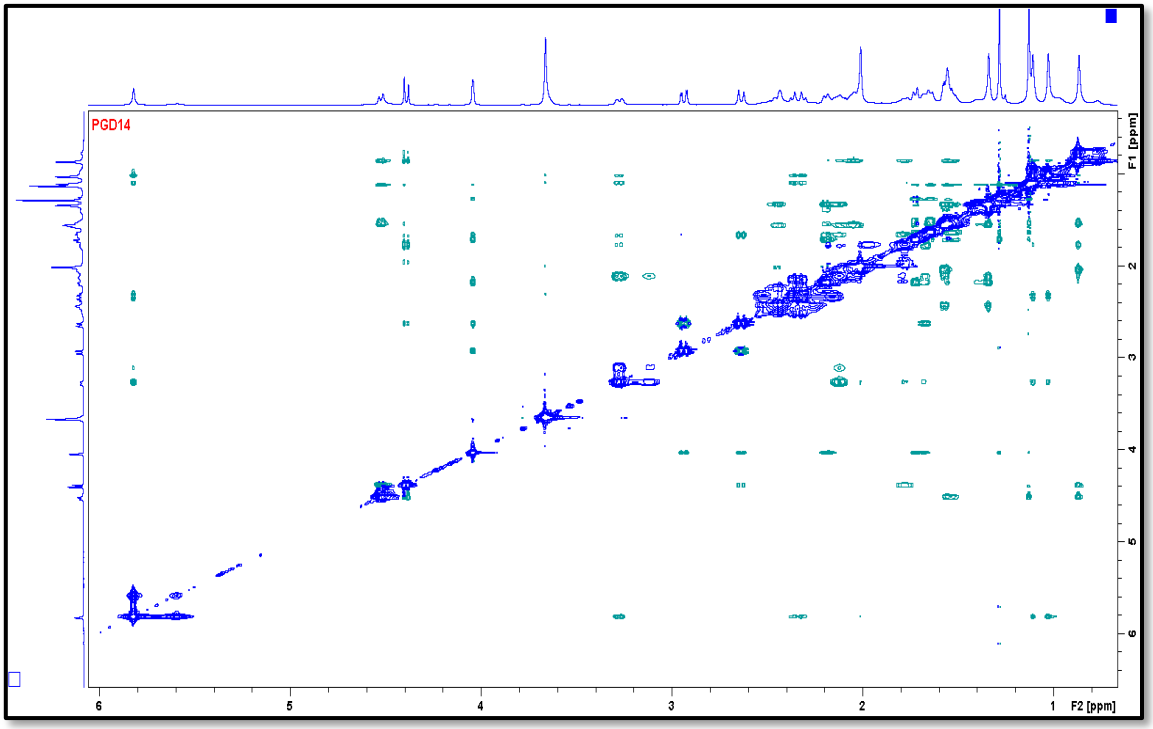

Figure S48: NOESY spectrum of Picraviane P (**14**) in $CDCl_3$ (600 MHz).

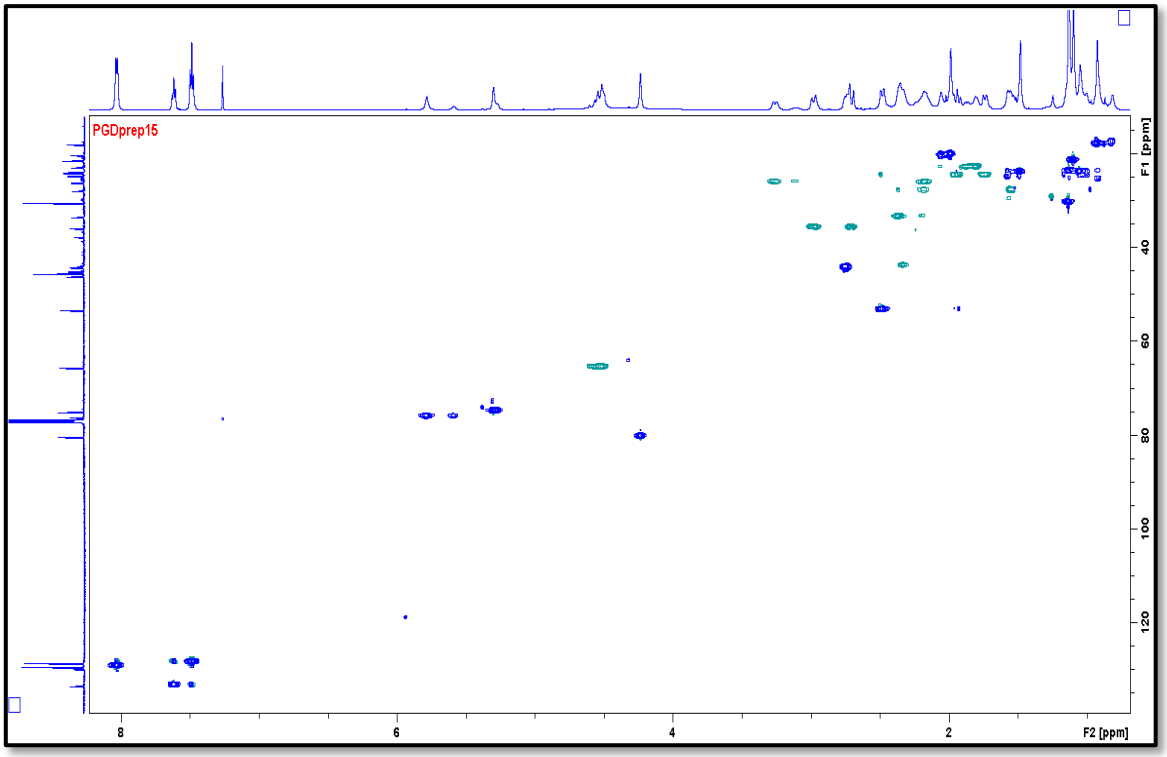

Figure S49: HSQC spectrum of Picraviane Q (**15**) in $CDCl_3$ (600 MHz).

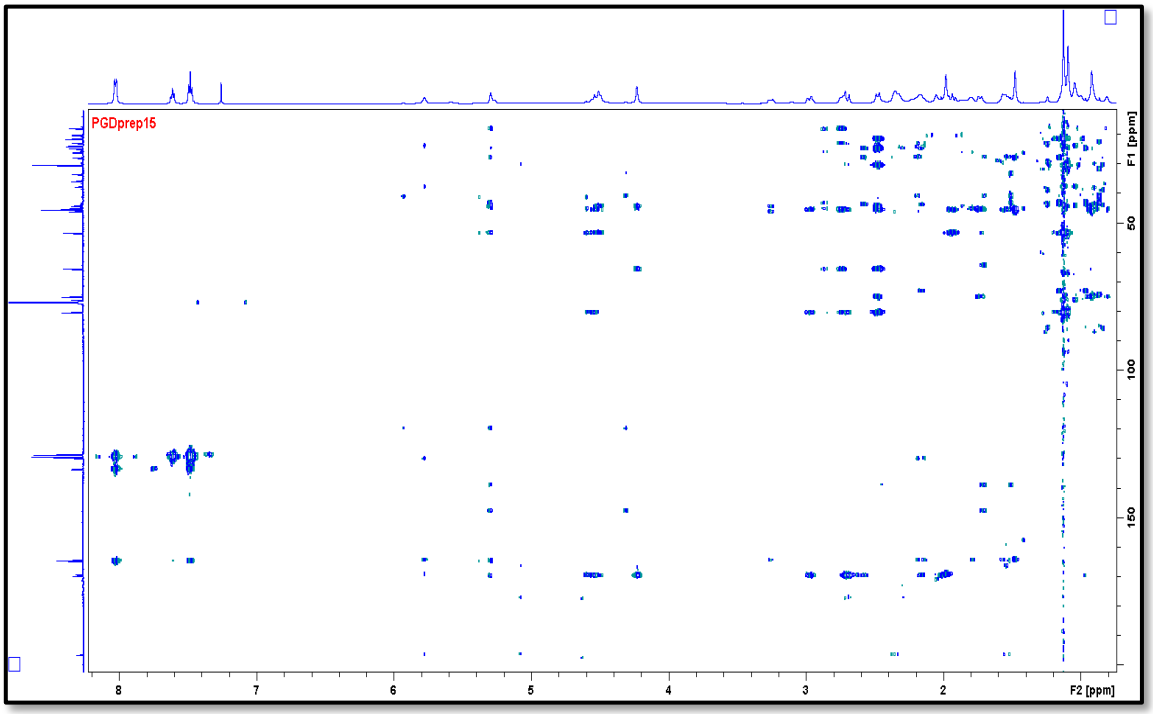

Figure S50: HMBC spectrum of Picraviane Q (**15**) in $CDCl_3$ (600 MHz).

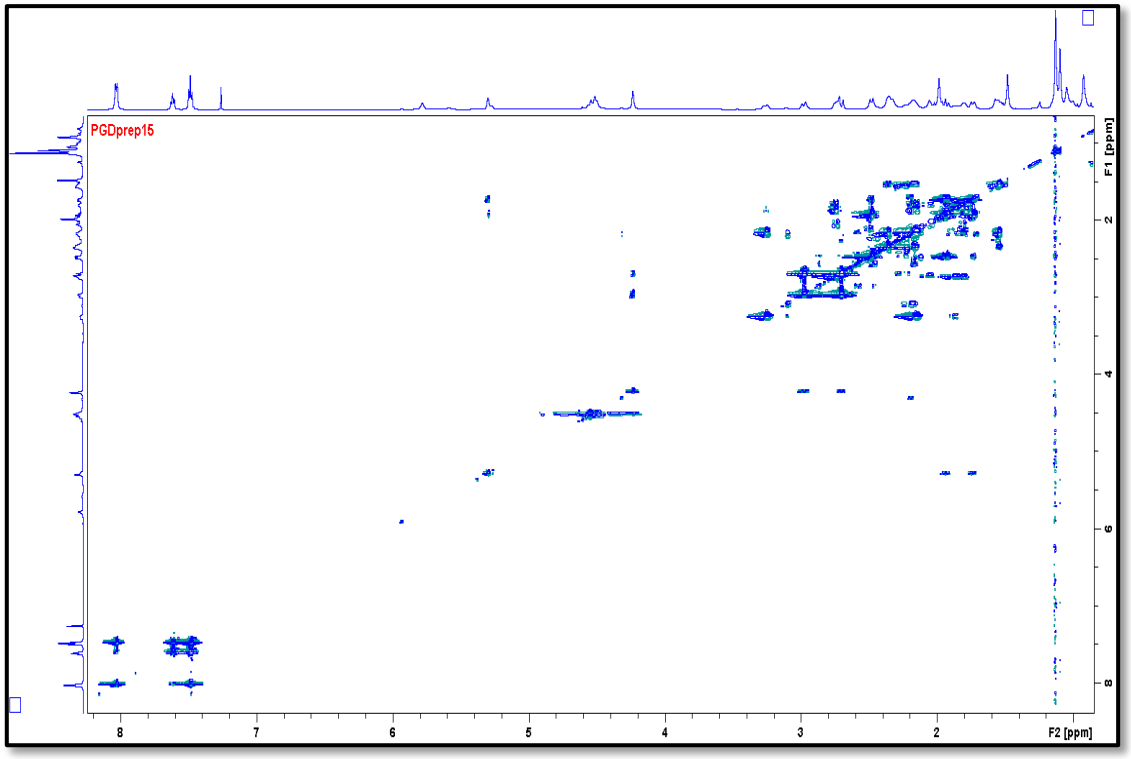

Figure S51: ^{1}H-^{1}H COSY spectrum of Picraviane Q (**15**) in $CDCl_3$ (600 MHz).

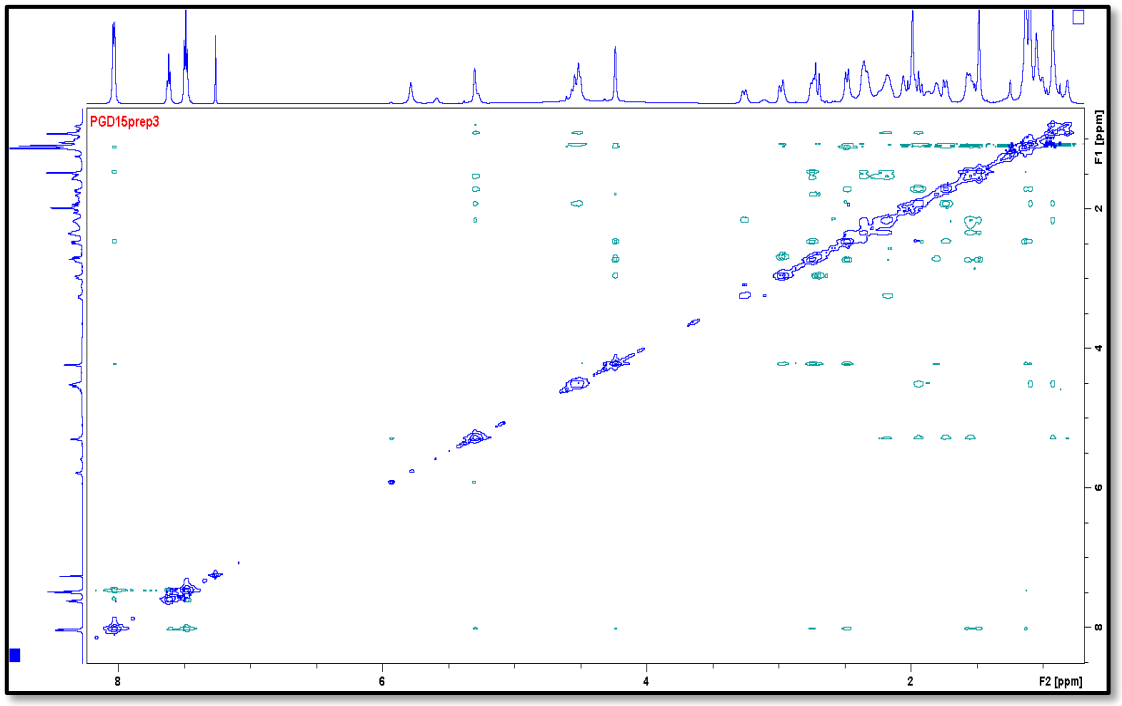

Figure S52: ROESY spectrum of Picraviane Q (**15**) in $CDCl_3$ (600 MHz).

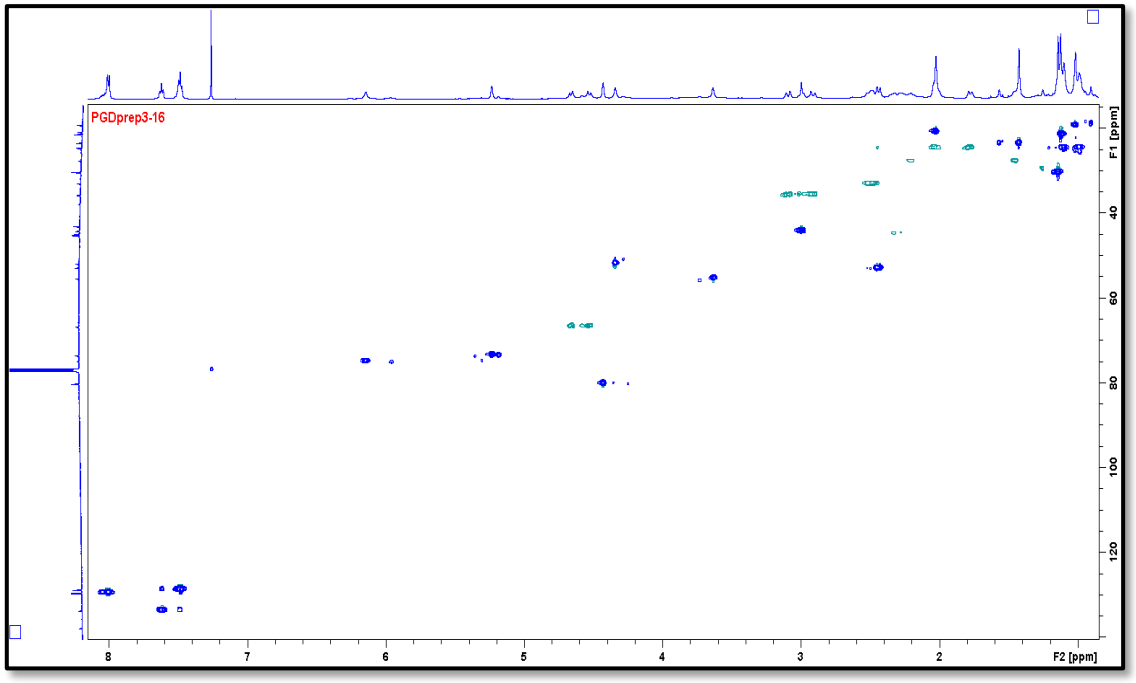

Figure S53: HSQC spectrum of Picraviane R (**16**) in $CDCl_3$ (600 MHz).

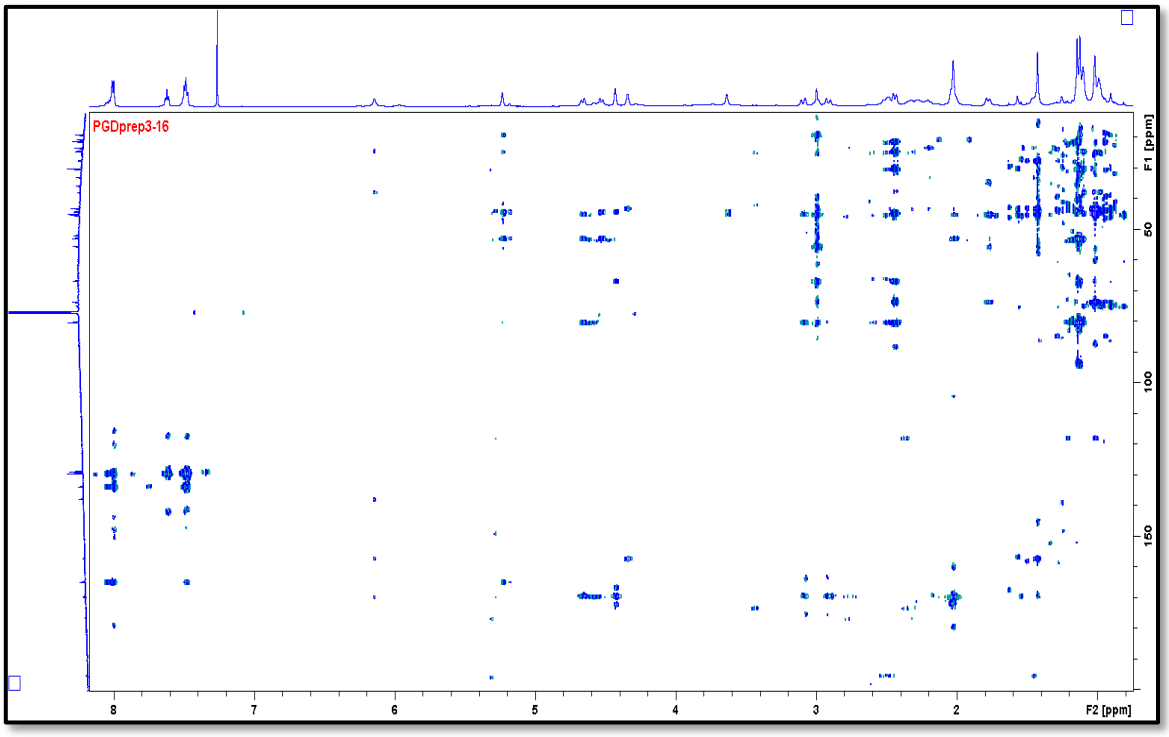

Figure S54: HMBC spectrum of Picraviane R (**16**) in $CDCl_3$ (600 MHz).

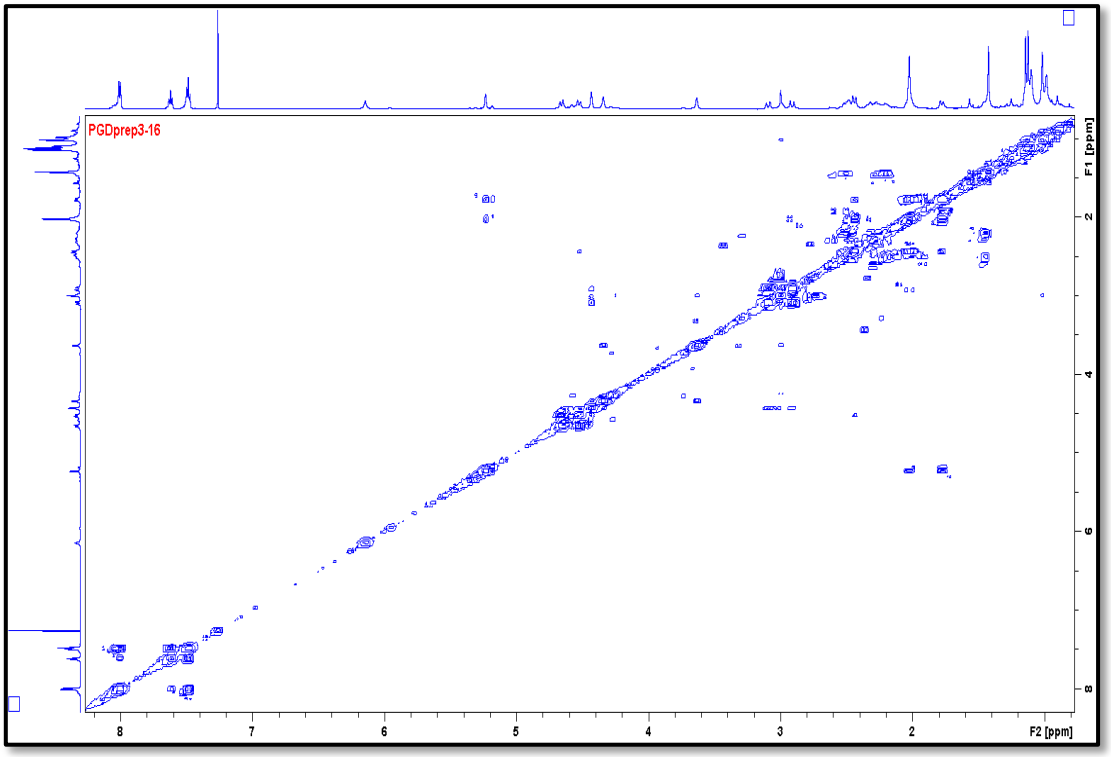

Figure S55: ^{1}H-^{1}H COSY spectrum of Picraviane R (**16**) in $CDCl_3$ (600 MHz).

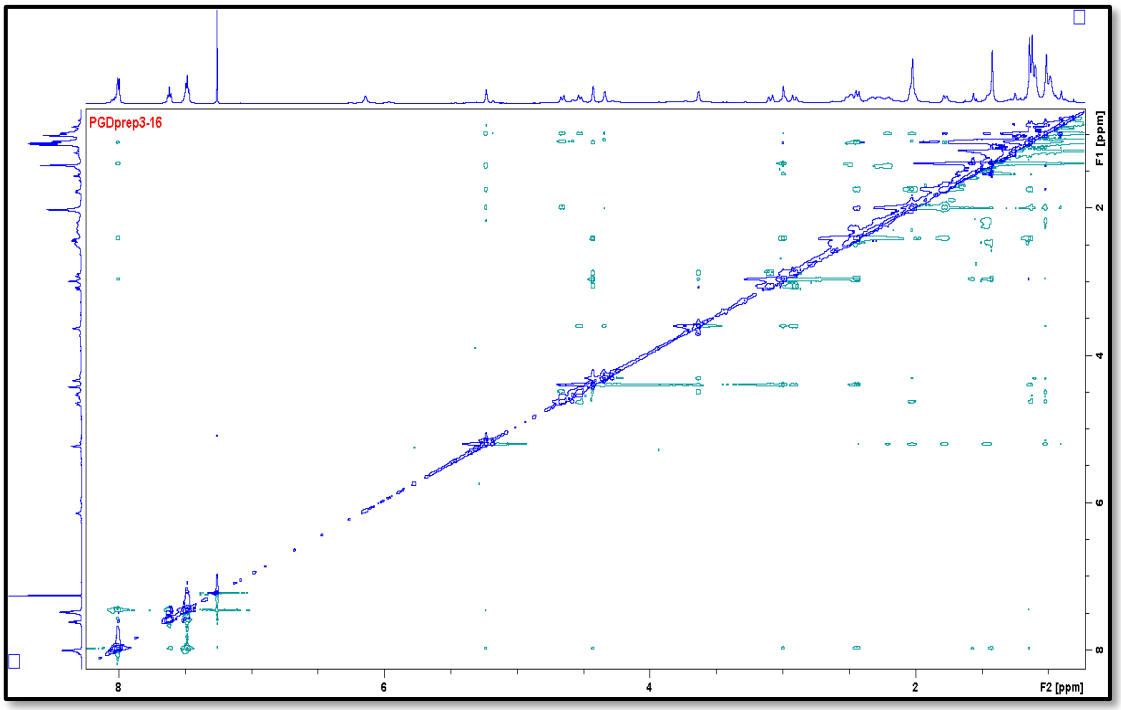

Figure S56: ROESY spectrum of Picraviane R (**16**) in $CDCl_3$ (600 MHz).

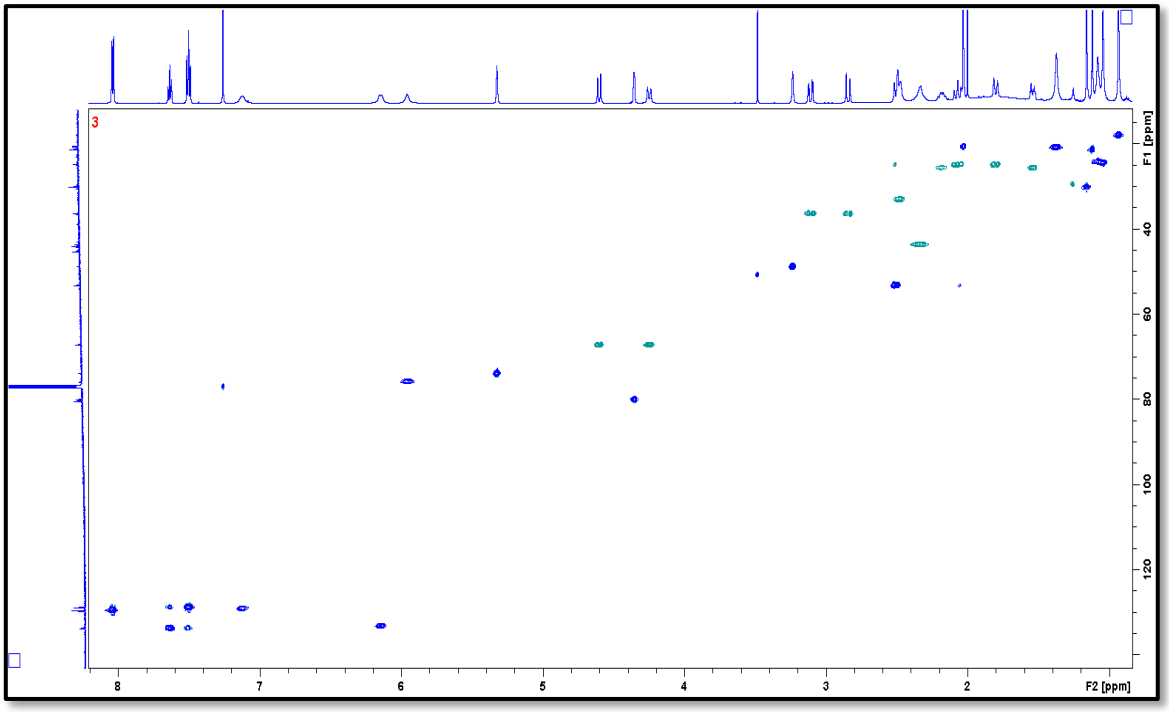

Figure S57: HSQC spectrum of Picraviane S (**17**) in $CDCl_3$ (600 MHz).

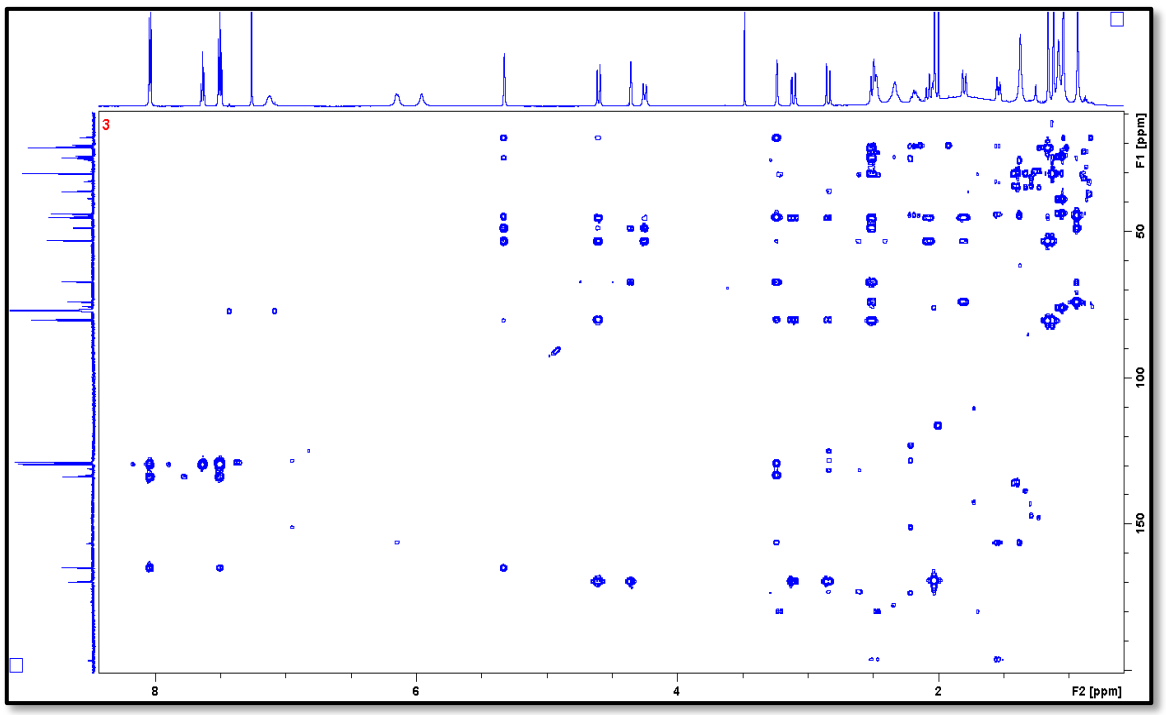

Figure S58: HMBC spectrum of Picraviane S (**17**) in $CDCl_3$ (600 MHz).

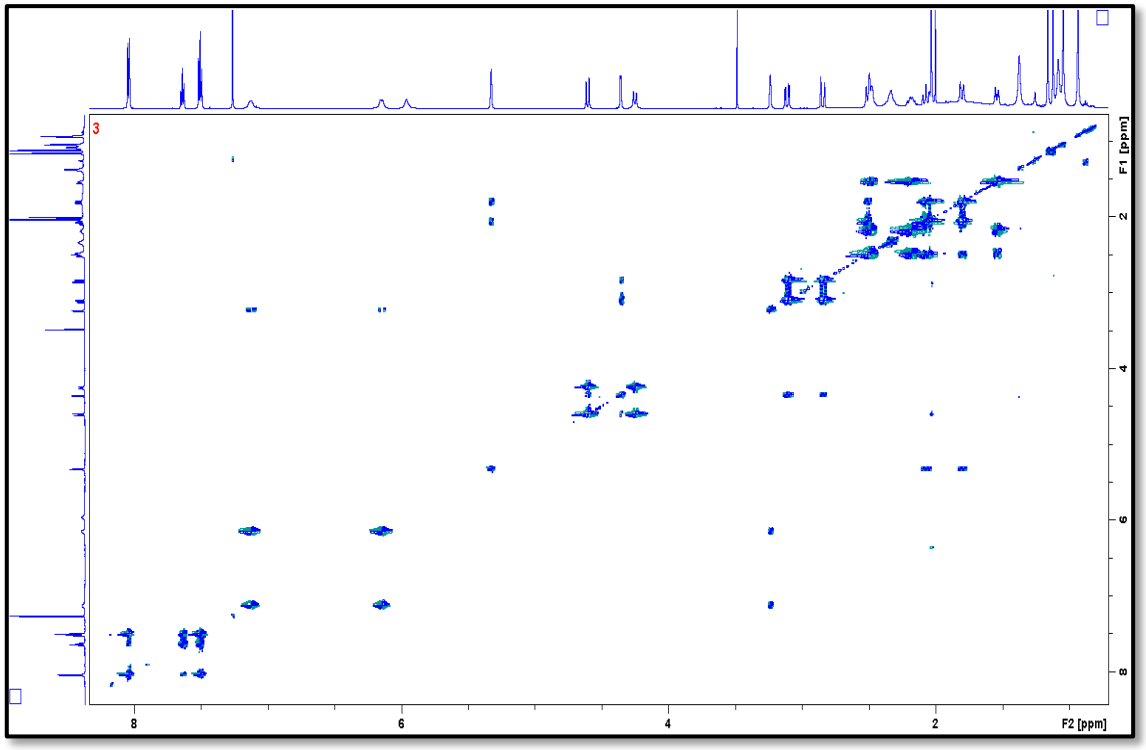

Figure S59: ^{1}H-^{1}H COSY spectrum of Picraviane S (**17**) in $CDCl_3$ (600 MHz).

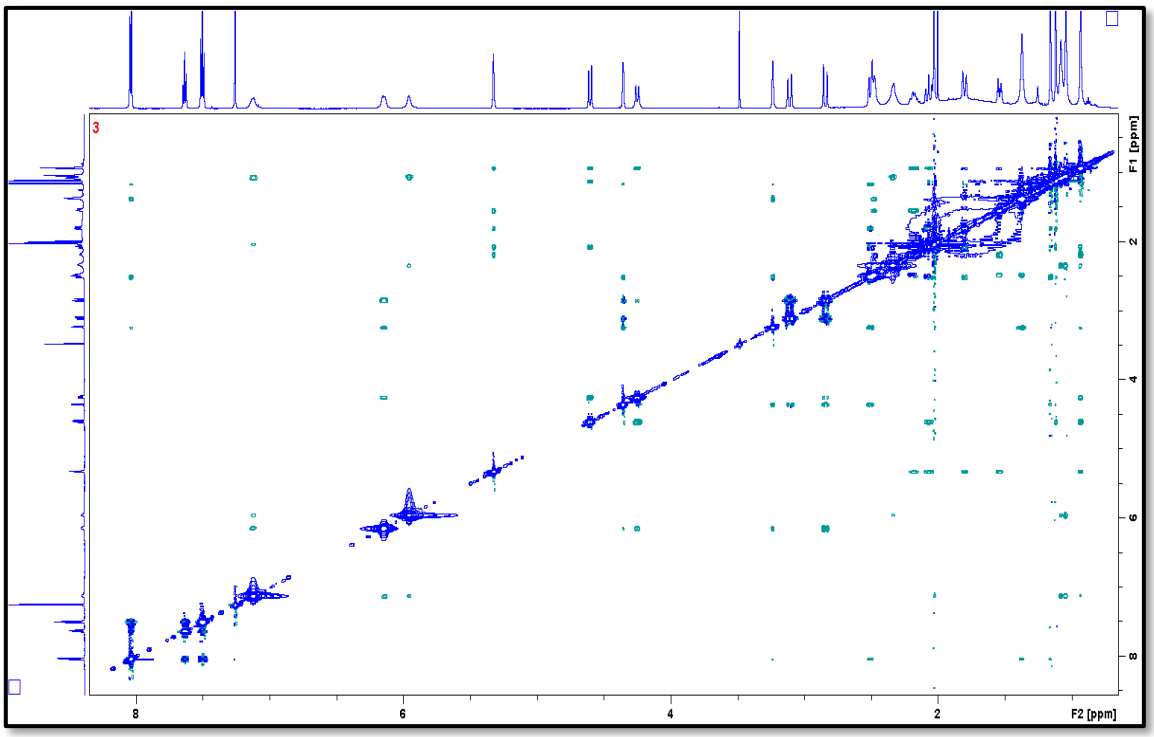

Figure S60: NOESY spectrum of Picraviane S (**17**) in $CDCl_3$ (600 MHz).

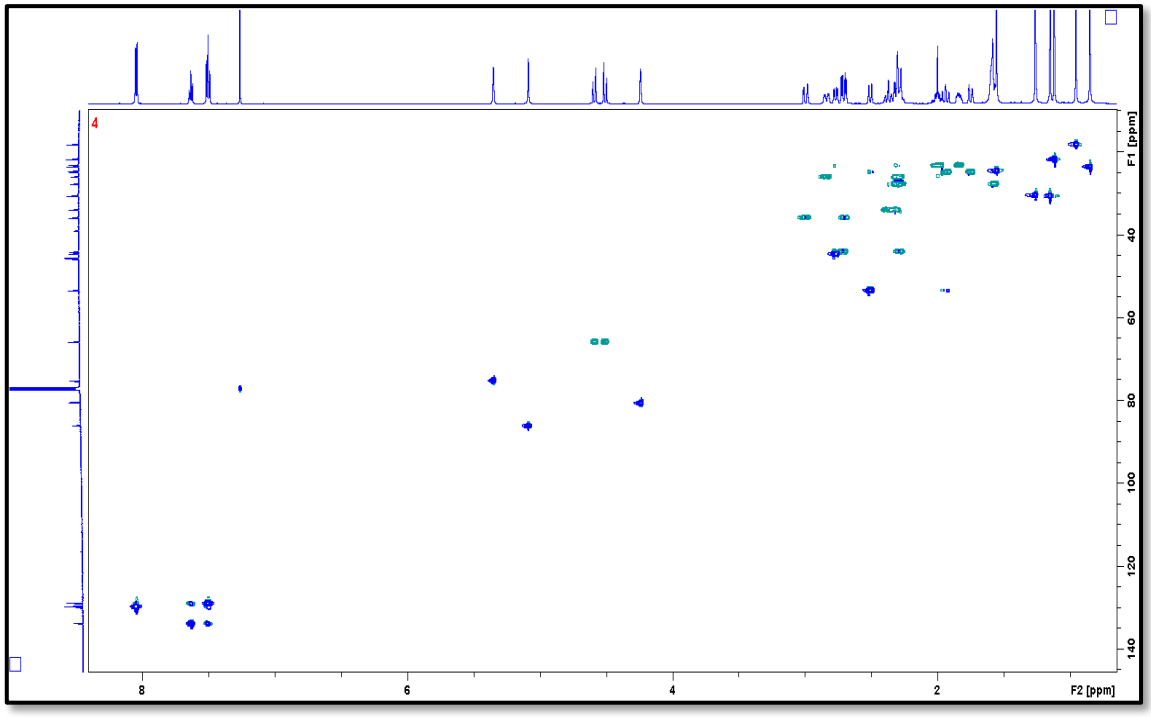

Figure S61: HSQC spectrum of Picraviane F (**18**) in $CDCl_3$ (600 MHz).

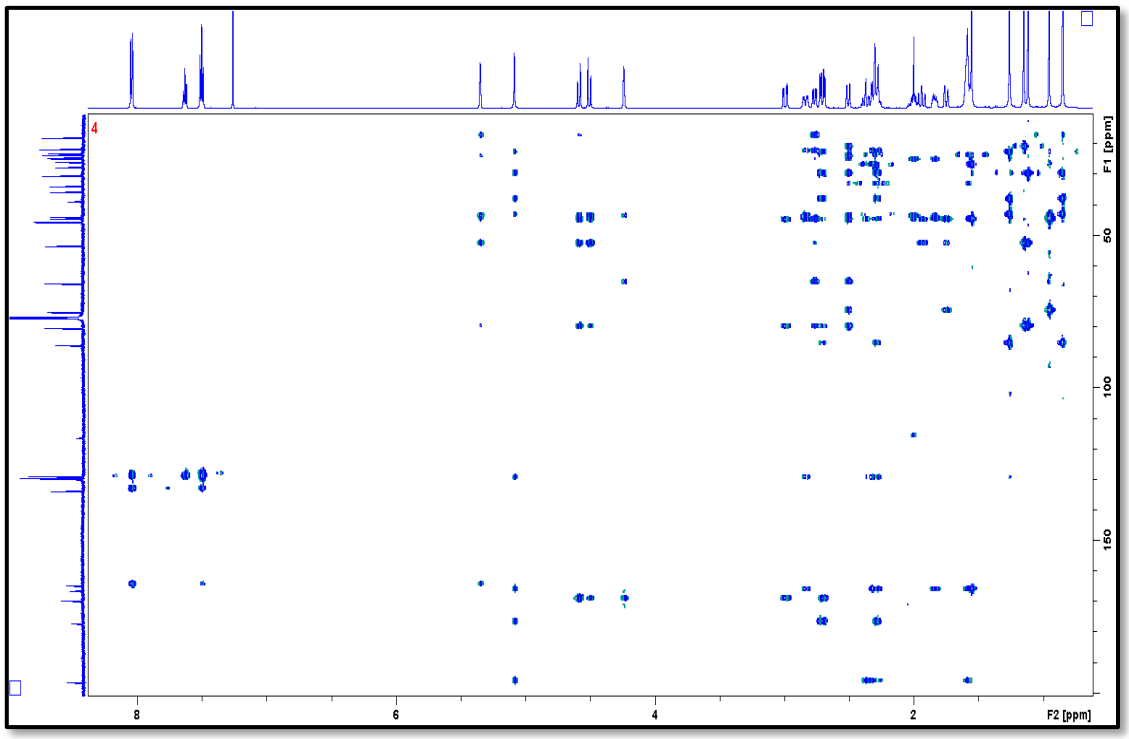

Figure S62: HMBC spectrum of Picraviane F (**18**) in $CDCl_3$ (600 MHz).

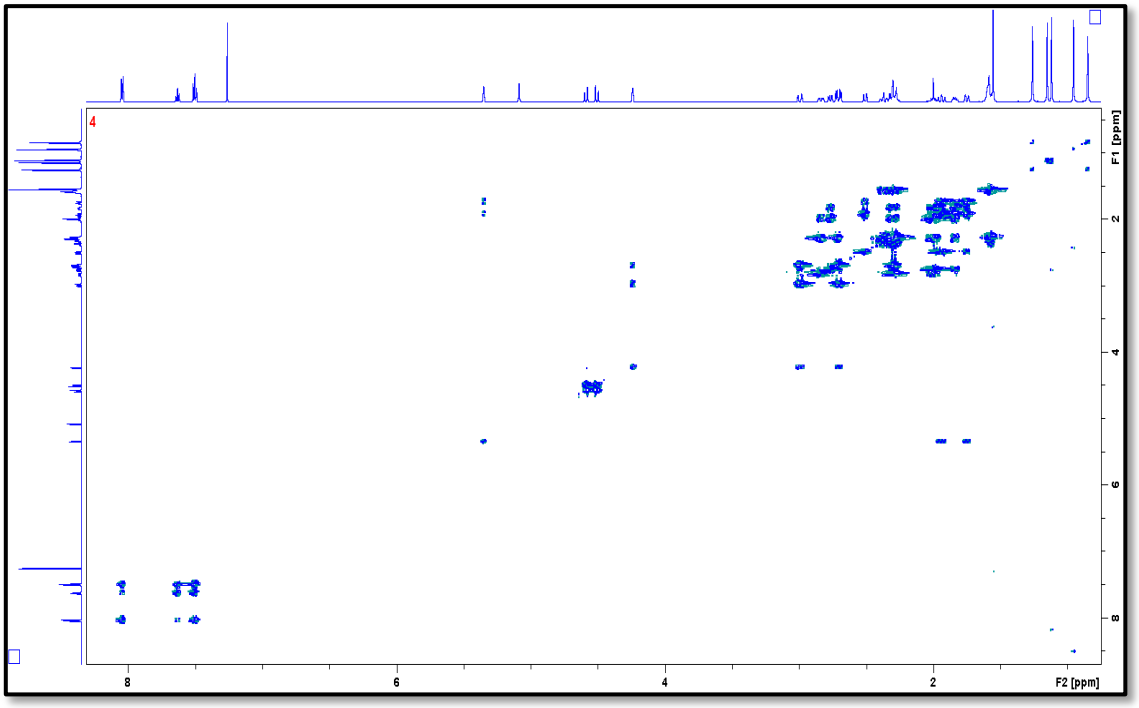

Figure S 63: ^{1}H-^{1}H COSY spectrum of Picraviane F (**18**) in $CDCl_3$ (600 MHz).

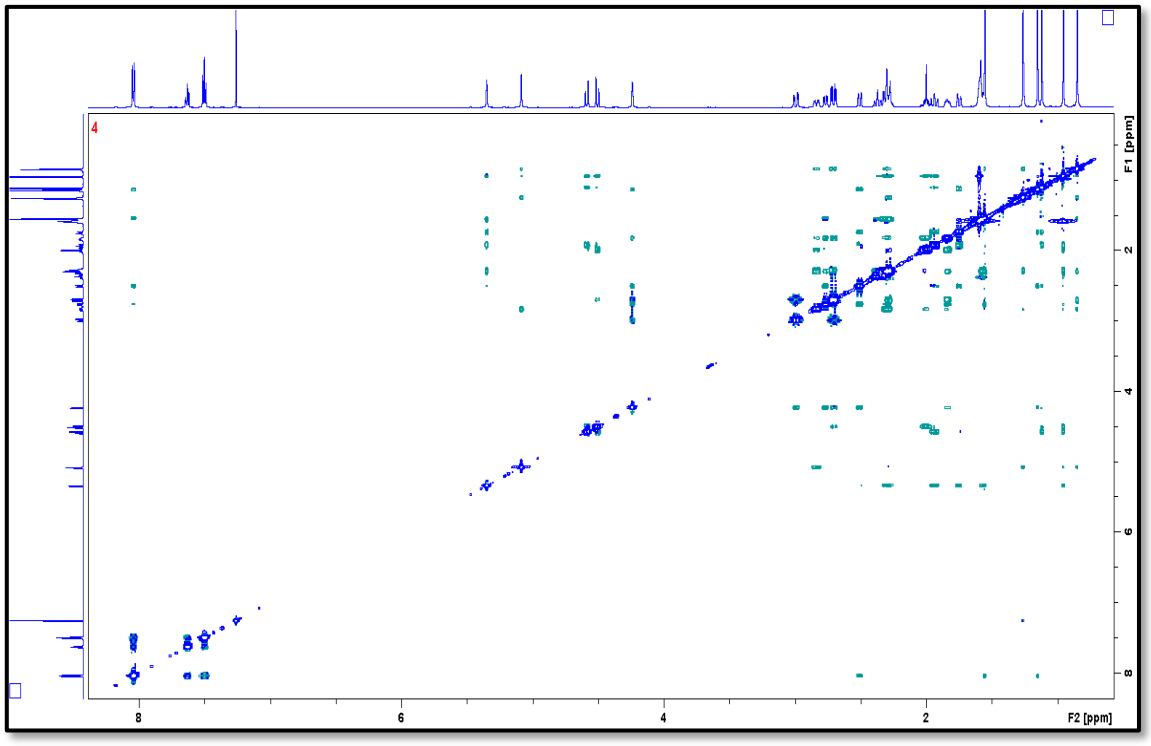

Figure S64: NOESY spectrum of Picraviane F (**18**) in $CDCl_3$ (600 MHz).

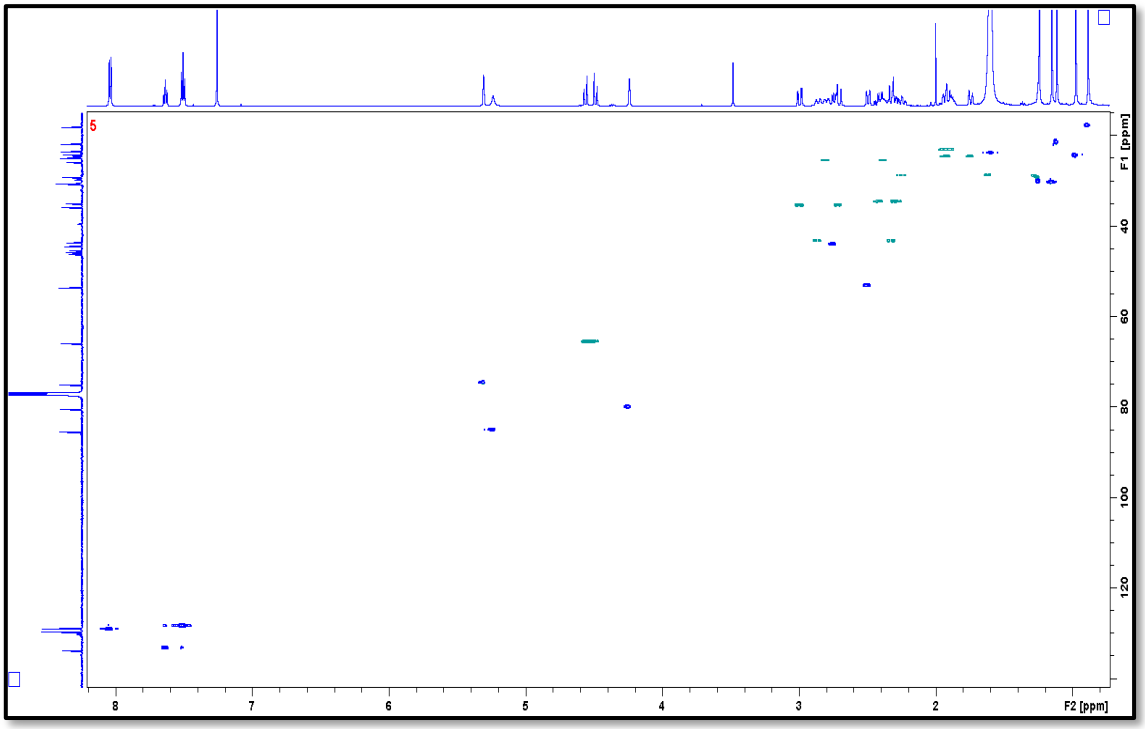

Figure S65: HSQC spectrum of Picraviane G (**19**) in $CDCl_3$ (600 MHz).

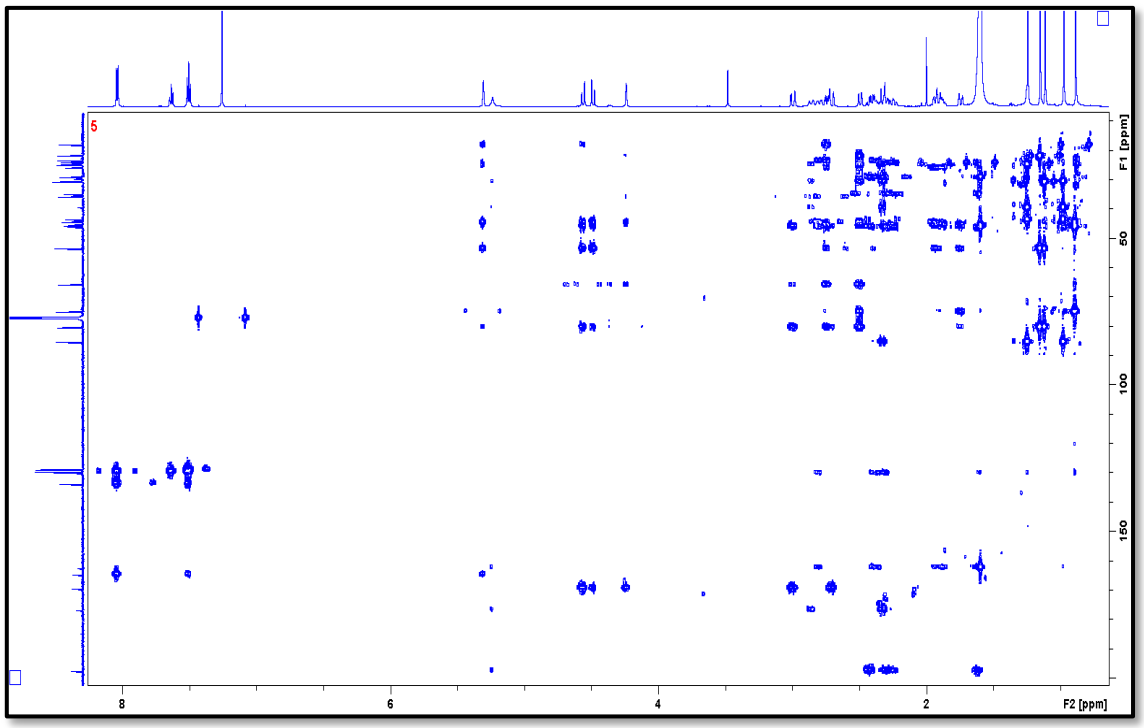

Figure S66: HMBC spectrum of Picraviane G (**19**) in $CDCl_3$ (600 MHz).

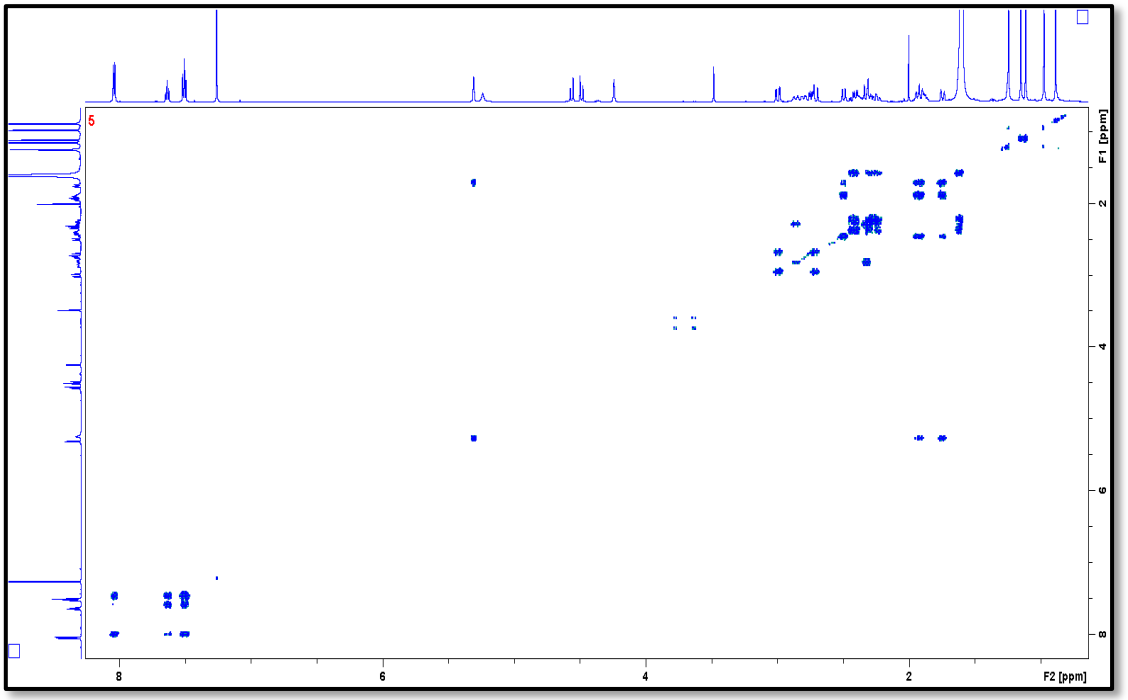

Figure S67: ^{1}H-^{1}H COSY spectrum of Picraviane G (**19**) in $CDCl_3$ (600 MHz).

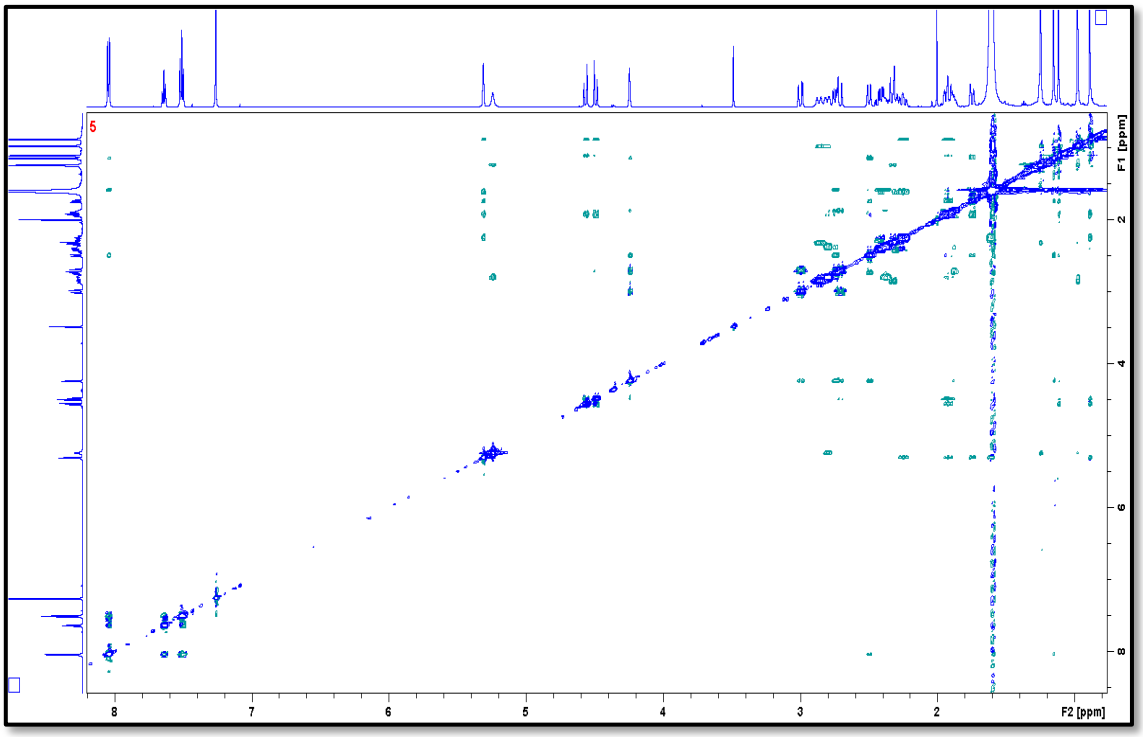

Figure S68: NOESY spectrum of Picraviane G (**19**) in $CDCl_3$ (600 MHz).

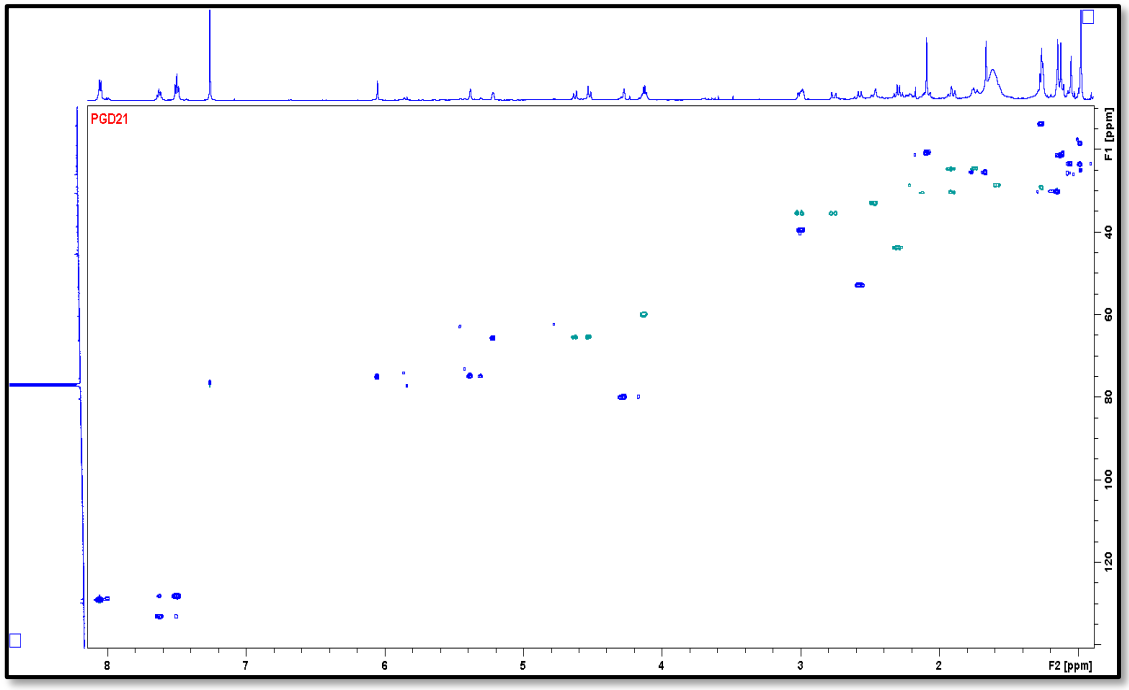

Figure S69: HSQC spectrum of Picraviane U (**21**) in $CDCl_3$ (600 MHz).

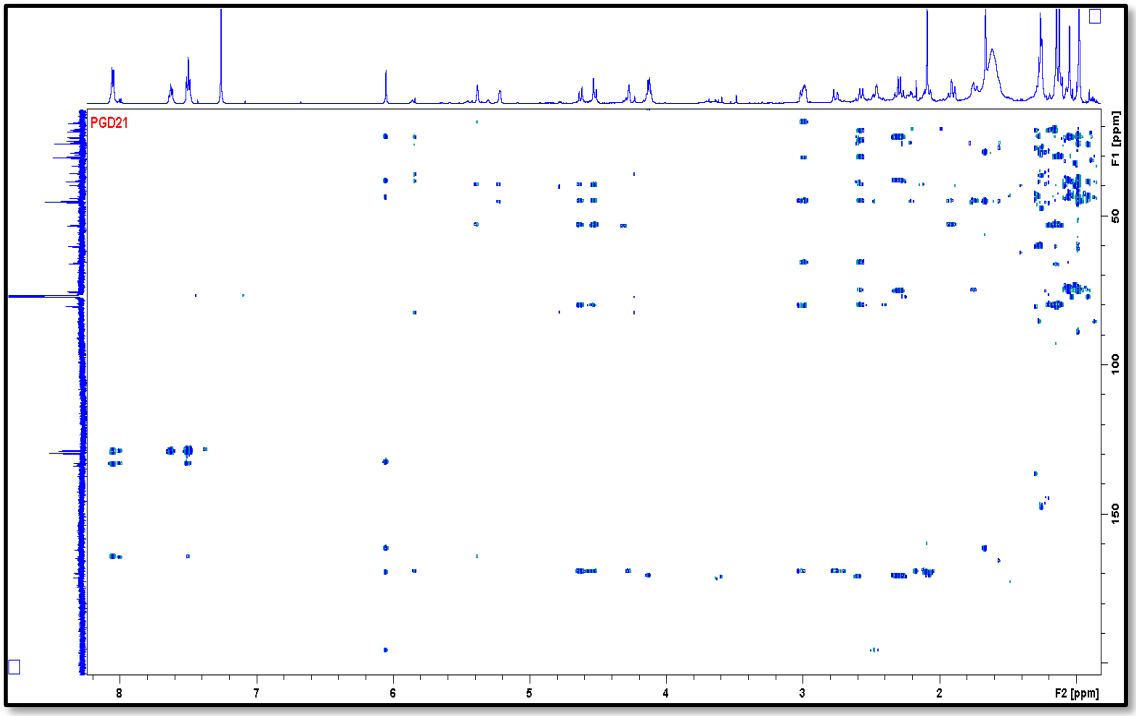

Figure S70: HMBC spectrum of Picraviane U (**21**) in $CDCl_3$ (600 MHz).

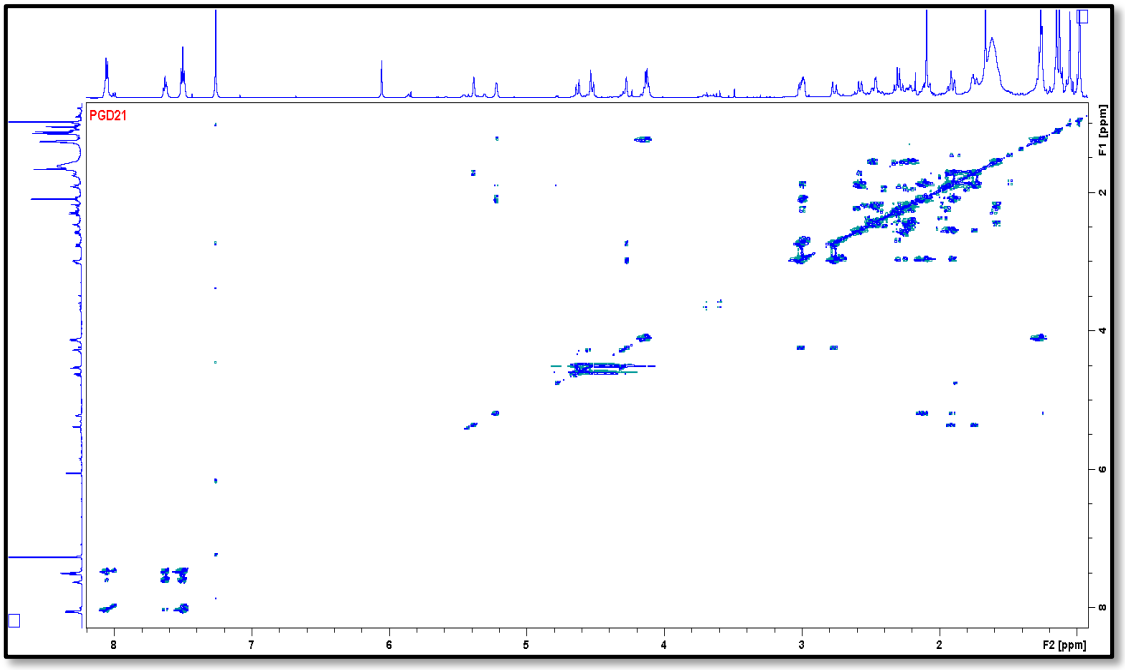

Figure S71: ^{1}H-^{1}H COSY spectrum of Picraviane U (**21**) in $CDCl_3$ (600 MHz).

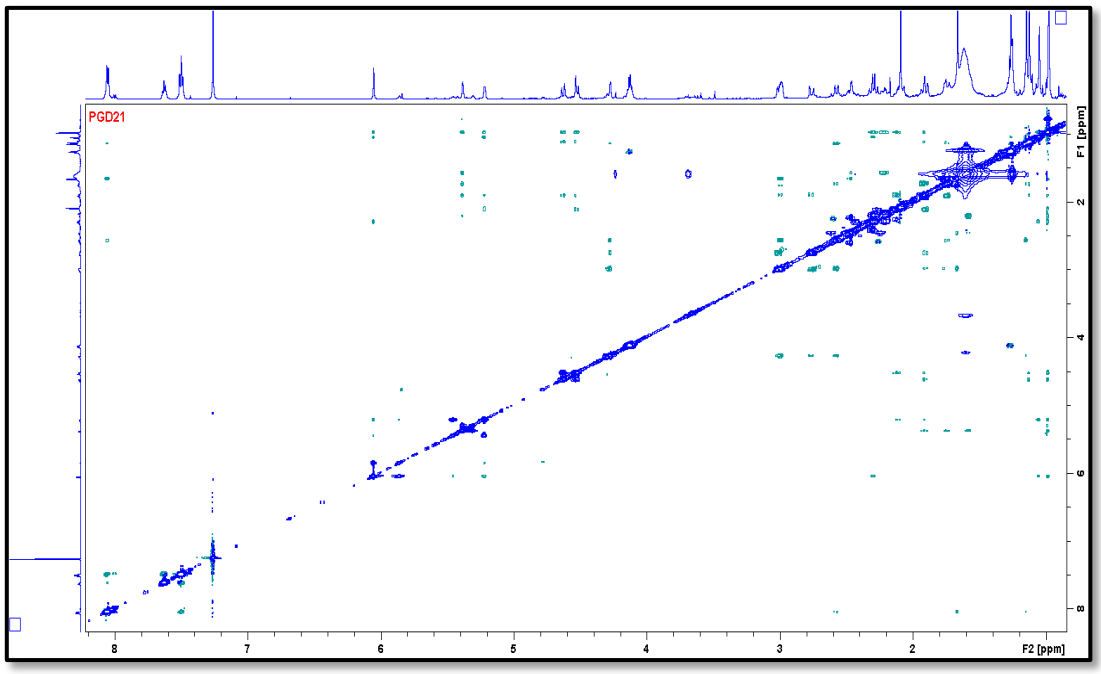

Figure S72: NOESY spectrum of Picraviane U (**21**) in $CDCl_3$ (600 MHz).

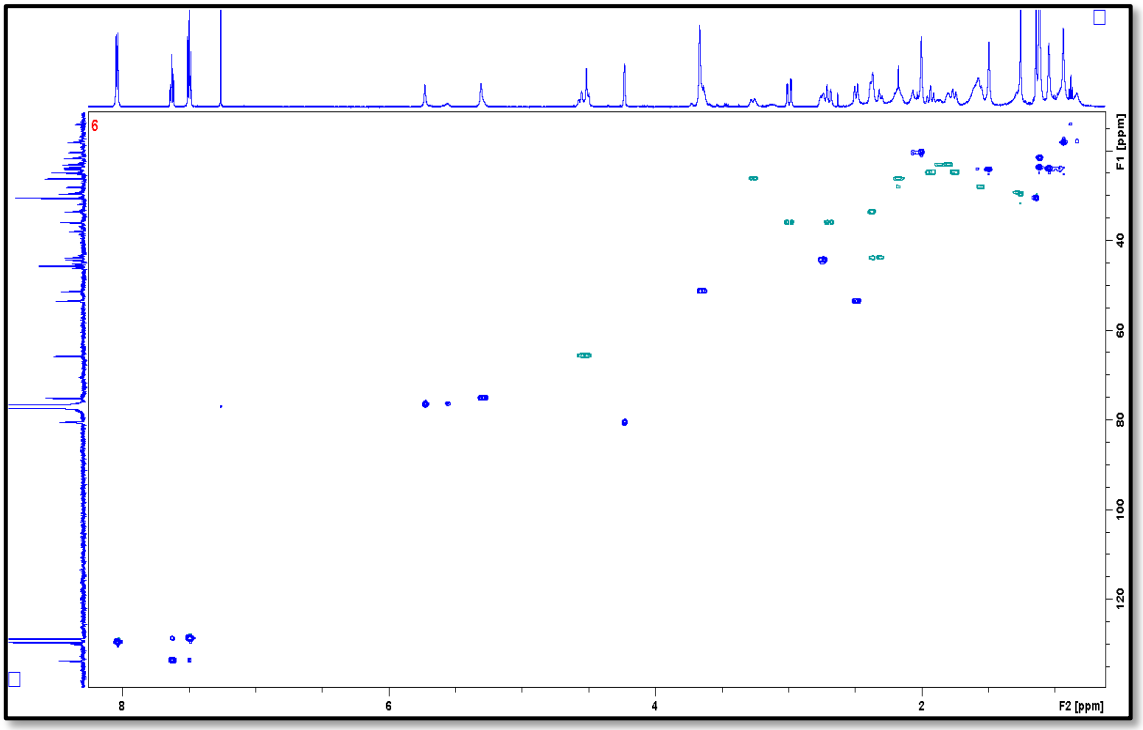

Figure S73: HSQC spectrum of Picraviane T (**22**) in $CDCl_3$ (600 MHz).

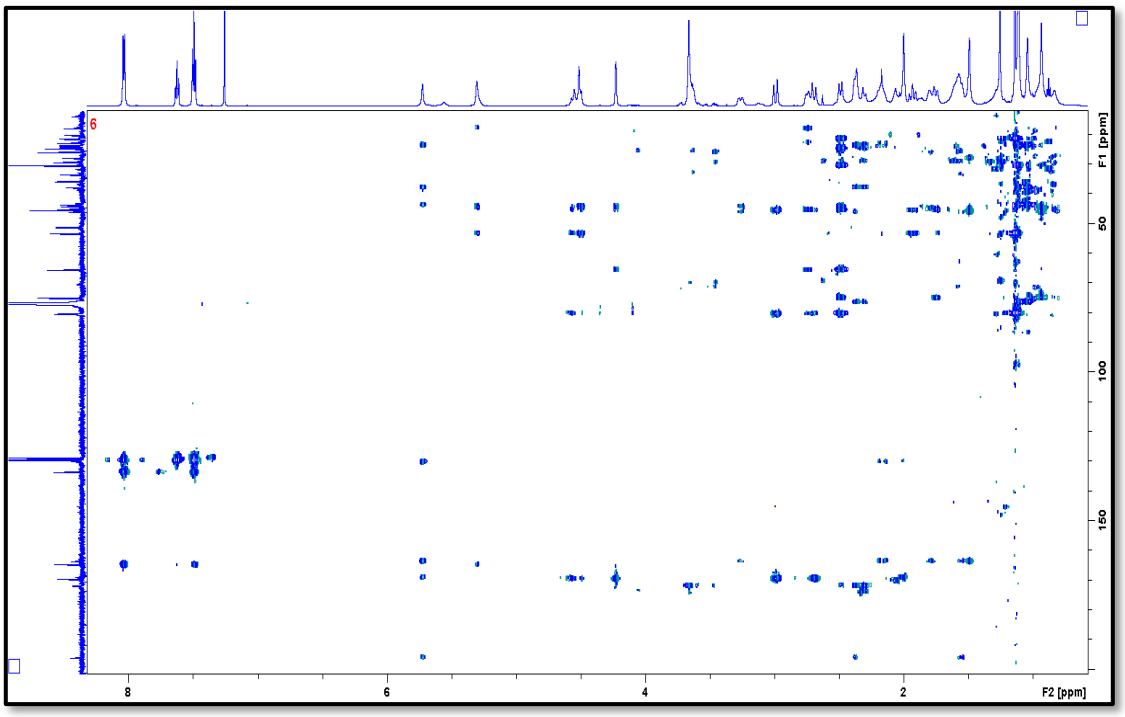

Figure S74: HMBC spectrum of Picraviane T (**22**) in $CDCl_3$ (600 MHz).

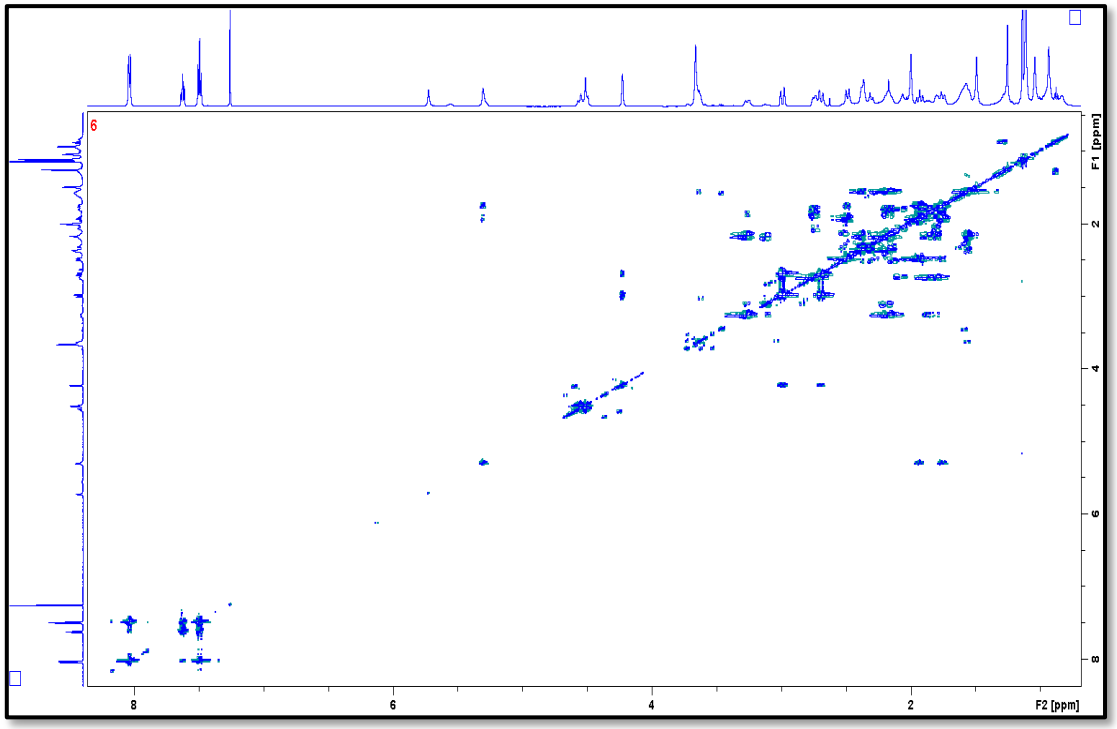

Figure S75: 1H-1H COSY spectrum of Picraviane T (**22**) in $CDCl_3$ (600 MHz).

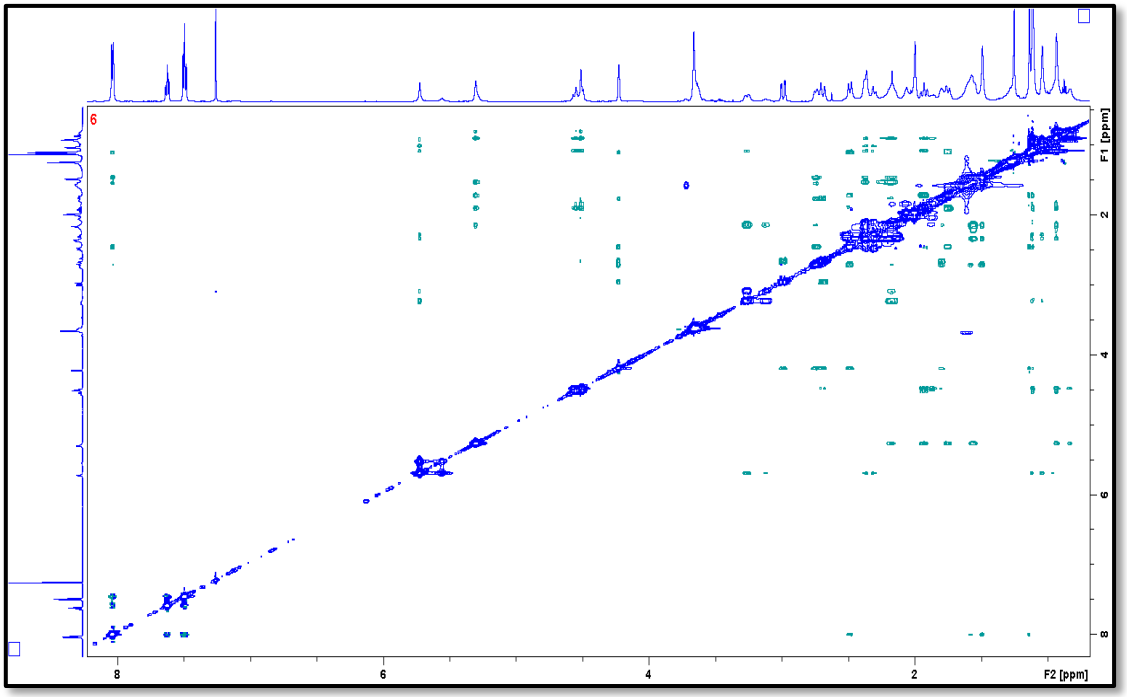

Figure S76: NOESY spectrum of Picraviane T (**22**) in $CDCl_3$ (600 MHz).

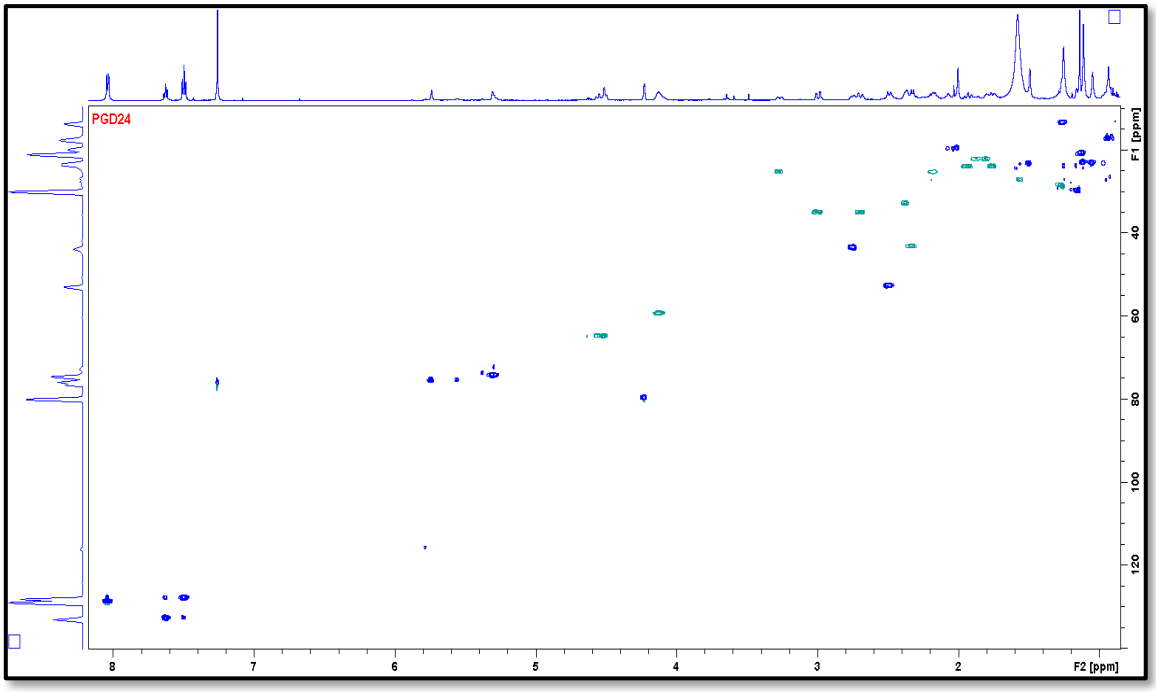

Figure S77: HSQC spectrum of Picraviane V (**24**) in $CDCl_3$ (600 MHz).

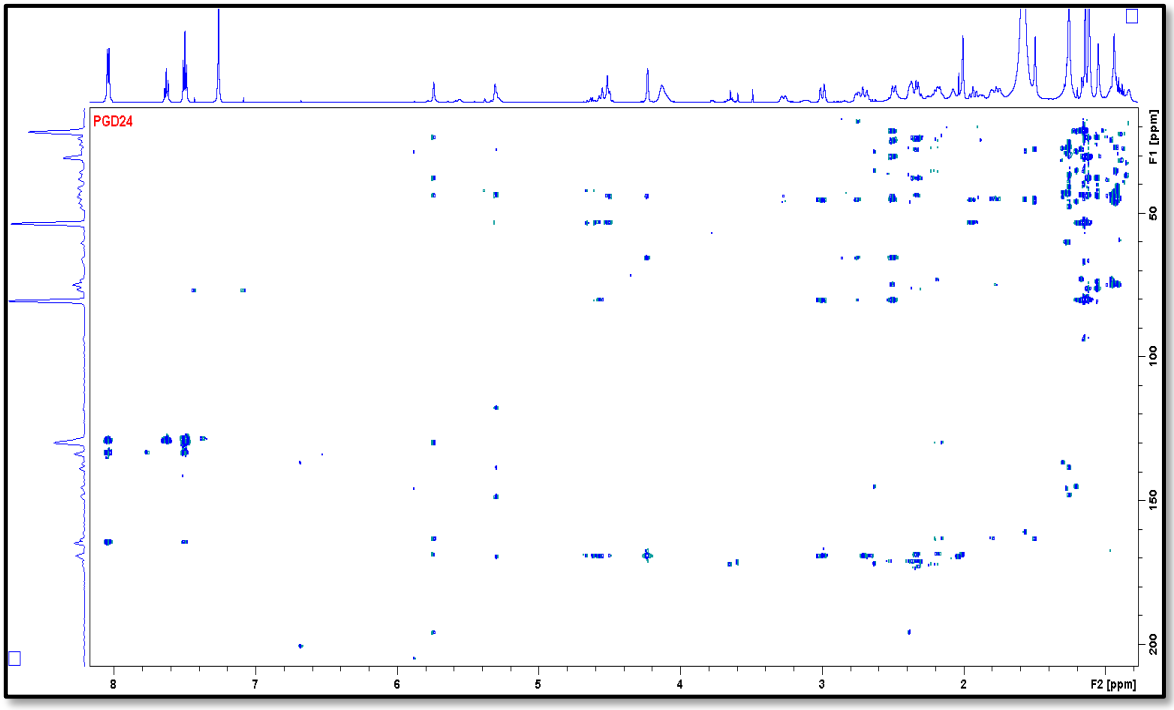

Figure S78: HMBC spectrum of Picraviane V (**24**) in $CDCl_3$ (600 MHz).

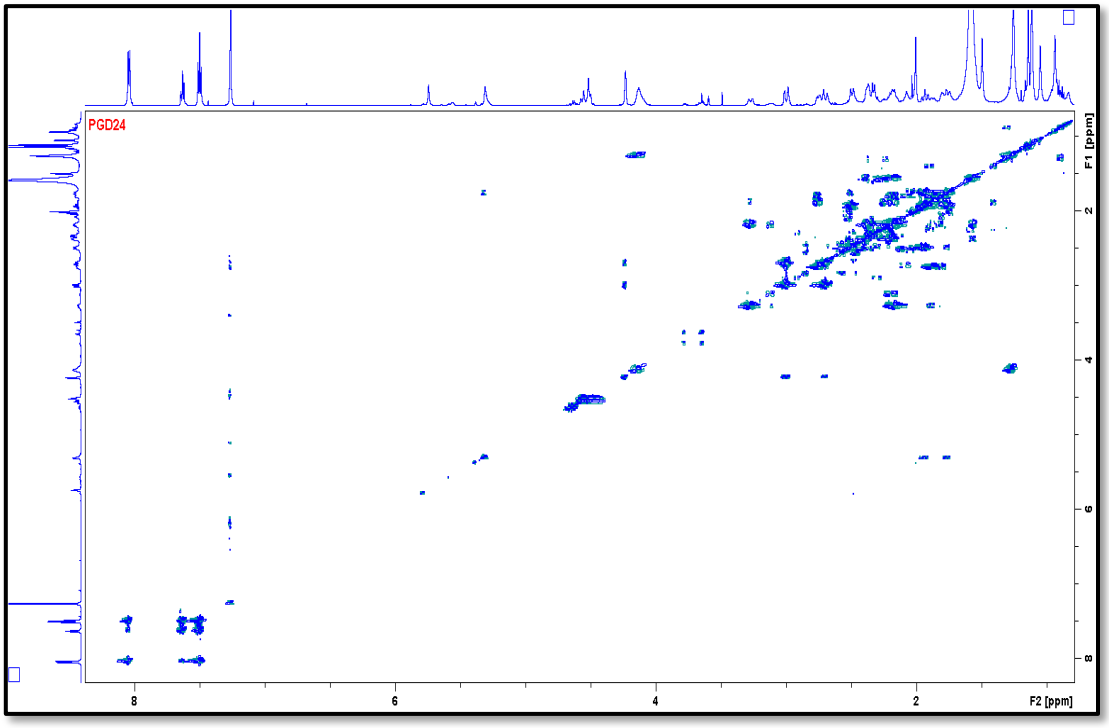

Figure S79: ^{1}H-^{1}H COSY spectrum of Picraviane V (**24**) in $CDCl_3$ (600 MHz).

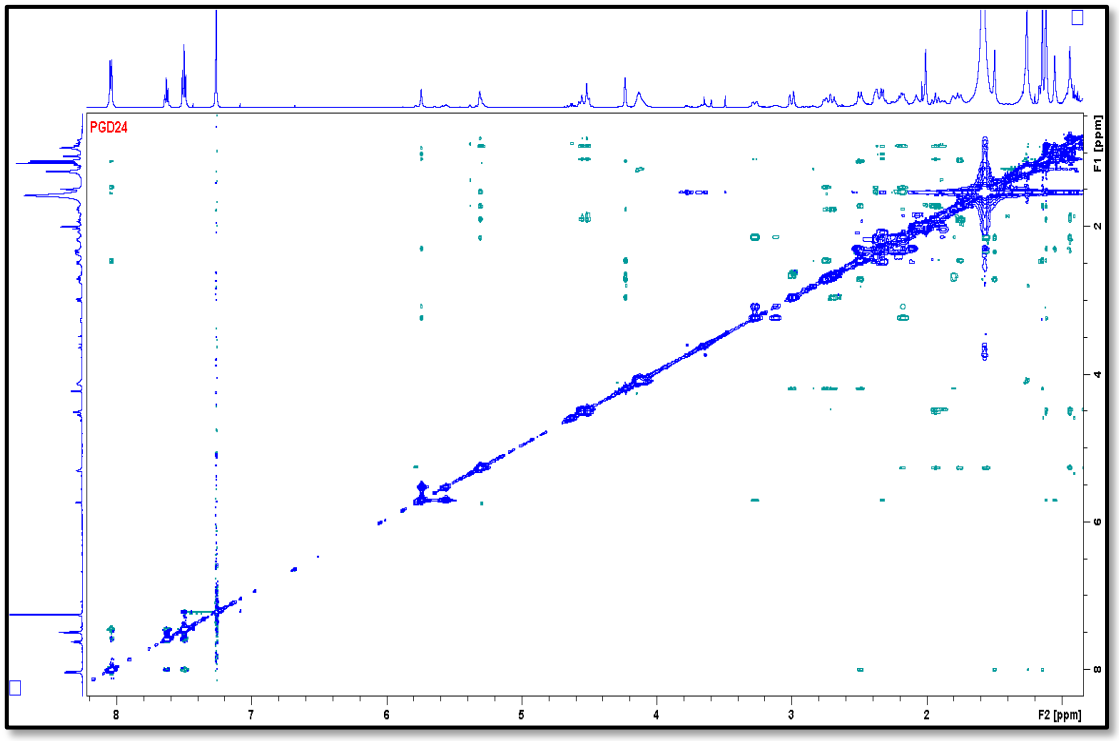

Figure S80: NOESY spectrum of Picraviane V (**24**) in $CDCl_3$ (600 MHz).

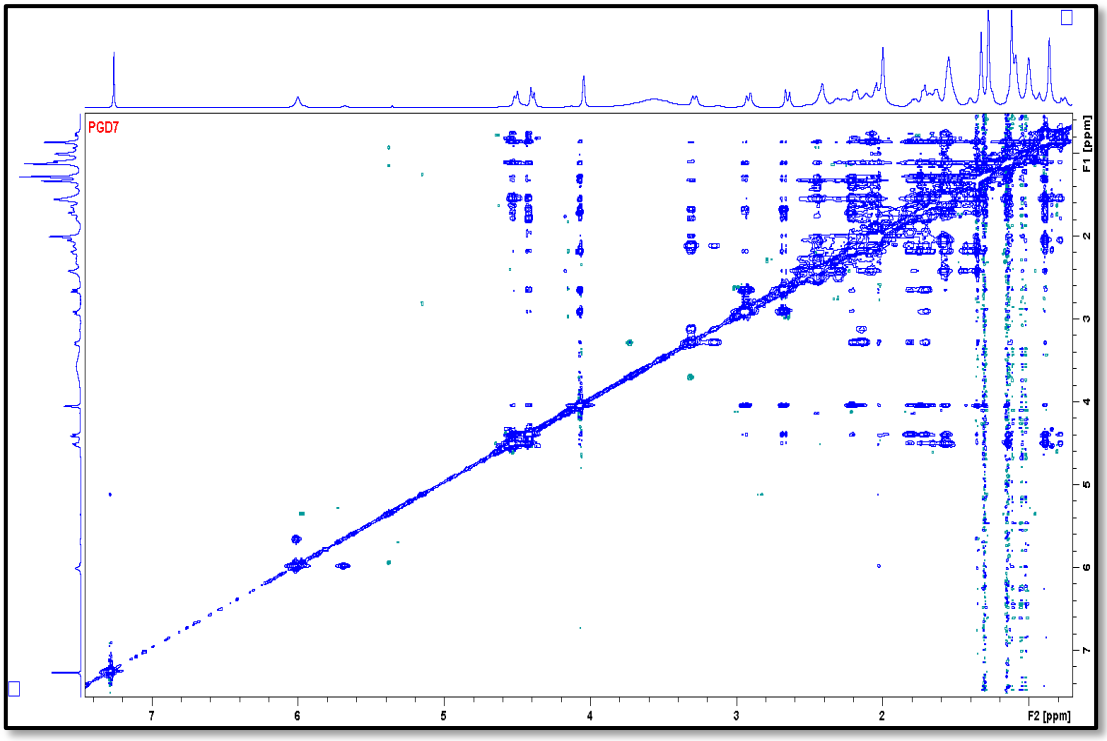

Figure S81: NOESY spectrum of Picraviane N (**07**) in $CDCl_3$ (600 MHz).

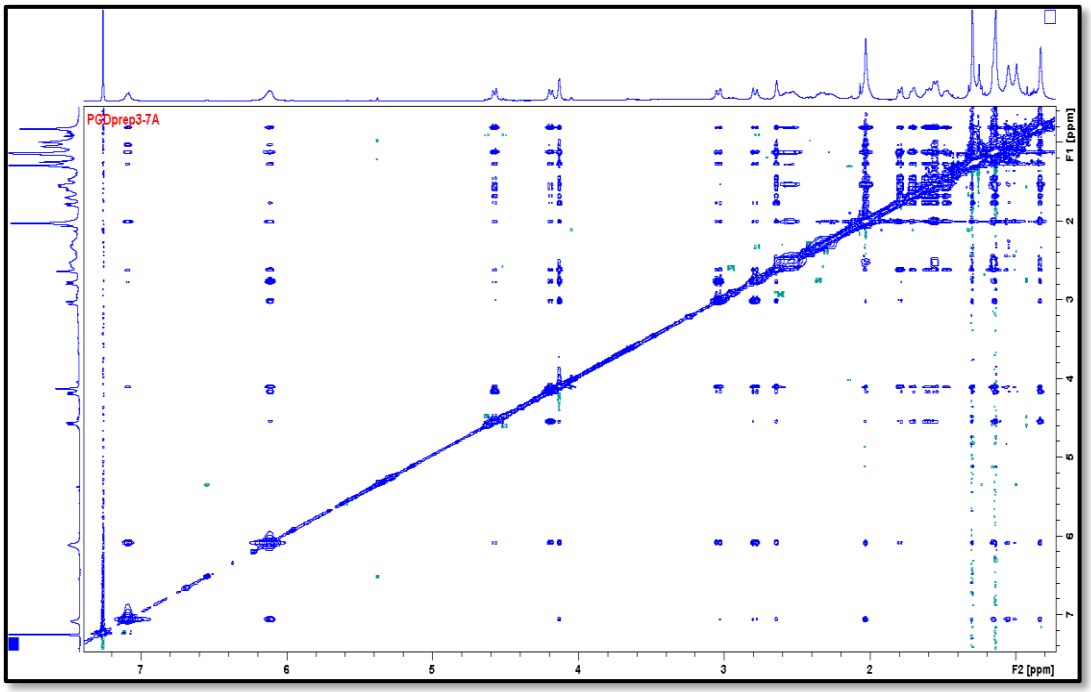

Figure S82: NOESY spectrum of Picraviane O (**07a**) in $CDCl_3$ (600 MHz).

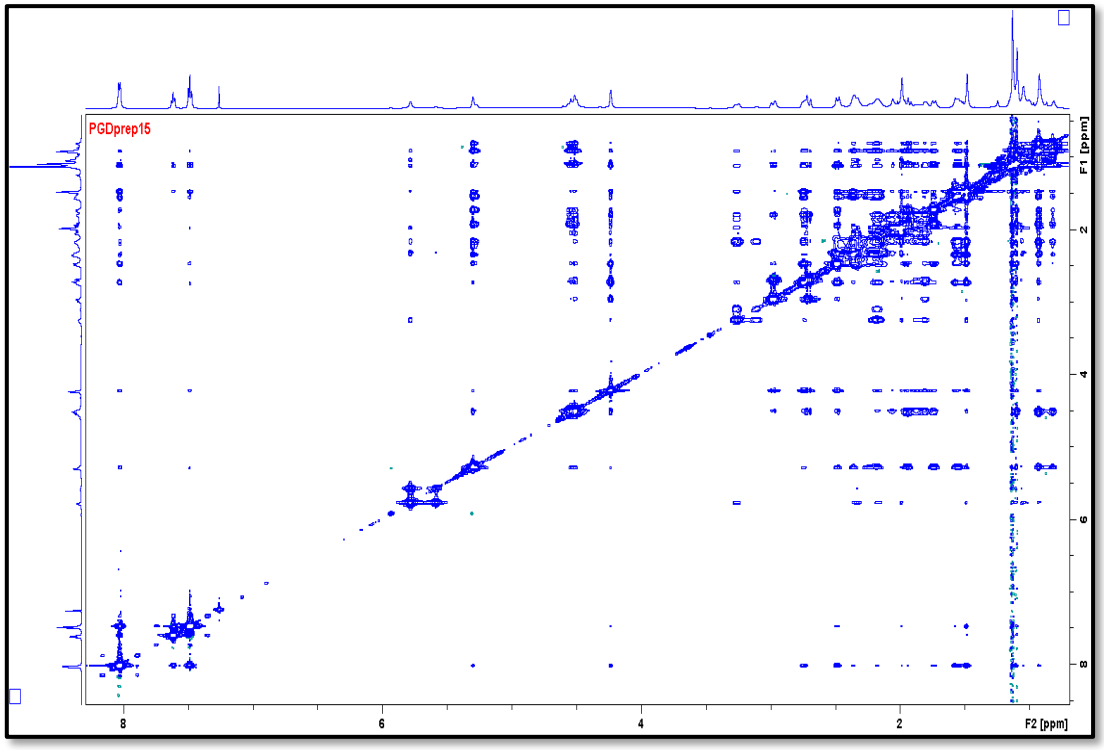

Figure S83: NOESY spectrum of Picraviane Q (**15**) in $CDCl_3$ (600 MHz).

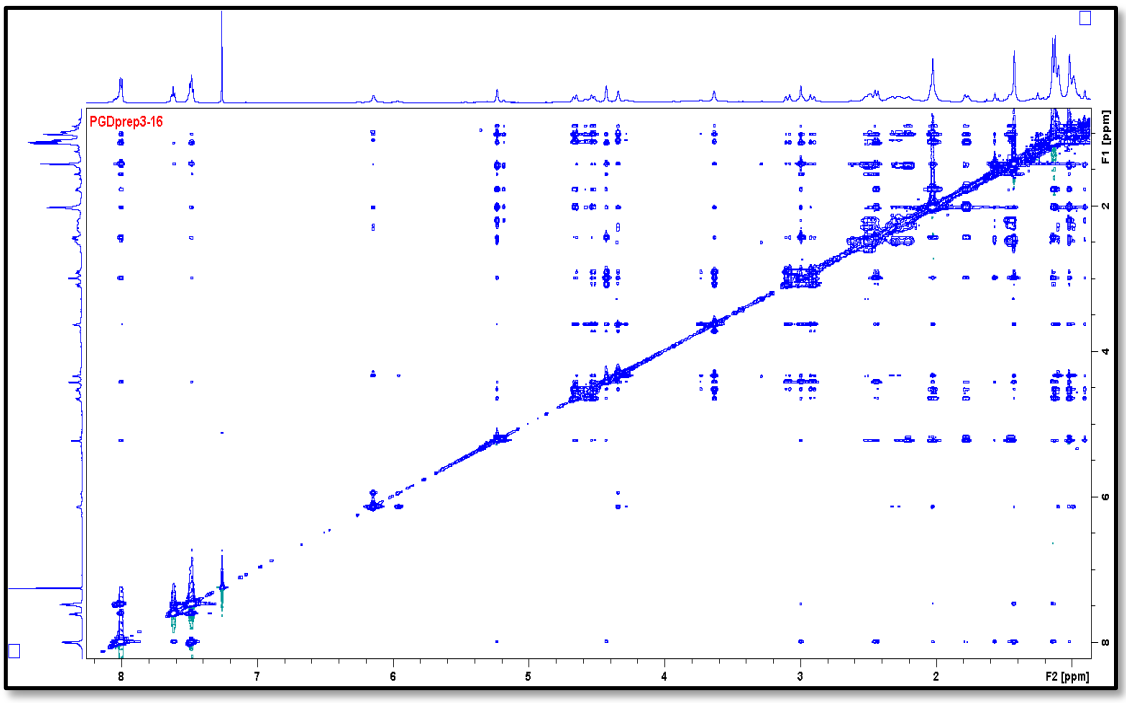

Figure S84: NOESY spectrum of Picraviane R (**16**) in $CDCl_3$ (600 MHz).